

Synthesis of Aza heterocycles from various substituted aromatic amines and dialdehyde

A Thesis Submitted

for the Degree of

DOCTOR OF PHILOSOPHY

In Chemistry

by

ARUNAVA MISRA

DR. MOHABUL ALAM MONDAL

(Research Guide)

to the



DEPARTMENT OF CHEMISTRY

JADAVPUR UNIVERSITY

KOLKATA- 700032

INDIA

March, 2024

Dedicated to my beloved Boro Pisimoni

CANDIDATE'S DECLARATION

I hereby declare that the work contained in the thesis entitled "Synthesis of Aza heterocycles from various substituted aromatic amines and dialdehyde" submitted for Ph.D. degree to the Jadavpur University Kolkata, India has been carried out in the Department of Chemistry under the supervision of Dr. Mohabul Alam Mondal. The work is original and has not been submitted in part or full by me for any degree or diploma to this or any other institute.

In keeping with general practice of reporting scientific observations, due acknowledgements have been made wherever the work described is based on the findings of other investigators.

March, 2024

Arunava Misra
15.03.2024
Arunava Misra

Research Scholar
Department of Chemistry
Jadavpur University
Kolkata- 700032, West Bengal

যাদবপুর বিশ্ববিদ্যালয়
কলকাতা - ৭০০ ০৩২, ভারত



JADAVPUR UNIVERSITY
KOLKATA-700 032, INDIA

FACULTY OF SCIENCE : DEPARTMENT OF CHEMISTRY : ORGANIC CHEMISTRY SECTION

CERTIFICATE FROM THE SUPERVISOR

This is to certify that the thesis entitled “**Synthesis of Aza heterocycles from various substituted aromatic amines and dialdehyde**” submitted by Sri Arunava Misra who got his name registered on 29/08/2019 for the award of Ph. D. (Science) Degree of Jadavpur University, is absolutely based upon his own work under the supervision of Dr. Mohabul Alam Mondal and that neither this thesis nor any part of it has been submitted for either any degree/diploma or any other academic award anywhere before.

Mohabul Alam Mondal
15/03/2024
DR MOHABUL ALAM MONDAL
Assistant Professor
Department of Chemistry
Jadavpur University
Kolkata-700032, India



(Signature of the Supervisor

Date with official seal)

ACKNOWLEDGEMENTS

I take this opportunity to thank and express my gratitude to all who have contributed in the successful completion of this thesis. First and foremost, I would like to thank and bow my head to my Gurudev Ostad Ji, who provided me with the strength to work hard and overcome the toughest situations and the ability to complete this thesis work successfully. Also, my heartfelt thanks and gratitude go to my family for their unconditional love and support.

It is a great pleasure to express my deepest thanks and gratitude to my advisor, Dr. Mohabul Alam Mondal, for providing me with the continuous support during my PhD study and research, for his patience, motivation, enthusiasm, and immense knowledge. His guidance helped me during the course of research and writing of this thesis. I also wish to express my appreciation to his family members for their affection.

I would like to acknowledge the past Heads of the Department and the present Head of the Department Prof. Kajal Krishna Rajak for their timely academic and administrative help and for providing me with the departmental facilities during my research work. I am deeply thankful to my course instructors Prof. Sanjay Bhar, Dr. Samit Guha, Dr. Arunabha Thakur, Dr. Amit Saha, Dr. Mohabul Alam Mondal, Prof. Tanurima Bhaumik, Prof. Rina Ghosh, Prof. Umasis Jana, Prof. Umesh Chandra Haldar and Dr. Gourhari Maiti for teaching the essence of chemistry to me. I will always miss the versatile teaching approach of Dr. Mohabul Alam Mondal and I would like to thank him for igniting the love of learning organic chemistry within me. I extend my sincere word of thanks to all the other faculty members for their kind help at various phases during the course of my doctoral studies.

I am grateful to the members of my Research Advisory Committee, Prof. Arindam Talukdar and head of the department for their valuable suggestions and cooperation during my research work.

This work would not have been possible without the help and support from the spectrometer operators Raju Babu, and Mrs. Baby di for 300 and 400 MHz NMR experiments. I thank Mr. Dyutiman Chakraborty, Mr. Mrityunjay for their constant help to regularise my CSIR fellowship and all other academic and technical staff members of the department of chemistry. I thank the former and the present Vice-Chancellor of Jadavpur University respectively, for providing me with the institutional facilities for my research and allowing me to present this work in the form of a thesis. I am grateful to Council of Scientific and Industrial Research (CSIR), India for the financial support granted through research fellowships.

I would like to extend heartfelt acknowledgment and appreciation to Ms. Sudipta Mondal, my special sister and lab mate, for her unwavering support and camaraderie throughout my PhD journey. Sudipta's dedication, encouragement, and collaborative spirit have been invaluable, creating a positive and motivating environment in the laboratory. I am truly grateful for the shared moments of success, the collaborative problem-solving, and the enduring friendship that has made the PhD journey all the more meaningful. Thank you, Sudipta, for being an exceptional lab mate and an even more exceptional sister.

I extend my wholehearted thanks to Sunny, Subhendu, Manas, Debabrata, Sushanta, Sourav, Hassan da, Rupsa, Sahanaz Di, and my juniors Soumya, Rwitabrita, Sourav, Susmita, Sayan, Pintu, Bidya and gratefully thank to Sushanta and Pintu for their help in analysing crystallographic data.

I am grateful to all the professors of the department of chemistry at Gour Banga University, Malda for their excellent teaching and guidance in my Master's Program for their constant encouragement and inspirations. I would like to thank Dr. Abul Hassan Sir and Dr. Subhankar Chowdhury at my Undergraduate course at Malda college, who kindled my passion in organic chemistry.

I express my heartfelt gratitude to my grandfather, Prof. Dr. Bhupendra Nath Misra, who has been a guiding light and a constant source of inspiration since my childhood. His unwavering support, motivation, and encouragement have played a pivotal role in shaping my academic journey, particularly in the pursuit of higher studies in organic chemistry. His wisdom, passion for knowledge, and dedication to the field have instilled in me a deep appreciation for the subject and a commitment to academic excellence. I am truly thankful for the invaluable lessons and encouragement he has provided, which have been instrumental in my academic and personal growth.

I express my sincere gratitude to all members of "We are Brothers" including Alik, Rantu, Prince, Bobin, Debraj, Ankur, Supriya, Pritam, Shrish, Dipanjan, Shreshtha, Prapan, Arka, Abir and many others for their companionship, moral support, and inspiration. A special acknowledgment to Sanu Da, crucial contributor who have played a significant role in changing my life and believing in my potential for success in research. I extend heartfelt thanks to Kana, my better half, for making a profound difference in my life, motivating and inspiring every aspect of my journey towards new possibilities.

Finally, I would like to acknowledge my late grandparents (Hiren and Shila), my beloved parents, my uncles, aunties and my in-laws for their love and blessings. I owe a lot of gratitude to my sisters Munai and Nanda for their constant guidance, cooperation and support. They have always been an inspiration to me and I feel lucky to have them as a sister. Arushi's enthusiasm for learning and her constant curiosity have served as a source of inspiration for me. Her presence in my life has reminded me of the importance of curiosity, perseverance, and joy in the pursuit of knowledge. They are blessed and loved by many.

Arunava Misra

LIST OF ABBREVIATIONS

Å	Angstrom(s)
Ac	Acetyl (CH ₃ C=O)
AcOH	Acetic Acid
aq	aqueous
Ar	Aryl
bp	Boiling point
Bu, ⁿ Bu	Normal (primary) butyl
°C	Degrees Celsius
calcd	Calculated
cat	Catalytic
CCDC	The Cambridge Crystallographic Data Centre
CD	Circular Dichroism
CDCl ₃	Deuterated chloroform
CIF	Crystallographic Information Framework
cm ⁻¹	Wavenumber(s)
COSY	Correlation spectroscopy
ct	Calf Thymus
δ	Chemical shift in parts per million
d	Doublet
DBU	1,8-diazabicyclo [5.4.0]undec-7-ene
DCM	Dichloromethane
dd	Doublet of a doublet
DMF	<i>N,N</i> -Dimethylformamide
DMSO	Dimethyl sulfoxide
DNA	Deoxyribonucleic acid
<i>E</i>	Entgegen
EB	Ethidium bromide
EDG	Electron-donating group
equiv	Equivalent(s)
Eq.	Equation

ESI	Electrospray ionization
Et	Ethyl
EWG	Electron-withdrawing group
h	Hour(s)
HMBC	Heteronuclear multiple bond correlation
HOMO	Highest Occupied Molecular Orbital
HRMS	High-Resolution Mass Spectrometry
HST	Hoechst
HSQC	Heteronuclear single quantum coherence spectroscopy
HT	Hydride Transfer
Hz	Hertz
IR	Infrared
<i>J</i>	Coupling constant (in NMR spectrometry)
LCMS	Liquid chromatography mass spectrometry
LUMO	Lowest unoccupied molecular orbital
μ	Micro
m	Multiplet
mg	Milligram
M	Molar
Me	Methyl
MHz	Megahertz
min	Minute(s)
mL	Milliliter
mmol	Milimole(s)
mp	Melting point
m/z	Mass-to-charge ratio
N	Normal
NaHCO ₃	Sodium bicarbonate
Naph	Naphthyl
NBS	<i>N</i> -bromosuccinimide
nm	nanometer
NMR	Nuclear magnetic resonance
OD	Optical Density

OPA	<i>o</i> -Pthaladehyde
ORTEP	Oak Ridge Thermal Ellipsoid Plot
PAH	Polycyclic aromatic hydrocarbon
Ph	Phenyl
PL	Photoluminescence
Pd(OAc) ₂	Palladium Acetate
ppm	Part(s) per million
<i>p</i> -TsOH	<i>p</i> -Toluenesulfonic acid
Φ	Quantum Yield
%	Percentage
R	Alkyl group
R _f	Retention factor
rt	Room temperature
s	Singlet
t	Triplet
Temp	Temperature
TFA	Trifluoroacetic acid
THF	Tetrahydrofuran
TLC	Thin layer chromatography
TMS	Trimethylsilyl
TOF	Time of flight
UV	Ultraviolet
Vis	Visible
Z	Zusammen

SYNOPSIS

Name of Research Scholar: **Mr. Arunava Misra**

Index no: **101/19/Chem./26**

Degree for which submitted: **Ph.D.**

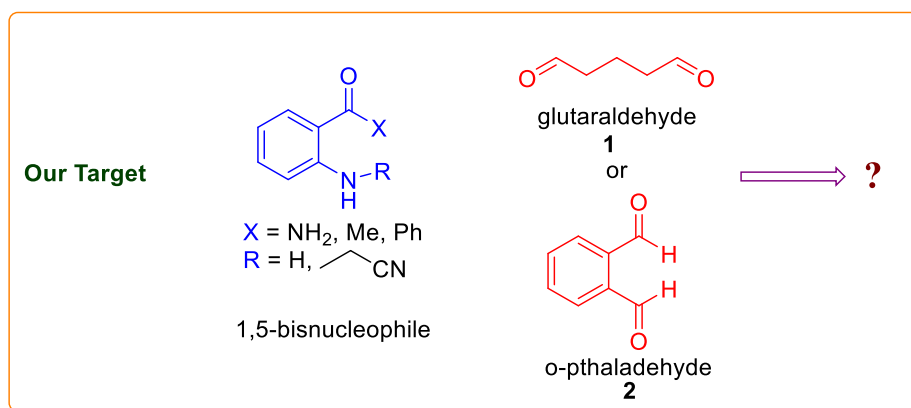
Department: **Chemistry**

Name of the Research Guide: **Dr. Mohabul Alam Mondal**

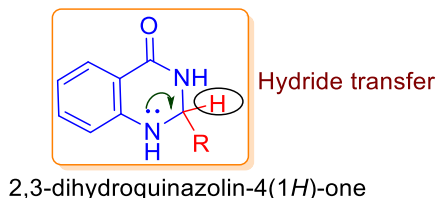
Thesis Title: Synthesis of Aza heterocycles from various substituted aromatic amines and dialdehyde.

Objectives:

- Design and synthesis of *N*-heteroatom-based fluorophores for various applications in the field of optoelectronics and bio imaging.
- Explore the reactivity of 1,5-bisnucleophile (2-aminoacetophenone & *anthranilamide*) with *o*-Pthalaldehyde to construct biologically important aza-heterocycles.



- We planned to synthesize functionalized quinazolinones for application in the area, such as interaction with biomaterials, photophysical study to explore biomedical applications, etc. We planned to investigate the scope of hydride transfer from 2,3-dihydroquinazolin-4(1*H*)-one to an electrophilic centre placed at the distal position within the same molecule.

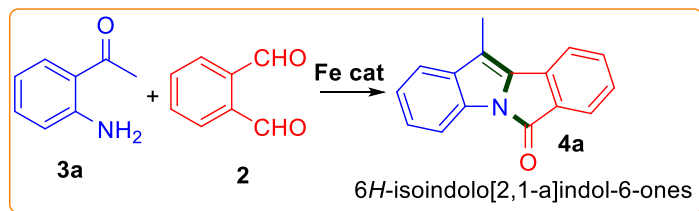


- Our objective was to explore the Lewis acidic property of Yttrium Nitrate to synthesize various functionalized aromatic aniline-based cyanoethylated products.

The thesis entitled above has been divided into three chapters as under:

Chapter 1: Transition Metal Catalyzed Annulative Coupling: Synthesis and Photophysical Properties of Isoindoloindolones

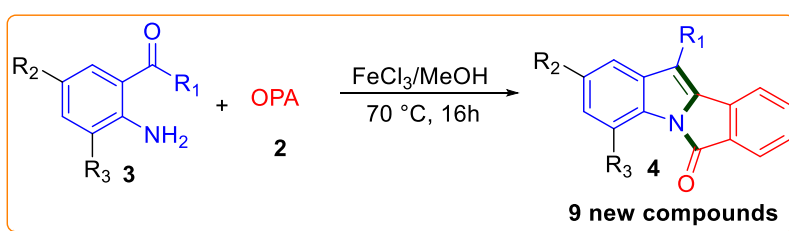
The first chapter describes a novel synthetic routes to access an array of 6*H*-isoindolo[2,1-*a*]indol-6-ones via one pot tandem cyclization of activated *o*-phthalaldehyde (**2**) with 2-amino acetophenone (**3a**) involving well-documented Lewis acidic behaviour or FeCl₃.



Scheme 1: Reactivity of OPA towards 2-aminoacetophenone

6*H*-isoindolo[2,1-*a*]indol-6-ones are an important class of nitrogen heterocycles that exhibit a wide range of biological activities. Consequently, finding an efficient route for synthesizing 6*H*-isoindolo[2,1-*a*]indol-6-ones **4** with different substituent groups would be highly desirable. Among the known synthetic routes, the intramolecular lactamization of 2-carboxylphenyl indole, intramolecular C-H coupling of *N*-benzoylindole and intramolecular Wittig reaction of *N*-phenylphthalimide derivatives are the most popular methods. However, most of these methods usually require multistep procedures under harsh reaction conditions and lead to a limited range of substrates.

With the optimized reaction conditions established, we set out to examine the generality of the reaction with various electron-withdrawing and electron donating substituents (**Scheme 2**).

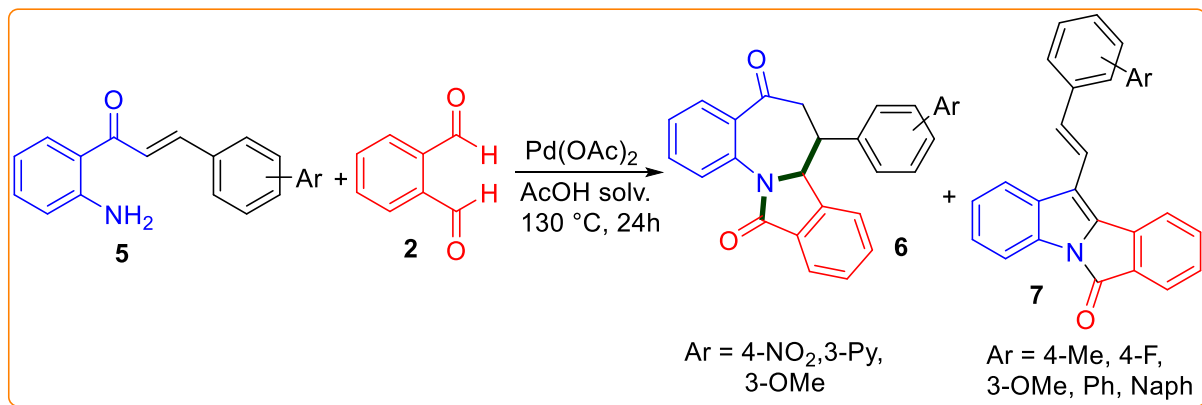


Scheme 2: Various substrate scope of the reaction

The green fluorescence properties of these isoindoloindolone compounds in solid as well as in the solution state was also observed.

Next, we targeted to synthesize another important class of heterocycles viz. 7-(4-nitrophenyl)-7,7a-dihydro-5*H*-benzo[6,7]azepino[2,1-*a*]isoindole-5,12(6*H*)-dione by changing the reactivity of the 1,5-bis nucleophile under appropriate reaction conditions (**Scheme 3**). In the reactions of structurally similar motif of 2-amino acetophenone **3a**, its chalcone with different

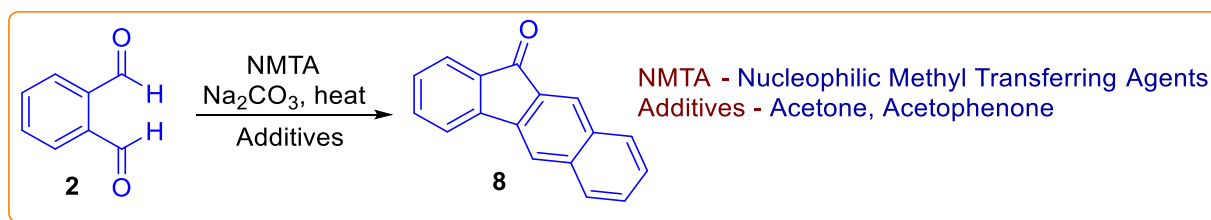
aromatic aldehydes. We anticipated that we got a very interesting heterocyclic moiety 7-(4-nitrophenyl)-7,7a-dihydro-5*H*-benzo[6,7]azepino[2,1-*a*]isoindole-5,12(6*H*)-dione along with isoindoloindolones with extended conjugation via 1,4- and 1,2 addition fashion. We optimized the reactions with different Lewis acids, solvents and varying temperature. Taking the optimization condition in hand we are able to find the substrate scopes of our reactions. We observed that incorporation of electron withdrawing substituents in chalcone portion favours 1,4-addition pathway, whereas electron donating substituents favours 1,2-addition pathway.



Scheme 3: Reaction between OPA and chalcones in presence of Pd(II) catalyst

Chapter 2: Studies towards the Synthesis of 11*H*-benzo[*b*]fluoren-11-one from *o*-Phthalaldehyde

In this chapter, we described a simple, economically viable method for synthesizing 11*H*-benzo[*b*]fluoren-11-one **8**, a dual-state organic fluorophore, starting from *ortho*-phthalaldehyde (OPA) **2** in different methyl transferring solvents (acetone, DMF, DMSO) (**Scheme 4**). Simple and rapid product isolation, high atom economy, short reaction time, and scalability are the attractive features of the method. During reaction condition optimization, DMSO, DMF and acetone in basic conditions contributed one carbon to form the compound, besides their solvent roles. LCMS analysis of the incomplete reaction mixture supported a proposed mechanism.

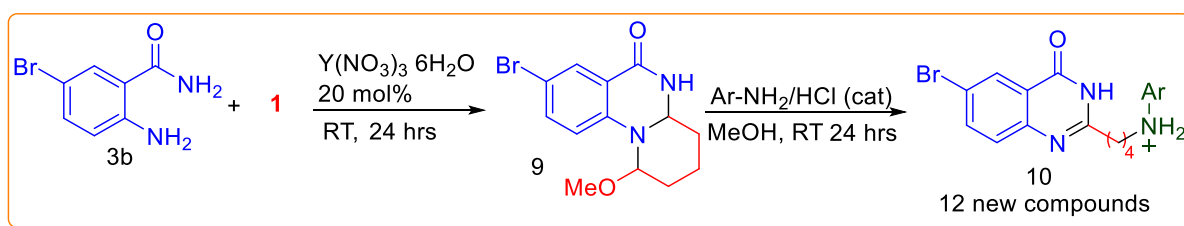


Scheme 4: One pot synthesis of benzo[fluorenone from OPA

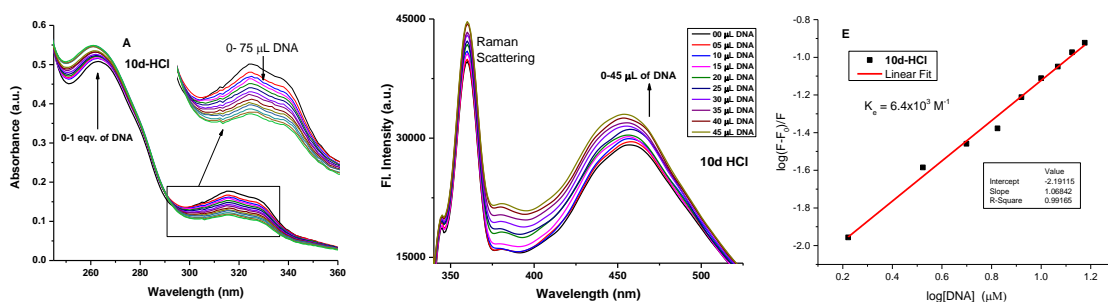
Chapter 3: Design, Synthesis, and Calf-Thymus DNA binding Studies of Highly Functionalized Quinazolinones

The third chapter of the thesis describes the one pot protocol for the synthesis of wide range of substituted quinazolinones **10** via a three component coupling reactions 4-bromoanthranalimide **3b**, glutaraldehyde **1** and various substituted anilines in presence of Yttrium nitrate as a catalyst.

A new strategy to access quinazolinones, a pharmaceutically active moiety, connected to a diverse array of amines linked through a five-carbon spacer via a facile intramolecular [1,5] hydride transfer reaction in a dihydroquinazolin-4(1*H*)-one moiety synthesized from anthranilamide, glutaraldehyde, and aromatic amines is described in isopropanol medium in the presence of catalytic HCl (**Scheme 5**). The use of isopropanol as a reaction medium at RT and isolation of the product without rigorous column purification make the process a step ahead towards sustainability. One of the synthesized compound was evaluated as a small molecule DNA binder. Detailed binding properties were investigated by the multi spectroscopy methods (**Figure 1**).



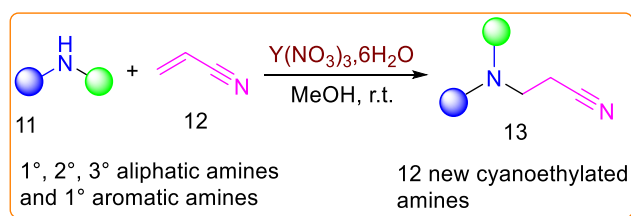
Scheme 5: Strategy to synthesize quinazolinone triggered by different aromatic amines



Chapter 4: Yttrium Nitrate Promoted Synthesis of Cyanoethyl Amines

The fourth chapter of this thesis describes the Lewis acidic behaviour of Yttrium nitrate in aza-Michael addition reaction of various aliphatic and aromatic amines with acrylonitrile in excellent yields.

Our preliminary study commenced with the reaction of aniline **11** with 10.0 equivalent of acrylonitrile **12** as a Michael acceptor for optimization of the reaction (**Scheme 6**). We optimized the reactions under various condition and we found that MeOH is the best solvent for this reaction. Taking the optimized condition in hand we have synthesised an array of cyanoethylated amine derivatives possessing electron donating as well as electron withdrawing substituents. Direct aqueous workup yielded cyanoethylation products up to 99.9% pure.



Scheme 6: $Y(NO_3)_3 \cdot 6H_2O$ mediated cyanoethylation of aniline by acrylonitrile

The method demonstrates selectivity towards mono-cyanoethylation, particularly targeting electron-rich primary aromatic amines, aliphatic secondary amines, and bulky primary aliphatic amines. An interesting aspect of this approach is its potential for use in biomaterial modification. This is supported by the stability and water solubility of the yttrium ion, which serves as a mild Lewis acid in the method. Furthermore, the yttrium ion can be easily removed from the final product, enhancing its biocompatibility. This suggests that the method could be a promising alternative for the modification of biomaterials, offering a controlled and selective means of introducing cyanoethyl groups while maintaining compatibility with the intricacies of biological systems.

CONTENTS

Entries	Page No.
Acknowledgements	i
List of Abbreviations	iv
Synopsis	vii
 Chapter 1: Transition Metal Catalyzed Annulative Coupling: Synthesis and Photophysical properties of Isoindoloindolones	
1.1. INTRODUCTION	2
1.2 LITERATURE REVIEW: A FOUNDATION FOR THE PRESENT WORK	5
1.3 PRESENT WORK	8
1.4 RESULT AND DISCUSSIONS	11
1.4.1 Synthesis of the Starting Material 29b-29j.....	13
1.4.2 Mechanistic Investigation	16
1.5 BROADENING THE SUBSTRATE SPECTRUM: ADDITIONAL INSIGHTS	18
1.5.1 Optimization of the reaction between chalcone and OPA	19
1.5.2 Mechanism of the formation of 29pa.....	21
1.6 PHOTOPHYSICAL PROPERTIES OF COMPOUND 6b	22
1.6.1 Absorption Spectroscopy Method.....	22
1.6.2 Photoluminescence Properties	22
1.6.3 Experimental Findings: Results and Insights	23
1.7 CONCLUSION	28
1.8 EXPERIMENTAL SECTION	29
1.8.1 General Procedures	29
1.8.2 Experimental Procedure and Analytical Data of the starting materials	30
1.8.3 Synthesis and characterization of the final compounds 6b-6j.....	37
1.9 CRYSTALLOGRAPHIC TABLE.....	93
1.10 REFERENCES	103

Chapter 2: Studies towards the Synthesis of 11*H*-benzo[b]fluoren-11-one from *o*-Phthalaldehyde

2.1 INTRODUCTION	109
2.2 LITERATURE BACKGROUND	112
2.3 PRESENT WORK	117
2.4 RESULTS AND DISCUSSION	117
2.5 MECHANISTIC STUDY	120
2.6 CONCLUSION	122
2.7 EXPERIMENTAL SECTION	122
2.7.1 Instruments and characterization	122
2.7.2 General procedure for the synthesis of compound 11 <i>H</i> -benzo[b]fluoren-11-one	122
2.7.3 Analytical spectroscopic data of 11 <i>H</i> -benzo[b]fluoren-11-one (40)	123
2.8 SPECTRAS OF COMPOUND 11 <i>H</i> -Benzo[b]fluoren-11-one (40)	125
2.9 REFERENCES	127

Chapter 3: Aromatic Amine attached Quinazolinones: Synthesis Characterization and DNA Binding Properties

3.1 INTRODUCTION	132
3.2 LITERATURE BACKGROUND	135
3.3 LITERATURE BACKGROUND & CONTRIBUTION FROM OUR GROUP	139
3.4 RESULT AND DISCUSSION	141
3.5 CALF-THYMUS DNA (ctDNA) BINDING STUDY	146
3.5.1 Techniques employed to study drug–DNA interactions	148
3.5.1.1 UV–visible spectroscopy	148
3.5.1.2 Fluorescence Spectroscopy	148
3.5.1.3 KI quenching studies	150
3.5.1.4 Thermal denaturation studies	150
3.5.1.5 Competitive displacement assays	151
3.5.1.6 Time Resolved Fluorescence	152

3.5.1.7 Circular Dichroism Spectra Study	154
3.5.2 ctDNA binding study with our synthesized molecule 86k-HCl.....	155
3.6 CONCLUSION	159
3.7 EXPERIMENTAL SECTION	159
3.7.1 General information	159
3.7.2 Experimental Procedure for Synthesis of Quinazolinones and Spectral Data	159
3.7.3. DNA Interaction Study: Experimental Methods and Findings	165
3.8 REFERENCES	191

Chapter 4: Yttrium Nitrate Promoted Synthesis of Cyanoethyl Amines

4.1 INTRODUCTION	198
4.2 LITERATURE BACKGROUND.....	199
4.3 Present Work.....	201
4.4 MECHANISM OF AZA-MICHAEL ADDITION CATALYZED BY $Y(NO_3)_3 \cdot 6H_2O$	204
4.5 CONCLUSIONS.....	205
4.6 EXPERIMENTAL SECTION	205
4.6.1 General information	205
4.6.2 Experimental Procedure and Spectral Data.....	206
4.7 REFERENCES	225

APPENDICES

List of Publications	228
Publications Abstract	229
Oral Presentation in Conference	231
List of Seminar Attended	231

Chapter 1

Transition Metal Catalyzed Annulative Coupling: Synthesis and Photophysical properties of Isoindoloindolones

Part of the work described in this chapter is published in

Tetrahedron 155 (2024) 133887; DOI: 10.1016/j.tet.2024.133887

Transition Metal Catalyzed Annulative Coupling: Synthesis and Photophysical properties of Isoindoloindolones

1.1. INTRODUCTION

Heterocyclic chemistry plays a pivotal role in organic chemistry, with compounds incorporating a heterocyclic core serving crucial functions in both industrial and biological contexts. Over 80% of developed drug molecules feature heterocyclic structures, mainly comprising nitrogen, oxygen, or sulfur atoms in five or six-membered rings. These compounds serve as fundamental building blocks in medicines, natural products, and biomolecules, contributing significantly to pharmaceutical and biological research. Researchers are keenly interested in their synthetic aspects, leveraging their multifaceted roles in functionalization, catalysis, and intermediacy for complex molecule synthesis.

Isoindole and saturated analogue of isoindole unit with their carbonyl moiety is called as isoindolinone molecule, has interesting properties for synthetic and medicinal chemistry. Isoindolinones are found in certain pharmaceuticals and can serve as versatile building blocks in organic synthesis. The significance of these compounds lies in their ability to serve as key intermediates in the synthesis of more complex molecules, contributing to the richness of heterocyclic chemistry.

Isoindole **1** is isomeric with Indole **2** which comprise a benzene ring fused with pyrrole nucleus. The parent compound and the 2-unsubstituted derivatives can tautomerize with the 1*H*-isomer, i.e. isoindolenine or (1*H*-isoindole)-**3**. Isoindole is much more unstable compared with indole and undergoes rapid oxidation in air to form polymers. Isoindole is thermodynamically more stable than its isoindolenine isomer at room temperature. The next stable reduction state of isoindole is isoindoline **4**. Isoindolinone (phthalimidine) **5** is the more stable derivative of isoindole¹. Isoindolinone system is expressed by a bicyclic nucleus which is deduced through the blending of γ -lactam ring and benzene ring. These types of compounds are also named as phthalimidines which are inner amides of the correlative γ -amino carboxylic acid. Isoindole **1** is a bicyclic 10 π electron array and complies with the Huckel ($4n + 2$) rule for aromatic stabilization. The distribution of charge density around the isoindole nucleus was calculated based on the LACO-MO method or the 'frontier electron concept', and the relatively high electron density found at position 1. Therefore, the expectation is that electrophilic substitution on carbon will occur most readily at this position. The semiempirical calculations of Dewar and Polansky et al. estimate a substantial degree of resonance stabilization for isoindole with a value of about 56 kcal mol⁻¹ which is significantly larger than the value of pyrrole and is close

to that ascribed for indole. Isoindole **1** should be favoured over its tautomer, isoindolenine **3** by about 8 kcal mol⁻¹ according to a molecular orbital calculation of Veber and Lwowski².

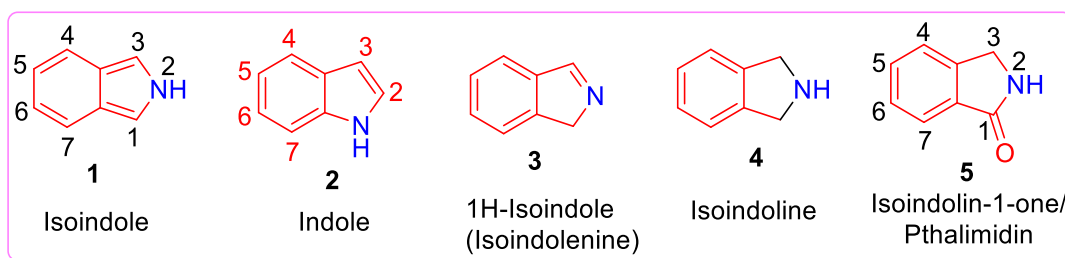


Figure 1.1 Isoindole and its other analogue

Due to the chemical instability of isoindole **1**, its isolation and detailed characterization were challenging and not achieved until 1972.³ Researchers likely faced difficulties in isolating the compound due to its reactivity and tendency to undergo side reactions. Despite the challenges with isoindole, the first isoindole derivative, *N*-methylisoindole was successfully prepared in 1951⁴.

Decoration of Isoindoline-1-one ring in proper position via their important pharmacophore unit generated to many natural and pharmaceutical products which exhibited bioactivity such as antifungal, antibacterial, antiparasitic, antiviral, anti-inflammatory, anticancer, antimalarial and enzyme inhibitor. The fusion of indole at the 2,3 positions can have significant implications for the compound's reactivity, stability, and biological activity. This modification may lead to the creation of a scaffold **6** with specific characteristics desirable for various applications, such as drug discovery or materials synthesis that make it valuable for further investigation.

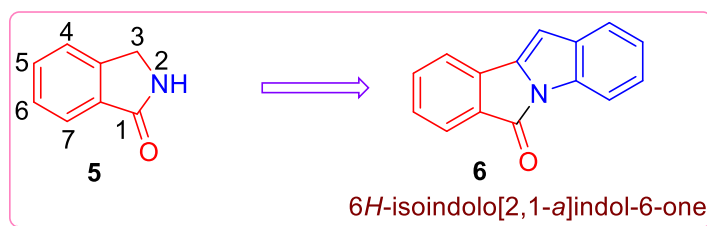


Figure 1.2 Isoindoloindolone designed from isoindoline-1-one

Inspired by the natural importance, we have concentrated on the pharmaceuticals utility of isoindoloindoles in this chapter. 6*H*-Isoindolo[2,1-*a*]indol-6-one (**6**) is a core structure for a number biologically active compounds. Indole-based structures derived from heterocyclic systems resembling 6*H*-isoindolo[2,1-*a*]indol-6-one **6** have been used as potential anti-tumor agents⁵ **7** and melatonin MT₃ ligands⁶ **8** as well as intermediate **9** in the synthesis of bacterial NorA efflux pump inhibitors^{7, 8}. Melatonin is a neurohormone derived from indole and is synthesized in the pineal gland of all mammalian species. There are two well-studied melatonin receptors in the human body, known as MT₁ and MT₂. However, a third receptor, MT₃, has

been discovered and requires further investigation. The MT₃ receptor has been found to interact with isoindolo compounds, particularly those with a core structure similar to compound **6**. This discovery opens up possibilities for in-depth studies on the binding properties of the MT₃ receptor. Isoindolo compounds have demonstrated cytotoxicity against carcinoma cells at low micromolar concentrations. Valuable in anticancer drug design, isoindolo compounds, are crucial for synthesizing drugs and have diverse applications. They hold potential in developing libraries of potential anticancer agents and as NorA efflux pump inhibitors, enhancing antibiotic effectiveness. A convenient synthetic route for isoindolo compounds, resembling compound **6**, is significant for pharmaceutical advancements, potentially leading to novel antibacterial drugs.

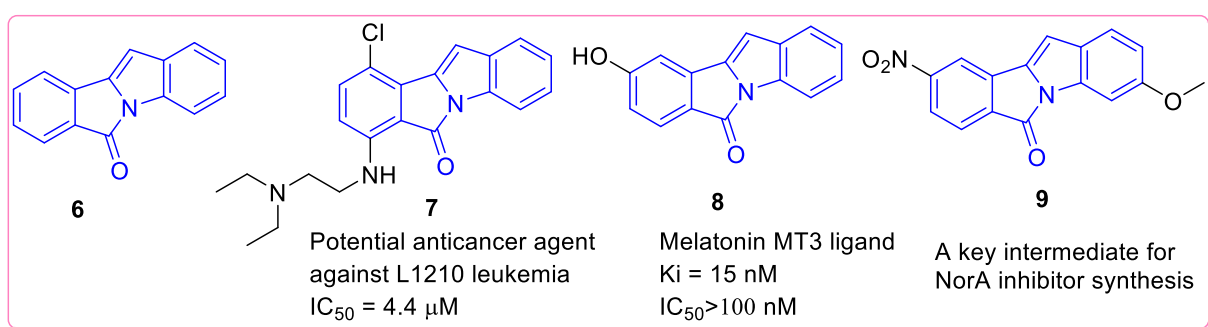


Figure 1.3 Some biologically relevant analogues of 6*H*-Isoindolo[2,1-*a*]indol-6-one

Extensive π -conjugation in multi-fused ring reduced the band gaps and also increased the charge transporting mobilities due to more electronic coupling and systematic intermolecular π - π overlapping. The tetracyclic aromatic ring containing compound **6** is a very good example of fluorophore. High fluorescence quantum yields and good photo stability, made them very charming for their various utilizations such as photosensitizers for organic photovoltaics and fluorescent markers in case of bio-imaging. The current fluorescence imaging techniques employed in biomedical research predominantly rely on fluorescent dyes and nanoparticles due to the insufficient fluorescence of biological objects⁹

The development of fluorophore having high photoluminescence (PL) properties in monomeric form as well as in aggregated form (dual-state emission or DSEgens) has recently become an attractive field of research for application in fluorescence imaging technologies to decipher complex biological processes and specific molecular targets, and optoelectronic properties but the area remains its infancy.¹⁰ Most of the existing organic dyes show either aggregation-induced emission or quenching. The common strategies for designing dual-state emission material are installing a twisted and bulky functional group onto a known organic fluorescent structure to reduce π - π stacking or keeping the chromophore isolated, along with the donor-

acceptor molecular architecture. Considering their broad range of applications, the development and design of multi-fused pyrroles has attracted the most demanding areas in organic chemistry and medicinal field. We described in chapter 1, a one-pot tandem protocol for constructing a linear tetracyclic aromatic core **6** via FeCl₃-mediated annulative coupling of 2-aminoacetophenones with *ortho*-phthalaldehyde and try to find out the photophysical properties of these molecules.

1.2 LITERATURE REVIEW: A FOUNDATION FOR THE PRESENT WORK

Reported synthesis of the core unit of the compound **6** require multiple synthetic steps.⁶ Only a limited numbers of one-pot methods to construct the tetracyclic core are available in the literature that used advanced/complex starting materials¹¹ along with transition metal complexes and difficult experimental condition,¹²⁻¹⁴ such as flash vacuum pyrolysis of methyl 2-(indol-1-yl)benzoate at 900° C.¹⁵

Syntheses typically entail multi-step processes and can be categorized by disconnecting individual bonds in the isoindoloindolone skeleton (Figure 1.4). The majority of established protocols involve C-N bond formation (path a) and isoindolo ring formation through C-C coupling (path b). An alternative approach utilizes condensation reactions or Heck coupling in constructing the indole ring (path c). Additionally, intramolecular cyclization (path d) and carbonylation (path e) offers a different avenue to access the indole substructure. These reported syntheses are multistep in nature and complex starting materials and expensive metal catalysts were used. One-pot methods involving easily available commercial starting materials are limited. Several one-pot methods described intramolecular and intermolecular bond formation reactions using tandem Pd-Catalyzed aminocarbonylation/lactamization and C-H activation to form bonds a, b and d required expensive palladium catalyst.

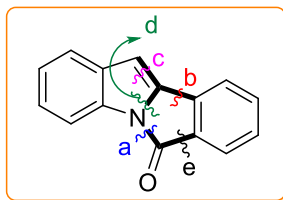
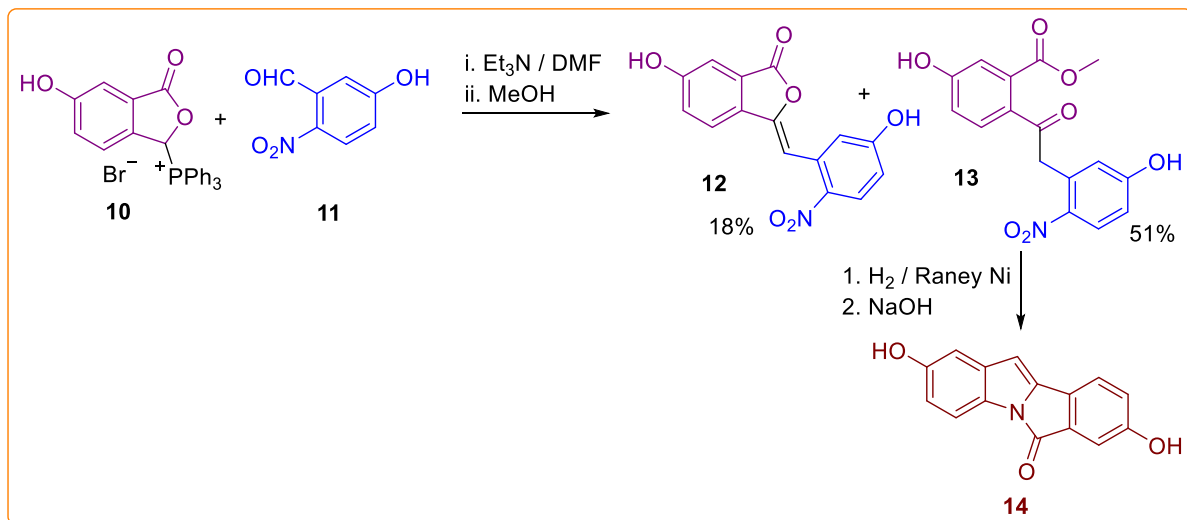


Figure 1.4 Synthetic methods of 6*H*-isoindolo[2,1-*a*]indol-6-ones

The literature reports for the syntheses of isoindoloindolones are discussed here in detail.

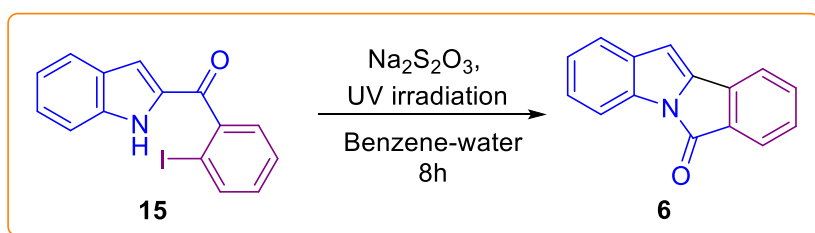
Boussard et al. outlined a multi-step method for synthesizing **14**. Methanol treatment of the crude Wittig reaction mixture derived from **10** and **11** resulted in the partial methanolysis of

the lactone, as illustrated in Scheme 1.1. The isolations of compounds **12** (as anticipated) and **13** were accomplished with a low yield. Subsequent reduction of **13** using Raney nickel, followed by base treatment, directly produced the expected dihydroxy isoindoloindole **14** (Scheme 1.1).⁶



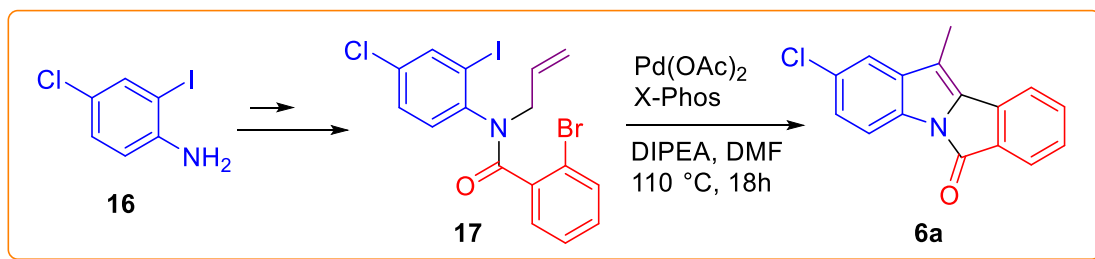
Scheme 1.1 Synthesis of compound 3,8-dihydroxy-isoindolo(1,2-a)indol-10-one **14**

Carruthers and his team demonstrated a photocyclization process involving iodo-aromatic compounds for the synthesis of diverse polycyclic structures. A combination of 1-*o*-iodo-benzoylindole **15** and sodium thiosulphate in a benzene-water mixture was exposed to light from the Phillips high-pressure lamp under reflux conditions through Pyrex. After 8 hours, the resulting product was isolated through preparative layer chromatography, yielding a 25% recovery (Scheme 1.2).¹¹



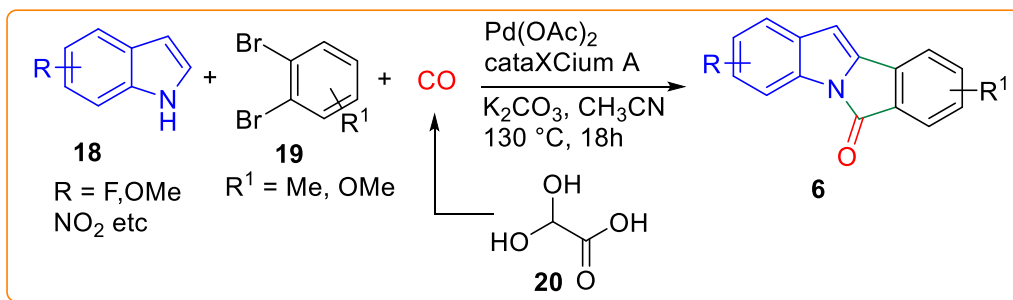
Scheme 1.2 Synthesis of 6*H*-isoindolo[2,1-a]indol-6-one **6** by photocyclization

Manojit et al. detailed a one-step synthesis of 11-substituted-6*H*-isoindolo[2,1-a]indol-6-ones through a Pd-mediated process, involving a sequential intramolecular Heck reaction of the corresponding dihalo *N*-allyl-substituted-*N*-arylbenzamide derivatives. The sequential intramolecular Heck reaction was investigated using *N*-allyl-2-bromo-*N*-(4-chloro-2-iodophenyl)benzamide **17**, employing Pd(OAc)₂, X-Phos and DIPEA in DMF, resulting in the desired product with a yield of 71% (Scheme 1.3).¹²



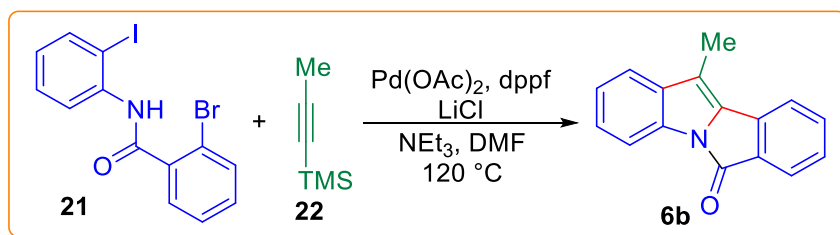
Scheme 1.3 Pd-catalyzed synthesis of 11-substituted 6*H*-isoindolo[2,1-*a*]indol-6-one

Koós et al. devised a unified catalytic system for a tandem Pd-catalyzed aminocarbonylation and C-C cross-coupling via C-H activation. They employed glyoxylic acid monohydrate as a surrogate for CO. The reaction involved subjecting substituted 1,2-dibromobenzene **19** and indole **18** to Pd(OAc)₂ (0.05 equiv) and cataXCium A (0.06 equiv) as catalysts in acetonitrile at elevated temperature, resulting in the desired substituted isoindoloindolones in **6** (Scheme 1.4).¹⁶



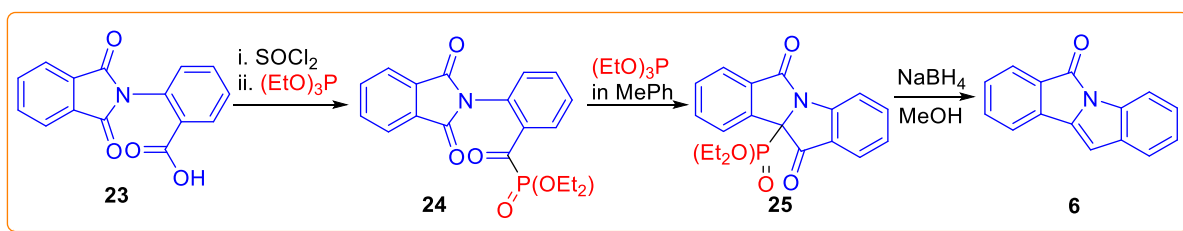
Scheme 1.4 Synthesis of **6** Pd-catalyzed aminocarbonylation and C-C cross-coupling

Liang et al reported a palladium-catalyzed domino Larock annulation/dearomative Heck reaction of *N*-bromobenzoyl *o*-iodoaniline and 1-(trimethylsilyl)-1-propyne, the targeted tetracyclic indoline **6b** was isolated in 53% yield at 120 °C in DMF for 2 h by using Pd(OAc)₂ as a catalyst, dppf as a ligand, LiCl as an additive, and NEt₃ as a base (Scheme 1.5).¹⁷



Scheme 1.5 Pd-catalyzed synthesis of 11-methyl-6*H*-isoindolo[2,1-*a*]indol-6-one (**6b**)

Philip et al demonstrated a convenient route to isoindolo[2,1-*a*]indol-6-ones starting from the appropriate 2-(*N*-phthaloyl)benzoic acids **23**. Formation of the acid chlorides with thionyl chloride followed by heating with triethyl phosphite in a suitable solvent resulted in a multistep reaction giving tetracyclic β-ketophosphonates that on reduction with sodium borohydride gave the required indolones (Scheme 1.6).¹⁸

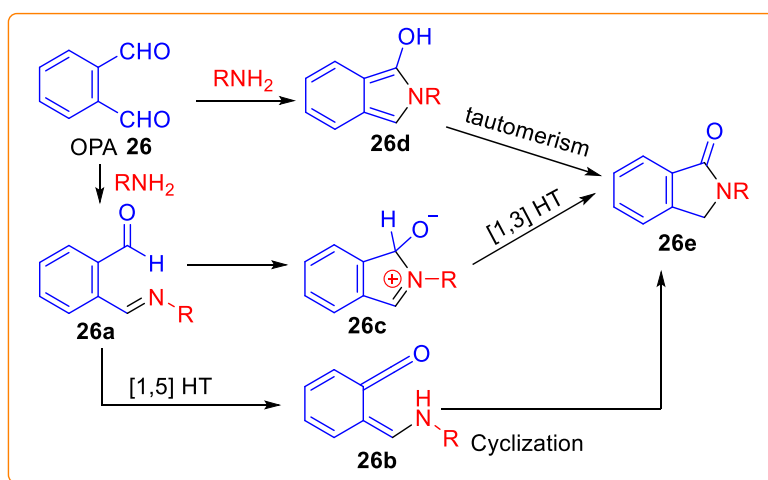


Scheme 1.6 Intramolecular Wittig reaction of *N*-phenylphthalimide derivatives

During our literature survey, we observed that the majority of these methods often necessitate multi-step procedures conducted under harsh reaction conditions, leading to a restricted scope of substrates. In contrast, a strategy based on a one-pot tandem approach could offer a more straightforward route to 6*H*-isoindolo[2,1-*a*]indol-6-ones, and evaluated them as DSEgens.¹⁹ We assumed that placing twisted and bulky groups on the skeleton of **6** would retain its PL properties in the aggregated state by keeping the basic chromophore units isolated.

1.3 PRESENT WORK

The reaction of OPA **26** with amine has been used to develop robust strategies for crosslinking biomolecules,^{20, 21} attaching markers to biomolecules²² or cells.²³ Though the reaction is successfully used for bio-conjugation, the synthetic applications were less devolved because of their complex reactivity pattern of OPA.²⁴ In a few cases, OPA had shown chemical reactivity similar to other aromatic aldehydes. Most often, it exhibited typical reactivity²⁵ due to the close proximity of two reactive aldehyde groups. Three different mechanisms (Scheme 1.7), namely intramolecular hydride transfer (via the intermediate **26c** or **26b**) and tautomerism (via **26d**), had been proposed for the formation of phthalimidine **26e** from amine and OPA **26**.²⁶ Thus, further study of the mechanistic aspects of the reaction would widen the scope of the reaction.



Scheme 1.7 The reported mechanistic explanations of phthalimidine (**26e**) formation

On viewing this attractive reactivity of OPA, we want to explore the reactivity of OPA with 1,5-bisnucleophile (2-aminoacetophenone and anthranilamide) to construct aza-heterocycles and other targets of contemporary interest. We anticipated that 11-methyl-6*H*-isoindolo[2,1-*a*]indol-6-one and 11-phenyl-6*H*-isoindolo[2,1-*a*]indol-6-one could easily be synthesized through tandem condensation cyclization. The results for the syntheses are discussed in this chapter of this thesis in detail.

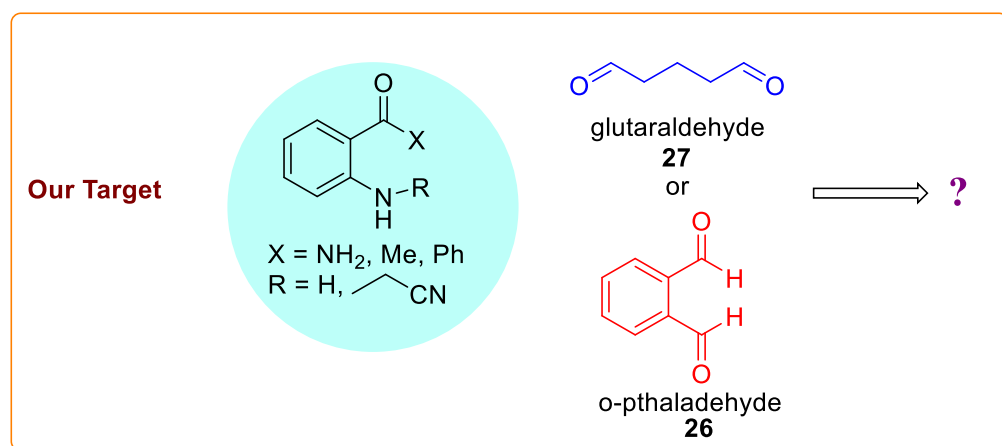
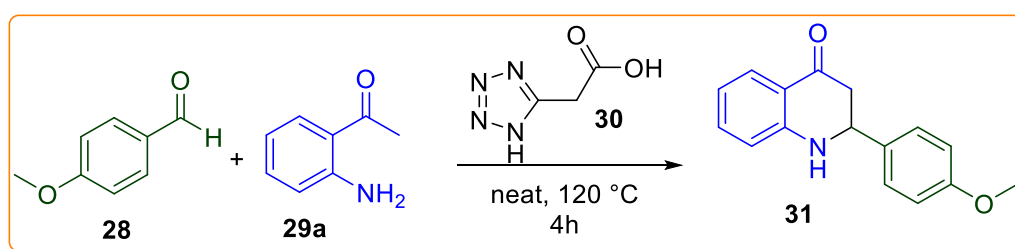


Figure 1.5 The reactivity of 1,5-bisnucleophile with dialdehyde

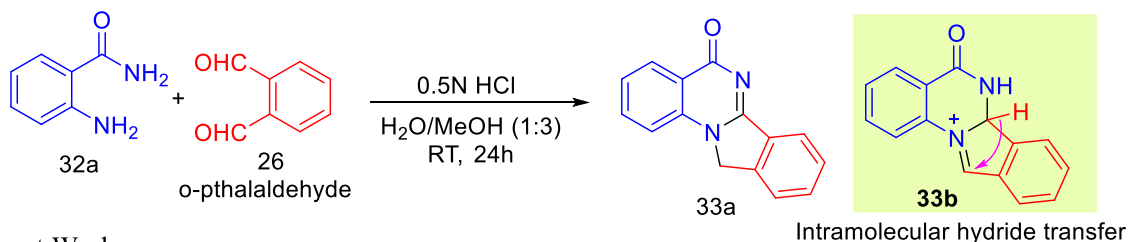
Our group previously reported a reaction between 1,5-bisnucleophile; 2-aminoacetophenone **29a** with 4-methoxybenzaldehyde **28** in presence of 1*H*-Tetrazole 5-acetic acid (TAA) **30**, which has been explored as a new organocatalyst for the synthesis of 2-aryl-2,3-dihydroquinolin-4(1*H*)-ones **31** derivatives from 2-aminoacetophenone under solvent free conditions.²⁷



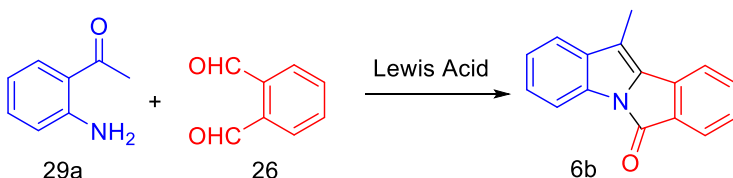
Scheme 1.8 Synthesis of 2-aryl-2,3-dihydroquinolin-4(1*H*)-ones from 2-aminoacetophenone

Our group also reported an one pot reaction between 1,5-bisnucleophile; 2-aminobenzamide (anthranilamide) **32a** with an aromatic dialdehyde (*o*-phthalaldehyde **26**) to synthesis of isoindole fused quinazolin 4-ones via intramolecular 1,3 hydride transfer in the presence of acid catalyst.²⁵

Previous Work from our group

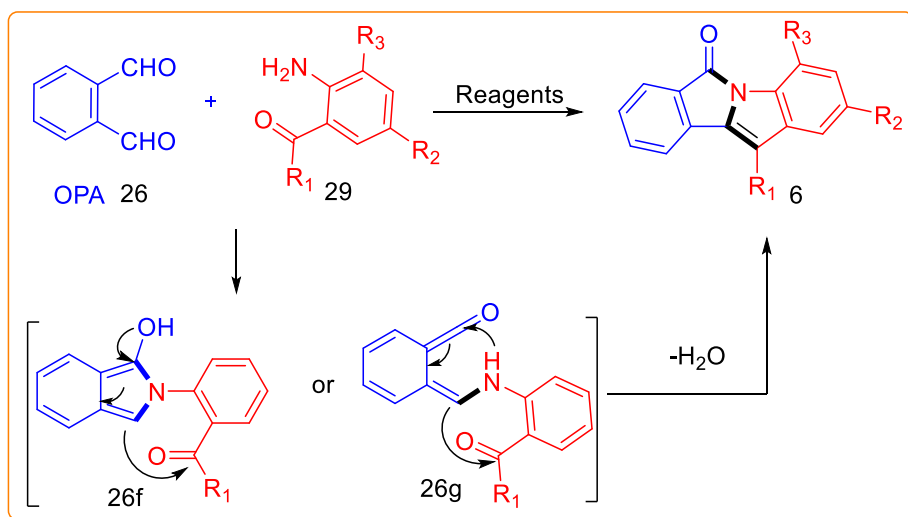


Present Work



Scheme 1.9 Synthesis of isoindolo[2,1-a]quinazolin-5(11H)-one from 2-aminobenzamide

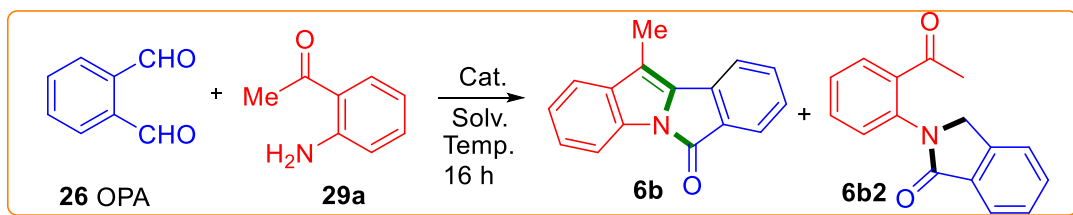
In the present chapter we developed a simple strategy to access of this isoindoloindolones skeleton with extensive scope for structural and functional diversification. We have investigated the reactions of 2-aminoacetophenone with *o*-phthalaldehyde in presence of FeCl_3 as a catalyst (Scheme 1.10). Notably, our findings reveal an unexplored reactivity of OPA towards 2-aminoacetophenone, a unique combination for which there are currently no reported reactions in the literature. This underscores a promising avenue for further exploration and detailed studies to elucidate the reaction mechanisms and potential applications of the resulting products.



Scheme 1.10 Present Work on one-pot tandem reaction for synthesis of **6**

1.4 RESULT AND DISCUSSIONS

At the beginning of the project, we treated 2-aminoacetophenone **29a** with OPA **26** in methanol for 16 hours and found that the solution turned into a purple colour and the majority of the **29a** remained intact. At the elevated temperature (entries 1&2) the mixture quickly turned to a brown solution with the formation of a large number of unidentified products. The complex reactions of OPA with **29a** in methanol have been studied by Klaus et al.²⁸ and suggested the formation of a large number of equilibrating products by the participation of the functional groups of starting materials (aldehyde, amine, keto) and the solvents methanol. The complexity of the reaction remained unaltered when it was attempted in the presence of mild Lewis acid $Y(NO_3)_3 \cdot H_2O$ ^{25, 29} and weak acid AcOH (entries 3 and 4). The slow reactivity of **29a** and *O*-substituted amine towards OPA³⁰ is because of the specific conformation of the *ortho*-substituent of the aromatic ring attached to the amidine **6b2**^{31, 32} which retards the formation of the transition state required for the formation of **6b**.³¹ However, a relatively stronger Lewis acid $CuCl_2$ or neat AcOH or aq. HCl resulted in a more complex reaction mixture (entries 5-7) within 2-3 hours. The results of entries 1-7 (Table 1.1) led us to search for a suitable promoter of intermediate reactivity that could help to bring all the function groups in a plane. The alkaline condition was inappropriate for the transformation as it produced a different product³³, which will discuss in the next section of this chapter. After several attempts under acid conditions, we found that the presence of $Pd(OAc)_2$ in AcOH led to the exclusive formation of **6b** instead of coloured tar formation. However, the carbonyl functional group remained inactive. Compound **6b** was characterized by NMR and Mass, and all the data agree with its structure. Use of $FeCl_3$ in methanol in RT observed the formation of product **6b** in 35% yield along with the tarification. The best result was obtained when the reaction was carried out in the presence of $FeCl_3$ ³⁴ in methanol at 65 °C (entry 10). Presence of a strong acidic reagent like $BF_3 \cdot OEt_2$ or TFA resulted in the complex polymerization with a reduced yield of **6b**. The use of aprotic solvent toluene was found to be inappropriate for the reaction. Thus, $FeCl_3$ promoted the annulative coupling reaction between OPA and 2-aminoacetophenone in methanol under refluxing condition.

Table 1.1 Optimization of the reaction

Entry	Catalyst	Solvent	T °C	Results
1	-	MeOH	RT	29a intact
2	-	MeOH	65	Complex mixture
3	Y(NO ₃) ₃ ·6H ₂ O	MeOH	65	complex mixture
4	AcOH	DCE	80	complex mixture
5	CuCl ₂	DCM	80	complex mixture
6	-	AcOH	120	complex mixture
7	Aq. HCl	MeOH	RT	complex mixture
8	Pd(OAc) ₂	AcOH	120	6b2: Yield 90%
9	FeCl ₃	MeOH	RT	6b: Yield 35%
10	FeCl ₃	MeOH	65	6b: Yield 76%
11	FeCl ₃	Toluene	RT	6b: Yield 25%
12	TFA	DCE	80	Complex reaction
13	BF ₃ ·OEt ₂	Toluene	RT	Complex reaction

After optimizing the reaction condition, we have selected a few substrates (**29b-i**) for the annulation reaction, and their synthesis is described in detail in the Experimental Section of this chapter.

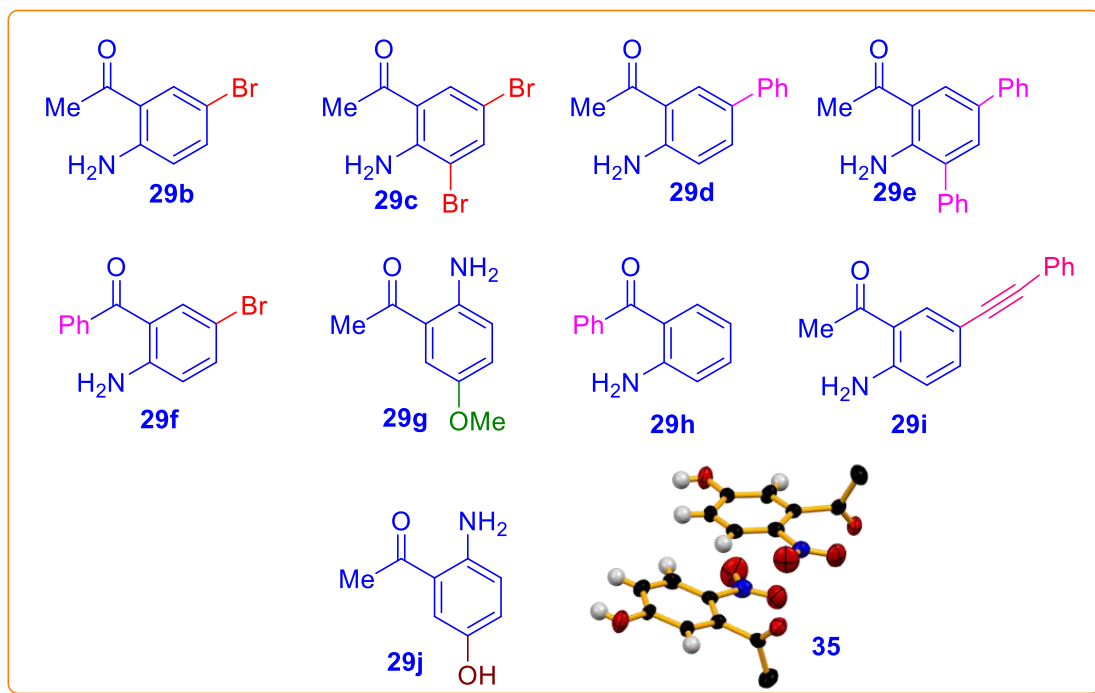
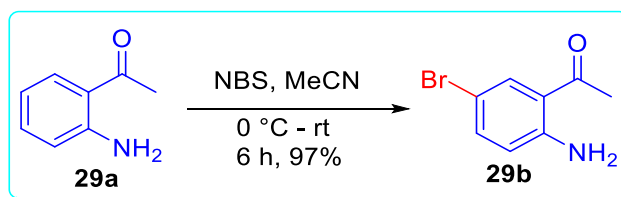


Figure 1.6 Structure of the compound **29** and ORTEP diagram of nitro derivative of **29j**

1.4.1 Synthesis of the Starting Material **29b-29j**

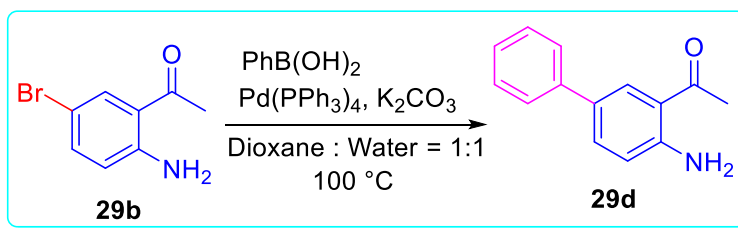
Compound **29b** and **29c** are obtained from 1-(2-aminophenyl)ethanone **29a** by *N*-bromosuccinimide mediated bromination (Scheme 1.11).³⁵

29f was also prepared by the same method of bromination of 2-aminobenzophenone **29h** by following the literature procedure.^{36, 37}



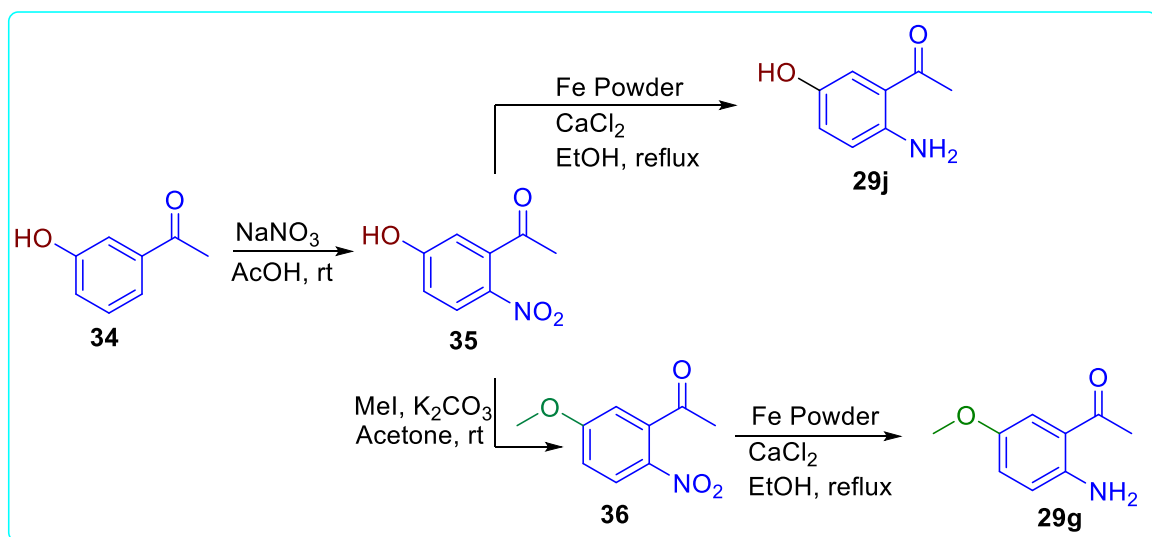
Scheme 1.11 Synthesis of 5-bromo derivative of 2-aminoacetophenone

The compound **29d** and **29e** was previously reported in the literature and prepared from **29b** and **29c** respectively by Pd(0) mediated Suzuki coupling reaction between 5-bromo derivative of 2-aminoacetophenone and phenylboronic acid (Scheme 1.12).³⁸



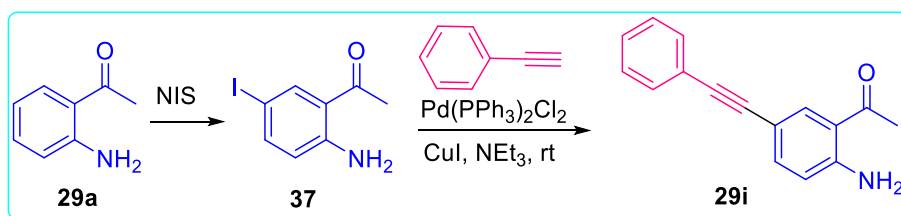
Scheme 1.12 Synthesis of **29d** by Suzuki coupling

Compound **29g** was synthesized from 3-hydroxy acetophenone following a synthetic sequence: nitration³⁶ followed by methylation and subsequent reduction of the nitro group, according to the reported procedure³⁹. Nitration of 3-hydroxyacetophenone followed by reduction of nitro group resulted the formation of the compound **29j**. The position of the nitration and hence amine group is confirmed by NMR and XRD of the nitro compound **35** (CCDC 2292561).



Scheme 1.13 Synthesis of 5-methoxy and 5-hydroxy derivative of 2-aminoacetophenone

Commercially available compound **29h** and its monobromoderivative **29f** were used for the annulation reaction. Compound **29i** was synthesized monoiododerivation of **29h** followed by Sonogashira coupling with phenyl acetylene (Scheme 1.14).⁴⁰



Scheme 1.14 Synthesis of 5-phenylethynyl derivative of compound 29a

The compounds **29b-j** were then reacted with OPA **26** under the condition optimized for the compound **29a** (Table 1.1, Entry 10). Isolated yields of the product **6b-j** varied from 41-76%. It appeared that the presence of substituents at substrate **29** slowed the process. The dibromo

compound **29c** reacted with OPA and produced compound **6d**, along with an intermediate product **6d2**. All the compounds (**6b-j**) were characterized by the NMR spectroscopy and HRMS spectrometry. Compound **6b** and **6i** are highly crystalline, and single crystals obtained from a mixed solvent CHCl_3 , MeOH & H_2O were subjected to XRD study, and their structure was solved. The Crystal structure of **6b** and **6i** and the crystal packing are shown in Figure 1.13. The phenolic $-\text{OH}$ in **29j** interferes in the conversion in $\text{FeCl}_3/\text{MeOH}$ reaction condition and did not produce the expected product.

The ^1H -NMR of **6b2** and **6d2** suggested that the C-N rotation is restricted, and the diastereotopic proton H_a & H_b (4.56, d, $J = 16.0$ Hz; 4.90, d, $J = 16.0$ Hz) appeared at different chemical shift with large germinal H-H spin coupling (16 Hz). While the C-N free rotation in **6b2** is not restricted at ambient temperature, and both the CH_2 protons resonated at 4.80 ppm (Figure 1.7).

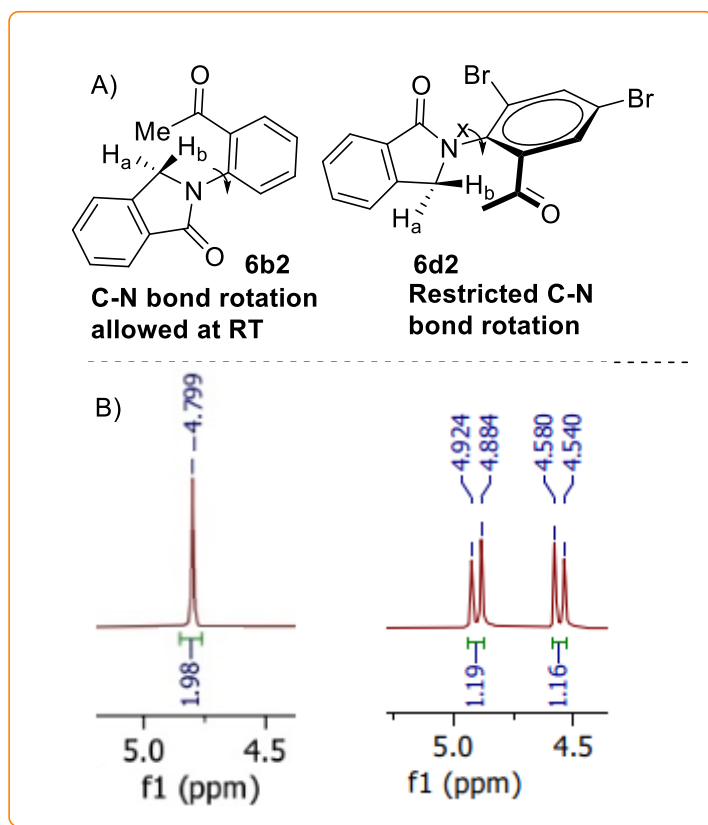


Figure 1.7 A) Restricted C-N bond rotation in **6b2** and **6d2**. B) the peak position of the H_a and H_b protons of **6b2** and **6d2** in ^1H -NMR in 400 MHz in CDCl_3

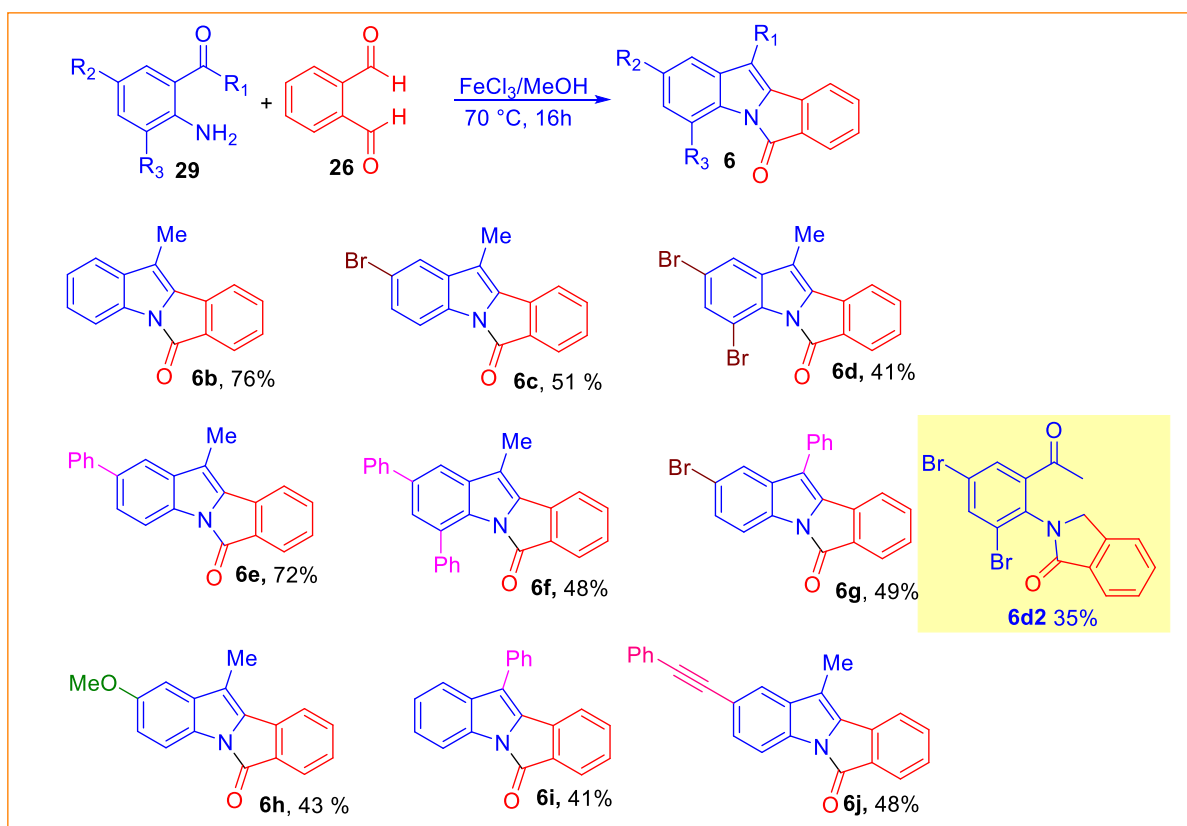
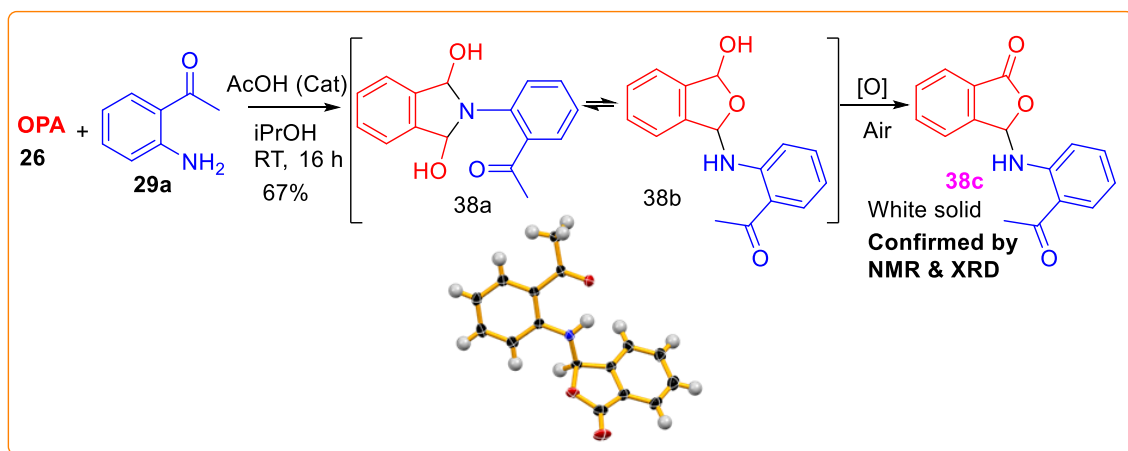


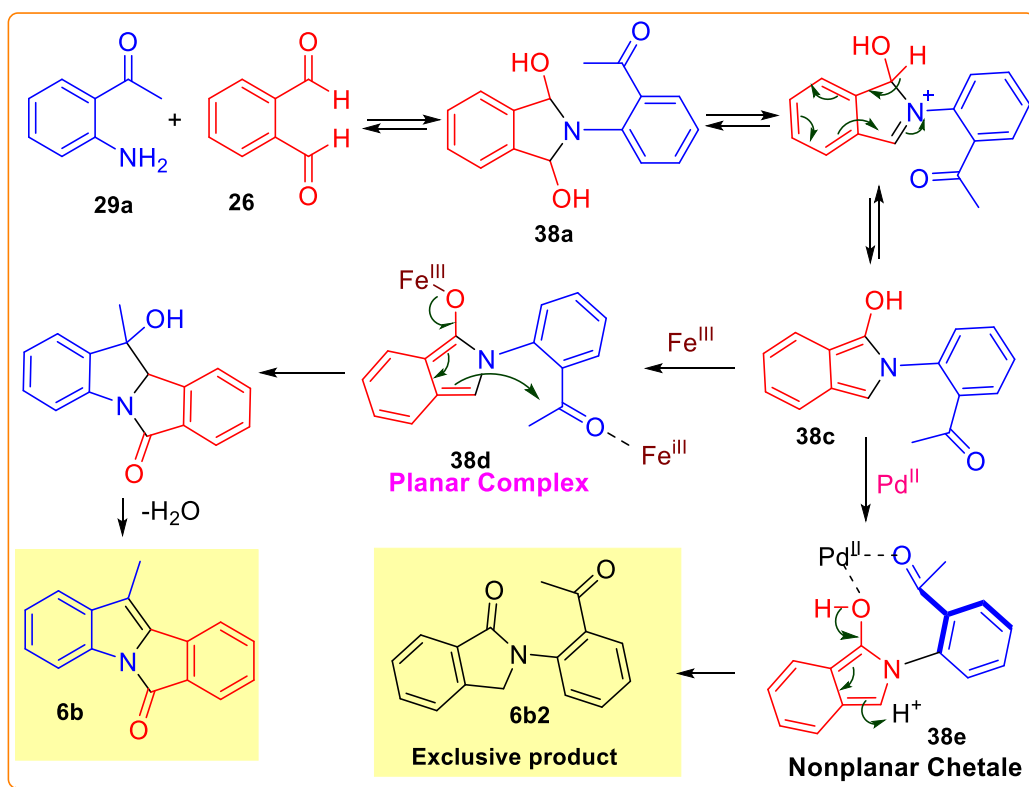
Figure 1.8 Substrate scope studies

1.4.2 Mechanistic Investigation

Formation of compound **6b** in one pot requires multiple synthetic stems in a cascade manner. To visualize the nature of different intermediates involved during the reaction's progress, we have reacted OPA **26** with **29a** in different solvent and catalytic conditions. To our surprise, the presence of catalytic AcOH in *i*PrOH at RT led to the formation of a white solid **38c** in 67% yield (Scheme 1.15).

Scheme 1.15 Isolation of intermediate **38c** and its XRD structure

All the spectroscopic data support the structure **38c**. The compound **38c** was converted into **6b** by FeCl_3 treatment in MeOH or $i\text{PrOH}$ at RT. Hence, it was an intermediate during the formation of **6b**. Based on the experimental results described above and previous reports,²⁶ a plausible mechanistic explanation for the formation compound **6b** is shown in Scheme 1.16. We also confirmed the initial formation **38c** in the presence of FeCl_3 in methanol. The reactivity of the intermediate **38c** was found to be dependent on the metal ion present. In the presence of FeCl_3 , the formation **6b** was a major reaction pathway, while $\text{Pd}(\text{OAc})_2$ produced compound **6b2** exclusively.^{41,42} This difference in reactivity of **38c** towards $\text{Fe}(\text{III})$ and $\text{Pd}(\text{II})$ may be due to the different modes of complexation with metals. The $\text{Fe}(\text{III})$ allows the formation of a planar complex **38d**, which is essential for C=C bond formation with the carbonyl group, while Pd, due to its large size, forms a weak chelate **38e**, which is essentially nonplanar. Thus, intermediate **38d** led to product **6b** via intramolecular aldol-type reaction while **38e** converted into **6b2** by taking a proton from the medium. The requirement of planarity in the structure of **38c** to form **6b** also supports the formation of **6d2** from the hindered dibromo compound **29c**.



Scheme 1.16 Plausible mechanistic pathway to 11-methyl-6H-isoindolo[2,1-a]indol-6-one

1.5 BROADENING THE SUBSTRATE SPECTRUM: ADDITIONAL INSIGHTS

Chalcone has found extensive application in organic synthesis for the creation of highly functionalised Michael adducts. The conjugate addition of a stabilized carbanion nucleophile to α,β -unsaturated carbonyl compounds stands out as one of the most significant C–C bond-forming reactions in organic chemistry. The chemoselective formation of intricate carbo- and heterocyclic skeletons from a multifunctional substrate through a chemical cascade process represents an appealing strategy in modern organic synthesis. Adjusting the chemoselectivity of such a reaction in a straightforward and predictable manner has gained increasing attention. The synergistic interplay of electronic and steric effects in the reactants holds the potential to achieve the desired chemoselectivity. In this section, our objective is to regulate the 1,2- versus 1,4-addition of a carbon nucleophile on an enone-containing amino acetophenone, facilitating the construction of new C–C and C–O bonds.

Inspired by our initial findings in the reaction of stoichiometric *ortho*-phthalaldehyde **26** with 2-aminoacetophenone **29a**, leading to the formation of 11-methyl-6*H*-isoindolo[2,1-*a*]indol-6-one **6b**, we sought to broaden the substrate scope of this reaction. To achieve this, a range of chalcones (**29k-29q**) were synthesized⁴³ and subjected to reactions with OPA **26**, employing a procedure involving catalytic Pd(II) salts.

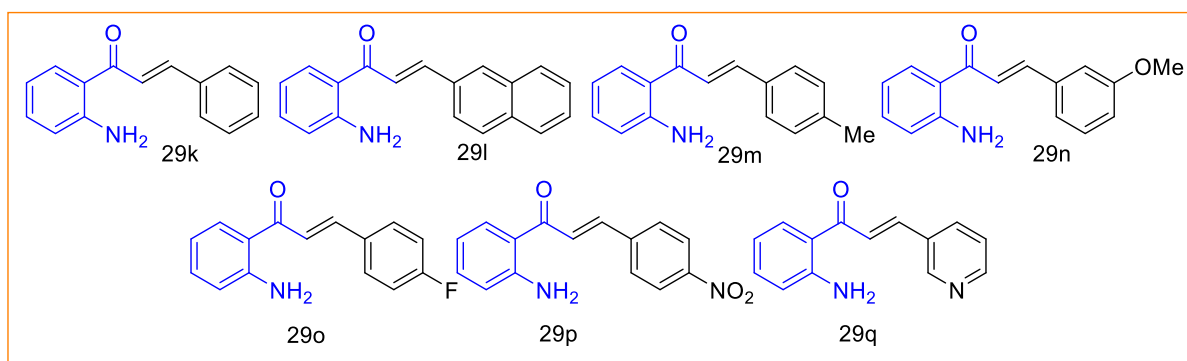


Figure 1.9 Various synthesised chalcones from 2-aminoacetophenone

To validate our hypothesis, we commenced our inquiry utilizing **29p** and OPA **26** as starting substrates, intending to synthesize isoindoloindolones. Surprisingly, we observed that the nitro-substituted chalcone **29p** yielded a highly intriguing molecule instead of the anticipated isoindoloindolones. Instead, it led to the formation of a benzoazepinoisoindole-(6*H*)-dione scaffold, featuring consecutive chiral centres.

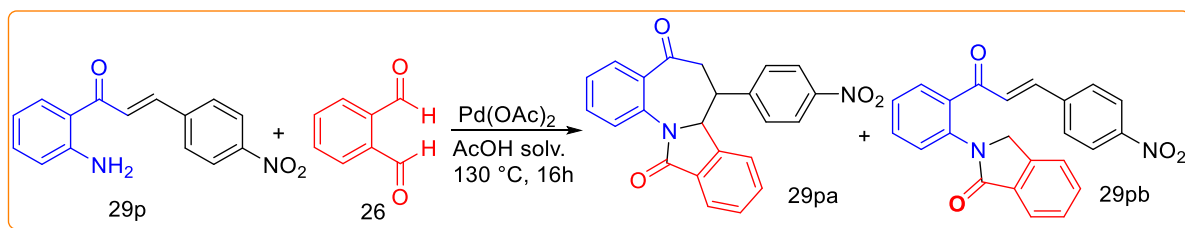
1.5.1 Optimization of the reaction between chalcone and OPA

To validate our hypothesis, we commenced our inquiry utilizing **29p** and OPA **26** as starting substrates, intending to synthesize isoindoloindolones.

According to our previous experience and planned route, OPA was treated with (*E*)-1-(2-aminophenyl)-3-(4-nitrophenyl)prop-2-en-1-one **29p** in acetic acid in the presence of morpholine and observed the formation of the compound **29pa** in 10% yield. We have noted a rapid and complex reaction pattern of OPA in AcOH. However, we observed a better result with a much cleaner reaction when we used FeCl₃ in methanol at refluxing condition, but we did not observe the expected **29pa** rather it leads a mixture of compounds **29pa** along with **29pb** (observed in NMR). It is worth noting strong Lewis acid like BF₃·OEt₂ in toluene dominates the decomposition of OPA and results in reduced yield however at elevated temperature (120 °C) it leads to a mixture of **29pa** and **29pb** in different proportion. Aprotic solvent toluene was found to be inappropriate for the reaction. Protic solvent methanol favoured the reaction. The best result was obtained when the reaction was carried out in the presence of Pd(OAc)₂ in acetic acid. To our surprise, the use of Pd(OAc)₂ in acetic acid gave exclusively compound **29pa** in 65% of yield.

Surprisingly, we observed that the nitro-substituted chalcone **29p** yielded a highly intriguing molecule instead of the anticipated isoindoloindolones. Instead, it led to the formation of a benzoazepinoisoindole-(6*H*)-dione scaffold, featuring consecutive chiral centres. The structure **29pa** was confirmed unambiguously by NMR (¹H, ¹³C) and X-ray crystallographic experiment.

Table 1.2 Optimization of the reaction



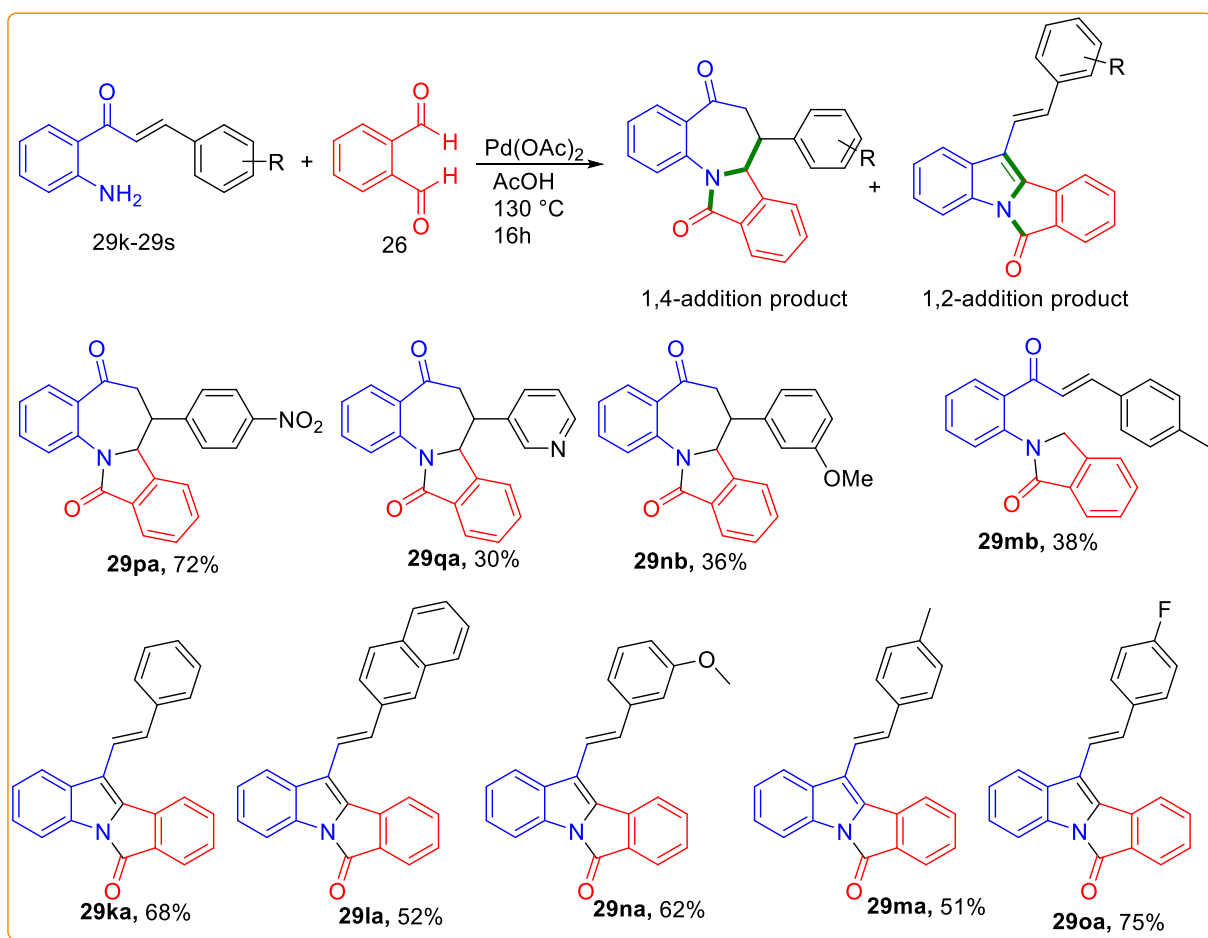
Entry	Catalyst	Solvent	Temp °C	Time (h)	Yield (%)
1	Morpholine	AcOH	130	16	29pa, 10%
2	-	AcOH	130	48	Complex mixture
3	FeCl ₃	MeOH	65	16	Complex mixture
4	FeCl ₃	Toluene	120	16	Mix of 29pa+29pb
5	CuI	DMF	140	16	Complex mixture

6	PdCl ₂	DCE	80	16	Complex mixture
7	^c Pd(OAc) ₂	AcOH	130	16	(29pa) 65%
8	Pd(OAc) ₂	MeOH	65	16	(29pa) 30%
9	Zn(OTf) ₂	DCM	rt	24	No reaction
10	BF ₃ -OEt ₂	Toluene	rt	24	Complex mixture
11	BF ₃ -OEt ₂	Toluene	120	24	Mix of 29pa+29pb
12	BF ₃ -OEt _s	MeOH	65	24	Trace 29pa

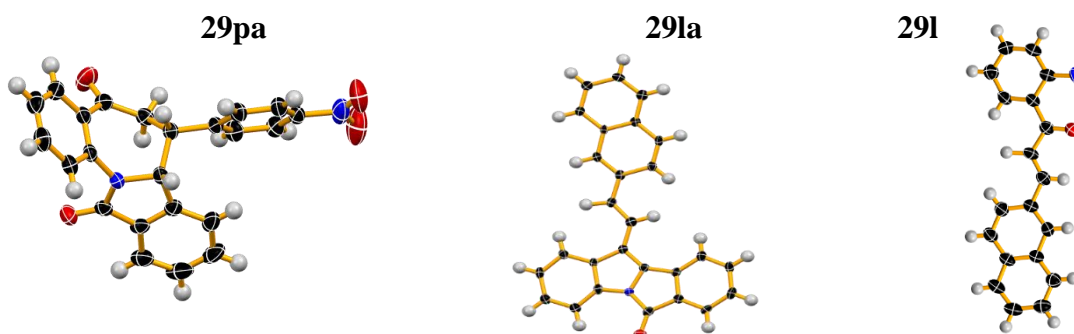
Note: 29p and 26 react in 1:1 molar ratio, 20 mol% ^cPd(OAc)₂ was used

Under the optimized reaction conditions outlined in entry 7 of Table 1.2, we conducted an exploration of the reaction's scope. A wide variety of substitutions on the aryl moiety of the substrate, and their synthesis is described in the Experimental Section of this chapter were examined and demonstrated the generality in terms of yields and chemoselectivity. Different electron-withdrawing groups, including nitro (29p), pyridine (29q), and fluoro (29o), as well as electron-donating groups such as methyl (29m) and 3-methoxy (29n) smoothly participated in the reaction. The structure of one of our chalcone substrate 29l is confirmed by NMR and XRD. Isolated yields of the product 29ka-29qa varied from 30-72% (Scheme 1.17). It appeared that there are two sets of product found under the optimized condition depending upon the electronic factor presence of substituents in chalocones. The 4-methyl chalcone compound 29m reacted with OPA and produced compound isoindoloindolone 29ma, along with an intermediate product 29mb. All the compounds (29ka-29qa) were characterised by the NMR spectroscopy and HRMS spectrometry. Compound 29pa and 29la are highly crystalline, and single crystals obtained from a mixed solvent CHCl₃ & CCl₄ were subjected to XRD study, and their structure was solved. The Crystal structure of 29pa and 29la and the crystal packing are shown in Figure 1.10. The resulted in two distinct sets of products, differing in their modes of reactions—one via 1,2-direct addition and another via 1,4-conjugate addition. The observation revealed that electron-donating substituted chalcones, when reacting with OPA, yield isoindoloindolones through a 1,2-fashion addition. In contrast, electron-withdrawing tailored chalcones lead to the formation of benzoazepinoisoindole-(6*H*)-dione compounds through a 1,4-conjugate addition fashion.

Isoindoloindolones (29ka-29oa) compounds exhibit remarkably intense fluorescence, prompting a keen interest in investigating their photophysical properties and assessing their potential utility in the realm of optoelectronics.



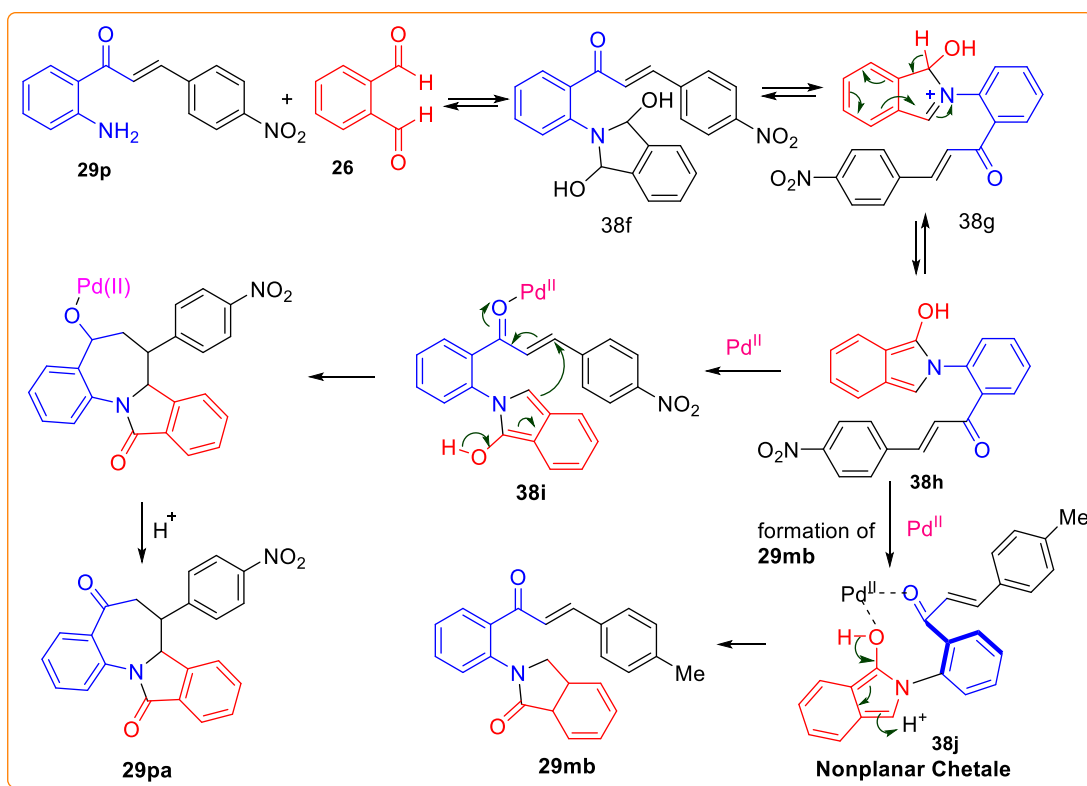
Scheme 1.17 Substrate scope studies

Figure 1.10 The single crystal XRD structure of **29pa**, **29la** & **29l**

1.5.2 Mechanism of the formation of **29pa**

Based on the experimental results described above and previous reports,²⁶ a plausible mechanistic explanation for the formation compound **29pa** is shown in Scheme 1.18. The formation of 1,2-addition products, specifically **29ka-29oa**, is analogous to the generation of **6b** as depicted in Scheme 1.16. Pd(II) ions in AcOH accelerate the formation of the intermediate **38h** through isoindanol **38g**. Another vital role of the Palladium ion in the proposed mechanism is the activation of the carbonyl in the intermediate **38i** to produce **29ka**

via 1,4-conjugate addition. Palladium acetate in acetic acid is also capable of producing intermediate **38j** in case of 4-Me chalcone under this condition, compound **29mb** formed via tautomerism.



Scheme 1.18 Plausible mechanistic pathway

1.6 PHOTOPHYSICAL PROPERTIES OF COMPOUND **6b**

In this investigation, a series of synthesized compounds were subjected to a comprehensive analysis of their photophysical properties. The primary focus of this study includes the examination of UV-Vis absorption spectra and fluorescence emission spectra.

1.6.1 Absorption Spectroscopy Method

For the UV-Visible absorption spectra measurements Shimadzu spectrophotometer (model UV-1800, Japan) with 1cm × 1cm quartz cuvette was used. The UV-Visible absorption spectra of **6b-6j** were recorded in the wavelength range of 200–600 nm. The experiment was conducted at a defined concentration of all the compounds (1 mM) in a fixed volume (3 ml) of chloroform.

1.6.2 Photoluminescence Properties

Steady-state fluorescence: Fluorescence emission spectra of **6b-6j** were recorded on a Shimadzu spectrofluorometer-5000 (Japan) equipped with a Xenon flash lamp using 1.0 cm quartz cells. Excitation was fixed at 375 nm and emission spectra were recorded from 385 nm

to 600 nm after setting the widths of both the excitation and the emission slits at 5 nm. The fluorescence was carried out by keeping the concentration of **6b-6j** constant (10 μ M).

The fluorescence quantum yield serves as a direct measurement of the proportion of excited molecules that revert to the ground state by emitting fluorescence photons. Simply put, it represents the ratio of the number of emitted photons to the number of absorbed photons. The fluorescence quantum yield (Φ_F) is determined using the given equation-

$$\frac{\Phi(\text{sample})}{\Phi(\text{ref})} = \frac{\text{Area}(\text{sample})}{\text{Area}(\text{ref})} \times \frac{1 - 10^{-\text{abs}(\text{ref})}}{1 - 10^{-\text{abs}(\text{sample})}} \times \frac{\eta^2(\text{sample})}{\eta^2(\text{ref})}$$

Φ = Quantum yield; η = Index of refraction.

The fluorescence quantum yield stands out as a pivotal parameter in spectroscopic analysis. It furnishes crucial insights into excited states, radiation less transitions, and the coupling of electronic to vibronic states. Additionally, fluorescence quantum yields play a significant role in estimating chemical structures, sample purity, and the suitability of laser media. Numerous researchers have computed fluorescence quantum yields for diverse molecules to delve into aspects such as solute-solvent interactions, solvent polarity-induced structural changes, and their use as standards.

While measuring fluorescence quantum yield using an absolute method requires sophisticated instrumentation, the relative method offers a more straightforward approach. In the relative method, the fluorescence quantum yield of a molecule is calculated by comparing it to a standard reference with a known fluorescence quantum yield. The single-point method involves comparing the integrated, spectrally corrected fluorescence intensity of a dilute fluorescence solution with that of a standard reference under the same experimental conditions. In our work, we also adopted the single-point method for estimating fluorescence quantum yield.

Time-resolved fluorescence decay measurement: Fluorescence lifetime measurements were conducted on Horiba Jobin Yvon Fluoro Log spectrofluorometer (HORIBA, Les Ulis, France) with the excitation wavelength at 385 nm. Maximum emission wavelength was 475 nm in room temperature. The concentration of **6b** was fixed at 30 μ M.

1.6.3 Experimental Findings: Results and Insights

A broad unstructured band at 375 nm is a characteristic feature of all the compounds **6b-j** in UV-Vis spectra (Figure 1.11). All synthesized compounds **6b-j** in dilute solution exhibited

photoluminescence in the visible range; among them, **6b** (QY = 0.57) and **6i** (QY = 0.44) were the most prominent (Figure 1.11B). The absorption and emission properties of the compound are shown in Table 1.3. The non-mirror image symmetry between absorption and emission spectra implies electronic transitions in emission spectra different from that of absorption spectra.⁴⁴ The structured emission spectra of **6c**, **6d** & **6h** are due to the vibronic transitions and show bands at 384, 407, 332, and 457 nm. However, for the compound **6e**, **6f**, **6g** and **6j** another new band appeared at 506 nm, which was most prominent for the compound **6b** and **6i**. The large Stokes shift of the 506 nm band must come from the subtle change in geometry in the excited state of the compound **6b** and **6i** and this change is not permitted in the structures **6c**, **6d** & **6h** and partially allowed in **6e**, **6f**, **6j** & **6g**. Experimental results suggested that any substituent on the moiety of **6b** resulted in decreased intensities of the 506 nm emissions band, especially the Br or OMe group, which suppressed the 506 nm band completely. Thus the emission 506 nm band is highly sensitive to the substituent attached to the moiety of **6b**. The unstructured band at 506 nm in solid state PL is probably because of the formation a new species in the excited state. Rapid conversion into a stable planar intramolecular charge transfer (PICT) state is probably the reason for the appearance of the band at 506 nm, which is absent or very weak in the solid state fluorescence (Figure 1.11D & 1.11E). The Structural rigidity in the solid state does not allow to the change of dipole moment and significant structure deformation and hence PICT formation.⁴⁵ Therefore, in the solid state, emission bands (368, 410) were only from the locally excited states of **6b**. A similar pattern was observed in the emission spectra of **6i** in solid with slight bathochromic shift.

Furthermore, the emission band red shifted with increasing solvent polarity (Figure 1.12A). While, the absorption spectra at 100 μM in different solvents revealed that the position of absorption maxima was less sensitive to solvent polarity and suggesting the absorption band at 375 is of $\pi \rightarrow \pi^*$ nature (Figure 1.12B).

We also measured emission at different concentrations to gain further insight into the kinetics of forming the new excited state from the locally excited state. Figure 1.12C shows that the broad band intensity at 475 nm varies linearly at low concentrations (up to $0.6 \times 10^{-7} \text{M}$) and above $0.6 \times 10^{-7} \text{M}$ concentration, linearity breaks, and a red shifts observed (Figure 1.12C). As the intermolecular process to form the new excited species is unlikely to be happened at low concentration, it might be an intramolecular in nature. Most likely, it is due to an intramolecular charge transfer (ICT) state.

The possible reason for red-shifts is the increase of polarity of the medium with an increasing concentration of **6i**. Similar ICT state formation is common for amide structure³¹ and *N*-benzoyl indoles.⁴⁶

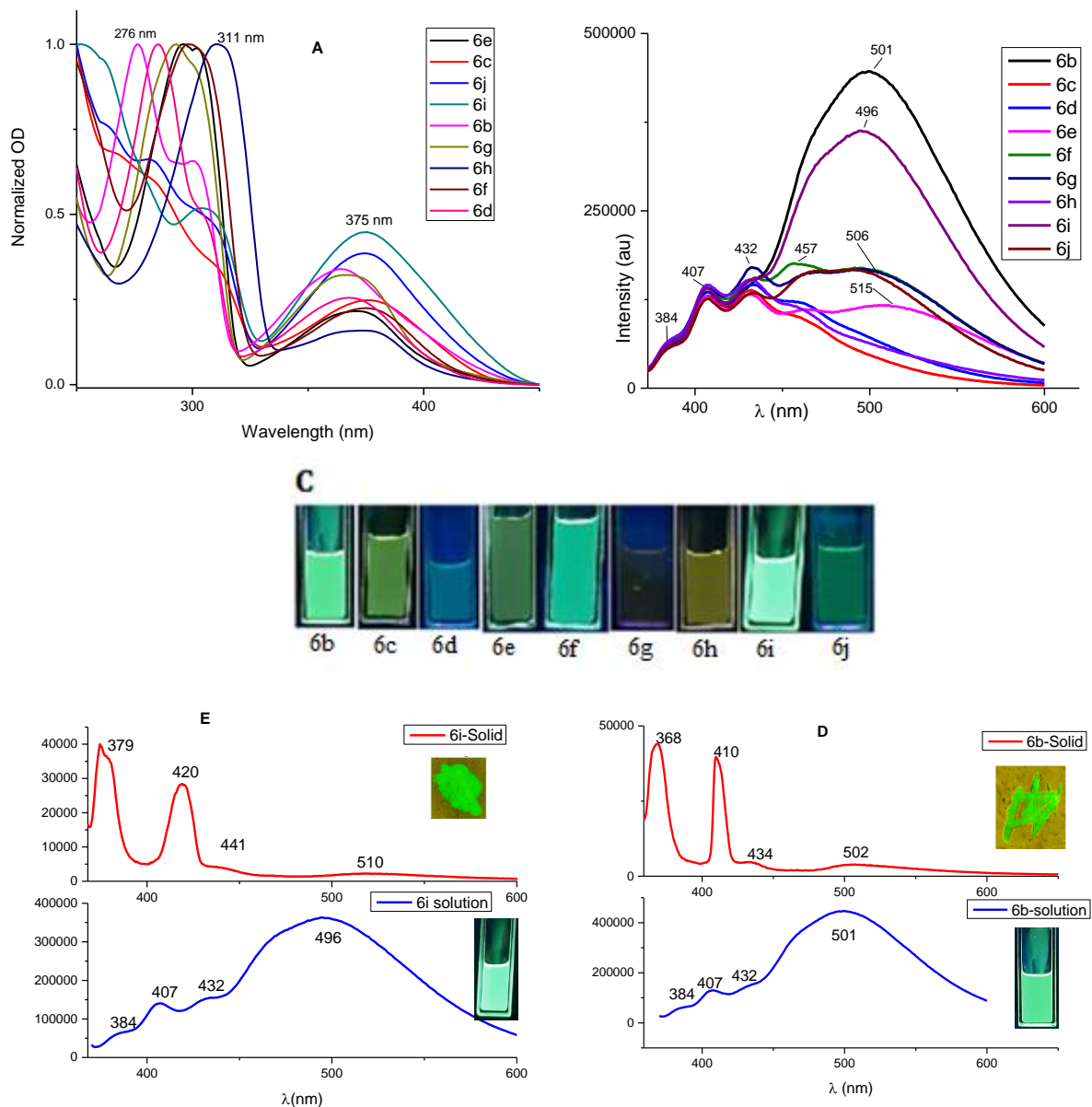


Figure 1.11: (A) Normalized absorption spectra in CHCl_3 (conc. = 1mM), (B) Fluorescence spectra of CHCl_3 (Conc. 3.3 μM), (C) Photograph of a 1mM solution of the fluorophore in CHCl_3 under 364 nm UV light. (D) The fluorescence spectra of **6b** in solid (excitation $\lambda = 340$ nm, upper panel) and in solution (CHCl_3 at conc. 3.3 μM , $\lambda = 360$ nm, lower panel). Insets show the fluorescence microscopic image (at 10X, blue Channel for DAPI) of the crystalline **6b** and CHCl_3 Solution at 364 nm UV light. (E) The fluorescence spectra of **6i** in solid (excitation $\lambda = 340$ nm, upper panel) and in solution (CHCl_3 at conc. 3.3 μM , $\lambda = 360$ nm, lower panel). Insets show the fluorescence microscopic image (at 10X, blue Channel for DAPI) of the crystalline **6i** and CHCl_3 Solution at 364 nm UV light.

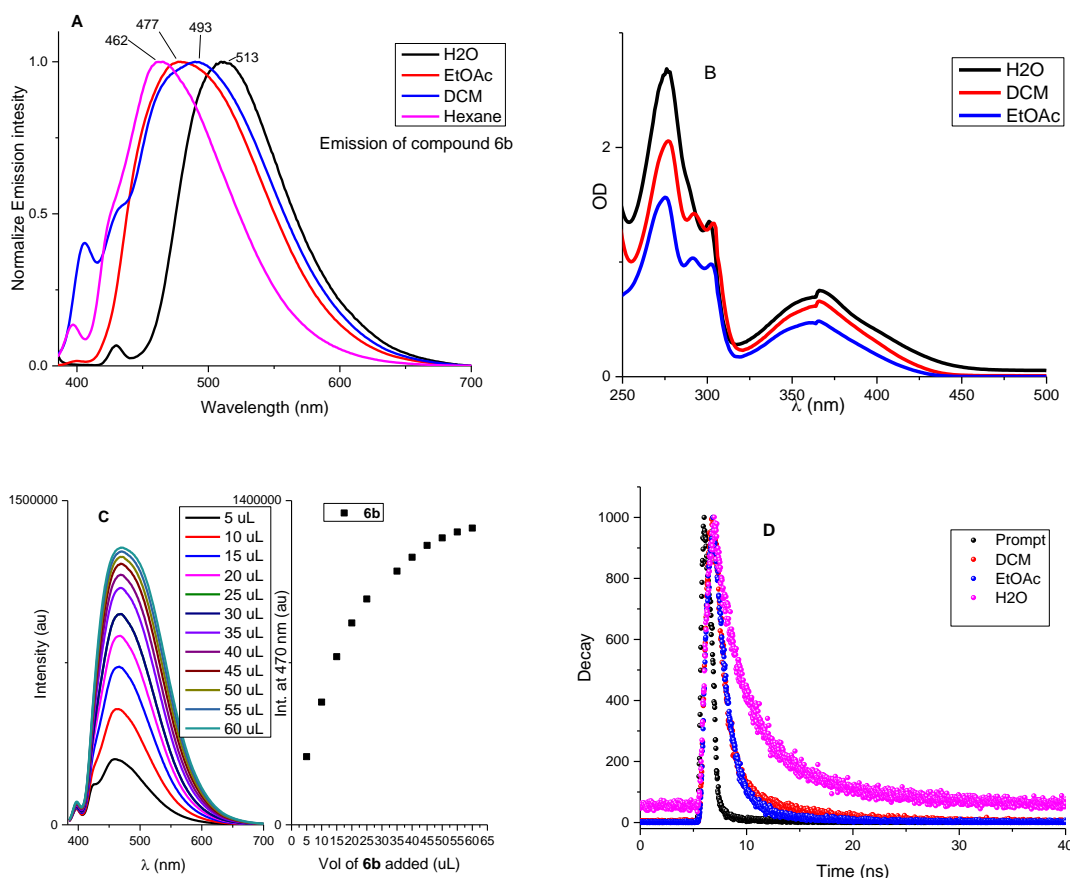


Figure 1.12 A) Normalized fluorescence spectra of **6b** (conc. 3.3 μ M) in different solvents, B) UV-Vis spectra of **6b** (conc. 1 mmol) in different solvents, C) Emission spectra of compound **6b** in hexane, obtained by adding 5 μ L stock (66 μ M) into 3 mL hexane in each step, D) Time-resolved fluorescence decay at 506 nm of **6b** in different solvents.

The possibility of ICT is further supported by the Time-correlated single photon counting (TCSPC) spectra (Figure 1.12). The TCSPC data are best fitted with a double exponential equation as shown in Table 1.3. A short-lived excited state characterized by T1 half-life is the significant contributing state for PL properties of **6b** in all the solvents (64 to 94%). However, on increasing polarity, T1 increases while decreasing its contribution to the overall PL properties (T1: 1 ns to 1.6 ns). In comparison, another excited state characterized by T2 remained unaltered with increasing solvent polarity. These data support that the excited state characterized by T1 half-life is an ICT state. It is stabilized by the polar solvent water and overall reduction of PL properties by enhancing the rate of the non-radiative process. The 506 nm band of **6b** in said is nearly suppressed. This data further supports the charge transfer nature of the band at 506 nm. Formation of ICT requires a change of bond length, and hence dipole moment and this change cannot be accommodated in the crystalline state.

Table 1.3 Decay parameters of **6b** in different solvents

Solvent	T1	T2
EtOAc	1.0486 (93)	4.70815 (03)
DCM	0.855914 (94)	5.83278 (06)
H ₂ O	1.65646 (64)	5.39465 (36)
Counts = A+ B1*exp(-i/T1)+ B2*exp(-i/T2) The value in the bracket shows Normalized pre expo factor		

Table 1.4 Absorption and emission data for 6b-j in CHCl₃ at 25 °C

Product	$\lambda_{\text{max}}(\text{nm})/\epsilon \times 10^{-5}$	$\lambda^{\text{em}}(\text{nm})$	QY
6b	366/1.2	384,407,432, 457, 501	0.57
6c	378/1.6	384,407,432, 457	0.15
6d	369/1.8	384,407,432, 457	0.16
6e	369/1.1	384,407,432, 457,515	0.29
6f	378/1.1	384,407,432, 457, 506	0.3
6g	366/1.1	384,407,432, 457, 506	0.24
6h	377/1.6	384,407,432, 457	0.16
6i	375/1.1	384,407,432, 457,496	0.44
6j	375/1.4	384,407,432, 457, 506	0.19
Note: ϵ is the coefficient ($\text{M}^{-1} \text{cm}^{-1}$) at λ_{max} , excitation λ 375 nm, QY is the quantum yield calculated using Quinine sulfate in 1 (N) H ₂ SO ₄ (QY 0.546) as a reference.			

The XRD structure of **6b** (CCDC 2292567) and **6i** (CCDC 2297371) are shown in Figure 1.13. The **6b** molecules are packed in a Herringbone⁴⁷ pattern formed by slip-stacked and displaced pairs. The interplanar distance between two adjacent slip-stacked **6b** molecules was 3.338 Å. Although the 3.338 Å is sufficiently close for π - π stacking, a slip-stack resulted in a small area of the aromatic rings overlapping with its nearest molecule, which does not allow quenching of PL in the crystalline state. Therefore, the PL property of **6b** in a solid crystalline form is very similar to the single molecule. Compound **6i** packed in a head-to-tail fashion, making the interplanar distance between two adjacent molecules 3.489 Å. The twisted (torsion angle 43.7°) phenyl ring of **6i** does not allow aggregation-induced quenching of fluorescence properties. The hexagonal arrangement of stacked **6i** molecules created a void space, which was occupied by solvent molecules as shown in Figure 1.13C (packing view along c axis). Thus, compounds **6b** and **6i** exhibited strong PL properties in solid and solution states.

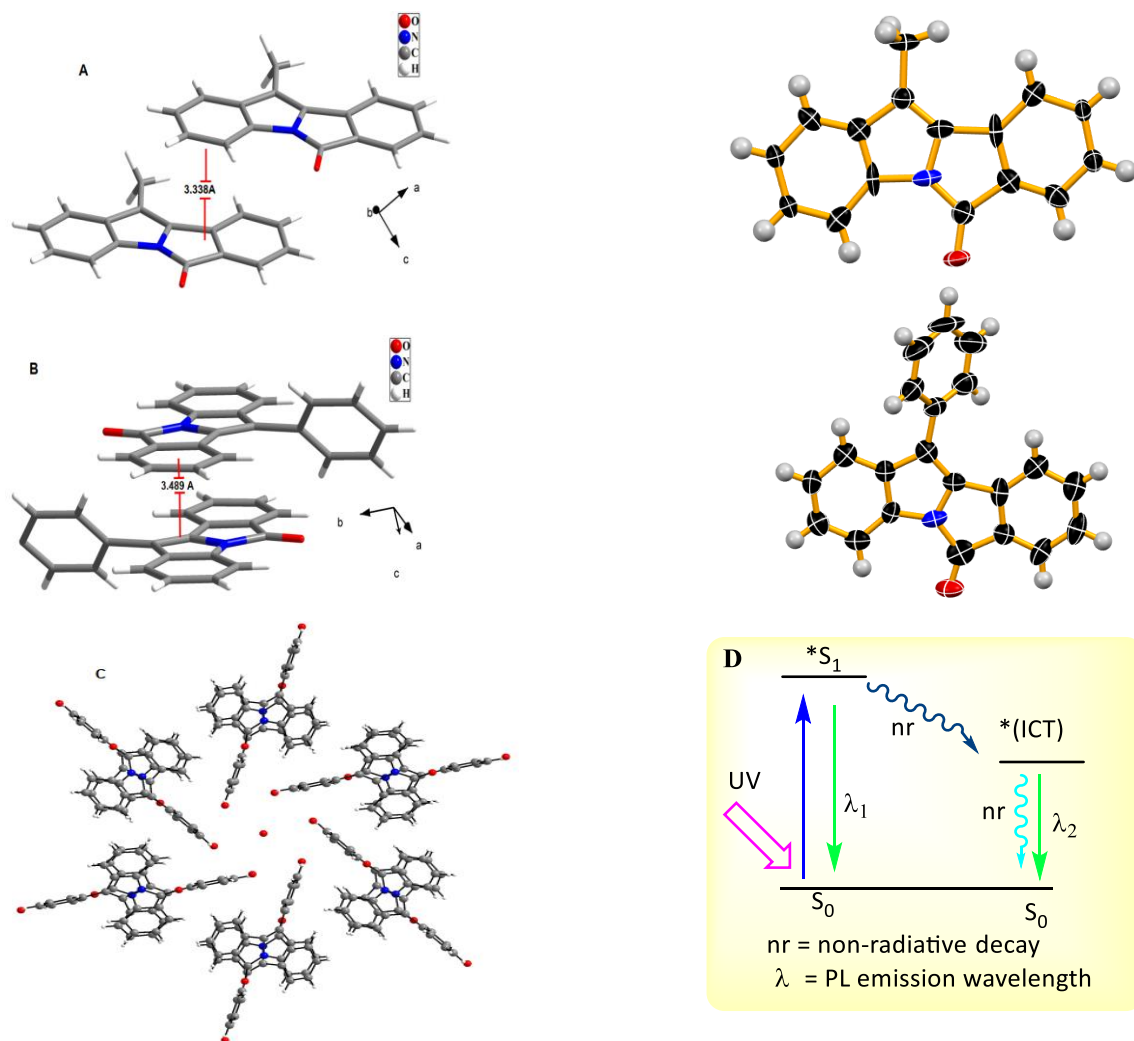


Figure 1.13 XRD Structure and packing **6b** and **6i**, and overall photochemistry

Thus, compound **6b** stands out to be a unique molecule where the interplay between ICT and locally excited state makes the materials a potential fluorophore. The overall photochemistry is shown in Figure 1.13D

1.7 CONCLUSION

In conclusion, we have explored a one-pot process mediated by inexpensive FeCl_3 in an alcoholic solvent for synthesizing tetracyclic aromatic compound isoindoloindolones. Detailed substrate scope and the photophysical properties of the synthesized compounds revealed that fluorescence quantum yield reduces on placing a group at the terminal aromatic ring of the isoindoloindolone moiety contributing from 2-aminoacetophenone residue. However, the presence of only methyl and twisted phenyl group at the 11 position of isoindoloindolone produced a novel material capable of showing Photoluminescence properties in solution and the solid state. The study of concentration-dependent PL properties in hexane suggested an ICT

state formation. Thus, **6b** appeared to be unique material for optoelectronics and bio-imaging technologies. Furthermore, the photophysical properties can be tuned by placing a suitable functional group at the place of methyl of **6b** for improvement of PL properties. We also devised and implemented a one-pot process mediated by Pd(OAc)₂ in an acidic solvent for the synthesis of tetracyclic aromatic compounds, specifically isoindoloindolones via 1,2-addition, and benzoazepinoisoindole-(6*H*)-dione derivatives via 1,4-addition. A thorough exploration of the substrate scope for the synthesized compounds unveiled that the introduction of a substituent at the terminal aromatic ring of the chalcone, originating from the aldehyde residue, significantly influences product selectivity. Electron-donating substituents tend to yield products via 1,2-direct addition resulting in the predominant formation of Isoindoloindolones, while electron-withdrawing substituents prefer 1,4-conjugated addition. Isoindoloindolones compounds demonstrate pronounced fluorescence characteristics, thus stimulating a desire to delve into their photophysical behaviour and ascertain their applicability within the domain of optoelectronics. Currently, these investigations are ongoing.

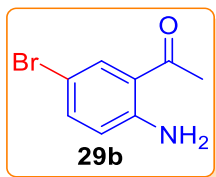
1.8 EXPERIMENTAL SECTION

1.8.1 General Procedures

The analytical thin layer chromatography (TLC) was carried out for monitoring the progress of the reactions using silica gel 60 F254 precoated plates. Visualizations of the spots were accomplished with a UV lamp or I₂ stain. Unless otherwise mentioned, all of the reactions were carried out in oven-dried glassware under an atmosphere of nitrogen or argon using normal solvent. All of the commercial reagents were used as received without further purification unless otherwise mentioned. Yields refer to the isolated product as mentioned in the experimental section. Proton nuclear magnetic resonance (¹H NMR) were recorded at Bruker 300 MHz and 400 MHz. The chemical shifts were recorded in parts per million (ppm, δ) using tetramethylsilane (δ 0.00) as the internal standard. All coupling constants (*J*) are absolute values and are expressed in Hz. Splitting patterns of the ¹H NMR are mentioned as singlet (s), doublet (d), doublet of doublet (dd), doublet of triplet (dt), triplet (t), multiplet (m) etc. Proton-decoupled carbon nuclear magnetic resonance ¹³C NMR spectra were recorded at 75 MHz and 100 MHz. HRMS were obtained using (ESI) mass spectrometer (TOF). The melting point measurements were made using a hot stage apparatus and are reported as uncorrected.

1.8.2 Experimental Procedure and Analytical Data of the starting materials

Synthesis of 1-(2-amino-5-bromophenyl)ethan-1-one (**29b**)⁴⁸

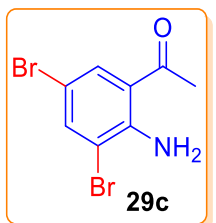


To a 50 mL round-bottom flask, 1-(2-aminophenyl)ethanone **29a** (0.5 g, 3.7 mmol) and 5 mL CH₃CN were added. *N*-Bromosuccinimide (0.66 g, 3.7 mmol) in 5 mL CH₃CN was slowly added to this solution at 0 °C under stirring. The mixture was allowed to warm to room temperature and stirred for 3 h. The solvent was removed in *vacuo* and the crude residue was filtered through a short plug of silica (washed with petroleum ether : ethyl acetate = 5: 1). The filtrate was concentrated in *vacuo* to afford 1-(2-amino-5-bromophenyl)ethanone **29b** as a dark yellow solid (0.76 g, 96 % yield). The product need not to be further purified.

29f was also prepared by the same method of bromination of 2-aminobenzophenone **29h** by following the literature procedure.^{36, 37}

¹H NMR (300 MHz, CDCl₃) δ 2.58 (s, 3H), 6.58 (d, J = 8.7 Hz, 1H), 7.34 (dd, J = 2.4 Hz, 9 Hz, 1H), 7.82 (d, J = 2.4 Hz, 1H).

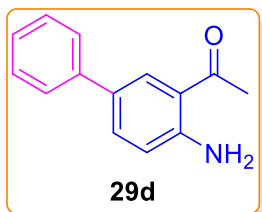
Synthesis of 1-(2-amino-3,5-dibromophenyl)ethanone: (**29c**)³⁸



To a 50 mL round-bottom flask, 1-(2-aminophenyl)ethanone **29a** (0.5 g, 3.7 mmol) and 5 mL CH₃CN were added. *N*-Bromosuccinimide (1.3 g, 7.7 mmol) in 20 mL CH₃CN was slowly added to this solution at 0 °C under stirring. The mixture was allowed to warm to room temperature and stirred for 24 h. The solvent was removed in *vacuo* and the crude residue was filtered through a short plug of silica (washed with petroleum ether : ethyl acetate = 5: 1). The filtrate was concentrated in *vacuo* to afford 1-(2-amino-3,5-dibromophenyl)ethanone **29c** 1.08 g (97%) as a brown solid. All the spectral data were found to be matching with the reported compound.³⁸

¹H NMR (300 MHz, CDCl₃) δ 2.60 (s, 3H), 7.70 (d, J = 2.4 Hz, 1H), 7.82 (d, J = 2.1 Hz, 1H).

Synthesis of 1-(4-amino-[1,1'-biphenyl]-3-yl)ethan-1-one (**29d**)³⁵

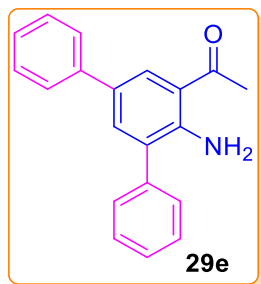


This compound was previously reported in the literature and prepared from **29b** using a modified procedure from the literature. In a 50 ml sealed tube, 1-(2-amino-5-bromophenyl)ethan-1-one (250 mg, 1.167 mmol), phenyl boronic acid (170.8 mg, 1.401 mmol), K₂CO₃ (484.1 mg,

3.50 mmol), and $\text{Pd(PPh}_3)_4$ (67.4 mg, 0.05 mmol) were combined in the presence of 3 ml H_2O and 3 ml dioxane. The tube was evacuated and backfilled with N_2 three times. The mixture was then stirred at 100 °C for 3 hours. After completion of the reaction, the mixture was washed with 50 ml ethyl acetate, and the organic layer was separated, washed with brine, dried over Na_2SO_4 , concentrated in vacuo, and the crude residue was purified through column chromatography (petroleum ether:ethyl acetate = 98:2). This process yielded the product **29d** as a yellow solid (210 mg, 85% yield)

^1H NMR (300 MHz, CDCl_3) δ 2.67 (s, 3H), 6.76 (d, J = 9 Hz, 1H), 7.33 (t, J = 9 Hz, 1H), 7.45 (J = 9 Hz, 2H), 7.55- 7.58 (m, 3H), 7.95 (d, J = 2.1 Hz, 1H); **^{13}C NMR (75 MHz, CDCl_3)** δ 27.9, 117.7, 117.8, 118.4, 126.3, 126.6, 128.8, 129.0, 130.3, 133.3, 140.5, 149.5, 200.8.

Synthesis of 1-(4'-amino-[1,1':3',1''-terphenyl]-5'-yl)ethan-1-one (**29e**)³⁸

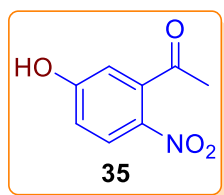


This compound was literature-known and prepared from **29c** according to a modified literature procedure.³⁸ To a 50 ml seal tube was added 1-(2-amino-3,5-dibromophenyl)ethan-1-one (250 mg, 0.853 mmol), phenyl boronic acid (121.9 mg, 2.13 mmol) in presence of K_2CO_3 (294.8 mg, 2.13 mmol) and Pd(OAc)_2 (9.5 mg, 0.042 mmol) in 5 ml H_2O . The tube was evacuated and backfilled with N_2 for three times. The mixture

was then stirred at 100 °C for 30 min. Upon completion of the reaction the mixture was washed with 50 ml ethyl acetate and the organic layer was separated and washed with brine, dried over Na_2SO_4 and concentrated in *vacuo* and the crude residue was purified through a column chromatography (petroleum ether : ethyl acetate = 94 : 6) gave the product **29e** as a yellow solid (198 mg, 80 % yield).

^1H NMR (300 MHz, CDCl_3) δ 2.73 (s, 3H), 6.01 (s, 2H), 7.34 (t, J = 7.2 Hz, 1H), 7.43-7.50 (m, 6H), 7.52-7.55 (m, 2H), 7.59 (d, J = 6.9 Hz, 2H), 8.01 (d, J = 2.1 Hz, 1H); **^{13}C NMR (75 MHz, CDCl_3)** δ 28.3, 118.3, 126.3, 126.6, 127.9, 128.3, 128.8, 129.2, 129.31, 129.36, 129.87, 129.93, 134.2, 138.1, 140.4, 147.1.

Synthesis of 1-(5-hydroxy-2-nitrophenyl)ethan-1-one (**35**)³⁷

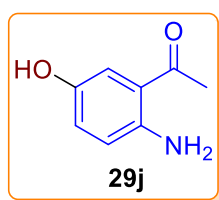


This compound was literature-known and prepared from commercially available 3-hydroxyacetophenone **34** according to a modified literature procedure. To a glacial acetic acid (20 ml) 3-hydroxyacetophenone (22.03 mmol) was added. Add NaNO_3 (44.06 mmol) portion wise into it The mixture was allowed to stir at room temperature for 72 h. After completion of the reaction

NaOH pellets was added to basic pH. The reaction mixture then washed with (3×50.0 mL) ethyl acetate and the organic layer was separated and washed with brine, dried over Na_2SO_4 and concentrated in *vacuo* and the crude residue was purified through a short column chromatography (EtOAc : Pet ether = 5 : 95) to afford 40% of the nitro compound **35**. No need for further purification. The position of the nitration is confirmed by NMR and XRD of the compound **35** (CCDC 2292561).

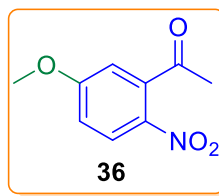
^1H NMR 400 MHz, CDCl_3) δ 2.55 (s, 3H), 6.75 (d, $J = 2.8$ Hz, 1H), 6.96 (dd, $J = 9.2$ Hz, 2.8 Hz 1H), 8.12 (d, $J = 9.2$ Hz, 1H).

Synthesis of 1-(2-amino-5-hydroxyphenyl)ethan-1-one (**29j**)^{37, 39}



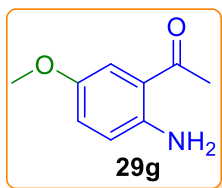
The compound **29j** was prepared by the reduction of **35**. The reduction of **35** was carried out by Fe powder and CaCl_2 following the protocol described by Chandrappa et al.³⁹ The mixture of nitro product **35** (250.0 mg, 1.38 mmol) Fe powder and CaCl_2 in ethanol was taken in a dried single-necked round bottom flask under the nitrogen atmosphere and was then stirred at 80°C for two hours. After completion of the reaction, the mixture was allowed to cool at room temperature and filtered it off through the Whatmann-40 filter paper. The filtrate was collected and the solvent was removed under reduced pressure to afford the title product **29j** in quantitative yield. No need to purify the mixture.

Synthesis of 1-(5-methoxy-2-nitrophenyl)ethan-1-one (**36**)

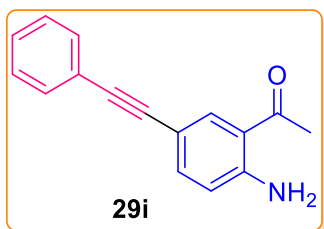


To a 50 mL round-bottom flask, 5-hydroxy 2-nitro acetophenone **35** (100 mg, 0.55 mmol) in 10 mL acetone was taken. Anhydrous K_2CO_3 (190.7 mg, 1.38 mmol) was added to it and stirred for 5 min; next, MeI (156.7 mg, 1.10 mmol) was slowly added to this solution at rt under stirring. The mixture was allowed to stir for 6 h. The solvent was removed in *vacuo* and the crude residue was filtered through a short plug of silica (washed with petroleum ether : ethyl acetate = 1 : 1) to afford the product 3-methoxy 5-nitroacetophenone **36** as a yellow compound (97 mg, 0.496 mmol, 90 % yield).

^1H NMR 300 MHz, CDCl_3) δ 2.45 (s, 3H), 3.85 (s, 3H), 6.70 (d, $J = 2.7$ Hz, 1H), 6.92 (dd, $J = 9.3$ Hz, 2.7 Hz 1H), 8.07 (d, $J = 9.3$ Hz, 1H).

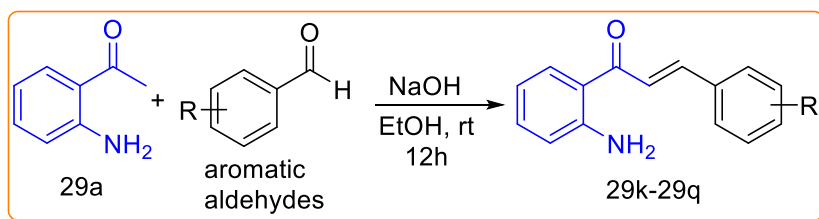
Synthesis of 1-(2-amino-5-methoxyphenyl)ethan-1-one (29g)^{36, 39}

The title compound was prepared by the reduction of **36**. The Reduction of 1-(2-nitro-5-hydroxyphenyl)ethan-1-one **36** was carried out in the same manner by Fe powder.³⁹ A mixture of 1-(2-nitro-5-hydroxyphenyl)ethan-1-one (200 mg, 1.024 mmol), Fe powder (572.3 mg, 10.248 mmol) and CaCl₂ (113.6 mg, 1.028 mmol) was allowed to reflux in ethanol (12 ml) for 16 h. After completion of the reaction, the reaction mixture was allowed to cool at room temperature and filtered it off through the Whatmann-40 filter paper. The filtrate was collected and the solvent was removed under reduced pressure to afford the title product **29g** in quantitative yield. No need to purify the mixture.

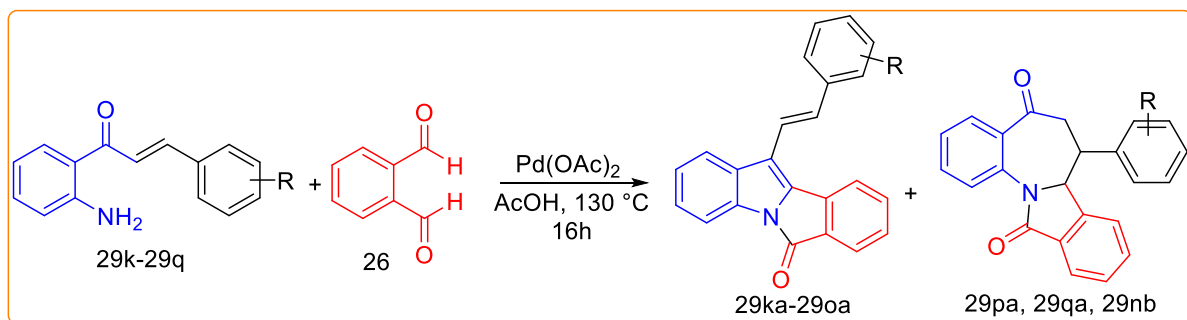
Synthesis of 1-(2-amino-5-(phenylethynyl)phenyl)ethan-1-one (29i)⁴⁰

This compound was literature-known and synthesized from **37** following a modified procedure.⁴⁰ To a well-stirred solution of 1-(2-amino-5-iodophenyl)ethan-1-one **37** (0.766 mmol, 1 equiv.) in Et₃N (1.5 mL) was added PdCl₂(PPh₃)₂ (5 mg, 0.007 mmol, 1 mol %) and CuI (2.9 mg, 0.01 mmol, 2 mol %) and the whole reaction mixture was stirred for 5 minutes under argon. A solution of phenylacetylene (0.766 mmol, 1 equiv) dissolved in Et₃N (2 mL) was then added dropwise for 5 minutes. The resulting solution was then stirred at room temperature overnight. When the reaction was found to be completed (TLC), the reaction mixture was then quenched by addition of water (2 mL), extracted with ethyl acetate (3 x 40 mL) and the combined organic extracts were dried over anhydrous Na₂SO₄ and concentrated under reduced pressure, then purified through silica gel (100–200 mesh) column chromatography (3–4% ethyl acetate–petroleum ether) to afford the requisite product **29i** in 85% yield.

¹H NMR (300 MHz, CDCl₃) δ 2.53 (s, 3H), 6.39 (s, 2H), 6.54 (d, *J* = 8.4 Hz, 1H), 7.22–7.30 (m, 3H), 7.34 (dd, *J* = 6.6 Hz, 2.1 Hz, 1H), 7.42–7.46 (m, 2H), 7.85 (d, *J* = 2.1 Hz, 1H); **¹³C NMR (75 MHz, CDCl₃)** δ 26.8, 86.2, 88.2, 109.1, 116.3, 116.9, 122.5, 126.8, 127.3, 130.3, 134.7, 136.1, 149.0, 199.2.

General procedure (A) for the synthesis of various 2-amino aryl chalcones:⁴³

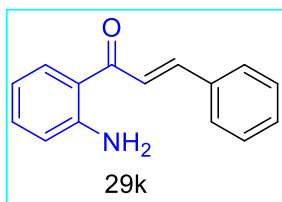
2-amino-aryl chalcones **29k-29q** were prepared according to our previous reported procedure.⁴³ A round bottom flask containing a magnetic stirring bar was charged with 2-aminoacetophenone (250mg, 1 equiv) in ethanol and 5 equiv. of NaOH (15 mL). Then the mixture was stirred for 5 min and then corresponding ethanolic solutions of arylaldehyde (1 equiv, 5 ml) was added dropwise. The reaction mixture was kept stirring for 12 h and after addition of distilled water corresponding yellow solid chalcones were precipitated out. The Solid was filtered through Whatman-41 paper and without further purification by column chromatography the chalcone derivatives were utilised in subsequent reactions.

Representative Procedure (B) for Synthesis of 6*H*-isoindolo[2,1-*a*]indol-6-one derivatives

The mixture of chalcone **29k-29q** (1.0 equiv), **26** (1.0 equiv) and anhydrous Pd(OAc)₂ (0.2 equiv) in acetic acid (1.0 mL) were taken under nitrogen atmosphere in a round bottom flask. The reaction mixture was stirred at 130 °C for 16 h. After completion of the reaction, the reaction mixture was quenched with water, extracted with ethyl acetate (3 × 15.0 mL) and dried over anhydrous Na₂SO₄. The solvent was removed under reduced pressure and the crude product was purified by column chromatography on silica gel (100–200 mesh) using 2% ethyl acetate in petroleum ether to afford the pure product **29ka-29oa** as a light green fluorescent solid and in some cases another product **29pa, 29qa** and **29nb** was purified by column chromatography on silica gel (100–200 mesh) using 15% ethyl acetate in pet ether as a brown solid.

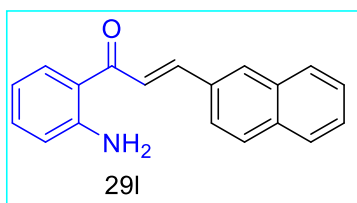
Characterization of the Analytical data of the starting chalcones

(*E*)-1-(2-aminophenyl)-3-phenylprop-2-en-1-one (29k)



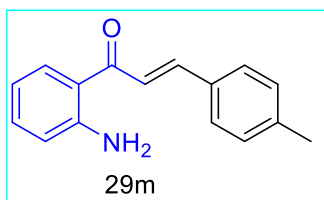
The chalcone **29k** was prepared according to the above mentioned general procedure A. Yellow solid; yield 88% (390 mg). ^1H NMR (400 MHz, CDCl_3) δ 6.35 (bs, 2H), 6.71-6.74 (m, 2H), 7.29-7.34 (m, 1H), 7.41-7.45 (m, 3H), 7.26-7.67 (m, 3H), 7.77 (d, $J = 15.6$ Hz, 1H), 7.89 (dd, $J = 8.4$ Hz, 1.6 Hz, 1H); ^{13}C NMR (100 MHz, CDCl_3) δ 116.0, 117.4, 119.3, 123.4, 128.3, 129.0, 130.2, 131.1, 134.4, 135.5, 143.0, 151.1, 191.8.

(*E*)-1-(2-aminophenyl)-3-(naphthalen-2-yl)prop-2-en-1-one (29l)



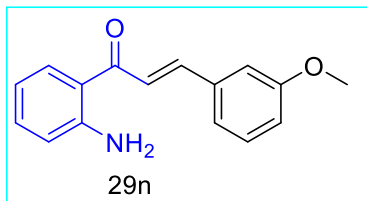
The chalcone **29l** was prepared according to the above mentioned general procedure A. Yellow solid; yield 92% (465 mg). ^1H NMR (300 MHz, CDCl_3) δ 6.38 (bs, 2H), 6.72-6.78 (m, 2H), 7.33 (dt, $J = 6.8$ Hz, 1.5 Hz, 1H), 7.51-7.57 (m, 2H), 7.75 (d, $J = 15.6$ Hz, 1H), 7.79-7.96 (m, 6H), 8.04 (s, H); ^{13}C NMR (75 MHz, CDCl_3) δ 115.9, 117.3, 119.1, 123.3, 123.8, 126.7, 127.1, 127.8, 128.60, 128.66, 130.1, 131.0, 132.7, 133.4, 134.2, 134.5, 143.0, 151.0, 191.6.

(*E*)-1-(2-aminophenyl)-3-(p-tolyl)prop-2-en-1-one (29m)

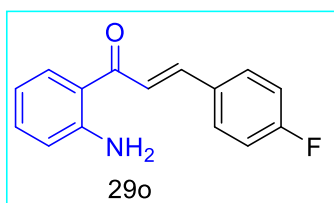


The chalcone **29m** was prepared according to the above mentioned general procedure A. Yellow solid; yield 88% (390 mg). ^1H NMR (400 MHz, CDCl_3) δ 2.30 (s, 3H), 6.22 (bs, 2H), 6.59-6.63 (m, 2H), 7.13 (d, $J = 6.6$ Hz, 2H), 7.17-7.21 (m, 1H), 7.43-7.50 (m, 3H), 7.64 (d, $J = 15.2$ Hz, 1H), 7.77 (d, $J = 6.0$ Hz, 1H); ^{13}C NMR (100 MHz, CDCl_3) δ 21.4, 115.8, 117.2, 119.2, 122.2, 128.2, 129.6, 131.0, 132.5, 134.1, 140.5, 143.0, 150.9, 191.8.

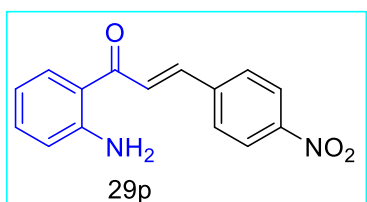
(*E*)-1-(2-aminophenyl)-3-(4-methoxyphenyl)prop-2-en-1-one (29n)



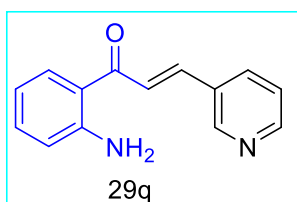
The chalcone **29n** was prepared according to the above mentioned general procedure A. Yellow solid; yield 84% (395 mg). ^1H NMR (400 MHz, CDCl_3) δ 3.87 (s, 3H), 6.69-6.74 (m, 2H), 6.95-6.98 (m, 1H), 7.16 (t, $J = 1.6$ Hz, 1H), 7.23-7.26 (m, 1H), 7.28-7.36 (m, 2H), 7.61 (d, $J = 15.6$ Hz, 1H), 7.72 (d, $J = 16.4$ Hz, 1H), 7.87 (dd, $J = 1.6$ Hz, 8.4 Hz, 1H); ^{13}C NMR (100 MHz, CDCl_3) δ 55.3, 113.3, 115.84, 115.88, 117.3, 119.0, 120.9, 123.5, 129.8, 131.0, 134.3, 136.7, 142.8, 151.0, 159.9, 191.6.

(E)-1-(2-aminophenyl)-3-(4-fluorophenyl)prop-2-en-1-one (29o)

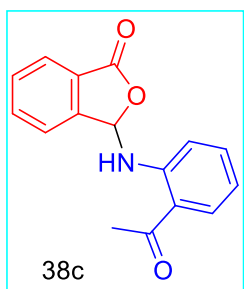
The chalcone **29o** was prepared according to the above mentioned general procedure A. Yellow solid; yield 88% (394 mg). **¹H NMR (400 MHz, CDCl₃)** δ 6.26 (bs, 2H), 6.59-6.64 (m, 2H), 6.99-7.05 (m, 2H), 7.21 (td, J = 8.7 Hz, 1.8 Hz, 1H), 7.46 (d, J = 15.6 Hz, 1H), 7.51-7.56 (m, 2H), 7.62 (d, J = 15 Hz, 1H), 7.77 (dd, J = 8.4 Hz, 1.8 Hz, 1H); **¹³C NMR (100 MHz, CDCl₃)** δ 114.8, 115.1, 116.3, 117.9, 121.7, 121.8, 129.0, 129.1, 129.9, 133.3, 140.6, 150.0, 161.1, 164.4, 190.4.

(E)-1-(2-aminophenyl)-3-(4-nitrophenyl)prop-2-en-1-one (29p)

The chalcone **29p** was prepared according to the above mentioned general procedure A. Brown solid yield 92%. **¹H NMR (400 MHz, CDCl₃)** δ 6.32 (bs, 2H), 6.61-6.65 (m, 2H), 7.24 (t, J = 8.0 Hz, 2H), 7.64-7.69 (m, 4H), 7.76 (d, J = 8.8 Hz, 1H), 8.18 (d, J = 7.6 Hz, 2H); **¹³C NMR (100 MHz, CDCl₃)** δ 115.9, 117.4, 118.5, 124.1, 127.1, 128.6, 130.9, 134.8, 139.6, 141.5, 148.3, 151.3, 190.6.

(E)-1-(2-aminophenyl)-3-(pyridin-3-yl)prop-2-en-1-one (29q)

The chalcone **29q** was prepared according to the above mentioned general procedure A. Yellow solid; yield 91% (378 mg). **¹H NMR (300 MHz, CDCl₃)** δ 6.43 (bs, 2H), 6.68-6.73 (m, 2H), 7.28-7.38 (m, 2H), 7.70 (s, 1H), 7.85 (dd, J = 14.1 Hz, 1.2 Hz, 1H), 7.94 (td, J = 7.8 Hz, 2.1 Hz, 1H), 8.61 (dd, J = 4.8 Hz, 1.8 Hz, 1H), 8.84 (d, J = 1.5 Hz, 1H); **¹³C NMR (100 MHz, CDCl₃)** δ 114.8, 116.3, 117.5, 122.7, 124.0, 129.9, 130.0, 133.4, 133.6, 137.9, 148.7, 149.6, 150.2, 189.8.

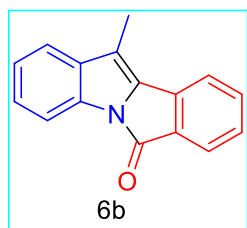
Synthesis of an Intermediate 38c**3-((2-acetylphenyl)amino)isobenzofuran-1(3H)-one (38c)**

A mixture of OPA **26** (65 mg, 0.84 mmol) and 2-amino acetophenone **29a** (66 mg, 0.84 mmol) in *i*PrOH (1 mL) was stirred at RT for 16 hours in the presence of 10 mg AcOH. The white precipitate formed was collected by filtration, dried under vacuum (78 mg, 64%) and characterized by NMR. **¹H NMR (300 MHz, CDCl₃)** δ 9.58 (d, J = 8.0

Hz, 1H), 7.96 (d, $J = 7.2$ Hz, 1H), 7.87 (d, $J = 7.8$ Hz, 1H), 7.82 – 7.73 (m, 1H), 7.68 (s, 2H), 7.54 (t, $J = 7.4$ Hz, 1H), 7.32 (d, $J = 8.2$ Hz, 1H), 6.94 (t, $J = 7.3$ Hz, 1H), 6.84 (d, $J = 8.5$ Hz, 1H), 2.61 (s, 3H). ^{13}C NMR (75 MHz, CDCl_3) δ 28.2, 85.5, 113.9, 118.6, 119.8, 123.1, 125.7, 127.7, 130.8, 132.5, 134.7, 135.3, 145.3, 147.4, 169.2, 201.8.

1.8.3 Synthesis and characterization of the final compounds 6b-6j

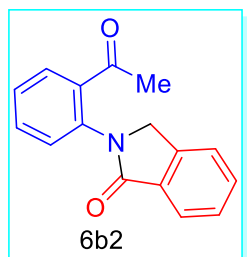
11-methyl-6H-isoindolo[2,1-a]indol-6-one (6b)



The mixture of **29a** (50.0 mg, 0.369 mmol, 1.0 equiv), **26** (49.4 mg, 0.369 mmol, 1.0 equiv) and anhydrous FeCl_3 (0.073 mmol, 0.2 equiv) in dry MeOH (1.5 mL) was taken in a dried double necked round bottom flask under nitrogen atmosphere and was then stirred at 70 °C for 16 h.

After completion of the reaction, the reaction mixture was cooled to rt and the solvent was removed under reduced pressure, extracted with ethyl acetate (3×15.0 mL) and dried over anhydrous Na_2SO_4 . The solvent was removed under reduced pressure which was purified by flash column chromatography on silica gel (100–200 mesh) using 2% ethyl acetate in petroleum ether as the eluent to obtain the pure major product **6b** as a yellow solid in 76% yield. mp 150 °C; ^1H NMR (300 MHz, CDCl_3) δ 2.45 (s, 3H), 7.18 (t, $J = 9$ Hz, 1H), 7.32 (t, $J = 6.9$, 2H), 7.39 (d, $J = 7.8$ Hz, 1H), 7.49–7.59 (m, 1H), 7.77 (d, $J = 7.5$ Hz, 1H), 7.87 (d, $J = 7.8$, 1H); ^{13}C NMR (75 MHz, CDCl_3) δ 9.4, 113.2, 115.3, 120.1, 121.1, 123.5, 125.2, 126.5, 128.0, 133.4, 133.5, 133.9, 134.5, 135.0, 135.7, 162.2; HRMS (ESI-TOF) m/z : $[\text{M}+\text{H}]^+$ Calcd for $\text{C}_{16}\text{H}_{11}\text{NOH}$ 234.0919; Found 234.0909.

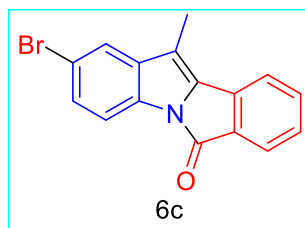
2-(2-acetylphenyl)isoindolin-1-one (6b2)



The mixture of **29a** (50.0 mg, 0.369 mmol, 1.0 equiv), OPA **26** (49.4 mg, 0.369 mmol, 1.0 equiv) and $\text{Pd}(\text{OAc})_2$ (0.073 mmol, 0.2 equiv) in acetic acid (2 mL) was taken in a dried double necked round bottom flask under nitrogen atmosphere and was then stirred at 130 °C for 16 h. After completion of the reaction, the reaction mixture was cooled to rt and aqueous NaHCO_3 was added, extracted with ethyl acetate (3×15.0 mL) and dried over anhydrous Na_2SO_4 . The solvent was removed under reduced pressure which was purified by flash column chromatography on silica gel (100–200 mesh) using 35% ethyl acetate in petroleum ether as the eluent to obtain the pure major product **6b2** (83.4 mg, 0.332 mmol) as a white solid in 90 % yield.

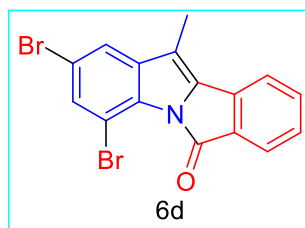
¹H NMR (300 MHz, CDCl₃) δ 2.50 (s, 3H), 4.79 (s, 2H), 7.27 (dd, J = 6.6 Hz, 1.2 Hz, 1H), 7.33 (td, J = 7.8, 1.2 Hz, 1H), 7.39-7.46 (m, 2H), 7.48-7.55 (m, 2H), 7.60 (dd, J = 7.8 Hz, 1.8 Hz, 1H), 7.81 (d, J = 7.2, 1H); **¹³C-NMR (75 MHz, CDCl₃)** δ 27.6, 51.9, 121.7, 123.2, 125.7, 126.1, 127.2, 127.3, 130.8, 131.0, 131.1, 134.3, 136.6, 140.3, 167.199.5; **HRMS (ESI-TOF) m/z : [M+H]⁺** Calcd for C₁₆H₁₃NO₂ 252.1025; Found 252.1017.

2-bromo-11-methyl-6H-isoindolo[2,1-a]indol-6-one (6c)



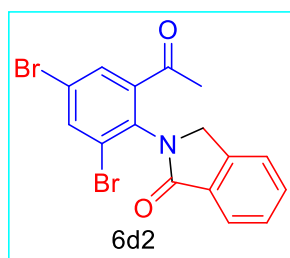
Prepared from **29b** (50.0 mg, 0.233 mmol, 1.0 equiv) and OPA **26** (31.3 mg, 0.233 mmol, 1.0 equiv) following the procedure described for **6b**. **Yield** (37 mg, 0.119 mmol) 51% yield. mp 166-168 °C; **¹H NMR (300 MHz, CDCl₃)** δ 2.39 (s, 3H), 7.31-7.39 (m, 2H), 7.48-7.54 (m, 3H), 7.73 (dd, J = 13.2 Hz, 4.8 Hz, 2H); **¹³C NMR (75 MHz, CDCl₃)** δ 9.4, 114.3, 114.4, 116.7, 121.3, 123.1, 125.4, 128.5, 129.1, 132.1, 133.72, 133.74, 134.7, 135.6, 137.5, 162.1; **HRMS (ESI-TOF) m/z : [M+H]⁺** Calcd for C₁₆H₁₀BrNO 312.0024; Found 312.0013.

2,4-dibromo-11-methyl-6H-isoindolo[2,1-a]indol-6-one (6d)



Prepared from **29c** (100.0 mg, 0.341 mmol, 1.0 equiv) and OPA **26** (50.3 mg, 0.375 mmol, 1.1 equiv) following the procedure described for **6b**. Compound **6d** and **6d2** were isolated from the reaction of **29c**. **Yield:** (54 mg, 0.139 mmol), 41% yield. mp 180 °C; **¹H NMR (400 MHz, CDCl₃)** δ 2.30 (s, 3H), 7.28 (dt, J = 1.2, 7.6 Hz, 1H), 7.33 (d, J = 2.0 Hz, 1H), 7.45-7.51 (m, 4H) [3H], 7.68 (d, J = 7.6 Hz, 1H); **¹³C NMR (100 MHz, CDCl₃)** δ 9.2, 106.3, 113.3, 116.8, 121.1, 121.5, 125.7, 128.9, 133.2, 133.4, 133.7, 133.9, 137.6, 139.9, 160.6; **HRMS (ESI-TOF) m/z : [M+H]⁺** Calcd for C₁₆H₉Br₂NO 391.9109; Found 391.9101.

2-(2-acetyl-4,6-dibromophenyl)isoindolin-1-one (6d2)

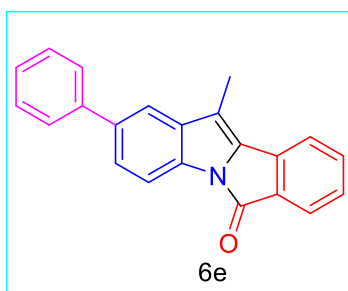


Yield 6d2: (47 mg, 0.119 mmol), 35% yield.; **¹H NMR (400 MHz, CDCl₃)** δ 2.44 (s, 3H), 4.56 (d, J = 16.0 Hz, 1H), 4.90 (d, J = 16.0 Hz, 1H), 7.43 (t, J = 7.6 Hz, 2H), 7.55 (t, J = 7.6 Hz, 1H), 7.66 (t, J = 2.0 Hz, 1H), 7.82 (d, J = 8.0 Hz, 1H), 7.90 (t, J = 2.4 Hz, 1H); **¹³C NMR (100 MHz, CDCl₃)** δ 28.0, 51.0, 121.5, 122.0, 123.3, 125.1,

127.1, 129.3, 130.3, 131.2, 132.9, 137.1, 140.8, 141.4, 167.7, 197.5; **HRMS (ESI-TOF) m/z :** $[M+2+Na]^+$ Calcd for $C_{16}H_{11}Br_2NO_2$ 431.9034; Found 431.7048.

11-methyl-2-phenyl-6*H*-isoindolo[2,1-*a*]indol-6-one (6e)

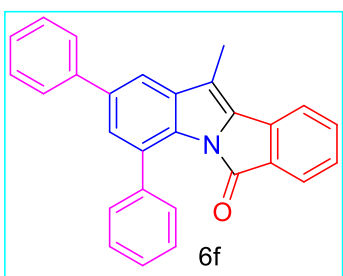
Prepared from **29d** (50.0 mg, 0.236 mmol, 1.0 equiv), and OPA **26** (31.6 mg, 0.236 mmol, 1.0 equiv) following the procedure described for **6b**.



Yield (56 mg, 0.170 mmol) 72% yield. mp 162 °C; **1H NMR (300 MHz, $CDCl_3$)** δ 2.50 (s, 3H), 7.32-7.40 (m, 2H), 7.46-7.56 (m, 4H), 7.59 (s, 2H), 7.64 (d, J = 6 Hz, 2H), 7.79 (d, J = 6 Hz, 1H), 7.93 (d, J = 6 Hz, 1H); **^{13}C NMR (75 MHz, $CDCl_3$)** δ 9.5, 113.4, 115.5, 118.8, 121.2, 125.3, 125.9, 127.0, 127.1, 128.1, 128.7, 132.8, 133.4, 133.9, 135.0, 135.2, 136.3, 137.1, 141.3,

162.2; **HRMS (ESI-TOF) m/z :** $[M+Na]^+$ Calcd for $C_{22}H_{15}NO$ 332.1051; Found 332.1137.

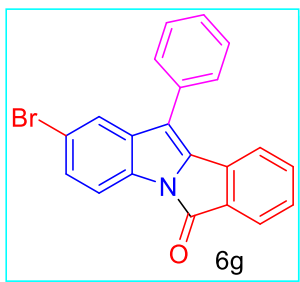
11-methyl-2,4-diphenyl-6*H*-isoindolo[2,1-*a*]indol-6-one (6f)



Prepared from **29e** (50.0 mg, 0.173 mmol, 1.0 equiv), and OPA **26** (23.3 mg, 0.173 mmol, 1.0 equiv) following the procedure described for **6b**. **Yield** (31 mg, 0.083 mmol) as a yellow solid in 48% yield. mp 170 °C; **1H NMR (300 MHz, $CDCl_3$)** δ 2.48 (s, 3H), 7.20 (m, 1H), 7.30 (t, J = 7.5 Hz, 1H), 7.37-7.47 (m, 10H), 7.55 (d, J = 7.2 Hz, 2H), 7.60 (d, J = 5.7 Hz, 2H); **^{13}C NMR**

(75 MHz, $CDCl_3$) δ 8.4, 114.0, 116.3, 119.8, 124.4, 126.1, 126.2, 126.41, 126.45, 127.1, 127.3, 127.7, 128.4, 128.5, 130.5, 132.3, 132.7, 133.5, 135.6, 135.9, 136.4, 139.6, 139.9, 159.8; **HRMS (ESI-TOF) m/z :** $[M+H]^+$ Calcd for $C_{28}H_{19}NO$ 386.1545; Found 386.1537.

2-bromo-11-phenyl-6*H*-isoindolo[2,1-*a*]indol-6-one (6g)

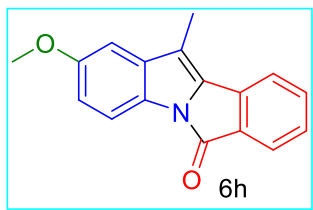


Prepared from **29f** (100.0 mg, 0.362 mmol, 1.0 equiv), and OPA (48.5 mg, 0.362 mmol, 1.0 equiv) following the procedure described for **6b**. **Yield** (66 mg, 0.177 mmol) as a yellow solid in 49 % yield. mp 170 °C; **1H NMR (400 MHz, $CDCl_3$)** δ 7.28 (t, J = 7.6 Hz, 1H), 7.35-7.38 (m, 2H), 7.42 (d, J = 7.2 Hz, 1H), 7.50 (t, J = 7.6 Hz, 3H), 7.60 (d, J = 6.8 Hz, 3H), 7.72 (d, J = 7.6 Hz, 1H), 7.76 (d, J = 8.4 Hz,

1H); **^{13}C NMR (100 MHz, $CDCl_3$)** δ 113.6, 116.2, 118.5, 120.4, 122.9, 124.5, 127.5, 127.8,

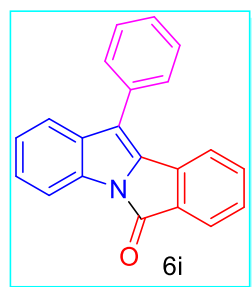
128.1, 128.5, 130.5, 131.3, 132.6, 132.8, 133.3, 134.1, 134.6, 161.3; **HRMS (ESI-TOF) m/z :** **$[M+H]^+$** Calcd for $C_{21}H_{12}BrNO$ 374.0181; Found 374.0171.

2-methoxy-11-methyl-6*H*-isoindolo[2,1-*a*]indol-6-one (6h)



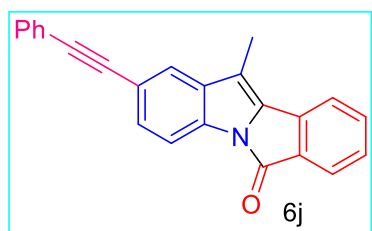
Prepared from **29g** (80.0 mg, 0.484 mmol, 1.0 equiv), and OPA (64.9 mg, 0.484 mmol, 1.0 equiv) following the procedure described for **6b**. Yield (54 mg, 0.202 mmol) as a yellow solid in 43% yield. mp 155 °C; **1H NMR (300 MHz, $CDCl_3$)** δ 2.43 (s, 3H), 3.88 (s, 3H), 6.88-6.91 (m, 2H), 7.32 (d, $J = 7.5$, 1H), 7.49 (d, $J = 7.5$ Hz, 1H), 7.55 (t, $J = 6.6$ Hz, 1H), 7.45-7.78 (m, 2H); **^{13}C NMR (75 MHz, $CDCl_3$)** δ 9.5, 55.8, 104.3, 113.80, 113.85, 115.2, 121.0, 125.2, 128.0, 128.2, 133.2, 134.1, 135.0, 135.5, 136.8, 156.7, 161.9; **HRMS (ESI-TOF) m/z :** **$[M+H]^+$** Calcd for $C_{17}H_{13}NO_2$ 264.1025; Found 264.1015.

11-phenyl-6*H*-isoindolo[2,1-*a*]indol-6-one (6i)

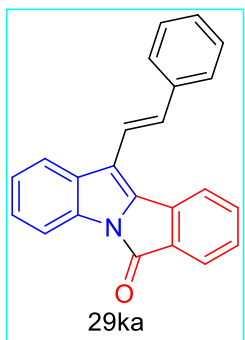


Prepared from **29h** (100.0 mg, 0.507 mmol, 1.0 equiv), and OPA (68.0 mg, 0.507 mmol, 1.0 equiv) following the procedure described for **6b**. Yield (61 mg, 0.208 mmol) as a yellow solid in 41 % yield. mp 174 °C; **1H NMR (300 MHz, $CDCl_3$)** δ 7.21 (t, $J = 7.5$ Hz, 1H), 7.36 (q, $J = 7.5$, 2H), 7.44 (t, $J = 7.5$ Hz, 1H), 7.50 (d, $J = 6.9$, 1H), 7.56-7.63 (m, 4H), 7.73 (d, $J = 8.1$ Hz, 2H), 7.82 (d, $J = 6.9$, 1H), 8.00 (d, $J = 8.1$, 1H); **^{13}C NMR (75 MHz, $CDCl_3$)** δ 112.4, 119.4, 120.13, 120.17, 122.9, 124.3, 125.7, 127.2, 127.7, 127.8, 127.9, 131.1, 132.5, 132.6, 132.7, 132.9, 133.1, 133.6, 161.5; **HRMS (ESI-TOF) m/z :** **$[M+H]^+$** Calcd for $C_{21}H_{13}NO$ 296.1075; Found 296.1075.

11-methyl-2-(phenylethynyl)-6*H*-isoindolo[2,1-*a*]indol-6-one (6j)

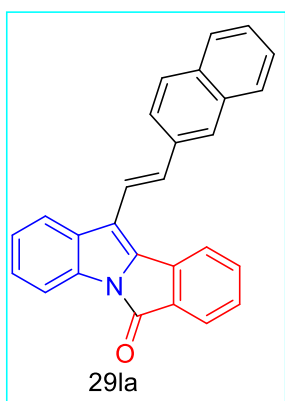


Prepared from **29i** (50.0 mg, 0.212 mmol, 1.0 equiv), and OPA (28.5 mg, 0.212 mmol, 1.0 equiv) following the procedure described for **6b**. Yield (34 mg, 0.104 mmol) as a yellow solid in 48% yield. mp 178 °C; **1H NMR (400 MHz, $CDCl_3$)** δ 2.48 (s, 3H), 7.34-7.38 (m, 4H), 7.50 (dd, $J = 6.4$ Hz, 1.6 Hz, 1H), 7.54-7.58 (m, 3H), 7.62 (d, $J = 6.8$ Hz, 2H), 7.80 (d, $J = 7.6$ Hz, 1H), 7.87 (d, $J = 8.0$ Hz, 1H); **^{13}C NMR (100 MHz, $CDCl_3$)** δ 8.4, 87.6, 88.7, 112.2, 113.0, 113.9, 115.8, 117.4, 120.3, 122.3, 122.5, 124.4, 127.1, 127.3, 129.0, 130.5, 132.6, 133.9, 134.8, 161.1; **HRMS (ESI-TOF) m/z :** **$[M+H]^+$** Calcd for $C_{24}H_{15}NO$ 334.1232; Found 334.1225.

(E)-11-styryl-6H-isoindolo[2,1-a]indol-6-one (29ka)

The mixture of chalcone **29k** (100 mg, 1.0 equiv), **26** (53.1 mg, 0.365 mmol, 1.0 equiv) and anhydrous Pd(OAc)₂ (0.2 equiv) in acetic acid (3.0 mL) were taken under nitrogen atmosphere in a round bottom flask. The reaction mixture was stirred at 130 °C for 16 h. After completion of the reaction, the reaction mixture was quenched with NaHCO₃ and water, extracted with ethyl acetate (3 × 15.0 mL) and dried over anhydrous Na₂SO₄. The solvent was removed under reduced pressure and the crude product was purified by column chromatography on silica gel (100–200 mesh) using 2% ethyl acetate in petroleum ether to afford the pure product **29ka** as a light yellowish green fluorescent solid in 68% yield.

¹H NMR (300 MHz, CDCl₃) δ 7.18 (m, 1H) (superimposed with CDCl₃), 7.24–7.31 (m, 3H), 7.33–7.38 (m, 4H), 7.45–7.54 (m, 3H), 7.67 (d, J = 7.8 Hz, 1H), 7.74 (dd, J = 7.5 Hz, 3 Hz, 2H), 7.89 (d, J = 8.1 Hz, 1H); **¹³C NMR (75 MHz, CDCl₃)** δ 100.0, 113.6, 117.6, 119.0, 121.8, 121.9, 124.1, 125.5, 126.5, 126.9, 128.3, 128.6, 128.9, 132.8, 132.9, 133.6, 134.1, 134.4, 135.4, 137.1, 162.3; **HRMS (ESI-TOF) m/z : [M+H]⁺** Calcd for C₂₃H₁₅NO 322.1232; Found 322.1234.

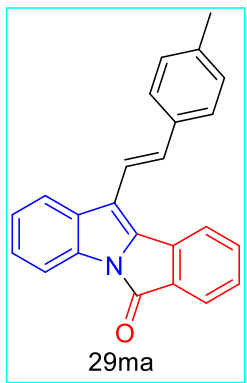
(E)-11-(2-(naphthalen-2-yl)vinyl)-6H-isoindolo[2,1-a]indol-6-one (29la)

The compound **29la** was prepared according to the above mentioned general procedure B was followed when compound **29l** (60.0 mg, 0.219 mmol, 1.0 equiv) was reacted with OPA **26** (58 mg, 1.0 equiv) and anhydrous Pd(OAc)₂ (0.2 equiv) in acetic acid (3.0 mL) were taken under nitrogen atmosphere in a round bottom flask. The reaction mixture was stirred at 130 °C for 16 h, the crude product was purified by column chromatography on silica gel (100–200 mesh) using 2% ethyl acetate in petroleum ether to afford the pure product **29la** as a yellow fluorescent solid in 52% yield.

¹H NMR (400 MHz, CDCl₃) δ 7.27–7.31 (m, 1H) (superimposed with CDCl₃), 7.37–7.41 (m, 2H), 7.49–7.54 (m, 2H), 7.56–7.62 (m, 3H), 7.80–7.85 (m, 3H), 7.86–7.92 (m, 4H), 7.95 (s, 1H), 7.99 (d, J = 6.0 Hz, 1H); **¹³C NMR (100 MHz, CDCl₃)** δ 113.6, 117.7, 119.2, 121.9, 122.0, 123.0, 124.2, 125.6, 126.3, 126.6, 126.9, 127.0, 127.8, 128.1, 128.6, 132.8, 133.0, 133.3, 133.7,

134.1, 134.4, 134.5, 135.5, 162.3; **HRMS (ESI-TOF) m/z :** $[M+H]^+$ Calcd for $C_{27}H_{17}NO$ 372.1388; Found 372.1375.

(E)-11-(4-methylstyryl)-6H-isoindolo[2,1-a]indol-6-one (29ma)

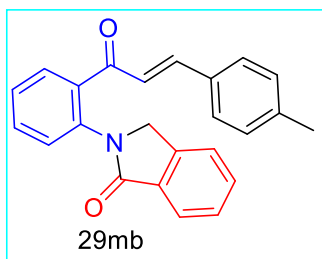


The compound **29ma** was prepared according to the above mentioned general procedure B was followed when compound **29m** (100 mg, 1.0 equiv), OPA **26** (54 mg, 1.0 equiv) and anhydrous $Pd(OAc)_2$ (0.2 equiv) in acetic acid (3.0 mL) were taken under nitrogen atmosphere in a round bottom flask. The reaction mixture was stirred at 130 °C for 16 h. The crude product was purified by column chromatography on silica gel (100–200 mesh) using 2% ethyl acetate in petroleum

ether to afford the pure product **29ma** as a light yellowish green fluorescent solid in 51% yield along with **29mb**.

1H NMR (300 MHz, $CDCl_3$) δ 2.33 (s, 3H), 7.13–7.18 (m, 3H) (superimposed with $CDCl_3$), 7.24–7.29 (m, 4H), 7.40–7.49 (m, 3H), 7.64 (d, $J = 7.8$ Hz, 1H), 7.70–7.74 (m, 2H), 7.87 (d, $J = 7.5$ Hz, 1H); **^{13}C NMR (75 MHz, $CDCl_3$)** δ 21.3, 100.0, 113.6, 117.92, 117.99, 121.8, 122.0, 124.1, 125.5, 126.4, 126.9, 128.5, 129.6, 132.92, 132.97, 133.62, 133.67, 134.14, 134.36, 134.50, 135.1, 138.3, 162.3; **HRMS (ESI-TOF) m/z :** $[M+H]^+$ Calcd for $C_{24}H_{17}NO$ 336.1388; Found 335.2593.

(E)-2-(2-(3-(p-tolyl)acryloyl)phenyl)isoindolin-1-one (29mb)

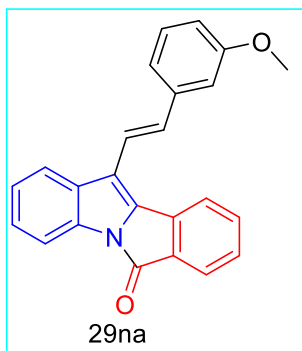


Yellowish brown solid, yield 38% **1H NMR (400 MHz, $CDCl_3$)** δ 2.26 (s, 3H), 4.74 (s, 2H), 6.92 (d, $J = 16.0$ Hz, 1H), 7.03 (d, $J = 8.0$ Hz, 2H), 7.27 (d, $J = 8.4$ Hz, 2H), 7.34–7.39 (m, 4H), 7.45–7.54 (m, 3H), 7.58 (dd, $J = 7.6$ Hz, 2.0 Hz, 1H), 7.77 (d, $J = 7.6$ Hz, 1H); **^{13}C NMR (100 MHz, $CDCl_3$)** δ 20.4, 52.6, 121.7, 123.2,

123.3, 126.4, 126.7, 127.1, 127.5, 128.2, 128.5, 130.6, 130.8, 130.9, 131.0, 135.3, 136.8, 140.0, 140.4, 145.4, 167.2, 192.9; **HRMS (ESI-TOF) m/z :** $[M+Na]^+$ Calcd for $C_{24}H_{19}NO_2$ 376.1616; Found 376.1302.

(E)-11-(4-methoxystyryl)-6H-isoindolo[2,1-a]indol-6-one (29na)

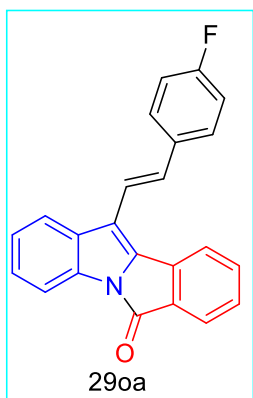
The compound **29na** was prepared according to the above mentioned general procedure B was followed when compound **29n** (100 mg, 1.0 equiv), **26** (55.5 mg, 1.0 equiv) and anhydrous $Pd(OAc)_2$ (0.2 equiv) in acetic acid (3.0 mL) were taken under nitrogen atmosphere in a round bottom flask. The reaction mixture was stirred at 130 °C for 16 h. The crude product was



purified by column chromatography on silica gel (100–200 mesh) using 2% ethyl acetate in petroleum ether to afford the pure product **29na** as a light yellowish green fluorescent solid in 62% yield along with compound **29nb**.

¹H NMR (300 MHz, CDCl₃) δ 3.82 (s, 3H), 6.82 (dd, J = 7.2 Hz, 2.1 Hz, 1H), 7.04 (t, J = 1.8 Hz, 1H), 7.12 (d, J = 7.5 Hz, 1H), 7.17–7.20 (m, J = 1H) (merged with CHCl₃), 7.25–7.31 (m, 5H), 7.47 (dt, J = 7.2 Hz, 1.2 Hz, 1H), 7.65 (d, J = 7.5 Hz, 1H), 7.73 (d, J = 8.4 Hz, 2H), 7.88 (d, J = 7.5 Hz, 1H); **¹³C NMR (100 MHz, CDCl₃)** δ 54.3, 111.1, 112.6, 113.0, 116.5, 118.2, 118.3, 120.8, 120.9, 123.1, 124.5, 125.9, 127.6, 128.8, 131.8, 132.6, 132.7, 133.1, 133.4, 134.5, 137.6, 138.2, 159.0, 161.3; **HRMS (ESI-TOF) m/z : [M+H]⁺** Calcd for C₂₄H₁₇NO₂ 352.1338; Found 353.1335.

(*E*)-11-(4-fluorostyryl)-6H-isoindolo[2,1-a]indol-6-one (29oa)

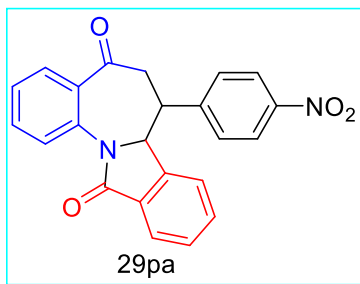


The compound **29oa** was prepared according to the above mentioned general procedure B was followed when compound **29o** (100 mg, 1.0 equiv), **26** (62 mg, 1.0 equiv) and anhydrous Pd(OAc)₂ (0.2 equiv) in acetic acid (3.0 mL) were taken under nitrogen atmosphere in a round bottom flask. The reaction mixture was stirred at 130 °C for 16 h. The crude product was purified by column chromatography on silica gel (100–200 mesh) using 2% ethyl acetate in petroleum ether to afford the pure product **29oa** as a light yellowish green fluorescent solid in 75%

yield

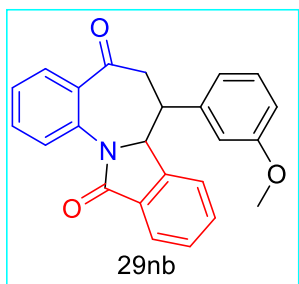
¹H NMR (400 MHz, CCl₄ + CDCl₃) δ 7.13 (t, J = 8.4 Hz, 2H), 7.21–7.27 (m, 1H) (merged with CDCl₃), 7.34–7.40 (m, 4H), 7.54–7.59 (m, 3H), 7.73 (d, J = 7.6 Hz, 1H), 7.81 (dd, J = 13.0 Hz, 8 Hz, 2H), 7.98 (d, J = 8.0 Hz, 1H); **¹³C NMR (100 MHz, CDCl₃ + CCl₄)** δ 113.7, 115.8, 116.0, 117.3, 118.82, 118.84, 121.73, 121.84, 124.1, 125.6, 126.9, 128.0, 128.08, 128.59, 131.6, 132.7, 133.36, 133.56, 133.77, 134.13, 134.48, 135.4; **HRMS (ESI-TOF) m/z : [M+H]⁺** Calcd for C₂₃H₁₄FN O 340.1138; Found 340.1133.

7-(4-nitrophenyl)-7,7a-dihydro-5H-benzo[6,7]azepino[2,1-a]isoindole-5,12(6H)-dione (29pa)



The compound **29pa** was prepared according to the above mentioned general procedure B was followed when compound **29p** (100 mg, 1.0 equiv), OPA **26** (62 mg, 2.0 equiv) and anhydrous Pd(OAc)₂ (0.2 equiv) in acetic acid (3.0 mL) were taken under nitrogen atmosphere in a round bottom flask. The reaction mixture was stirred at 130 °C for 16 h. The crude product was purified by column chromatography on silica gel (100–200 mesh) using 15–20% ethyl acetate in petroleum ether to afford the pure product **29pa** as a light yellowish green fluorescent solid in 52% yield. **¹H NMR (400 MHz, CDCl₃)** δ 2.86–2.98 (m, 2H), 3.99–4.04 (m, 1H), 5.17 (d, *J* = 6.8 Hz, 1H), 6.22 (d, *J* = 7.6 Hz, 1H), 7.16–7.19 (m, 2H) (with CDCl₃), 7.26 (t, *J* = 7.2 Hz, 1H), 7.36 (t, *J* = 7.6 Hz, 1H), 7.43 (t, *J* = 7.6 Hz, 1H), 7.65 (t, *J* = 8.0 Hz, 1H), 7.76–7.80 (m, 2H), 7.92 (d, *J* = 7.6 Hz, 1H), 8.06 (d, *J* = 8.8 Hz, 1H); **¹³C NMR (100 MHz, CDCl₃)** δ 42.7, 42.9, 64.1, 122.7, 122.9, 123.4, 126.3, 126.4, 127.1, 128.2, 128.4, 129.3, 131.0, 131.7, 132.0, 133.2, 136.9, 139.7, 144.6, 146.3, 167.6, 197.50, 197.52; **HRMS (ESI-TOF) *m/z*: [M+H]⁺** Calcd for C₂₃H₁₇N₂O₄ 385.1188; Found 385.1180.

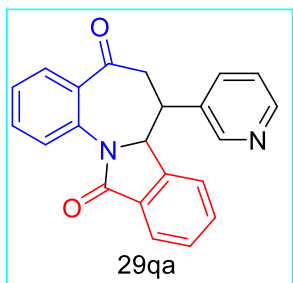
7-(4-methoxyphenyl)-7,7a-dihydro-5H-benzo[6,7]azepino[2,1-a]isoindole-5,12(6H)-dione (29nb)



The compound **29nb** was prepared according to the above mentioned general procedure B was followed when compound **29n** (100 mg, 1.0 equiv), OPA **26** (55 mg, 2.0 equiv) and anhydrous Pd(OAc)₂ (0.2 equiv) in acetic acid (3.0 mL) were taken under nitrogen atmosphere in a round bottom flask. The reaction mixture was stirred at 130 °C for 16 h. The crude product was purified by column chromatography on silica gel (100–200 mesh) using 15% ethyl acetate in petroleum ether to afford the pure product **29nb** as a Brown solid, yield 74%. **¹H NMR (400 MHz, CDCl₃)** δ 2.70 (dd, *J* = 16.4 Hz, 11.6 Hz, 1H), 2.91 (d, *J* = 16.0 Hz, 1H), 3.67 (s, 3H), 3.85–3.90 (m, 1H), 5.10 (d, *J* = 6.8 Hz, 1H), 6.05 (d, *J* = 7.6 Hz, 1H), 6.53 (s, 1H), 6.58 (d, *J* = 7.2 Hz, 1H), 6.77 (d, *J* = 8.0 Hz, 1H), 7.13–7.23 (m, 2H), 7.34 (t, *J* = 7.2 Hz, 1H), 4.45 (t, *J* = 7.6 Hz, 1H), 7.61–7.67 (m, 2H), 7.79 (d, *J* = 7.6 Hz, 1H), 7.93 (d, *J* = 8.0 Hz, 1H); **NMR (100 MHz, CDCl₃)** δ 42.8, 43.1, 55.2, 65.4, 113.2, 114.2, 120.8, 123.8, 124.9, 128.3, 128.4, 128.7,

129.6, 130.3, 131.5, 133.0, 133.7, 134.1, 137.7, 139.7, 141.1, 159.7, 168.7, 199.3; **HRMS (ESI-TOF) m/z : $[M+Na]^+$** Calcd for C₂₄H₁₉NO₃ 392.1263; Found 392.2426.

7-(pyridin-3-yl)-7,7a-dihydro-5H-benzo[6,7]azepino[2,1-*a*]isoindole-5,12(6H)-dione (29qa)



The compound **29qa** was prepared according to the above mentioned general procedure B was followed when compound **29q** (100 mg, 1.0 equiv), OPA **26** (68 mg, 2.0 equiv) and anhydrous Pd(OAc)₂ (0.2 equiv) in acetic acid (3.0 mL) were taken under nitrogen atmosphere in a round bottom flask. The reaction mixture was stirred at 130 °C for 16 h. The crude product was purified by column chromatography on silica gel (100–200 mesh) using 20% ethyl acetate in petroleum ether to afford the pure product **29qa** as a pale yellowish brown solid, yield 33%. **¹H NMR (300 MHz, CDCl₃)** δ 2.89-2.92 (m, 1H), 3.90-3.97 (m, 1H), 5.15 (d, J = 6.6 Hz, 1H), 6.27 (d, J = 7.5 Hz, 1H), 7.13-7.17 (m, 1H), 7.25-7.30 (m, 2H), 7.32-7.37 (m, 1H), 7.43 (dt, J = 1.5 Hz, 7.8 Hz, 1H), 7.64 (dt, J = 1.8 Hz, 8.1 Hz, 1H), 7.75-7.79 (m, 2H), 7.92 (dd, J = 1.5 Hz, 6.8 Hz, 1H); **¹³C NMR (100 MHz, CDCl₃)** δ 41.5, 44.0, 65.4, 123.4, 124.1, 124.3, 127.3, 128.0, 129.0, 130.3, 132.1, 132.8, 133.1, 133.9, 134.1, 135.7, 138.0, 141.1, 149.0, 149.9, 168.6, 198.8; **HRMS (ESI-TOF) m/z : $[M+H]^+$** Calcd for C₂₂H₁₆N₂O₂ 341.1290; Found 341.1285.

Copy of NMR and other Analytical Spectra

Chapter 1

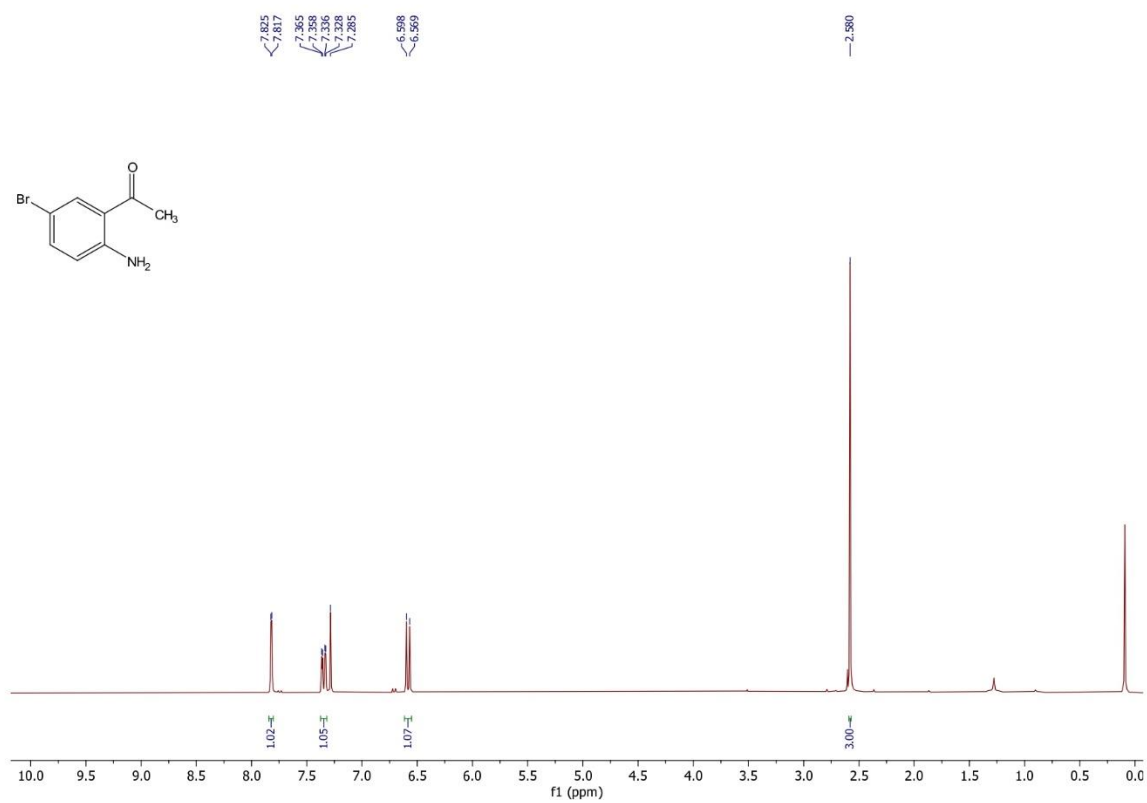


Figure 1.14 ¹H NMR spectrum of **29b** (300 MHz, CDCl₃)

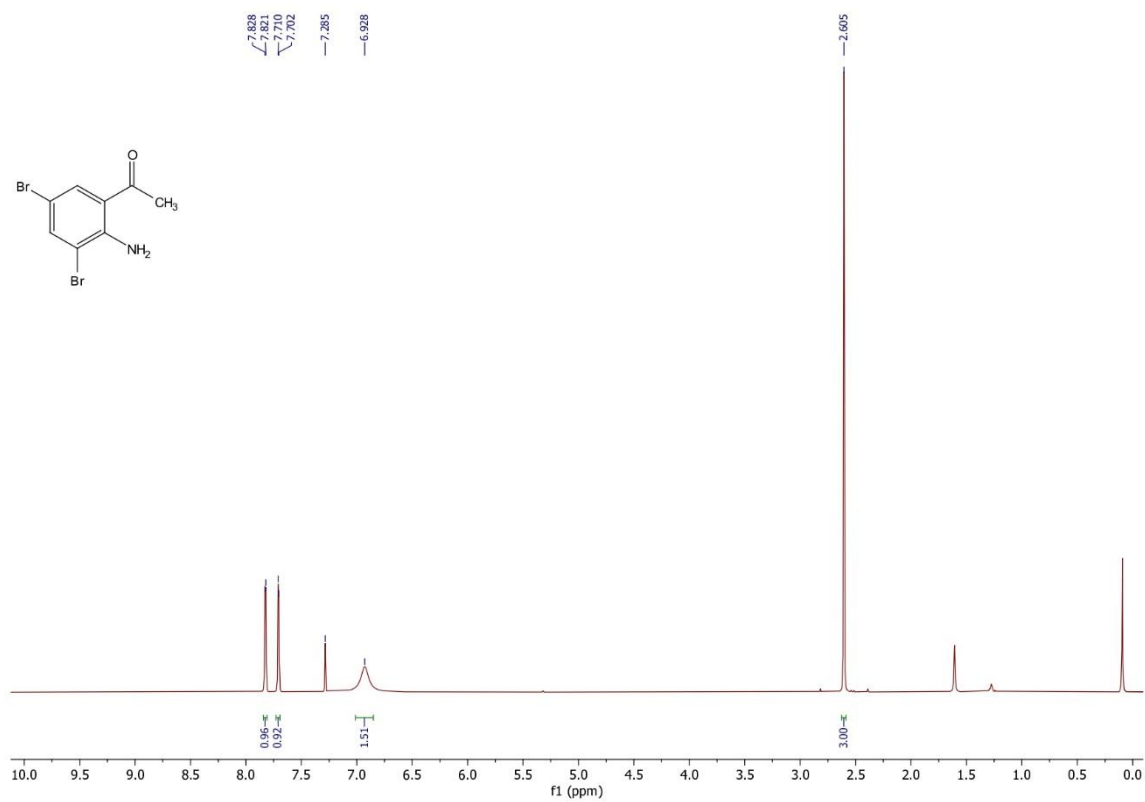


Figure 1.15 ¹H NMR spectrum of **29c** (300 MHz, CDCl₃)

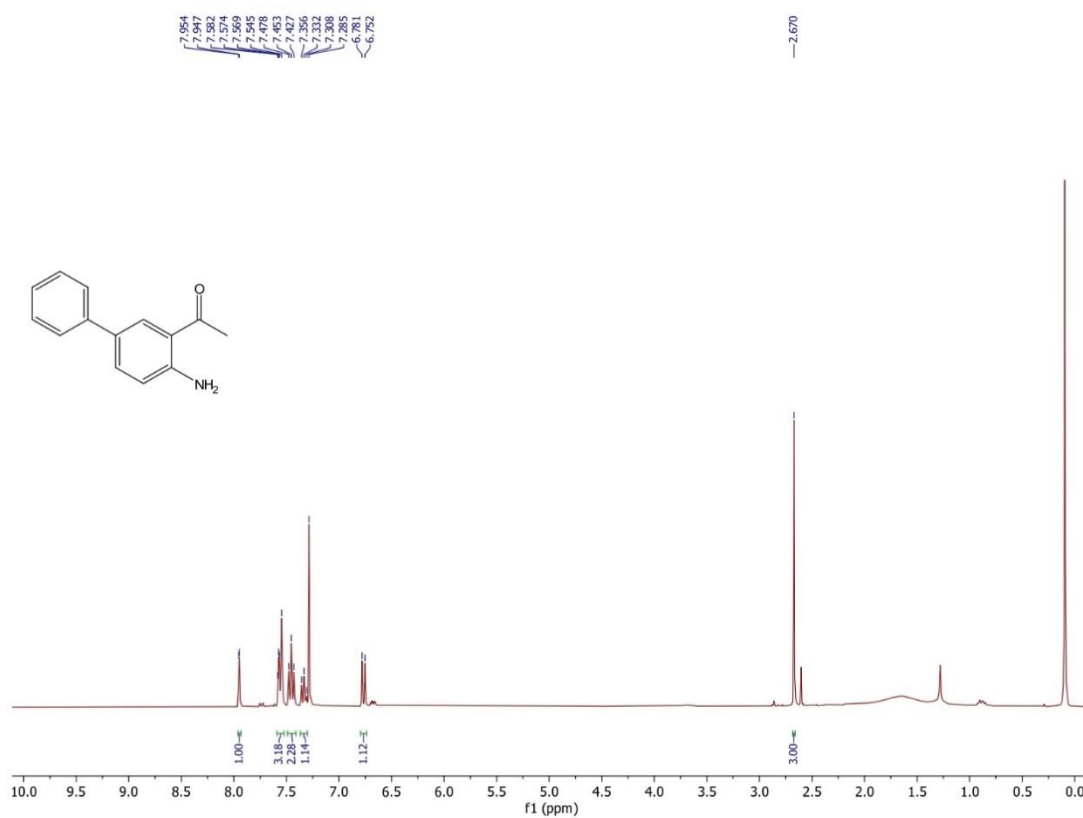


Figure 1.16 ¹H NMR spectrum of **29d** (300 MHz, CDCl₃)

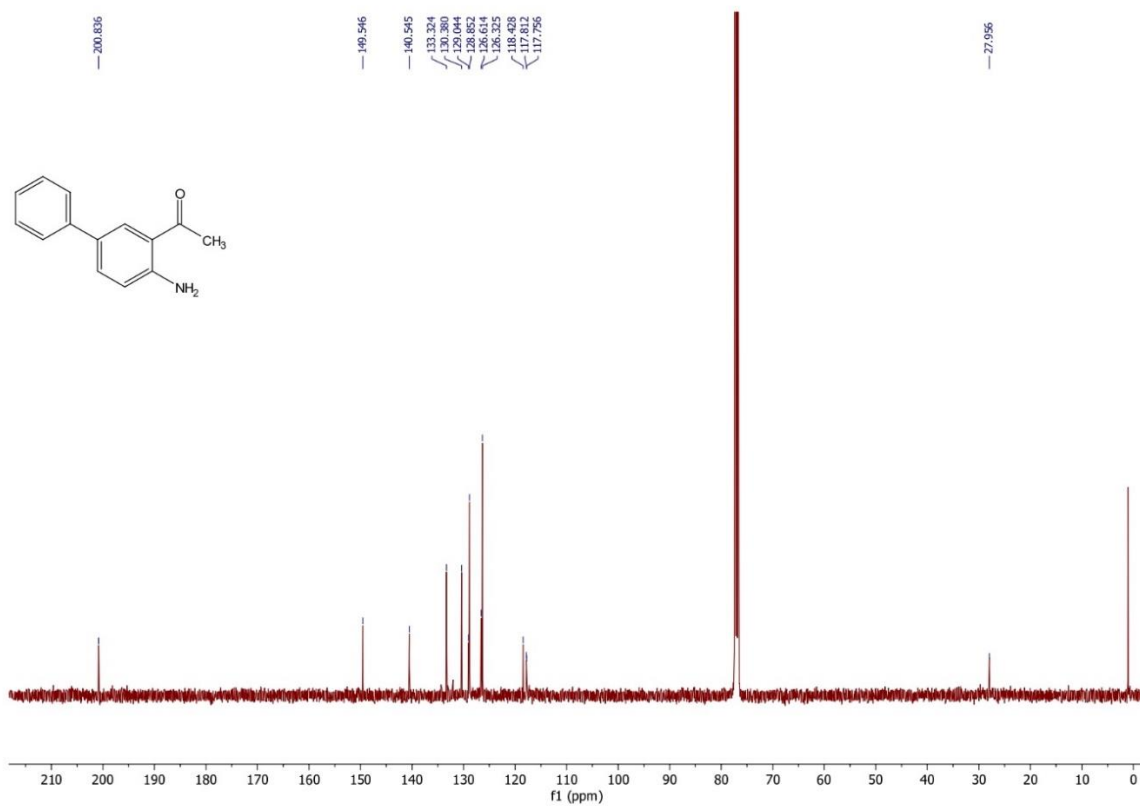


Figure 1.17 ¹³C NMR spectrum of **29d** (75 MHz, CDCl₃)

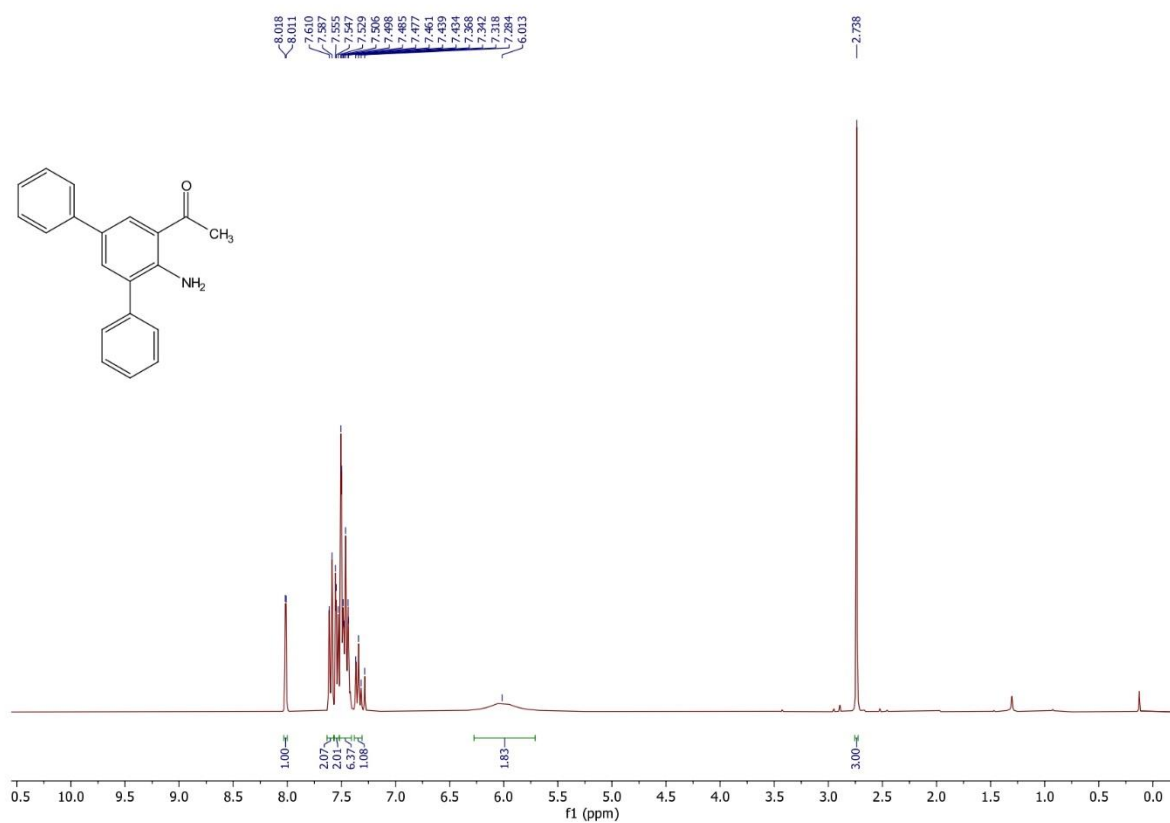


Figure 1.18 ¹H NMR spectrum of **29e** (300 MHz, CDCl₃)

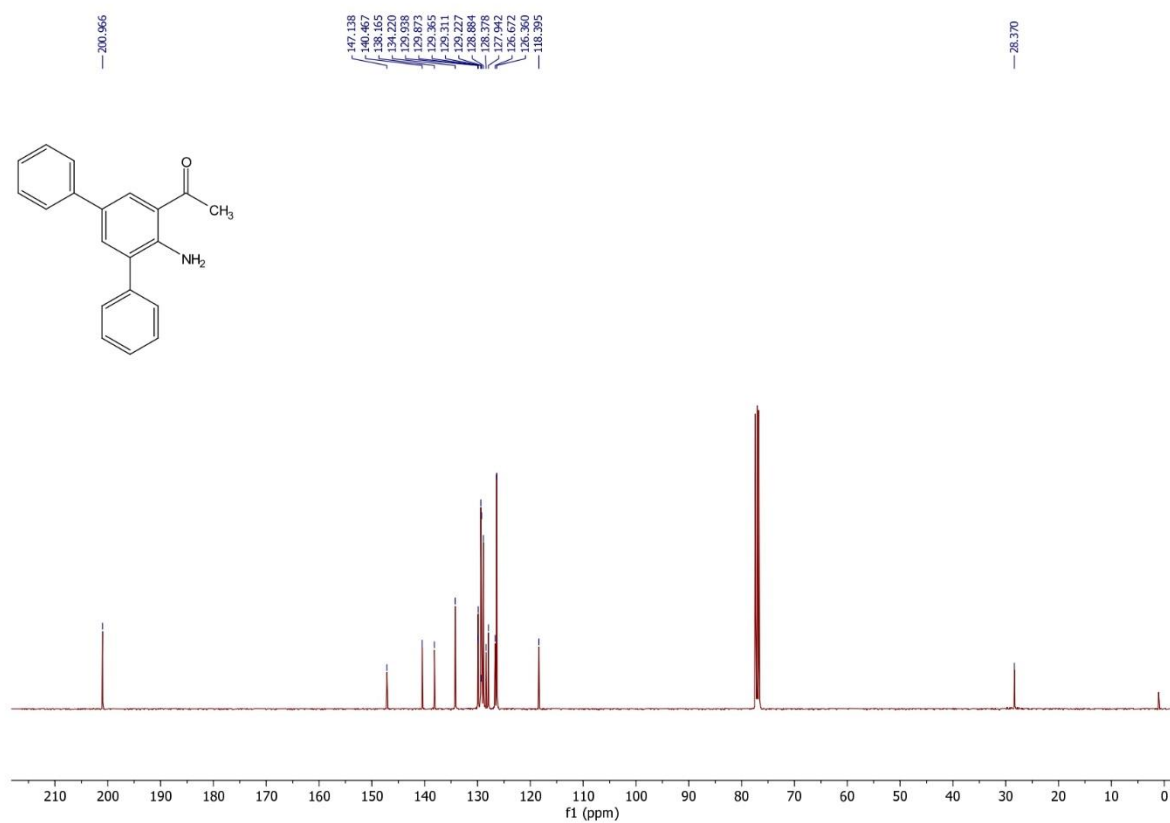


Figure 1.19 ¹³C NMR spectrum of **29e** (75 MHz, CDCl₃)

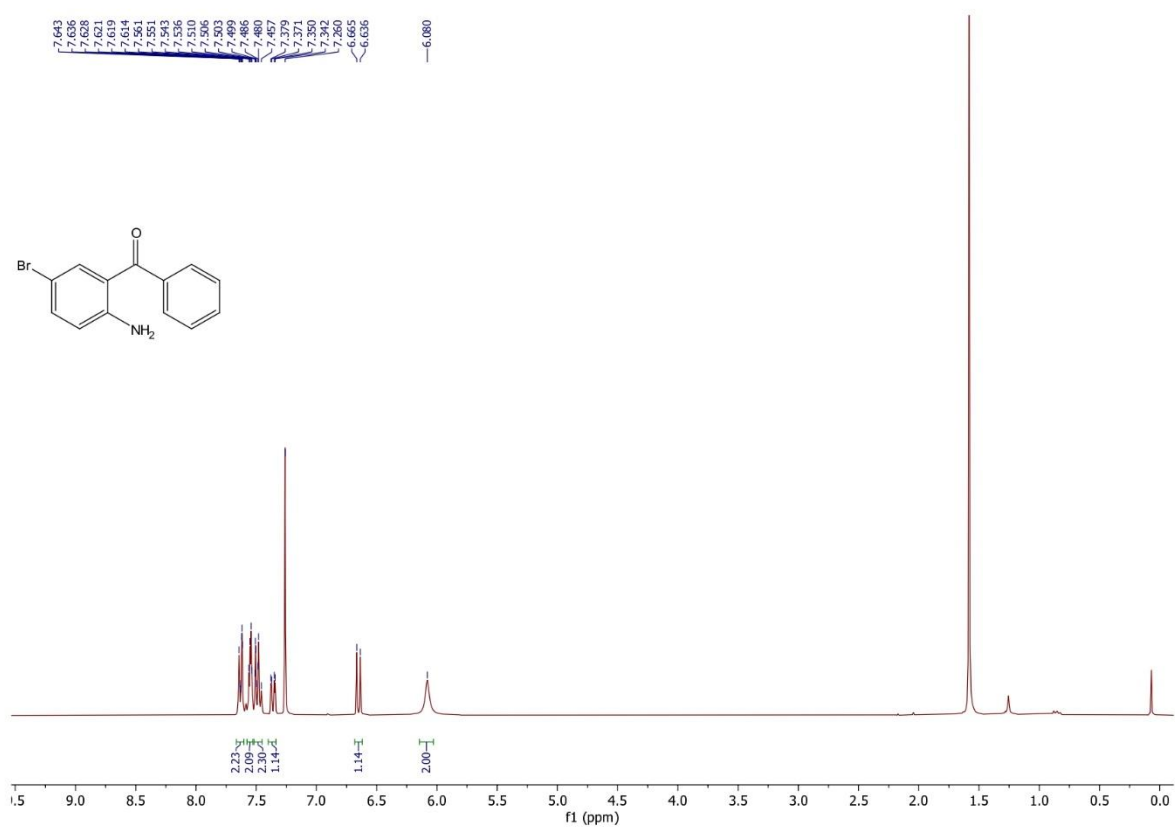


Figure 1.20 ¹H NMR spectrum of **29f** (300 MHz, CDCl₃)

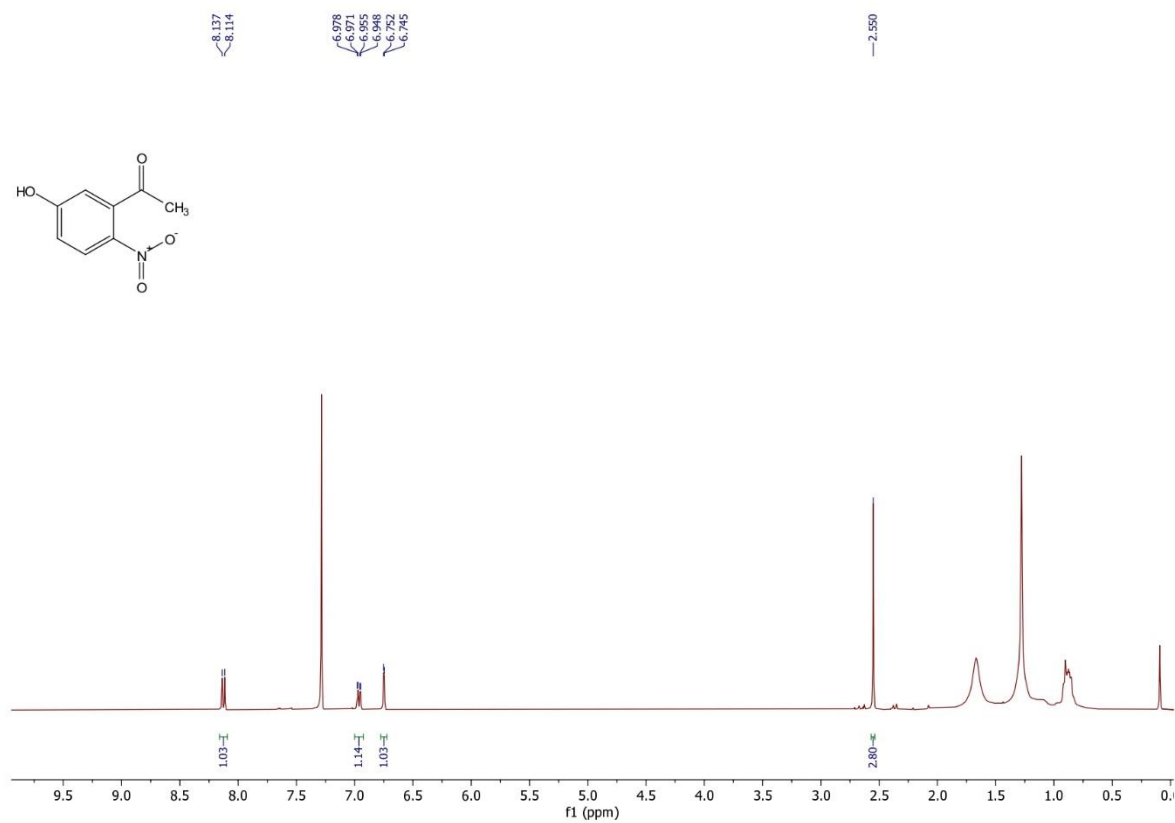


Figure 1.21 ¹H NMR spectrum of **35** (300 MHz, CDCl₃)

Chapter 1

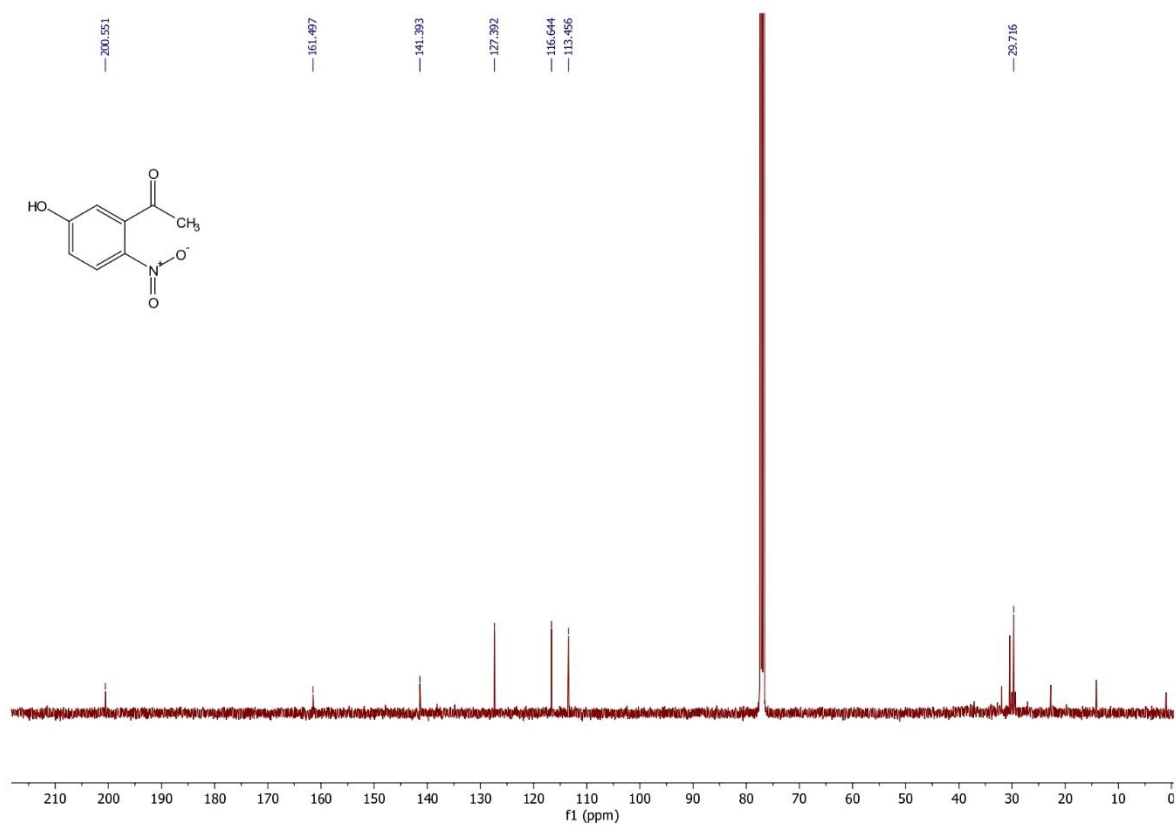


Figure 1.22 ¹³C NMR spectrum of **35** (75 MHz, CDCl₃)

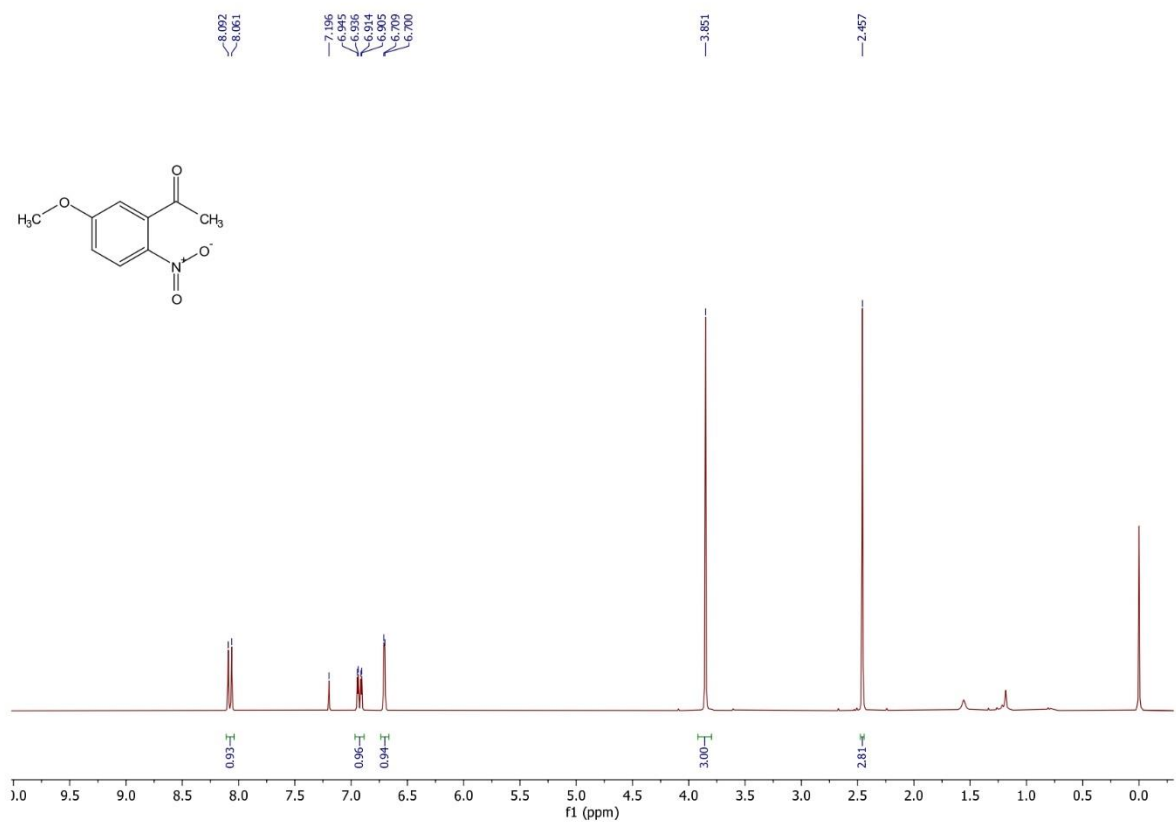


Figure 1.23 ¹H NMR spectrum of **3-Methoxy 5-nitroacetophenone 36** (300 MHz, CDCl₃)

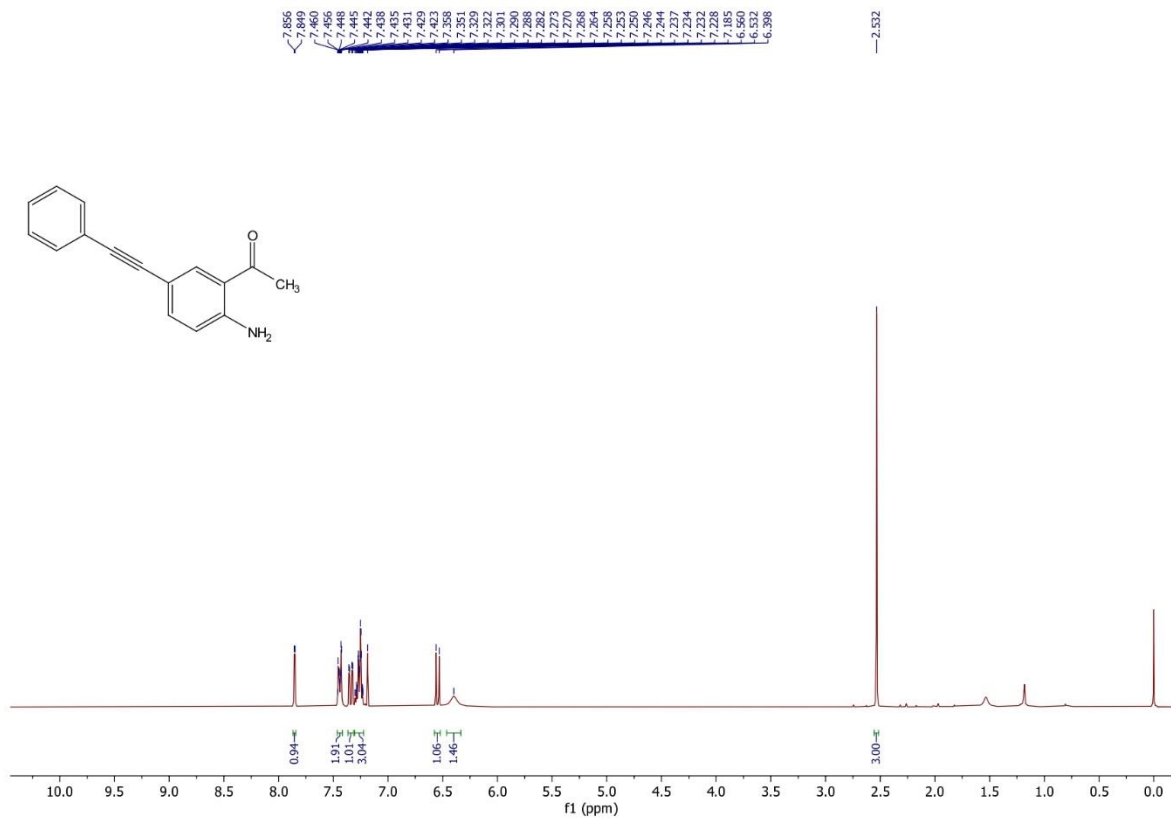


Figure 1.24 ^1H NMR spectrum of **29i** (300 MHz, CDCl_3)

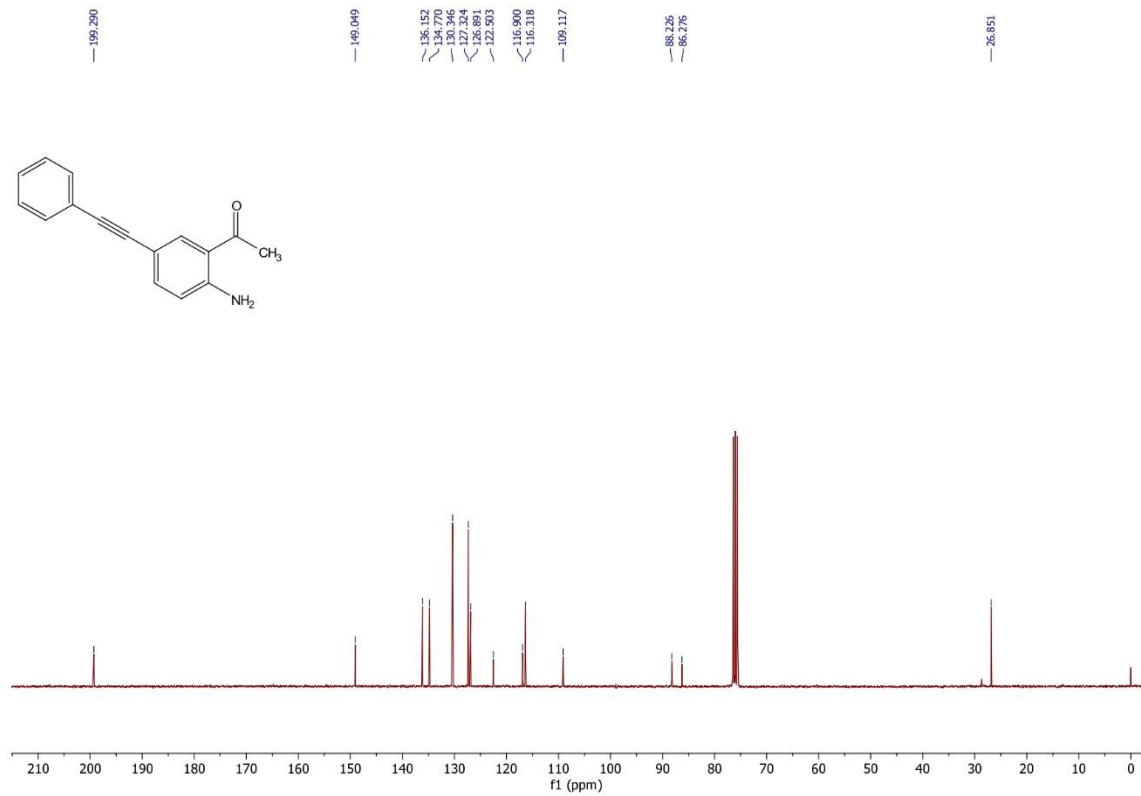


Figure 1.25 ^{13}C NMR spectrum of **29i** (75 MHz, CDCl_3)

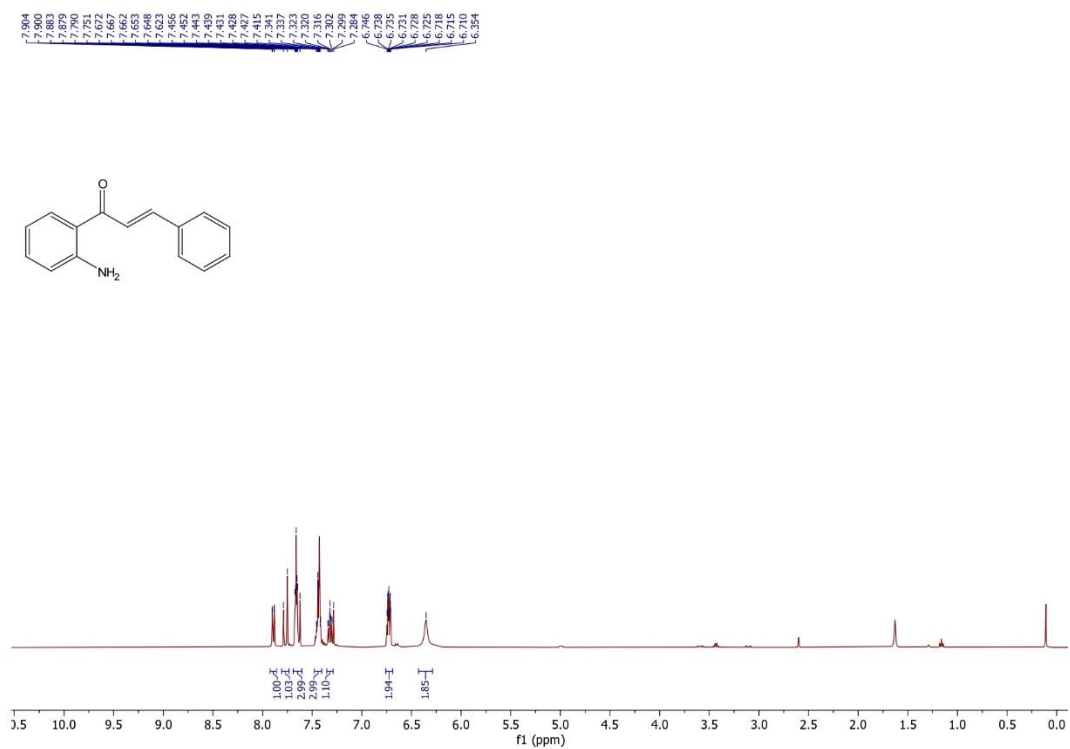


Figure 1.26 ¹H NMR spectrum of **29k** (400 MHz, CDCl₃)

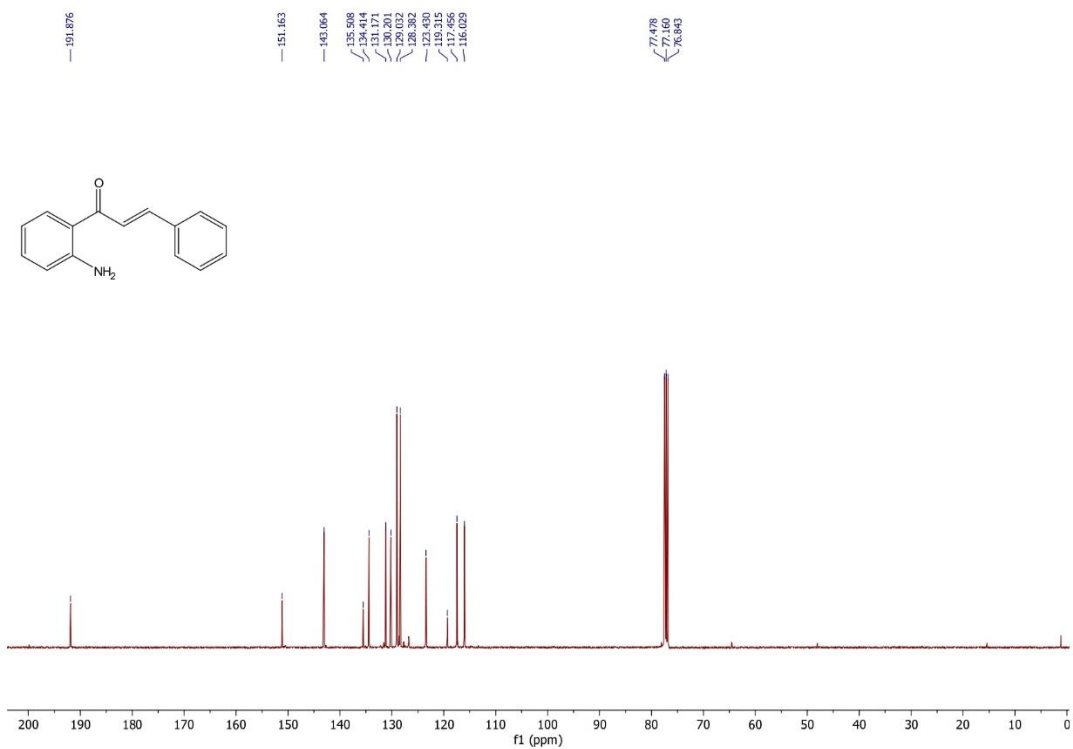


Figure 1.27 ¹³C NMR spectrum of **29k** (100 MHz, CDCl₃)

Chapter 1

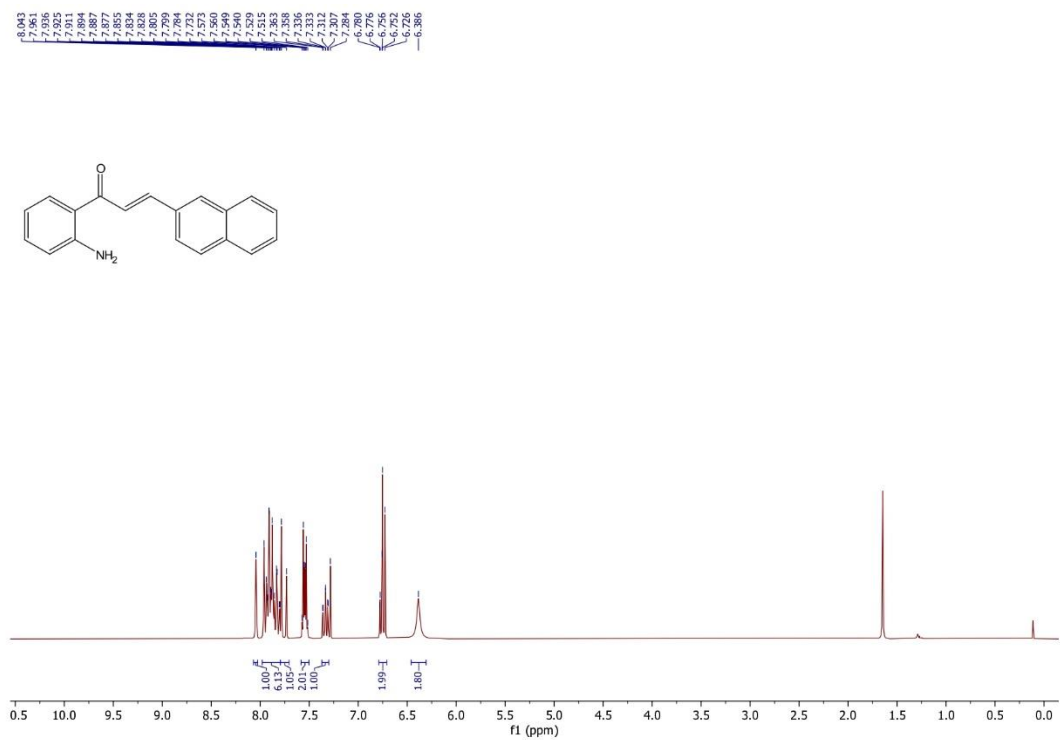


Figure 1.28 ¹H NMR spectrum of **29I** (300 MHz, CDCl₃)

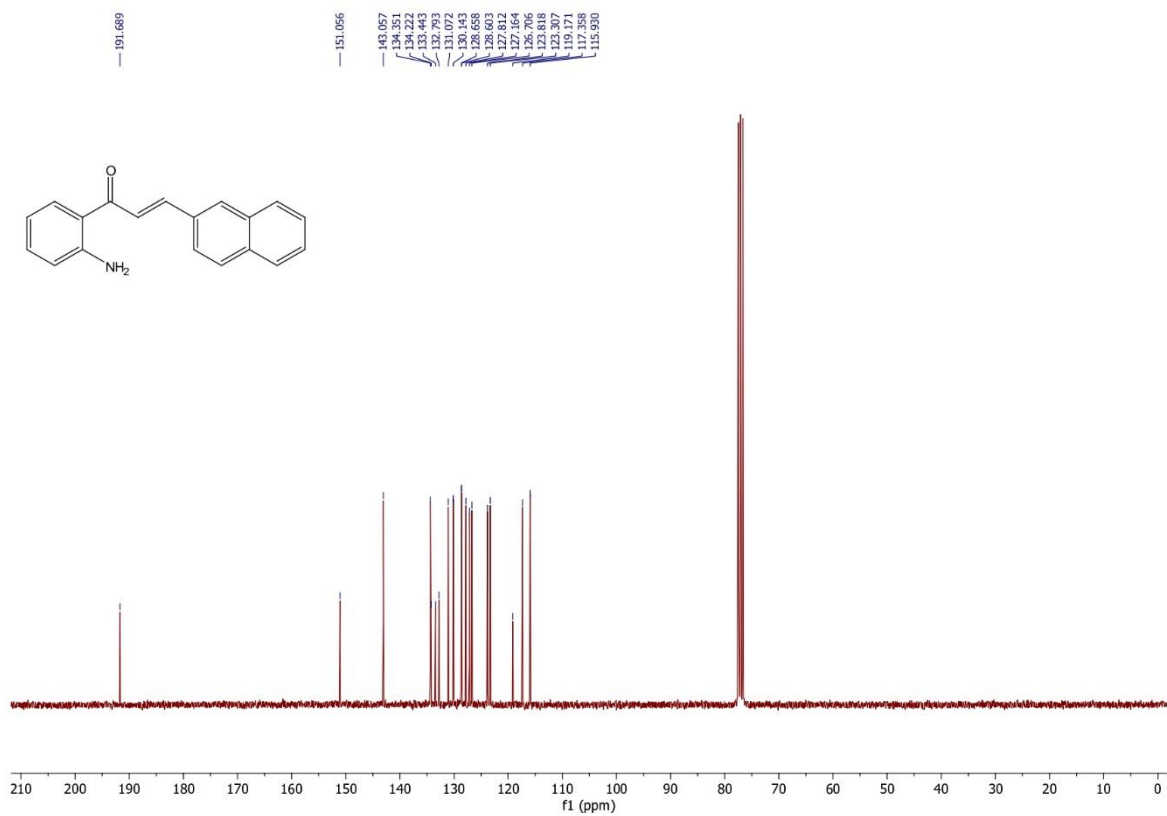


Figure 1.29 ¹³C NMR spectrum of **29I** (75 MHz, CDCl₃)

Chapter 1

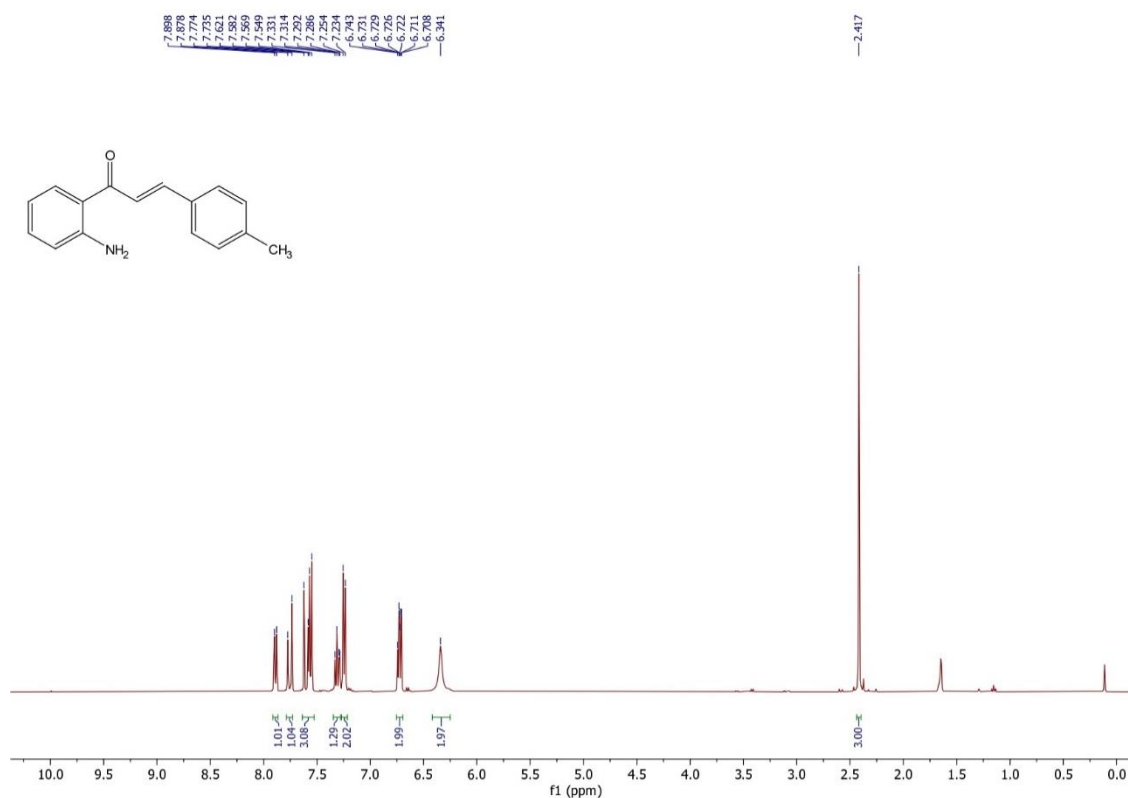


Figure 1.30 ¹H NMR spectrum of **29m** (400 MHz, CDCl₃)

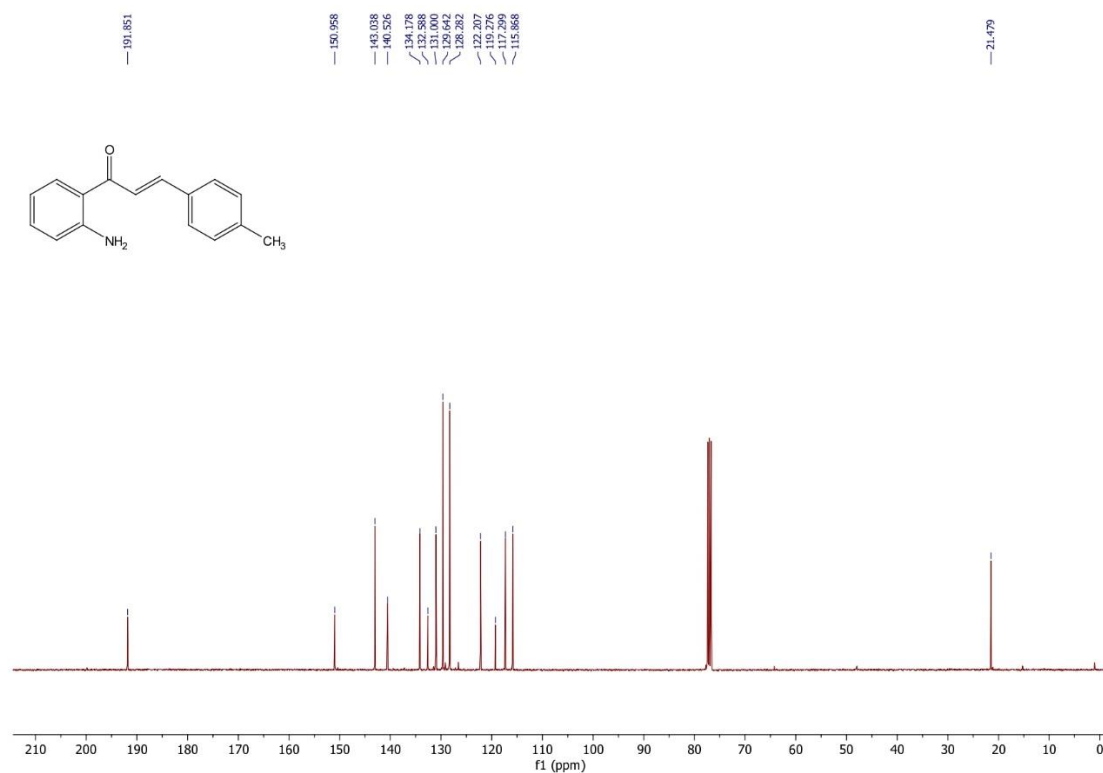


Figure 1.31 ¹³C NMR spectrum of **29m** (100 MHz, CDCl₃)

Chapter 1

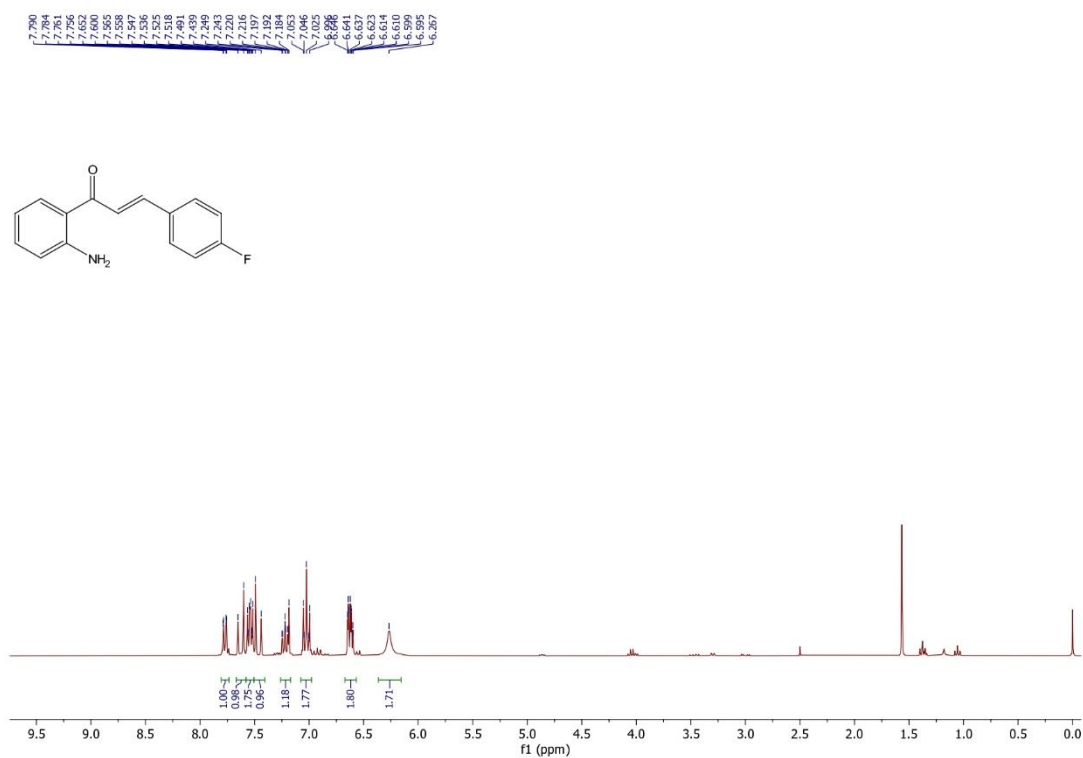


Figure 1.34 ¹H NMR spectrum of **29o** (400 MHz, CDCl₃)

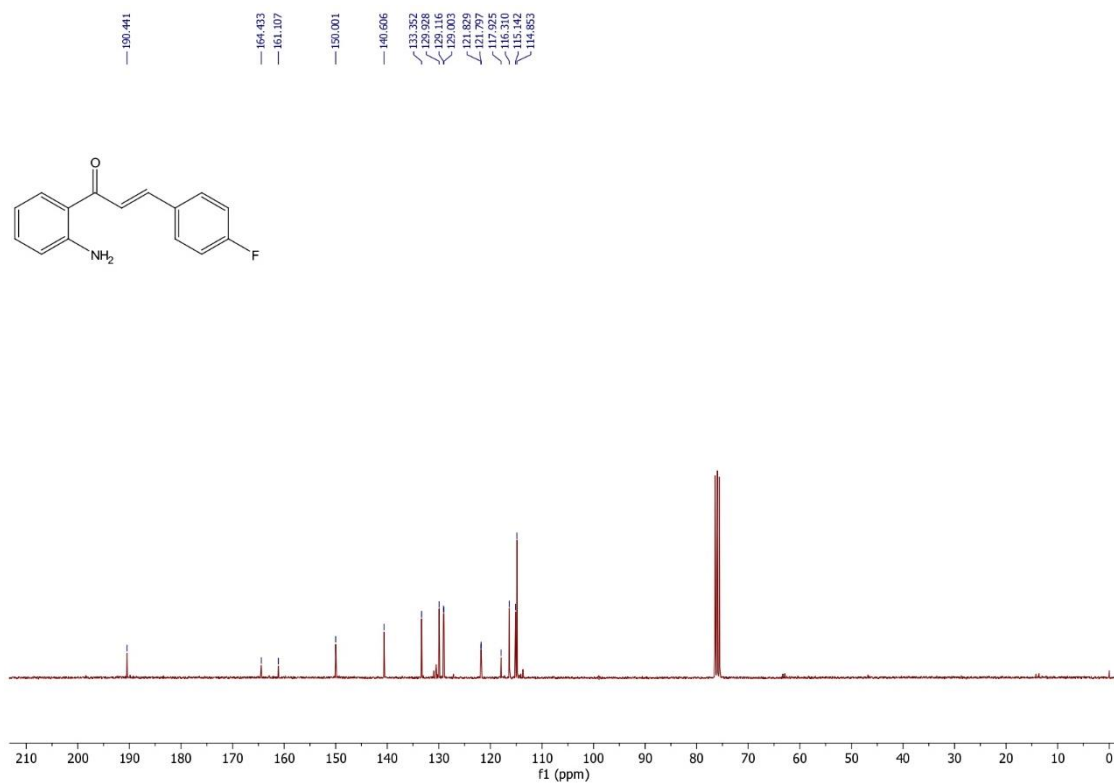


Figure 1.35 ¹³C NMR spectrum of **29o** (100 MHz, CDCl₃)

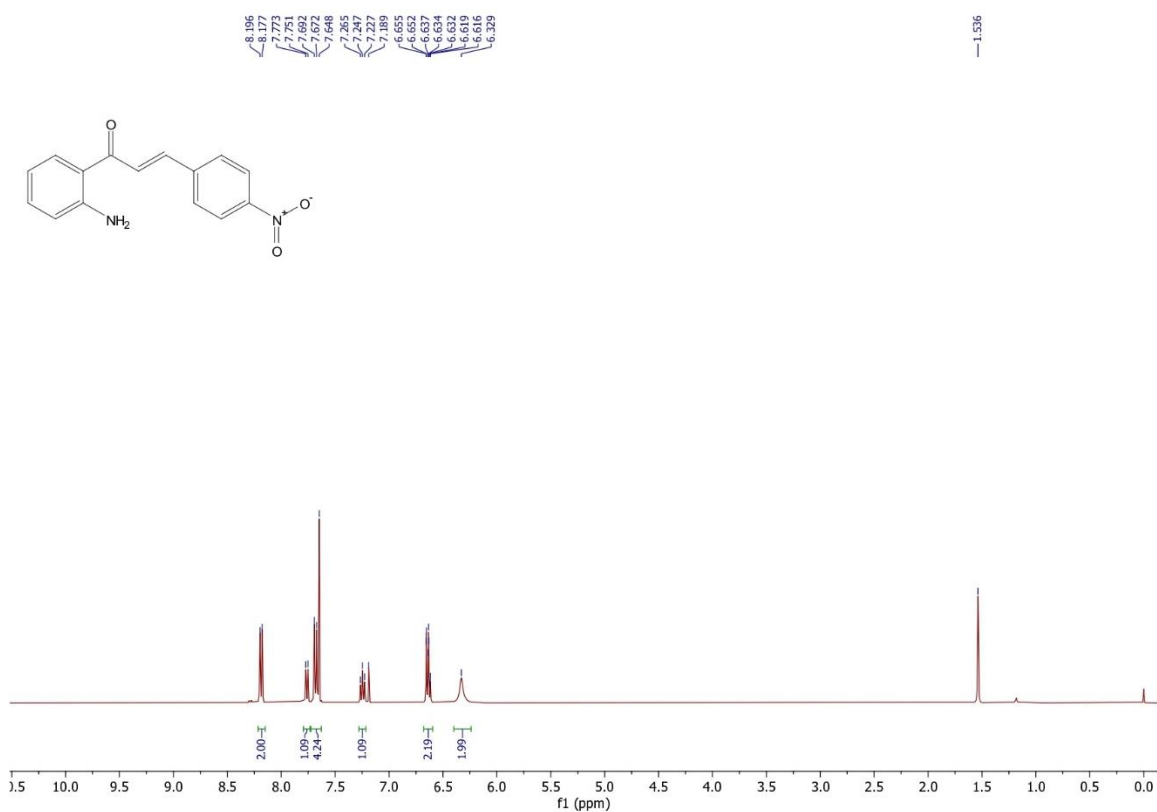


Figure 1.36 ¹H NMR spectrum of **29p** (400 MHz, CDCl₃)

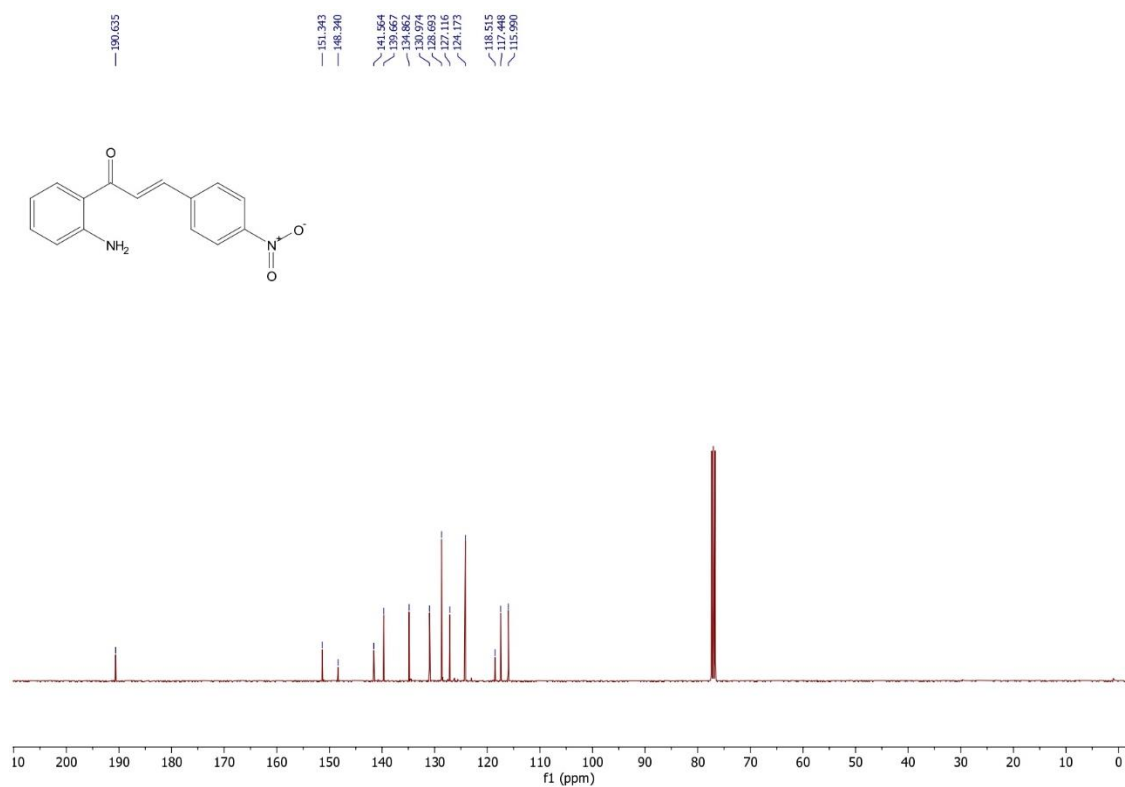


Figure 1.37 ¹³C NMR spectrum of **29p** (100 MHz, CDCl₃)

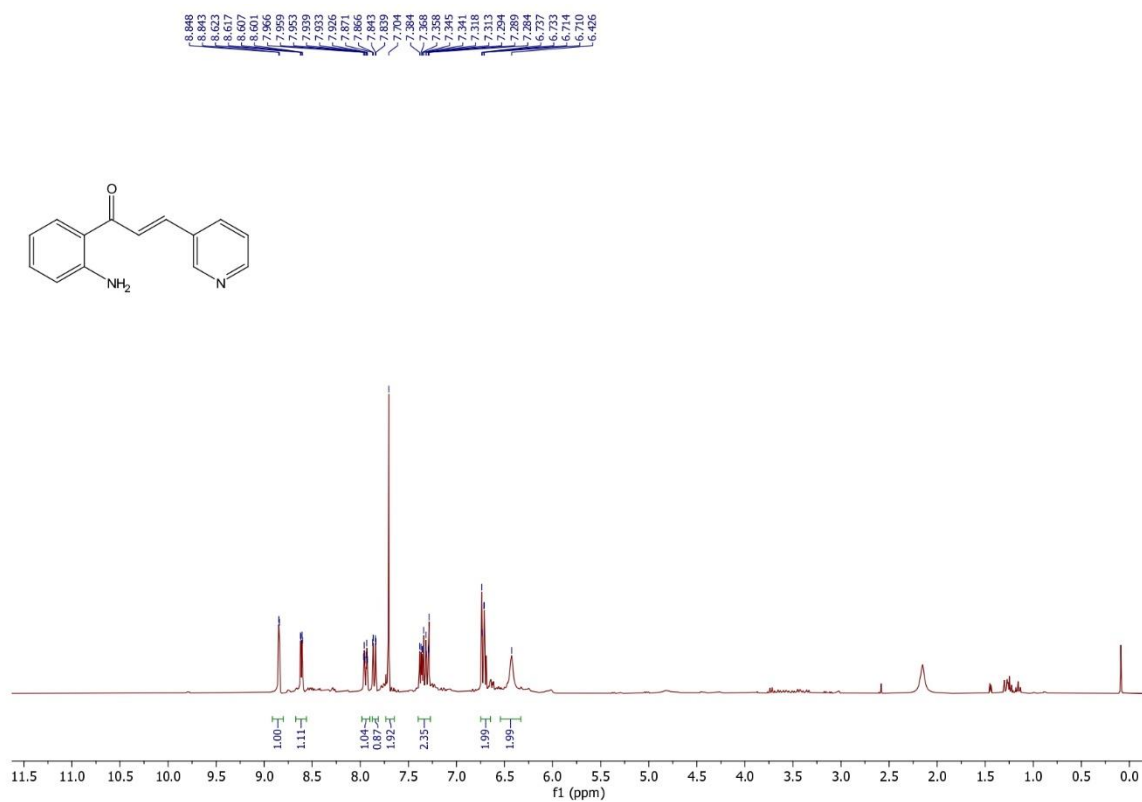


Figure 1.38 ¹H NMR spectrum of **29q** (300 MHz, CDCl₃)

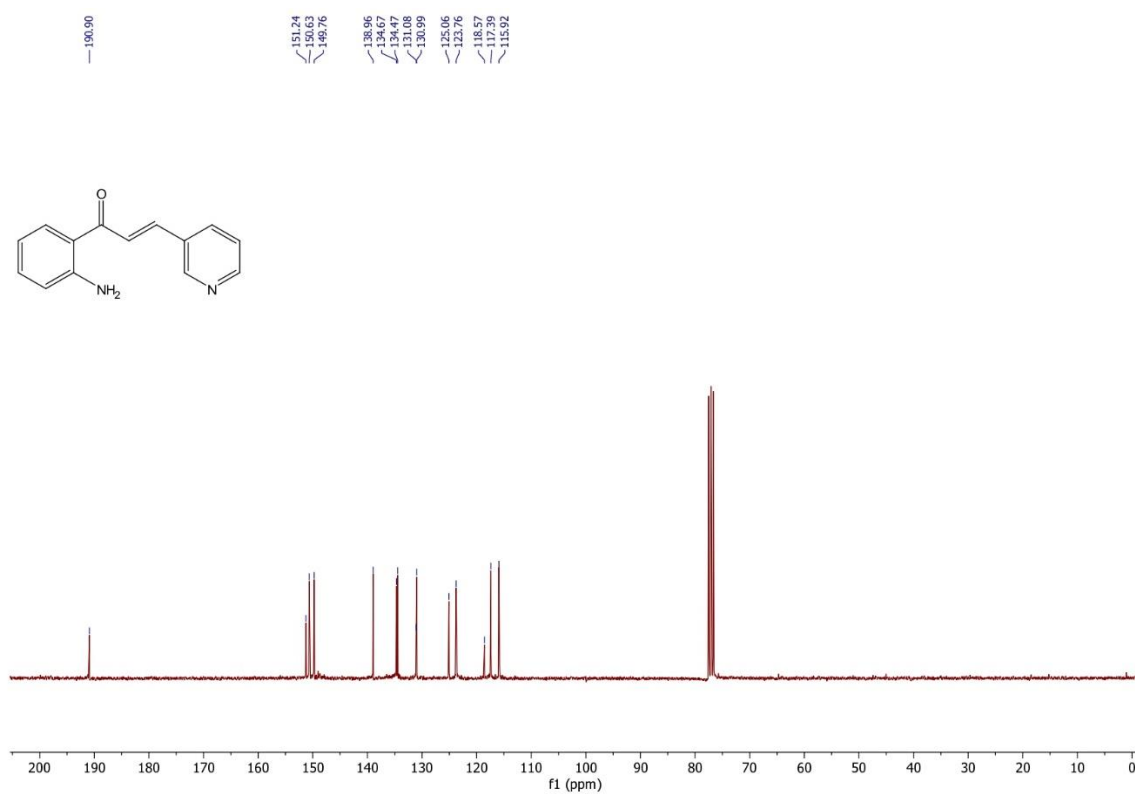


Figure 1.39 ¹³C NMR spectrum of **29q** (100 MHz, CDCl₃)

Chapter 1

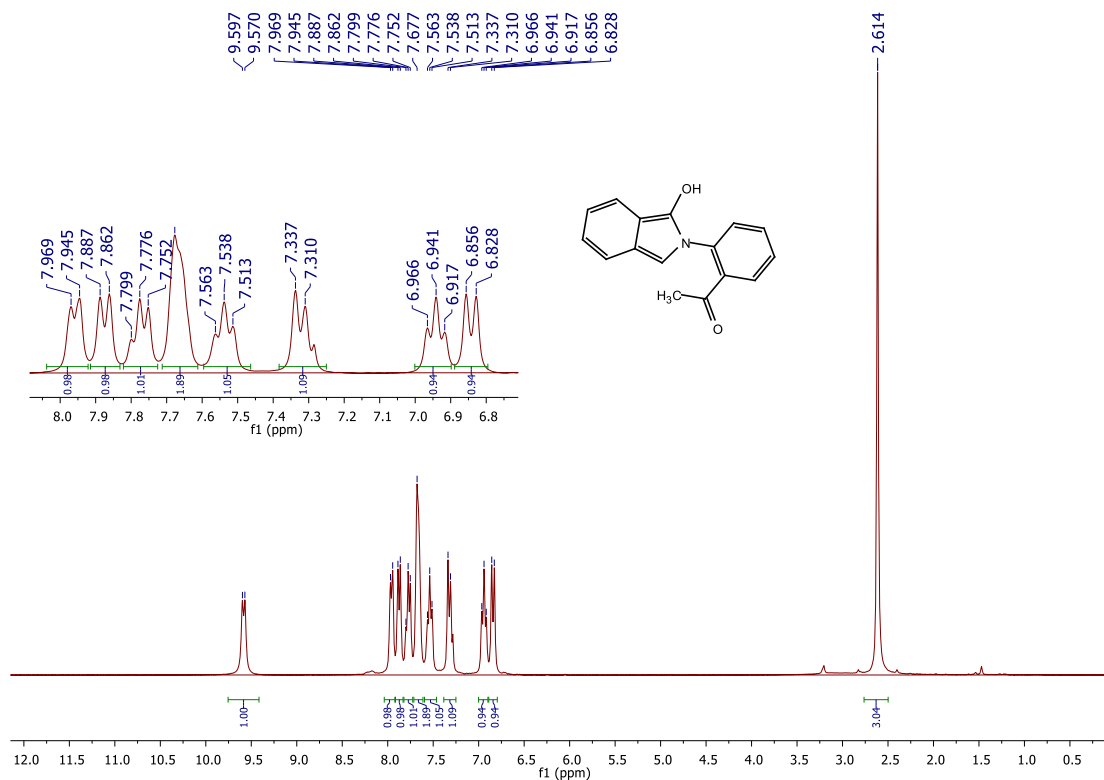


Figure 1.40 ¹H NMR spectrum of **38c** (300 MHz, CDCl₃)

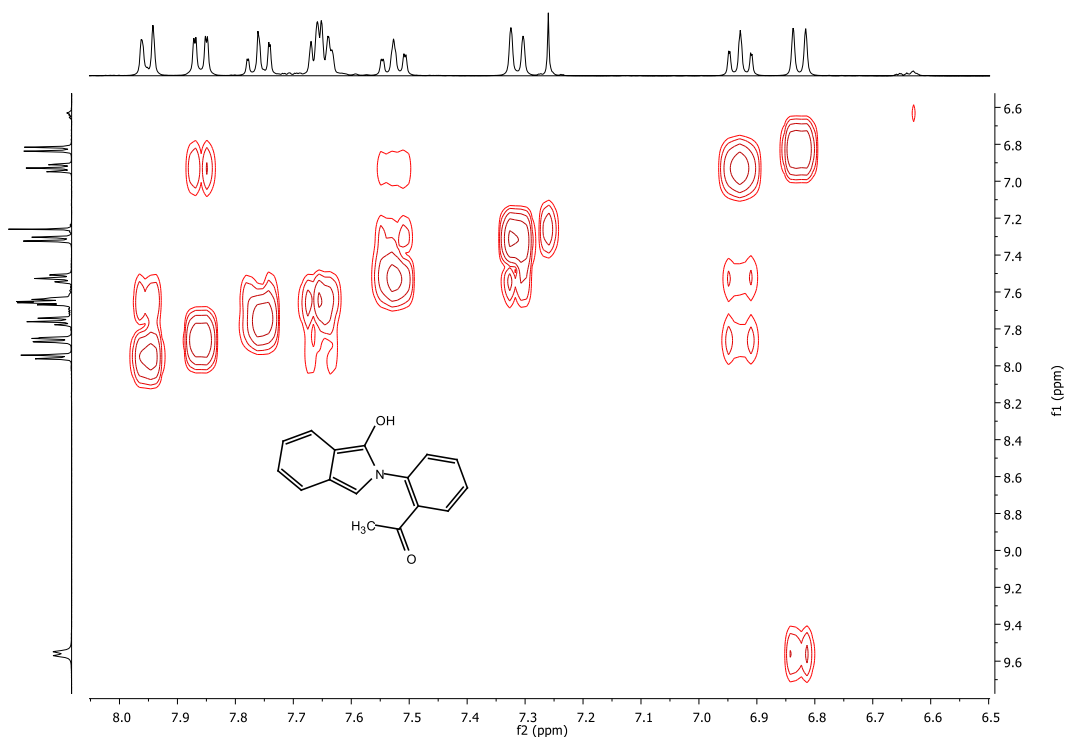


Figure 1.41 ¹H-¹H COSY NMR spectrum of **38c** (400 MHz, CDCl₃)

Chapter 1

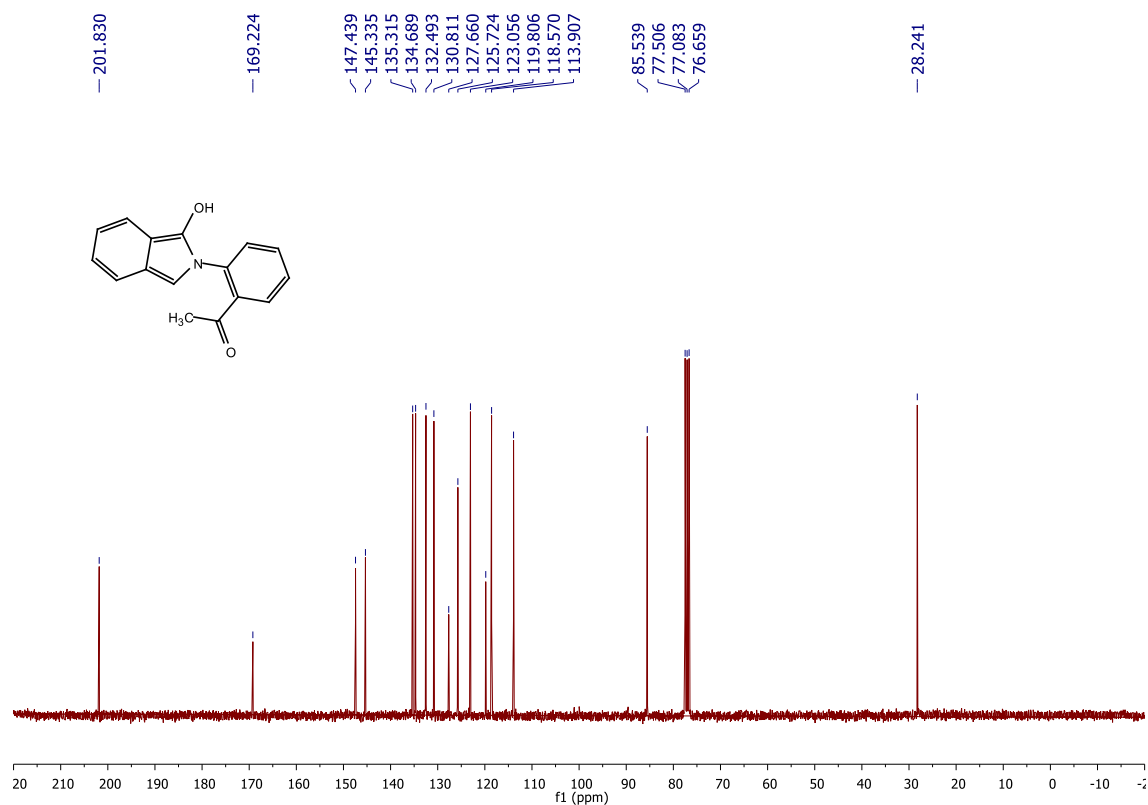


Figure 1.42 ¹³C NMR spectrum of **38c** (75 MHz, CDCl₃)

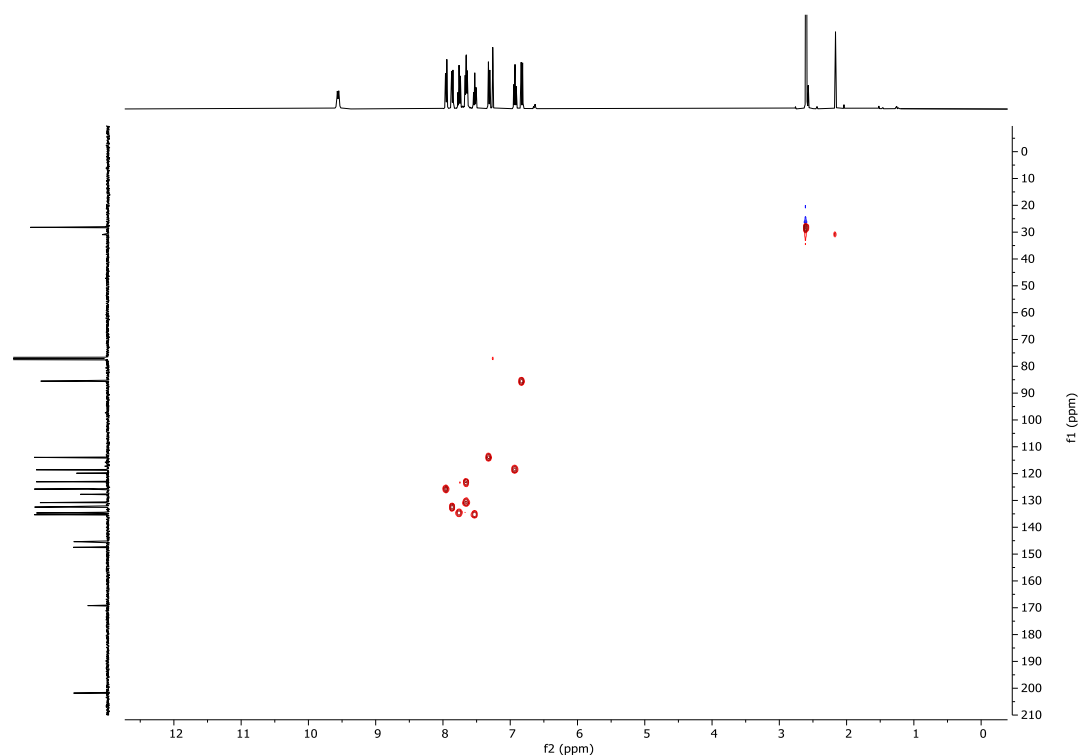


Figure 1.43 HSQC NMR spectrum of **38c** (400 MHz, CDCl₃)

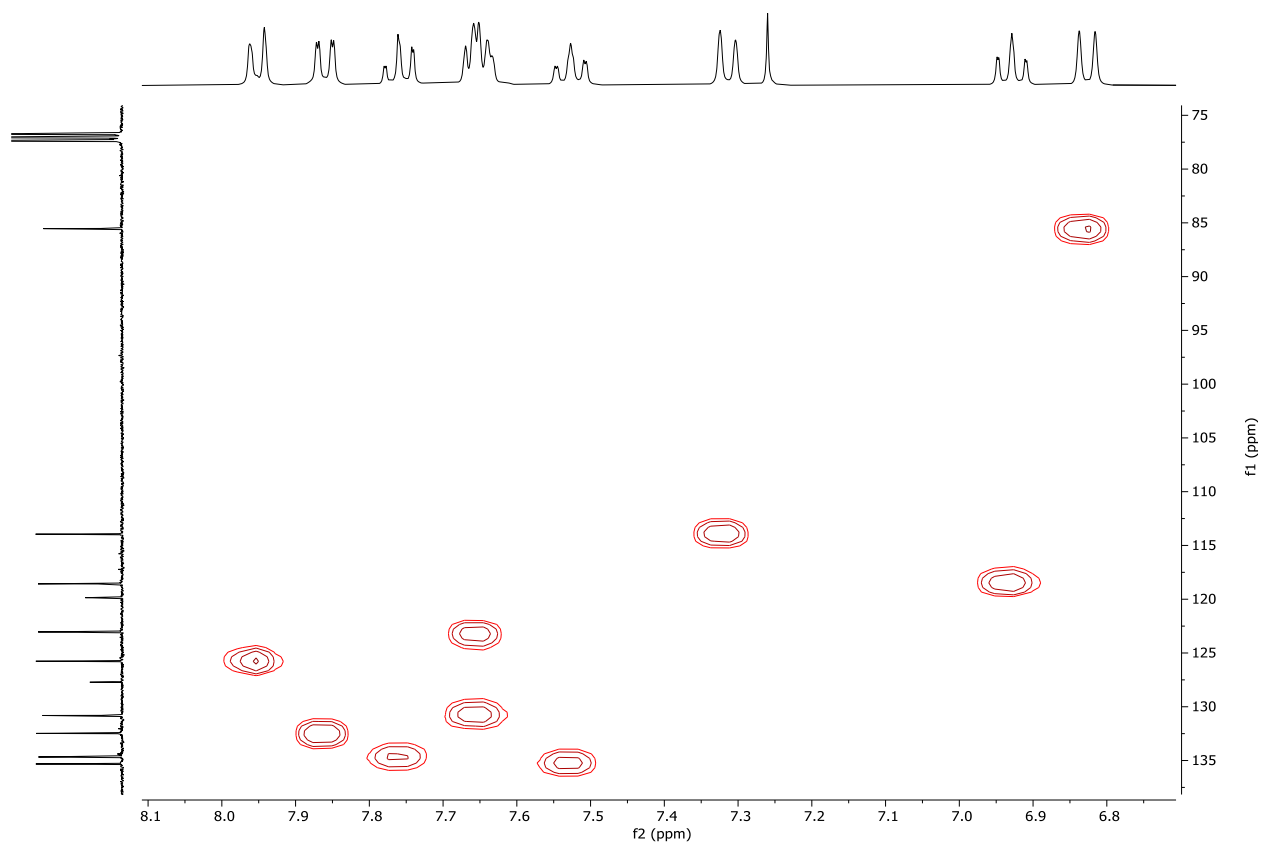


Figure 1.44 HSQC NMR spectrum of **38c** expansion

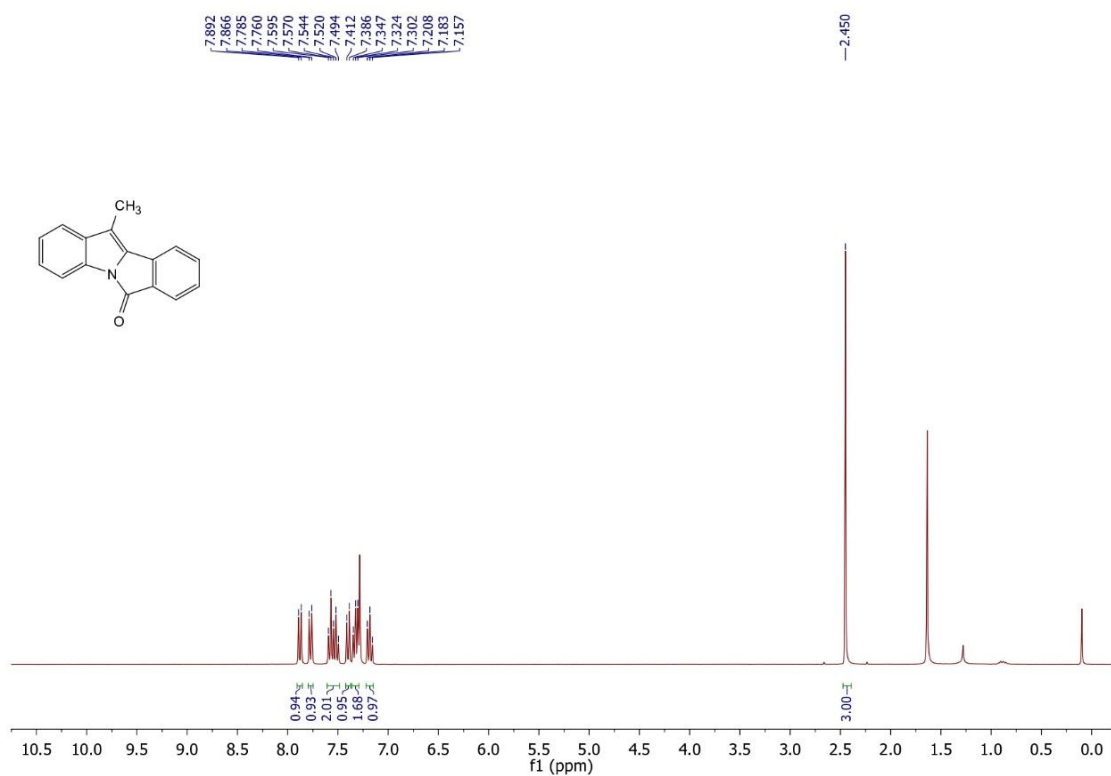


Figure 1.45 ^1H NMR spectrum of **6b** (300 MHz, CDCl_3)

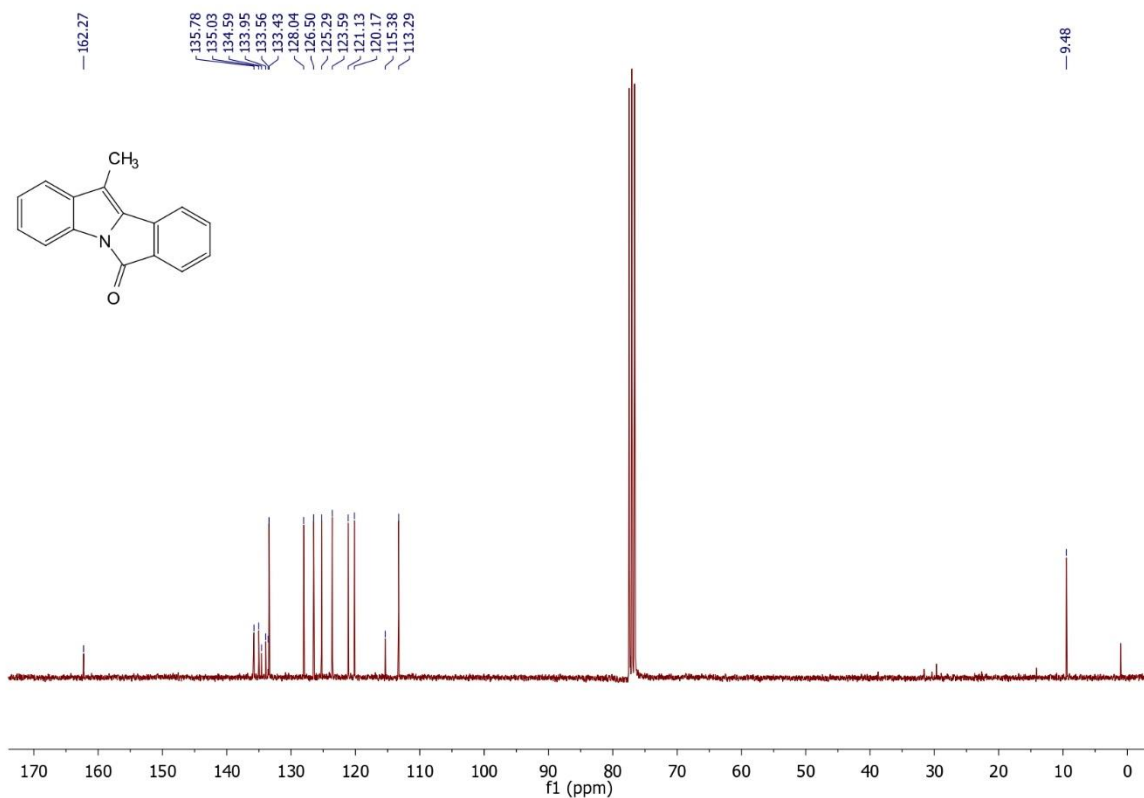


Figure 1.46 ^{13}C NMR spectrum of **6b** (75 MHz, CDCl_3)

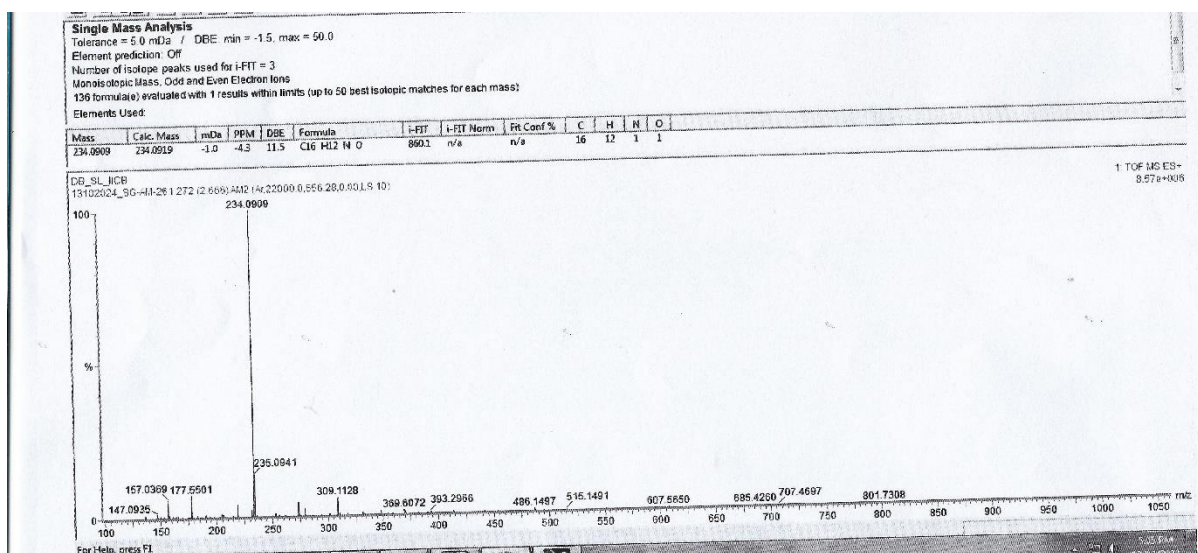


Figure 1.47 Mass spectrum of **6b** (ESI-TOF) m/z: $[\text{M}+\text{H}]^+$

Chapter 1

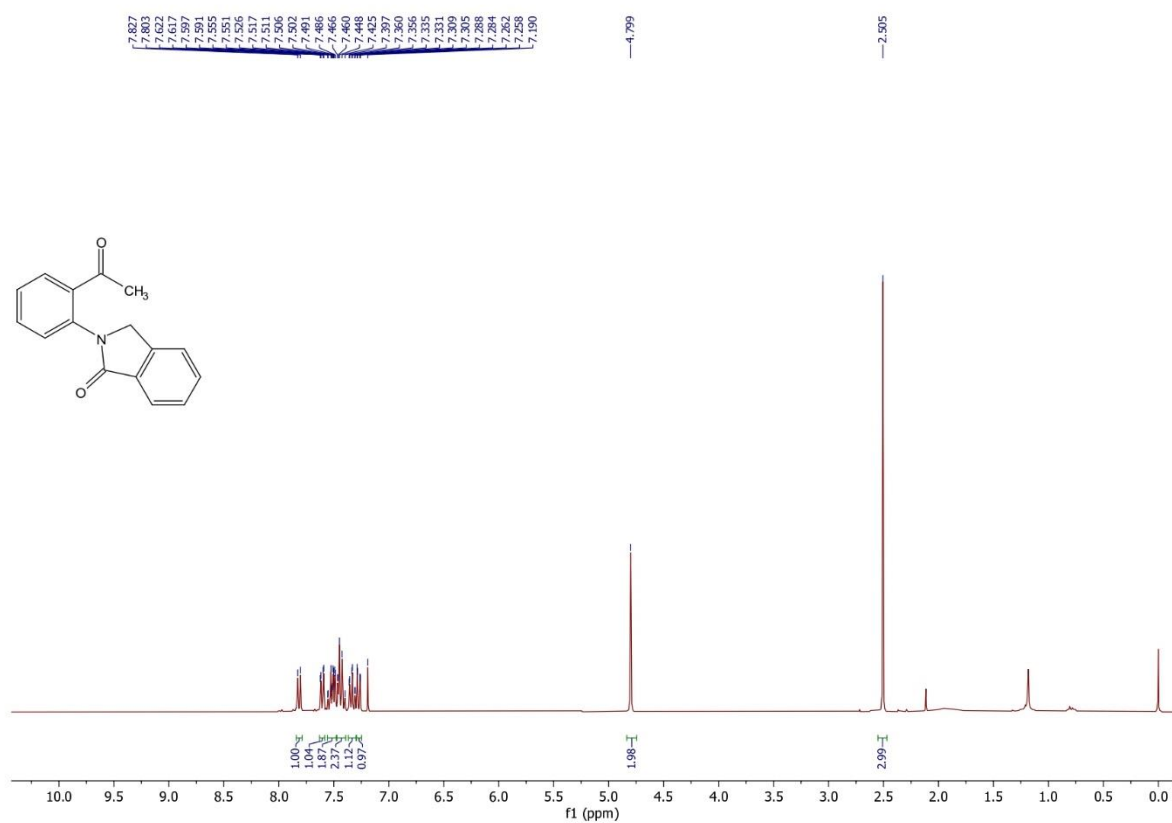


Figure 1.48 ¹H NMR spectrum of **6b2** (300 MHz, CDCl₃)

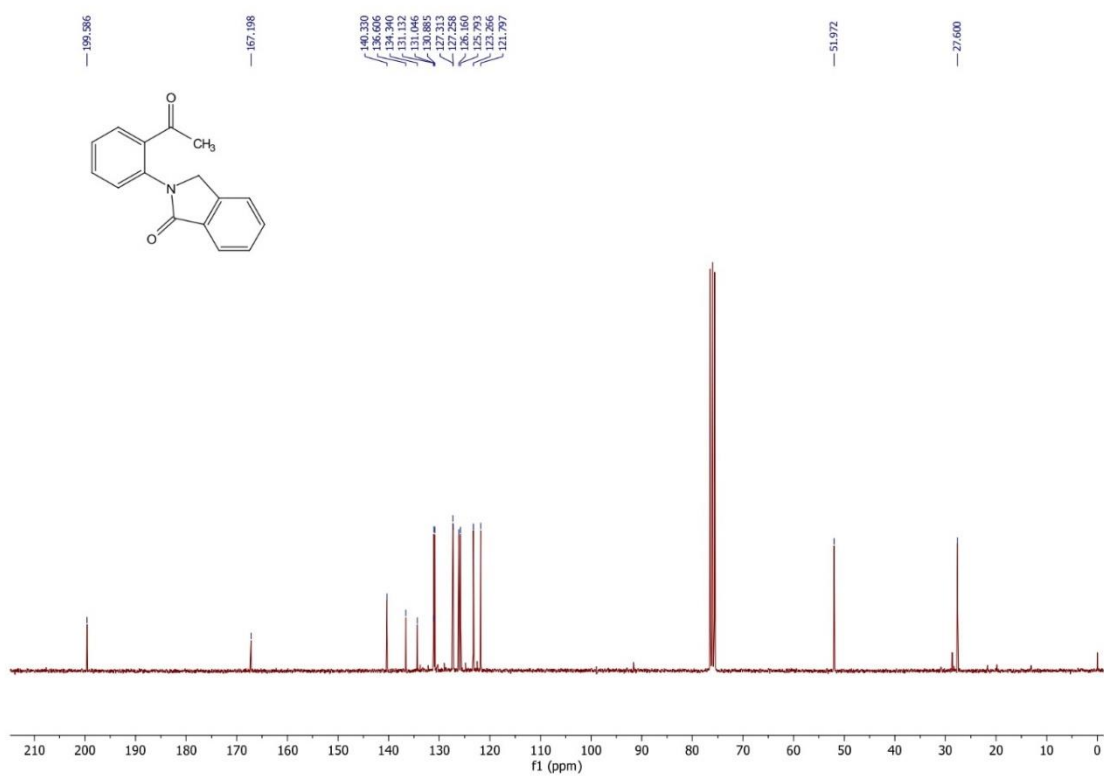


Figure 1.49 ¹³C NMR spectrum of **6b2** (300 MHz, CDCl₃)

Chapter 1

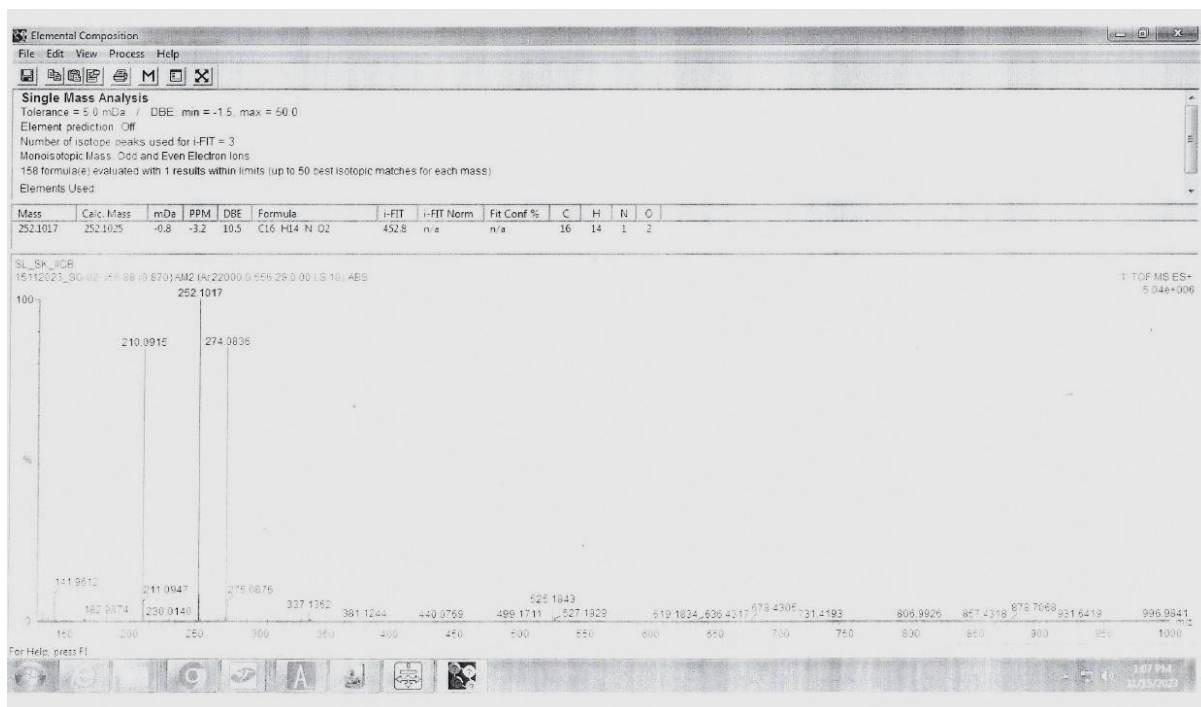


Figure 1.50 Mass spectrum of **6b2** (ESI-TOF) m/z : $[M+H]^+$

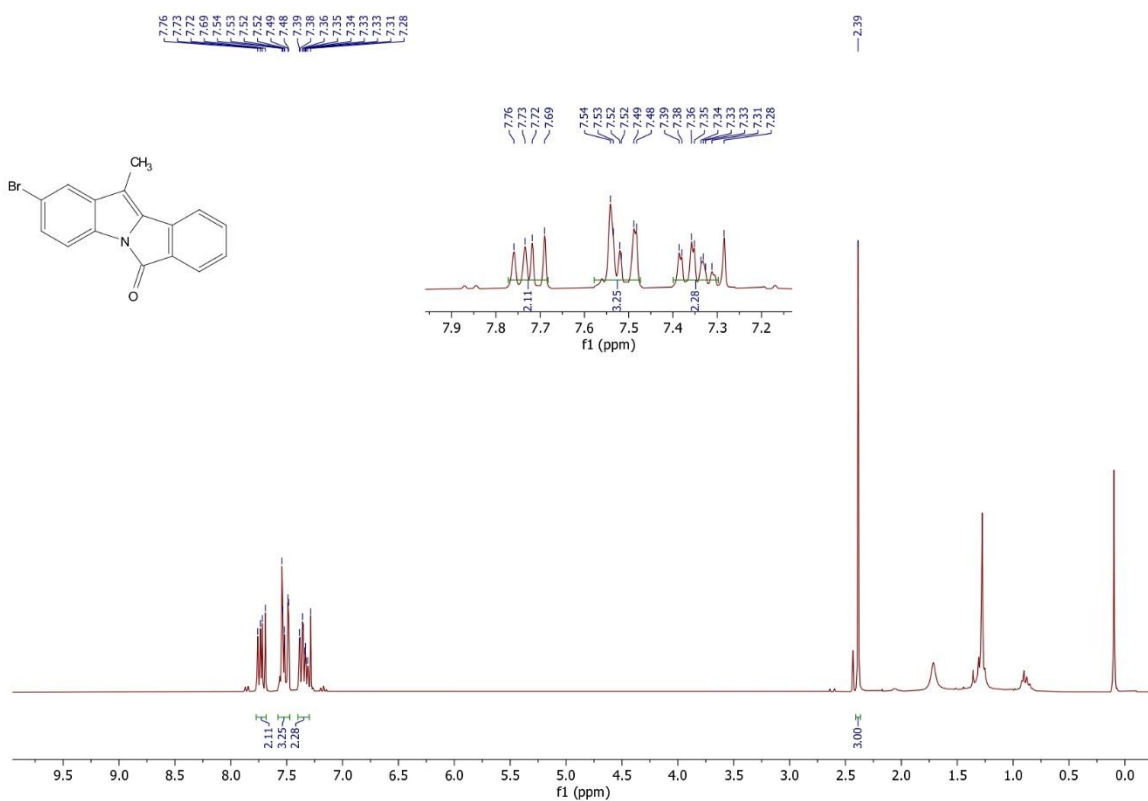


Figure 1.51 ^1H NMR spectrum of **6c** (300 MHz, CDCl_3)

Chapter 1

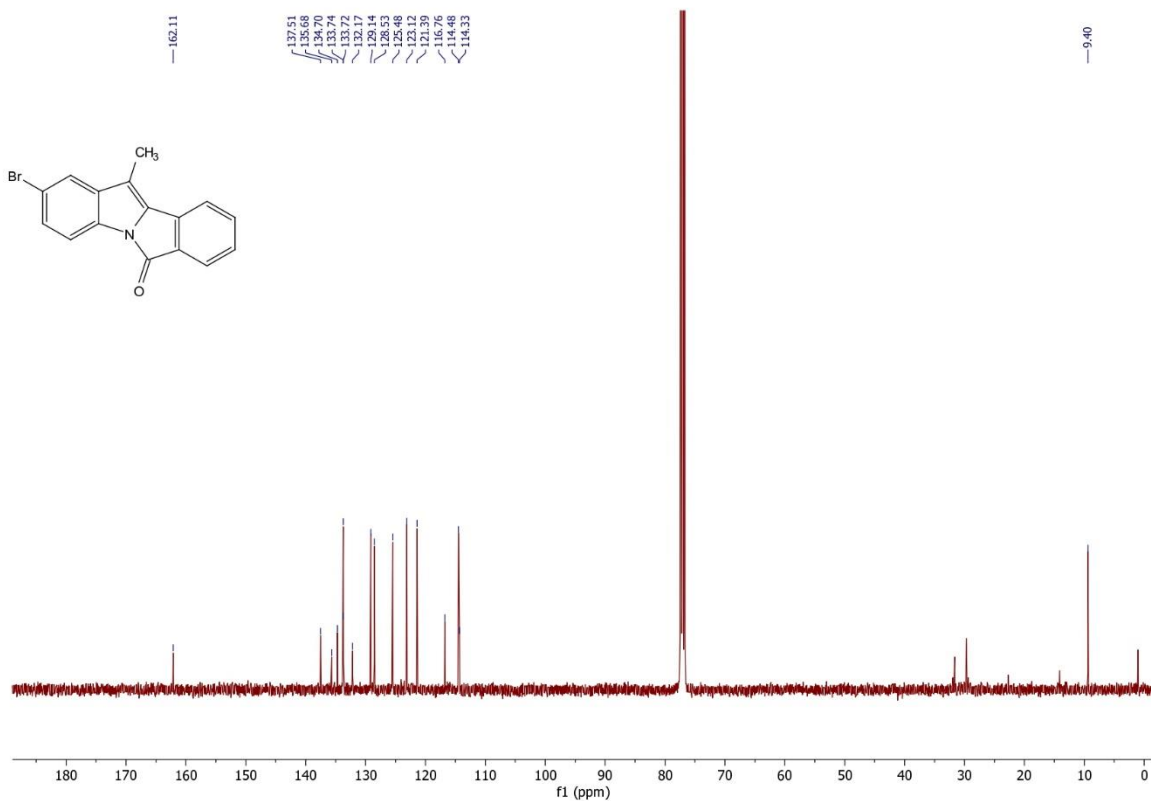


Figure 1.52 ¹³C NMR spectrum of 6c (75 MHz, CDCl₃)

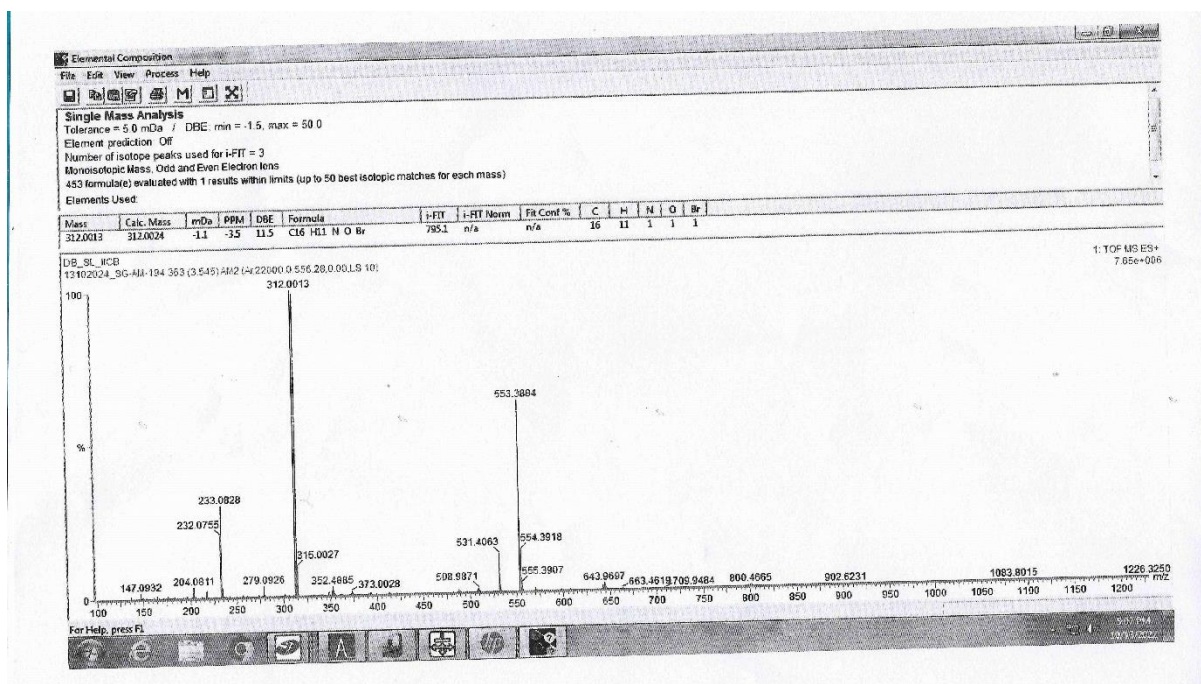


Figure 1.53 Mass spectrum of 6c (ESI-TOF) m/z: [M+H]⁺

Chapter 1

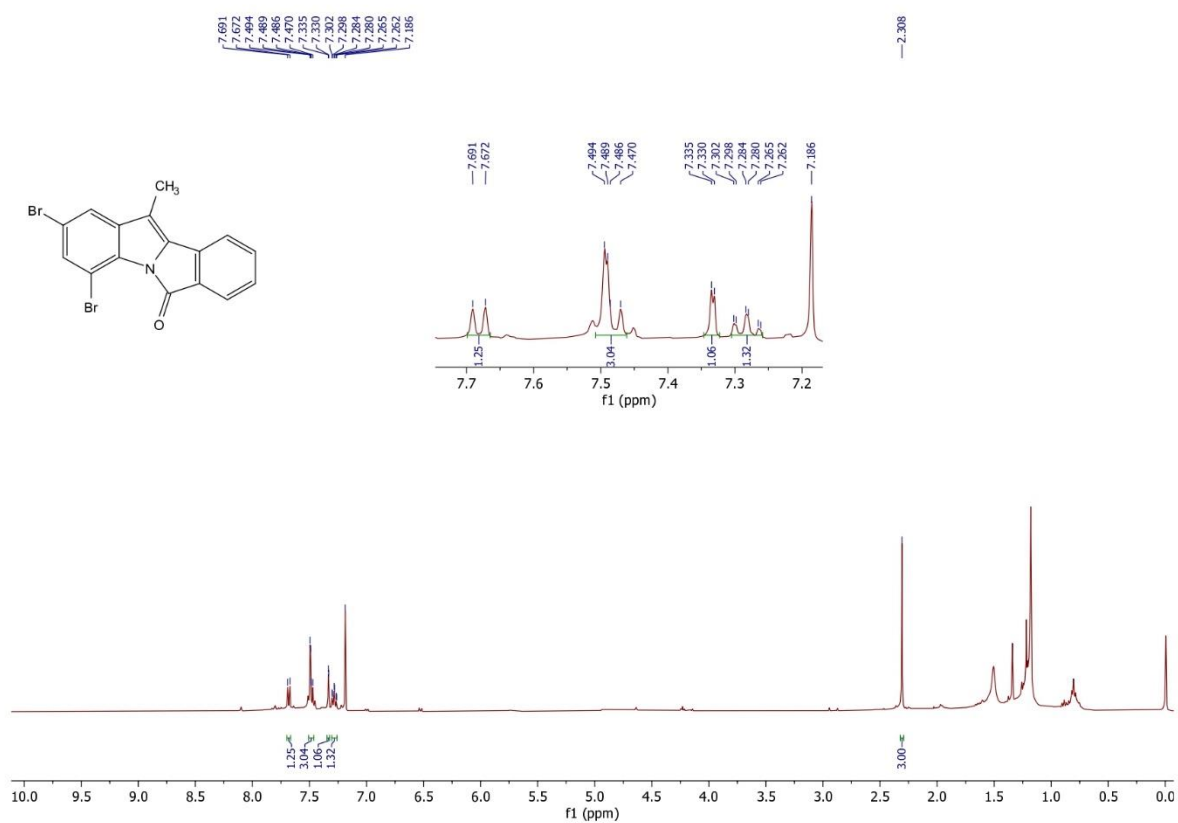


Figure 1.54 ^1H NMR spectrum of **6d** (400 MHz, CDCl_3)

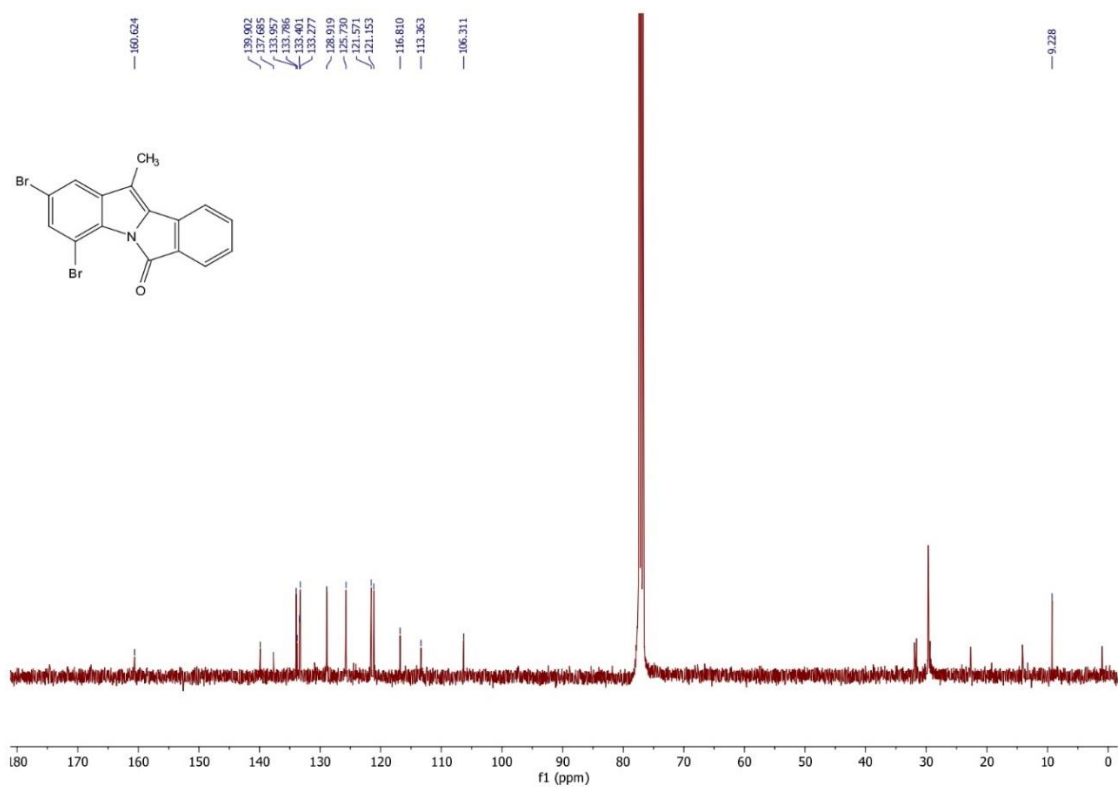


Figure 1.55 ^{13}C NMR spectrum of **6d** (100 MHz, CDCl_3)

Chapter 1



Figure 1.56 Mass spectrum of **6d** (ESI-TOF) m/z : $[\text{M}+\text{H}]^+$

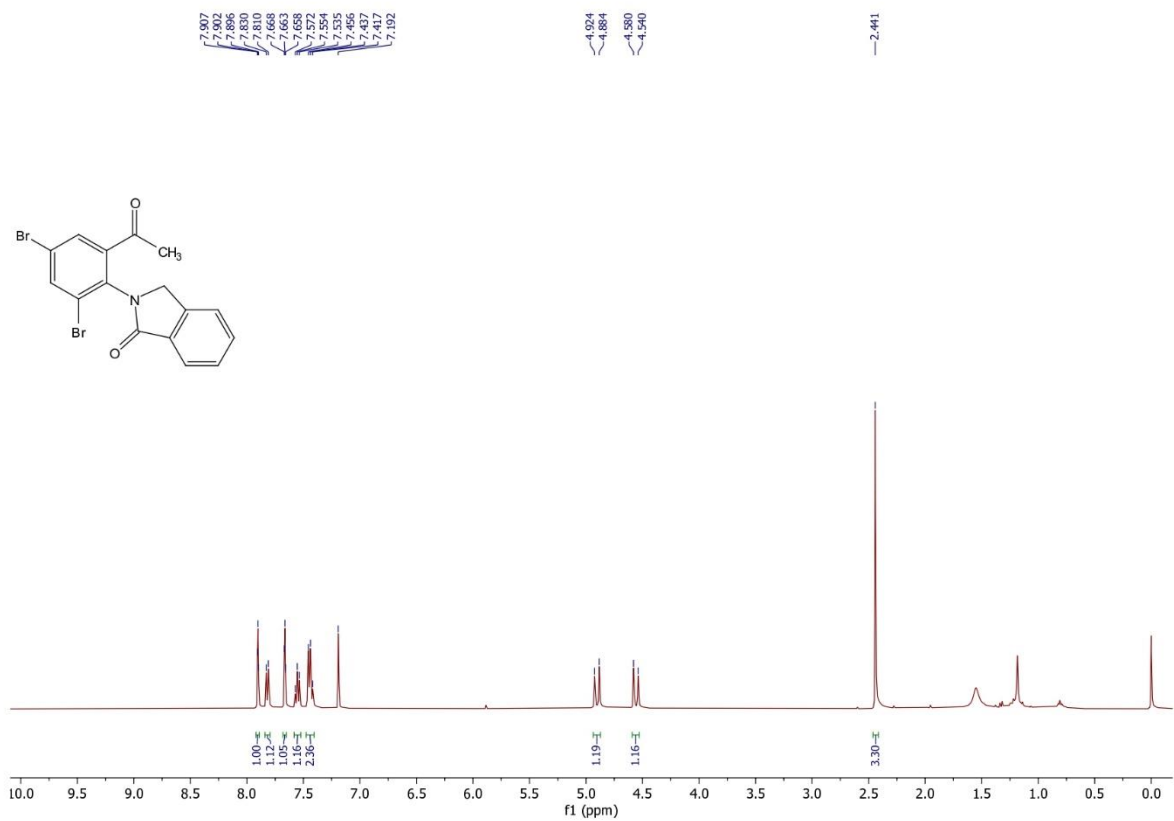


Figure 1.57 ^1H NMR spectrum of **6d** (400 MHz, CDCl_3)

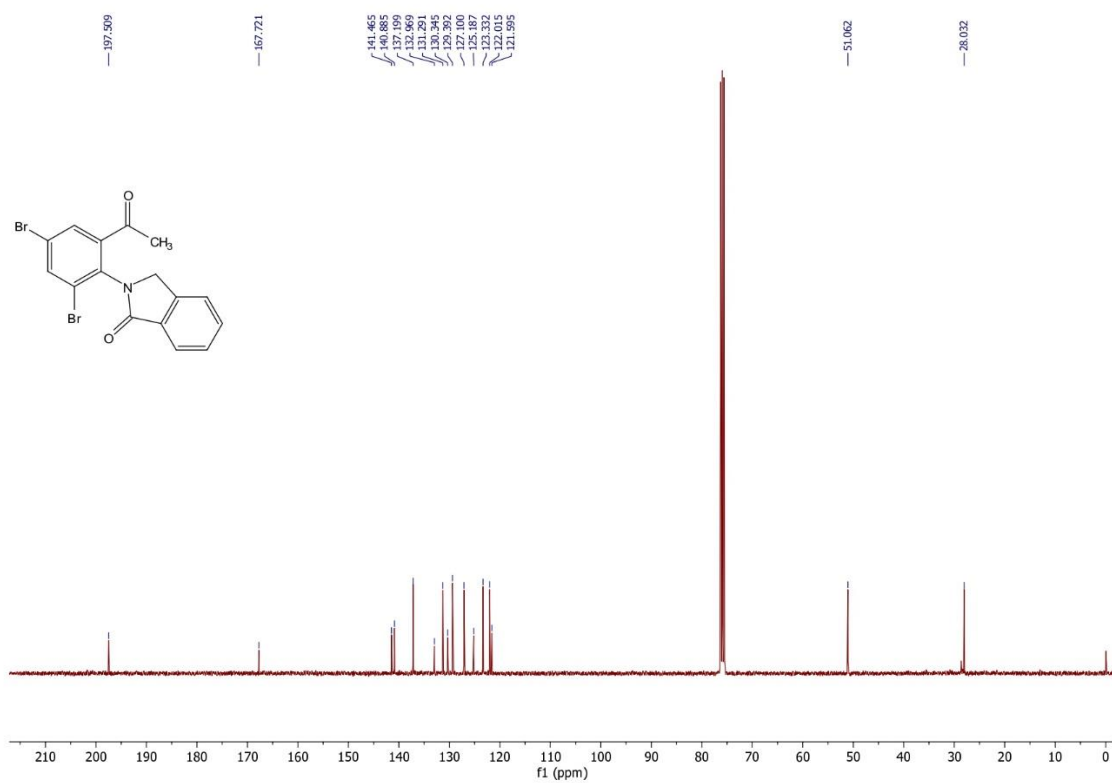


Figure 1.58 ¹³C NMR spectrum of **6d2** (100 MHz, CDCl₃)

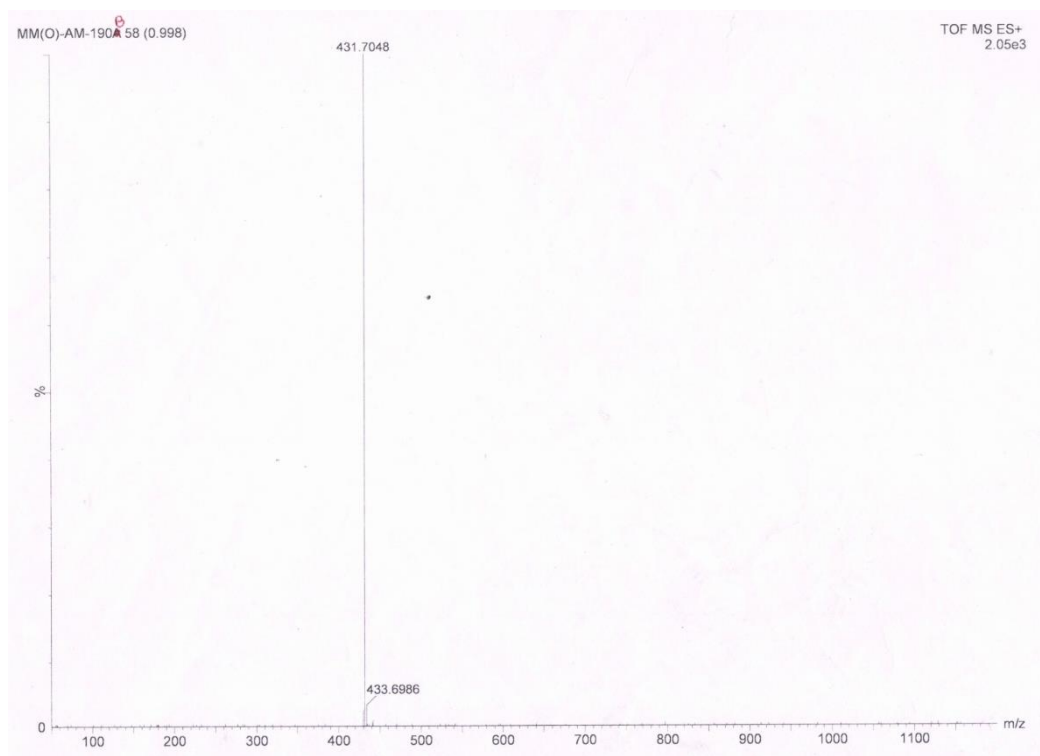


Figure 1.59 Mass spectrum of **6d2** (ESI-TOF) m/z: [M+2+Na]⁺

Chapter 1

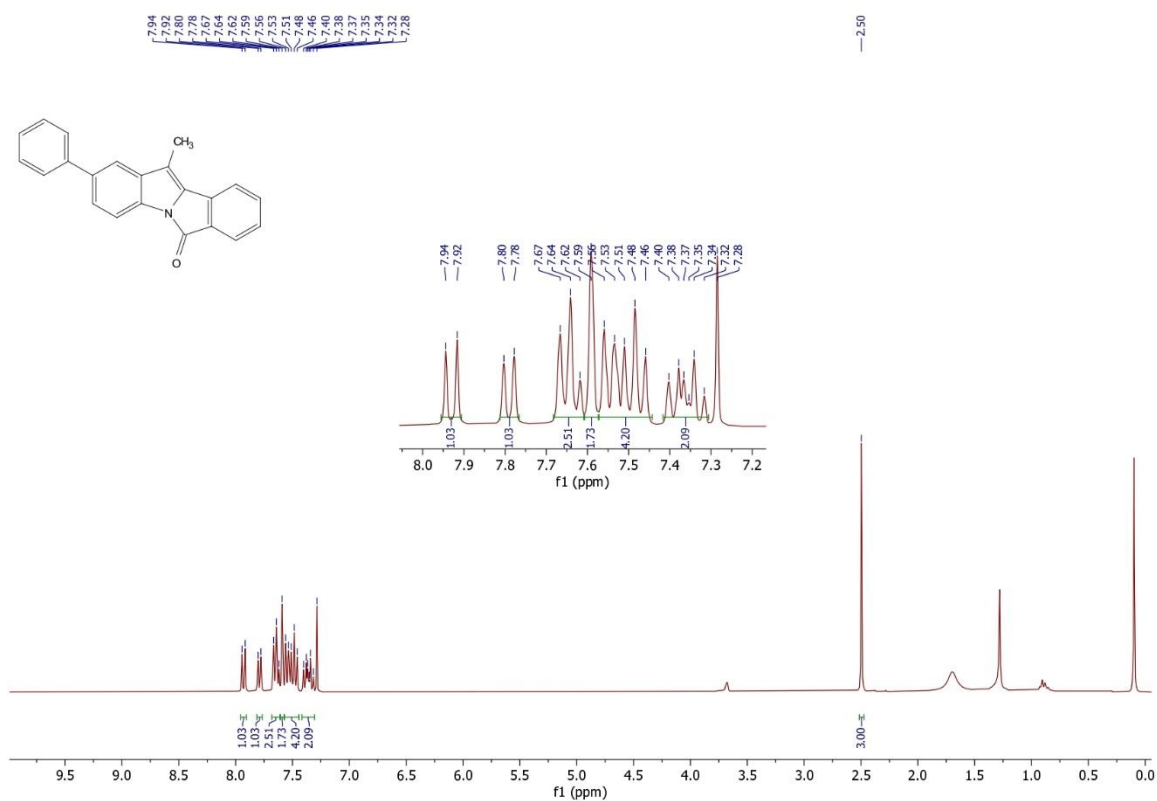


Figure 1.60 ¹H NMR spectrum of **6e** (300 MHz, CDCl₃)

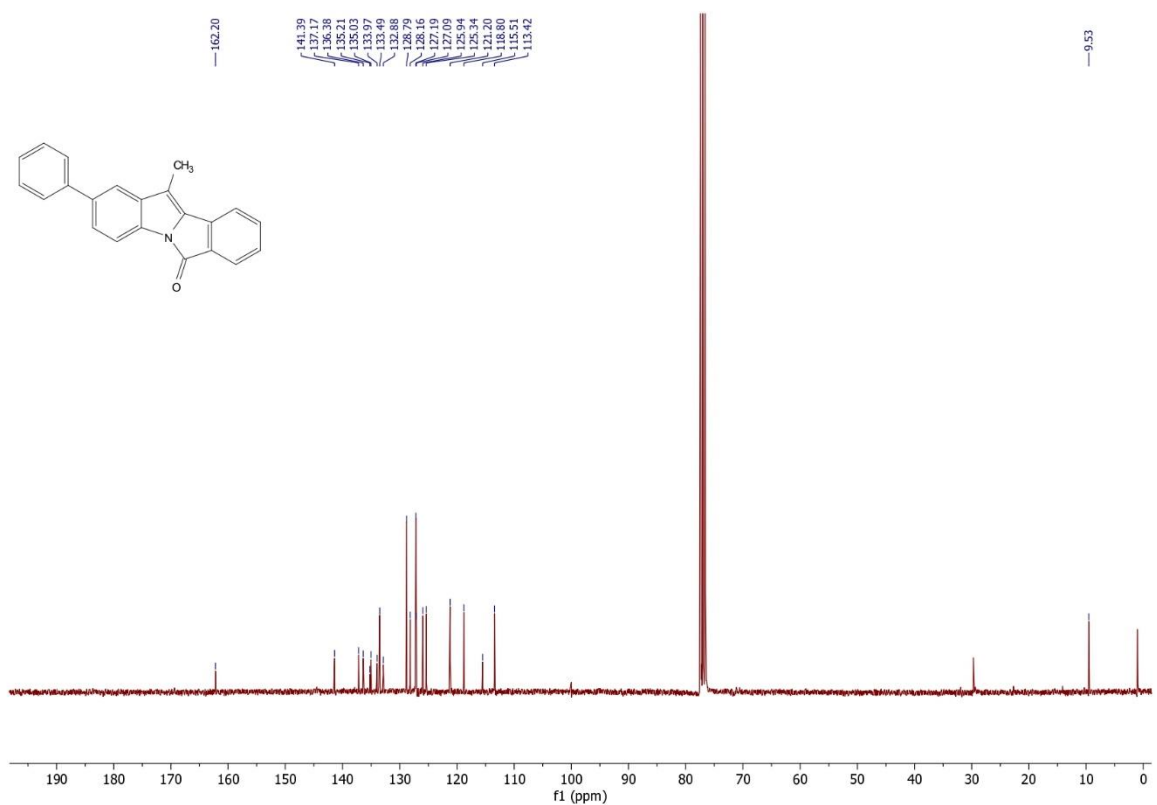


Figure 1.61 ¹³C NMR spectrum of **6e** (75 MHz, CDCl₃)

Chapter 1

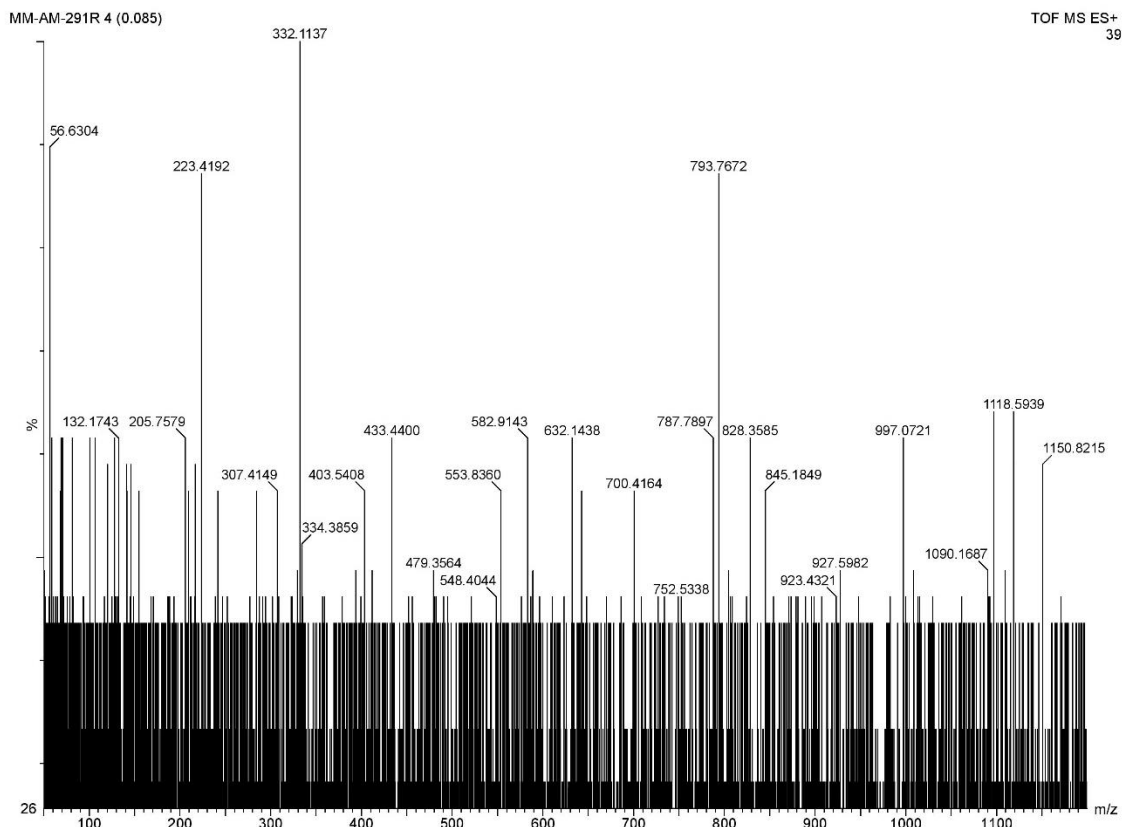


Figure 1.62 Mass spectrum of **6e** (ESI-TOF) m/z : $[M+Na]^+$

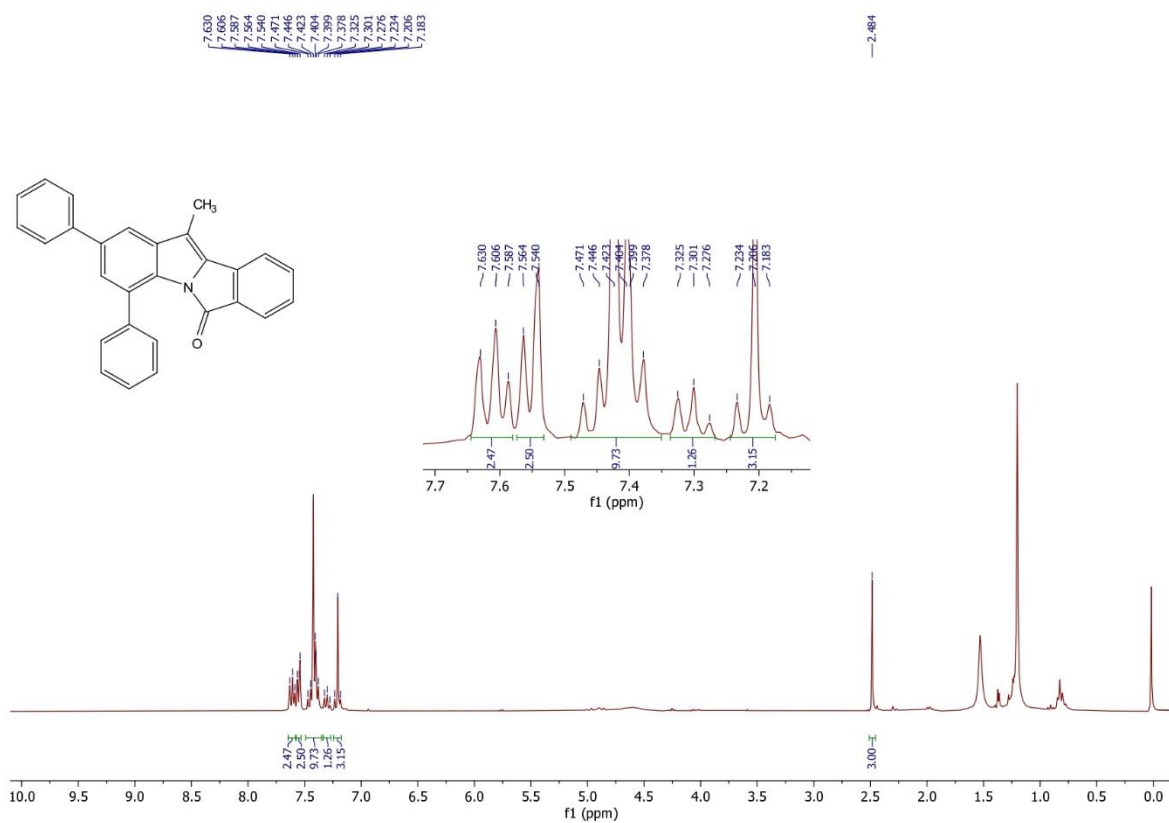


Figure 1.63 1H NMR spectrum of **6f** (300 MHz, $CDCl_3$)

Chapter 1

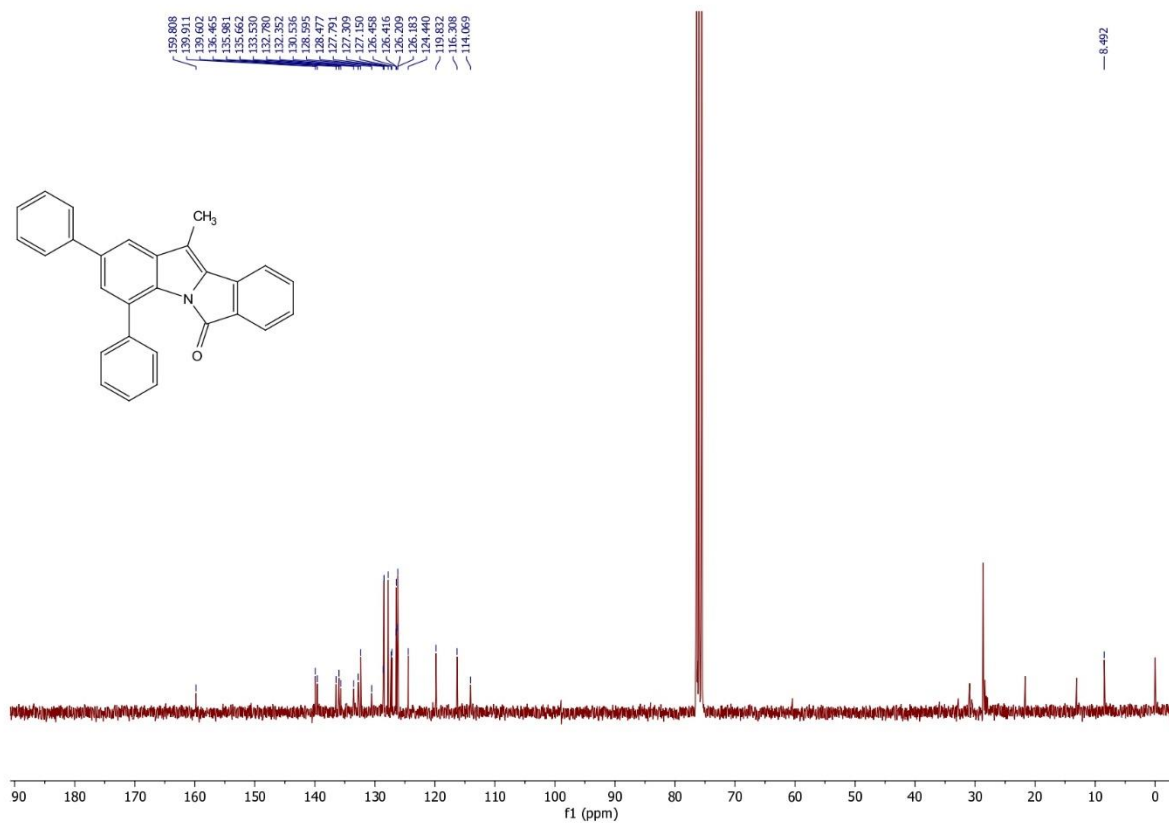


Figure 1.64 ¹³C NMR spectrum of **6f** (75 MHz, CDCl₃)

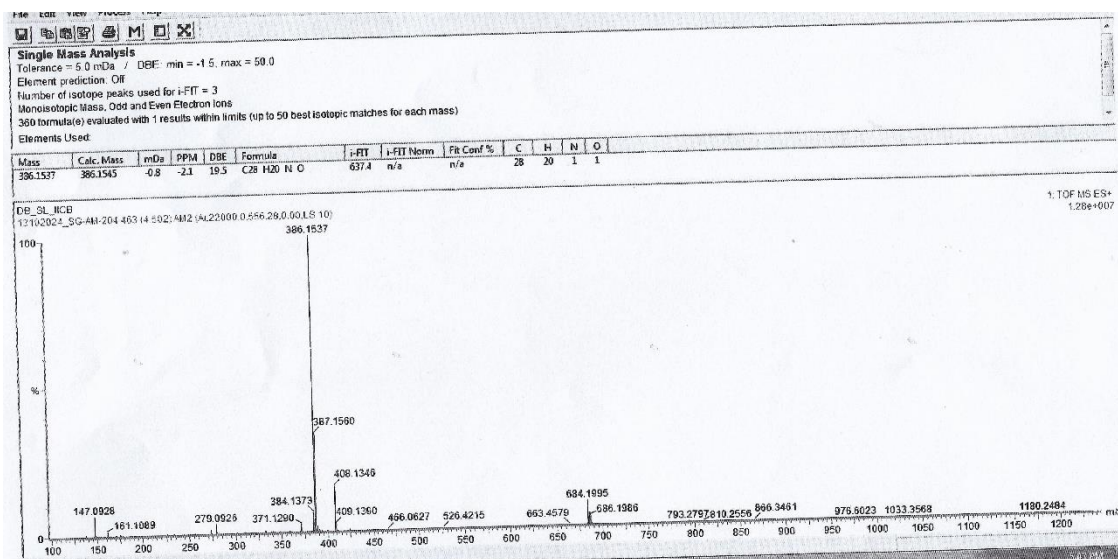


Figure 1.65 Mass spectrum of **6f** (ESI-TOF) m/z: [M+H]⁺

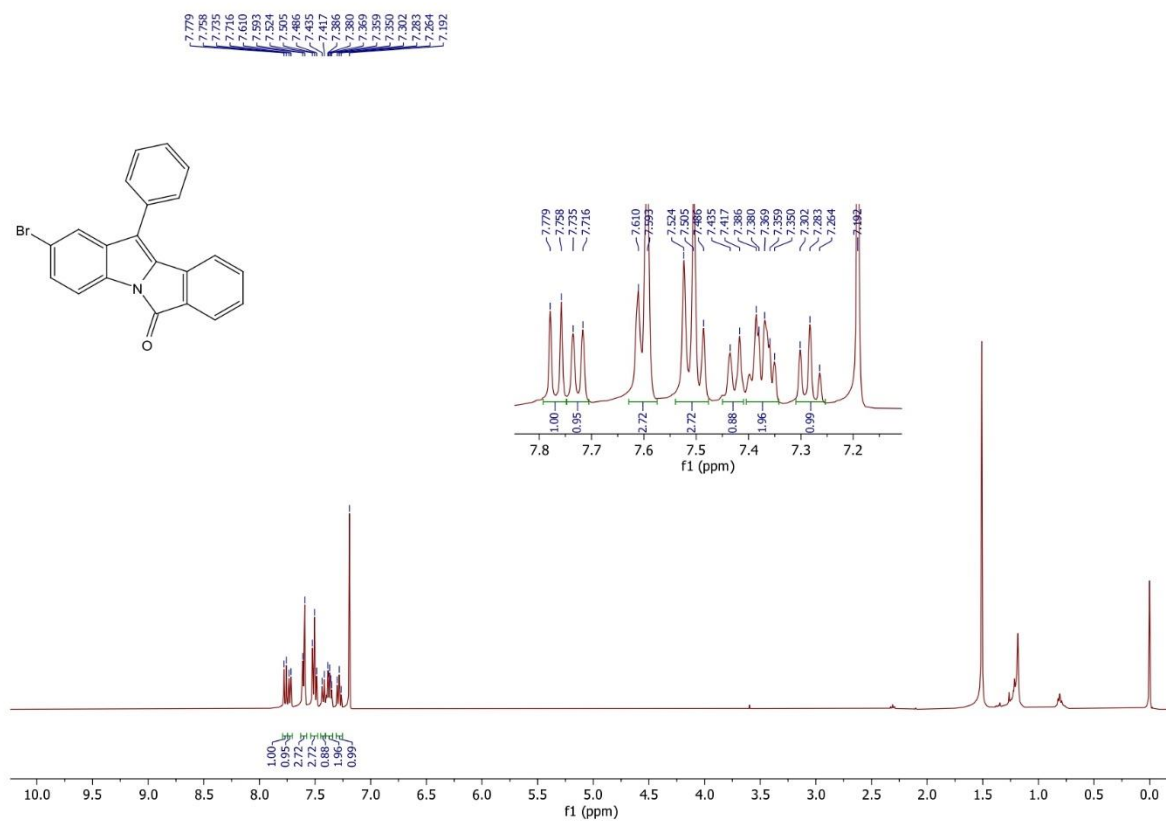


Figure 1.66 ¹H NMR spectrum of **6g** (400 MHz, CDCl₃)

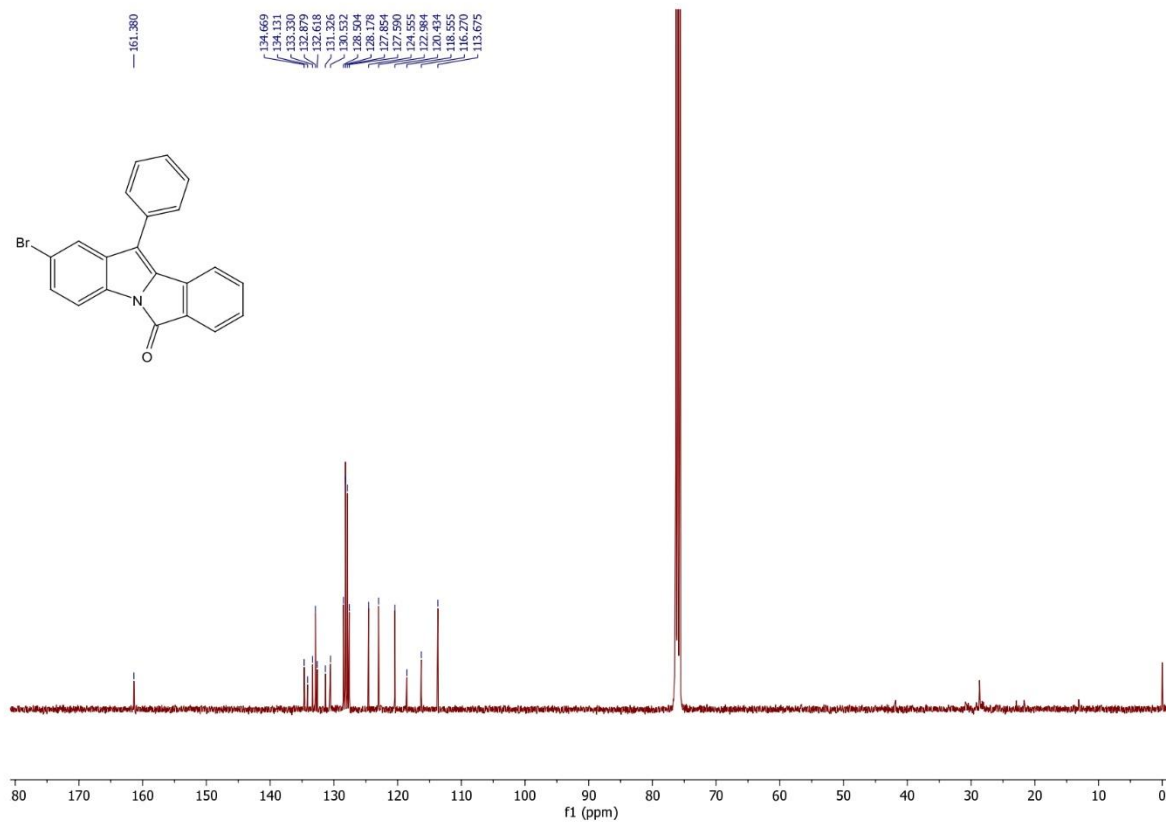


Figure 1.67 ¹³C NMR spectrum of **6g** (100 MHz, CDCl₃)

Chapter 1

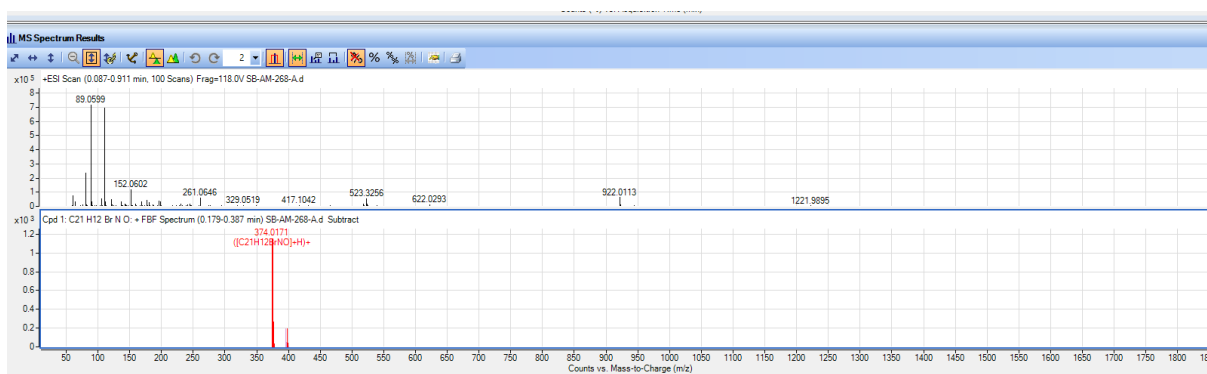


Figure 1.68 Mass spectrum of **6g** (ESI-TOF) m/z: $[M+H]^+$

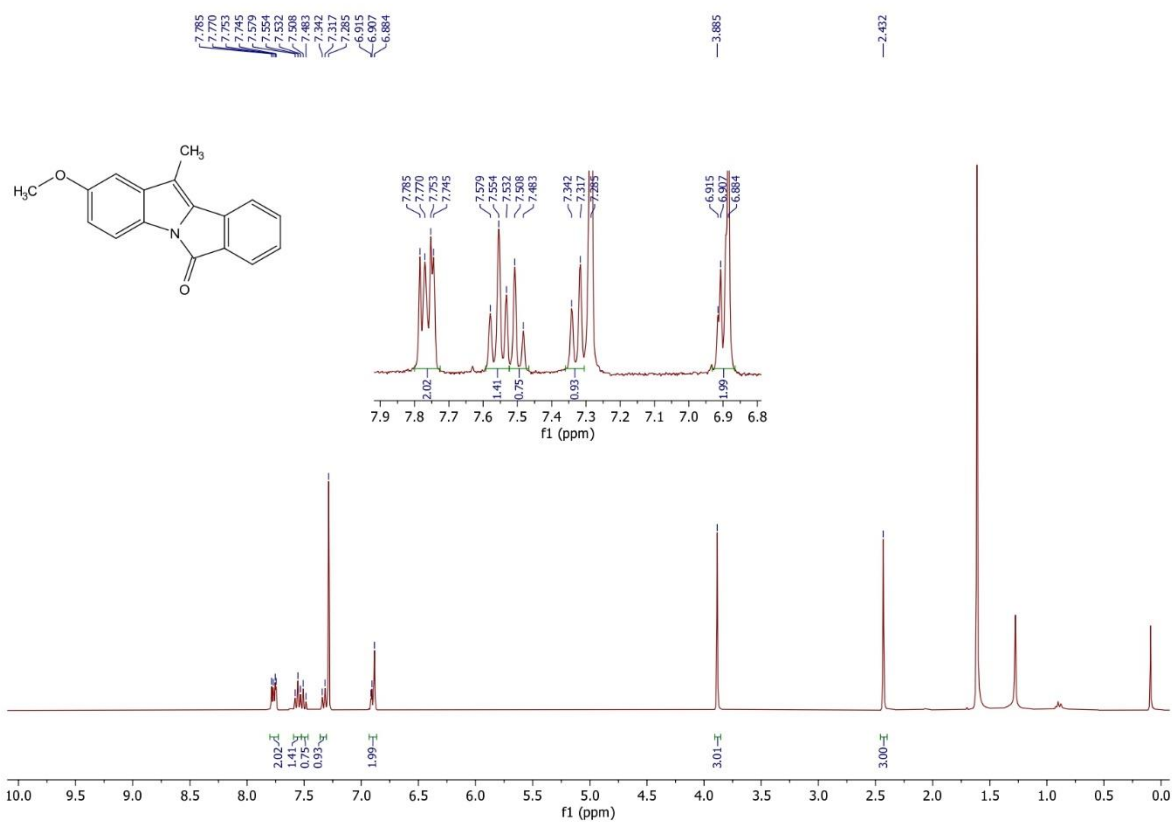


Figure 1.69 ^1H NMR spectrum of **6h** (300 MHz, CDCl_3)

Chapter 1

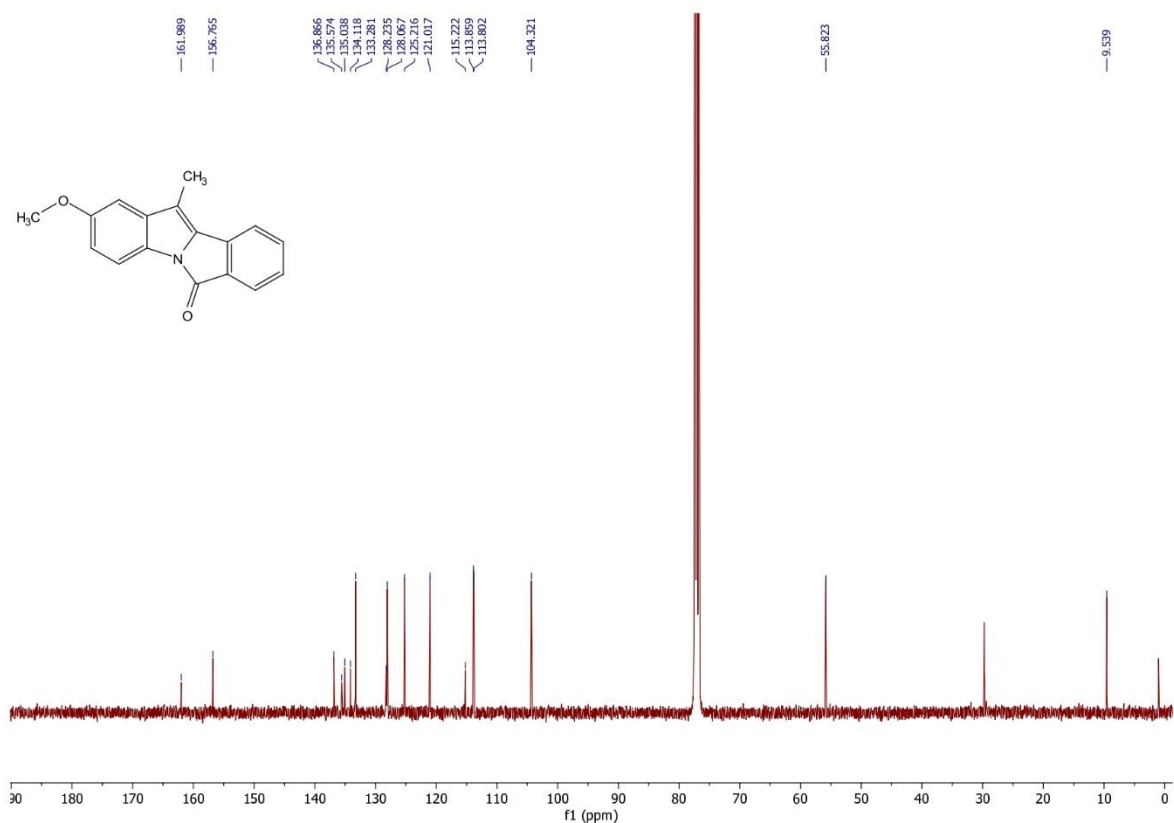


Figure 1.70 ^{13}C NMR spectrum of **6h** (75 MHz, CDCl_3)

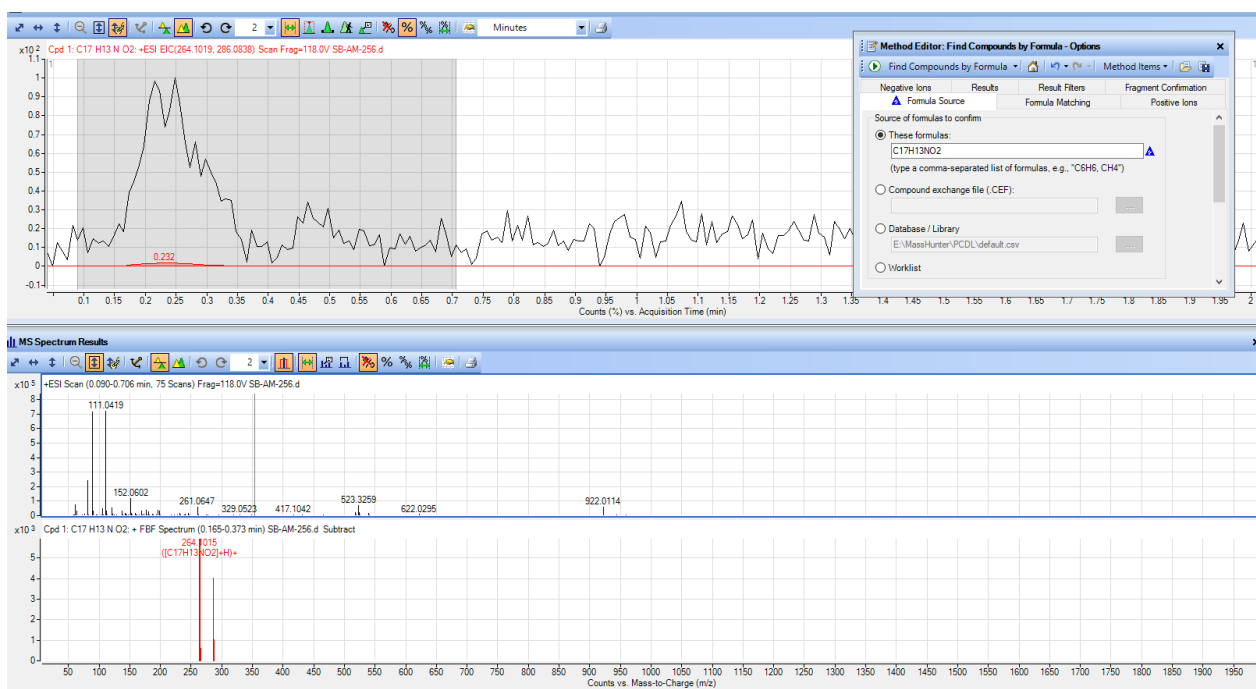


Figure 1.71 Mass spectrum of **6h** (ESI-TOF) m/z : $[\text{M} + \text{H}]^+$

Chapter 1

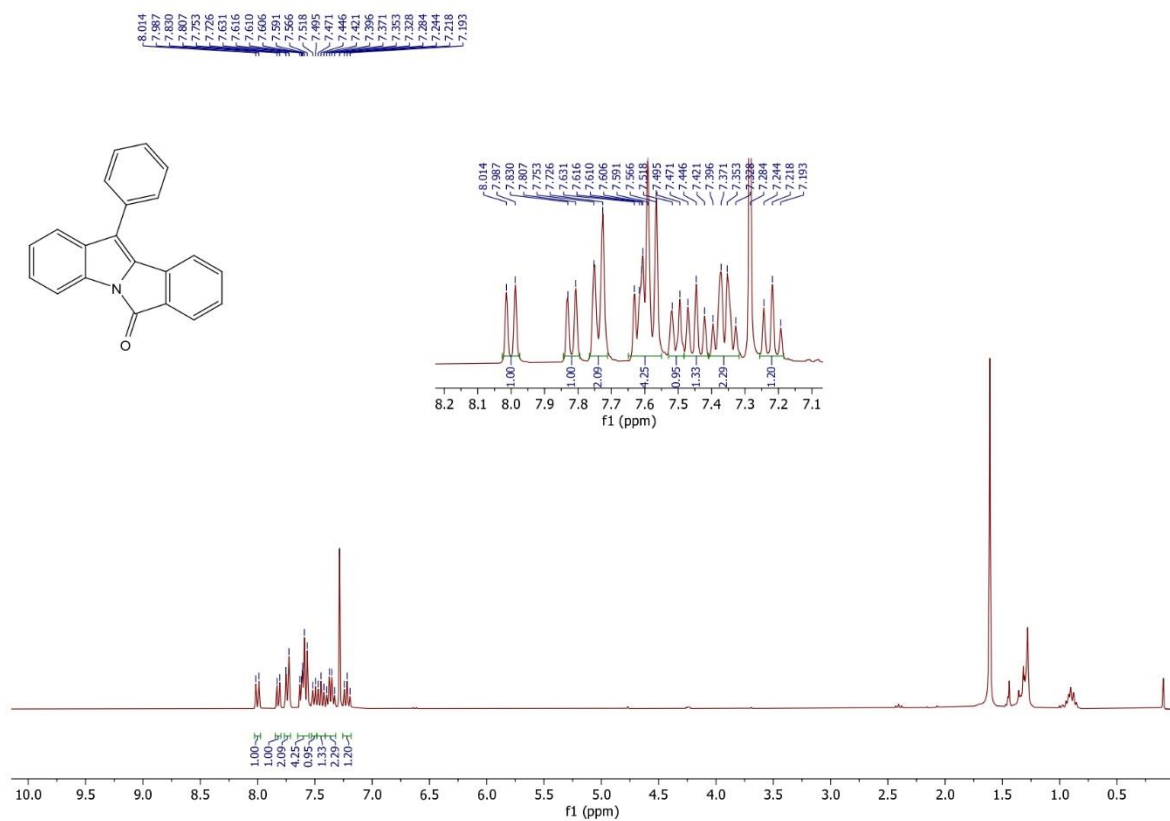


Figure 1.72 ¹H NMR spectrum of **6i** (300 MHz, CDCl₃)

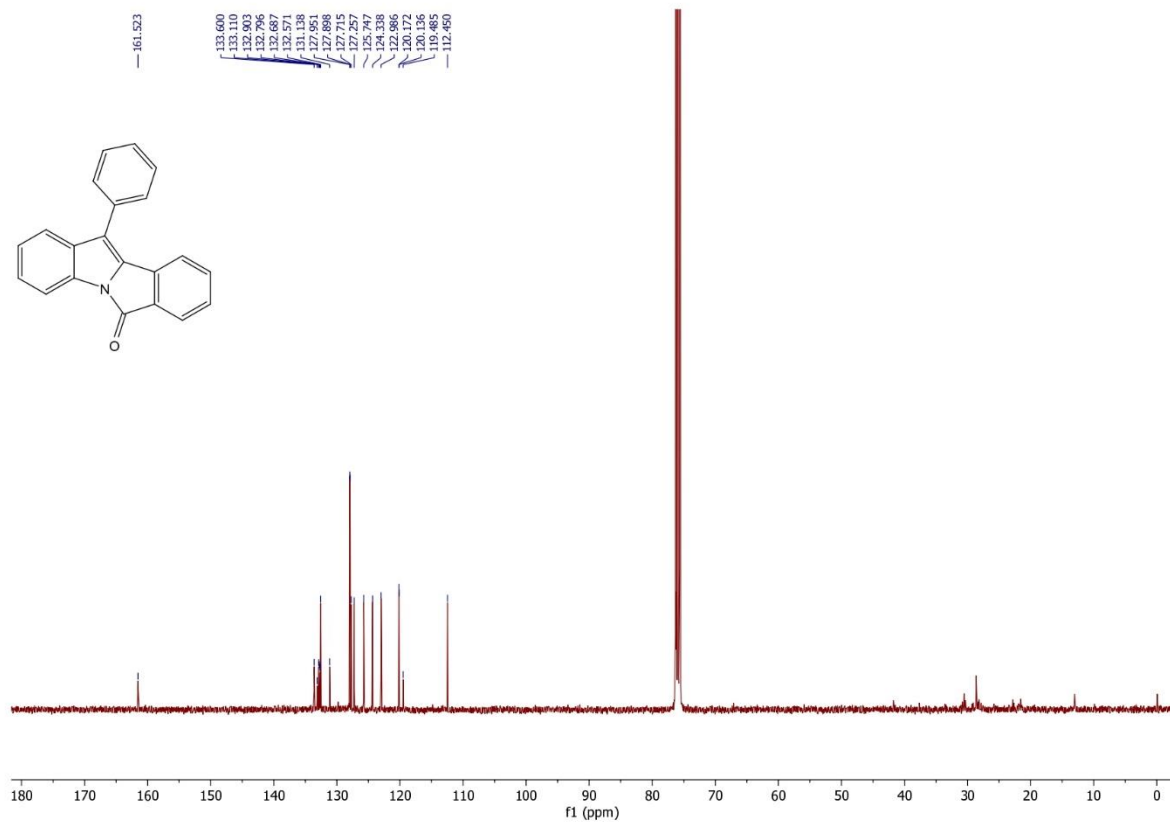


Figure 1.73 ¹³C NMR spectrum of **6i** (75 MHz, CDCl₃)

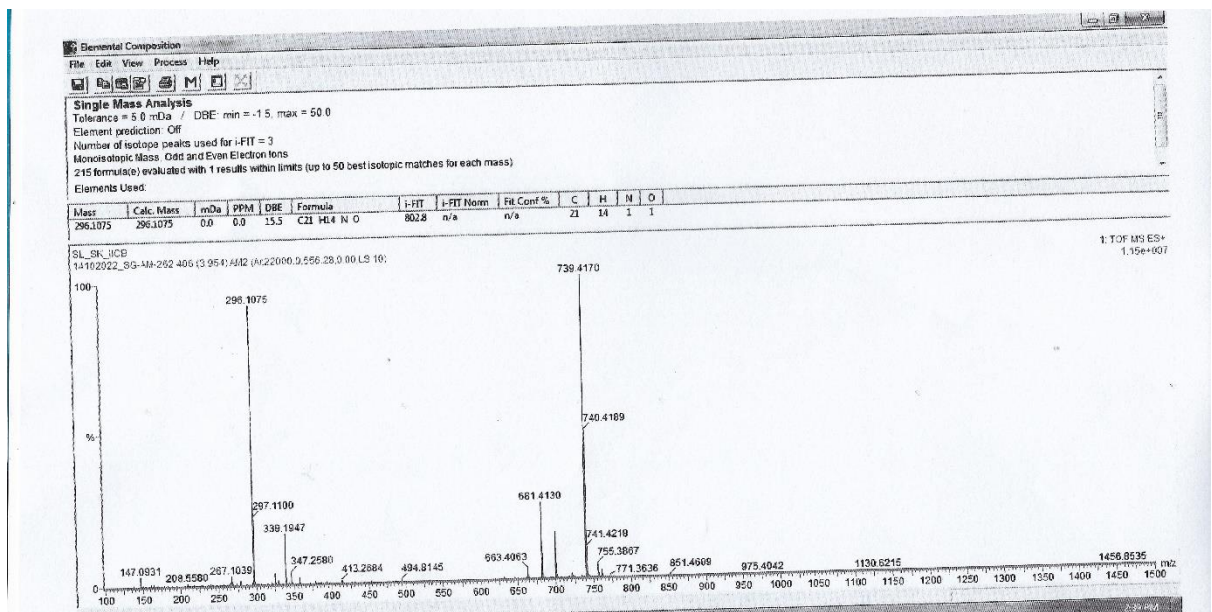


Figure 1.74 Mass spectrum of **6i** (ESI-TOF) m/z: $[M+H]^+$

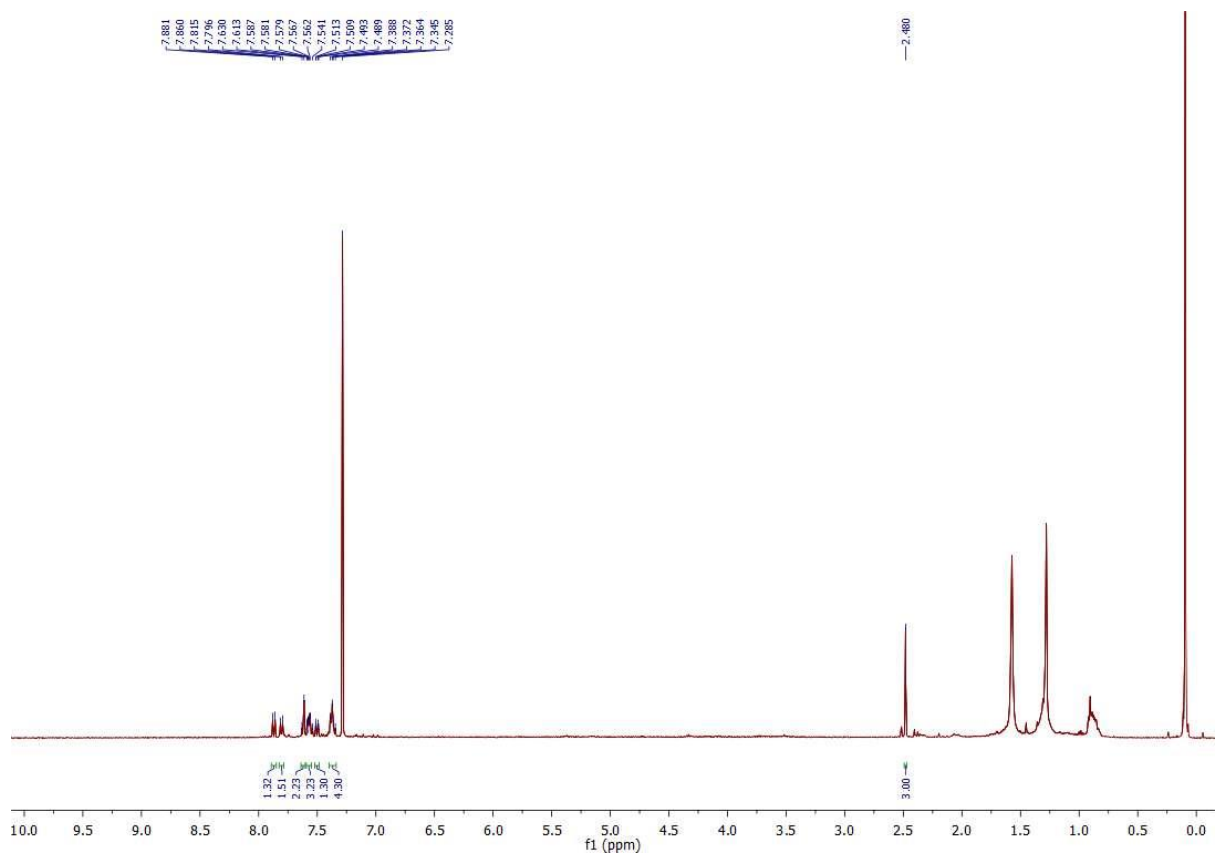


Figure 1.75 ¹H NMR spectrum of **6j** (400 MHz, CDCl₃)

Chapter 1

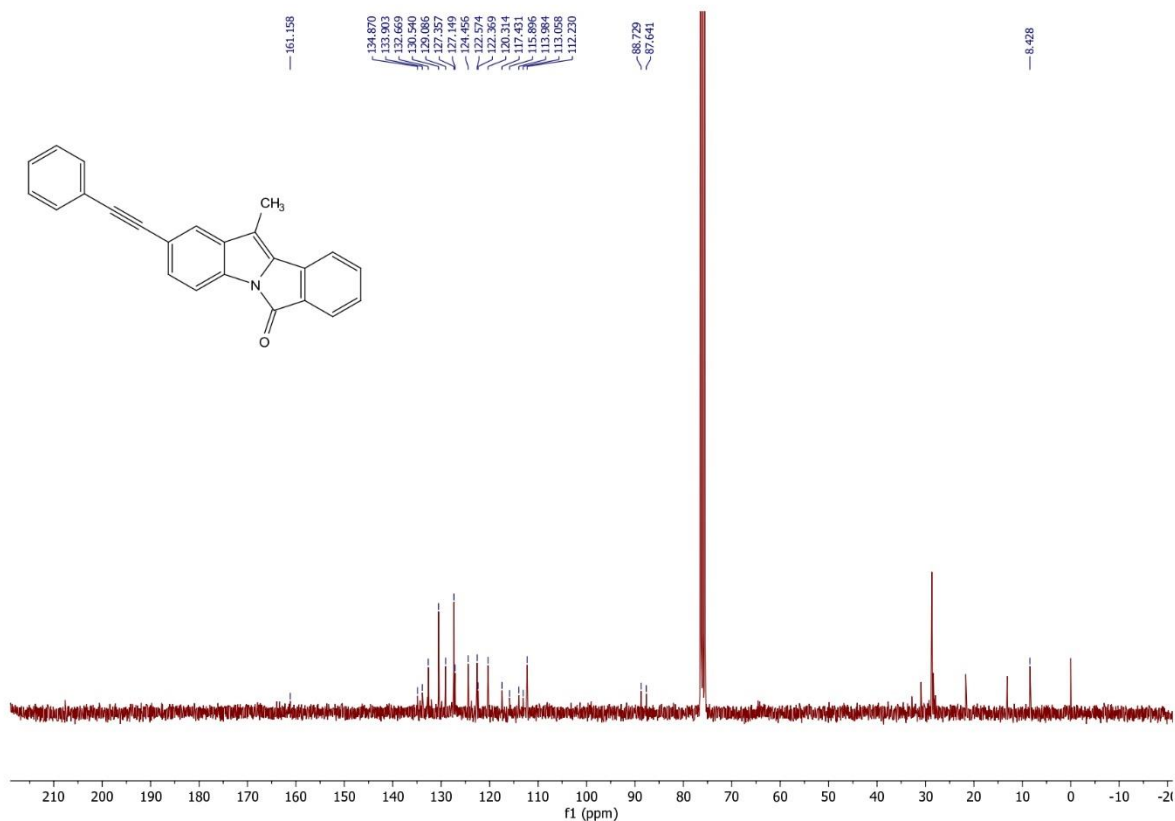


Figure 1.76 ¹³C NMR spectrum of **6j** (100 MHz, CDCl₃)

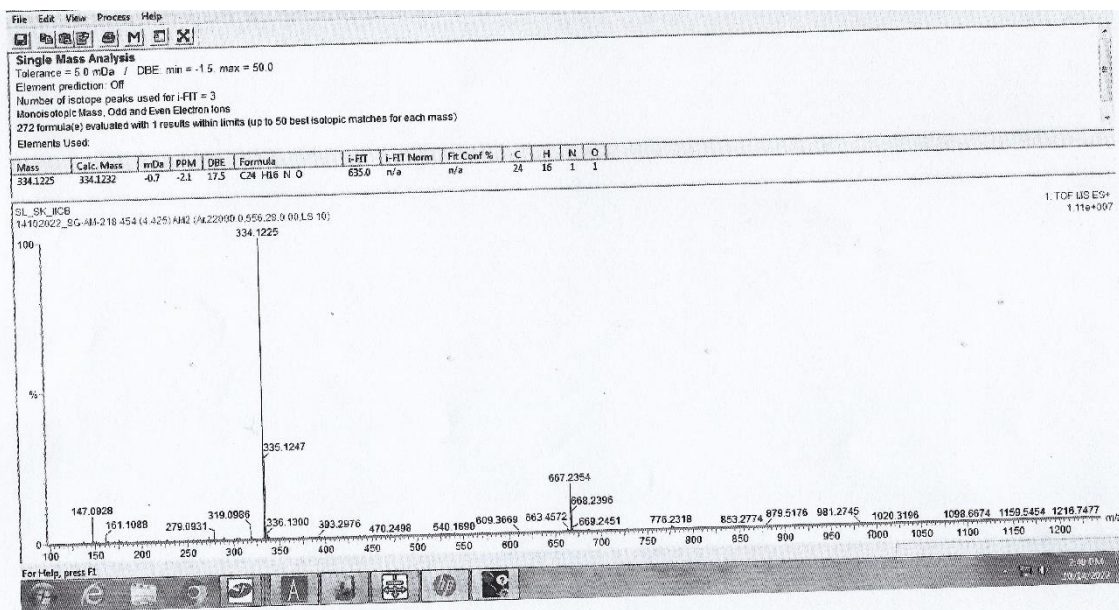


Figure 1.77 Mass spectrum of **6j** (ESI-TOF) m/z : [M+H]⁺

Chapter 1

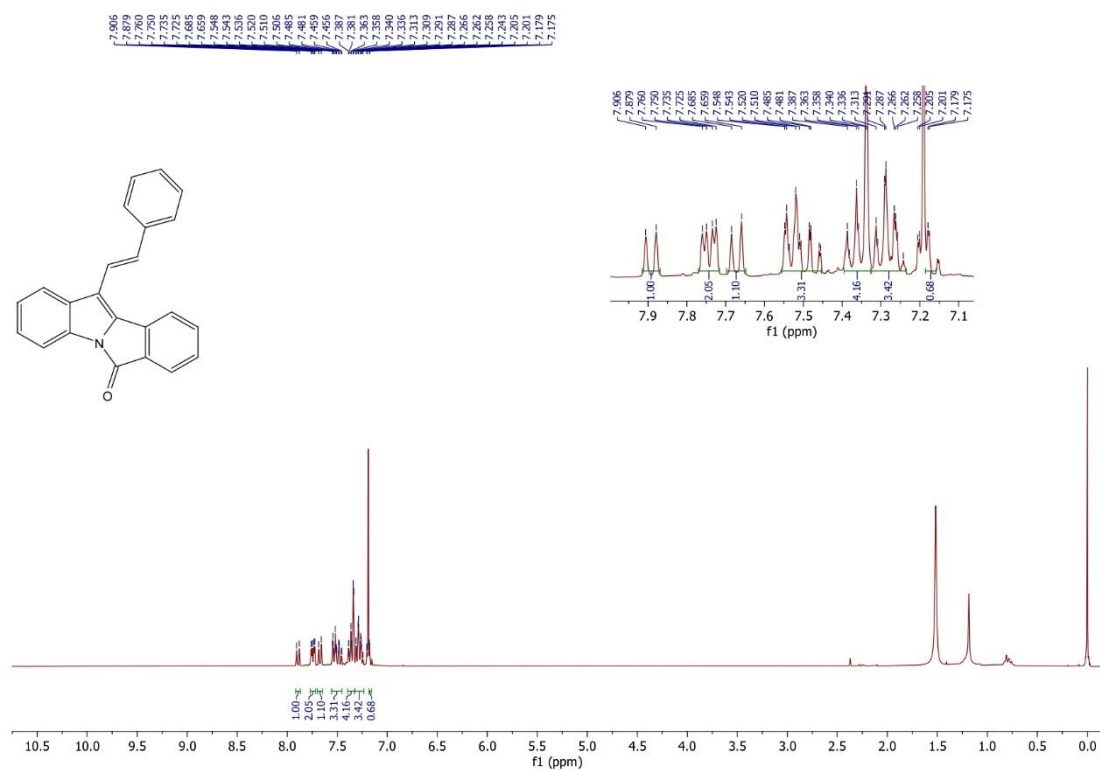


Figure 1.78 ¹H NMR spectrum of **29ka** (300 MHz, CDCl₃)

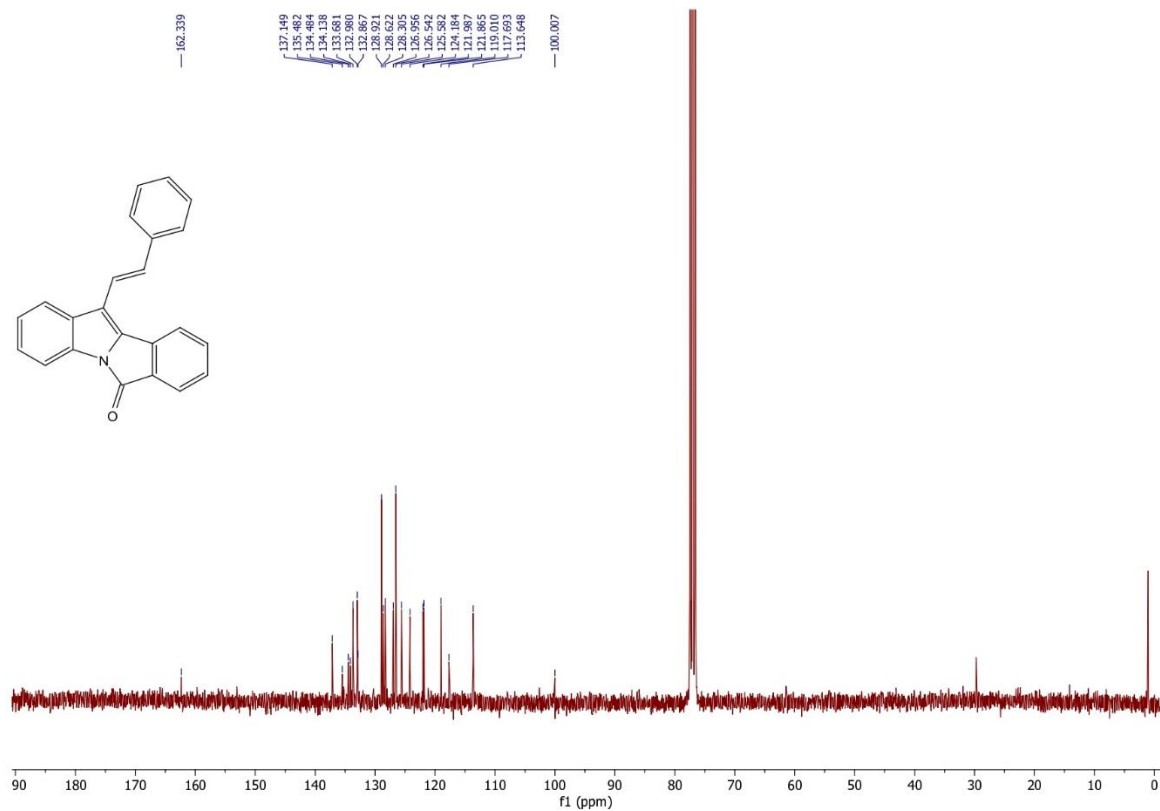


Figure 1.79 ¹³C NMR spectrum of **29ka** (75 MHz, CDCl₃)

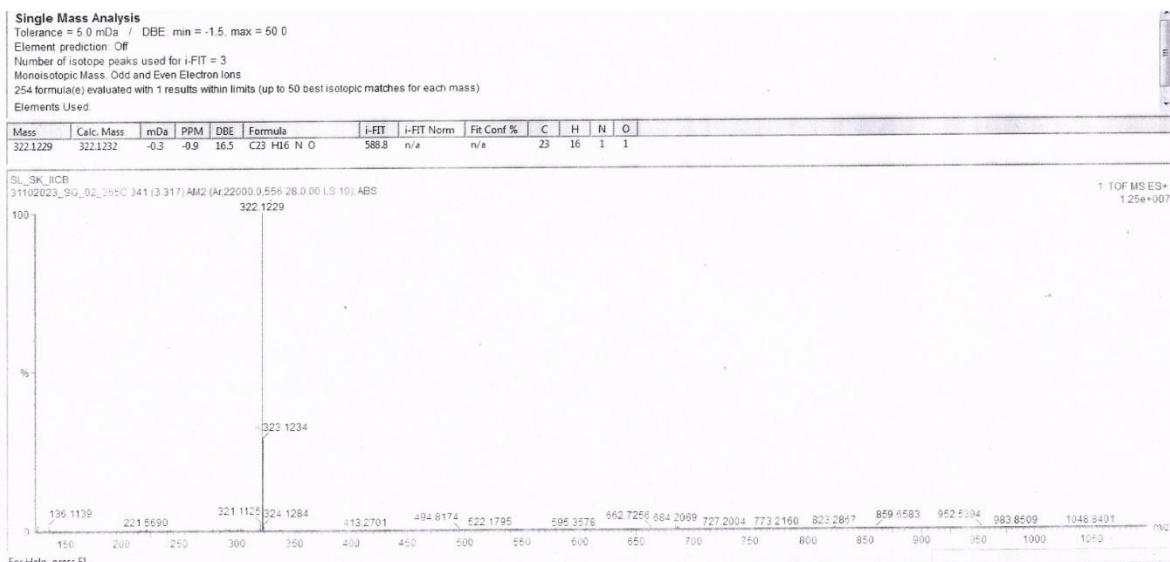


Figure 1.80 Mass spectrum of **29ka** (ESI-TOF) m/z: [M+H]⁺

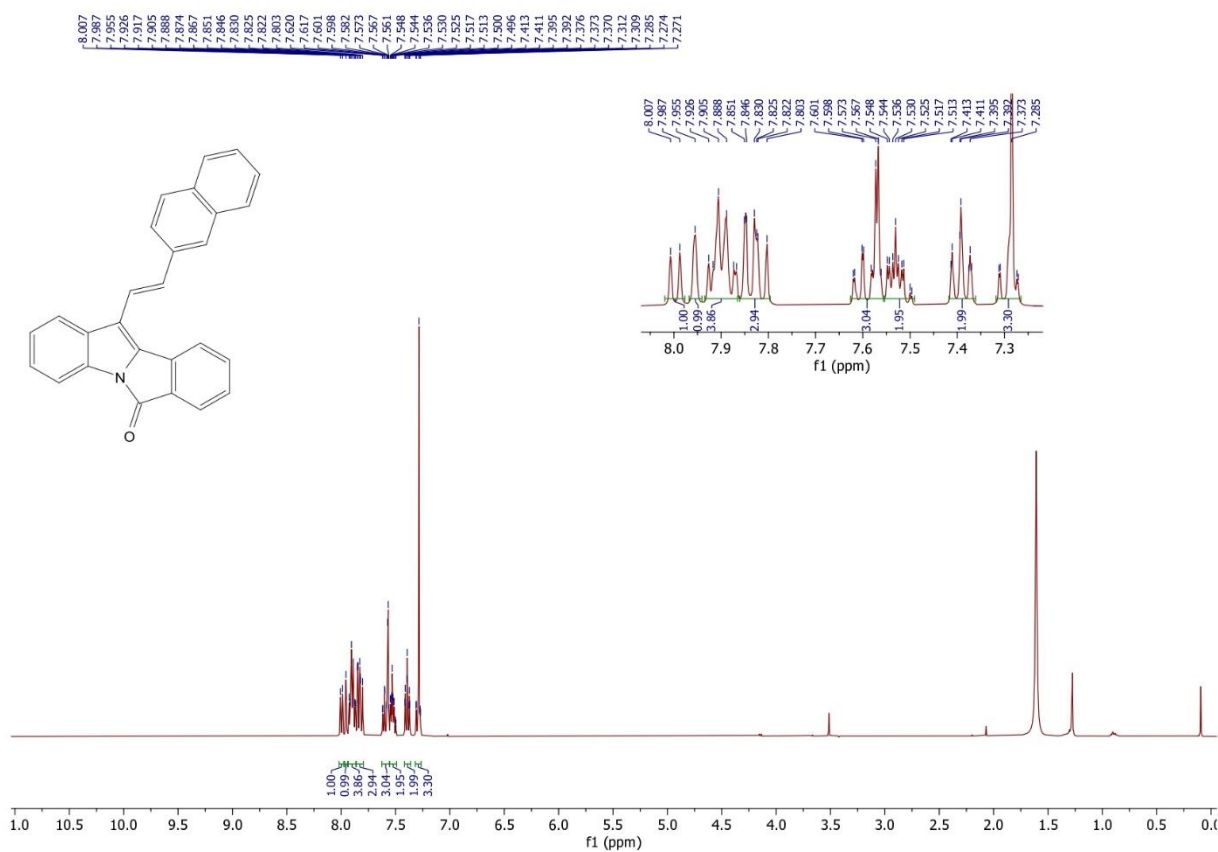


Figure 1.81 ^1H NMR spectrum of **29la** (400 MHz, CDCl_3)

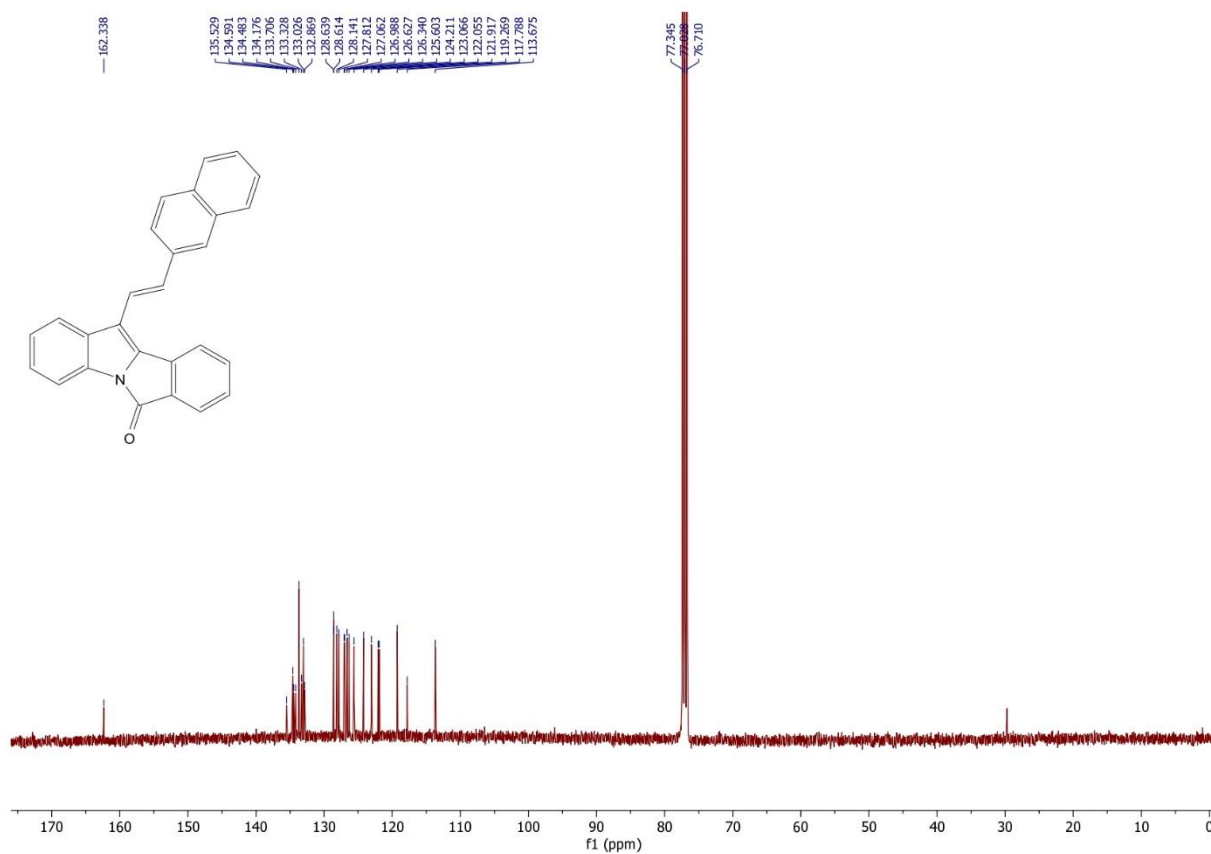


Figure 1.82 ¹³C NMR spectrum of **13la** (400 MHz, CDCl₃)

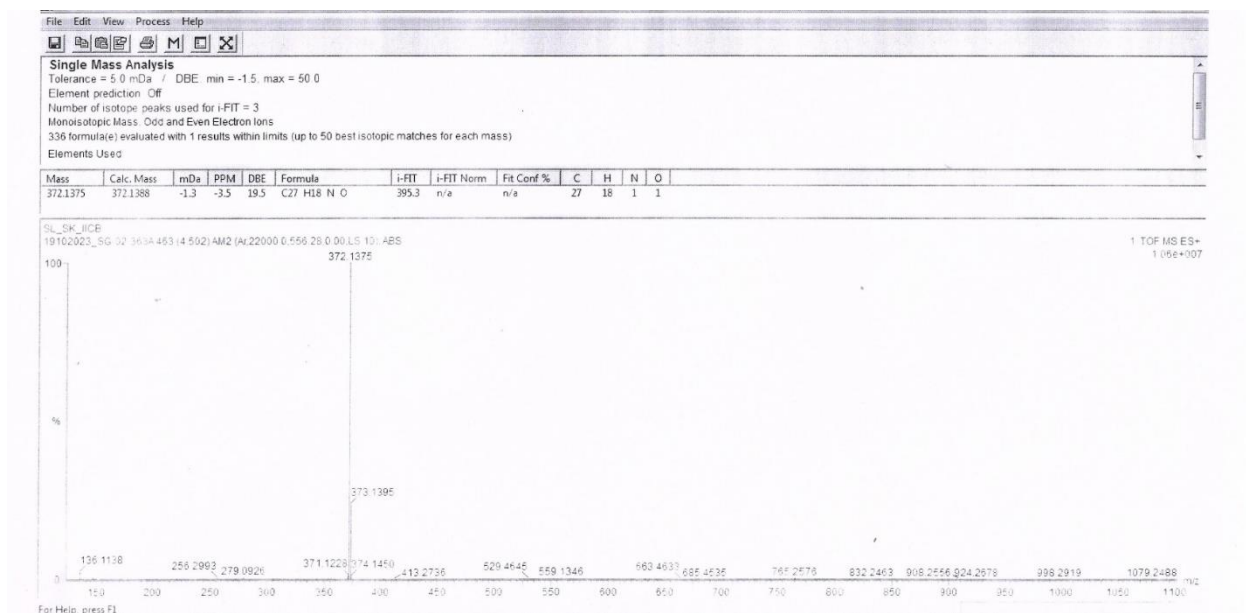


Figure 1.83 Mass spectrum of **29la** (ESI-TOF) m/z: [M+H]⁺

Chapter 1

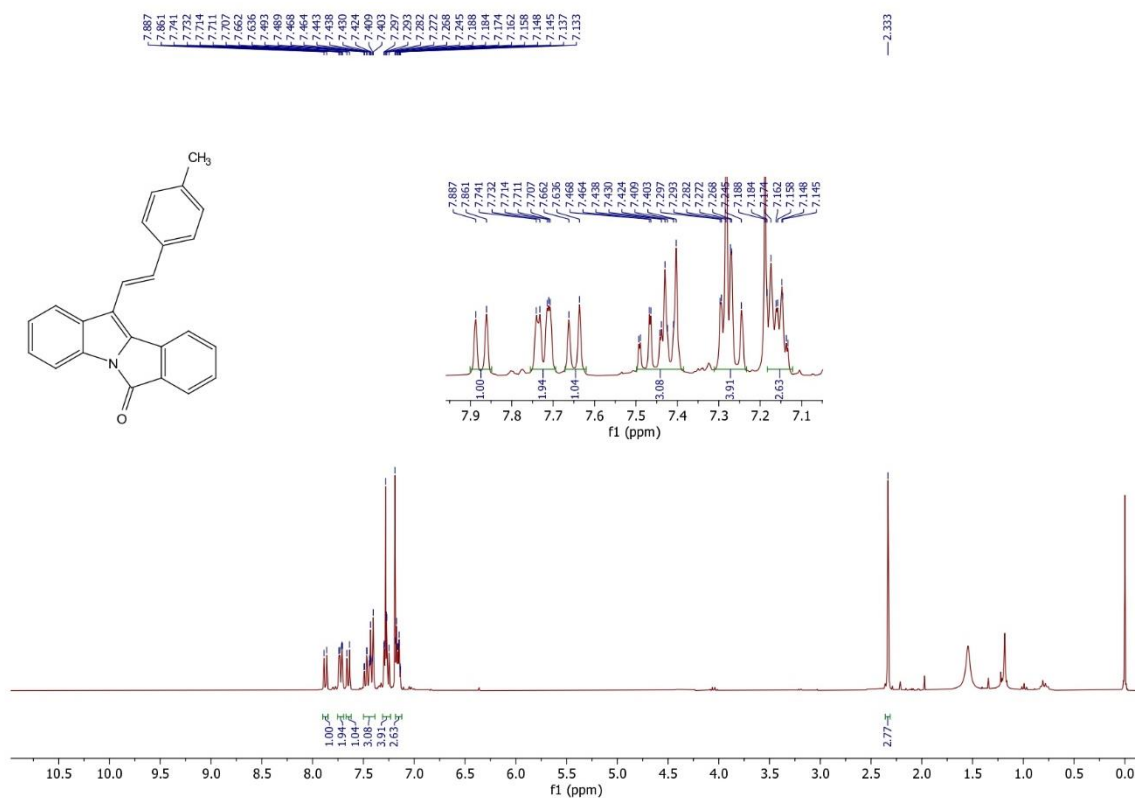


Figure 1.84 ¹H NMR spectrum of **29ma** (300 MHz, CDCl₃)

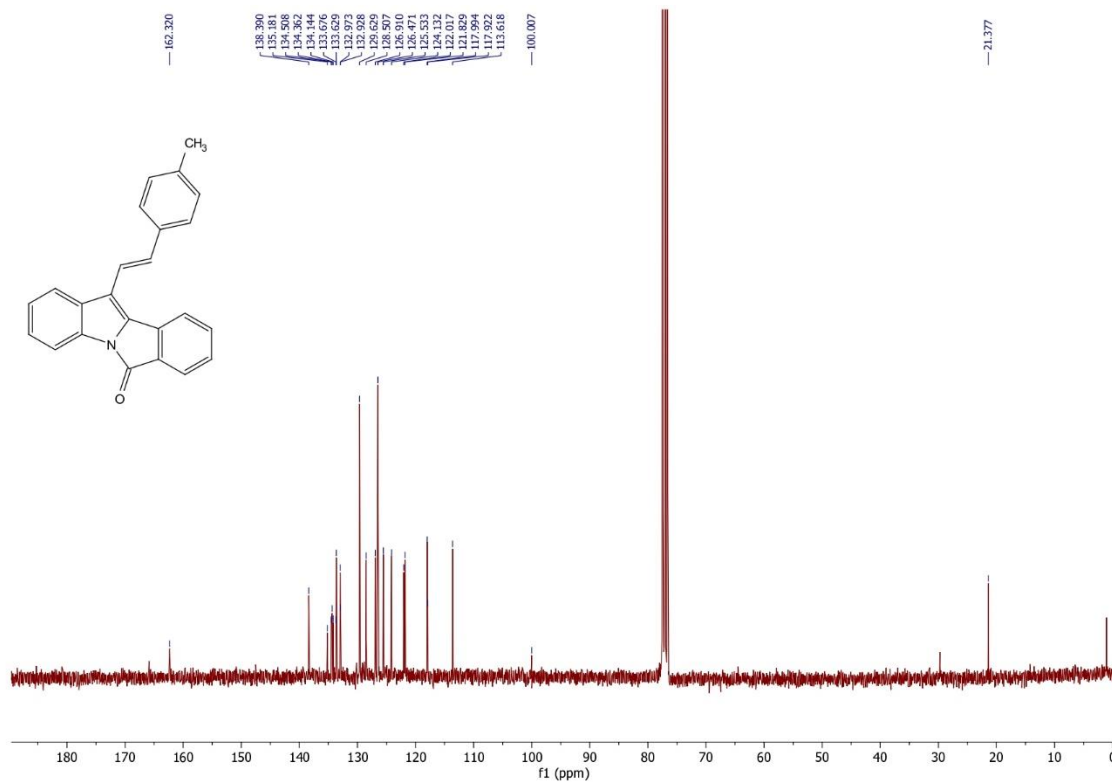


Figure 1.85 ¹³C NMR spectrum of **29ma** (75 MHz, CDCl₃)

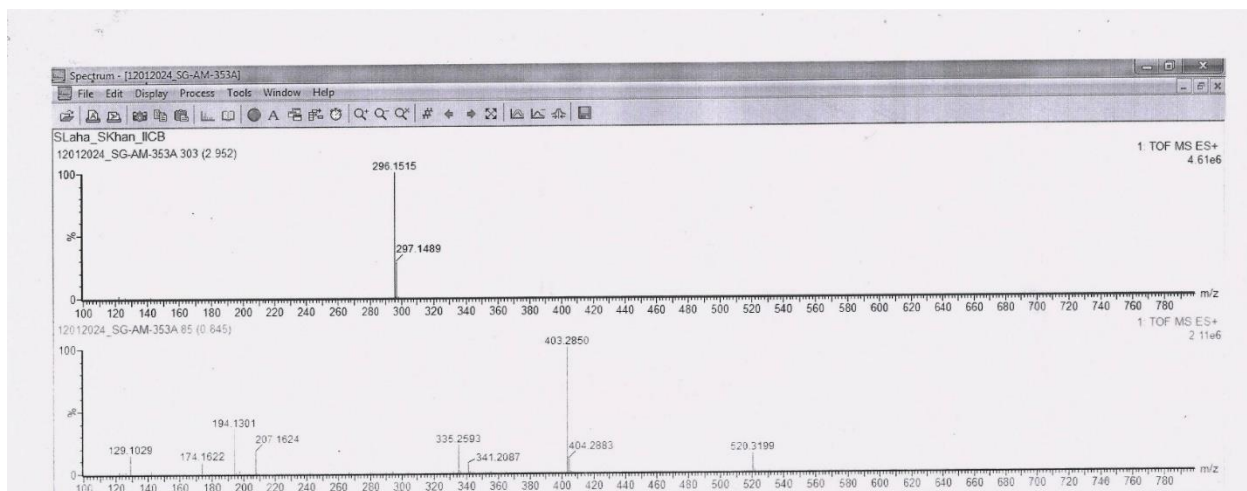


Figure 1.86 Mass spectrum of **29ma** (ESI-TOF) m/z: M^+

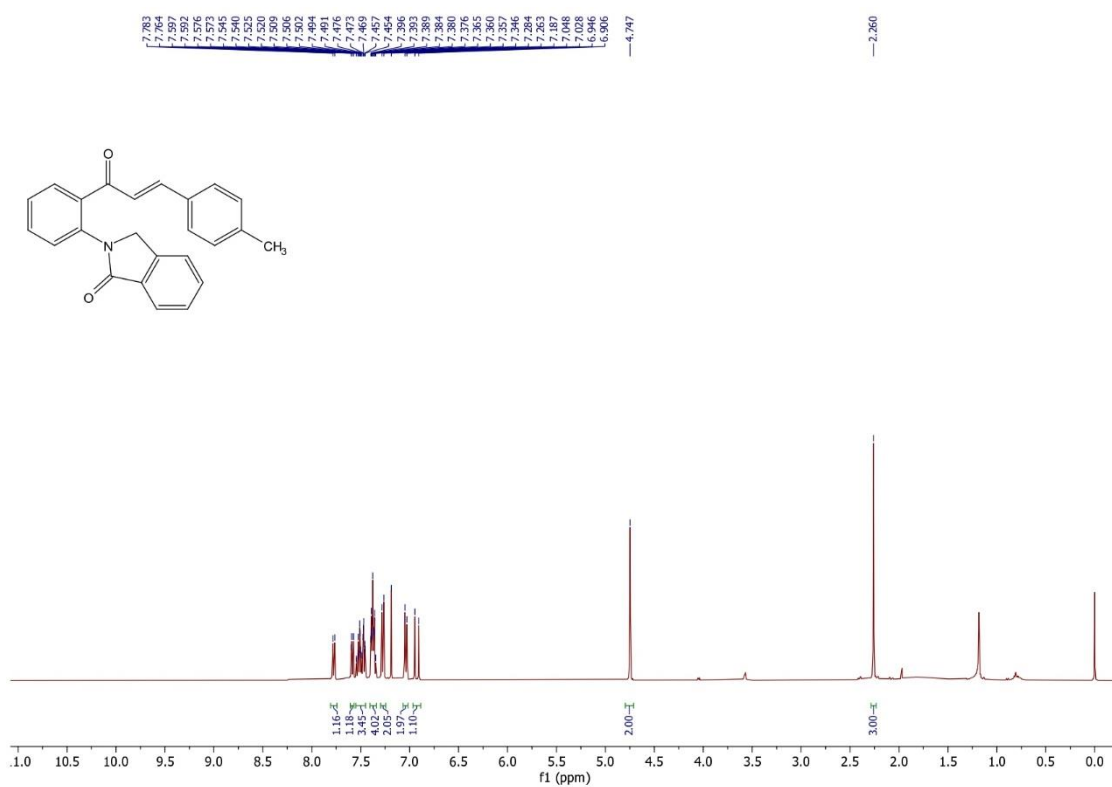


Figure 1.87 1H NMR spectrum of **29mb** (400 MHz, $CDCl_3$)

Chapter 1

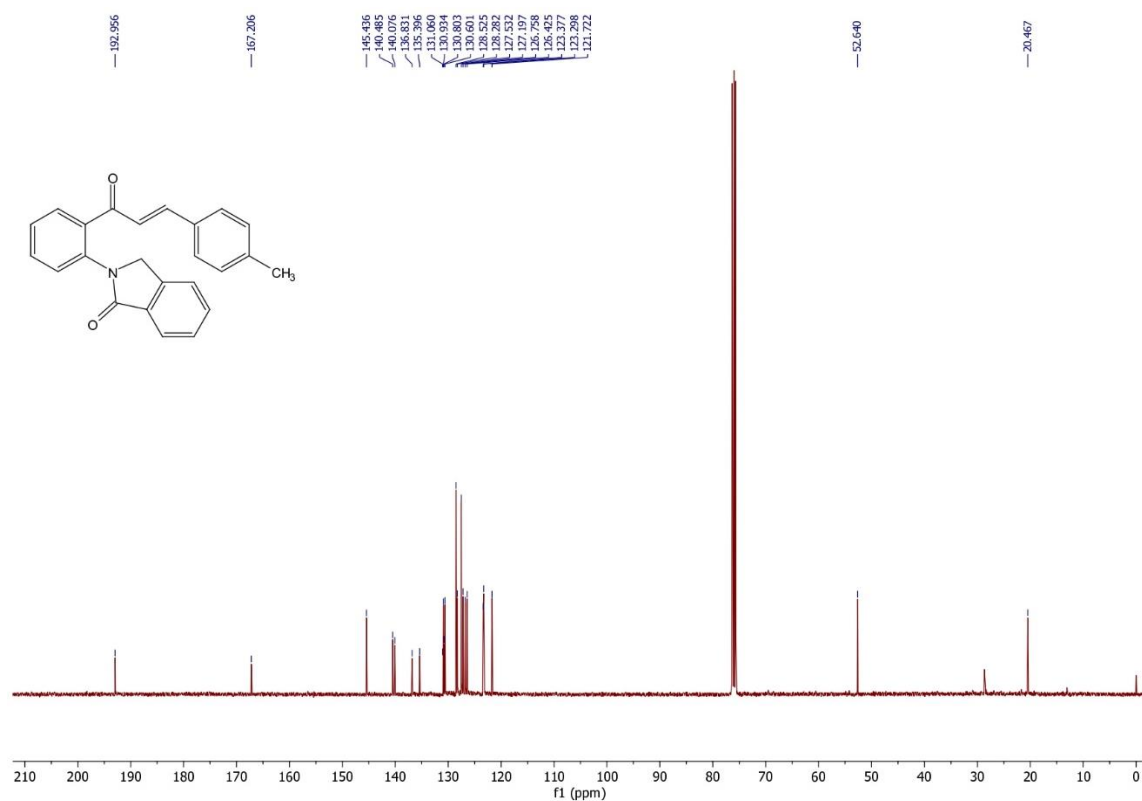


Figure 1.88 ¹³C NMR spectrum of **29mb** (75 MHz, CDCl₃)

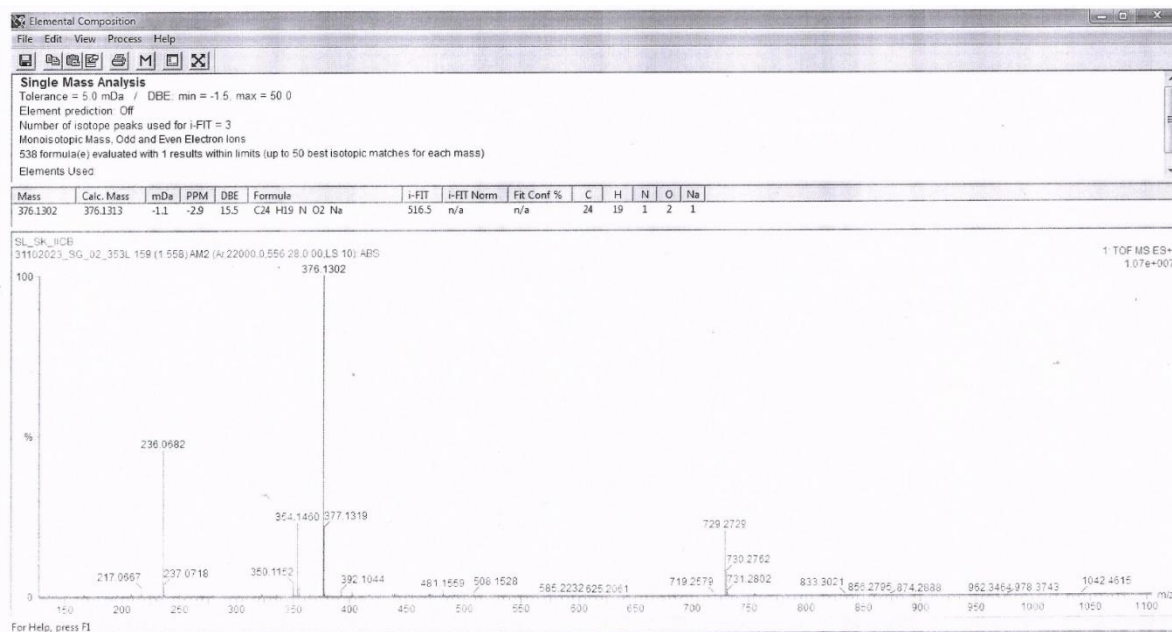


Figure 1.89 Mass spectrum of **29mb** (ESI-TOF) m/z: [M+Na]⁺

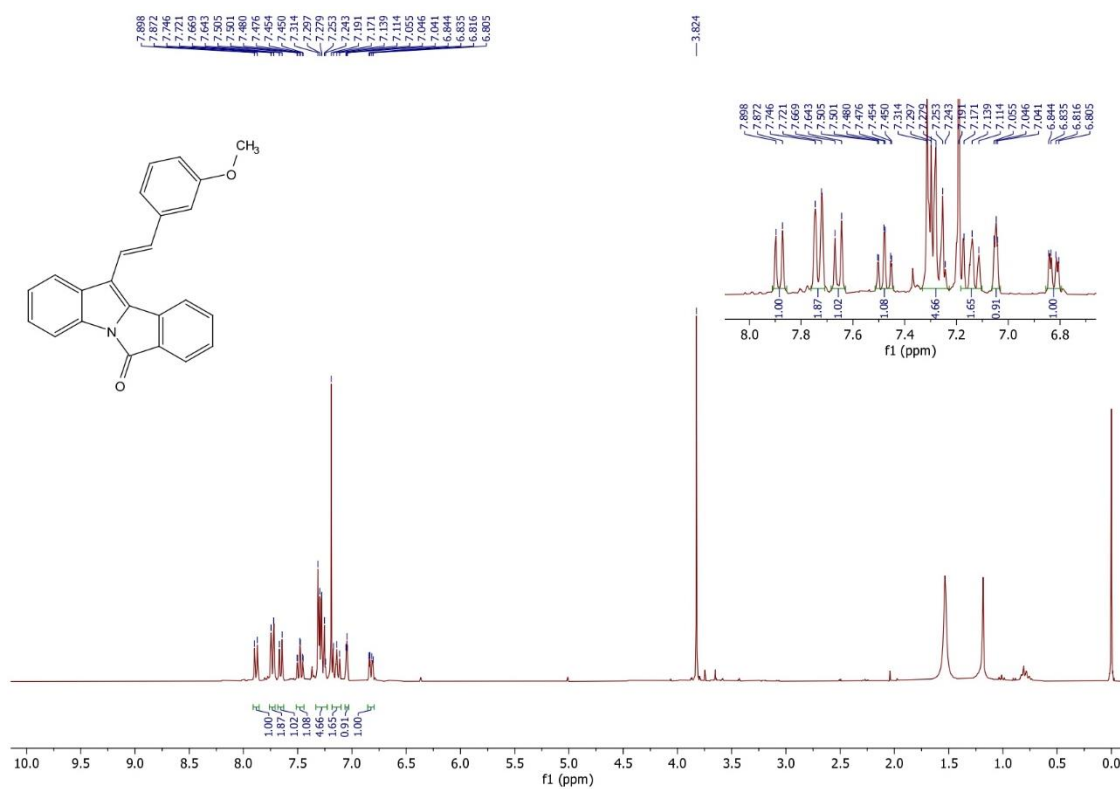


Figure 1.90 ¹H NMR spectrum of **29na** (300 MHz, CDCl₃)

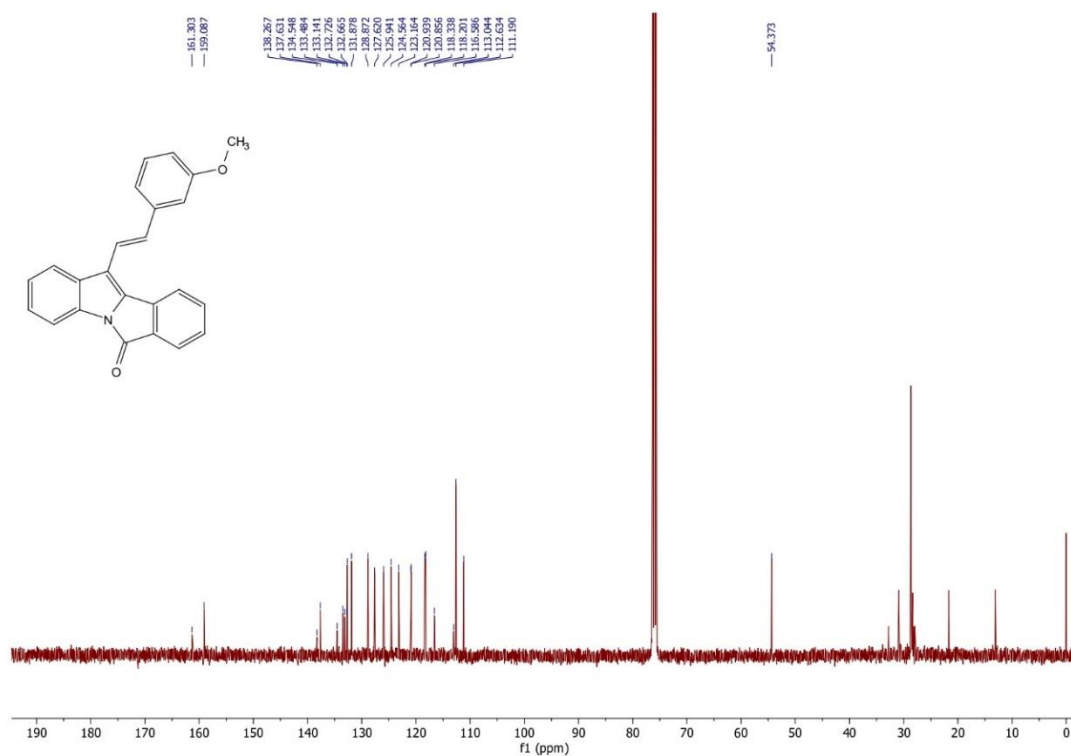


Figure 1.91 ¹³C NMR spectrum of **29na** (100 MHz, CDCl₃)

Chapter 1

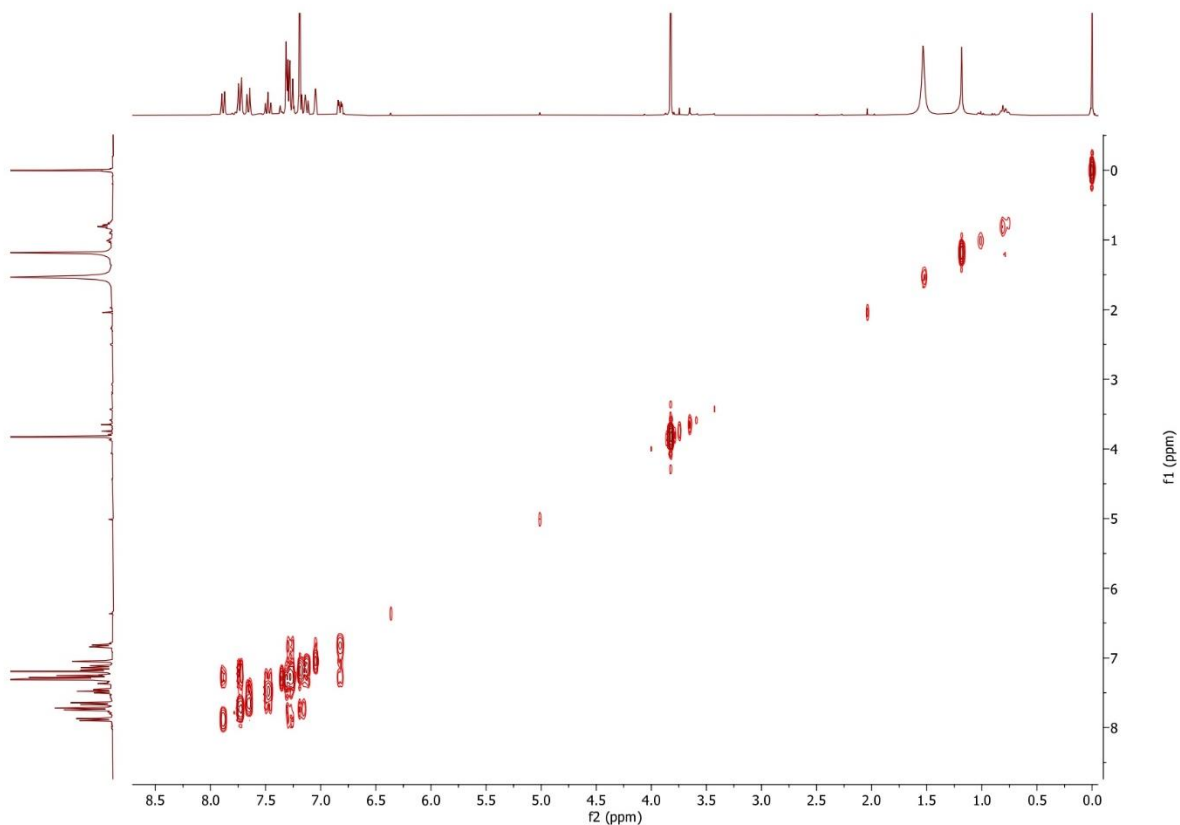


Figure 1.92 ^1H - ^1H COSY NMR spectrum of **29na** (400 MHz, CDCl_3)

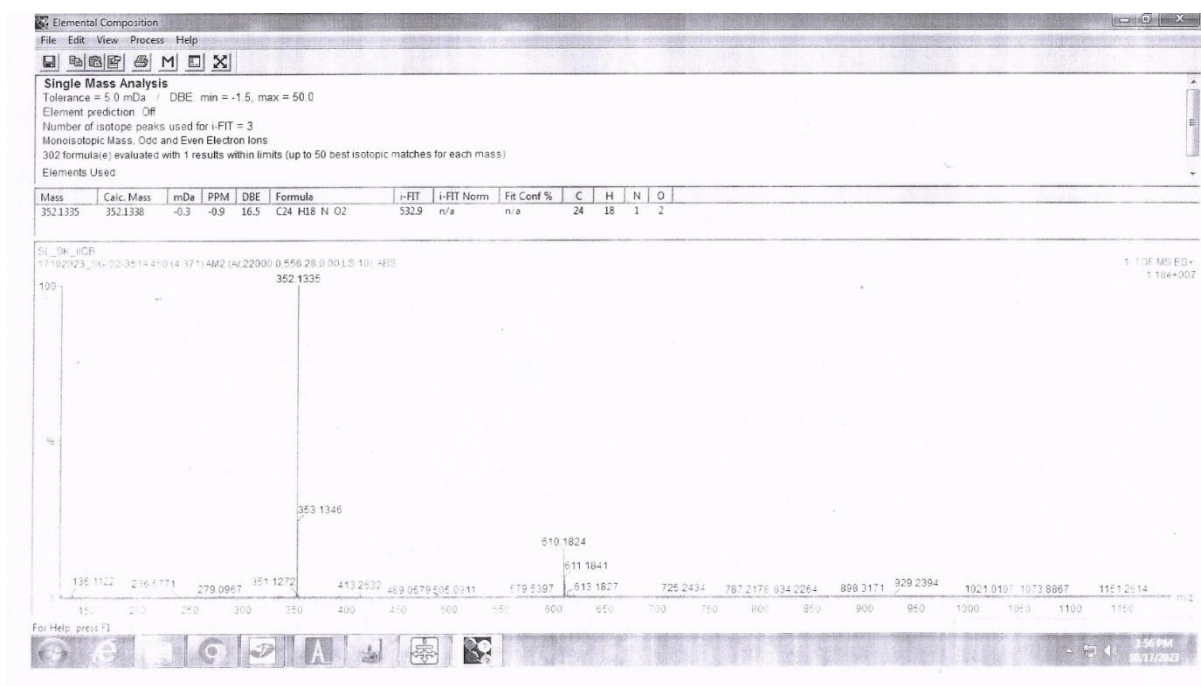


Figure 1.93 Mass spectrum of **29na** (ESI-TOF) m/z : $[\text{M}+\text{H}]^+$

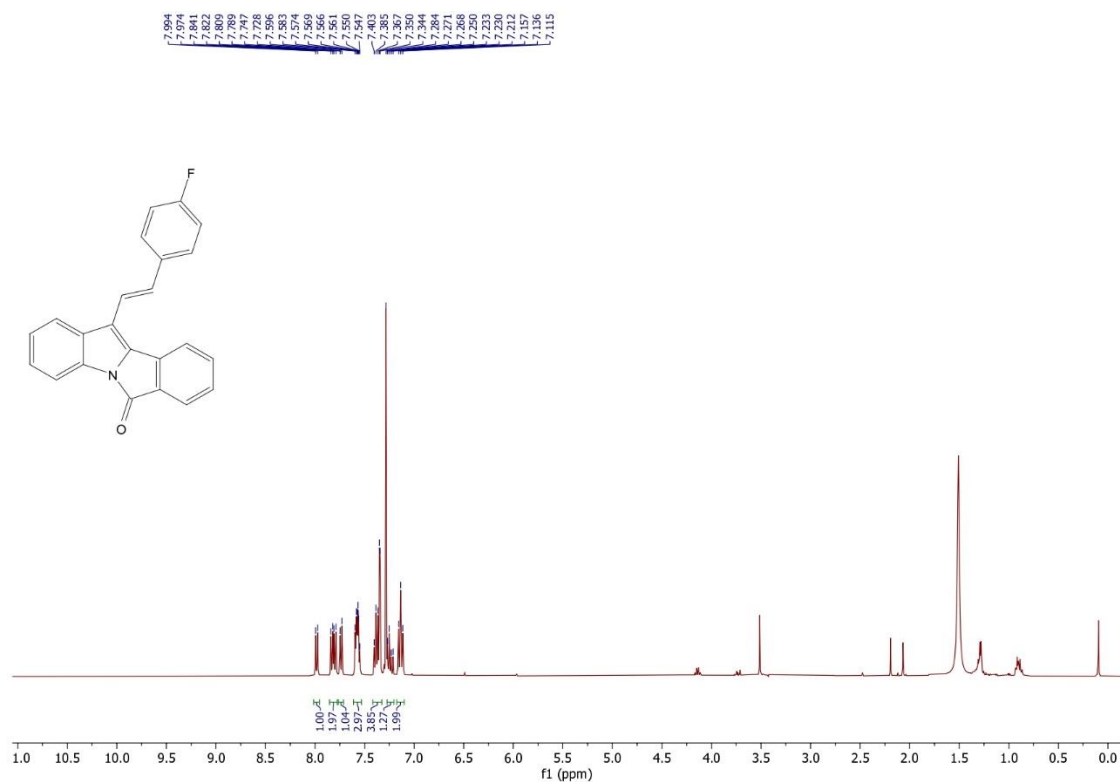


Figure 1.94 ¹H NMR spectrum of **29oa** (400 MHz, CCl₄+CDCl₃)

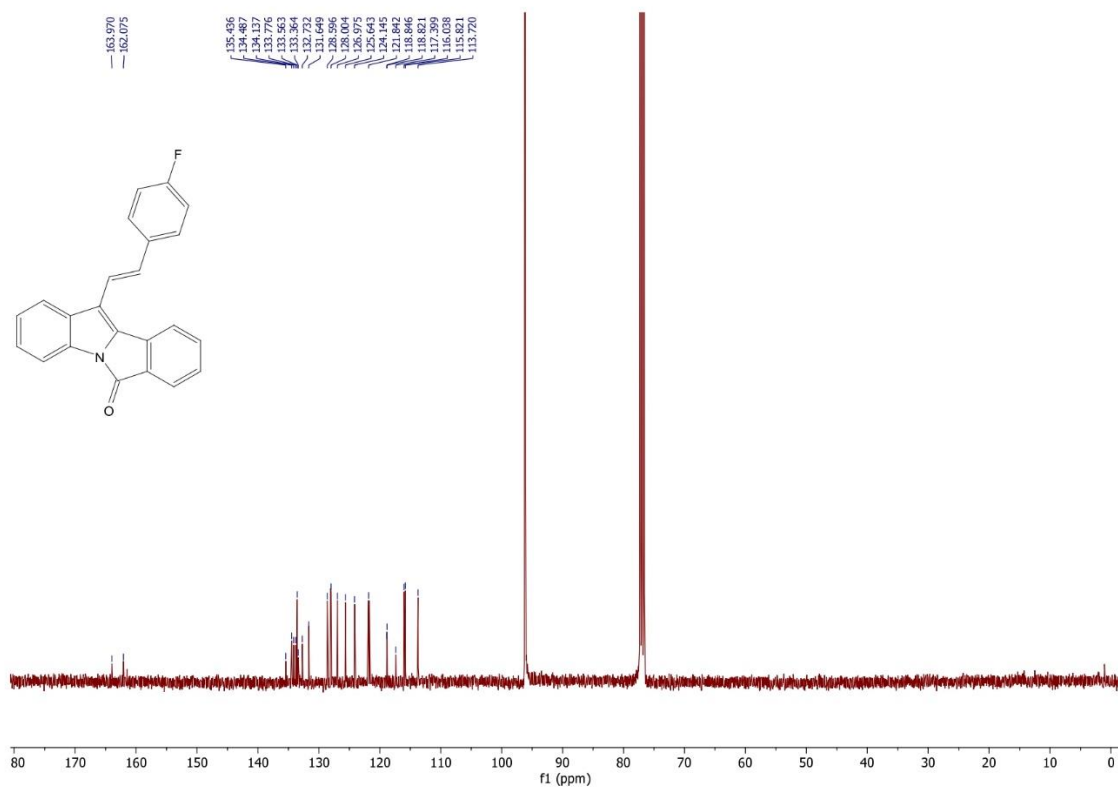


Figure 1.95 ¹³C NMR spectrum of **29oa** (100 MHz, CCl₄+CDCl₃)

Chapter 1

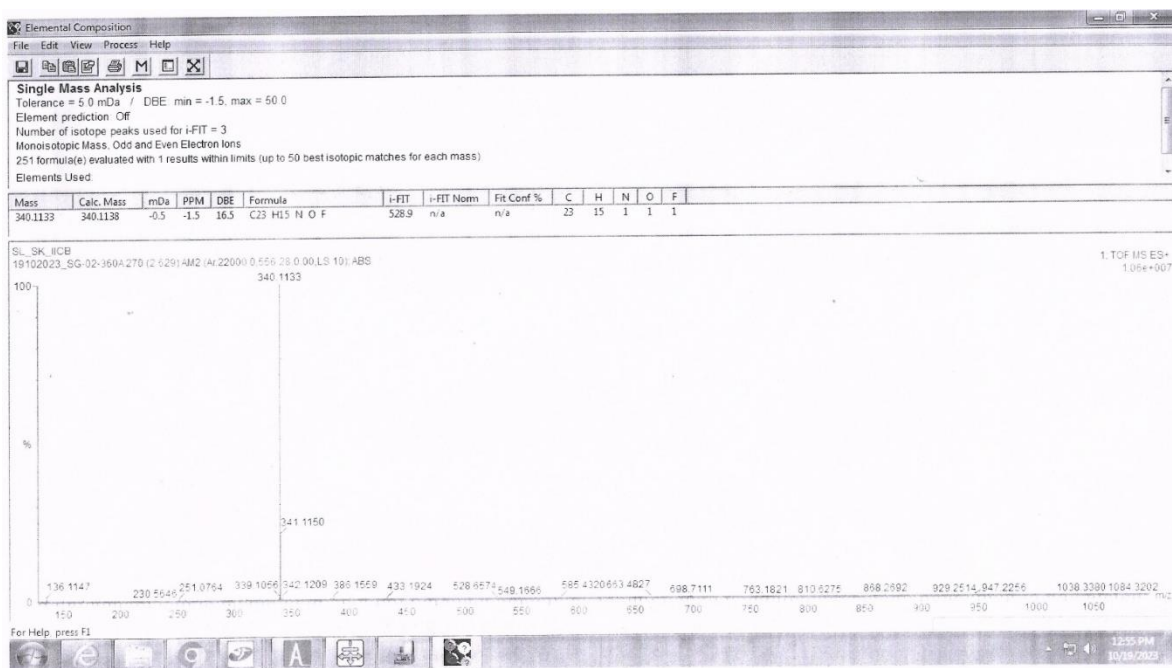


Figure 1.96 Mass spectrum of **290a** (ESI-TOF) m/z : $[M+H]^+$

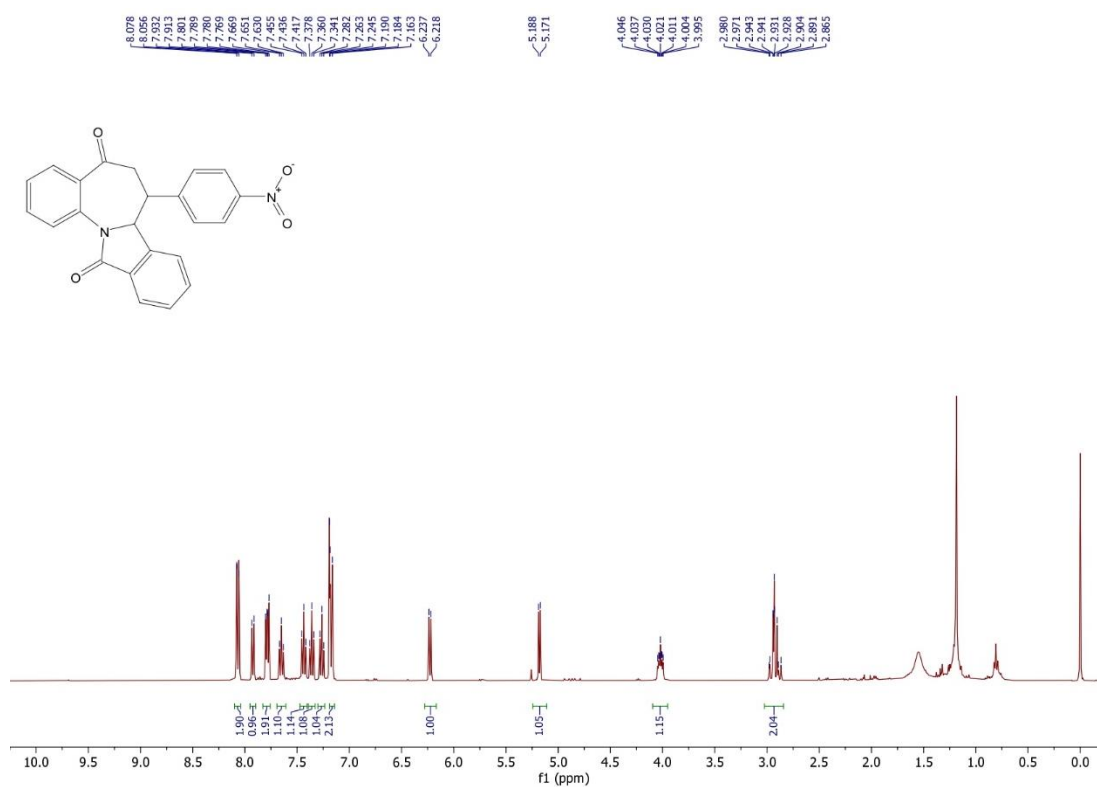


Figure 1.97 ^1H NMR spectrum of **29pa** (400 MHz, CDCl_3)

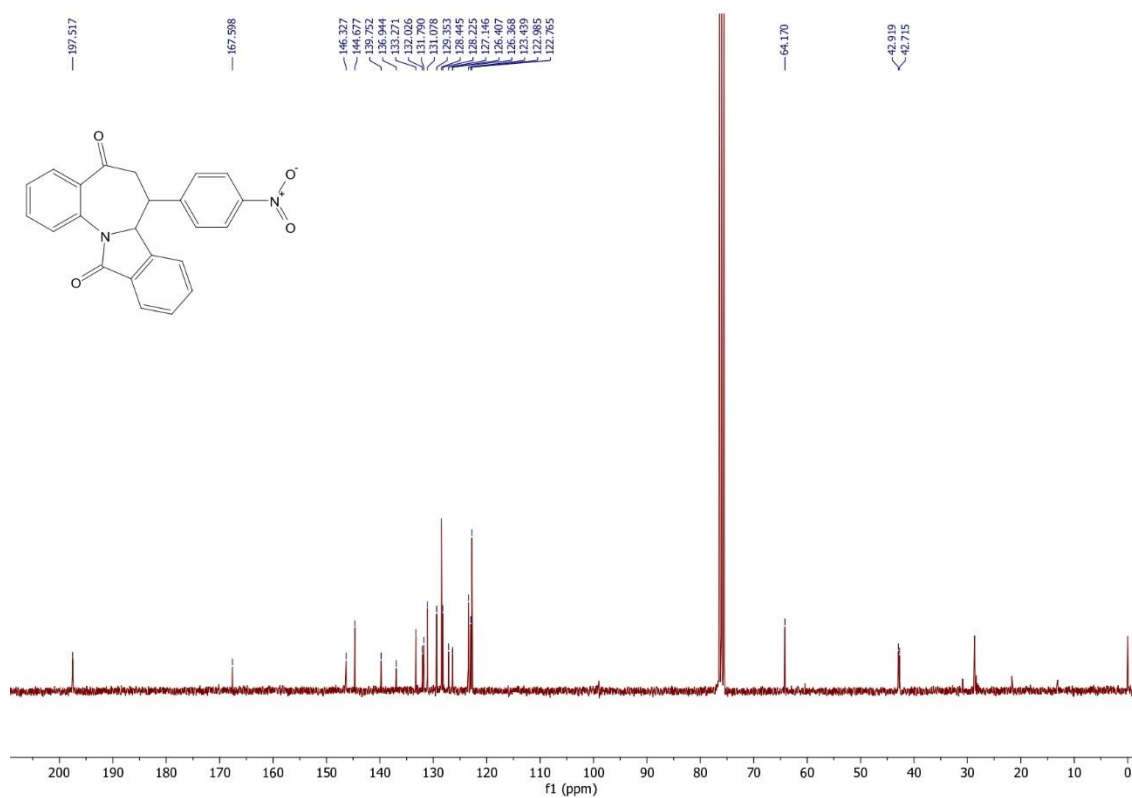


Figure 1.98 ^{13}C NMR spectrum of **29pa** (75 MHz, CDCl_3)

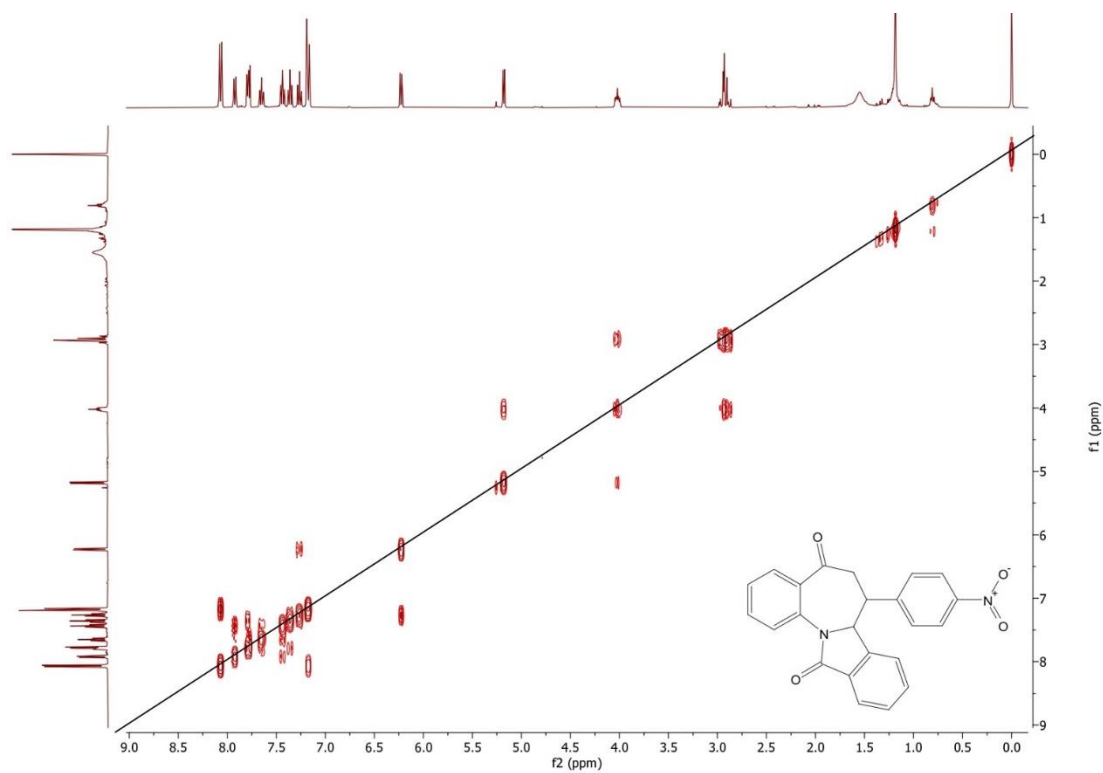


Figure 1.99 ^1H - ^1H COSY NMR spectrum of **29pa** (400 MHz, CDCl_3)

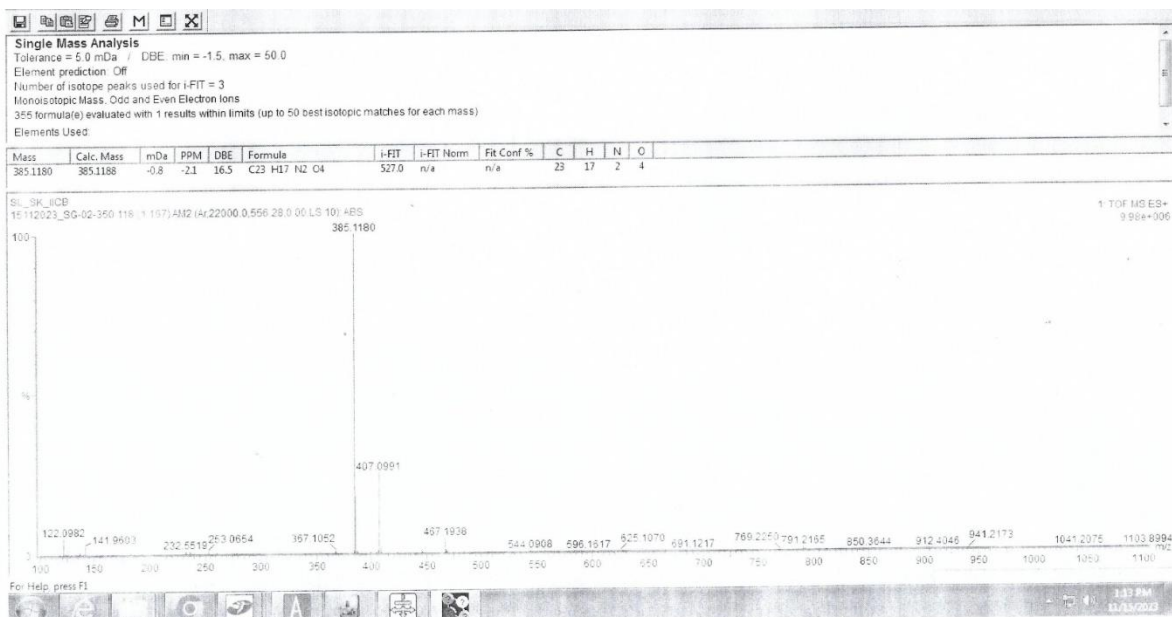


Figure 1.100 Mass spectrum of **29pa** (ESI-TOF) m/z: [M+H]⁺

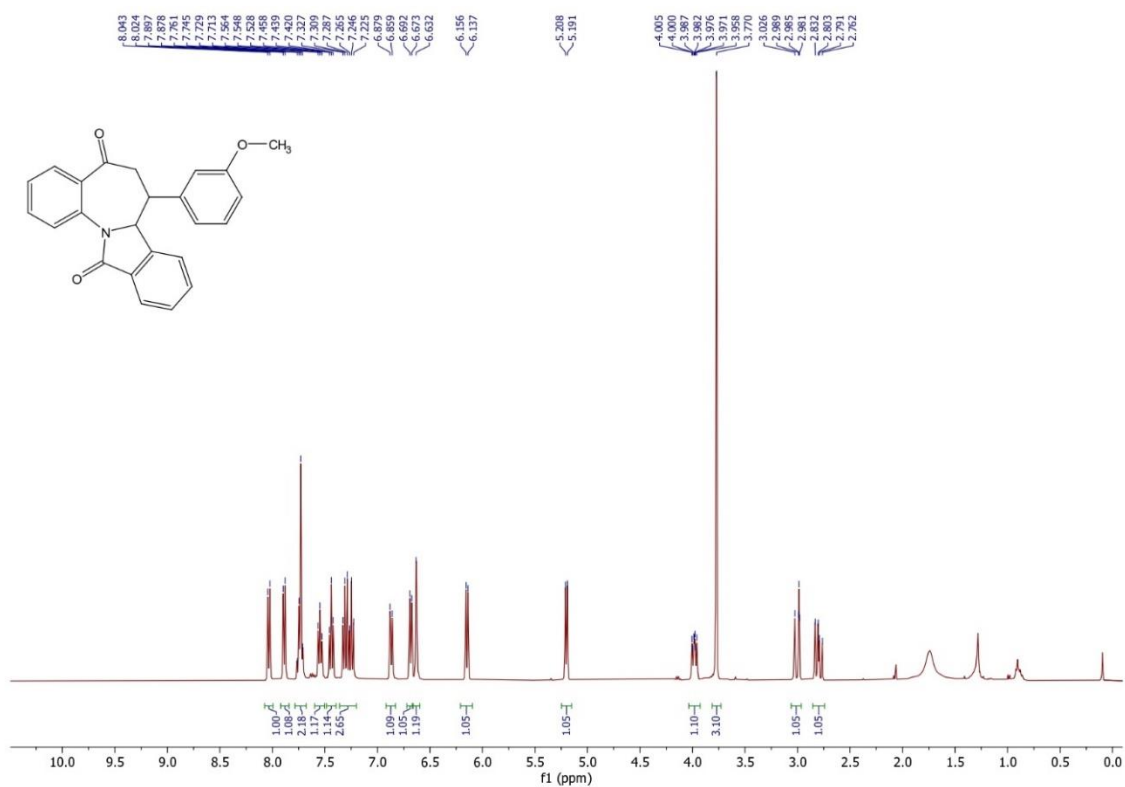


Figure 1.101 ^1H NMR spectrum of **29nb** (400 MHz, CDCl_3)

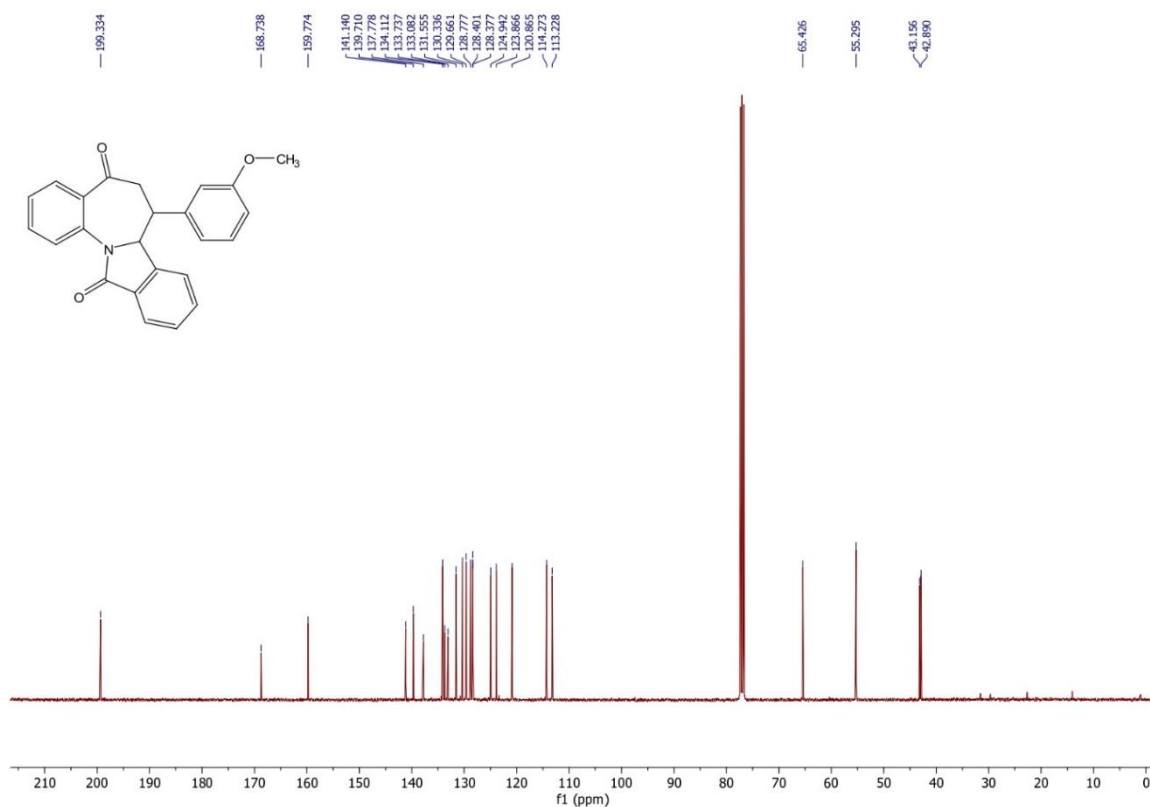


Figure 1.102 ^{13}C NMR spectrum of **29nb** (100 MHz, CDCl_3)

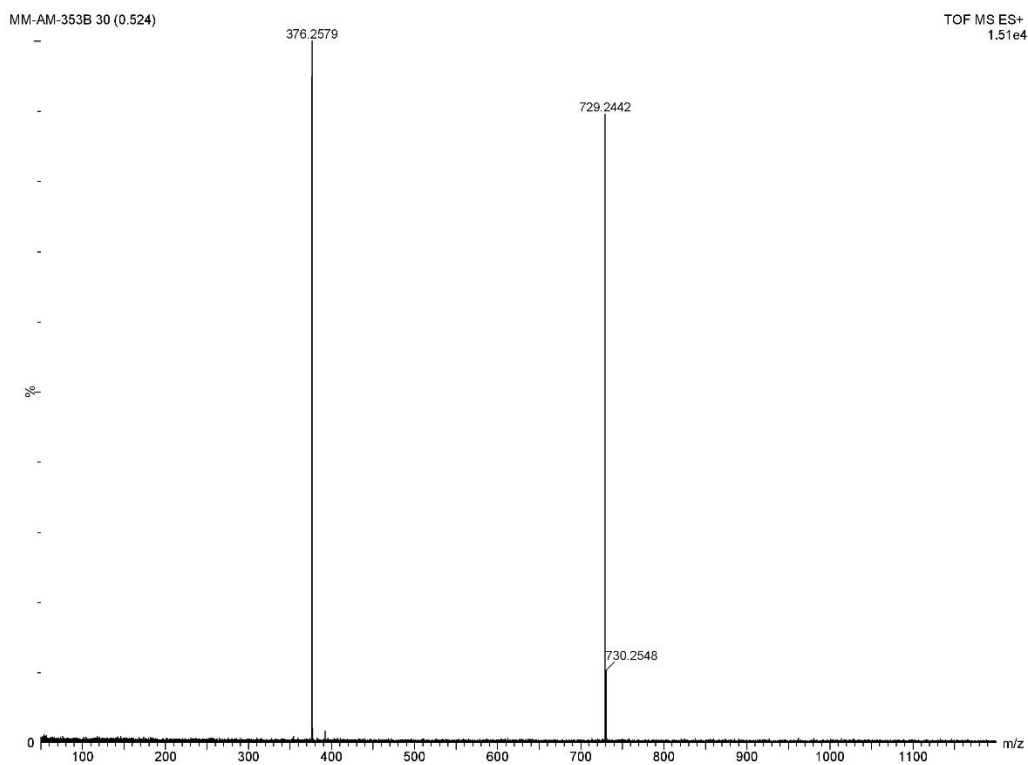
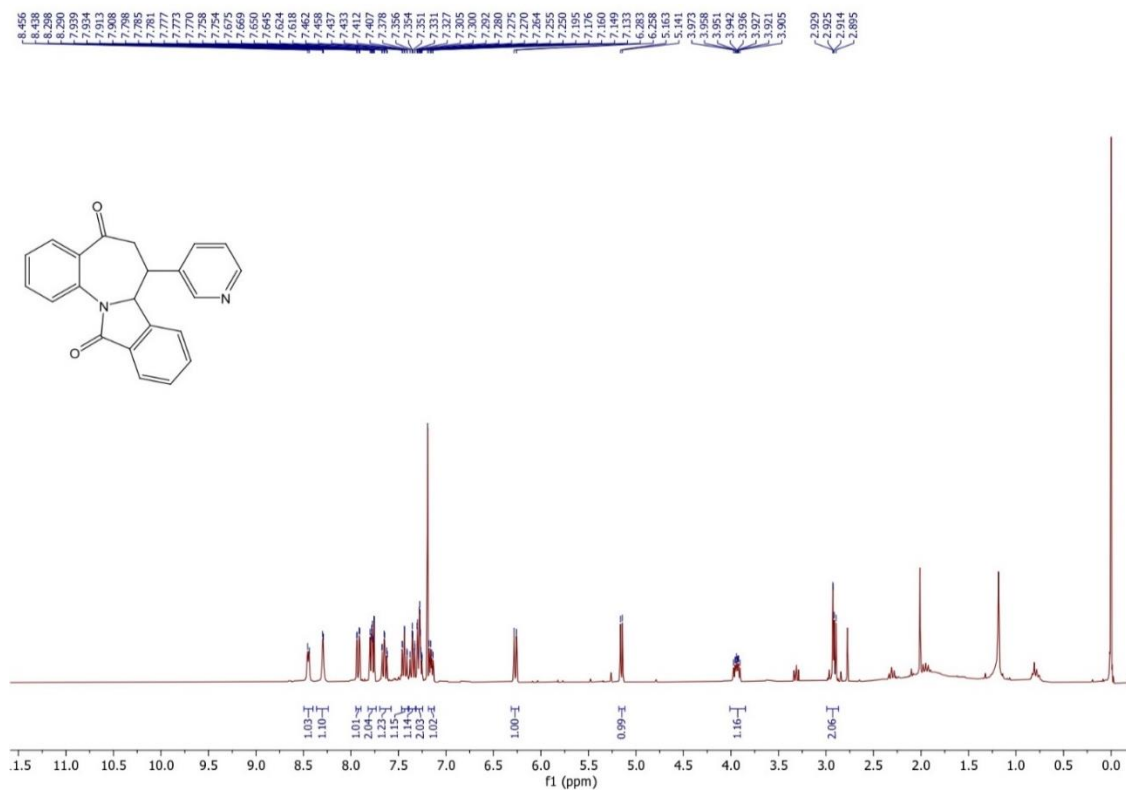
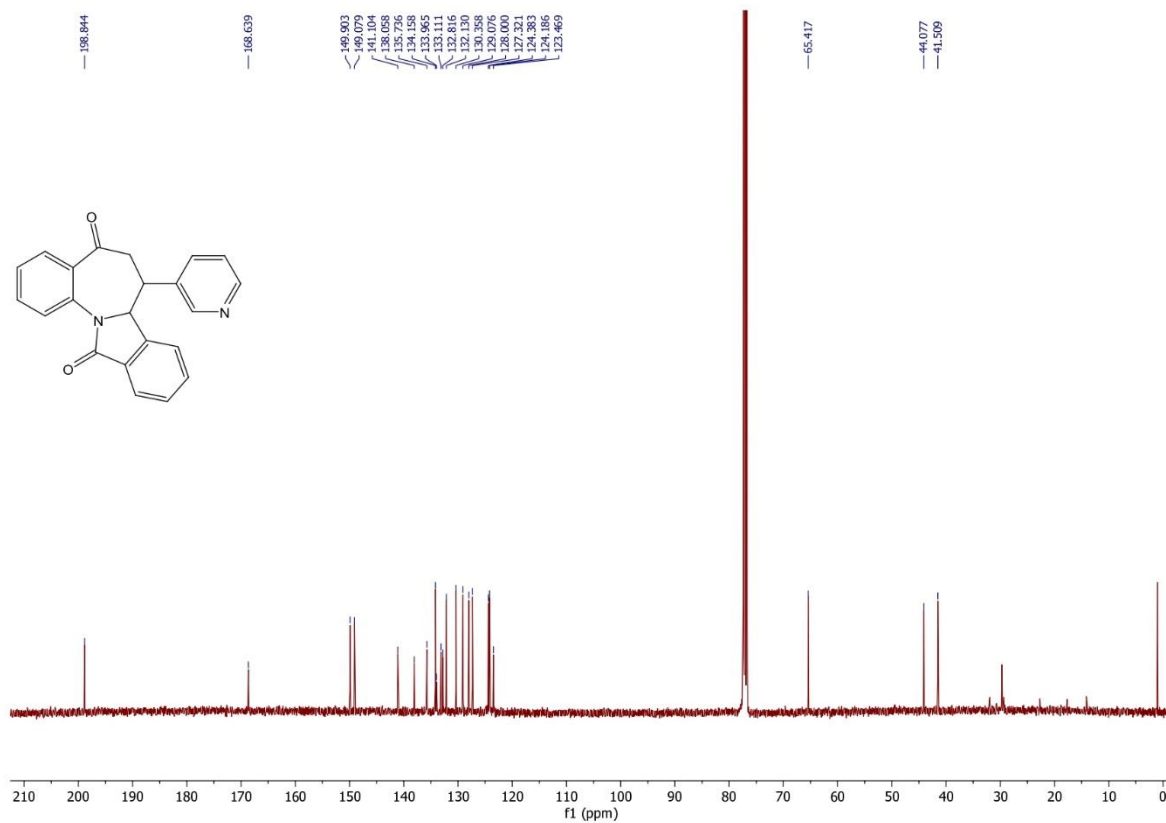


Figure 1.103 Mass spectrum of **29nb** (ESI-TOF) m/z: [M+Na]⁺

Figure 1.104 ¹H NMR spectrum of **29qa** (300 MHz, CDCl₃)Figure 1.105 ¹³C NMR spectrum of **29qa** (100 MHz, CDCl₃)

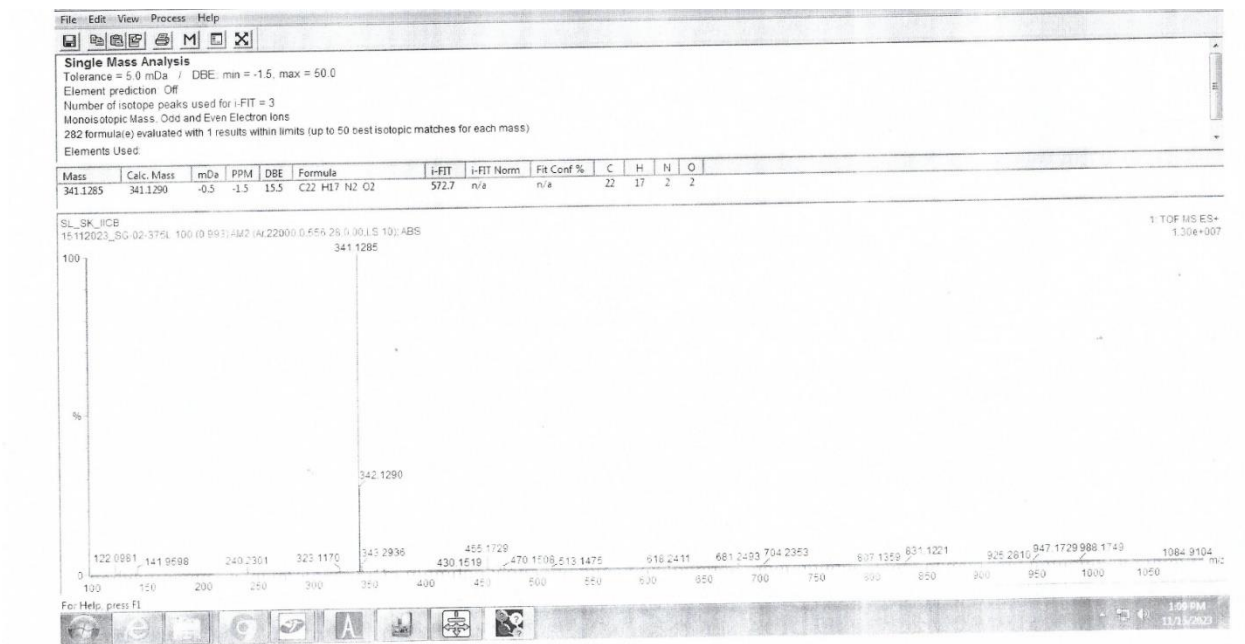


Figure 1.106 Mass spectrum of **29qa** (ESI-TOF) m/z: [M+H]⁺

1.9 CRYSTALLOGRAPHIC TABLE

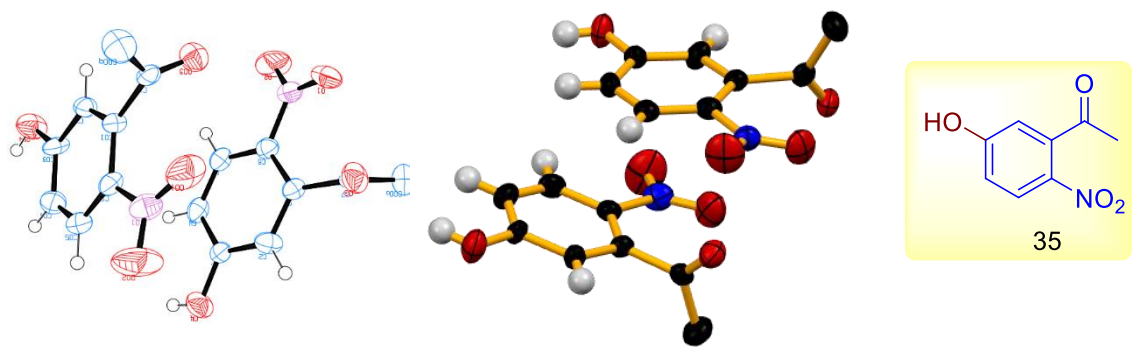


Figure 1.107 ORTEP diagram of **35** (CCDC 2292561)

Table 1.5 Crystallographic and structure refinement parameters for **35**

Emperical formula	C8 H4 N O4
Formula weight	178.12
Crystal system	Triclinic,
space group	P -1
<i>a</i> / Å	7.7827(15)
<i>b</i> /Å	9.695(2)
<i>c</i> / Å	11.087(2)

Chapter 1

$\alpha/^{\circ}$	84.192(5)
$\beta/^{\circ}$	79.572(5)
$\gamma/^{\circ}$	78.353(5)
$V/\text{\AA}^3$	804.0(3)
Z	4
Limiting Indices	$-8 \leq h \leq 8, -11 \leq k \leq 11, -12 \leq l \leq 12$
$D_c/\text{Mg/m}^3$	1.472
μ/mm^{-1}	0.121
T/K	273(2)
θ range/ $^{\circ}$	1.872- 23.867
λ (MoK α) / \AA	0.71073
Reflections collected / unique	17375 / 2474 [R(int) = 0.0880]
Completeness to $\theta = 23.86$	99.5 %
Refinement method	Full-matrix least-squares on F^2
Data / restraints / parameters	2474 / 0 / 235
Goodness-of-fit on F^2	1.572
R indices ($I > 2\sigma(I)$)	$R_1 = 0.1562, wR_2 = 0.3702$
R indices (all data)	$R_1 = 0.1748, wR_2 = 0.3874$
Largest diff. peak and hole	1.332 and -0.522 e. \AA^{-3}

$R_1 = \sum ||F_0| - |F_c|| / \sum |F_0|$; $wR_2 = [\sum [w(F_0^2 - F_c^2)^2] / \sum [w(F_0^2)^2]]^{1/2}$. $w = 1/[\sigma^2(F_0^2) + (aP)^2 + bP]$,
 $P = [\max.(F_0^2, 0) + 2(F_c^2)]/3$, where $a = 0.0560$ and $b = 0.8626$

Crystal Data of Compounds 6b

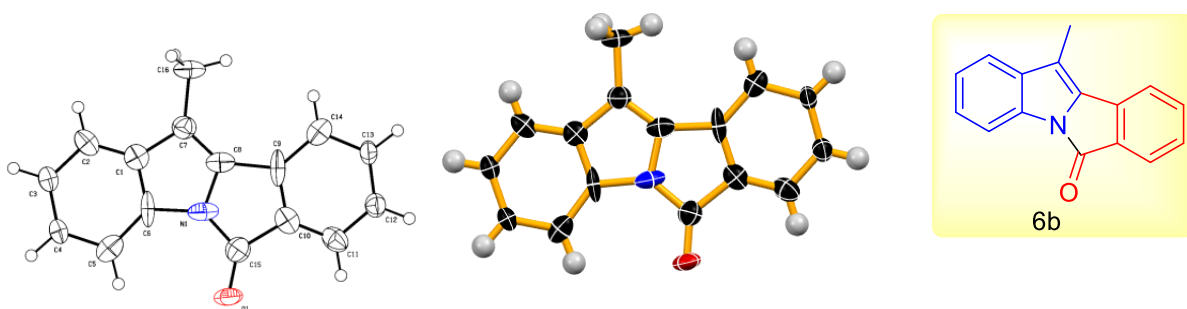
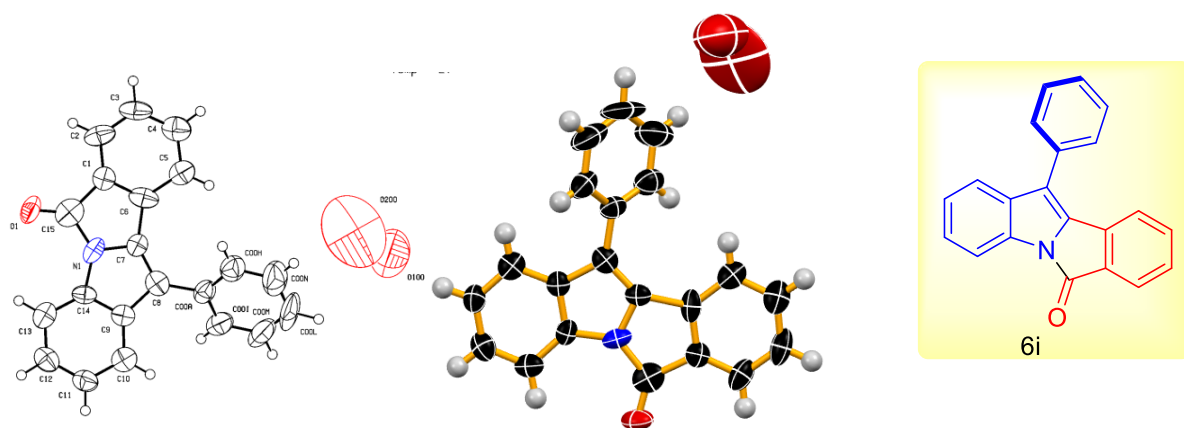


Figure 1.108 ORTEP diagram of **6b** (CCDC 2292567)

Table 1.6 Crystallographic and structure refinement parameters for **6b**

Empirical formula	C ₁₆ H ₁₁ N O
Formula weight	233.26
Crystal system	Orthorhombic,
space group	P 21 21 21
<i>a</i> / Å	5.7595(5)
<i>b</i> /Å	13.2684(13)
<i>c</i> / Å	14.8659(14)
α /°	90
β /°	90
γ /°	90
<i>V</i> /Å ³	1136.04(18)
<i>Z</i>	4
Limiting Indices	-6<= <i>h</i> <=6, -15<= <i>k</i> <=15, -17<= <i>l</i> <=16
<i>D_c</i> /Mg/m ³	1.364
μ /mm ⁻¹	0.677
<i>T</i> /K	100(2)
θ range/°	4.466-63.696
λ (MoK α)/Å	1.54178
Reflections collected / unique	20752 / 1796 [R(int) = 0.0540]
Completeness to θ = 63.696	96.1 %
Refinement method	Full-matrix least-squares on <i>F</i> ²
Data / restraints / parameters	1796 / 0 / 164
Goodness-of-fit on <i>F</i> ²	1.063
R indices(<i>I</i> > 2 σ (<i>I</i>))	R ₁ = 0.0896, wR ₂ = 0.2104
R indices (all data)	R ₁ = 0.0900, wR ₂ = 0.2110
Largest diff. peak and hole	0.745 and -0.267 e. Å ⁻³
$R_1 = \sum F_0 - F_c / \sum F_0 ; wR_2 = [\sum [w(F_0^2 - F_c^2)^2] / \sum [w(F_0^2)^2]]^{1/2}. w = 1/[\sigma^2(F_0)^2 + (aP)^2 + bP],$ $P = [\max.(F_0^2, 0) + 2(F_c^2)]/3, \text{ where } a = 0.0560 \text{ and } b = 0.8626]$	

Crystal Data of Compounds 6i

Figure 1.109 ORTEP diagram of **6i** (CCDC 2297371)Table 1.7 Crystallographic and structure refinement parameters for **6i**

Empirical formula	C ₂₁ H ₁₃ N O _{2.33}
Formula weight	316.66
Crystal system	Trigonal
space group	R -3 :H
<i>a</i> / Å	31.295(4)
<i>b</i> /Å	31.295(4)
<i>c</i> / Å	9.0210(16)
α /°	90
β /°	90
γ /°	120
<i>V</i> /Å ³	7651(3)
<i>Z</i>	18
Limiting Indices	-29<= <i>h</i> <=29, -29<= <i>k</i> <=29, -8<= <i>l</i> <=8
<i>D_c</i> /Mg/m ³	1.237
μ /mm ⁻¹	0.081
<i>T</i> /K	273(2)
θ range/°	2.254-19.828
λ (CuK α) /Å	0.71073
Reflections collected / unique	27994 / 1553 [R(int) = 0.1873]
Completeness to theta = 19.828	99.8 %

Refinement method	Full-matrix least-squares on F ²
Data / restraints / parameters	1553 / 0 / 220
Goodness-of-fit on F ²	1.152
R indices(<i>I</i> > 2σ(<i>I</i>))	R1 = 0.1329, wR2 = 0.3329
R indices (all data)	R1 = 0.1748, wR2 = 0.3663
Largest diff. peak and hole	0.718 and -0.278 e. Å ⁻³

$$R_1 = \frac{\sum ||F_0| - |F_c||}{\sum |F_0|}; wR_2 = \frac{[\sum [w(F_0^2 - F_c^2)^2]]}{\sum [w(F_0^2)^2]}^{1/2}. w = 1/[\sigma^2(F_0)^2 + (aP)^2 + bP],$$
$$P = [\max.(F_0^2, 0) + 2(F_c)^2]/3, \text{ where } a = 0.0560 \text{ and } b = 0.8626]$$

Crystal Structure of 38c

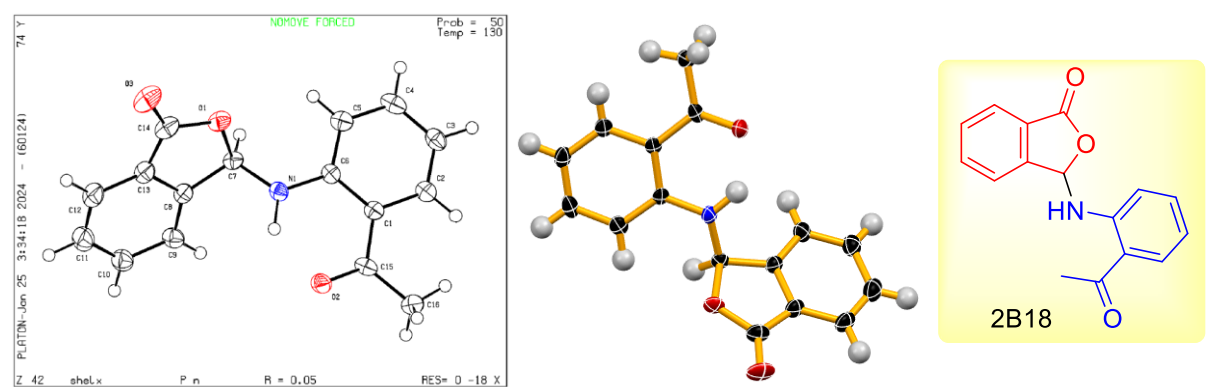


Figure 1.110 ORTEP diagram of 38c

Table 1.8 Crystallographic and structure refinement parameters for 38c

Emperical formula	C16 H13 N O3
Formula weight	267.27
Crystal system	Monoclinic
space group	P n
<i>a</i> / Å	3.9320(7)
<i>b</i> / Å	7.3433(13)
<i>c</i> / Å	21.730(4)
α /°	90
β /°	94.257(9)
γ /°	90
<i>V</i> / Å ³	625.71(19)

Chapter 1

Z	2
Limiting Indices	$-4 \leq h \leq 4, -8 \leq k \leq 8, -24 \leq l \leq 24$
$D_c/\text{Mg/m}^3$	1.419
μ/mm^{-1}	0.809
T/K	130(2)
θ range/ $^\circ$	10.185 to 62.536
λ (CuK α)/ \AA	1.54178
Reflections collected / unique	4557 / 1651 [R(int) = 0.0719]
Completeness to $\theta = 62.536$	96.3 %
Refinement method	Full-matrix least-squares on F^2
Data / restraints / parameters	1651 / 2 / 189
Goodness-of-fit on F^2	1.064
R indices ($I > 2\sigma(I)$)	R1 = 0.0537, wR2 = 0.1385
R indices (all data)	R1 = 0.0541, wR2 = 0.1389
Largest diff. peak and hole	0.247 and -0.297 e. \AA^{-3}

$R_1 = \Sigma ||F_0| - |F_c|| / \Sigma |F_0|$; $wR_2 = [\Sigma [w(F_0^2 - F_c^2)^2] / \Sigma [w(F_0^2)^2]]^{1/2}$. $w = 1/[\sigma^2(F_0)^2 + (aP)^2 + bP]$,
 $P = [\max.(F_0^2, 0) + 2(F_c^2)]/3$, where $a = 0.0560$ and $b = 0.8626$

Crystal Structure of 29l

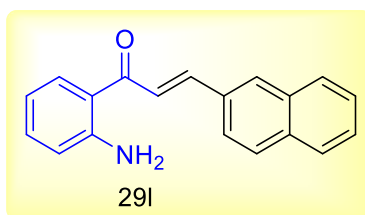
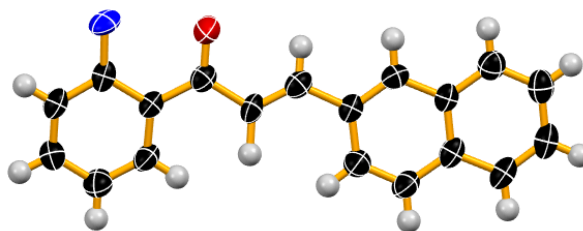
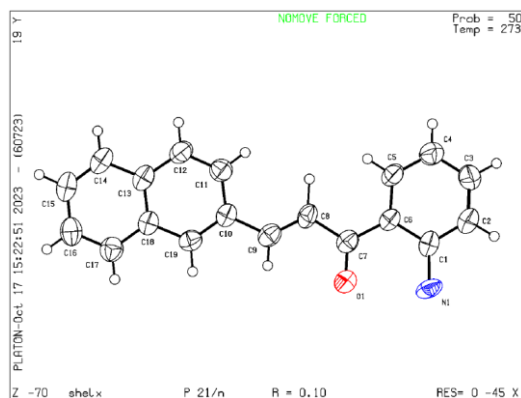


Figure 1.111 ORTEP diagram of 29l

Table 1.9 Crystallographic and structure refinement parameters for **29l**

Empirical formula	C ₁₉ H ₁₅ N O
Formula weight	273.32
Crystal system	Monoclinic,
space group	P 2 ₁ /n
<i>a</i> / Å	13.6027(11)
<i>b</i> /Å	5.1419(3)
<i>c</i> / Å	20.1968(17)
α /°	90
β /°	99.593(3)
γ /°	90
<i>V</i> /Å ³	1392.89(18)
<i>Z</i>	4
Limiting Indices	-15 ≤ <i>h</i> ≤ 15, -5 ≤ <i>k</i> ≤ 5, -23 ≤ <i>l</i> ≤ 23
<i>D_c</i> /Mg/m ³	1.303
μ /mm ⁻¹	0.080
<i>T</i> /K	273(2)
θ range/°	1.683 to 24.170
λ (MoK α)/Å	0.71073
Reflections collected / unique	17508 / 2218 [R(int) = 0.1941]
Completeness to θ = 24.170	99.9 %
Refinement method	Full-matrix least-squares on <i>F</i> ²
Data / restraints / parameters	2218 / 0 / 202
Goodness-of-fit on <i>F</i> ²	1.097
R indices (<i>I</i> > 2 σ (<i>I</i>))	R ₁ = 0.0985, wR ₂ = 0.1742
R indices (all data)	R ₁ = 0.1863, wR ₂ = 0.2078
Largest diff. peak and hole	0.319 and -0.210 e. Å ⁻³
$R_1 = \sum F_0 - F_c / \sum F_0 ; wR_2 = [\sum [w(F_0^2 - F_c^2)^2] / \sum [w(F_0^2)^2]]^{1/2}. w = 1/[\sigma^2(F_0)^2 + (aP)^2 + bP],$ $P = [\max.(F_0^2, 0) + 2(F_c)^2]/3, \text{ where } a = 0.0560 \text{ and } b = 0.8626]$	

Crystal Structure of 29la

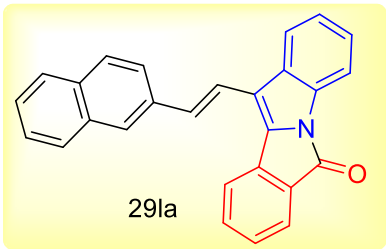
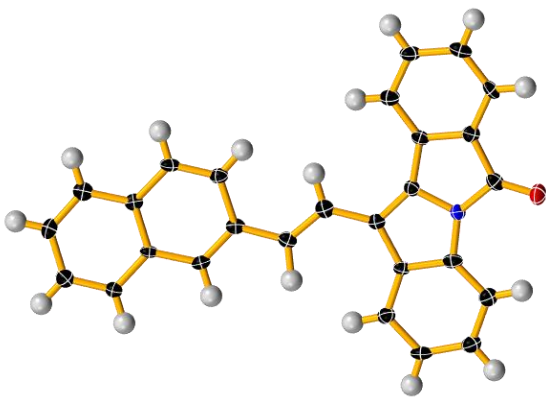
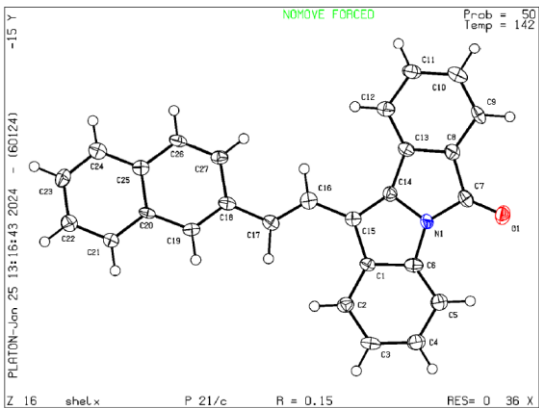


Figure 1.112 ORTEP diagram of 29la

Table 1.10 Crystallographic and structure refinement parameters for 29la

Emperical formula	C27 H17 N O
Formula weight	371.42
Crystal system	Monoclinic
space group	P 21/c
<i>a</i> / Å	20.84(6)
<i>b</i> / Å	5.833(17)
<i>c</i> / Å	15.13(4)
α /°	90
β /°	98.30(11)
γ /°	90
<i>V</i> / Å ³	1820(9)
<i>Z</i>	4
Limiting Indices	-23<= <i>h</i> <=23, -6<= <i>k</i> <=6, -17<= <i>l</i> <=17
<i>D_c</i> /Mg/m ³	1.355

Chapter 1

μ / mm^{-1}	0.641
T/K	142(2)
$\theta \text{ range}/^\circ$	2.142 to 63.050
$\lambda (\text{MoK}\alpha)/\text{\AA}$	1.54184
Reflections collected / unique	62891 / 2911 [R(int) = 0.1152]
Completeness to theta = 63.050	98.7 %
Refinement method	Full-matrix least-squares on F^2
Data / restraints / parameters	2911 / 0 / 270
Goodness-of-fit on F^2	1.155
R indices ($I > 2\sigma(I)$)	R1 = 0.1462, wR2 = 0.4447
R indices (all data)	R1 = 0.1508, wR2 = 0.4458
Largest diff. peak and hole	0.824 and -0.701 e. \AA^{-3}

$$R_1 = \frac{\sum ||F_0| - |F_c||}{\sum |F_0|}; wR_2 = \left[\frac{\sum [w(F_0^2 - F_c^2)^2]}{\sum [w(F_0^2)^2]} \right]^{1/2}. w = 1/[\sigma^2(F_0)^2 + (aP)^2 + bP],$$

$$P = [\max.(F_0^2, 0) + 2(F_c)^2]/3, \text{ where } a = 0.0560 \text{ and } b = 0.8626]$$

Crystal Structure of 29pa

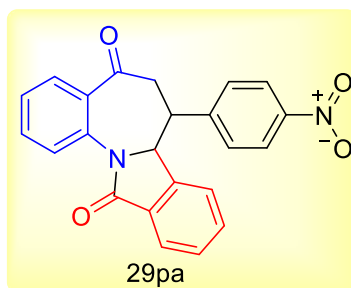
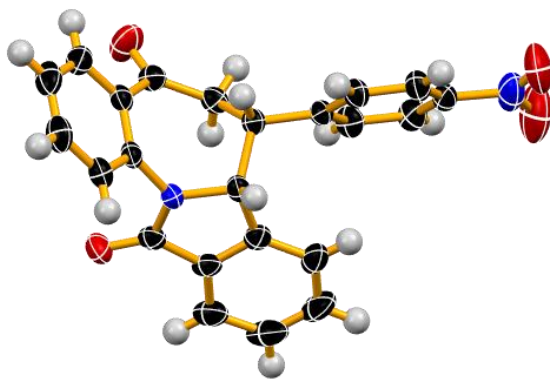
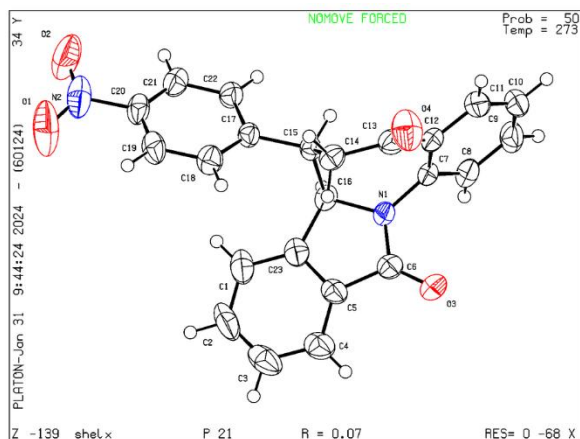


Figure 1.113 ORTEP diagram of **29pa**

Table 1.11 Crystallographic and structure refinement parameters for **29pa**

Emperical formula	C23 H16 N2 O4
Formula weight	384.38
Crystal system	Monoclinic
space group	P 21
$a/\text{\AA}$	7.4598(3)
$b/\text{\AA}$	10.1286(5)
$c/\text{\AA}$	12.0302(5)
$\alpha/^\circ$	90
$\beta/^\circ$	94.8620(10)
$\gamma/^\circ$	90
$V/\text{\AA}^3$	905.70(7)
Z	2
Limiting Indices	$-9 \leq h \leq 9, -13 \leq k \leq 13, -15 \leq l \leq 15$
$D_c/\text{Mg/m}^3$	1.410
μ/mm^{-1}	0.098
T/K	273(2)
θ range/ $^\circ$	2.011 to 27.618
λ (MoK α)/ \AA	0.71073
Reflections collected / unique	32322 / 4192 [R(int) = 0.0641]
Refinement method	Full-matrix least-squares on F^2
Data / restraints / parameters	4192 / 1 / 262
Goodness-of-fit on F^2	1.176
R indices ($I > 2\sigma(I)$)	R1 = 0.0655, wR2 = 0.1439
Largest diff. peak and hole	0.225 and -0.22 e. \AA^{-3}

$R_1 = \Sigma ||F_0| - |F_c|| / \Sigma |F_0|$; $wR_2 = [\Sigma [w(F_0^2 - F_c^2)^2] / \Sigma [w(F_0^2)^2]]^{1/2}$. $w = 1/[\sigma^2(F_0)^2 + (aP)^2 + bP]$,
 $P = [\max.(F_0^2, 0) + 2(F_c^2)]/3$, where $a = 0.0560$ and $b = 0.8626$

1.10 REFERENCES

1. Barton, D.; Barton, D.; Jones, D. N.; Ollis, W. D., *Comprehensive Organic Chemistry: The Synthesis and Reactions of Organic Compounds. Sulphur, selenium, silicon, boron, organometallic compounds. Vol. 3.* Pergamon Press: 1979.
2. Veber, D. F.; Lwowski, W., 1-Arylisoindoles. *Journal of the American Chemical Society* **1964**, 86 (19), 4152-4158.
3. Bonnett, R.; Brown, R. F. C., Isoindole. *Journal of the Chemical Society, Chemical Communications* **1972**, (7), 393-395.
4. Wittig, G.; Tenhaeff, H.; Schoch, W.; Koenig, G., Einige Synthesen über Ylide. **1951**, 572 (1), 1-22.
5. Guillaumel, J.; Léonce, S.; Pierré, A.; Renard, P.; Pfeiffer, B.; Arimondo, P. B.; Monneret, C., Synthesis and biological activity of 6H-isoindolo[2,1-a]indol-6-ones, analogues of batracylin, and related compounds. *Eur J Med Chem* **2006**, 41 (3), 379-86.
6. Boussard, M.-F.; Truche, S.; Rousseau-Rojas, A.; Briss, S.; Descamps, S.; Droual, M.; Wierzbicki, M.; Ferry, G.; Audinot, V.; Delagrangé, P.; Boutin, J. A., New ligands at the melatonin binding site MT3. *European Journal of Medicinal Chemistry* **2006**, 41 (3), 306-320.
7. Ambrus, J. I.; Kelso, M. J.; Bremner, J. B.; Ball, A. R.; Casadei, G.; Lewis, K., Structure-activity relationships of 2-aryl-1H-indole inhibitors of the NorA efflux pump in *Staphylococcus aureus*. *Bioorganic & medicinal chemistry letters* **2008**, 18 (15), 4294-7.
8. Samosorn, S.; Bremner, J. B.; Ball, A.; Lewis, K., Synthesis of functionalized 2-aryl-5-nitro-1H-indoles and their activity as bacterial NorA efflux pump inhibitors. *Bioorganic & medicinal chemistry* **2006**, 14 (3), 857-65.
9. Klymchenko, A. S., Solvatochromic and Fluorogenic Dyes as Environment-Sensitive Probes: Design and Biological Applications. *Accounts of Chemical Research* **2017**, 50 (2), 366-375.
10. Belmonte-Vázquez, J. L.; Amador-Sánchez, Y. A.; Rodríguez-Cortés, L. A.; Rodríguez-Molina, B., Dual-State Emission (DSE) in Organic Fluorophores: Design and Applications. *Chemistry of Materials* **2021**, 33 (18), 7160-7184.
11. Carruthers, W.; Evans, N., Photolysis of 1-benzoyl- and 1- and 3-o-Iodobenzoyl-indole. *Journal of the Chemical Society, Perkin Transactions 1* **1974**, (0), 1523-1525.

12. Nallapati, S. B.; Adepu, R.; Ashfaq, M. A.; Sreenivas, B. Y.; Mukkanti, K.; Pal, M., A Pd-catalyzed direct entry to 11-substituted 6H-isoindolo[2,1-a]indol-6-one derivatives as potential anticancer agents. *RSC Advances* **2015**, 5 (108), 88686-88691.
13. Huang, Q.; Han, Q.; Fu, S.; Yao, Z.; Su, L.; Zhang, X.; Lin, S.; Xiang, S., Rhodium-Catalyzed NH-Indole-Directed C–H Carbonylation with Carbon Monoxide: Synthesis of 6H-Isoindolo[2,1-a]indol-6-ones. *The Journal of Organic Chemistry* **2016**, 81 (24), 12135-12142.
14. Yoo, J. M.; Ho, S. L.; Cho, C. S., Synthesis of 6H-Isoindolo[2,1-a]indol-6-ones via Palladium-Catalyzed Carbonylative Cyclization of 2-(2-Bromophenyl)-1H-indoles. *Synlett* **2016**, 27 (09), 1383-1386.
15. Crawford, L. A.; Clemence, N. C.; McNab, H.; Tyas, R. G., Isoindolo[2,1-a]indol-6-one—a new pyrolytic synthesis and some unexpected chemical properties. *Organic & Biomolecular Chemistry* **2008**, 6 (13), 2334-2339.
16. Čarný, T.; Markovič, M.; Gracza, T.; Koós, P., One-Step Synthesis of Isoindolo[2,1-a]indol-6-ones via Tandem Pd-Catalyzed Aminocarbonylation and C–H Activation. *The Journal of Organic Chemistry* **2019**, 84 (19), 12499-12507.
17. Liang, R.-X.; Xu, D.-Y.; Yang, F.-M.; Jia, Y.-X., A Pd-catalyzed domino Larock annulation/dearomative Heck reaction. *Chemical Communications* **2019**, 55 (53), 7711-7714.
18. Duncanson, P.; Cheong, Y.-K.; Motevalli, M.; Griffiths, D. V., A novel approach to isoindolo[2,1-a]indol-6-ones. *Organic & Biomolecular Chemistry* **2012**, 10 (21), 4266-4279.
19. Thiele, J.; Schneider, J., Ueber Condensationsproducte des o-Phthalaldehyds. **1909**, 369 (3), 287-299.
20. Xiong, J.; Chu, J. C. H.; Fong, W.-P.; Wong, C. T. T.; Ng, D. K. P., Specific Activation of Photosensitizer with Extrinsic Enzyme for Precise Photodynamic Therapy. *Journal of the American Chemical Society* **2022**, 144 (23), 10647-10658.
21. Cheung, C. H. P.; Chong, T. H.; Wei, T.; Liu, H.; Li, X., Guanidine Additive Enabled Intermolecular ortho-Phthalaldehyde-Amine-Thiol Three-Component Reactions for Modular Constructions. **2023**, 62 (10), e202217150.
22. Wang, J.-H.; Tang, Y.-L.; Gong, Z.; Jain, R.; Xiao, F.; Zhou, Y.; Tan, D.; Li, Q.; Huang, N.; Liu, S.-Q.; Ye, K.; Tang, C.; Dong, M.-Q.; Lei, X., Characterization of protein unfolding by fast cross-linking mass spectrometry using di-ortho-phthalaldehyde cross-linkers. *Nature Communications* **2022**, 13 (1), 1468.

23. Chu, J. C. H.; Shao, C.; Ha, S. Y. Y.; Fong, W.-P.; Wong, C. T. T.; Ng, D. K. P., One-pot peptide cyclisation and surface modification of photosensitiser-loaded red blood cells for targeted photodynamic therapy. *Biomaterials Science* **2021**, 9 (23), 7832-7837.
24. Zuman, P., Reactions of Orthophthalaldehyde with Nucleophiles. *Chemical Reviews* **2004**, 104 (7), 3217-3238.
25. Mondal, M. A.; Mondal, S.; Khan, A. A., A mechanistic insight into the acid catalyzed, one-pot synthesis of isoindole-fused quinazolin 4-ones. *Journal of Chemical Sciences* **2020**, 132 (1), 63.
26. Alajarín, M.; Sánchez-Andrada, P.; López-Leonardo, C.; Álvarez, Á., On the Mechanism of Phthalimidine Formation via o-Phthalaldehyde Monoimines. New [1,5]-H Sigmatropic Rearrangements in Molecules with the 5-Aza-2,4-pentadienal Skeleton. *The Journal of Organic Chemistry* **2005**, 70 (19), 7617-7623.
27. Mondal, A. M.; Khan, A. A.; Mitra, K., Tetrazole 5-Acetic Acid Catalyzed Synthesis and Photophysical Study of 2-Aryl-2,3-dihydroquinolin-4(1H)-ones. *Letters in Organic Chemistry* **2019**, 16 (3), 176-184.
28. Görlitzer, K., Untersuchungen an 1,3-Dicarbonylverbindungen, 8. Mitt.: Zur Cyclisierung von Phthalaldehyd mit Acetophenonen. **1976**, 309 (5), 356-366.
29. Khan, A. A.; Mitra, K.; Mandal, A.; Baildya, N.; Mondal, M. A., Yttrium nitrate catalyzed synthesis, photophysical study, and TD-DFT calculation of 2,3-dihydroquinazolin-4(1H)-ones. **2017**, 28 (4), e21379.
30. Takahashi, I.; Nishiwaki, Y.; Saitoh, K.; Matsunaga, T.; Aratake, A.; Morita, T.; Hosoi, S., Exploration of Moderate Conditions and Substrate Variation in the Direct Condensation between Phthalide and Primary Amine Catalyzed by GaCl₃. Are Aliphatic Amines Less Reactive than Aromatic Ones? *HETEROCYCLES* **2019**, 99.
31. Azumaya, I.; Kagechika, H.; Fujiwara, Y.; Itoh, M.; Yamaguchi, K.; Shudo, K., Twisted intramolecular charge-transfer fluorescence of aromatic amides: conformation of the amide bonds in excited states. *Journal of the American Chemical Society* **1991**, 113 (8), 2833-2838.
32. Shvo, Y.; Taylor, E. C.; Mislow, K.; Raban, M., Chemical shift nonequivalence of diastereotopic protons due to restricted rotation around aryl-nitrogen bonds in substituted amides. *Journal of the American Chemical Society* **1967**, 89 (19), 4910-4917.
33. Misra, A.; Mondal, S.; Mondal, M. A., Synthesis of 11H-Benzo[b]Fluoren-11-One via an Unprecedented Cascade Reaction of O-Phthalaldehyde. *Polycyclic Aromatic Compounds*, 1-8.

34. Mondal, M. A.; Khan, A. A.; Mitra, K., Iron(III)-catalyzed selective direct olefination of dihydropyrimidinone with aromatic aldehyde. *Journal of Chemical Sciences* **2018**, *130* (11), 151.
35. Lou, Z.; Zhang, S.; Chen, C.; Pang, X.; Li, M.; Wen, L., Concise Synthesis of 1-Naphthols under Mild Conditions through a Copper-Catalyzed Arylation of Methyl Ketones. **2014**, *356* (1), 153-159.
36. Wang, J.; Chen, W.; Zuo, S.; Liu, L.; Zhang, X.; Wang, J., Direct Exchange of a Ketone Methyl or Aryl Group to Another Aryl Group through C–C Bond Activation Assisted by Rhodium Chelation. **2012**, *51* (49), 12334-12338.
37. Gabriele, B.; Mancuso, R.; Salerno, G.; Ruffolo, G.; Plastina, P., Novel and Convenient Synthesis of Substituted Quinolines by Copper- or Palladium-Catalyzed Cyclodehydration of 1-(2-Aminoaryl)-2-yn-1-ols. *The Journal of Organic Chemistry* **2007**, *72* (18), 6873-6877.
38. Banik, T.; Kaliappan, K. P., A Serendipitous One-Pot Cyanation/Hydrolysis/Enamide Formation: Direct Access to 3-Methyleneisindolin-1-ones. **2021**, *27* (2), 628-633.
39. Chandrappa, S.; Vinaya, K.; Ramakrishnappa, T.; Rangappa, K. S., An Efficient Method for Aryl Nitro Reduction and Cleavage of Azo Compounds Using Iron Powder/Calcium Chloride. *Synlett* **2010**, *2010* (20), 3019-3022.
40. Bichovski, P.; Haas, T. M.; Kratzert, D.; Streuff, J., Synthesis of Bridged Benzazocines and Benzoxocines by a Titanium-Catalyzed Double-Reductive Umpolung Strategy. **2015**, *21* (6), 2339-2342.
41. Min, C.; Lin, Y.; Seidel, D., Catalytic Enantioselective Synthesis of Mariline A and Related Isoindolinones through a Biomimetic Approach. **2017**, *56* (48), 15353-15357.
42. Derayea, S. M.; Nagy, D. M.; Badr El-Din, K. M.; Attia, T. Z.; Samir, E.; Mohamed, A. A.; Hamad, A. A., Green innovative fluorescence approach for the feasible and reliable assay of thiol-containing drugs; captopril as a model. *RSC Advances* **2022**, *12* (27), 17607-17616.
43. Bera, S. K.; Maharana, R. R.; Samanta, K.; Mal, P., CBr₄ catalyzed activation of α,β -unsaturated ketones. *Organic & Biomolecular Chemistry* **2022**, *20* (35), 7085-7091.
44. Catalán, J., On the photophysics of a polyene dissolved in n-alkanes when the temperature drops from 293 to 77 K. **2020**, *33* (10), e4097.
45. Northey, T.; Stacey, J.; Penfold, T. J., The role of solid state solvation on the charge transfer state of a thermally activated delayed fluorescence emitter. *Journal of Materials Chemistry C* **2017**, *5* (42), 11001-11009.

46. Disanayaka, B. W.; Weedon, A. C., Charge transfer fluorescence of some N-benzoylindoles. *Canadian Journal of Chemistry* **1987**, 65 (2), 245-250.
47. Guijarro, A.; Vergés, J. A.; San-Fabián, E.; Chiappe, G.; Louis, E., Herringbone Pattern and CH- π Bonding in the Crystal Architecture of Linear Polycyclic Aromatic Hydrocarbons. **2016**, 17 (21), 3548-3557.
48. Huang, Z.; Yang, Y.; Xiao, Q.; Zhang, Y.; Wang, J., Auto-Tandem Catalysis: Synthesis of Acridines by Pd-Catalyzed C=C Bond Formation and C(sp²)-N Cross-Coupling. **2012**, 2012 (33), 6586-6593.

Chapter 2

Studies towards the Synthesis of 11*H*-benzo[*b*]fluoren-11-one from *o*-Phthalaldehyde

Part of the work described in this chapter is published in

Polycyclic Aromatic Compounds (2023); DOI: 10.1080/10406638.2023.2270124

2.1 INTRODUCTION

Various synthetic routes towards polycyclic aromatic hydrocarbons and their derivatives were studied. All of these compounds are not readily available and the literature lacks facile, efficient, and scalable syntheses. Fluorenone (**39**) is a polycyclic aromatic hydrocarbon (PAH) and a ketone derivative of fluorene. It is a crystalline compound with a molecular formula $C_{13}H_8O$, consisting of a central carbonyl group ($C=O$) attached to a polycyclic aromatic ring structure. The polycyclic aromatic ring system in fluorenone is composed of three fused benzene rings, which gives it its characteristic structure.

Key features of fluorenone (**39**) include its aromatic nature and carbonyl functional group, which imparts unique chemical and physical properties. The compound is often recognized for its role in organic chemistry, where it serves as a valuable intermediate in the synthesis of various organic compounds. Fluorenone **39** also serves as a precursor for the preparation of various core structure in various bioactive^{1, 2}, optical and electronic material. Fluorenone falls within the category of polycyclic aromatic hydrocarbons (PAHs) due to its fused benzene ring system. PAHs are compounds composed of multiple aromatic rings and are of interest in environmental chemistry, as some are known environmental pollutants. Understanding the properties and applications of fluorenone contributes to its significance in both academic and industrial research, particularly in the synthesis of diverse organic compounds.

In the year 1985, C_{60} , commonly known as the buckyball or buckminsterfullerene **43**, was serendipitously discovered by H. W. Kroto from the University of Sussex, UK, along with R. F. Curl and R. E. Smalley, both affiliated with Rice University, USA.³ Their groundbreaking contribution to the discovery of **C60** earned them the Nobel Prize in Chemistry in 1996. Notably, Science recognized **C60** as the "Molecule of the Year" in 1991,⁴ underscoring its significance in the scientific community.

Since its discovery, **C60** has been the focal point of extensive research endeavors, investigating its chemical reactivities and physical properties. Researchers have also dedicated efforts to devising novel synthetic routes for the production of **C60**. The remarkable attention bestowed upon buckyball and its broader fullerene family is evident in the widespread interest from physicists, material scientists, and experts in both inorganic and organic chemistry. The multifaceted exploration of **C60** showcases its exceptional appeal and the diverse avenues it opens for scientific investigation and technological applications. The synthesis of buckminsterfullerene **C60** and other higher fullerenes continues to pose a challenge for

chemists. One widely adopted synthetic strategy aimed at overcoming the challenges in buckminsterfullerene **C60** and higher fullerene synthesis involves the initial preparation of curved hydrocarbon fragments, often referred to as buckybowls. These buckybowls possess carbon frameworks that mirror the surface structure of the buckyball. Recently, the flash vacuum pyrolysis (FVP) method⁵ has emerged as a successful approach, offering a more direct route to obtaining corannulene⁶ and various other buckybowls. The high-temperature requirement in FVP presents both advantages and challenges.^{5, 6} On one hand, the method provides a rapid and direct pathway to the desired buckybowls. On the other hand, the extreme temperatures can lead to low yields and introduce difficulties in maintaining the structural integrity of the synthesized molecules. Indeed, synthesizing buckybowls with a structure consisting of five-membered rings surrounded by six-membered rings can be facilitated by considering benzofluorenone (**40** & **41**) and its derivatives as potential precursors.⁷ A comparison of their structures with corannulenes **42** and other buckybowls reveals a resemblance that suggests the feasibility of utilizing benzofluorenone-based compounds in the synthesis process.

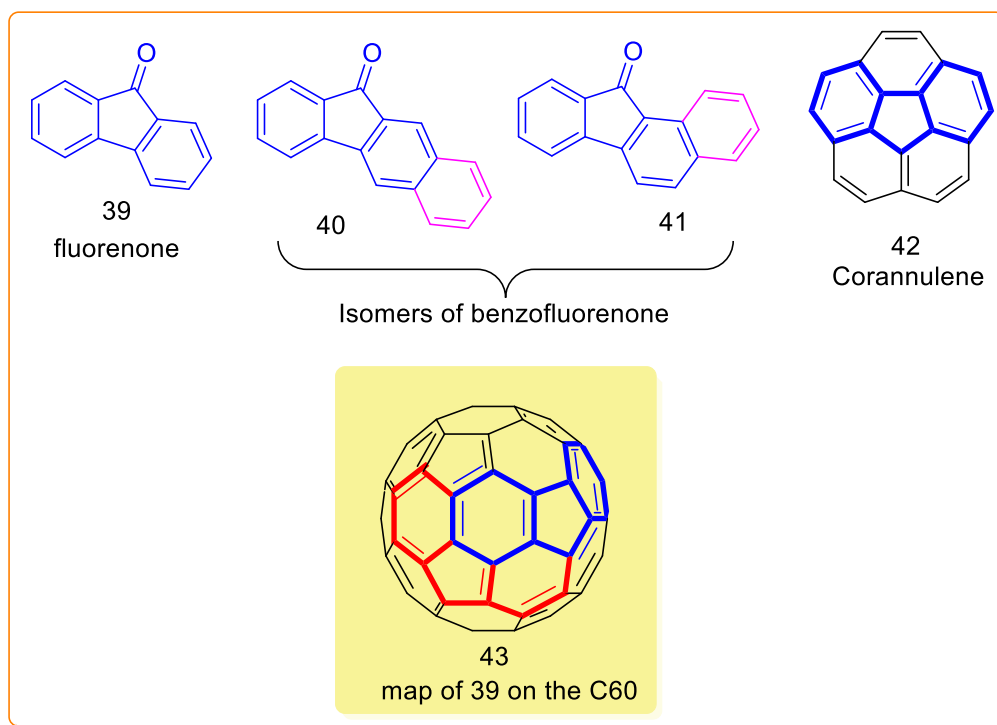


Figure 2.1 Structures of fluorenone and other PAH

The structural similarities between benzofluorenone and the desired buckybowls make these compounds attractive starting materials. The incorporation of five-membered and six-membered rings in benzofluorenone-derived molecules provides a suitable framework for the

formation of the curved and strained geometries characteristic of buckybowls. By manipulating and functionalizing benzo[fluorene]-based compounds, researchers can explore tailored pathways for the controlled assembly of buckybowls, advancing the field of fullerene chemistry.

11*H*-Benzo[**b**]fluorenone **40** and its derivatives attracted our interest because of their potentiality to be used as precursors for the synthesis of polycyclic aromatic hydrocarbons with carbon frameworks represented on the surface of C60.

This chapter unfolds with a detailed exploration of the reaction mechanisms and key steps involved in transforming *ortho*-phthalaldehyde (OPA) into 11*H*-benzo[**b**]fluorene-11-one **40**.

Ortho phthalaldehyde (OPA) is an attractive aromatic dialdehyde mostly used as a reagent for biochemical studies such as the detection of biomolecules through the formation of a fluorogenic isoindolone moiety by the reaction of amines group of the biomolecules.⁸ It is also used as a photoresist material in the polymeric form.⁹ The synthetic application of OPA is limited due to its complex reactivity. In many cases, the adjacent aldehyde groups of OPA exhibited chemical properties similar to the aromatic aldehyde,¹⁰ but, in some instances, due to the presence of proximity of the aldehyde groups, it shows typical reactivity.¹¹ In this chapter, we have observed a typical reactivity of OPA with a nucleophilic methyl source in the presence of a base to form benzo[fluorenone] **40**, an attractive polycyclic aromatic hydrocarbon¹² and core structure of benzo[fluorene] antibiotics.¹³

Compound **40** had been used as a starting material for designing and synthesis of valuable organic materials such as AIEgens having solid-state $\Phi_F = 99.8\%$ and the CIE coordinates are 0.152, 0.048, which is close to the European Broadcasting Union standard blue (0.15, 0.06),¹⁴ material for organic electroluminescent device, curable resin composition etc. Moreover, the other derivatives, such as bromo or isomerization¹⁵ led to varieties of benzo[fluorenones] (Figure 2.2).

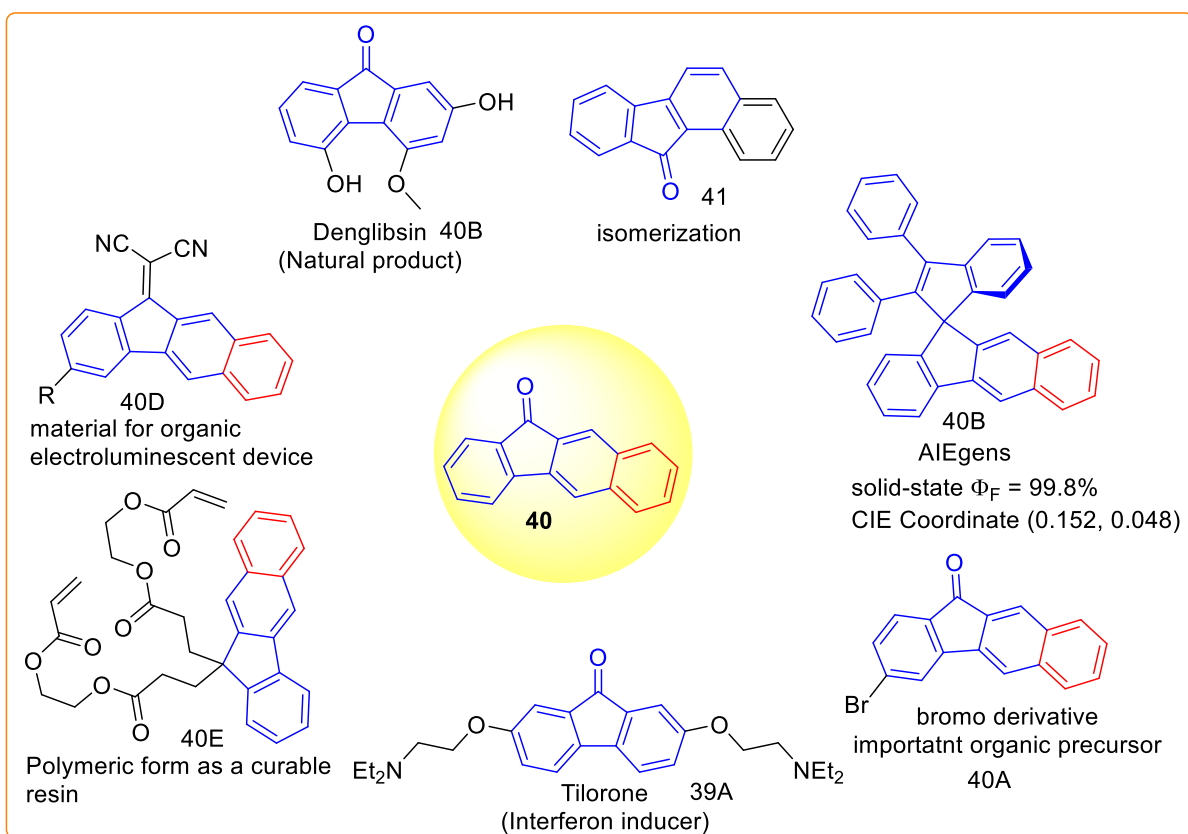


Figure 2.2: Use of compound **40** for designing valuable organic materials.

2.2 LITERATURE BACKGROUND

Despite the immense significance of 11H-benzo[b]fluoren-11-one, only a few reports are known for their syntheses that proceeded through the formation of **b** and **c** bonds (Figure 2.3).

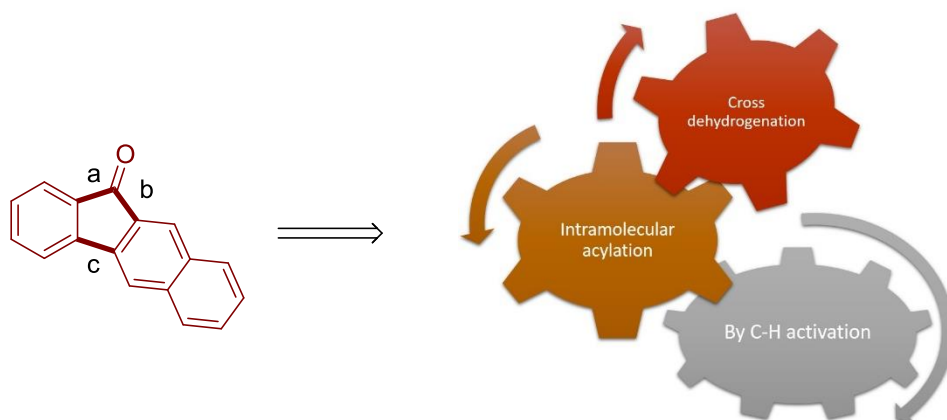
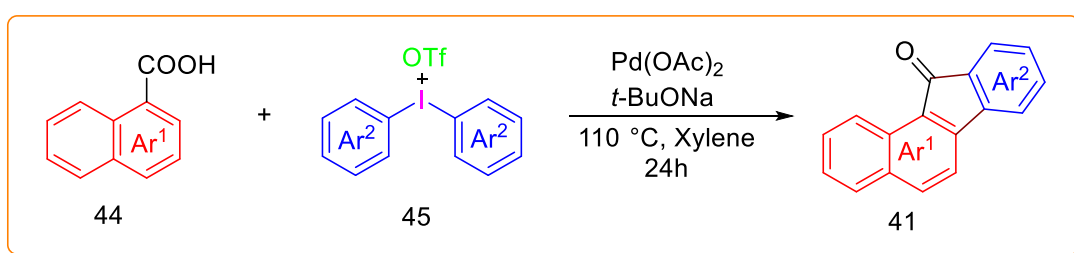


Figure 2.3 Strategy of the synthesis of 11H-benzo[b]fluoren-11-one

For example, via palladium-catalyzed, one-pot arylation cascade reactions,¹⁶⁻¹⁸ a cobalt-catalyzed MHP-directed [3+2] annulation/ring-opening/dehydration sequence,¹⁹ palladium catalyzed domino C-H activation reaction of aryl aldehydes with dihaloarene² or oxidation of

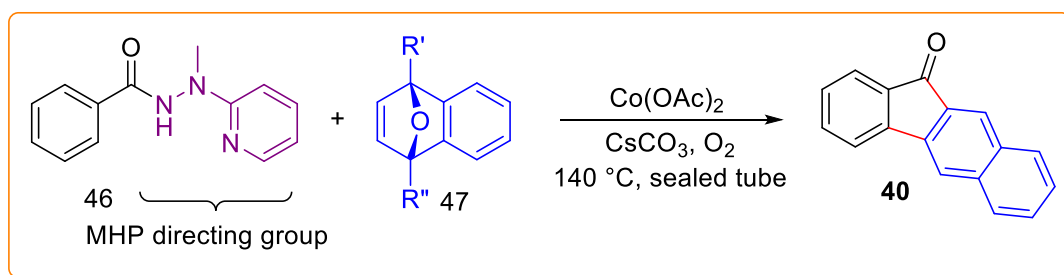
benzylic $-\text{CH}_2-$ to installed $\text{C}=\text{O}$ bond²⁰⁻²² of the hydrocarbon or formation of the bond b, for example, the acid-catalyzed intramolecular acylation,^{23, 24} Pd catalyzed domino reaction²⁵ and decarboxylative cyclization²⁶ or formation of the five-membered ring by carbonylation reaction to form the bonds a and b²⁷ or cross dehydrogenation reaction to form the bond c.²⁸ Reported synthetic methods and application fluorenones are reviewed.¹²

Han and his group reported a method of synthesis of compound **41**, isomer of our targeted fluorenone **40** via palladium-catalyzed, one-pot arylative cascade reactions started from 1-naphthoic acid **44**, diaryliodonium salts **45**, $\text{Pd}(\text{OAc})_2$ and $t\text{-BuONa}$ in xylene at $110\text{ }^\circ\text{C}$ for 24 h to afford **41** in 85% yield (Scheme 2.1).¹⁶



Scheme 2.1 Synthesis of 11H-benzo[a]fluoren-11-one starting from 1-naphthoic acid

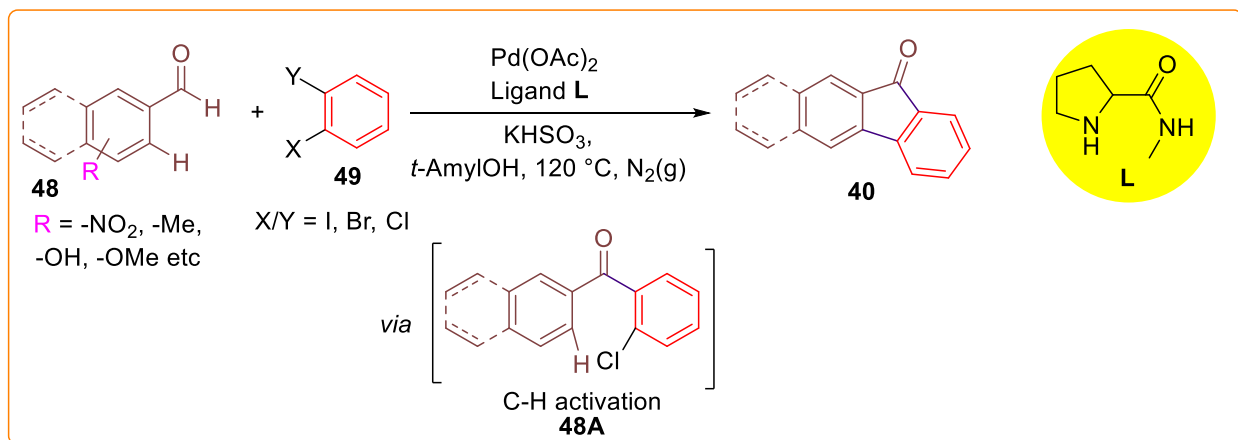
Zhai and his group developed a one-pot synthesis of benzo[b]fluorenones via a cobalt-catalyzed [3+2] annulation of oxabicyclic alkenes followed by a ring-opening/dehydration sequence with the use of 2-(1-methylhydrazinyl)pyridine (MHP) as the bidentate directing group in C–H functionalization of benzoic hydrazides (Scheme 2.2).¹⁹



Scheme 2.2 Synthesis of 11H-benzo[b]fluoren-11-one starting from benzoic hydrazides

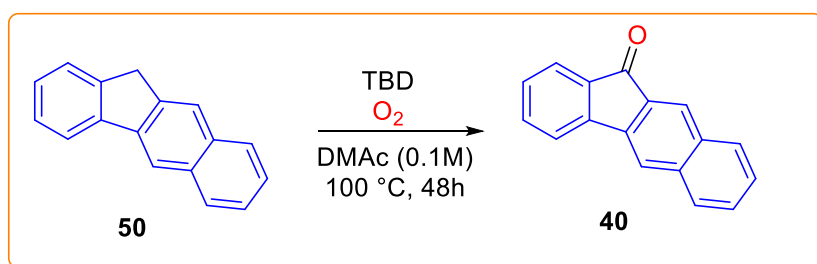
Chikhalia Group demonstrated a one-pot palladium catalyzed domino C-H activation reaction of aryl aldehydes with dihaloarene to access 9-fluorenone molecules. They have examined several bidentate ligands for the reaction of arylaldehyde **48** and 2-bromoiodobenzene **49** in the presence of $\text{Pd}(\text{OAc})_2$ and KHCO_3 under N_2 gas in $t\text{-AmylOH}$. Pyrrolidinylamide ligand **L** was

found most fruitful for the proposed reaction to afford desired 9-fluorenone derivative (**40**) in excellent yield (Scheme 2.3).²



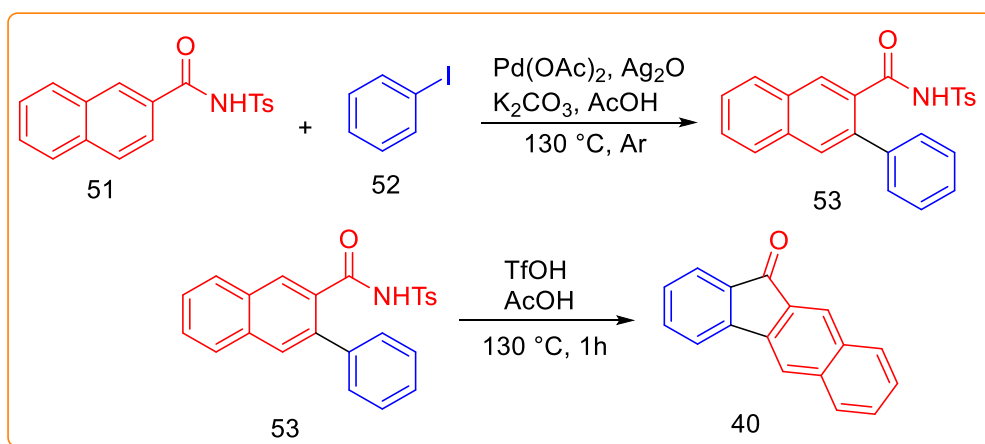
Scheme 2.3 Synthesis of 11*H*-Benzo[b]fluoren-11-one via double C-H bond activation

Jang group reported an aerobic oxidation of 11*H*-benzo[b]fluorine **50** using 1,5,7-triazabicyclo[4.4.0]dec-5-ene (TBD), a guanidine-type base, to afford 11*H*-Benzo[b]fluoren-11-one underwent oxidation to afford desired product **40** in 85% yield (Scheme 2.4).²⁰



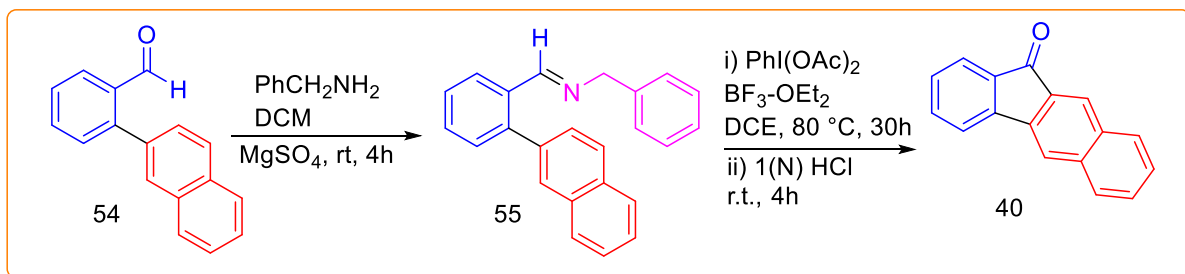
Scheme 2.4 Synthesis of 11*H*-Benzo[b]fluoren-11-one via aerobic oxidation

Large et al. illustrated a reaction of Pd-catalysed C–H arylation of naphthalene tailoring with *N*-tosyl carboxamides group. Their strategy relies on the dual functionality of *N*-tosyl carboxamides, which collaboratively serve as a directing group during the initial C–H arylation step and as a precursor for the "CO" or "CO–NH" fragment in the subsequent synthesis of naphthalene-based fluorenone or phenanthridinone derivatives. In the first step of their approach was C-H arylation of naphthalenes **51** installation of the phenyl group by using Ag_2O , K_2CO_3 and $Pd(OAc)_2$ in the presence of iodobenzene **52** for 24 hours to get **53** followed by electrophilic cyclisation by using TfOH in AcOH to afford the final fluorenone product **40** in 40% yield (Scheme 2.5).²³



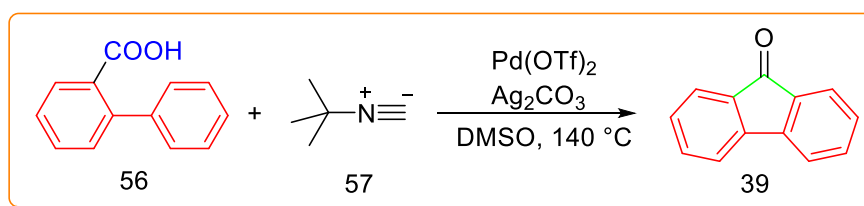
Scheme 2.5 Pd-catalysed C–H arylation/acid catalyzed intramolecular acylation protocol

Satinath et al. reported $\text{PhI}(\text{OAc})_2\text{-BF}_3\text{-OEt}_2$ mediated domino synthesis of fluorenones. The reaction proceeds through imine activation, intra-molecular C–C bond formation and β -elimination sequences. In order to synthesize fluorenones, they took 2-(naphthalen-2-yl)benzaldehyde **54** which converted into the key intermediate aldimine **55** by treating with benzylamine. Which then undergoes domino C–C bond formation followed by β -elimination to give the ketimine intermediate. The hydrolysis of the resultant ketimine produce 11*H*-Benzo[b]fluoren-11-one (Scheme 2.6).²⁵



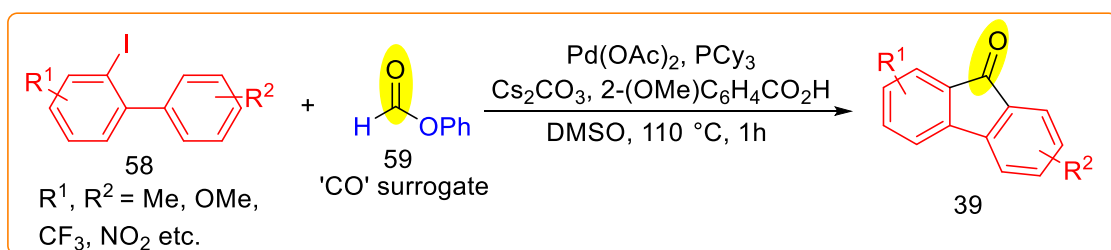
Scheme 2.6 Synthesis of 11*H*-benzo[b]fluoren-11-one via domino reaction

Cai et al reported a one-pot palladium-catalyzed synthesis of fluoronones via decarboxylative cyclization by using 2-phenylbenzoic acid **56** and tert-butyl isocyanide **57** which was treated with $\text{Pd}(\text{OAc})_2$ along with Ag_2CO_3 as an additive in DMSO (50% aq) at 140 °C for 24 hours to afford product **39** in 80% yield (Scheme 2.7).²⁶



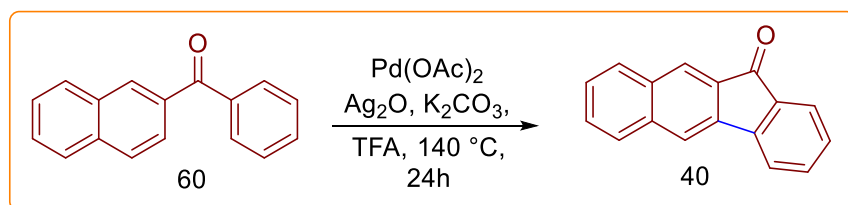
Scheme 2.7 Synthesis of fluorenone via via decarboxylative cyclization

The Pd-catalyzed carbonylation reaction showcased by the Manabe group facilitates the production of fluoren-9-ones from 2-halogenated biphenyls, employing phenyl formate as a surrogate for carbon monoxide. using 2-iodobiphenyl **58** as a model substrate and phenyl formate **59** as a CO surrogate in presence of $\text{Pd}(\text{OAc})_2$ as an active catalyst (Scheme 2.8).²⁷



Scheme 2.8 Formation of the five-membered ring by carbonylation reaction

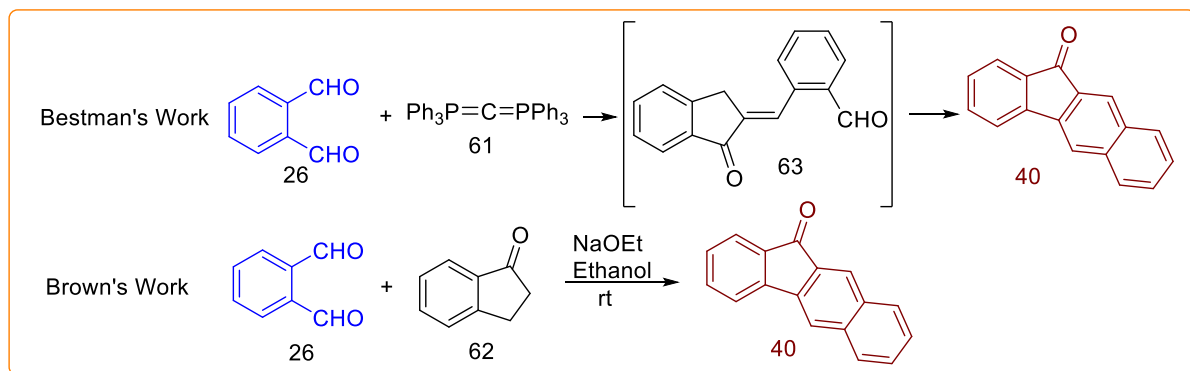
Zhang and his group illustrated a Palladium-catalyzed dual C–H functionalization of 2-naphthylphenylketone **60** to form benzofluorenone **40** by oxidative dehydrogenative cyclization. 2-naphthylphenylketone **60** was subjected to react with trifluoroacetic acid (TFA) in presence of $\text{Pd}(\text{OAc})_2$, Ag_2CO_3 , K_2CO_3 , were treated with at 140°C for 24 h to give the product 30 in 48% yield (Scheme 2.9).²⁸



Scheme 2.9 Synthesis of benzofluorene by oxidative dehydrogenative cyclisation

Brown et al. were intrigued by Bestman's investigation into phosphonium ylide. Bestman's team initially discovered an inexplicable reaction involving o-phthalaldehyde and hexaphenylcarbodiphosphorane, yielding 11*H*-benzo[*b*]fluorenone.²⁹ This compound could be generated even more easily through the chalcone condensation of 1-indanone with

phthalaldehyde in ethanolic sodium ethoxide at room temperature,¹⁵ as illustrated in Scheme 2.10.



Scheme 2.10 A closely related method used hexaphenylcarbodiphosphorane and OPA to form compound **40**

2.3 PRESENT WORK

Because of the commercial importance of compound **40**, a simple and inexpensive way of synthesis without the use of complex starting materials, expensive transition metals catalysts, and restricted experimental conditions is desirable to meet the demand. A closely related method used hexaphenylcarbodiphosphorane and OPA to form compound **40**, as shown in Scheme 2.10.¹⁵

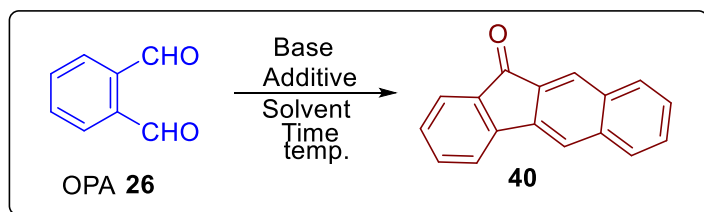
In continuation of our present interest in the reactivity study of OPA,³⁰ we observed an unprecedented reaction of OPA with the nucleophilic methyl transferring agents such as acetone, DMSO, DMF, and acetophenone in the presence of a base to form a commercially valuable material 11H-benzo[b]fluoren-11-one **40** (Scheme 2.11). The results for the synthesis of 11H-benzo[b]fluoren-11-one **36** are discussed in this chapter in detail.

2.4 RESULTS AND DISCUSSION

Initially, we treated OPA in an acetone medium in the presence of aqueous sodium hydroxide at RT to study the reactivity of OPA toward an aqueous base. Under this condition, we observed the immediate formation of many unidentified products. The aqueous base promotes several chemical transformations of OPA because of the dual nature (nucleophilic and Basic) of the OH^- ion.³¹ However, with the use of acetone as a solvent in the presence of sodium carbonate, the reactivity of OPA toward acetone was sluggish. After heating the reaction mixture, we observed the formation of compound **40** in 27% yield. The structure of compound **40** is confirmed by NMR, mass, and single crystal XRD³² and is matched with the reported data.¹⁹

It is necessary to mention that the number of carbon in the OPA is eight, and that of structure **40** is 17, one more than the multiple of 8. We assumed that the source of the extra carbon apart from the carbons of the two units of OPA is the solvent molecule.

To study the behavior of OPA towards different solvents, OPA was treated with DMF, DMSO, acetonitrile, methanol, and water in the presence of Na_2CO_3 , and the results are shown in Table 2.1. Both DMSO and DMF reacted with OPA in the presence of Na_2CO_3 to produce compound **40**. Whereas acetonitrile, methanol, and water solvents failed to produce compound **40**. No significant improvement was observed when K_2CO_3 was used instead of Na_2CO_3 . The non-nucleophile base, like DBU, gave a better yield of compound **40**, though it was required a longer reaction time (entries 7, 8 & 9, Table 2.1). These results suggested that the solvent DMF, DMSO, and acetone served as a reagent along with the conventional role of solvent. The nucleophilic properties of α carbon of acetone³³ and DMSO³⁴ under basic condition is common. Beyond the role of solvent, DMF have been used as a source of $-\text{HCO}_2$, $-\text{O}-$, CO , H^+ , $-\text{H}$, $-\text{NMe}_2$, $-\text{CONMe}_2$, CHO , to a lesser extent, as a methyl transferring agent.³⁵ We explored here DMF as source of a methyl transferring agent.



Scheme 2.11 Optimization of the reaction condition

Table 2.1: Optimization of the reaction condition

Entry	Solvent	Base	Additive	Temp. °C	Time (h)	Yield
1.	Acetone	Na_2CO_3	-	60	24	11
2.	DMF	Na_2CO_3	-	130	72	12
3.	DMSO	Na_2CO_3	-	130	24	13
4.	MeOH	Na_2CO_3	-	70	24	0
5.	CH_3CN	Na_2CO_3	-	85	24	0
6.	H_2O	Na_2CO_3	-	100	24	0

Chapter 2

7.	DMF	DBU	-	130	48	22
8.	DMSO	DBU	-	130	48	30
9.	Acetone	DBU	-	60	48	23
10.	MeOH	DBU	-	70	48	0
11.	DMF	Na ₂ CO ₃	PhCOCH ₃	130	12	35
12.	DMSO	Na₂CO₃	PhCOCH₃	130	12	42
13.	CH ₃ CN	Na ₂ CO ₃	PhCOCH ₃	60	24	25
14.	Acetone	Na ₂ CO ₃	PhCOCH ₃	85	24	27
15.	DMSO	Na₂CO₃	Acetone	130	3	48

Note: The yields mentioned are isolated, and it was calculated based on the amount of OPA used. Maximum yield expected to be 50% as two OPA molecules are involved in the formation of 2. For entries 1-14, column chromatography was used to get pure product, while for entry 15, no column purification was needed.

The reaction was also performed in the presence of an equimolar amount of acetophenone, which can serve as a source of nucleophilic carbon, and observed significant yield improvement (Table 2.1, entry 11-14). Acetonitrile alone cannot act as a source of nucleophilic carbon in the presence of Na₂CO₃. However, CH₃CN can be used as a solvent in the presence of acetophenone (entries 5 & 13). Among acetone, DMSO, DMF, and acetonitrile, DMSO solvent gave the best result (up to 42 % yield). Careful analysis of TLC of the reaction mixture containing OPA, Acetophenone, and Na₂CO₃ in DMSO indicated that a significant portion of acetophenone remained unreacted. The OPA decomposed rapidly before coupling with acetophenone. Therefore, we have carried out the reaction in DMSO in the presence of more reactive acetone (Table 2.1: Entry 15). To our surprise, the reaction was completed within three hours, and analytically pure product **40** was isolated by filtration after dilution of the DMSO reaction mixture with water. The reaction was performed with the 1-gram batch, and the method was found to be equally efficient as observed with the small scale. Thus, we have developed a potential alternative method for synthesizing 11*H*-benzo[*b*]fluoren-11-one with high atom economy using DMSO as a solvent³⁶ without column purification.

Developing organic fluorophores that preserve emission properties in aggregated solid state as well as in dilute solution has been a growing research field in the recent past.³⁷ Most of the

organic fluorescence exhibited either aggregation-induced fluorescence enhancement or quenching. Compound **40** in pure crystalline form retains its fluorescent properties. Although the crystal structure is known **CCDC 977770**,³² we used single-crystal XRD to confirm the structure, as shown in Figure 2.4. Compound **40** shows greenish-yellow fluorescence in the solid and solution state (Figure 2.4b, c).

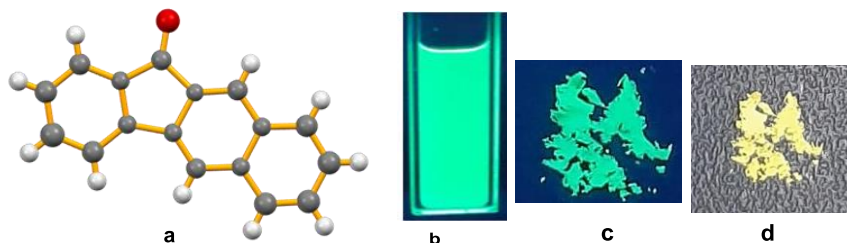


Figure 2.4 (a) X-ray crystal structure of **40** (b) Image of chloroform solutions (100 μ M) of compound **40** under UV light at 365 nm. (c) Image of the solid compound under UV light at 365 nm. (d) Image of the solid compound under visible light.

2.5 MECHANISTIC STUDY

The LCMS analysis of the incomplete reaction mixture was used to identify the intermediates formed during the progress of the reaction. An equimolar mixture of OPA and acetophenone in DMSO was heated at 130 $^{\circ}$ C for 4 hrs., and the mixture was partitioned between ethyl acetate and water. Both the ethyl acetate and the aqueous layers were analyzed separately by LCMS. The ethyl acetate layer (Figure 2.5) shows mainly compound **40** (MW:230.07) in 96% purity.

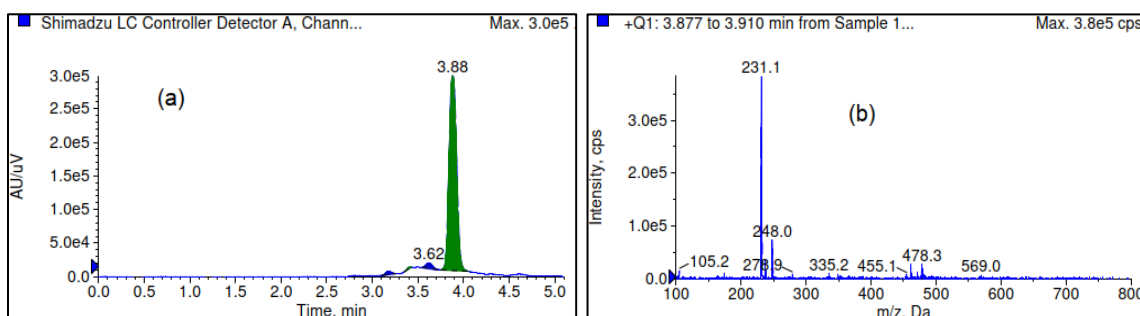


Figure 2.5: LCMS of the ethyl acetate layer (a) Liquid chromatogram of 5 minutes run using column X-Bridge (4.6×50 mm, 5 μ m), NH_4OAc (10 mM):ACN :: 90:10, detected by a UV detector at 260 nm (b) Mass spectra of the fraction eluted at 3.88 min.

While the chromatogram of the aqueous layer indicated the formation of a number of products (Figure 2.6) provided valuable information to predict the mechanism. The LCMS analysis of the range 3.877 min to 3.910 min suggested the presence of an ion peak at m/z 236.8 due to the formation of the initial aldol product **64a** or its isomeric structure **64d** (Scheme 2.12). Further analysis of the eluents from 3.008 min to 3.041 min led to the identification of the crucial intermediate **64e** (m/z 352.9) and the benzoic acid **64h** (m/z 122.8).

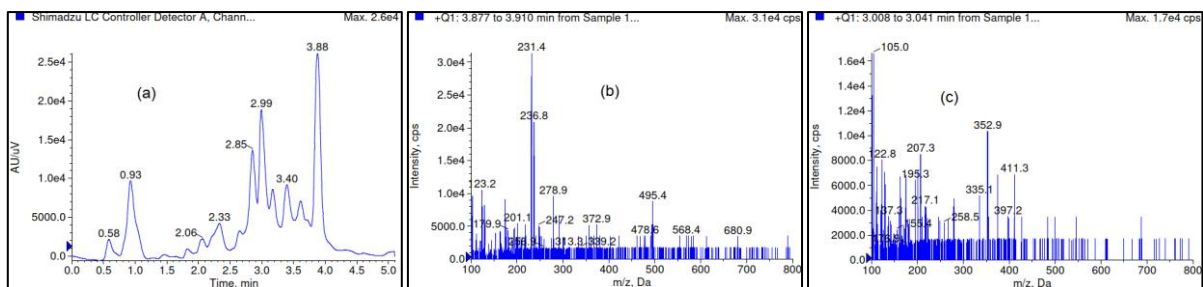
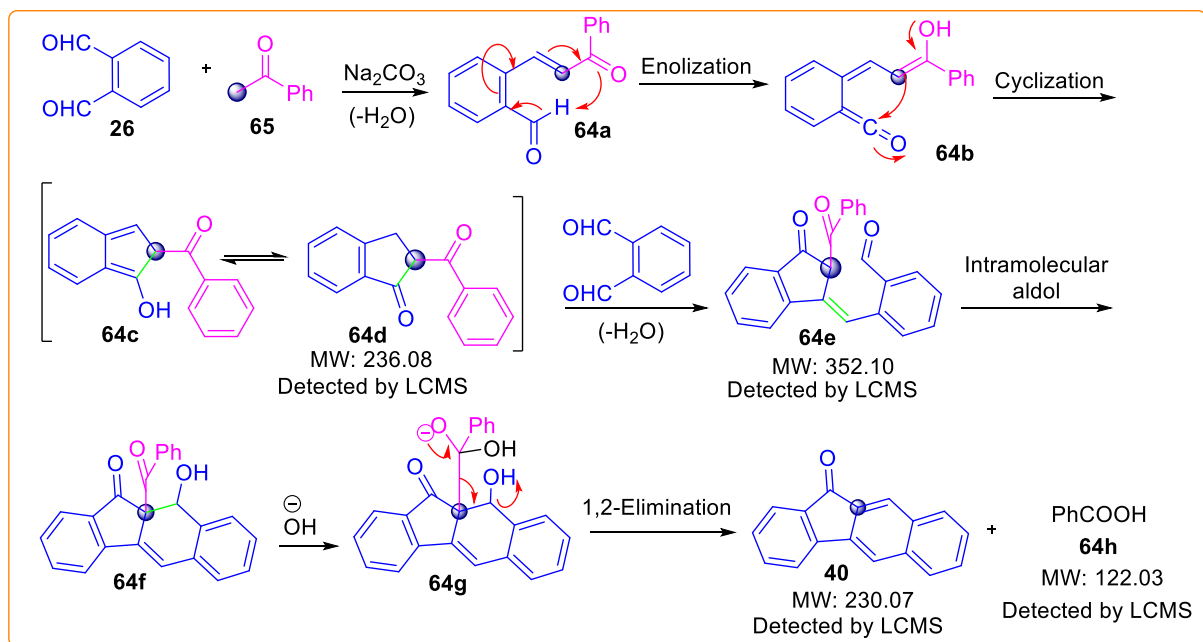


Figure 2.6 LCMS analysis of the aqueous layer. The aqueous layer was acidified with dilute HCl and extracted with ethyl acetate, and the organic layer was subjected to LCMS (a) Liquid chromatogram of 5 minutes run using column X-Bridge (4.6×50 mm, $5 \mu\text{m}$), NH_4OAc (10 mM): $\text{ACN}::90:10$, detected by a UV detector at 260 nm (b) Mass spectra of the fraction eluted at 3.877-3.910 min. (c) Mass spectra of the fraction eluted at 3.008-3.041 min.

Based on the evidence of forming the intermediate **64a**, **64e**, and **64h** from LCM and the solvent study, a probable mechanism involving multistep cascade reactions has been proposed in Scheme 2.12. The intermediate **64a** formed by the initial aldol condensation between OPA and acetophenone, underwent intramolecular cyclization via an extended enol intermediate **64b** to give the structure **64c**. Then, the active indenone intermediate **64d** reacted with another molecule of OPA in a tandem aldol condensation reaction and generated intermediate **64g** via intermediate **64e**. Finally, the base promoted 1,2 elimination of a molecule of benzoic acid led to the formation of compound **40**. Apart from the evidence from LCMS, the formation of **64d** was also supported by the work of Balasubramani et al.¹³



Scheme 2.12 Proposed mechanisms for the base-promoted reaction of OPA with acetophenone based on LCMS of the incomplete reaction mixture

2.6 CONCLUSION

We developed a simple and efficient method of synthesis of 11*H*-benzo[b]fluoren-11-one, a valuable organic material and the core unit of benzofluorene antibiotics. The in situ generated indenone intermediate, identified by LCMS, was found to be the key intermediate that undergoes tandem aldol condensation reaction to form the target compound. The most interesting part of this work is that DMF can serve as a source of nucleophilic carbon in the formation of benzofluorene. Although the method was optimized on ortho phthalaldehyde, it could be applicable for all the other ortho dialdehyde to get polycyclic benzofluorenones in a single step.

2.7 EXPERIMENTAL SECTION

2.7.1 Instruments and characterization

The progress of the reactions was monitored using the silica gel 60 F254 pre-coated TLC plate. All reactions were carried out in an open pot under atmospheric pressure using commercial-grade solvents and reagents. Proton nuclear magnetic resonance (¹H-NMR) was recorded at 300 MHz. The chemical shifts were recorded in parts per million (ppm, δ) using tetramethylsilane (δ 0.00) as the internal standard. Splitting patterns of the ¹H-NMR are mentioned as singlet (s), doublet (d), doublet of doublet (dd), doublet of triplet (dt), triplet (t), multiplet (m) etc. ¹³C-NMR spectra were recorded at 75 MHz. Chemical shifts are given in δ relative to TMS, the coupling constants *J* are given in Hz. Mass Spectra were obtained using an ESI-TOF mass spectrometer. LCMS taken using ZORBAXEXT (4.6 \times 50 mm, 5 μ) column, NH₄OAc (10 mM):CAN::90:10 for liquid chromatogram. Melting points were determined in open capillary tubes by a LabX India digital melting point apparatus.

Slow evaporation at RT of a solution of **40** in chloroform-methanol (1:1) produced a single crystal of compound **40**. A single crystal of **40** was attached to a glass fiber with epoxy glue and transferred to an X-ray diffractometer equipped with a graphite-monochromator. Diffraction data of product **40** were measured with MoK α radiation (λ = 0.71073 Å) at 273 K.

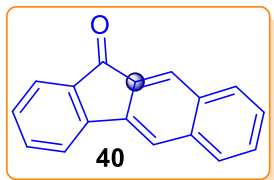
2.7.2 General procedure for the synthesis of compound 11*H*-benzo[b]fluoren-11-one

Method A: The mixture of OPA (200 mg, 1.49 mmol), acetophenone (180 mg, 1.49 mmol), and K₂CO₃ (618 mg, 4.5 mmol) in acetone (5 mL) were taken in a single-necked round bottom flask fitted with a reflux condenser under open atmosphere and heated the mixture at 60 °C to reflux for 24 hours. After completion of the reaction, the mixture was diluted with 30 mL water, extracted with ethyl acetate (3 \times 15 mL), and dried the organic layer over anhydrous Na₂SO₄.

The volatiles were removed, and the crude products were purified by flash column chromatography to get analytically pure compound **40** as a light yellow solid (143 mg). Yield: 42% (assuming maximum yield 50%), mp: 208 °C. All other experiments were performed similar way as described for acetophenone at different temperatures and times mentioned in Table 2.1.

Method B: A mixture of OPA (200 mg, 1.49 mmol), K₂CO₃ (618 mg, 4.5 mmol), and (acetone 433 mg, 7.46 mmol) is heated in 2 mL DMSO at 130 °C for three hours. After that, the mixture was cooled to RT and diluted with water (15 mL). The solid compound **40** was isolated by filtration (167 mg, 48%). Product isolated in this way was sufficiently pure for spectroscopic data.

2.7.3 Analytical spectroscopic data of 11*H*-benzo[*b*]fluoren-11-one (**40**)



R $\tilde{\nu}_{\text{max}}$ (cm⁻¹): 3398, 3058, 3010, 2955, 2921, 2851, 1705, 992, 640, 550; **¹H-NMR (300 MHz, CDCl₃)**: δ 7.35 (td, *J* = 0.9 Hz, 6.0 Hz, 1H), 7.45-7.50 (m, 1H), 7.53-7.59 (m, 2H), 7.70-7.77 (m, 2H), 7.82-7.91 (m, 3H), 7.81 (s, 1H); **¹³C-NMR (75 MHz, CDCl₃)**: δ 119.0, 121.0, 124.4, 125.7, 126.9, 128.7, 129.0, 129.1, 130.8, 132.7, 133.6, 135.0, 136.1, 136.9, 138.4, 144.8, 193.1; **HRMS (ESI-TOF)**: *m/z*: [M+Na]⁺ Calcd for C₁₇H₁₀NaO 253.0629; Found 253.0235.

Copy of NMR and other analytical spectra

Chapter 2

2.8 SPECTRAS OF COMPOUND 11*H*-Benzo[*b*]fluoren-11-one (40)

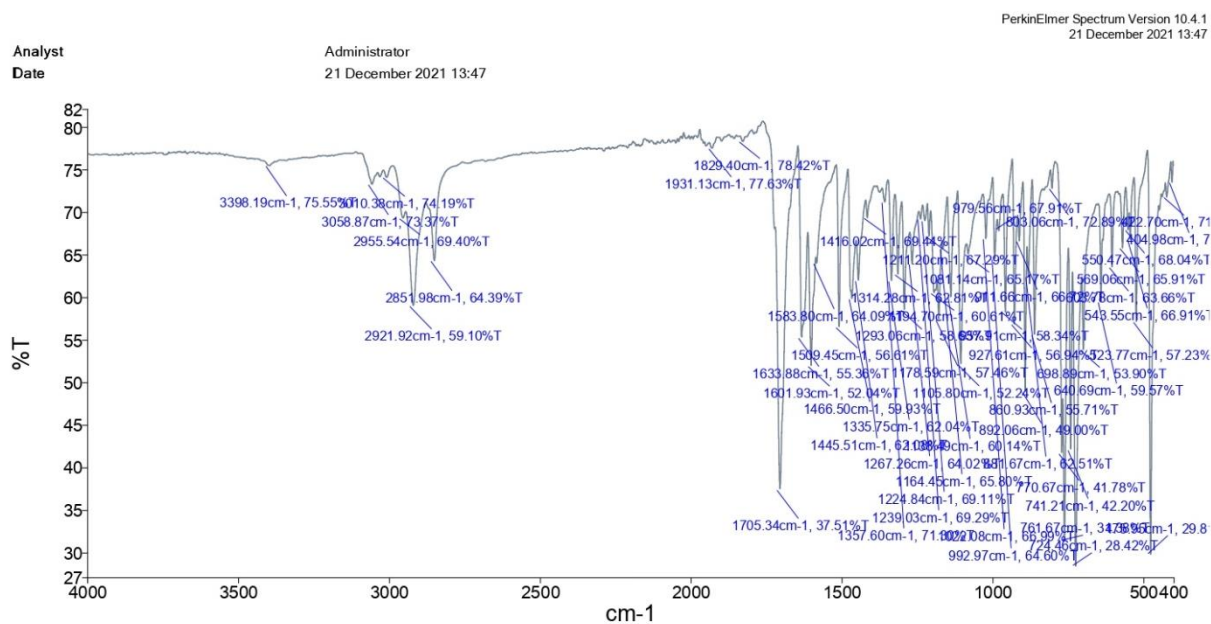


Figure 2.7 IR spectrum of 40

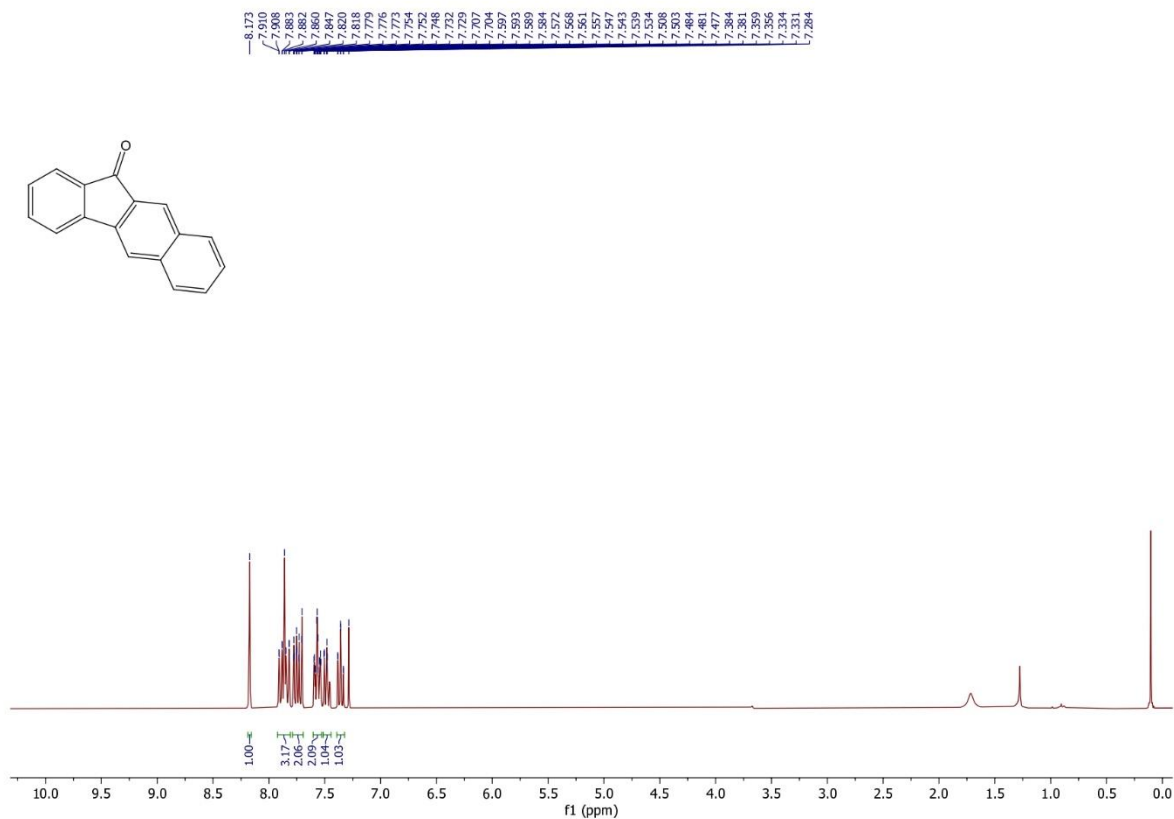


Figure 2.8 ¹H NMR spectrum of 40 (300 MHz, CDCl₃)

Chapter 2

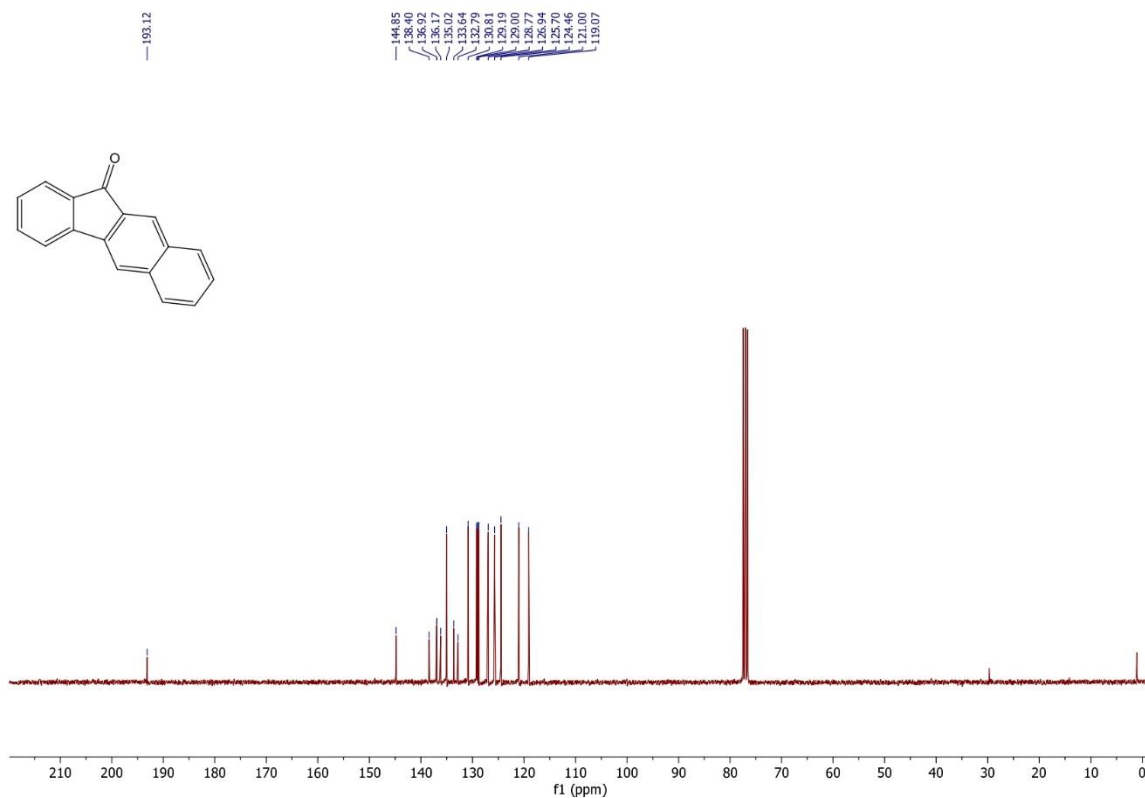


Figure 2.9 ¹³C NMR spectrum of **40** (75 MHz, CDCl₃)

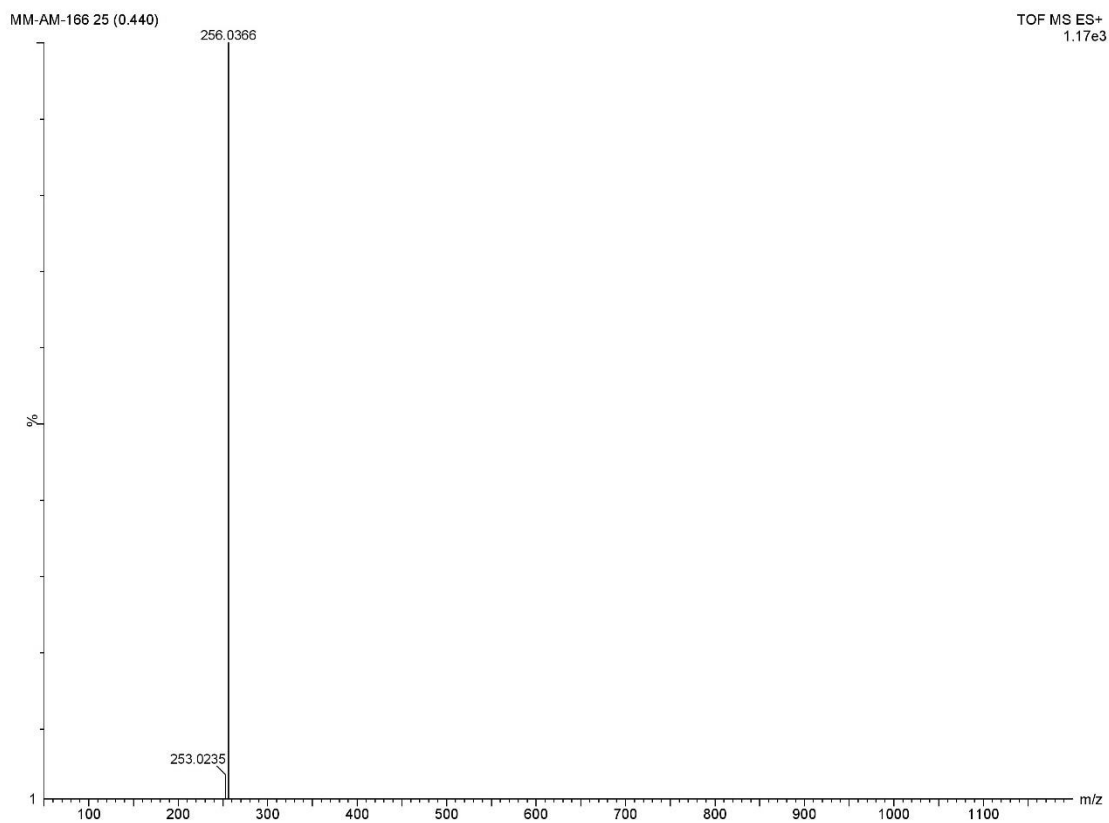


Figure 2.10 Mass spectrum of **40** (ESI-TOF) m/z: [M+Na]⁺

2.9 REFERENCES

1. Krueger, R. F.; Mayer, G. D., Tilorone Hydrochloride: An Orally Active Antiviral Agent. **1970**, *169* (3951), 1213-1214.
2. Patel, A.; Shaikh, M.; Chikhalia, K., Palladium catalyzed domino C-H activation strategy: An access to 9-fluorenones. *Tetrahedron* **2019**, *75* (2), 236-245.
3. Kroto, H. W.; Heath, J. R.; O'Brien, S. C.; Curl, R. F.; Smalley, R. E., C₆₀: Buckminsterfullerene. *Nature* **1985**, *318* (6042), 162-163.
4. Culotta, E.; Koshland, D. E., Buckyballs: Wide Open Playing Field for Chemists. **1991**, *254* (5039), 1706-1709.
5. Mehta, G.; Rao, H. S. P., Synthetic studies directed towards bucky-balls and bucky-bowls. *Tetrahedron* **1998**, *54* (44), 13325-13370.
6. Scott, L. T.; Hashemi, M. M.; Meyer, D. T.; Warren, H. B., Corannulene. A convenient new synthesis. *Journal of the American Chemical Society* **1991**, *113* (18), 7082-7084.
7. Harvey, R. G.; Abu-Shaqara, E.; Yang, C. X., An efficient synthesis of the sterically strained hydrocarbon tetrabenzo[de,hi,mn,qr]naphthacene. *The Journal of Organic Chemistry* **1993**, *58* (21), 5866-5866.
8. Simons, S. S., Jr.; Johnson, D. F., Reaction of o-phthalaldehyde and thiols with primary amines: formation of 1-alkyl(and aryl)thio-2-alkylisoindoles. *The Journal of Organic Chemistry* **1978**, *43* (14), 2886-2891.
9. Tsuda, M.; Hata, M.; Nishida, R. I. E.; Oikawa, S., CHEMICALLY AMPLIFIED RESISTS IV. PROTON-CATALYZED DEGRADATION MECHANISM OF POLY(PHTHALALDEHYDE). *Journal of Photopolymer Science and Technology* **1993**, *6* (4), 491-494.
10. Sail, B. S.; Naik, V. H.; Kamli, M. R.; Prasanna, B. M., Synthesis, spectral, in vitro microbial and DNA cleavage studies of isatin bishydrozone metal complexes. *Journal of Molecular Structure* **2023**, *1277*, 134837.
11. Zhang, M.; Zhao, M.; Wang, Y.; Chen, L.; Li, G.; Liu, B.; You, X.; Sun, W.; Hong, L., Synthesis and Biological Evaluation of Phthalideisoquinoline Derivatives. *The Journal of Organic Chemistry* **2023**, *88* (3), 1720-1729.
12. Patel, S.; Rathod, B.; Regu, S.; Chak, S.; Shard, A., A Perspective on Synthesis and Applications of Fluorenones. *ChemistrySelect* **2020**, *5* (34), 10673-10691.

13. Balasubramani, A.; Mehta, G., One-Pot Synthesis of Functionally Enriched Benzo[b]fluorenones: An Eco-Friendly Embedment of Diverse 1-Indanones into o-Bis-Ynones. *The Journal of Organic Chemistry* **2023**, 88 (2), 933-943.
14. Zhou, Z.; Xie, S.; Chen, X.; Tu, Y.; Xiang, J.; Wang, J.; He, Z.; Zeng, Z.; Tang, B. Z., Spiro-Functionalized Diphenylethenes: Suppression of a Reversible Photocyclization Contributes to the Aggregation-Induced Emission Effect. *Journal of the American Chemical Society* **2019**, 141 (25), 9803-9807.
15. Streitwieser, A., Jr.; Brown, S. M., Convenient preparation of 11H-benzo[a]fluorenone and 11H-benzo[b]fluorenone. *J. Org. Chem.* **1988**, 53 (4), 904.
16. An, G.; Wang, L.; Han, J., Palladium Catalyzed Regioselective Cyclization of Arylcarboxylic Acids via Radical Intermediates with Diaryliodonium Salts. *Org. Lett.* **2021**, 23 (22), 8688-8693.
17. Vignesh, A.; Kaminsky, W.; Dharmaraj, N., Expeditious Assembly of Fluorenones through Domino Reactions of Benzoyl Chlorides with Arylboronic Acids Catalyzed by ONO Pincer-like Palladium(II) Complexes. *ChemCatChem* **2016**, 8 (20), 3207-3212.
18. Sun, D.; Li, B.; Lan, J.; Huang, Q.; You, J., Chelation-assisted Pd-catalysed ortho-selective oxidative C-H/C-H cross-coupling of aromatic carboxylic acids with arenes and intramolecular Friedel-Crafts acylation: one-pot formation of fluorenones. *Chem. Commun. (Cambridge, U. K.)* **2016**, 52 (18), 3635-3638.
19. Qiu, S.; Zhai, S.; Wang, H.; Chen, X.; Zhai, H., One-pot synthesis of benzo[b]fluorenones via a cobalt-catalyzed MHP-directed [3+2] annulation/ring-opening/dehydration sequence. *Chem. Commun. (Cambridge, U. K.)* **2019**, 55 (29), 4206-4209.
20. Lee, S.; Kim, S. A.; Jang, H.-Y., Aerobic Oxidation of Benzylic Carbons Using a Guanidine Base. *ACS Omega* **2019**, 4 (18), 17934-17938.
21. Yang, F.; Zhou, B.; Chen, P.; Zou, D.; Luo, Q.; Ren, W.; Li, L.; Fan, L.; Li, J., Transition-metal-free C(sp³)-H oxidation of diarylmethanes. *Molecules* **2018**, 23 (8), 1922/1.
22. Nakai, S.; Uematsu, T.; Ogasawara, Y.; Suzuki, K.; Yamaguchi, K.; Mizuno, N., Aerobic Oxygenation of Alkylarenes over Ultrafine Transition-Metal-Containing Manganese-Based Oxides. *ChemCatChem* **2018**, 10 (5), 1096-1106.
23. Large, B.; Gigant, N.; Joseph, D.; Clavier, G.; Prim, D., Site-Selective Arylation of Naphthalenes: a Key Entry towards Extended Fluorenones and Phenanthridinones. *Eur. J. Org. Chem.* **2019**, 2019 (8), 1835-1841.

24. Luo, K.; Cao, T.; Jiang, H.; Chen, L.; Zhu, S., Gold-Catalyzed Ring Expansion of Enyne-Lactone: Generation and Transformation of 2-Oxoninonium. *Org. Lett.* **2017**, *19* (21), 5856-5859.
25. Sarkar, S.; Jana, M.; Tadigoppula, N., Metal-free directed ortho C-H iodination: synthesis of 2'-iodobiaryl-2-carbonitriles. *Eur. J. Org. Chem.* **2013**, *2013* (29), 6491-6495.
26. Cai, Z.; Hou, X.; Hou, L.; Hu, Z.; Zhang, B.; Jin, Z., One-Pot Palladium(II)-Catalyzed Synthesis of Fluorenones via Decarboxylative Cyclization. *Synlett* **2016**, *27* (3), 395-398.
27. Konishi, H.; Futamata, S.; Wang, X.; Manabe, K., Rapid Formation of Fluoren-9-ones via Palladium-Catalyzed External Carbon Monoxide-Free Carbonylation. *Adv. Synth. Catal.* **2018**, *360* (9), 1805-1809.
28. Li, H.; Zhu, R.-Y.; Shi, W.-J.; He, K.-H.; Shi, Z.-J., Synthesis of Fluorenone Derivatives through Pd-Catalyzed Dehydrogenative Cyclization. *Org. Lett.* **2012**, *14* (18), 4850-4853.
29. Bestmann, H. J., Old and new ylide chemistry. *Pure Appl. Chem.* **1980**, *52* (4), 771.
30. Mondal, M. A.; Mondal, S.; Khan, A. A., A mechanistic insight into the acid catalyzed, one-pot synthesis of isoindole-fused quinazolin 4-ones. *Journal of Chemical Sciences* **2020**, *132* (1), 63.
31. Zuman, P., Reactions of Orthophthalaldehyde with Nucleophiles. *Chemical Reviews* **2004**, *104* (7), 3217-3238.
32. Wang, J.; Xiang, J.; Wang, M.; Guan, J.; Wu, A., Synthesis of substituted naphthalenes from α -substituted ketones and 1,2-bis(halomethyl)benzenes including a rearrangement aromatization of benzo[c]oxepine. *Tetrahedron* **2014**, *70* (7), 1412-1417.
33. Hull, L. A., The Dibenzalacetone Reaction Revisited. *Journal of Chemical Education* **2001**, *78* (2), 226.
34. Bortolini, O.; Fantin, G.; Ferretti, V.; Fogagnolo, M.; Giovannini, P. P.; Massi, A.; Pacifico, S.; Ragno, D., Methylsulfinyl (Dimsyl) Anion as Umpolung Catalyst for the Chemoselective Cross-Benzoin Reaction of α -Diketones with Aldehydes. *Advanced Synthesis & Catalysis* **2013**, *355* (16), 3244-3252.
35. Zhao, M. N.; Hui, R. R.; Ren, Z. H.; Wang, Y. Y.; Guan, Z. H., Ruthenium-catalyzed cyclization of ketoxime acetates with DMF for synthesis of symmetrical pyridines. *Organic letters* **2014**, *16* (11), 3082-5.
36. Xie, W.; Li, T.; Chen, C.; Wu, H.; Liang, S.; Chang, H.; Liu, B.; Drioli, E.; Wang, Q.; Crittenden, J. C., Using the Green Solvent Dimethyl Sulfoxide To Replace Traditional Solvents Partly and Fabricating PVC/PVC-g-PEGMA Blended Ultrafiltration

- Membranes with High Permeability and Rejection. *Industrial & Engineering Chemistry Research* **2019**, 58 (16), 6413-6423.
37. Belmonte-Vázquez, J. L.; Amador-Sánchez, Y. A.; Rodríguez-Cortés, L. A.; Rodríguez-Molina, B., Dual-State Emission (DSE) in Organic Fluorophores: Design and Applications. *Chemistry of Materials* **2021**, 33 (18), 7160-7184.

Chapter 3

Aromatic Amine attached Quinazolinones: Synthesis Characterization and DNA Binding Properties

Part of the work described in this chapter is published in

ChemistrySelect 2024, 9, e202303740; DOI: 10.1002/slct.202303740

Aromatic Amine attached Quinazolinones: Synthesis Characterization and DNA Binding Properties

3.1 INTRODUCTION

Heterocyclic compounds containing nitrogen (N) atoms in their structures are considered a crucial class of heterocycles extensively utilized in medicinal chemistry.^{1, 2} Depending on the position of the N-atom(s) within the ring, they are known by different names such as Quinazolines, Quinazolinones, Quinolins, Pyrimidines, Pyrimidinones, Indoles, Isoindoles, Pyrazoles, Triazoles, Imidazoles, etc. Among these heterocyclic compounds, Quinazolinones, Pyrimidinones, and Isoindoles have garnered significant attention in various research sectors, including synthetic organic and medicinal chemistry. Due to their diverse applications, the synthesis of heterocyclic compounds has become a focal point in organic synthesis.

Quinazolines represent a subgroup within the quinoline alkaloids, characterized by a fused benzene and pyrimidine bicyclic structure **66a** (Figure 3.1). Quinazolinones, the oxidized form of quinazolines, are also encompassed within the quinoline alkaloids. Both naturally occurring and synthetically derived quinazolines and quinazolinones have garnered significant attention due to their diverse range of pharmacological activities. The arrangement of the oxygen and hydrogen on the nitrogen (NH) defines these structures, and the generally accepted numbering for quinazolines and quinazolinones is based on the quinazoline structure (Figure 3.1). The primary sub-classes of quinazolinones can be categorized as: (i) 4(3*H*)-quinazolinone (3*H*-1,3-quinazolin-4-one); **66b** (ii) 2(1*H*)-quinazolinone (1*H*-1,3-quinazolin-2-one); **66c** (iii) 2,4(1*H*,3*H*)-quinazolinedione (1*H*,3*H*-1,3-quinazoline-2,4-dione); **66d**.

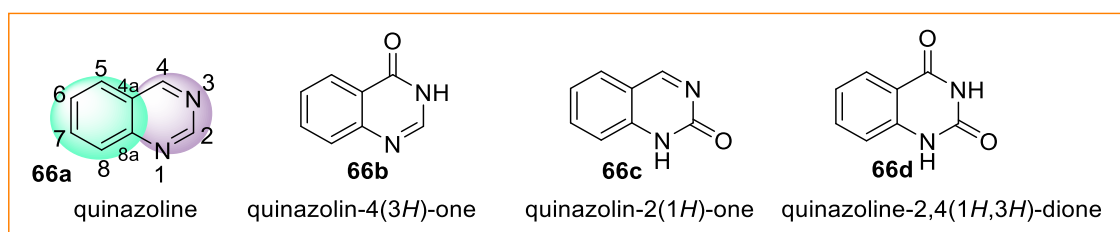


Figure 3.1 Core structure of quinazoline and quinazolinone

Of the three quinazolinone structures the 4(3*H*)-quinazolinones are most prevalent, either as intermediates, or as natural products in many proposed biosynthetic pathways. Quinazolinone serves as a foundational unit for approximately 200 naturally occurring alkaloids that have been identified to date. These alkaloids are found in various plant families, animals, and microorganisms. The initial discovery of a quinazoline alkaloid dates back to 1888 when vasicine (peganine **66e**) was isolated from the Indian medicinal tree *Adhatoda vasica*.

Subsequently, this alkaloid has been identified in other species along with additional quinazolinone alkaloids such as vasicinone (66f) and deoxyvasicinone (66g).^{3,4} Following the initial discovery, a diverse range of quinazoline and quinazolinone natural products have been isolated, characterized, and subsequently synthesized. The first quinazolinone, 2-cyanoquinazolinone (66h), was synthesized in the late 1860s from anthranilic acid and cyanogens (Figure 3.2).⁵ The interest in the medicinal chemistry of quinazolinone derivatives gained momentum in the early 1950s with the structural elucidation of a quinazolinone alkaloid, 3-[β -keto- γ -(3-hydroxy-2-piperidyl)-propyl]-4-quinazolinone (febrifugine, 66i), from an Asian plant *Dichroa febrifuga*. This alkaloid is an ingredient in a traditional Chinese herbal remedy effective against malaria. In the pursuit of discovering additional potential quinazolinone-based drugs, various substituted quinazolinones have been synthesized. This effort led to the creation of 2-methyl-3-o-tolyl-4-(3*H*)-quinazolinone (methaqualone 66j). Synthesized for the first time in 1951, methaqualone (66j) is the most well-known synthetic quinazolinone drug, renowned for its sedative–hypnotic effects.

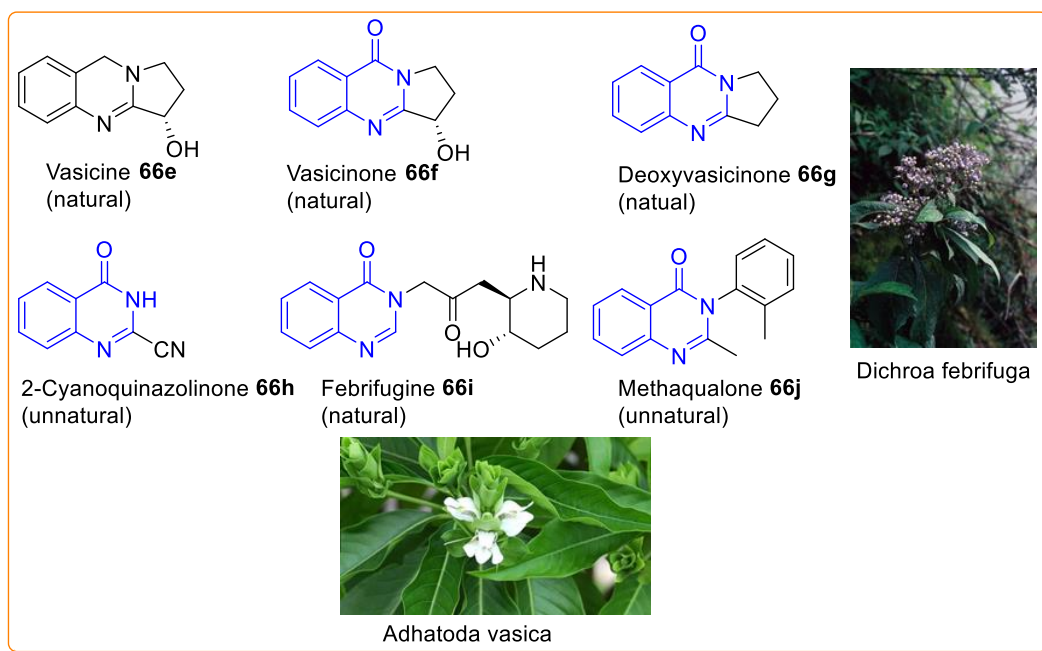


Figure 3.2 Natural and unnatural quinazolinones

Quinazolinones exhibit different varieties of chemical and biological properties. Even a single compound shows a diverse range of biological functions. Synthetic small molecule halofuginone **66r** (Figure 3.3) is a potent inhibitor of the critical steps in angiogenesis progression and tumor suppressor.^{6,7} Febrifugine **66s** derivatives have been used to treat malaria, inflammatory disease, fibrosis, and cancer.⁸ Other properties include inhibition-activity of many critical biological targets, e.g., tankyrase,⁹ COX-II,¹⁰ tubulins,¹¹

poly(adenosine-diphosphate-ribose)polymerase-1,¹² and CDK5/p25 kinase¹³ of quinazolinones are notably significant. Recently, compound **66k** was evaluated as a potential cytotoxic agent to human lung carcinoma cell line and the results are comparable with the standard drug cisplatin.¹⁴ Certainly, given its significance as a crucial pharmacophore and a foundational unit for numerous drugs and natural products¹⁵ (Figure 3.3), quinazolinone stands out as a focal point in our research. Recognizing its potential, we consider it a powerful structural motif for drug development endeavors. Therefore, synthesizing the diverse array of quianazolines and their use as ligands for tuning the biological process of biomolecules is a longstanding and continuous research interest.

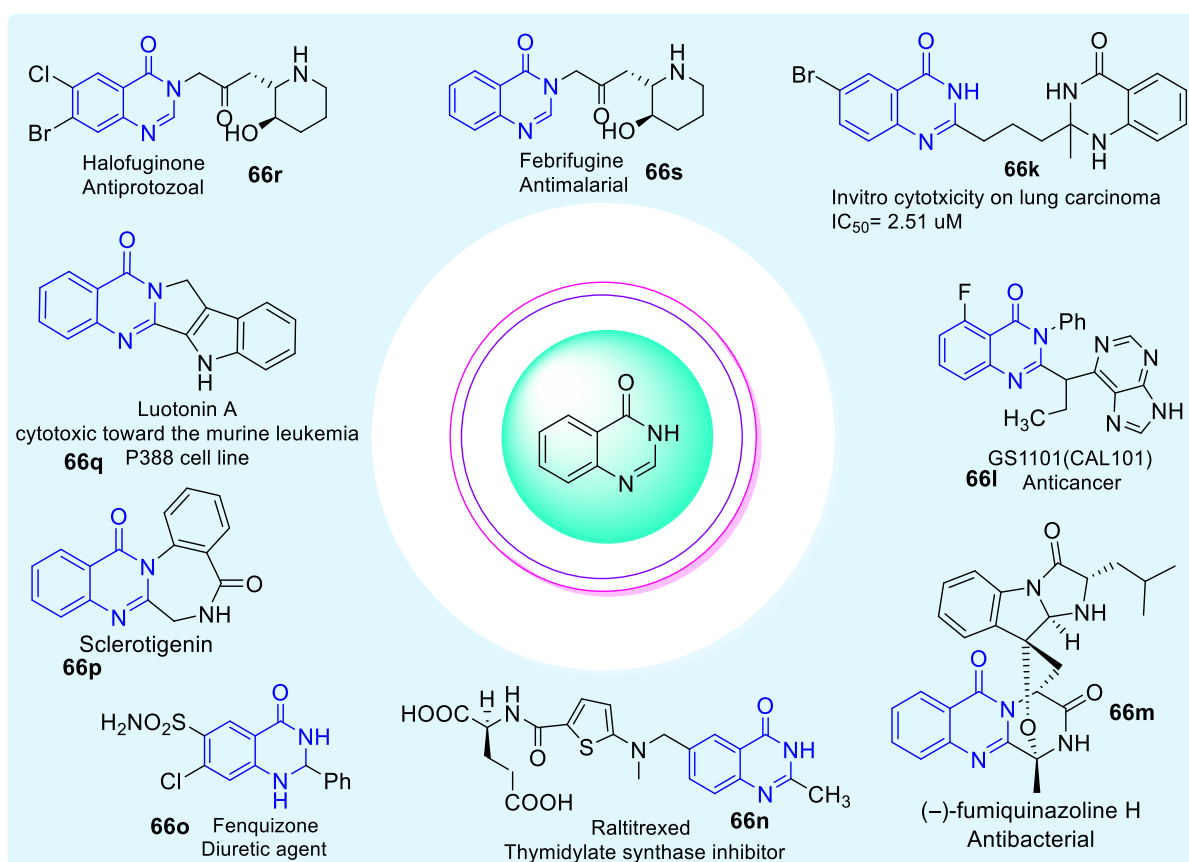


Figure 3.3 Pharmaceutically important Quinazolinone based drugs

Studies on quinazolinones reveal a notable lactam-lactim tautomeric interaction. The significance of these extended tautomeric effects lies in their ability to enhance the reactivity of substituted 4(3*H*)-quinazolinones.^{16, 17}

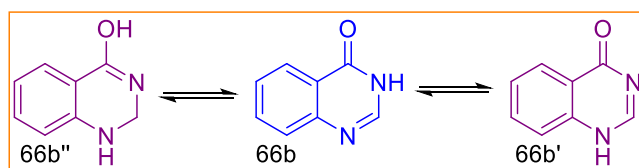


Figure 3.4 Diagram of the tautomeric states of 4(3*H*)-quinazolinone

Upon an in-depth review of the literature focusing on the chemical properties inherent in the structure of quinazolinones, a notable observation becomes apparent: the hydrogen atoms positioned at site-2 display a tendency to undergo hydride transfer towards a discernibly electropositive center. The use of hydride transfer (HT) in organic synthesis remains an expanding field of research. Intramolecular hydride transfer (HT) reactions, also referred to as redox-neutral reactions, are characterized by the migrated hydrogen not exchanging or combining with solvent protons. For a successful intramolecular hydride transfer (HT) reaction, a proximal acceptor center with an electron-deficient nature is essential to receive the transferred hydride. Electron-deficient functional groups like imine, carbonyl, C=C bond, α,β -unsaturated keto, or ester are commonly employed as acceptor centers with the assistance of an activator. Another crucial factor for the effective application of redox-neutral reactions is the presence of a non-bonded electron pair or an anionic center. Therefore, hydrogen located at the methylene/methine group adjacent to heteroatoms (e.g., N, O, S) readily serves as a hydride donor. Utilizing this protocol, numerous complex organic syntheses have been successfully achieved.

To the best of our knowledge, this less-explored area presents an interesting opportunity for the functionalization of quinazolinones or for carrying out various types of reactions using the hydride transfer (HT) protocol.

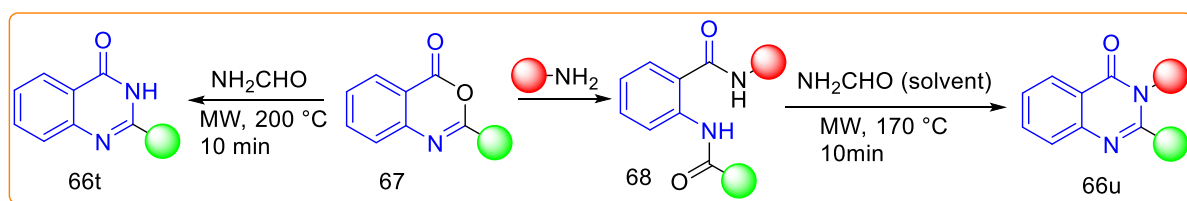
Continuing our previous interest in synthesizing heterocyclic moieties for developing small-molecule anticancer agents,¹⁸⁻²¹ we reported here an expeditious method for conjugating a quinazolinone moiety with an aromatic amine through a four-carbon spacer. The described method enabled quick access to diverse quinazolinones structurally similar to the reported anticancer agent **66k**. A study with one of the synthesized compounds (**86k-HCl**) revealed that the compound is a potential DNA binder. Detailed studies of binding interactions with ctDNA have been investigated by using UV/Vis absorption, fluorescence, and circular dichroism (CD) spectroscopy.

3.2 LITERATURE BACKGROUND

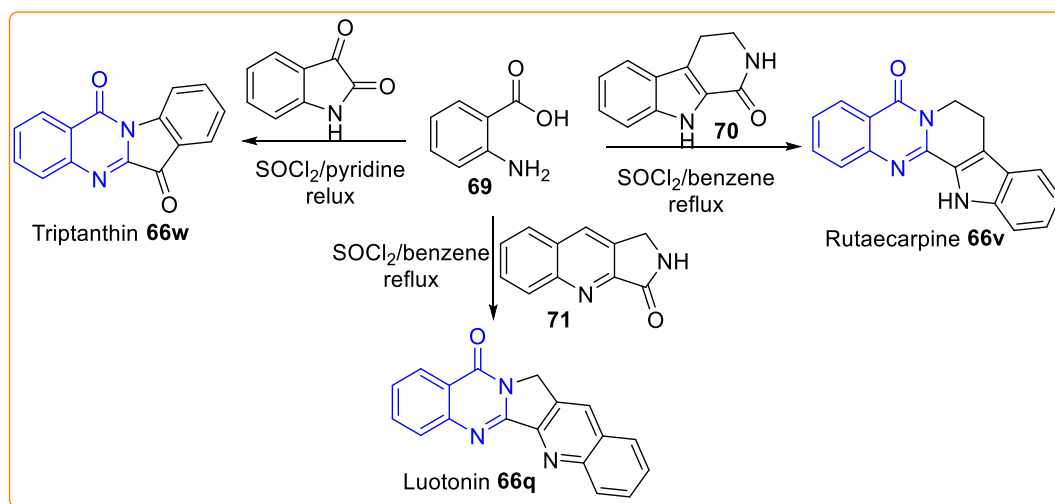
Even though quinazolinone chemistry is considered a well-established area, ongoing research continues to unveil newer and more complex variants of the quinazolinone structure. Significant progress in synthetic methodologies applicable to the synthesis of quinazoline alkaloids and related molecules has been reported in the literature. This section outlines some

of the important methodologies for the synthesis of quinazolinones and redox neutral [1,*n*]-hydride transfer methodologies.

Besson and his group developed an effective method for synthesizing 2,3-disubstituted-quinazolin-4(3*H*)-ones **66u** through microwave irradiation of linear diamides **68** in formamide solvent. Their findings underscored that the microwave-promoted decomposition of formamide under controlled power, temperature, and time was critical for using formamide as a highly convenient ammonia source in the preparation of 2-substituted-quinazolin-4(3*H*)-ones **66t** (Scheme 3.1).²²



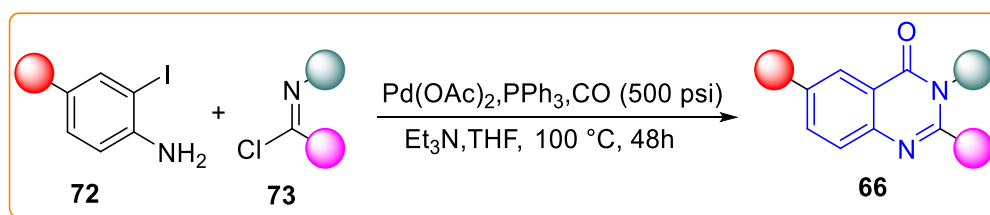
Scheme 3.1 Microwave-assisted synthesis of 2- and 2,3-disubstituted-quinazolin-4(3*H*)-one Jahng et al. demonstrated a one-pot synthesis of 2,3-disubstituted-4(3*H*)-quinazolinones from anthranilic acid, the corresponding lactam, and thionyl chloride in refluxing benzene or pyridine. They utilized this protocol for the one-step preparation of luotonin A (**66q**), rutaecarpine (**66v**) and tryptanthrin (**66w**) (Scheme 3.2).²³ The condensation reactions in this synthesis proceed through the corresponding *N*-sulfinylanthraniloyl chloride intermediate.



Scheme 3.2 One-pot synthesis of quinazolinone based alkaloids

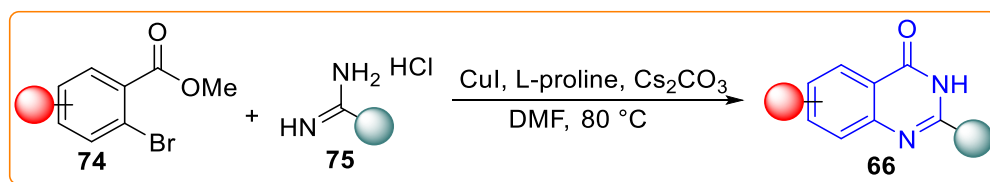
Alper and colleagues recently reported a palladium-catalyzed three-component cyclocarbonylation reaction involving *o*-iodoanilines **72**, imidoyl chlorides **73** and carbon monoxide. The reaction proceeds through the in-situ generation of an amidine, followed by oxidative addition of palladium, CO insertion, and intramolecular cyclization. This process

leads to the formation of substituted 2,3-disubstituted-quinazolin-4(3*H*)-ones **66**. The method is tolerant of various functional groups, providing the quinazoline-4(3*H*)-ones **66** in yields ranging from 63-91% (Scheme 3.3).²⁴



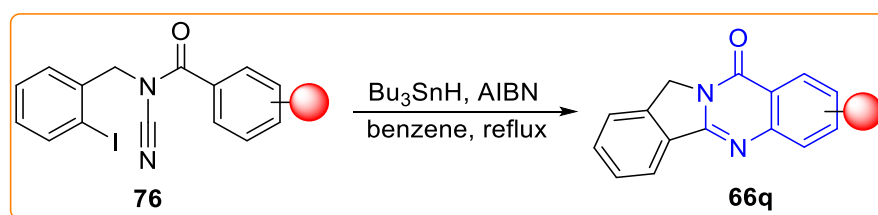
Scheme 3.3 Palladium-catalyzed carbonylation of *o*-iodoanilines

Zhao et al developed a general and efficient copper-catalyzed method for 2-substituted quinazoline-4(3*H*)-ones through a cascade reaction of amidine hydrochlorides with 2-halomethylbenzoate (Scheme 3.4). The reaction involves *ortho*-halomethylbenzoate **74** with amidine hydrochlorides **75** using copper iodide as a catalyst, L-proline as a ligand, and cesium carbonate as the base in DMF as a solvent at 110 °C, exclusively providing 2-substituted quinazoline-4(3*H*)-ones **66**.²⁵



Scheme 3.4 Cu(I)-catalyzed coupling of imidamides with *o*-haloaryl-carboxy compound

Fensterbank and colleagues illustrated a rapid synthesis of the natural alkaloid luotonin A **66q** via cascade radical cyclization of *N*-acylcyanamides process involves a domino mechanism that forms new C-C and C-N bonds via radical migration of hydrogen atoms or carbon substituents on the aromatic ring (Scheme 3.5).²⁶

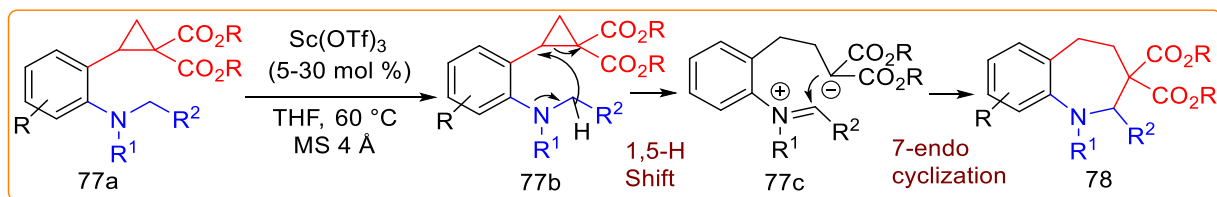


Scheme 3.5 Radical cyclization cascade of *N*-acyl-*N*-(2-iodobenzyl)cyanamides

In light of our interest in hydride transfer chemistry, we have contemplated a related approach for the general α -functionalization of amines. In this context, we have reviewed literature on intramolecular hydride transfer, and some of the related works are discussed below.

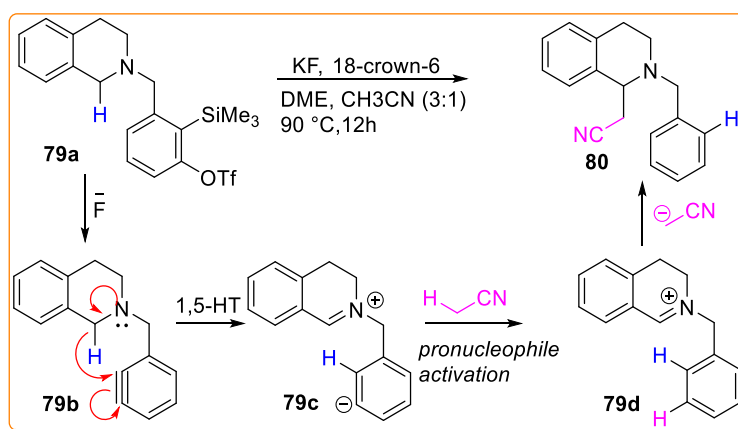
Kim et al proposed a reaction mechanism in which the interaction between a donor-acceptor cyclopropane containing cyclic amine **77a** and Lewis acid catalysts initiates a [1,5]-hydride

shift, resulting in the formation of the zwitterion **77c**. This is followed by a 7-endo cyclization, ultimately yielding the benzazepines **78** (Scheme 3.6).²⁷



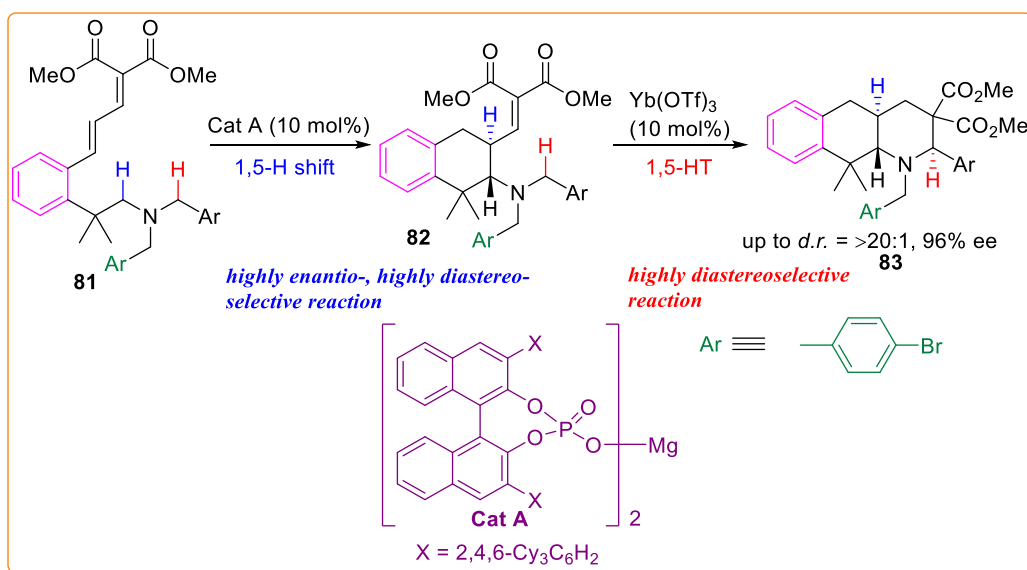
Scheme 3.6 Synthesis of Heterocycles via [1,5]-Hydride Shift Cyclization Sequences

Jones et al. described a transition metal-free and redox-neutral process for generating a new C-C bond alpha to nitrogen in a single step (Scheme 3.7). In their approach, they used 1,2,3,4-tetrahydroisoquinoline (THIQ) as the hydride donor and an aryne acceptor tethered to the amine donor using a 2-trimethylsilyl-3-trifluoromethanesulfonyl benzaldehyde precursor. Treatment of the *o*-silylaryl triflate precursor **79a** with fluoride generated an aryne **79b** that underwent intramolecular 1,5-hydride transfer from a C-H bond α to nitrogen. The resulting zwitterionic intermediate **79c** then deprotonated acetonitrile to form an iminium ion **79d** that underwent a Mannich-type addition to give the α -cyanomethylated amine **80**.²⁸



Scheme 3.7 Intramolecular hydride transfer onto aryne with THIQ derivatives.

Akiyama group developed an asymmetric double C(sp³)-H bond functionalization in presence of a chiral magnesium bisphosphate as a catalyst to afford a highly enantio- and diastereoselective synthesis of fused tricyclic piperidine derivatives. The reaction involves two successive stereoselective C(sp³)-H bond functionalizations, the first step is the highly enantio- and diastereoselective C(sp³)-H bond functionalization catalysed by the chiral magnesium phosphate via a [1,5]-hydride shift followed by an achiral catalyst mediated diastereoselective C(sp³)-H bond functionalization via second 1,5-hydride transfer methodology (Scheme 3.8).²⁹



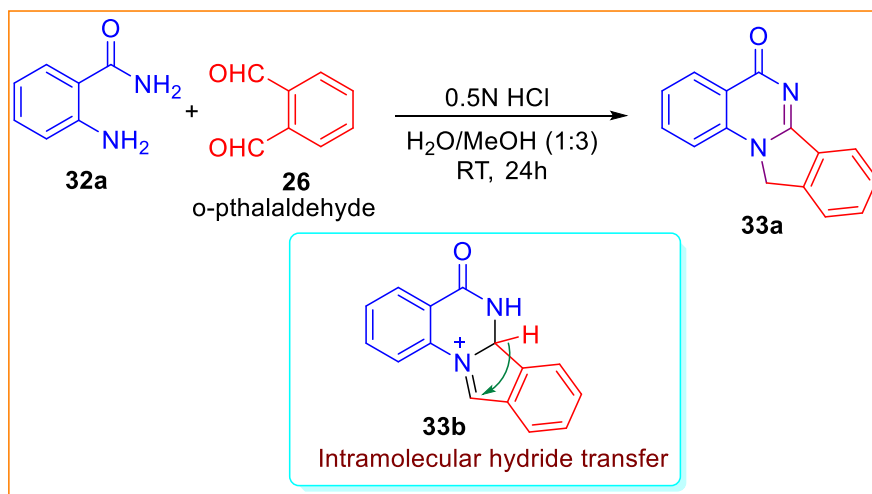
Scheme 3.8 Asymmetric double C(sp³)–H bond functionalization

In accordance with the principles of redox- and step-economy, we have disclosed a method involving intramolecular hydride transfer to distal imines, leading to the generation of highly functionalized quinazolinones. This synthetic approach aligns with the efficient utilization of redox reactions and the reduction of unnecessary steps, showcasing its potential value in organic synthesis.

3.3 LITERATURE BACKGROUND & CONTRIBUTION FROM OUR GROUP

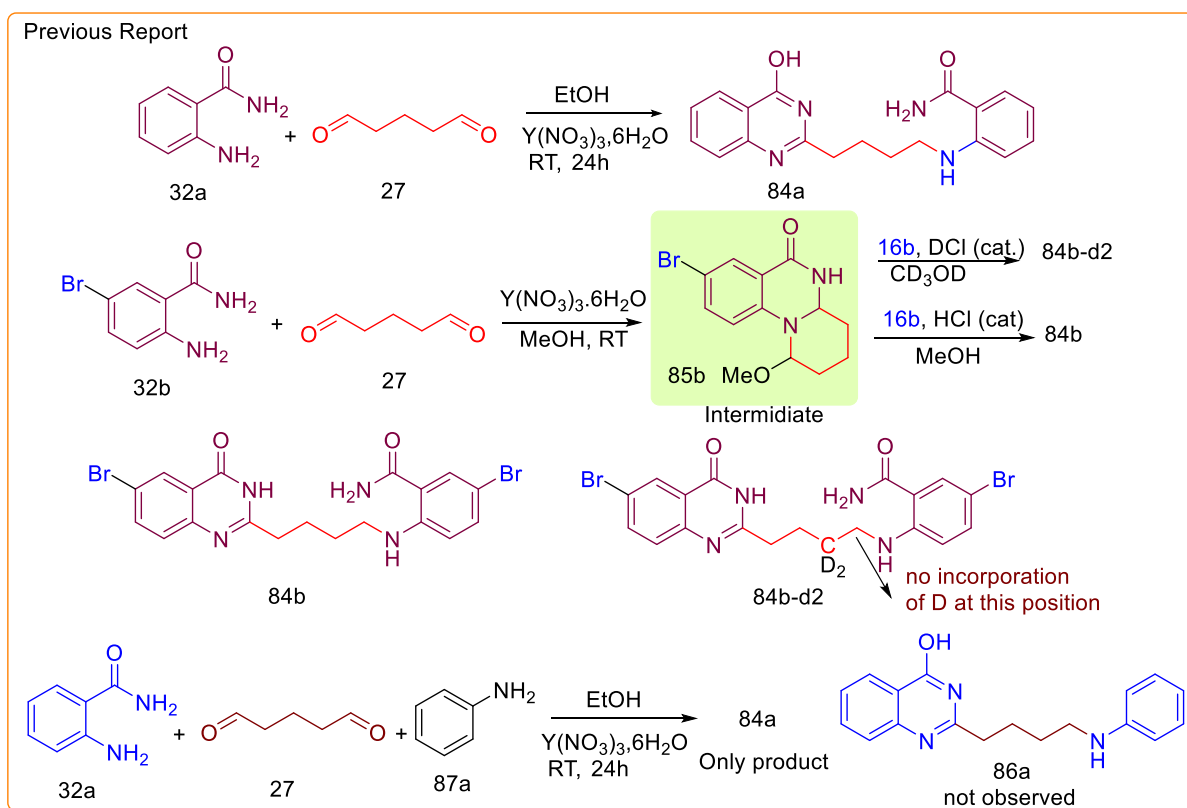
Building upon our prior investigation into the synthesis of quinazolinones derived from 1,5-bisnucleophile precursors like 2-aminobenzophenone and glutaraldehyde, our findings have uncovered a significant limitation in the methodology. Specifically, we observed the attachment of dimeric anthranalimide at both ends of the glutaraldehyde substrate.³⁰ Despite numerous attempts to modify the other end of the glutaraldehyde molecule, these efforts have unfortunately proven unsuccessful. This limitation highlights the necessity for further exploration and refinement of the synthetic approach to overcome these challenges and potentially enhance the versatility and applicability of the methodology.

When equimolar mixture of 2-amino benzamide **32a** and *ortho*-phthalaldehyde **26** in methanol and 2(N) aq. HCl (3:1) at room temperature gave the compound **33a** smoothly.²⁰



Scheme 3.9 Synthesis of isoindolo[2,1-a]quinazolin-5(11*H*)-one from 2-aminobenzamide. Primarily, two types of mechanistic pathways; namely, intramolecular hydride transfer (Path-A) and tautomerism (Path-B) have been proposed for the reaction of **26** with structurally identical 1,5-*N*-bisnucleophiles. Path-A involves intramolecular 1,3- hydride transfer without participation of solvent proton in the key step. Whereas, in the Path-B, multiple tautomeric sequences by which hydrogen atom transferring with the participation of solvent proton may lead to the compound 33bHCl. Deuterium experiment showed no deuterium incorporation in the structure of it 33bHCl.²⁰

After the above observations our group explored the reactivity of anthranilamide with aliphatic dialdehyde (glutaraldehyde). Primarily our group observed a complex reaction mixture when compound **32a** and glutaraldehyde **27** were subjected under the similar condition. However, 2:1 molar ratio of compound **32a** and **27** mixed with lower acid loading gave the compound **84a** as a white solid. The compound **84a** is a redox-neutral product, where an oxidation and reduction process is going on without adding any external oxidative or reducing agents. In this case, an imine functionality acted as the hydride accepting counterpart and facilitated the intramolecular redox reaction. The intermediate of this reaction **85** containing bromine was isolated under milder condition using Y(NO₃)₃·6H₂O in methanol. But the same product **84b** was isolated in methanol under their optimum condition i.e. 2(N) aq. HCl (3:1) at room temperature. When CD₃OD/DCl was used as a reaction medium compound **85** converted into a redox neutral product **84b-d2**. No deuterium incorporation was observed at the reduced site. This critical information led us to conclude that the hydride is being transferred from quinazolinone moiety to the reduced site without the participation of solvent protons.

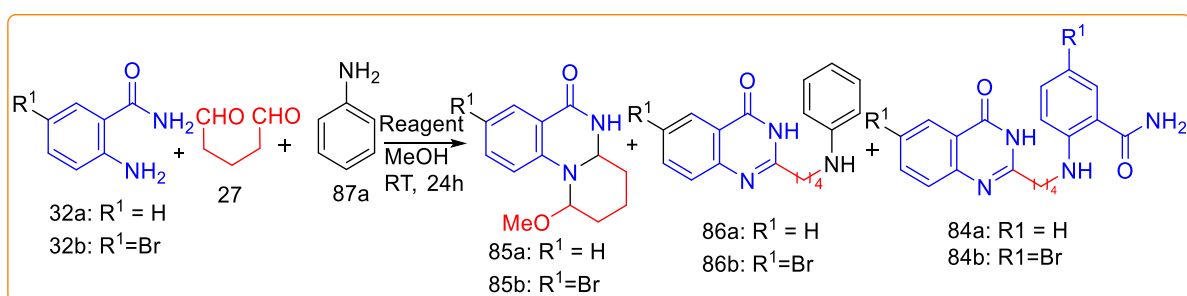


Scheme 3.10 Previous report from our group

3.4 RESULT AND DISCUSSION

We observed the spontaneous formation of compound **84a** via intramolecular 1,5 hydride transfer when glutaraldehyde is treated with excess anthranilamide **32a** in the presence of an acid catalyst. In the structure of compound **84a**, one unit of anthranilamide is involved in the quinazolinone ring formation at one terminal, whereas the second unit of anthranilamide is connected through the primary aromatic amine at the other terminal of glutaraldehyde.

In this context, we have explored the possibility of using one molecule of anthranilamide with another molecule of primary aromatic amine to synthesize quinazolinones **86**, having structurally different heteroatom-units at the terminals of glutaraldehyde spacer.



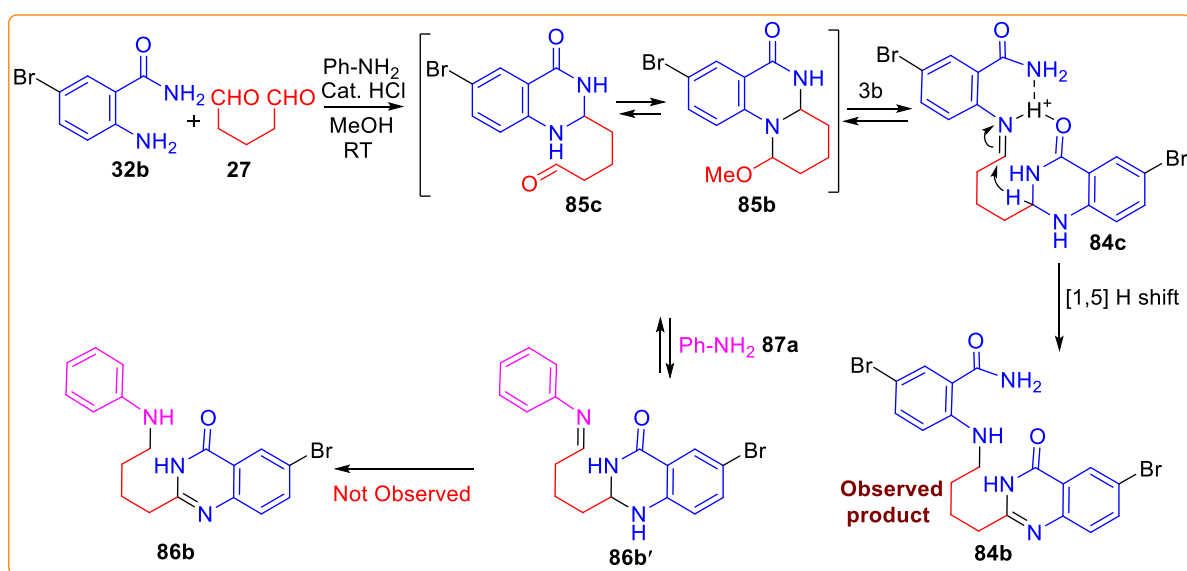
Scheme 3.11: Synthesis of the functionalized quinazolinones

Table 3.1: One-pot attempts to synthesized compound **86**

Entry	Starting compounds		Catalyst	Product (Yield %)		
	32	Aniline		84	85	86
1	32a (1 eqv.)	Aniline (1eqv.)	^d HCl	84a (32%)	-	-
2	32a(2 eqv.)	-	HCl	84a (91%)	-	-
3	32a (2 eqv.)	Aniline (1eqv.)	HCl	84a (85%)	-	-
4	32a(2 eqv.)	Aniline (1eqv.)	^c Y(NO ₃) ₃	84a (73%)	-	-
5	32b (2 eqv.)	Aniline (1eqv.)	HCl	84b (85%)	-	-
6	32b (2 eqv.)	Aniline (1eqv.)	Y(NO ₃) ₃		85b (63%)	
7	32b (1 eqv.)	-	Y(NO ₃) ₃		85b (84%)	
8	32a (1 eqv.)	-	Y(NO ₃) ₃	Complex Mixture		
9	32a (1 eqv.)	-	FeCl ₃	Complex Mixture		
Note						
a) All the reactions are run for 24 hours at ambient temperature in an open pot using the stoichiometry mentioned with 100 mg of 32b						
b) Isolated Yield						
c) 10 mol% Y(NO ₃) ₃ .6H ₂ O was used						
d) 67 µl of 36% HCl in 5 ml isopropanol was used to run the reaction						

Synthesis of compound **86a** requires the coupling of anthranilamide and an amine (Ar-NH₂) in the presence of glutaraldehyde. Initially, we attempted a one-pot method under different reaction conditions. A stoichiometric mixture of anthranilamide **32a**, glutaraldehyde **27** and aniline **87a** (equimolar ratio) in isopropanol in the presence of catalytic acid led to a complex reaction mixture from where compound **84a** was isolated in 32% yield. The formation of the cross-coupling product **86a** was not observed. However, the yield of the **84a** was enhanced up to 91% when 2:1 ratio of the starting compound **32a** and glutaraldehyde **27** was maintained (Entry 2, Table 3.1). Aniline **87a** did not participate in the reaction even in the presence of a mild Lewis acid Yttrium nitrate³¹ under competitive reaction conditions (Entry 4). A similar study with compound **32b** was carried out under various reaction conditions (Table 3.1; Entry 5, 6 & 7). Compound **32b**, in the presence of Y(NO₃)₃.6H₂O did not proceed to the end product **86b** or **84b**; instead, it resulted in the formation of an intermediate product **85b**.

We observed³⁰ that the intermediate product **85b** converted to the compound **84b** in the presence of catalytic HCl in isopropanol via a [1,5] hydride shift. The proposed mechanism involved the initial formation of intermediate **85c** or **85b**, followed by the formation of intermediate **84c**. An intramolecular hydride transfers in intermediate **84c** (Scheme 3.12), promoted by the acid or metal ion through the activation of imine, led to the formation of product **84b**. The nonparticipation of aniline in the one-pot reaction (Entry 1,3-6, Table 3.1) in the competitive reaction medium is attributed to the exclusive formation of imine intermediate **84c**. The intramolecular three-center hydrogen bonding³² in the intermediate **84c** facilitated such selectivity. This type of stabilization was absent in the intermediate **86b'** obtained from aniline **87a** (Scheme 3.12).

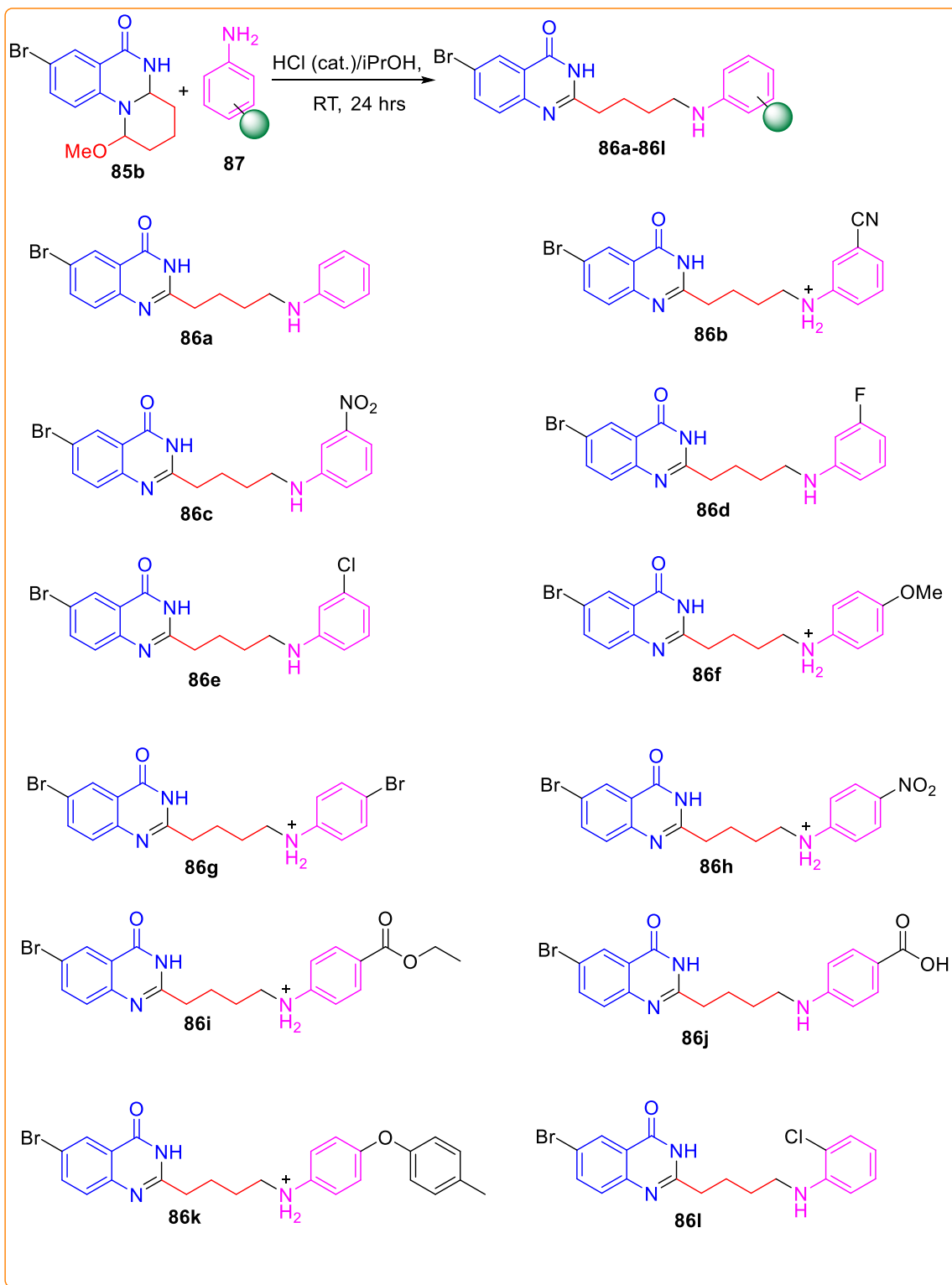


Scheme 3.12 Mechanistic explanation for selective formation of **84b** in the presence of aniline.

Then, we attempted to isolate compound **85a** from **32a** (Table 3.1, Entry 3, 4, 6, 7) using different catalysts, such as Y^{3+} , Fe^{3+} , and HCl. All attempts failed to isolate compound **85a**. Considering the importance of the compound **66k** reported by Nasrin et al.¹⁴ we have used compound **85b** to couple with different substituted aromatic amines as shown in the Scheme 3.13. Thus, we developed a two-step process to connect a quinazolinone moiety with aromatic amines under mildly acidic conditions. The use of less polar, non-toxic solvent *i*PrOH gave better results. However, in *i*PrOH condition, we isolated a few compounds (**86b**, **86f-i** and **86k**) in the form of HCl salt and characterized them as such without converting them into the salt-free state.

We have synthesized 12 (86a-86l) different products, as shown in Scheme 3.13 from compound **85b** by the reaction of aromatic amine in the presence of catalytic HCl, and the solid products isolated from the reaction mixture by filtration was used for spectroscopic data collection. The structure of the quinazolinone derivatives was confirmed by IR, NMR spectroscopy, and HRMS. The IR spectrum of compound **86a** is characterized³³ by the presence of a strong band at 1678 cm^{-1} due to the amide carbonyl stretching and an N-H stretching band at 3327 cm^{-1} . The N-H peaks in ^1H NMR at 11.79 ppm and the amide carbonyl carbon peak at 163 ppm in ^{13}C NMR of compound **86a** are in favor of the amide structure.

It was interesting to note that the NH peak of the quinazolinone ring of the compound 86b, 86f-86i and 86k did not appear in ^1H -NMR as it was observed around 12 ppm for the compounds 86a, 86c-e, 86j, and 86l. The first set of the compound were isolated in the form of HCl salt. This was confirmed by converting 86k-HCl into compound 86k by the treatment of aqueous NaHCO_3 solution. The point of protonation was confirmed by comparing the chemical shift of the PMR of 86k-HCl and 86k (Figure 3.5A). It appeared that the protons attached to the diaryl ether ring and the aliphatic $-\text{CH}_2-$ adjacent to the spacer nitrogen were most deshielded due the protonation. And the quinazolinone ring proton resonances remained unchanged in the PMR. Hence, the point of protonation was at the spacer nitrogen atom, not at the quinazolinone nitrogen atoms. The protons of the ammonium center were being rapidly exchanged (Figure 3.5B) with the quinazolinone heteroatom protons through the residual water molecule present in the NMR solvent.³⁴ Therefore, the heteroatom protons and the residual water peak of NMR solvent appeared as a broad singlet in the range 4-6 ppm in the PMR spectrum. The ^{13}C NMR of the salt shows a significant change in the carbon signals of the diaryl ether ring (Figure 3.5C). The boarding of the signal of $-\text{Me}$ (48.6 ppm) and the aromatic ring carbon (119.0, 121.6) of the 4-methylphenyl units of 86k-HCl was due to the rapid rotation of the ring. However, in the case of 86k the free rotation is restricted because of the extended conjugation of the nitrogen ether oxygen lone pair with the aryl rings of the diaryl ether unit.



Scheme 3.13 Synthesis of the quinazolinones

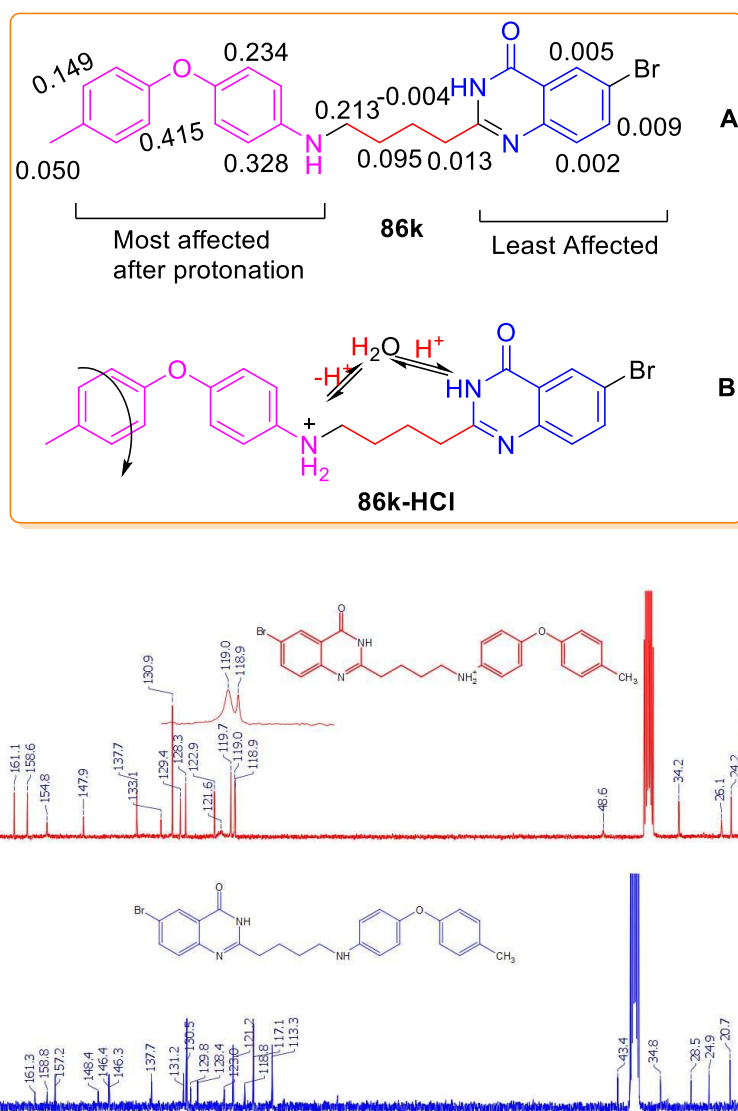


Figure 3.5 (A) Chemical shift difference of the individual protons sets of the compound 86k-HCl and 86k. (B) Rapid proton exchange mechanism. (C) ¹³C NMR of 86k-HCl (Red) and 86k (Blue)

3.5 CALF-THYMUS DNA (ctDNA) BINDING STUDY

It has been half a century since Watson and Crick made the ground breaking discovery that genetic material possesses a structural form known as the double helix, a concept now firmly established with well-defined characteristics. This pivotal revelation regarding the structure of DNA immediately underscored its significance in regulating cellular functions, leading to the recognition of DNA as an excellent target for addressing illnesses with genetic origins, particularly conditions like cancer. Cancer is one of the most prevailing disease conditions, which occurs due to uncontrolled cell division either due to natural mutation to the genes or due to changes induced by physical, chemical, or biological carcinogens. As per the World Health Organization (WHO), cancer stands as the second leading cause of death globally, with

a staggering 10 million reported deaths in the year 2020 alone. This alarming statistic underscores the urgent need for more effective chemotherapies, and DNA intercalators have emerged as a promising therapeutic avenue for cancer treatment.

DNA intercalating agents represent a class of compounds that reversibly intercalate with the double-helical structure of DNA. They achieve this by interacting with adjacent base pairs, disrupting the DNA structure and ultimately leading to cell death. Numerous anticancer drugs in clinical use leverage this mechanism of action through intercalation.

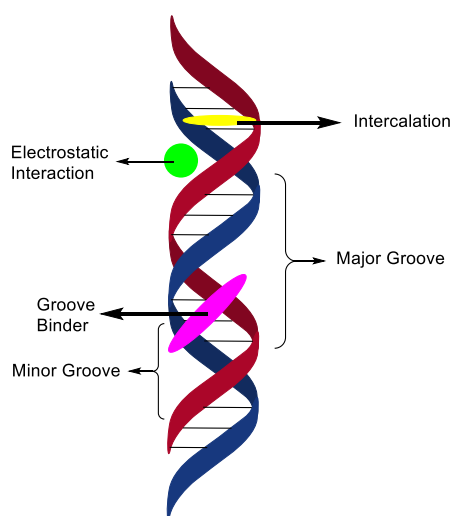


Figure 3.6 General picture of an intercalator and a groove binder

The intercalation process initiates with the transfer of an intercalating molecule from an aqueous environment to the hydrophobic space situated between two adjacent DNA base pairs as depicted in Figure 3.6. This transfer is thermodynamically favoured, primarily due to the positive entropy contribution resulting from the disruption of the organized shell of water molecules around the ligand, a phenomenon known as the hydrophobic effect. For the intercalating molecule to fit, DNA must undergo a conformational change involving an increase in the vertical separation between the base pairs, creating a cavity for the incoming chromophore. This conformational change causes a partial unwinding of the double helix, resulting in distortions of the sugar-phosphate backbone and alterations in the twist angle between successive base pairs. Once the intercalating molecule is sandwiched between the DNA base pairs, the stability of the complex is optimized through various non-covalent interactions. These interactions include van der Waals and π -stacking interactions, reduction of columbic repulsion between the DNA phosphate groups due to increased distance between the bases caused by helix unwinding, ionic interactions between positively charged groups of

the ligand and DNA phosphate groups, and hydrogen bonding. These intricate interactions collectively contribute to the stability of the intercalated complex within the DNA structure.

3.5.1 Techniques employed to study drug–DNA interactions

Intercalation, owing to its distinctive binding mode and specific properties, can be characterized using various biophysical methods. Some of these methods, briefly mentioned below, allow researchers to study and understand the intercalation process:

3.5.1.1 UV–visible spectroscopy

UV–visible absorption spectroscopy proves to be a simple, widely utilized, and highly effective method for detecting the interaction of small molecules with DNA. The stability of DNA during its interaction with small molecules can be easily investigated through UV–visible absorption measurements. Typically, the interaction of small molecules with DNA, leading to the formation of a new complex, induces changes in the UV–visible spectra³⁵. To elaborate on the method, both the band intensity and position of the spectra of the free small molecule and its complex with DNA are recorded. Any alteration in the band is indicative of complex formation³⁶. Another approach involves studying the change in the absorption spectra of DNA by gradually adding increasing concentrations of small molecules to a fixed concentration of DNA (where λ_{max} is typically at 260 nm). As the concentration of small molecules increases, any change in absorbance and shifts in the position of the peak are recorded and interpreted. Two major features in the spectra of DNA, known as the 'hyperchromic' effect and 'hypochromic effect,' are observed due to changes in its double helical structure³⁷. The hyperchromic effect arises from the destabilization of the secondary structure of DNA upon interaction with small molecules, while the hypochromic effect originates from the stabilization of the DNA secondary structure, either through electrostatic effects or intercalation of small molecules³⁸. Generally, absorption spectra of small molecules exhibit a bathochromic shift (red shift) and hypochromic effect upon intercalation into the DNA double helix³⁸. In cases of intercalation, the observed hypochromism and bathochromism in the presence of DNA are typically greater than 35% and 15 nm, respectively³⁶. For groove-binding molecules that attach to the outer surface of DNA, a smaller (6–8 nm) or no bathochromism is usually observed.

3.5.1.2 Fluorescence Spectroscopy

Fluorescence spectroscopy is among the most extensively employed techniques to investigate drug–DNA interactions. Generally, compounds that incorporate aromatic functional groups exhibit more pronounced fluorescence compared to small molecules containing aliphatic,

alicyclic carbonyl structures, or those with highly conjugated double bond structures. Notably, DNA itself possesses negligible fluorescence. Therefore, when studying drug–DNA interactions using fluorescence spectroscopy, researchers typically focus on examining changes in the intrinsic fluorescence of the drug in the presence of varying DNA concentrations.

The change in fluorescence intensity in drug–DNA interaction studies is often interpreted through Stern–Volmer plots, utilizing the Stern–Volmer equation:

$$F_0/F = 1 + K_{sv}[Q] \quad \dots\dots\dots (1)$$

Here, F_0 is the fluorescence intensity of the fluorophore in the absence of DNA, F is the fluorescence intensity in the presence of DNA, K_{sv} is the Stern–Volmer constant, and $[Q]$ is the concentration of DNA. A linear Stern–Volmer plot indicates the occurrence of either static or dynamic quenching processes. To distinguish between the two, the bimolecular quenching rate constant (K_q) is evaluated using the equation:

$$K_q = K_{sv}/\tau_0 \quad \dots\dots\dots (2)$$

where τ_0 is the lifetime of the biomolecule in the absence of the quencher. If K_q exceeds the limiting diffusion rate constant (around 2.0×10^{10}), the quenching process is static rather than dynamic.³⁹

The differentiation between static and dynamic quenching can also be based on the temperature dependence of K_{sv} values. An increase in temperature typically leads to a higher dynamic quenching process due to increased molecular motion. In contrast, static quenching processes may exhibit a decrease in K_{sv} values with rising temperature, reflecting a decrease in complex stability⁴⁰.

Fluorescence spectroscopy allows the calculation of intrinsic binding constants (K_b) using the equation:

$$\log \frac{F_0 - F}{F_0} = \log K_b + n \log [Q] \quad \dots\dots\dots (3)$$

Here, n is the number of binding sites, F_0 is the fluorescence intensity of the small molecule in the absence of DNA, F is the fluorescence intensity in the presence of DNA, and $[Q]$ is the concentration of the quenching molecule (DNA). K_b and n are determined from the double logarithmic regression curve⁴¹.

Fluorescence titration experiments, involving the gradual addition of a small molecule in the presence of single-stranded DNA (ssDNA) and double-stranded DNA (dsDNA), are commonly employed to elucidate the binding mode of these molecules with DNA³⁹ (as illustrated in Figure 3.6).

By carefully analysing the quenching patterns in the presence of ssDNA and dsDNA, researchers can deduce the binding mode of small molecules with DNA, providing valuable insights into the nature of the interaction and the specific binding sites involved.

3.5.1.3 KI quenching studies

Iodide quenching studies are commonly used to determine the binding mode of DNA with fluorescent drugs. Iodide ions, being negatively charged quenchers, can effectively quench the fluorescence of small molecules. The Stern–Volmer equation is used to evaluate accessibility, and differences in K_{sv} values in the absence and presence of DNA indicate the binding mode. Intercalation prevents anionic quenchers from approaching the fluorophore, resulting in a decrease in K_{sv} , while electrostatically bonded molecules and groove binders are exposed and may show minimal changes in K_{sv} values.³⁹

Therefore, iodide quenching studies, provide valuable information about the location of bound molecules, whether they are intercalated within the DNA helix or externally bound through electrostatic or groove-binding interactions. These studies aid in understanding the specific binding modes and interactions between small molecules and DNA.

3.5.1.4 Thermal denaturation studies

Thermal denaturation studies are a common method used to investigate the binding mode of small molecules with DNA. In these studies, the temperature of a DNA solution is gradually increased, leading to the denaturation of the DNA double helix and the generation of single-stranded regions. This denaturation process is monitored by observing changes in the absorbance of the DNA solution at 260 nm. The temperature at which 50% of the double-stranded DNA is denatured to single-stranded DNA is referred to as the midpoint denaturation or melting temperature (T_m).

To study the interaction of small molecules with DNA, the T_m of the DNA solution is recorded both in the absence and presence of small molecules or drugs. Small molecules that bind to DNA via intercalation typically stabilize the DNA structure, resulting in an increase in the T_m of DNA by approximately 5–8 °C⁴². This observed increase in T_m serves as an indicator of the

intercalative binding mode of these molecules. On the other hand, groove-binding molecules do not significantly alter the melting temperature of the DNA duplex⁴³.

3.5.1.5 Competitive displacement assays

Various well known DNA binding dyes are used to establish the mode of drug–DNA interactions. The use of DNA binding dyes, specifically focusing on ethidium bromide (EB), in competitive displacement assays to study the mode of interaction between small molecules and DNA. Ethidium bromide is a well-known fluorescence probe that binds to DNA in an intercalative fashion.⁴⁴ The competitive displacement assays involve pre-binding the fluorescent dye, such as ethidium bromide, to DNA. In this case, the fluorescence of ethidium bromide increases when it intercalates between DNA base pairs. Any small molecule that can displace ethidium bromide from the DNA helix will interact with DNA in a similar intercalative mode. The displacement of ethidium bromide by a competing molecule leads to a decrease in the fluorescence intensity of the DNA–EB system.

The extent of fluorescence quenching in the DNA–EB system can be used to determine the degree of intercalation between the competing molecule and DNA. Groove-binding and surface-binding molecules, which do not intercalate between base pairs, will not displace ethidium bromide, and therefore, they show no effect on the fluorescence intensity in this competitive assay.

The use of Hoechst 33342 as a fluorescent dye in competitive displacement studies to investigate the interaction between groove-binding molecules and DNA. Hoechst 33342 is known for its ability to bind specifically to the minor groove of double-stranded DNA, with a high specificity for AT-rich sequences⁴⁵. When Hoechst 33342 binds to DNA, there is an enhancement in the fluorescent intensity, and this fluorescence enhancement is used as a signal for the binding of the dye to the minor groove. Groove-binding molecules, which have the capability to interact with the minor groove of the DNA helix, can displace Hoechst 33342 from its binding site in the minor groove⁴⁶. This displacement results in a reduction in the fluorescent yield of the DNA–Hoechst system.

By measuring the extent of this reduction in fluorescence, we can assess the ability of different molecules to bind to the minor groove of DNA, helping to differentiate between groove-binding and intercalating modes.

3.5.1.6 Time Resolved Fluorescence

The fluorescence lifetime is a key measure indicating the time taken by excited fluorophores to decay exponentially to N/e (36.8%) of the original population due to energy loss through fluorescence and other processes. It helps understand how fluorescence intensity changes over time and how excited states transition to ground states. Photophysical processes vary widely in lifetime, from femtoseconds to seconds, with fluorescence being in the nanosecond range. In biological studies, particularly Drug-DNA interactions, fluorescence lifetime is crucial, revealing insights into photophysical events triggered by photon absorption.

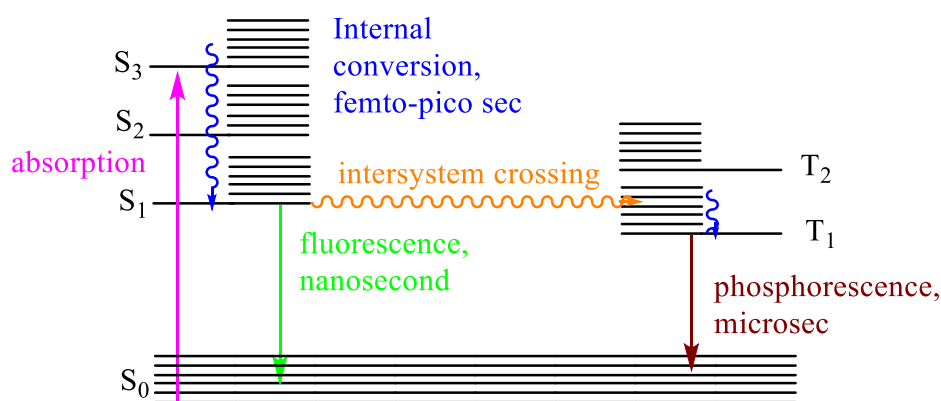


Figure 3.7 Jablonski diagram and time scale of photophysical processes

Understanding key events like internal conversion, vibrational relaxation, fluorescence, phosphorescence, and intersystem crossing is essential in studying how molecules behave upon light absorption, offering insights into their electronic structure, excited states, and emission characteristics. Each event occurs with a specific probability characterized by decay rate constants (k). The average time (τ) for molecules to transition from one state to another is inversely proportional to the decay rate, expressed as $\tau = 1/k$, commonly known as the mean lifetime or simply the lifetime of the process.

The fluorescence lifetime, an intrinsic property of a fluorophore, remains consistent regardless of the measurement method used. This ensures that the duration of time a fluorophore stays in an excited state is a fundamental feature unaffected by experimental conditions. Two common methods to measure fluorescence lifetime are time-domain and frequency-domain data acquisition. In the time-domain approach, the sample is excited with short pulses of light, typically less than 1-2 nanoseconds, and the fluorescence decay curve is analyzed to calculate the lifetime. Various light sources like flash lamps, pulsed lasers, laser diodes, or LEDs are utilized for excitation in this method.

$$F(t) = F_0 e^{-t/\tau} \quad \dots\dots\dots (4)$$

This expression represents a mathematical model used to describe the decay of fluorescence intensity over time in a time-resolved fluorescence measurement. Here, the variables have the following meanings:

$F(t)$: The fluorescence intensity at time t .

F_0 : The initial fluorescence intensity (at time $t = 0$).

e : The mathematical constant approximately equal to 2.71828.

τ : The fluorescence lifetime, representing the average time it takes for a fluorophore to transition from the excited state to the ground state.

In this model, the fluorescence intensity $F(t)$ decreases exponentially with time, and the rate of decay is governed by the fluorescence lifetime (τ). The term $e^{-t/\tau}$ describes the decay factor, where t is the time elapsed since the excitation.

This expression is derived from the general form of an exponential decay process, where the intensity at any given time is proportional to its initial intensity multiplied by the decay factor. In fluorescence, this decay factor is related to the fluorescence lifetime and characterizes how quickly the excited state population diminishes over time.

The relationship between the fluorescence lifetime (τ) and the sum of rate constants for radiative (k_r) and nonradiative (k_{nr}) processes, collectively known as quenching, is often expressed as an inverse proportionality. Mathematically, this relationship can be described as:

$$\tau = \frac{1}{k_r + k_{nr}} \quad \dots\dots\dots (5)$$

Here, τ represents the fluorescence lifetime, k_r is the rate constant for radiative processes, and k_{nr} is the sum of rate constants for nonradiative processes associated with quenching.

The inverse of the fluorescence lifetime is directly linked to the sum of rate constants for radiative and nonradiative processes, indicating that as these processes' total rate increases, the fluorescence lifetime decreases, and vice versa. Fluorescence lifetime is critical for understanding how long a fluorophore stays in an excited state before undergoing decay processes. Time-correlated single photon counting (TCSPC) has greatly simplified data collection and improved quantitative photon counting in fluorescence lifetime measurements. The versatility of fluorescence lifetime lies in its effectiveness in detecting biological

interactions and its usefulness in scenarios with multiple emitting species and overlapping spectra. By measuring fluorescence lifetimes at wavelength increments during the same data collection time, one can represent resulting measurements on an intensity-time axis, providing spectra at different times post-excitation.

The intrinsic fluorescence decay, $F(t)$, for a system with multiple non-interacting fluorophore species can be expressed as a sum of exponentials to describe how the sample's fluorescence intensity decreases with time. Mathematically, this can be represented as:

$$F(t) = A_1 e^{-t/\tau_1} + A_2 e^{-t/\tau_2} + \dots + A_n e^{-t/\tau_n} \quad \dots (6)$$

Here, each term in the sum corresponds to a distinct fluorophore species with its own amplitude (A_i) or pre exponential factor and fluorescence lifetime (τ_i). The fluorescence lifetime (τ_i) is the characteristic time it takes for the fluorescence intensity of each species to decrease by a factor of e .

Analysing the fluorescence lifetimes of the representative compound isoindoloindolones in the presence of ctDNA, as measured using a laser diode at 375 nm for excitation and monitoring fluorescence at 505 nm, allows for the monitoring of drug-DNA interactions. The interpretation of the decay curve, especially the change in lifetimes and their respective amplitudes, can provide insights into the binding kinetics and the nature of the drug-DNA complex.

The fluorescence lifetime method finds applications across diverse fields of study, including materials science, aeronautics, agriculture, forensics, biology, and medicine. The ability to gain insights into dynamic processes at the molecular level makes fluorescence lifetime a powerful and widely applicable technique. In the context of this thesis, the single photon counting technique has been employed as one of the techniques for measuring fluorescence lifetime. This method contributes to the precision and accuracy of the measurements in the investigation.

3.5.1.7 Circular Dichroism Spectra Study

The use of Circular Dichroism (CD) spectroscopy as a sensitive technique to detect changes in the secondary structure of polypeptides, proteins, and DNA when interacting with ligands. CD spectroscopy has been extensively employed to analyse changes in the DNA backbone upon binding with drugs, allowing researchers to identify alterations in DNA structure.

Calf thymus DNA (ctDNA) is commonly used as a representative model for studying interactions with various small molecules⁴⁶. In the CD spectrum of native calf thymus DNA, two major bands are observed at 277 nm (positive) and 243 nm (negative). The positive band

at 277 nm is attributed to base stacking, while the negative band at 243 nm is indicative of the helicity characteristic of DNA in the right-handed B form.

These CD spectral bands are highly sensitive to interactions between small molecules and DNA. Electrostatic binding and minor groove binding show little alteration in the CD spectra of calf thymus DNA. However, in the case of intercalation, both the positive and negative bands are significantly altered, providing a distinct CD signature for this mode of binding.

3.5.2 ctDNA binding study with our synthesized molecule 86k-HCl

After successful synthesis and characterization of some new quinazolinone compounds, to check the bioactivity of these molecule, we studied the DNA binding interaction with one of our compound 86k•HCl. In order to find the general affinity of 86k•HCl towards double stranded DNA (ds-DNA), we studied the titration of 86k•HCl with ctDNA by UV–Vis spectrophotometer. We have used UV-visible spectroscopy, the most common technique,⁴⁹ to investigate the binding study of the compound 86k-HCl with ctDNA. The intrinsic absorption spectra of the compound 86k-HCl showed weak bands 330, 315, 265 nm in UV-Vis spectra. On subsequent addition of ctDNA, a hypochromic effect of the weak bands in the range 315-325 nm was observed with no apparent shift in the position of the absorption maxima. An isosbestic point was noted near 290 nm (Figure 3.8). The hypochromic effect detected within the range of 315-325 nm in the UV-vis spectra indicates that the compounds interact with the dsDNA. The classical intercalation mode of binding is ruled out, as the hypochromic effect is relatively weak. Moreover, the presence of a clear isosbestic point in the UV-Vis spectra of DNA bound 86k-HCl indicated the presence of multiple modes of binding, or 1:1/drug:DNA stoichiometry was not maintained during the process.⁵⁰ The calculated binding constant with ctDNA was found to be a moderate range⁵¹ $1.2 \times 10^4 \text{ M}^{-1}$. These results implied that the quinazolinones 86k-HCl have significant potential to modulate dsDNA structure and these templates could be used for developing small molecule binders for cellular DNA to tune many cellular functions.

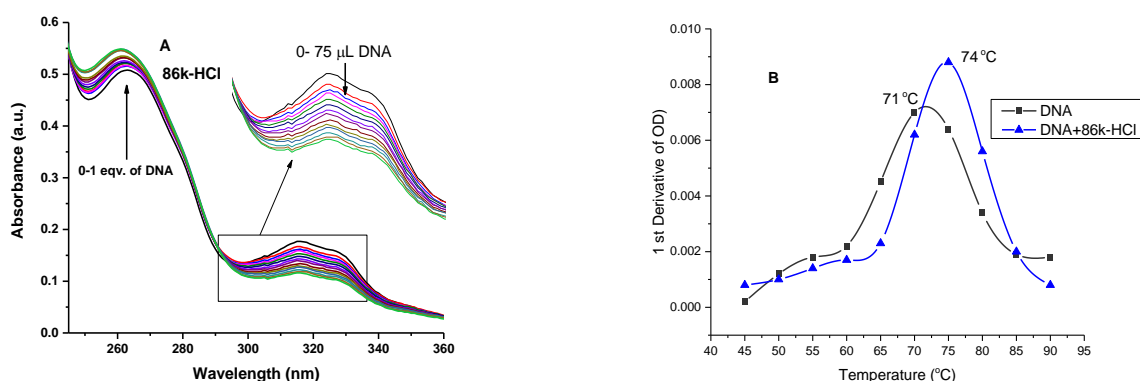


Figure 3.8(A) Titration of 86k-HCl by DNA (0-30 μM) monitored by UV-spectra. The arrow's direction indicates the change in absorption peak intensity by increasing DNA concentration. (B) Plot of 1st derivative of OD vs temperature of DNA in the absence and presence of 86k-HCl.

Thermal denaturation of DNA⁵² study revealed that presence of the small molecule 86k-HCl enhanced the DNA melting point by 3 degree. In general, melting temperature (T_m) is a thermodynamic parameter that is used to correlate the stability of dsDNA, and it depends on the length of DNA, % of GC base pairs,⁵³ ionic strength of the medium⁵⁴, and interaction with the small molecules.⁵⁵ Variation of dsDNA melting temperature correlated with the strength of interaction of the small molecules with the DNA when other factors are unaltered.⁵⁶ The influence of intercalative mode on the T_m of DNA is more significant than that of groove binding.⁵⁶ The moderate value of ΔT_m supported the minor groove binding of the 86k-HCl to the dsDNA.

We have also monitored the interaction of 86k-HCl with ctDNA in details by steady-state fluorescence spectroscopy. Intrinsic emission spectra of 86k-HCl in 10mM Tris-HCl buffer, at biological pH (7.2), showed a weak band at around 450 nm of the quinazoline 4-one moiety (Figure 3.9).⁵⁷ Because of fluorescence emission is weak due to the presence of heavy atom (bromine) in the molecule, the Raman scattering of water appeared prominently at around 365 nm.⁵⁸ Addition of ctDNA to a solution 86k-HCl resulted enhancement of the fluorescence intensity with no detectable shift of the emission band. The change in fluorescence intensity on the addition of DNA established the binding of the quinazolinone 86k-HCl with ctDNA. To understand the dynamic properties of binding, we have calculated the enhancement constant from the fluorescence titration. The enhancement ($6.4 \times 10^3 \text{ M}^{-1}$) constant (K_e) obtained from fluorescence titration is in good agreement with K_b obtained by UV-Vis spectra.

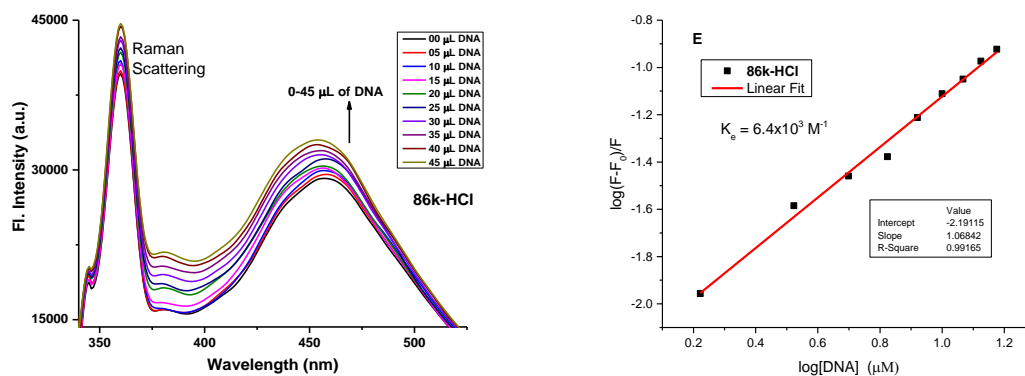


Figure 3.9 Titration of 86k-HCl by DNA (0-30 μM) monitored by fluorescence spectrometer. The arrow's direction indicates the change in emission intensity by increasing DNA concentration

The mode of binding was checked by a comparative displacement assay using two known dye Ethidium Bromide (EB)⁵⁹ and Hoechst 33342 (HST).⁶⁰ In general, molecule with similar binding mode displaces each other at low concentrations. Titration of the DNA-dye complexes by 86k-HCl revealed that HST was displacing more prominently than that of EB as shown in the Figure 3.10. From the fluorescence quenching titration, the values of the Stern-Volmer quenching constants were calculated for both the dye EB and HST, and the relative ratio of $K_{sv}(\text{HST})/K_{sv}(\text{EB})$ was 2.9 i.e. HST was displacing 2.9 times faster than EB. Therefore, binding mode of 86k-HCl was preferentially via minor groove binding. This result was further supported by iodide quenching study.

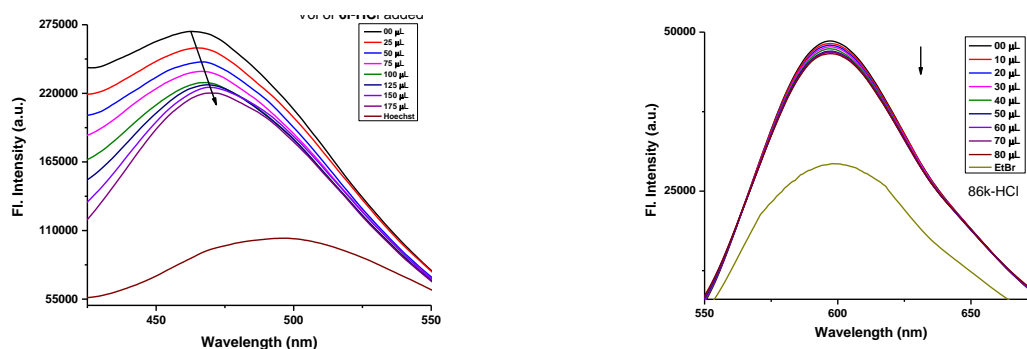


Figure 3.10 Competitive displacement assay study of **86k-HCl** with Hoechst (A) and EB (B)

The relative PL emission quenching properties in the free-state and DNA bound state by Iodide provide valuable information about the nature of the binding mode of interaction.⁶¹ However, the dynamic quenching⁶² property of the iodide is significantly reduced when the fluorophore molecule is within the base pair of the DNA via intercalation and become inaccessible to the iodide ion as it is repelled by the negatively charged phosphates of the DNA backbone.

However, the minor groove binder is easily accessible to the anionic quencher, even in the presence of DNA. The relative quenching behavior in the presence and absence of DNA towards iodide is monitored by measuring the $K_{sv}(\text{free})/K_{sv}(\text{Bound})$ which was found to be 1.8 (Figure 3.11). The relative quenching properties is in good agreement with the minor groove mode of binding nature.⁶³

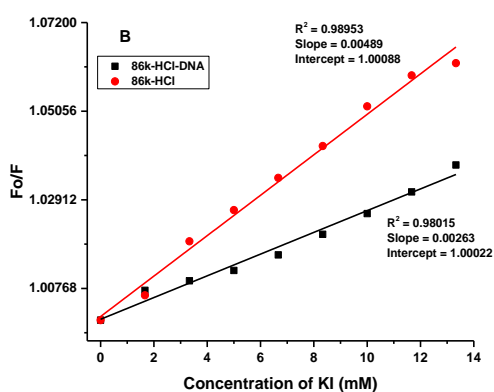


Figure 3.11 Relative quenching properties of 86k-HCl by iodide

Finally, the change of secondary structure of the dsDNA was measure by CD spectroscopy (Figure 3.12). The similarity in the overall pattern of the CD spectrum of the DNA complex with the DNA itself suggested that the overall secondary structure remained unaltered. However, the slight deviation in the ellipticity in the range 280 nm and 245 nm is due to the non-covalent interactions of the DNA helices with the quinazolinones. As minor groove binders do not significantly perturb the CD spectrum of DNA, the compounds under investigation mostly interacted via minor groove binding mode.

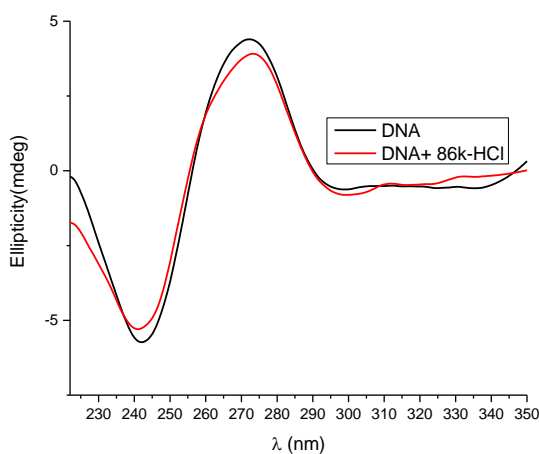


Figure 3.12 CD spectra of ctDNA (black line) and in the presence of 86k-HCl (red)

3.6 CONCLUSION

We have developed a synthetic method to obtain highly functionalized quinazoline derivatives coupled with an aromatic polar handle through a four-carbon spacer. The process involves an intramolecular hydride transfer mechanism promoted under mildly acidic conditions. We reported here twelve new compounds with their NMR and mass spectroscopic data. A few of the compounds were isolated in the HCl salt form, and one of the compounds in the salt form has been converted into the salt-free condition and established the point of proton attachment by NMR of the product. We assumed that the two aromatic/heterocyclic moieties within the molecules would show efficient binding interactions with dsDNA. The spacer would take a curved shape fit to the DNA topology. Hence, we have investigated DNA binding properties of a compound. Result suggested that the compound under investigation was a potential small molecule DNA binder. This strategy could be used for development of a multivalent system to probe cellular DNA.

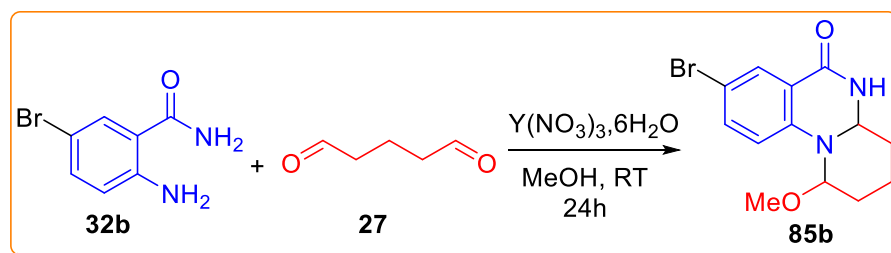
3.7 EXPERIMENTAL SECTION

3.7.1 General information

All NMR (^1H , ^{13}C , COSY, HMBC, HSQC) spectra were recorded with Bruker Avance III (300 or 400 MHz) spectrometers in deuterated solvent CDCl_3 . Chemical shifts are reported in parts per million (ppm, δ) relative to tetramethylsilane (TMS) and the solvent resonance was referenced to internal standard CDCl_3 (δ 7.28 ppm). All coupling constants are absolute values and are expressed in Hz. The descriptions of the signals are reported as follows: s = singlet, d = doublet, dd = double of doublet, t = triplet, m = multiplet and dt = doublet of triplets. ^{13}C NMR spectra were recorded using Bruker Avance III 300 (75 MHz), 400 (100 MHz) spectrometers as solutions in CDCl_3 with complete proton decoupling. High-resolution mass spectra were recorded on ESI-TOF mass spectrometry. Solvents, reagents, and chemicals were purchased from Aldrich, Merck, SRL, Spectrochem, and Process Chemicals. Commercially available (SRL India) calf thymus DNA (ctDNA), Hoechst 33258 and Ethidium bromide (EB), Tris-buffer were used without purification also. All the reactions were monitored by TLC (Silica Gel60 F254) and it was observed under UV light (254 nm). Yields refer to the isolated product as mentioned in the experimental section.

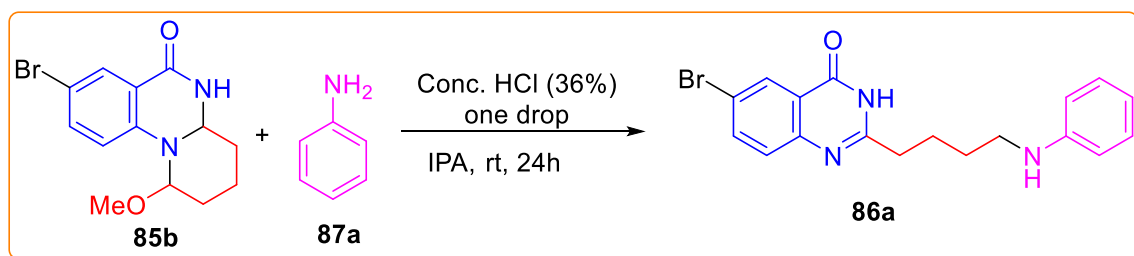
3.7.2 Experimental Procedure for Synthesis of Quinazolinones and Spectral Data

Compound 5-bromoanthranilamide **32b** was prepared according to the earlier reported procedure.³⁰

8-bromo-1-methoxy-1,2,3,4,4a,5-hexahydro-6H-pyrido[1,2-a]quinazolin-6-one (85b)**Scheme 3.14** Preparation of intermediate **85b**

To a mixture of 5-bromoanthranilamide **32b** (500 mg, 2.32 mmol) and glutaraldehyde **27** (0.5 mL, 2.32 mmol), $Y(NO_3)_3 \cdot 6H_2O$ (152 mg, 0.46 mmol) was added, and the mixture was stirred for 24 hrs at RT. After that the mixture was diluted with water and the solid that appeared was collected by filtration to get compound **85b** as a white solid. It was directly used for spectral data and subsequent reactions without further purification.

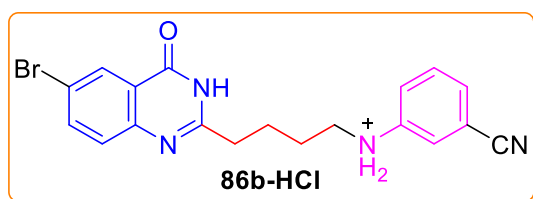
Yield: 90%; 1H NMR (300 MHz, DMSO- d_6) δ 1.55-1.65 (m, 4H), 1.91-2.06 (m, 2H), 3.27 (s, 3H), 4.75 (d, $J = 8$ Hz, 1H), 5.09 (s, 1H), 6.90 (d, $J = 8$ Hz, 1H), 7.54 (d, $J = 8$ Hz, 1H), 7.77 (s, 1H), 8.31 (s, 1H); ^{13}C NMR (100 MHz, DMSO- d_6 + $CDCl_3$) δ 161.4, 146.2, 135.2, 129.8, 119.16, 115.3, 110.2, 82.5, 63.17, 54.17, 30.72, 25.19, 15.49. ESI-TOF MS: Calculated for $C_{13}H_{15}BrN_2O_2 = 335.0194$, Obtained $[M+Na]^+ = 334.9499$.

6-bromo-2-(4-(phenylamino)butyl)quinazolin-4(3H)-one (86a).**Scheme 3.15** Preparation of intermediate **86a**

The compound **85b** (50 mg, 0.160 mmol, 1 equiv.) was taken in isopropanol (5.0 ml) in a round bottom flask, and one drop of conc. HCl (36%) was added as a catalyst, followed by dropwise addition of aniline (22mg, 0.240 mmol, 1.5 equiv.) at RT and stirred for 24 hrs. Upon addition of distilled water to the reaction mixture a precipitate was obtained. The solid product was collected by filtration and washed thoroughly with distilled water to afford the pure product **86a** (52.0 mg, 0.139 mmol) as an off-white solid in 86% yield. mp 156 °C;

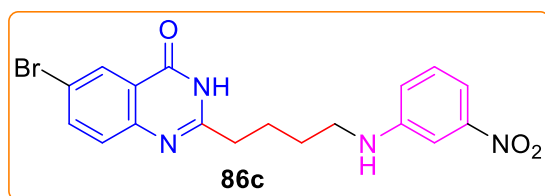
¹H NMR (300 MHz, CDCl₃) δ 1.81-1.86 (m, 2H), 1.99-2.09 (m, 2H), 2.85 (t, J = 7.5 Hz, 2H), 3.25 (t, J = 6.9 Hz, 2H), 6.62 (d, J = 7.8 Hz, 2H), 6.7 (t, J = 7.2 Hz, 1H), 7.17 (t, J = 7.8 Hz, 2H), 7.59 (d, J = 8.6 Hz, 1H), 7.86 (dd, J = 8.6, 3 Hz, 1H), 8.40 (d, J = 3 Hz, 1H), 11.79 (s, 1H); **¹³C NMR (75 MHz, CDCl₃)** δ 24.6, 28.7, 35.3, 43.4, 112.7, 117.3, 120.0, 121.9, 128.7, 129.1, 129.2, 138.0, 148.24, 148.21, 156.6, 163.0; **HRMS (ESI-TOF) m/z : [M+H]⁺** Calcd for C₁₈H₁₉BrN₃O 372.0711; Found 372.0719.

3-((4-(6-bromo-4-oxo-3,4-dihydroquinazolin-2-yl)butyl)amino)benzonitrile (86b-HCl).



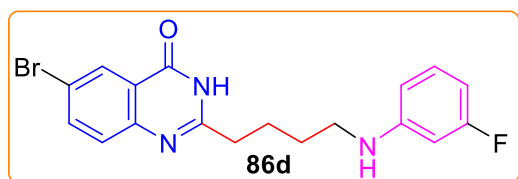
It was synthesized by the reaction of compound **85b** with 3-aminobenzonitrile following the procedure described for compound **86a**. Yield: 92%; mp 210 °C; **¹H NMR (300 MHz, DMSO-d₆)** δ 1.66-1.68 (m, 2H), 1.88-1.90 (m, 2H), 2.89 (t, J = 7.2 Hz, 2H), 3.12 (t, J = 6.3 Hz, 2H), 6.98-7.01 (m, 3H), 7.28 (t, J = 7.8 Hz, 1H) 7.82 (d, J = 8.7 Hz, 1H), 8.08 (d, J = 8.7 Hz, 1H) 8.21 (s, 1H) (The heteroatomic protons are merged with the DMSO water and appeared over a wide range 5.32 ppm); **¹³C NMR (75 MHz, DMSO-d₆)** δ 25.0, 27.5, 32.5, 43.0, 111.2, 115.5, 118.6, 119.8, 120.4, 120.5, 122.2, 124.8, 128.9, 130.5, 138.6, 141.6, 148.4, 159.7, 162.0; **HRMS (ESI-TOF) m/z : [M+H]⁺** Calcd. for C₁₉H₁₈BrN₄O 397.0664; Found 397.0668.

6-bromo-2-(4-((3-nitrophenyl)amino)butyl)quinazolin-4(3H)-one (86c).



It was synthesized by the reaction of compound **85b** with 3-nitroaniline following the procedure described for compound **86a**. Yield: 71%. mp 190 °C; **¹H NMR (300 MHz, DMSO-d₆)** δ 1.58-1.67 (m, 2H), 1.79-1.89 (m, 2H), 2.65 (t, J = 7.5 Hz, 2H), 3.12 (t, J = 6.3 Hz, 2H), 6.37 (bs, 1H), 6.94-6.98 (m, 1H), 7.30 (m, 3H) 7.52 (d, J = 8.4 Hz, 1H), 7.90 (dd, J = 8.7, 2.1 Hz, 1H), 8.15 (d, J = 2.1, 1H), 12.37 (s, 1H); **¹³C NMR (75 MHz, DMSO-d₆)** δ 24.7, 28.0, 34.6, 42.6, 106.4, 109.9, 118.5, 118.7, 122.9, 128.2, 129.6, 130.3, 137.5, 148.3, 149.3, 150.3, 158.6, 161.1; **HRMS (ESI-TOF) m/z : [M+H]⁺** Calcd for C₁₈H₁₈BrN₄O₃ 417.0562; Found 417.0566.

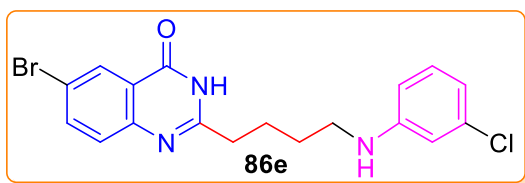
6-bromo-2-(4-((3-fluorophenyl)amino)butyl)quinazolin-4(3H)-one (86d):



It was synthesized by the reaction of compound **85b** with 3-fluoroaniline acid following the procedure described for compound **86a**.

Yield: 91%; mp 162 °C; ^1H NMR (300 MHz, DMSO- d_6) δ 1.59 (t, J = 6.6, 2H), 1.76-1.84 (m, 2H), 2.64 (t, J = 7.3 Hz, 2H), 3.03 (s, 2H), 5.90 (s, 1H), 6.21-6.30 (m, 2H), 6.36 (d, J = 8.1, 1H), 7.03 (q, J = 7.8 Hz, 1H), 7.54 (d, J = 8.7 Hz, 1H), 7.91 (dd, J = 8.7 Hz, 1H), 8.15 (s, 1H), 12.34 (s, 1H); ^{13}C NMR (75 MHz, DMSO- d_6) δ 24.7, 28.3, 34.6, 42.7, 98.3 (d, $^2J_{\text{C-F}}$ = 24Hz), 101.7 (d, $^2J_{\text{C-F}}$ = 21 Hz), 108.7 (d, $^4J_{\text{C-F}}$ = 2 Hz), 118.7, 122.9, 128.2, 129.3, 130.6 (d, $^3J_{\text{C-F}}$ = 6 Hz), 137.6, 148.4, 151.4 (d, $^3J_{\text{C-F}}$ = 11Hz), 158.6, 161.1, 162.4 (d, $^1J_{\text{C-F}}$ = 237 Hz); HRMS (ESI-TOF) m/z : $[\text{M}+\text{H}]^+$ Calcd for $\text{C}_{18}\text{H}_{18}\text{BrFN}_3\text{O}$ 390.0617; Found 390.0620.

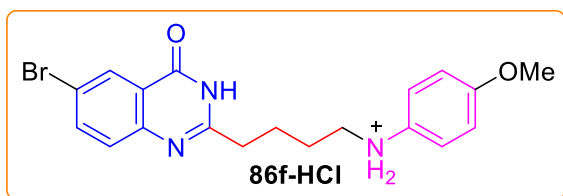
6-bromo-2-(4-((3-chlorophenyl)amino)butyl)quinazolin-4(3H)-one (86e).



It was synthesized by the reaction of compound **85b** with 3-chloroaniline acid following the procedure described for compound **86a**. Yield: 73.4%; mp 170 °C; ^1H NMR (300 MHz, DMSO- d_6) δ 1.59-1.61 (m, 2H), 1.79-1.90 (m, 2H), 2.64 (t, J = 7.5 Hz, 2H), 3.02 (t, J = 5.4 Hz, 2H), 5.91 (bs, 1H), 6.50 (m, 3H), 7.03 (t, J = 8.1 Hz, 1H), 7.55 (d, J = 8.4 Hz, 1H), 7.91 (dd, J = 8.7, 2.1 Hz, 1H), 8.15 (d, 1H); ^{13}C NMR (75 MHz, DMSO- d_6) δ 24.7, 28.2, 34.6, 42.6, 111.0, 111.3, 115.1, 118.7, 122.9, 128.2, 129.7, 130.7, 134.1, 137.5, 150.8, 158.6, 161.1

HRMS (ESI-TOF) m/z : $[\text{M}+\text{H}]^+$ Calcd for $\text{C}_{18}\text{H}_{18}\text{BrClN}_3\text{O}$ 406.0321; Found 406.0682.

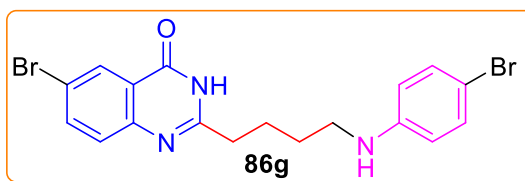
6-bromo-2-(4-((4-methoxyphenyl)amino)butyl)quinazolin-4(3H)-one (86f-HCl):



It was synthesized by the reaction of compound **85b** with 4-methoxyaniline acid following the procedure described for compound **86a**. Yield: 83%; mp 176 °C; ^1H NMR (300 MHz, DMSO- d_6) δ 1.80-1.87 (m, 4H), 2.80 (t, J = 7.2 Hz, 2H), 3.28 (t, J = 7.2 Hz, 2H), 3.88 (s, 3H), 7.05 (d, J = 8.7, 2H), 7.53 (d, J = 9 Hz, 2H), 7.72 (d, J = 8.7 Hz, 1H), 8.03 (dd, J = 8.4, 2.1 Hz, 1H), 8.19 (d, J = 2.1 Hz, 1H); ^{13}C NMR (75 MHz, DMSO- d_6) δ 24.2, 24.8, 32.8, 50.8, 55.9, 115.3, 119.9, 122.4, 124.9, 126.5, 128.7, 129.1, 138.3, 148.3, 159.7, 160.2, 160.4; HRMS (ESI-TOF) m/z : $[\text{M}+\text{H}]^+$ Calcd for $\text{C}_{19}\text{H}_{21}\text{BrN}_3\text{O}_2$ 402.0817; Found 402.0820.

HRMS (ESI-TOF) m/z : $[\text{M}+\text{H}]^+$ Calcd for $\text{C}_{19}\text{H}_{21}\text{BrN}_3\text{O}_2$ 402.0817; Found 402.0820.

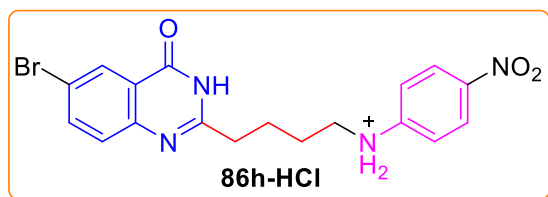
6-bromo-2-(4-((4-bromophenyl)amino)butyl)quinazolin-4(3H)-one (86g).



It was synthesized by the reaction of compound **85b** with 4-bromoaniline acid following the procedure described for compound **86a**. Yield: 80%; mp 172 °C; ^1H NMR (300 MHz, DMSO- d_6) δ

δ 1.63-1.71 (m, 2H), 1.79-1.89 (m, 2H), 2.74 (t, $J = 7.2$ Hz, 2H), 3.13 (t, $J = 7.2$ Hz, 2H), 6.89 (d, $J = 8.4$, 2H), 7.37 (d, $J = 8.7$ Hz, 2H), 7.66 (d, $J = 8.7$ Hz, 1H), 7.99 (dd, $J = 6.6$ Hz, 1H), 8.18 (d, $J = 2.1$ Hz, 1H) [The heteroatomic protons are merged with the DMSO water and appeared at 5.08 ppm]; ^{13}C NMR (75 MHz, DMSO- d_6) δ 24.6, 26.9, 33.5, 45.5, 118.5, 119.5, 122.6, 127.5, 128.5, 132.3, 138.0, 144.0, 145.3, 160.0, 160.5; HRMS (ESI-TOF) m/z : $[\text{M}+\text{H}]^+$ Calcd for $\text{C}_{18}\text{H}_{18}\text{Br}_2\text{N}_3\text{O}$ 449.9817; Found 449.9817.

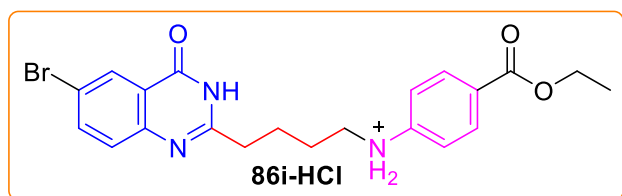
6-bromo-2-((4-((4-nitrophenyl)amino)butyl)quinazolin-4(3H)-one (86h-HCl).



It was synthesized by the reaction of compound **85b** with 4-nitroaniline following the procedure described for compound **86a**. Yield: 86%; mp 220 °C; ^1H NMR (300 MHz, DMSO- d_6) δ 1.56-

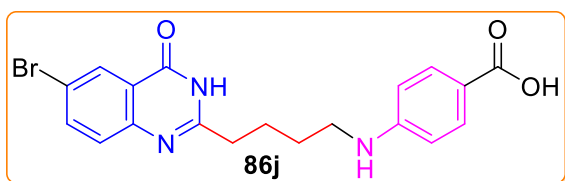
1.66 (m, 2H), 1.75-1.85 (m, 2H), 2.65 (t, $J = 7.8$ Hz, 2H), 3.18 (t, $J = 7.2$ Hz, 2H), 6.61 (d, $J = 9.3$ 2H), 7.54 (d, $J = 8.7$ Hz, 1H), 7.90-7.97 (m, 3H), 8.14 (s, 1H) [The heteroatomic protons are merged with the DMSO water and appeared at 3.54 ppm]; ^{13}C NMR (75 MHz, DMSO- d_6) δ 24.5, 27.9, 34.4, 42.3, 118.9, 122.75, 126.75, 126.81, 128.3, 129.2, 135.8, 137.7, 147.7, 154.9, 158.8, 161.2; HRMS (ESI-TOF) m/z : $[\text{M}+\text{H}]^+$ Calcd for $\text{C}_{18}\text{H}_{18}\text{BrN}_4\text{O}_3$ 417.0562 ; Found 417.0565.

Ethyl 4-((4-(6-bromo-4-oxo-3,4-dihydroquinazolin-2-yl)butyl)amino)benzoate (86i-HCl):



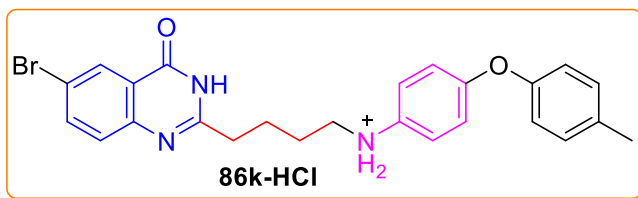
It was synthesized by the reaction of compound **85b** with ethyl 4-aminobenzoate acid following the procedure described for compound **86a**.

Yield: 87%; mp 190 °C; ^1H NMR (300 MHz, DMSO- d_6) δ 1.25 (t, $J = 7.2$ Hz, 3H), 1.59-1.61 (m, 2H), 1.78-1.80 (m, 2H), 2.63 (t, $J = 7.2$ Hz, 2H), 3.09 (t, $J = 8.1$ Hz, 2H), 4.18 (q, $J = 6.9$ Hz, 3H), 6.55 (d, $J = 8.7$, 2H), 7.54 (d, $J = 8.7$ Hz, 1H), 7.64 (d, $J = 8.7$ Hz, 2H), 7.90 (dd, $J = 8.7$ Hz, 1H), 8.14 (d, $J = 2.1$ Hz, 1H); ^{13}C NMR (75 MHz, DMSO- d_6) δ 14.8, 24.6, 28.1, 34.5, 42.3, 60.0, 111.2, 116.2, 118.8, 122.8, 128.2, 129.5, 131.4, 137.6, 148.1, 153.2, 158.7, 161.2, 166.4; HRMS (ESI-TOF) m/z : $[\text{M}+\text{H}]^+$ Calcd for $\text{C}_{21}\text{H}_{23}\text{BrN}_3\text{O}_3$ (considering ^{81}Br isotope) 446.0902; Found 446.0898.

4-((4-(6-bromo-4-oxo-3,4-dihydroquinazolin-2-yl)butyl)amino)benzoic acid (86j):

It was synthesized by the reaction of compound **85b** with 4-aminobenzoic acid following the procedure described for compound **86a**. Yield: 70%; mp 210 °C; ¹H NMR (300 MHz, DMSO-

d₆) δ 1.58-1.63 (m, 2H), 1.77-1.84 (m, 2H), 2.65 (t, *J* = 7.5 Hz, 2H), 3.10 (t, *J* = 6.9 Hz, 2H), 6.42 (bs, 1H, N-H), 6.55 (d, *J* = 8.7, 2H), 7.54 (d, *J* = 8.7 Hz, 1H), 7.65 (d, *J* = 4.2 Hz, 2H), 7.90 (dd, *J* = 8.7, 2.1Hz, 1H), 8.15 (d, *J* = 2.1, 1H), 11.9 (bs, 1H), 12.5 (bs, 1H); ¹³C NMR (75 MHz, DMSO-**d₆**) δ 24.7, 28.2, 34.6, 42.4, 111.1, 117.1, 118.1, 122.9, 128.2, 129.6, 131.6, 137.5, 148.3, 153.0, 158.6, 161.1, 167.9; HRMS (ESI-TOF) *m/z*: [M+H]⁺ Calcd for C₁₉H₁₉BrN₃O₃ 416.0609; Found 415.9635.

6-bromo-2-((4-((4-(*p*-tolxyloxy)phenyl)amino)butyl)quinazolin-4(3*H*)-one (86k-HCl).

It was synthesized by the reaction of compound **85b** with 4-(*p*-tolxyloxy)aniline following the procedure described for compound **86a**. Yield: 91%

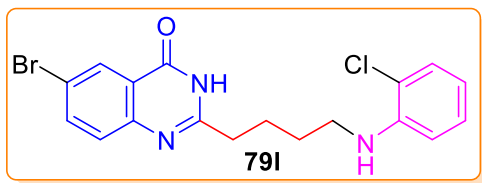
as an off-white solid. mp 160 °C; ¹H NMR (300 MHz, DMSO-**d₆**) δ 1.69-1.77 (m, 2H), 1.77-1.84 (m, 2H), 2.28 (s, 3H), 2.65 (t, *J* = 7.2 Hz, 2H), 3.21 (t, *J* = 7.2 2H), 6.88 (d, *J* = 8.4 Hz, 2H), 6.97 (d, *J* = 8.7 Hz, 2H), 7.17-7.25 (m, 4H), 7.56 (d, *J* = 8.7 Hz, 1H), 7.92 (dd, *J* = 8.7, 2.2 Hz, 1H), 8.16 (d, *J* = 2.2 Hz, 1H) (The heteroatomic protons are merged with the DMSO water and appeared over a wide range 3.54 ppm); ¹³C NMR (75 MHz, DMSO-**d₆**) δ 20.7, 24.2, 26.0, 34.2, 48.6, 118.90, 118.97, 119.7, 119.5, 121.6, 122.8, 128.3, 129.3, 130.8(2C) 133.0, 137.6, 147.8, 154.8, 158.5, 161.0; HRMS (ESI-TOF) *m/z*: [M+H]⁺ Calcd for C₂₅H₂₅BrN₃O₂ 478.1130; Found 478.1130.

Synthesis of compound of 86k: The compound **86k-HCl** was suspended in saturated sodium bicarbonate for 1 hour with vigorous stirring and then the solid was collected by filtration washed thoroughly with water to get **86k** as a white solid (yield 98%).

¹H NMR (300 MHz, DMSO-**d₆**) δ 12.40 (s, 1H), 8.16 (d, *J* = 2.4 Hz, 1H), 7.92 (dd, *J* = 8.7, 2.4 Hz, 1H), 7.56 (d, *J* = 8.7 Hz, 1H), 7.09 (d, *J* = 8.2 Hz, 2H), 6.76 (t, *J* = 8.8 Hz, 4H), 6.56 (d, *J* = 8.9 Hz, 2H), 5.50 (t, *J* = 5.6 Hz, 1H), 3.01 (q, *J* = 6.4 Hz, 2H), 2.65 (t, *J* = 7.5 Hz, 2H), 2.24 (s, 3H), 1.83 (m, 2H), 1.60 (m, 2H); ¹³C NMR (75 MHz, DMSO-**d₆**) δ 161.27, 158.78,

157.19, 148.45, 146.38, 146.26, 137.69, 131.21, 130.55, 129.79, 128.36, 122.98, 121.19, 118.83, 117.09, 113.30, 43.41, 39.99, 34.77, 28.55, 24.95, 20.67.

6-bromo-2-(4-((2-chlorophenyl)amino)butyl)quinazolin-4(3H)-one (86l):



It was synthesized by the reaction of compound **85b** with 2-chloroaniline acid following the procedure described for compound **86a**. Yield: 79.6%; mp 162 °C; ^1H NMR (300 MHz, DMSO- d_6) δ 1.59-1.61 (m, 2H), 1.76-1.85 (m, 2H), 2.63 (t, $J = 7.2$ Hz, 2H), 3.13 (t, $J = 5.1$ Hz, 2H), 6.53 (t, $J = 7.2$, 1H), 6.66 (m, 1H), 7.08 (t, $J = 7.2$ Hz, 1H), 7.19 (d, $J = 7.5$, 1H), 7.53 (d, $J = 8.7$, 1H), 7.89 (d, $J = 8.7$, 1H), 8.13 (s, 1H); ^{13}C NMR (75 MHz, DMSO- d_6) δ 24.6, 28.0, 34.5, 42.5, 111.5, 115.9, 116.6, 117.4, 118.1, 118.8, 122.7, 128.1, 128.2, 128.4, 129.4, 129.5, 137.6, 144.4, 148.1, 158.7, 161.3; HRMS (ESI-TOF) m/z : $[\text{M}+\text{H}]^+$ Calcd for $\text{C}_{18}\text{H}_{18}\text{BrClN}_3\text{O}$ 406.0321; Found 406.0666.

3.7.3. DNA Interaction Study: Experimental Methods and Findings

Sample Preparation: Stock solution of **86k-HCl** (1 mM) was prepared in DMSO. ctDNA stock solution was prepared in 10 mM Tris-HCl buffer with 1 mM EDTA (pH 7.2), and the concentration was measured spectrophotometrically using the molar extinction coefficient value of $6600 \text{ M}^{-1} \text{ cm}^{-1}$. The purity of the DNA solution was monitored by recording the absorbance ratio A_{260}/A_{280} . The measured ratio was between 1.8 and 1.9, and we used the DNA without further purification. Different concentration of ctDNA solution was prepared by dilution of the stock solution.

DNA-Binding Studies: We studied the binding parameters of the quinazoline derivatives to the DNA macromolecule by Spectroscopy (Absorption, fluorescence, CD) and DNA melting study.

Absorption Spectroscopy: For the UV-visible absorption spectra measurements, a Shimadzu spectrophotometer (model UV-1800, Japan) with $1 \text{ cm} \times 1 \text{ cm}$ quartz cuvette was used. The UV-visible absorption spectra of the compound **86k-HCl** in the free state and bound ctDNA complex were recorded in the wavelength range 200–400 nm. The experiment was conducted at a defined concentration of **86k-HCl** (30 μM) in a fixed volume (3 ml) and quantified by changing the concentration of ctDNA from 0 to 30 μM by adding multiple 5 μL DNA solution of concentration 1 mM.

Benesi-Hildebrand equation were used to calculate the binding constant K_b with help of the measures OD values of the ligand in absence (A_0) at 315 nm in the presence of ctDNA.

$$\frac{A_0}{A - A_0} = \frac{\epsilon_0}{\epsilon - \epsilon_0} + \frac{\epsilon_0}{\epsilon - \epsilon_0} \frac{1}{K_b} \frac{1}{[DNA]} \quad \text{Equation 7}$$

Steady-state fluorescence: Fluorescence emission spectra of **86k-HCl** were recorded on a Shimadzu spectrofluorometer-5000 (Japan) using 1.0 cm quartz cells. Excitation was fixed at 310-330 nm for different samples, and emission spectra were recorded from 320 nm to 600 nm after setting the widths of both the excitation and the emission slits at 5 nm. Appropriate blanks corresponding to the buffer were subtracted to correct the background fluorescence. The fluorescence titration was carried out by keeping the concentration of **86k-HCl** constant (30 μM) and varying DNA concentration up to 30 μM by adding multiple 5 μL of DNA of concentration 1 mM.

We have calculated the binding constant from the fluorescence titration by using the following equation-

$$\text{Log} \frac{F - F_0}{F} = \log K_e + n \log [DNA] \quad \text{Equation 8}$$

Where K_e is the enhancement constant, F and F_0 are the fluorescence emission intensity in the presence and absence of DNA respectively of the quinazolinones and n is the binding site size. The enhancement ($6.4 \times 10 \text{ M}^{-1}$) constant obtained from fluorescence titration is in good agreement with K_b obtained by UV-Vis spectra

Comparative binding study with known DNA binders: Displacement assay was done with EB and Hoechst 33342. In the case of EB displacement assay, we have monitored the emission spectra of ctDNA (50 μM) bound EB (50 μM) in the presence of changing amounts of **86k-HCl** (0–150 μM) to ensure the binding of **86k-HCl** with ctDNA. The binding displacement assay was carried out at excitation wavelength 476 nm for the EB-bound ctDNA molecule, and the corresponding emission spectra were recorded in between the range 500-680 nm. The Hoechst 33342 displacement assay was also performed similarly at an excitation wavelength 343 containing 50 μM of Hoechst 33258 and 50 μM of ctDNA; the fluorescence emission spectra were recorded between 375–600 nm by titrating with increasing concentrations of **86k-HCl** (0–150 μM). In all the above experiments, the final volume of the reaction mixture was made to 3 mL by adding 0.01M Tris-HCl buffer.

Calculation of relative quenching constant-

$$\frac{K_{sv(HST)}}{K_{sv(EB)}} = \frac{0.00455}{0.00155} = 2.9$$

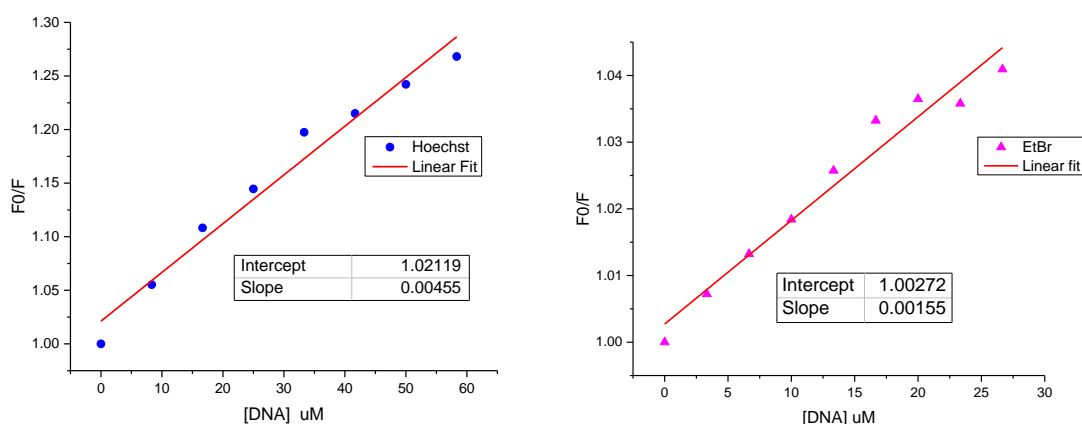


Figure 3.13 1st one is the F_0/F vs [DNA] at 460 nm of the titration Hoechst-DNA complex by 86k-HCl DNA. 2nd one is the F_0/F vs [DNA] at 600 nm of the titration EB-DNA complex by 86k-HCl. K_{sv} was calculated using the equation $F_0/F = 1 + K_{sv}[\text{DNA}]$.

Quenching experiment: The iodide quenching effect of the compound **86k-HCl** (50 μM) was observed in the absence and presence of DNA (50 μM) by fluorescence spectroscopy with increasing concentrations of KI between 0–10 μM . By the use of the equation $F_0/F = 1 + K_{sv}[\text{Q}]$, K_{sv} Stern-Volmer quenching constant was calculated from the slope of the $[F_0/F]$ vs $[\text{Q}]$ plot. [F_0 and F are the fluorescence intensity in the absence and presence of the anionic quencher $[\text{Q}]$ respectively]

$$\frac{K_{sv(86k\ HCl)}}{K_{sv(86k\ HCl-DNA)}} = \frac{0.00489}{0.00263} = 1.8$$

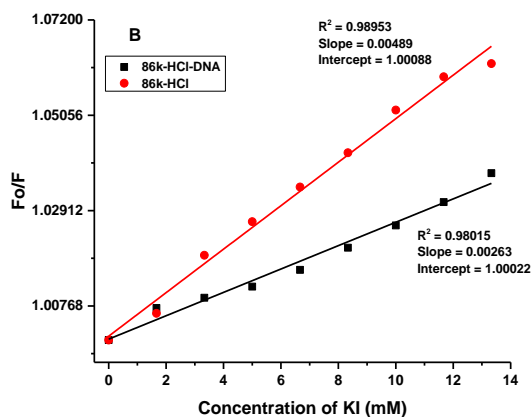


Figure 3.14 Effect of iodide on fluorescence emission of 86k-HCl

CD Spectroscopy: CD spectra of DNA alone and **86k-HCl** complex were recorded using an Applied Photophysics CD spectrophotometer (model CIRASCAN, U.K.) equipped with a Peltier temperature controller to keep the temperature of the sample constant at 25°C. All the CD spectra were recorded in a range from 200 nm to 350 nm with a scan speed of 100 nm/min with a spectral bandwidth of 10 nm. An average of three scans was taken in all experiments. The background spectrum of the buffer solution (10 mM Tris-HCl, pH 7.2) was subtracted from the spectra of DNA and 86k-HCl complex.

Melting Point Studies: DNA melting experiments were performed by monitoring the absorption of ctDNA (50 μ M) at 260 nm in the absence and presence of 86k-HCl (50 μ M) at various temperatures by using a UV-visible spectrophotometer fitted with a temperature-controlled Peltier. 10 mM Tris-HCl buffer (pH 7.2) was added to make the volume of the sample 3 ml. The absorbance was then plotted as a function of temperature ranging from 35°C to 90°C. The DNA melting temperature (T_m) was determined as the transition midpoint.

Copies of NMR and HRMS spectra

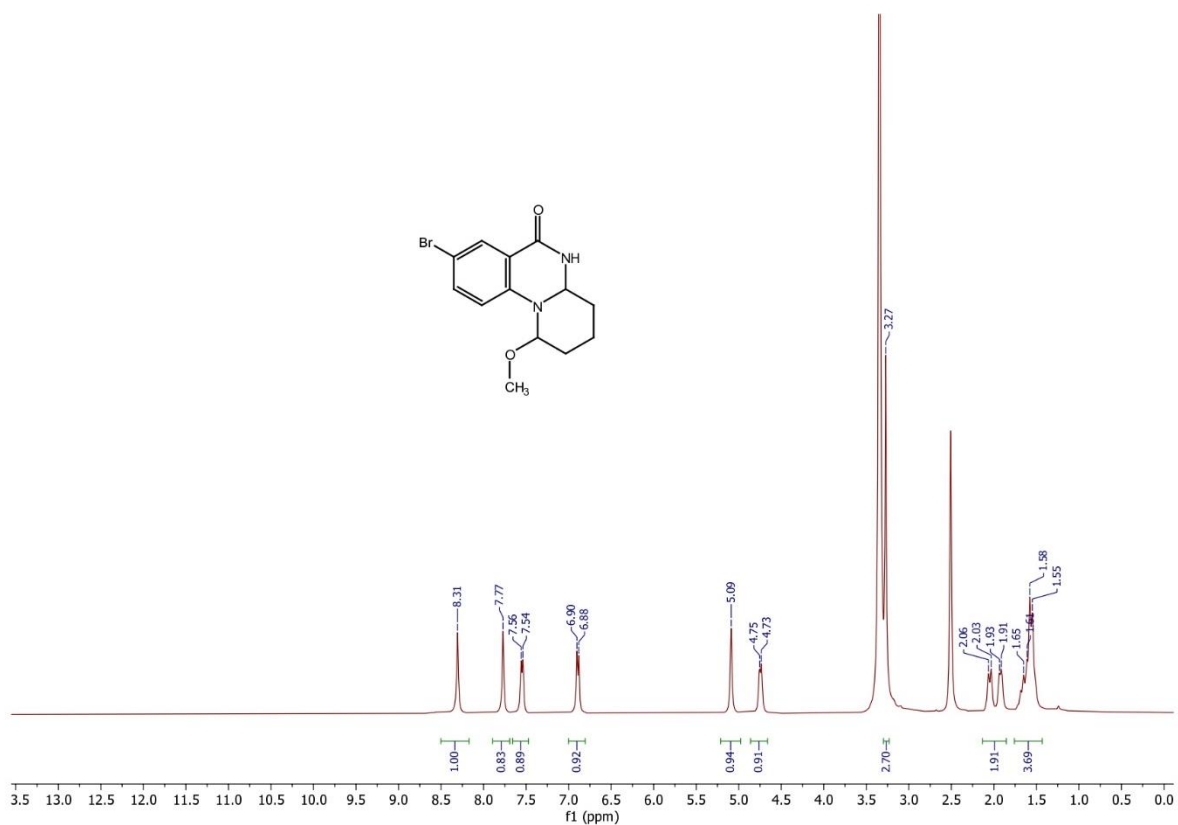


Figure 3.15 ¹H NMR spectrum of 85b (300 MHz, DMSO-d₆)

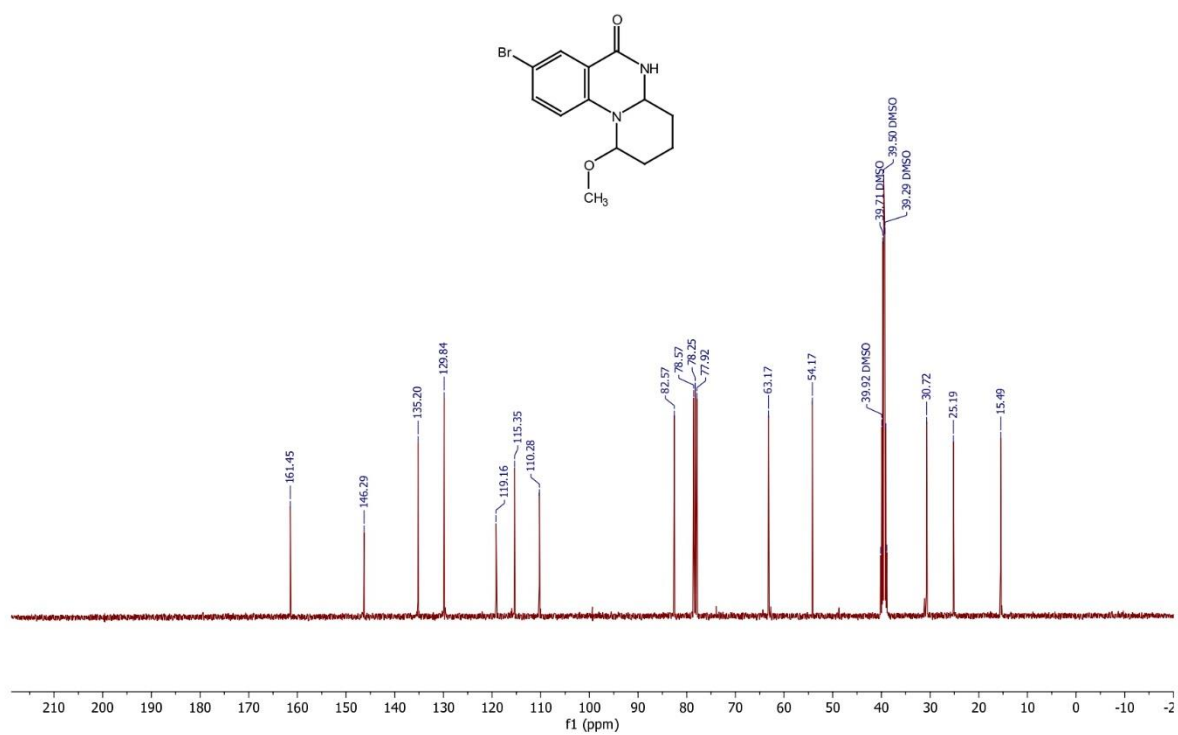


Figure 3.16 ¹³C NMR spectrum of 85b (300 MHz, DMSO-d₆)

Chapter 3

^1H NMR (300 MHz, CDCl_3) of the compound 6b

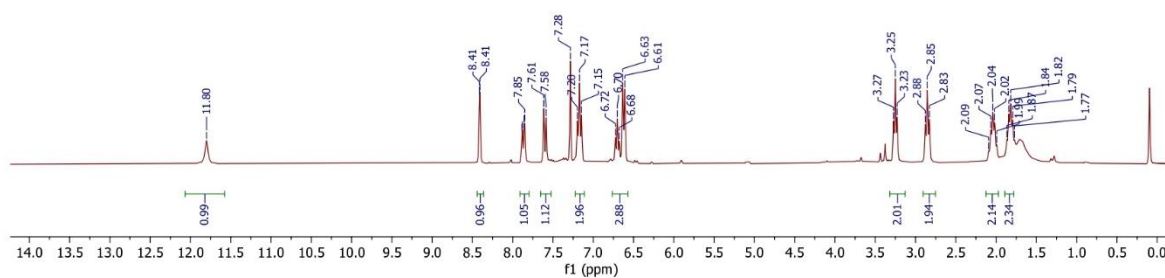
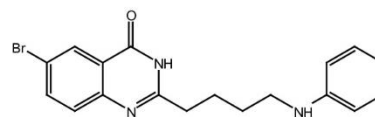


Figure 3.17 ^1H NMR spectrum of 86a (300 MHz, CDCl_3)

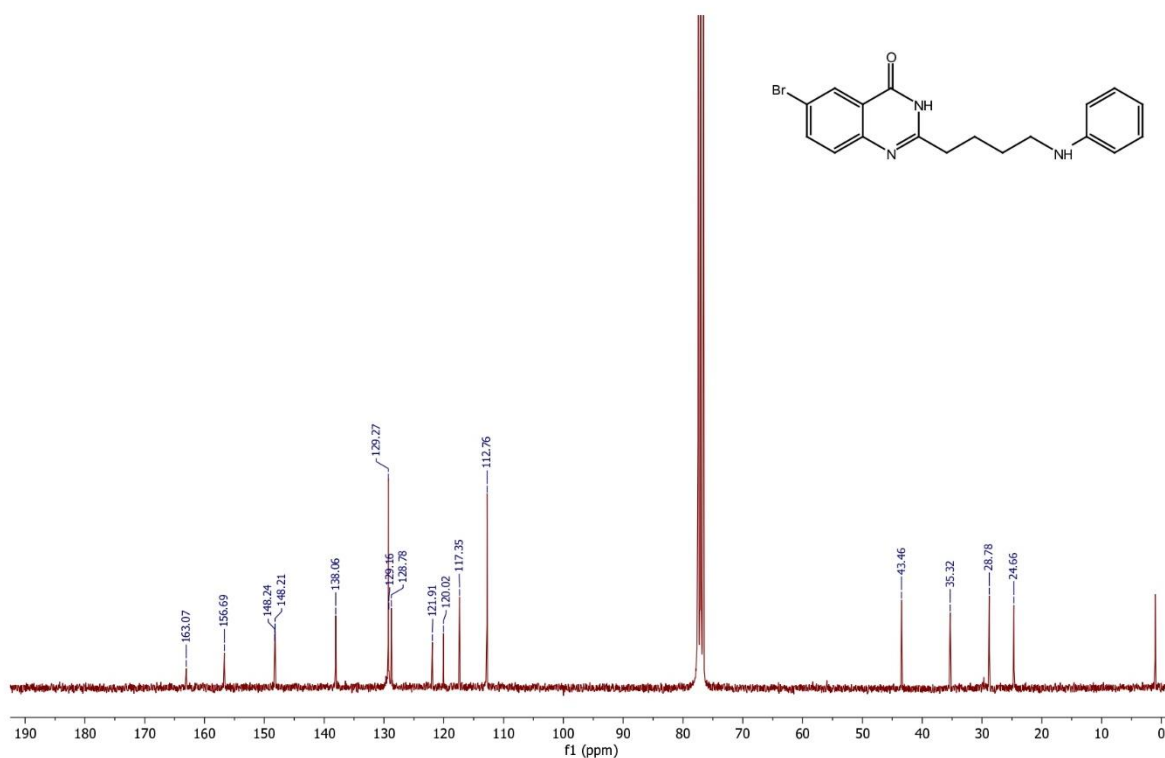


Figure 3.18 ^{13}C NMR spectrum of 86a (300 MHz, CDCl_3)

Chapter 3

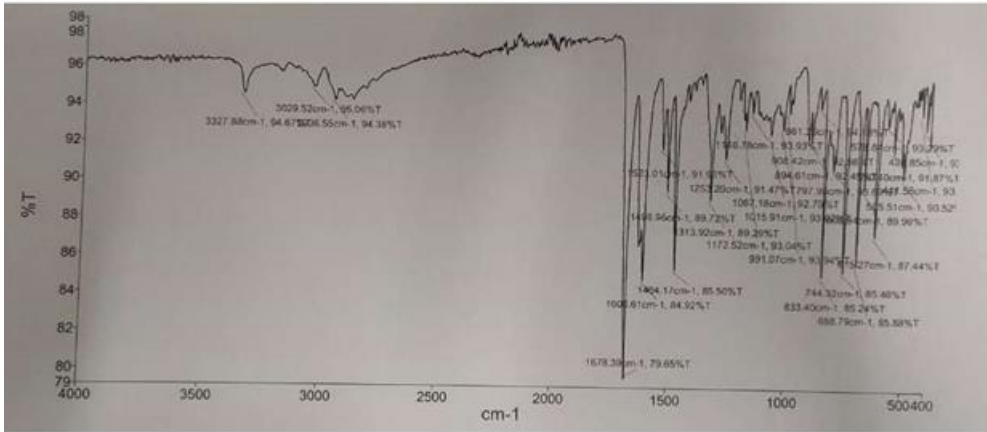
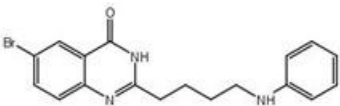


Figure 3.19 IR spectrum of 86a

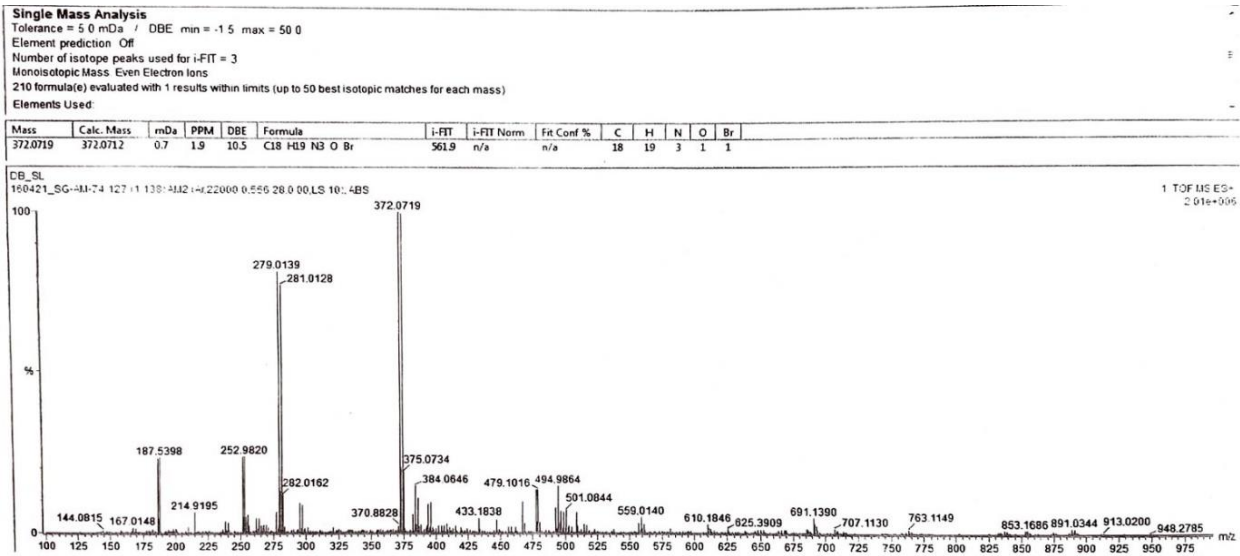


Figure 3.20 Mass spectrum of 86a (ESI-TOF), Calculated m/z for $[M+H]^+ = 372.0711$

Chapter 3

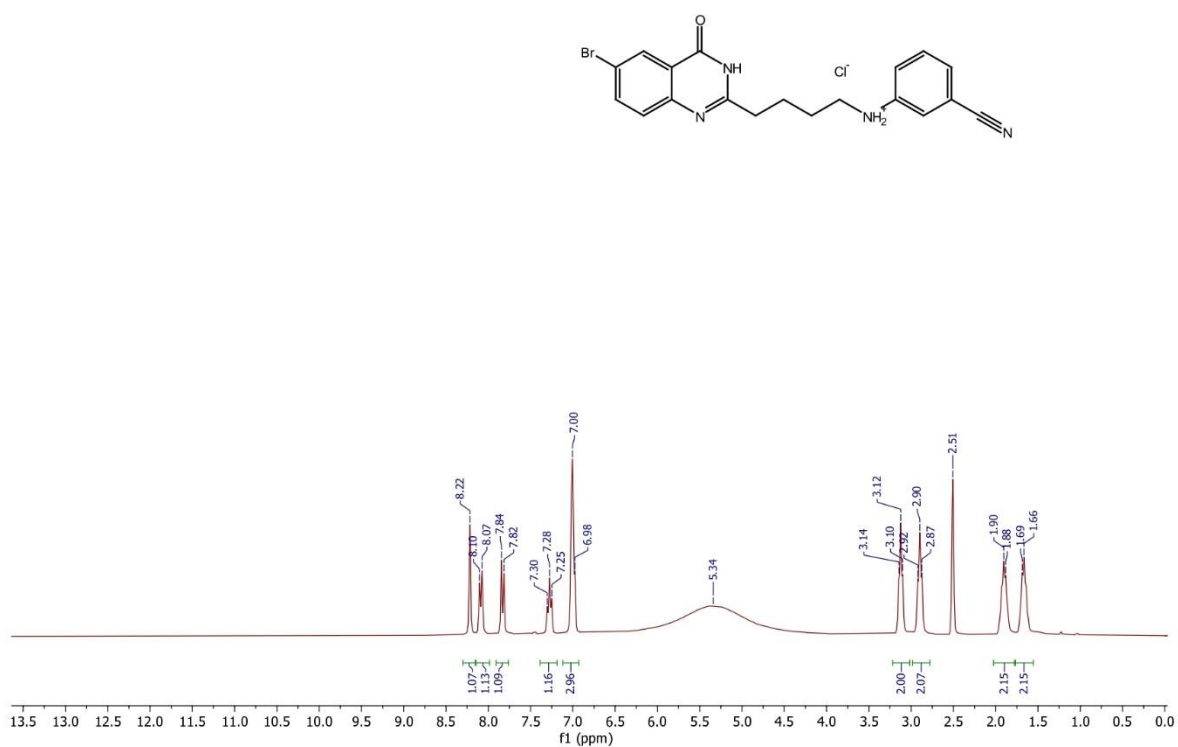


Figure 3.21 ^1H NMR spectrum of 86b-HCl (300 MHz, DMSO- d_6)

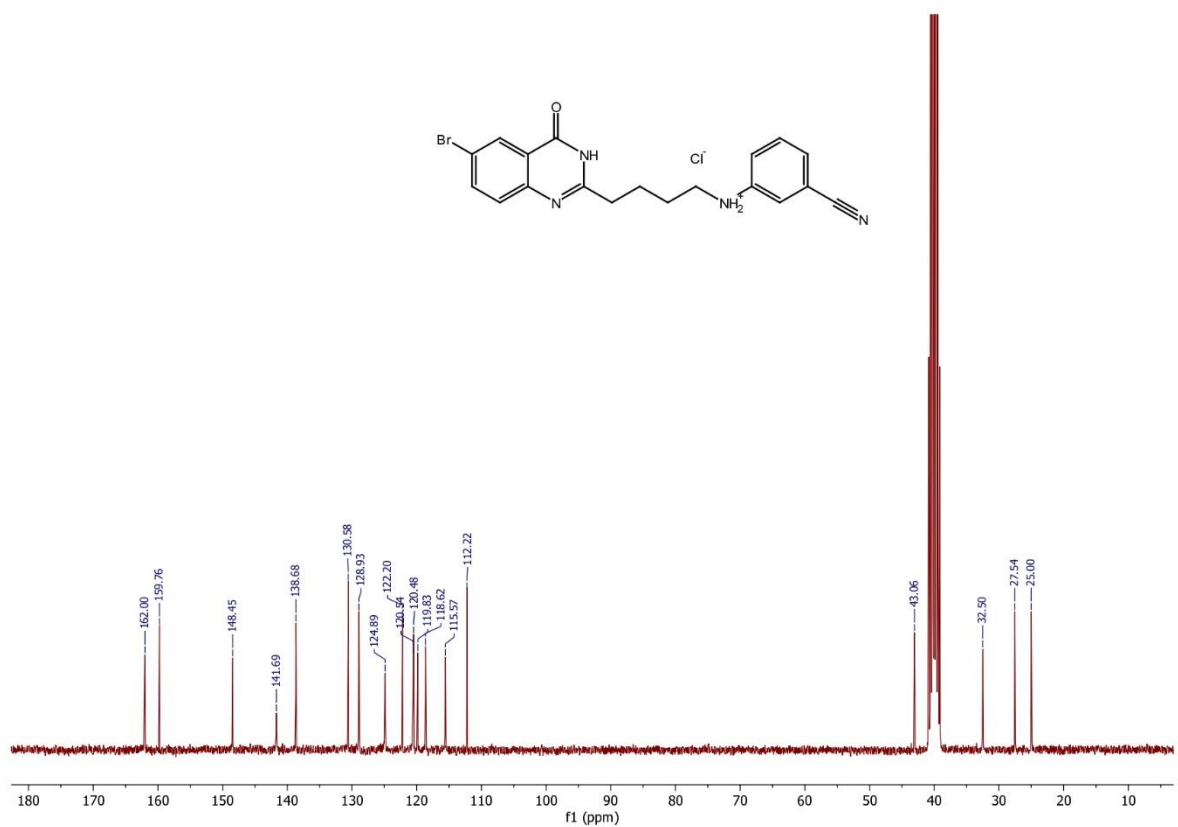


Figure 3.22 ^{13}C NMR spectrum of 86b-HCl (300 MHz, CDCl_3)

Chapter 3

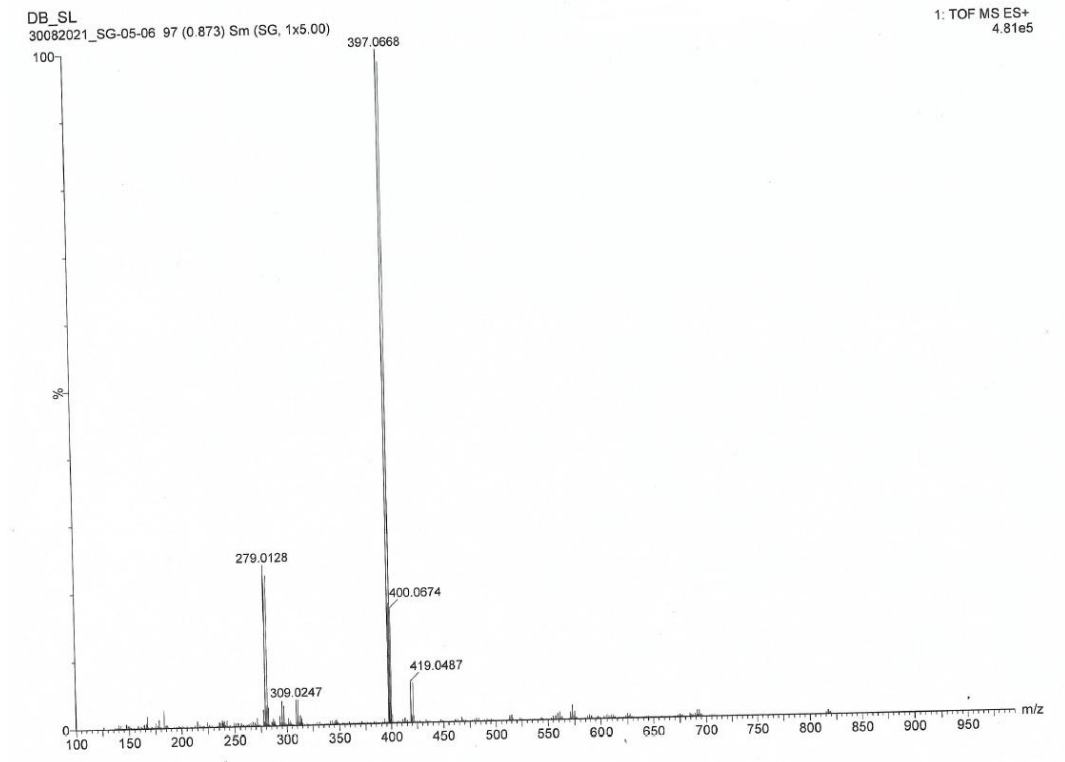


Figure 3.23 Mass spectrum of 86b-HCl (ESI-TOF), Calculated m/z for $[M+H]^+ = 397.0664$

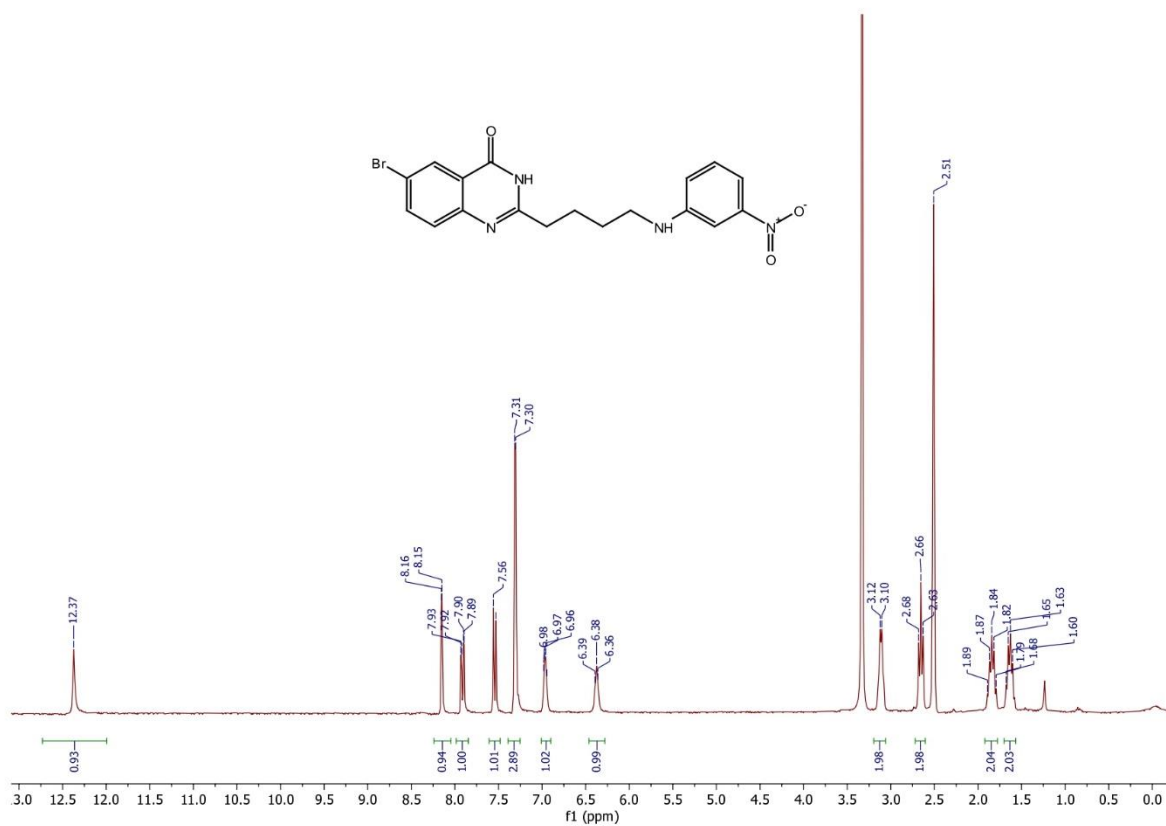
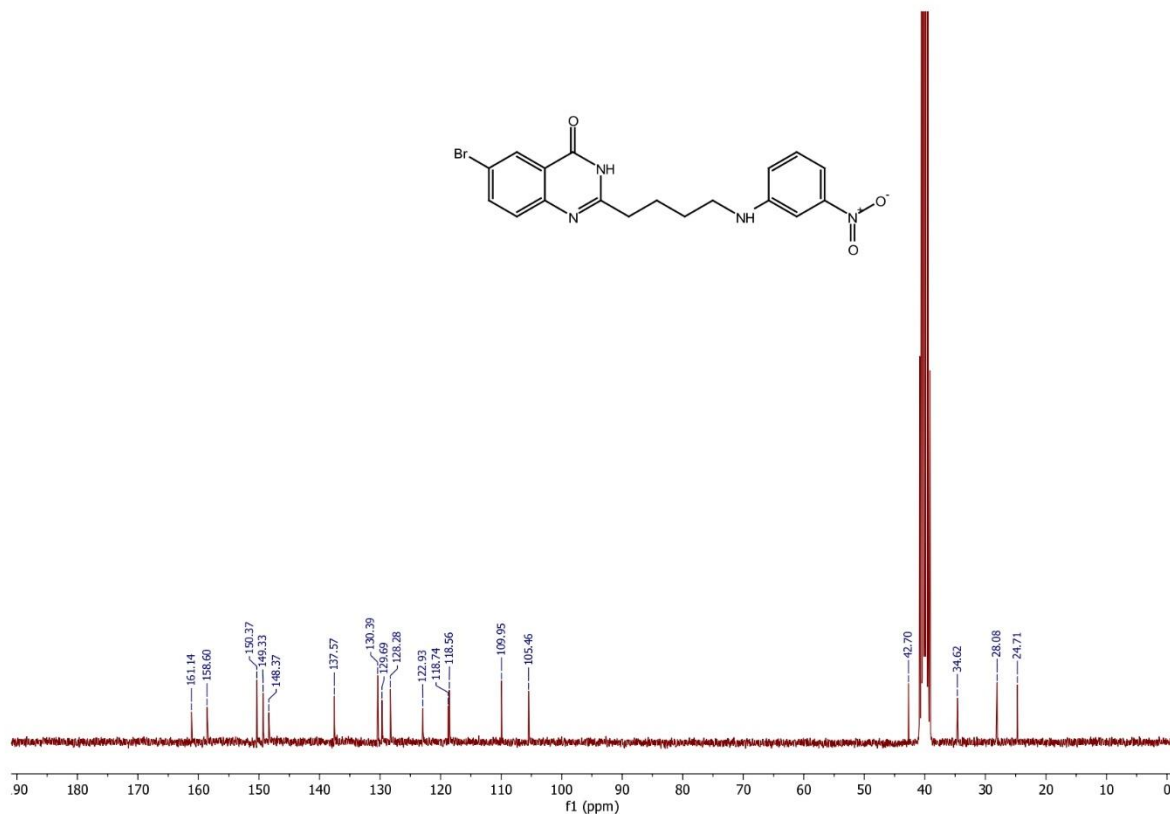
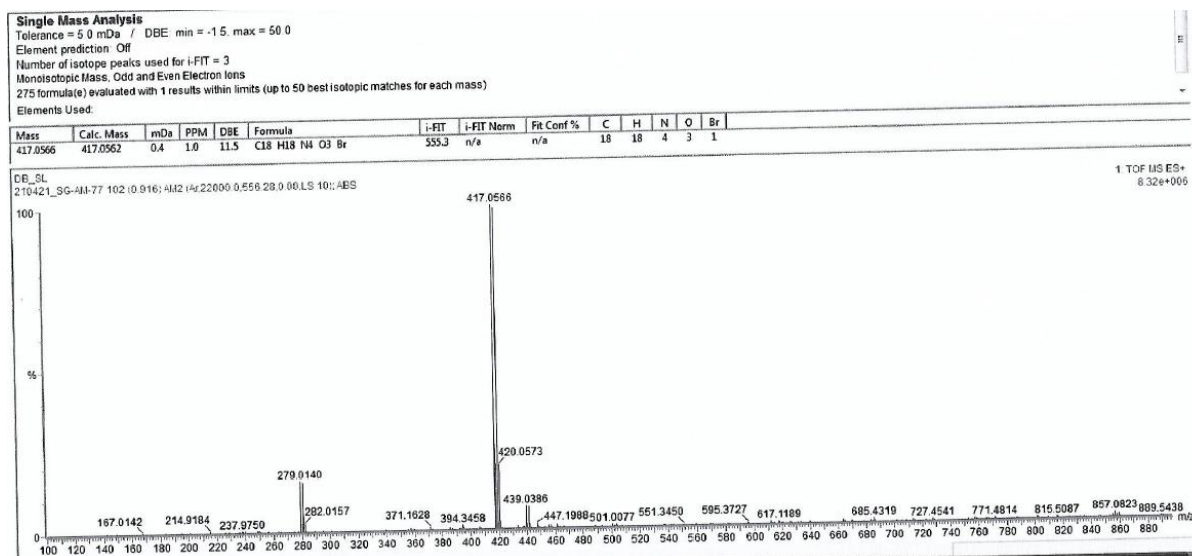


Figure 3.24 ^1H NMR spectrum of 86c (300 MHz, DMSO-d_6)

Figure 3.25 ¹³C NMR spectrum of 86c (300 MHz, DMSO-d₆)Figure 3.26 Mass spectrum of 86c (ESI-TOF), Calculated m/z for $[M+H]^+ = 417.0562$

Chapter 3

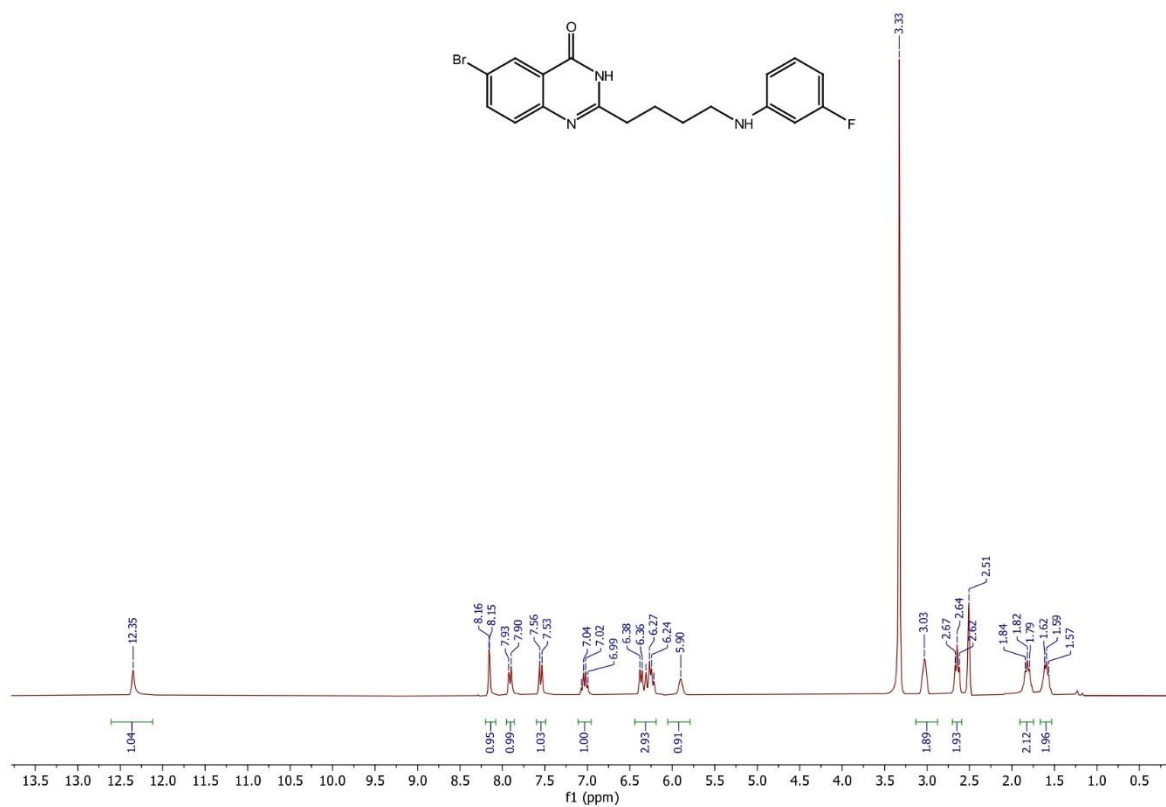


Figure 3.27 ¹H NMR spectrum of 86d (300 MHz, DMSO-d₆)

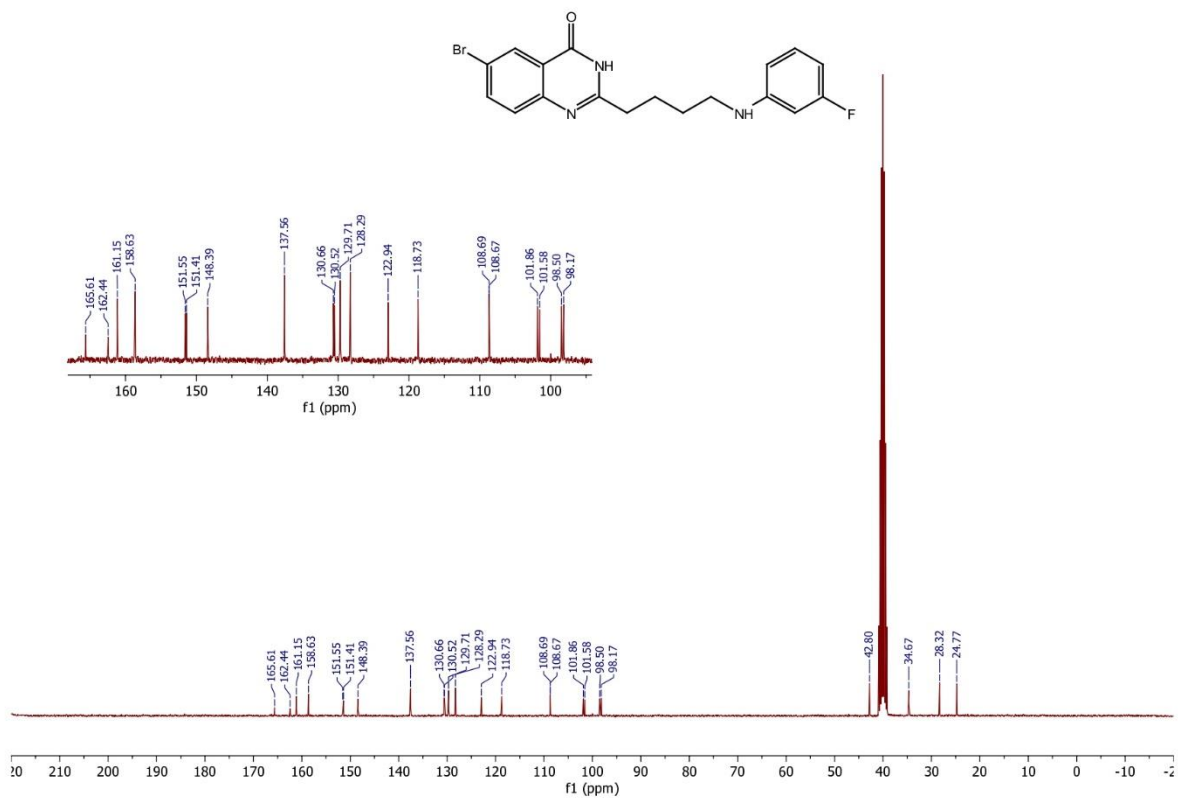


Figure 3.28 ¹³C NMR spectrum of 86d (300 MHz, DMSO-d₆)

Chapter 3

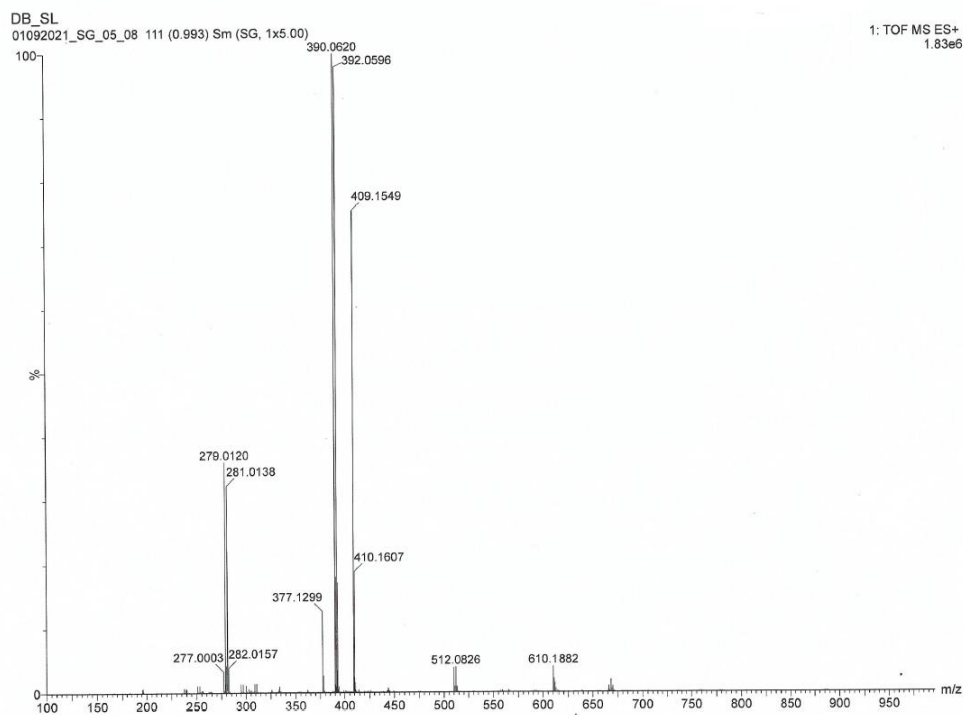


Figure 3.29 Mass spectrum of 86d (ESI-TOF), Calculated m/z for $[M+H]^+ = 390.0617$

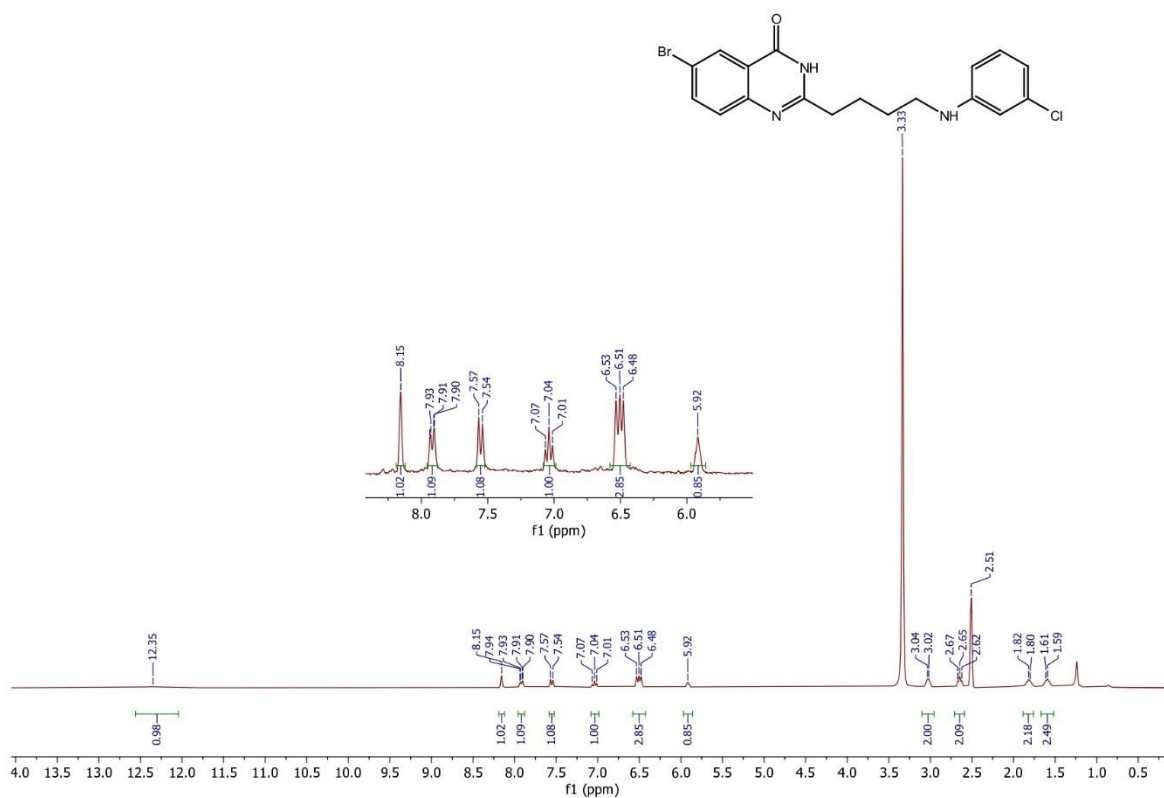


Figure 3.30 ^1H NMR spectrum of 86e (300 MHz, DMSO-d_6)

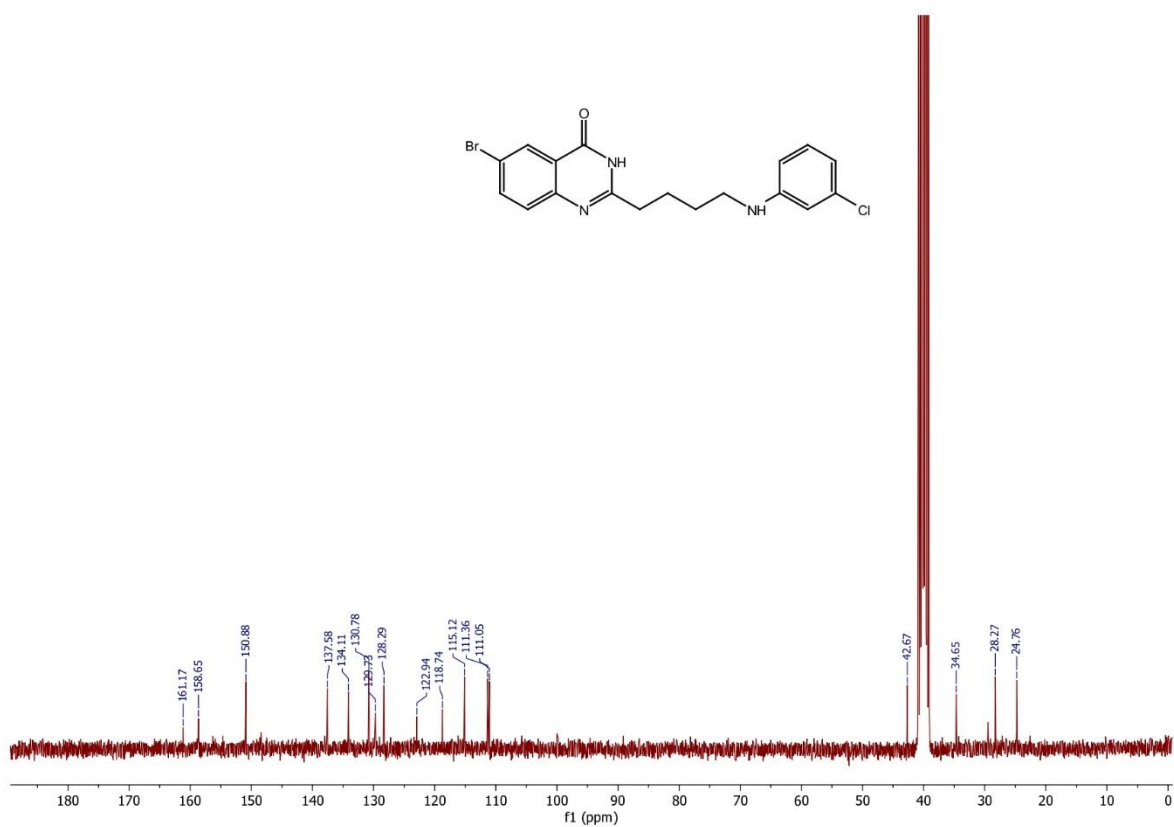


Figure 3.31 ¹³C NMR spectrum of 86e (300 MHz, DMSO-d₆)

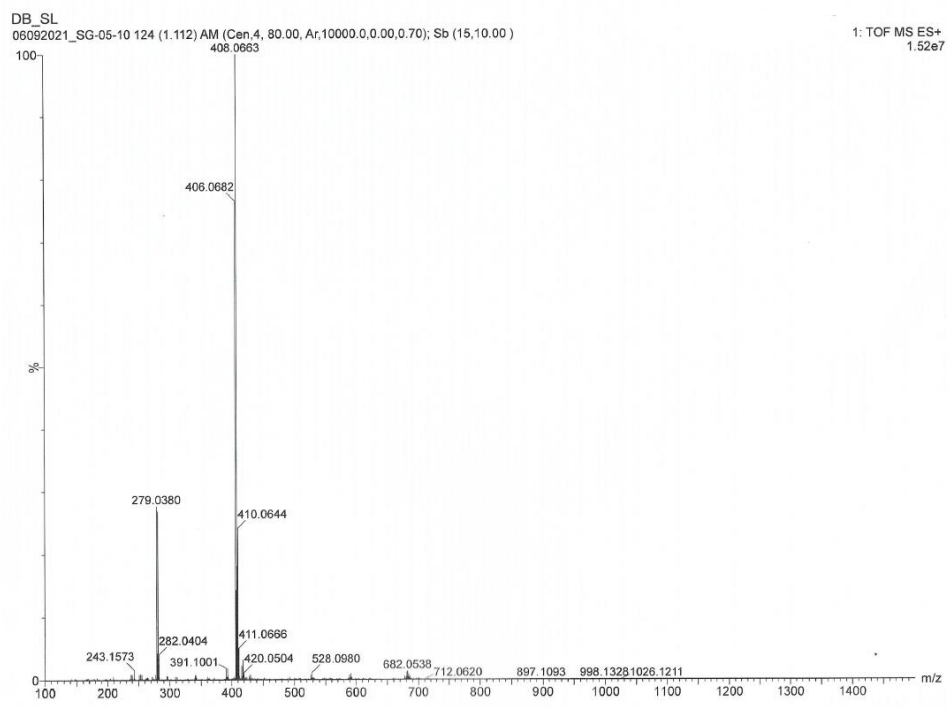


Figure 3.32 Mass spectrum of 86e (ESI-TOF), Calculated m/z for $[M+H]^+ = 406.0322$

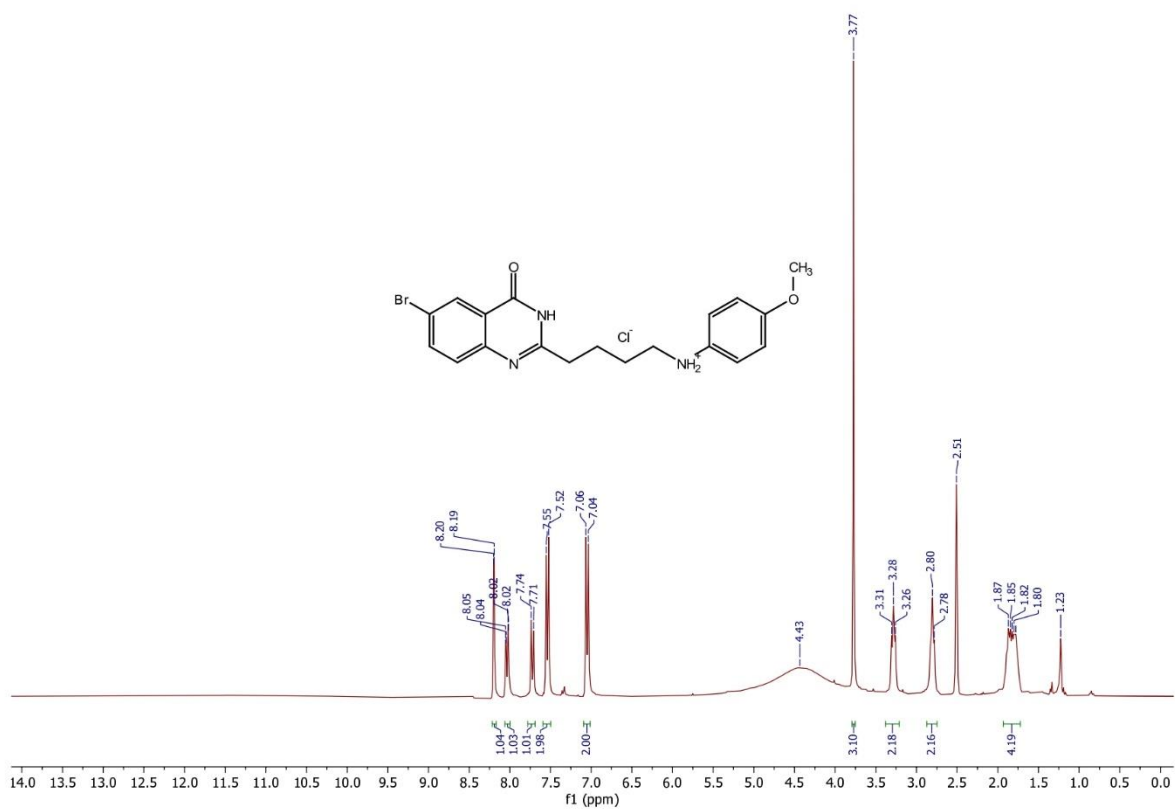


Figure 3.33 ¹H NMR spectrum of 86f (300 MHz, DMSO-d₆)

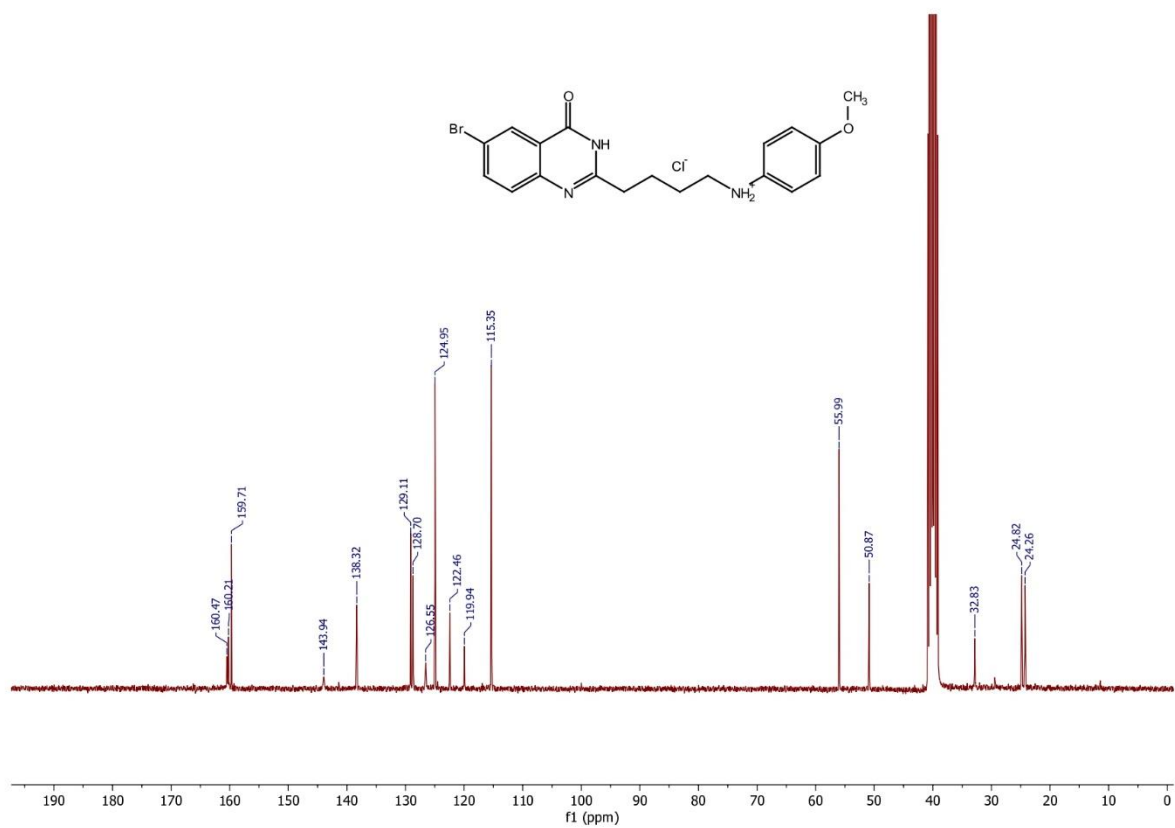


Figure 3.34 ¹³C NMR spectrum of 86f (300 MHz, DMSO-d₆)

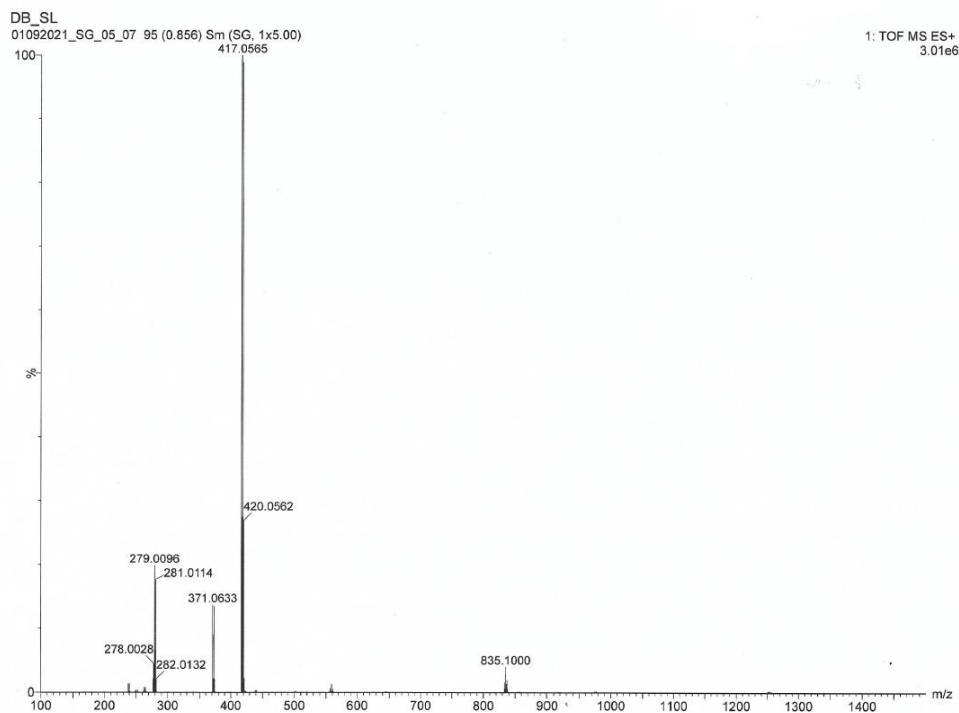


Figure 3.35 Mass spectrum of 86f (ESI-TOF), Calculated m/z for $[M+H]^+ = 417.0562$

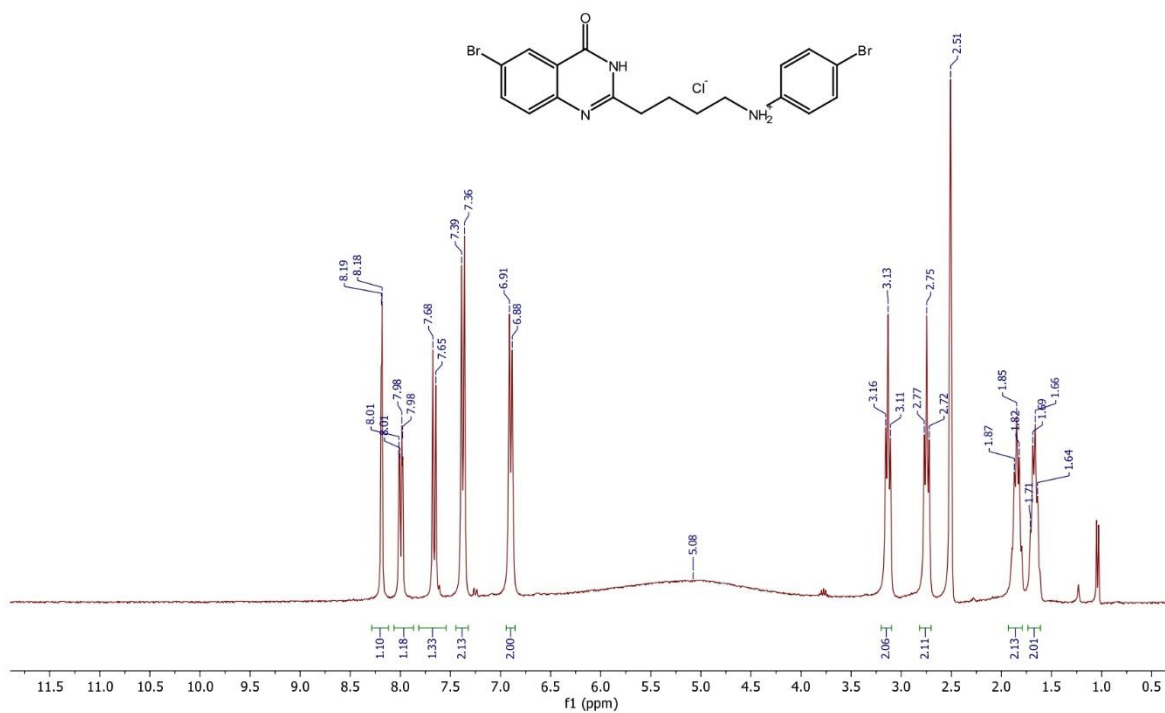


Figure 3.36 ^1H NMR spectrum of 86g-HCl (300 MHz, DMSO- d_6)

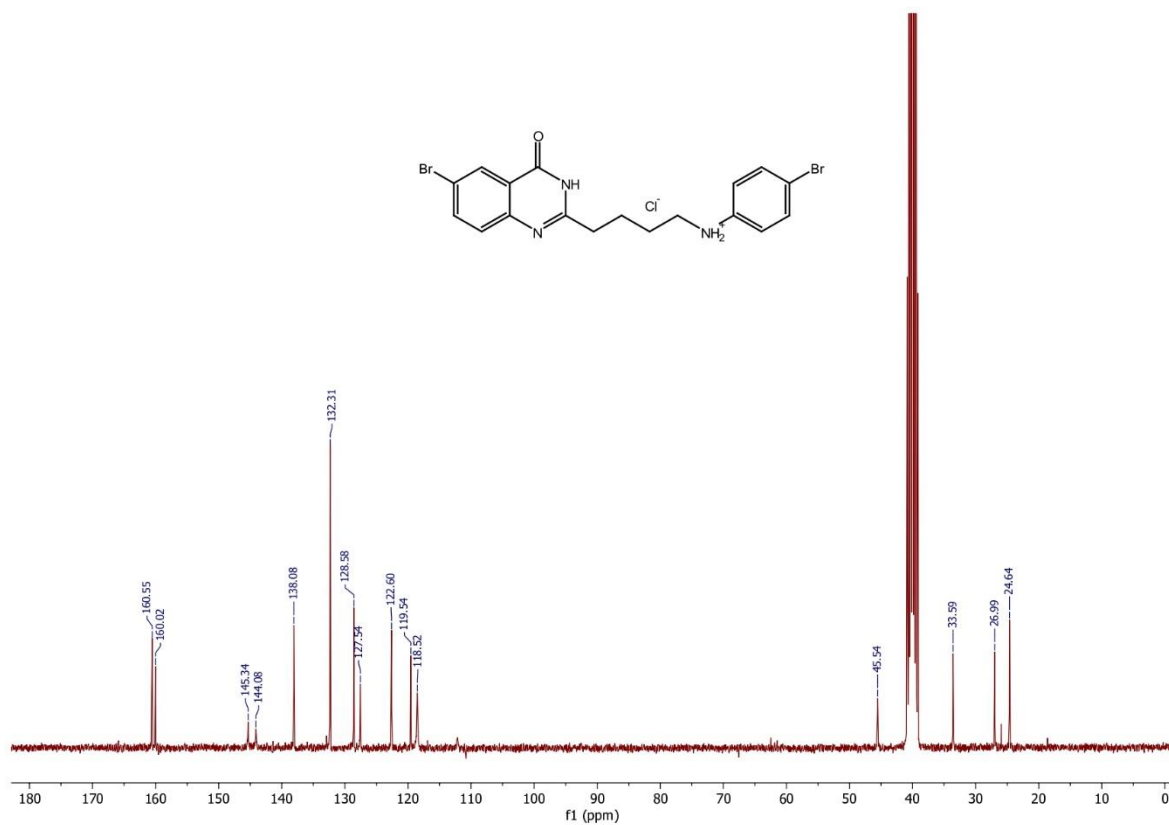


Figure 3.37 ¹³C NMR spectrum of 86g-HCl (300 MHz, DMSO-d₆)

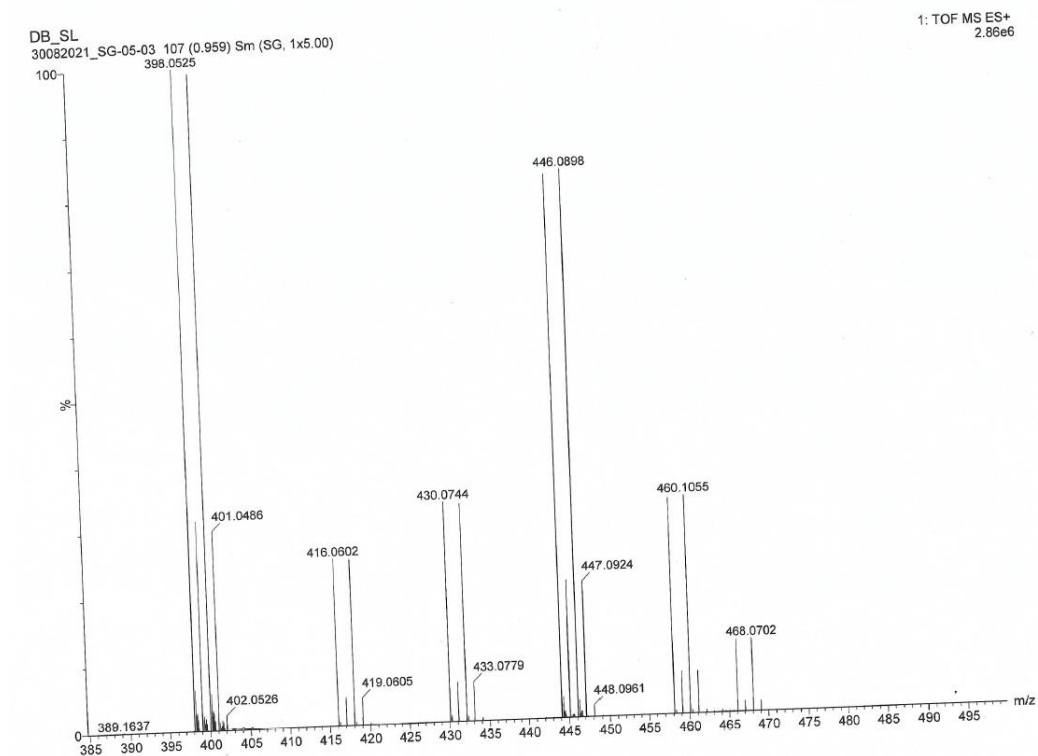


Figure 3.38 Mass spectrum of 86g-HCl (ESI-TOF), Calculated m/z for $[M+2+H]^+ = 446.0902$

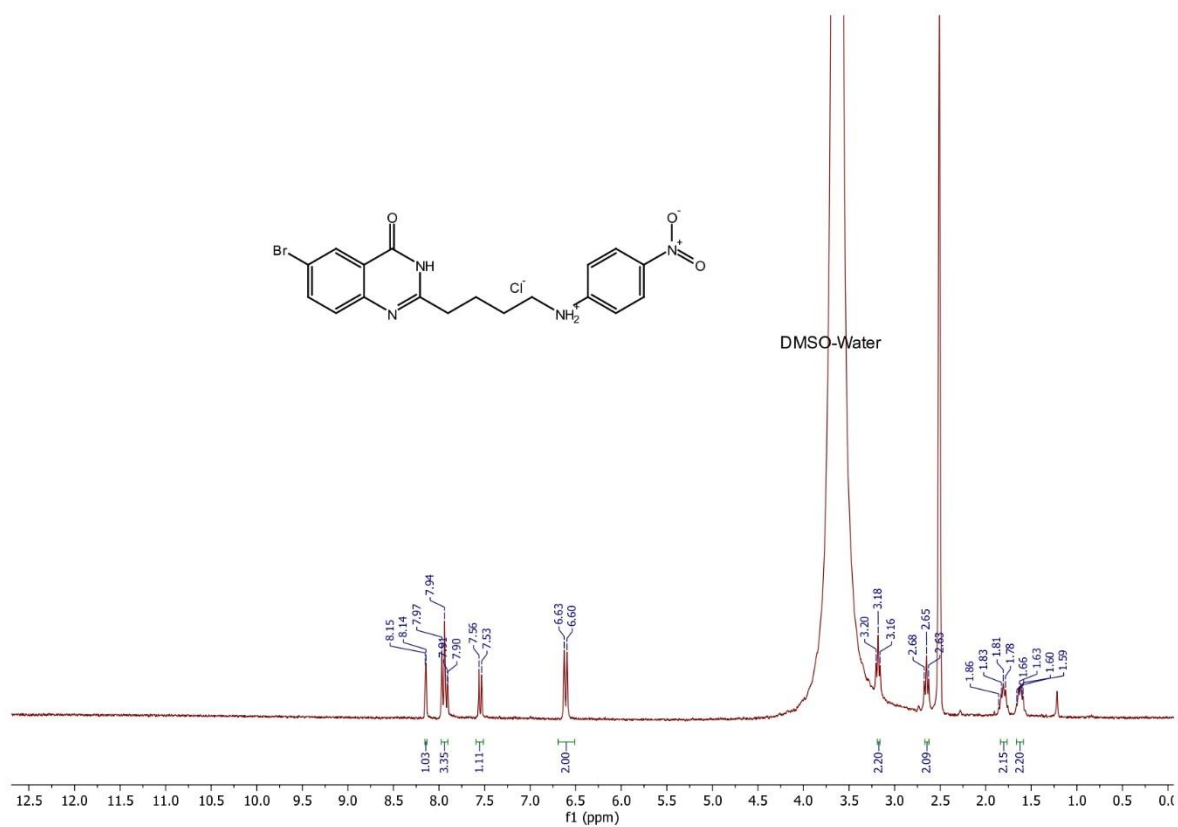


Figure 3.39 ¹H NMR spectrum of 86h-HCl (300 MHz, DMSO-d₆)

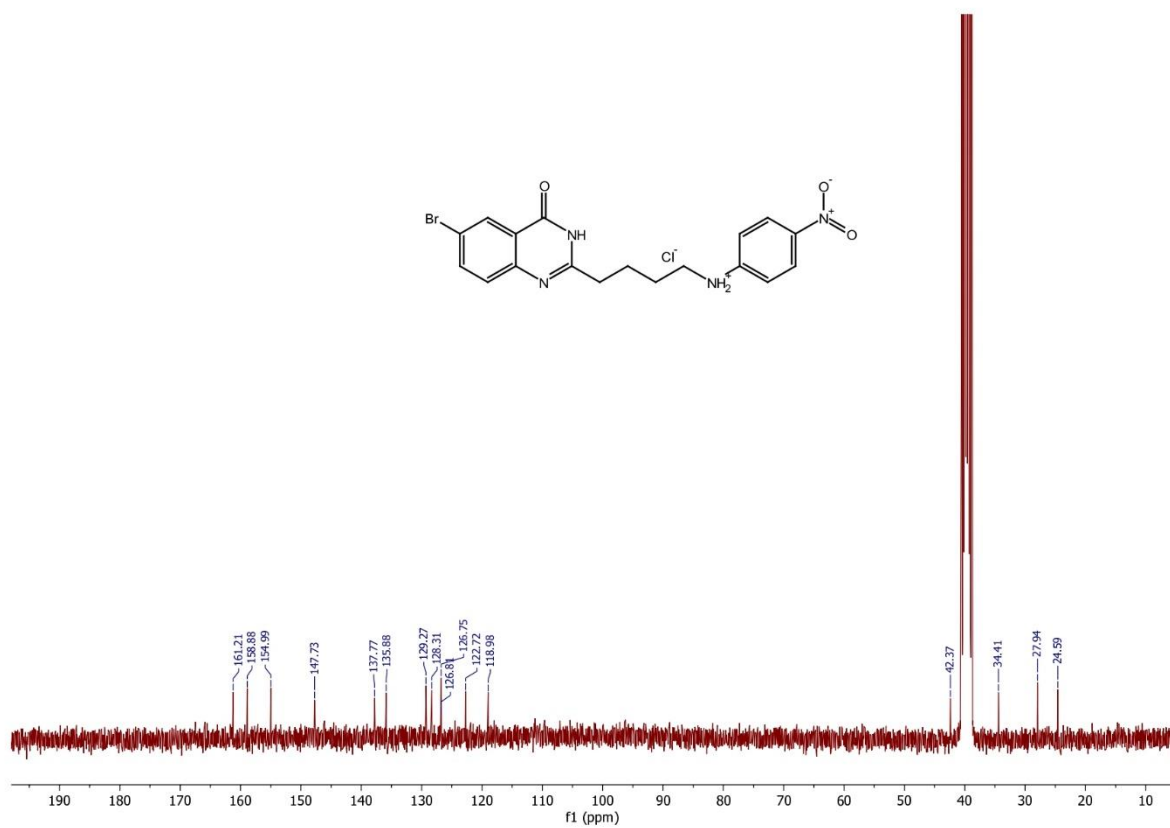


Figure 3.40 ¹³C NMR spectrum of 86h-HCl (300 MHz, DMSO-d₆)

Chapter 3

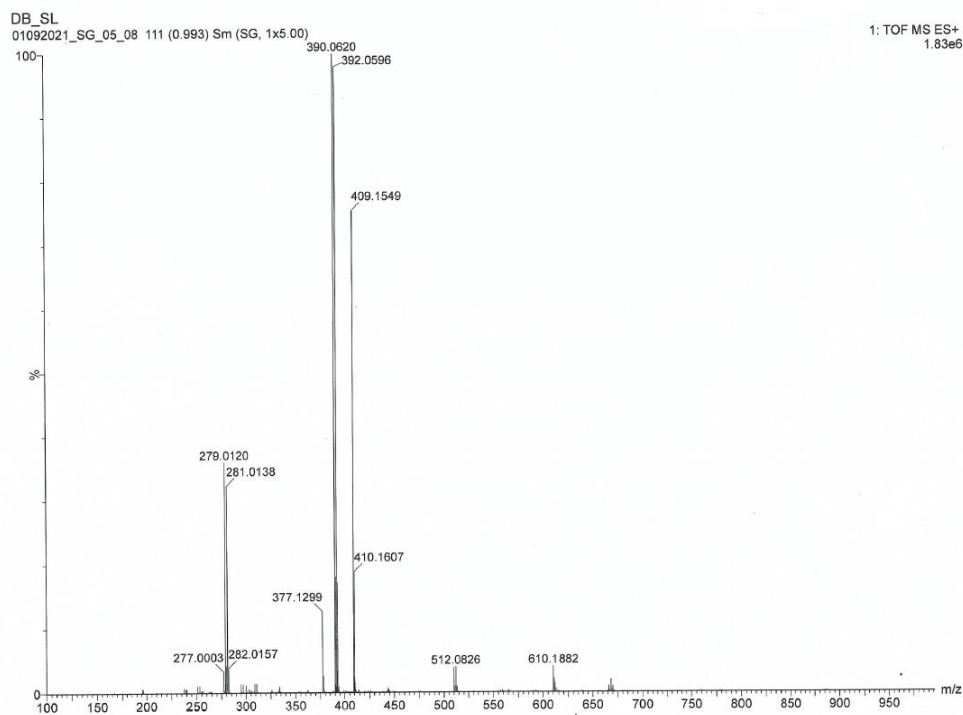


Figure 3.41 Mass spectrum of 86h-HCl (ESI-TOF), Calculated m/z for $[M+H]^+ = 390.0617$

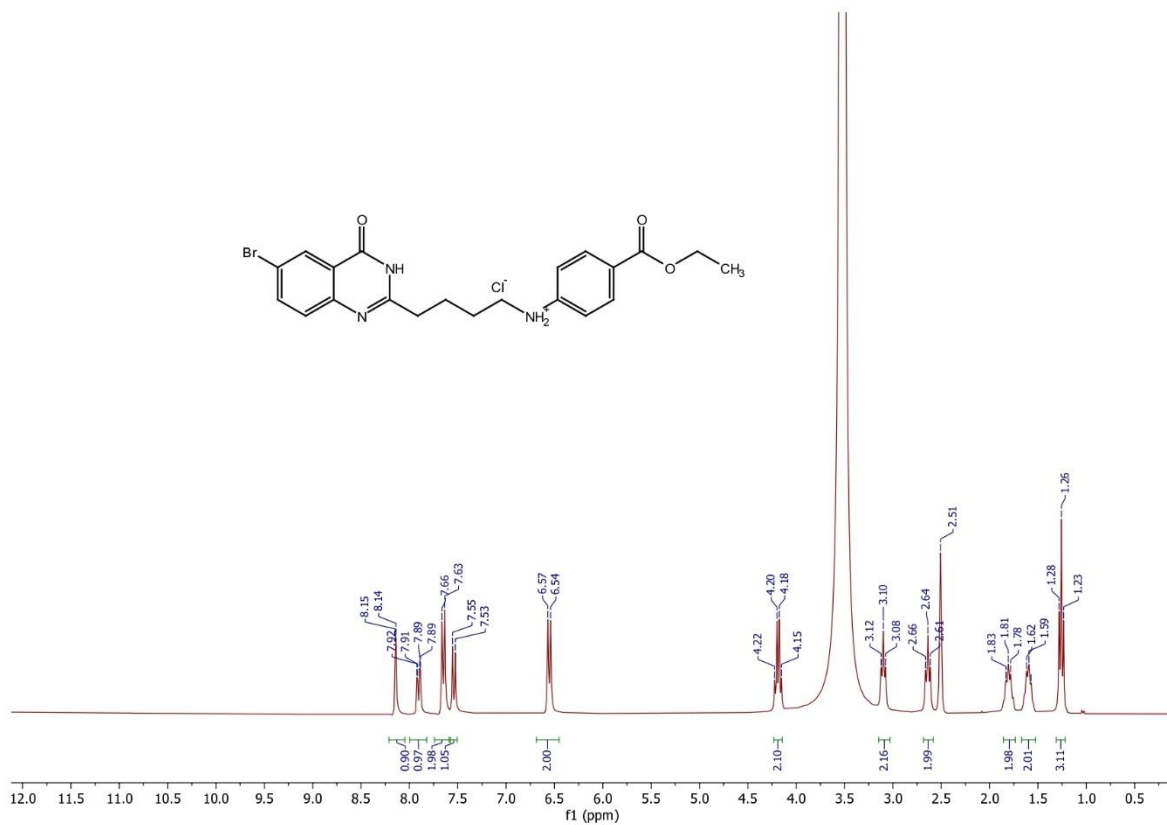


Figure 3.42 ^1H NMR spectrum of 86i-HCl (300 MHz, DMSO- d_6)

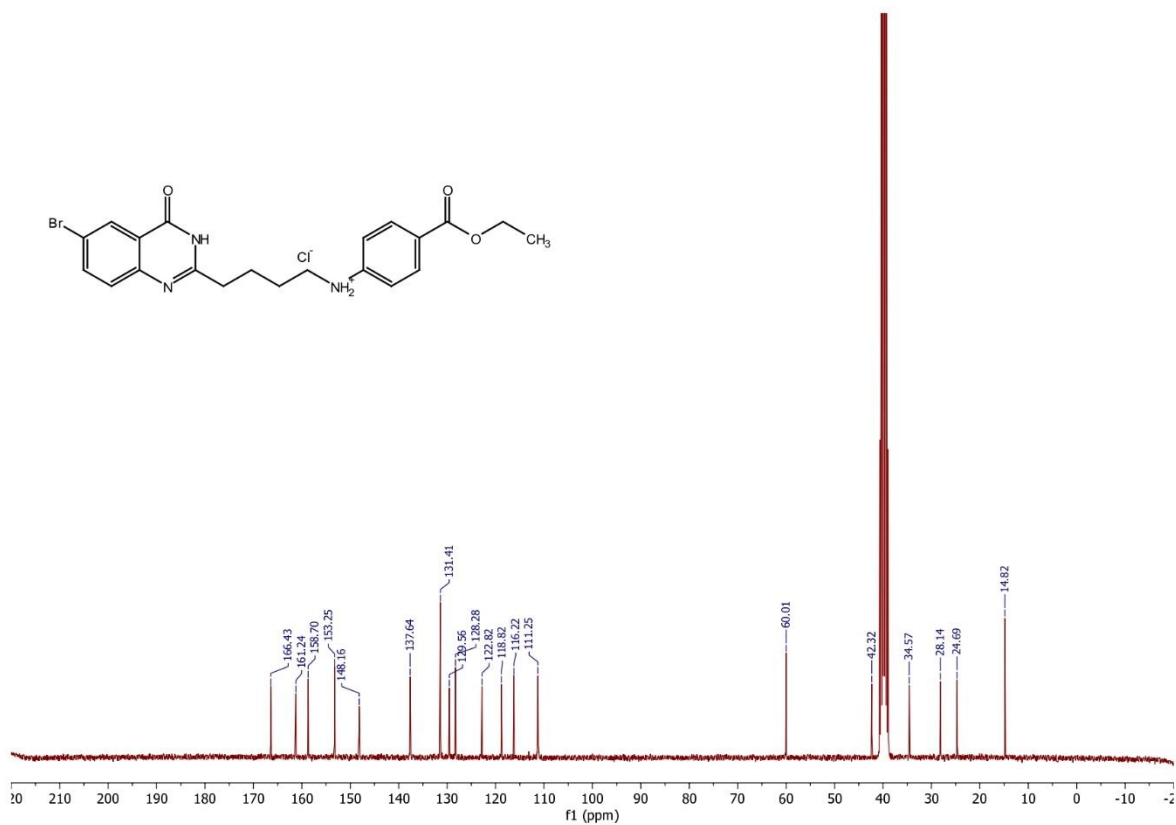


Figure 3.43 ¹³C NMR spectrum of 86i-HCl (300 MHz, DMSO-d₆)

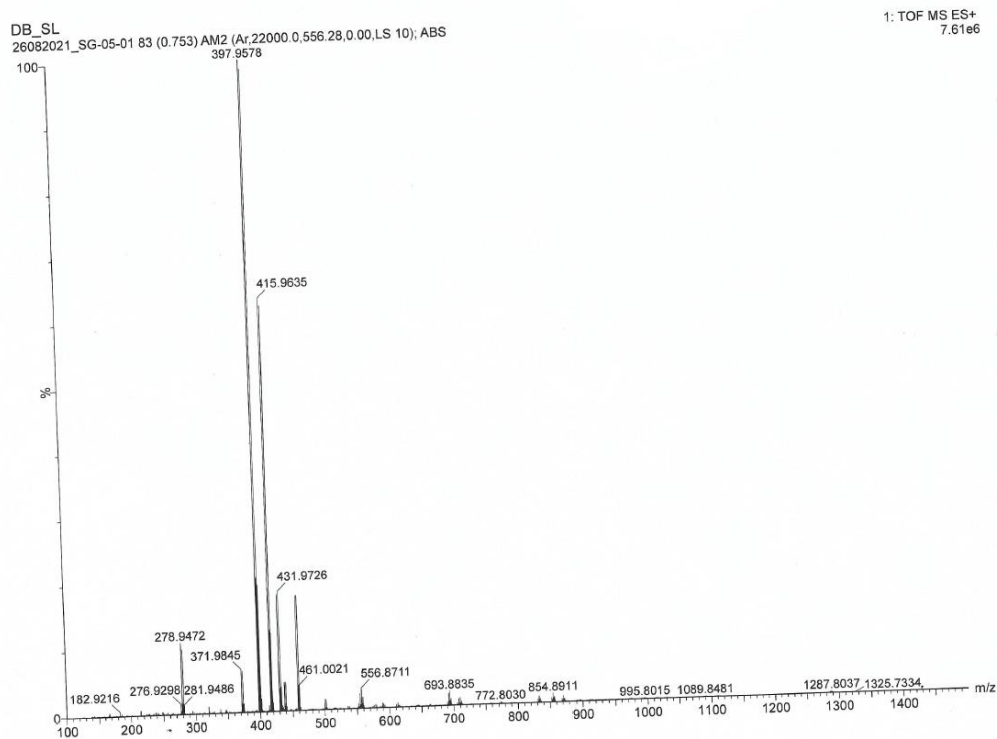


Figure 3.44 Mass spectrum of 86i-HCl (ESI-TOF), Calculated m/z for $[M+H]^+ = 416.0610$

Chapter 3

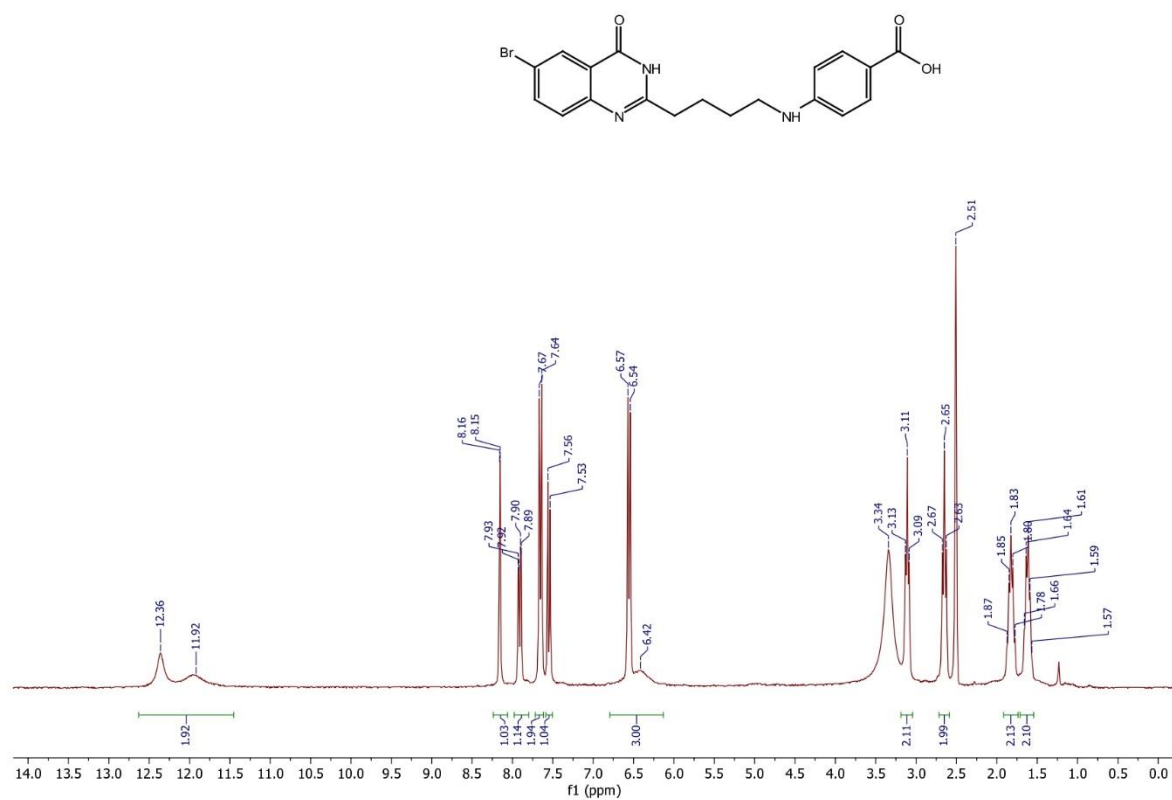


Figure 3.45 ¹H NMR spectrum of 86j (300 MHz, DMSO-d₆)

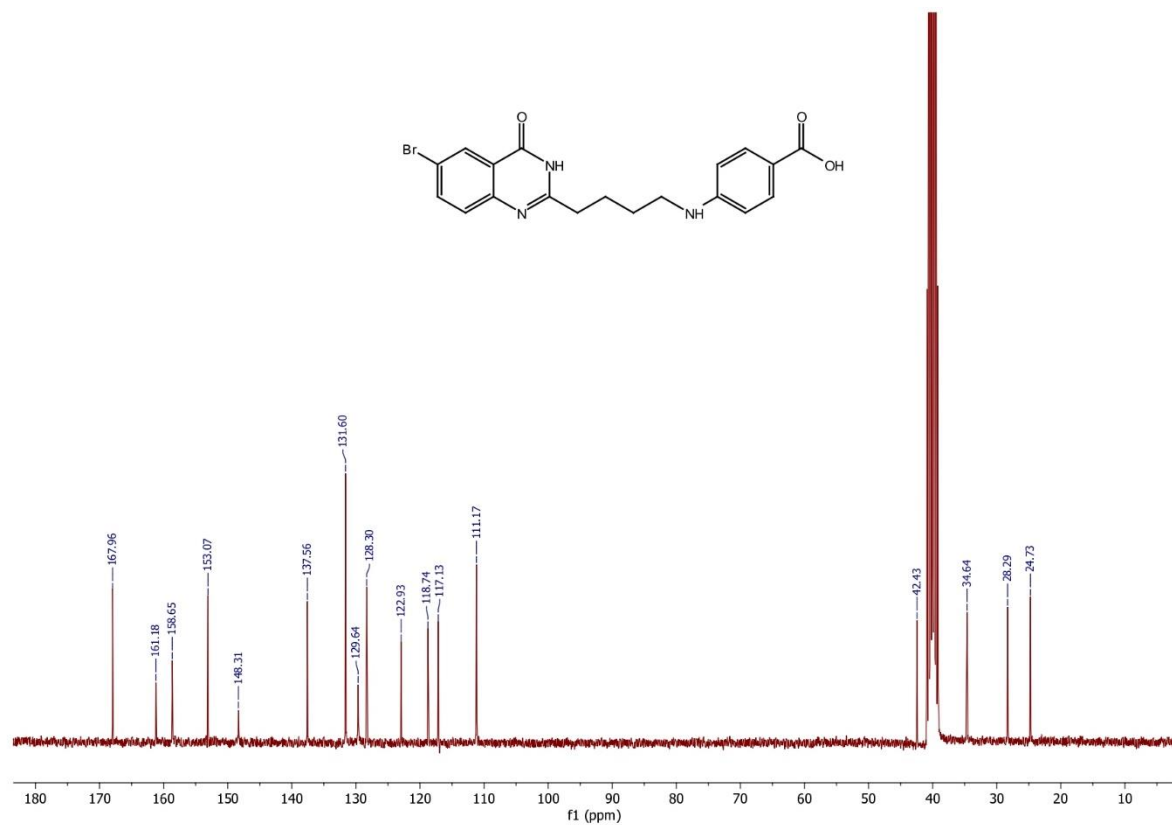


Figure 3.46 ¹³C NMR spectrum of 86j (300 MHz, DMSO-d₆)

Chapter 3

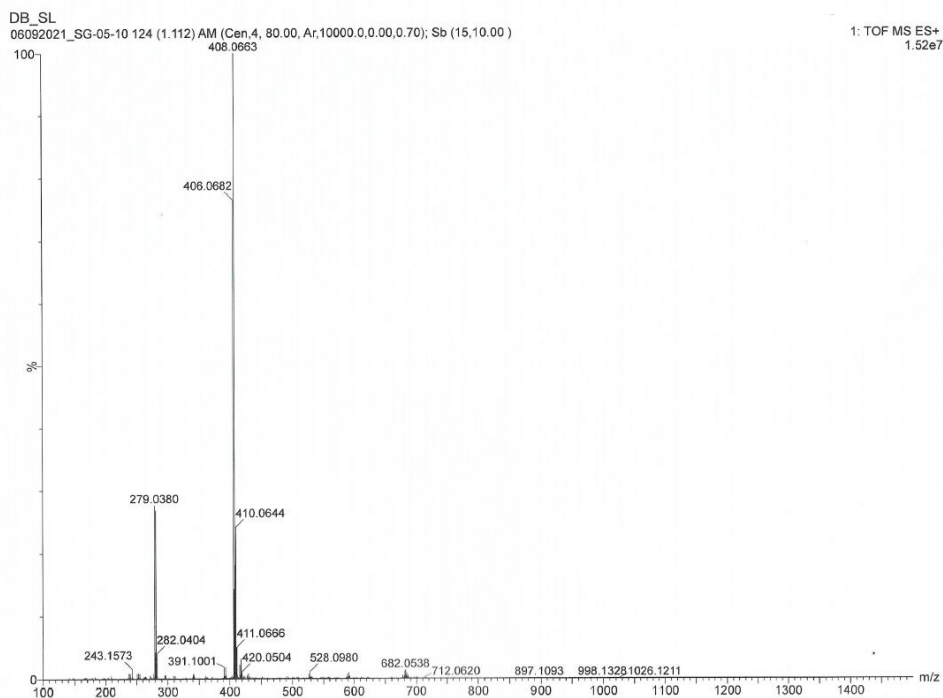


Figure 3.47 Mass spectrum of 86j (ESI-TOF), Calculated m/z for $[M+H]^+ = 406.0322$

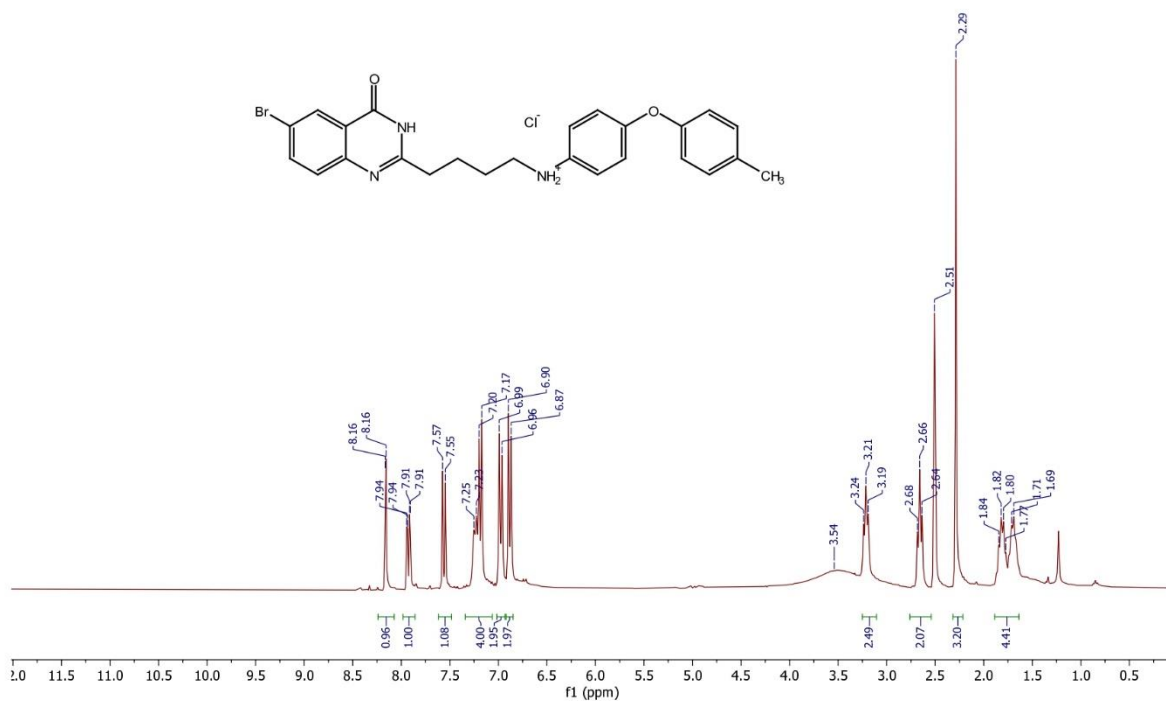


Figure 3.48 ^1H NMR spectrum of 86k-HCl (300 MHz, DMSO-d_6)

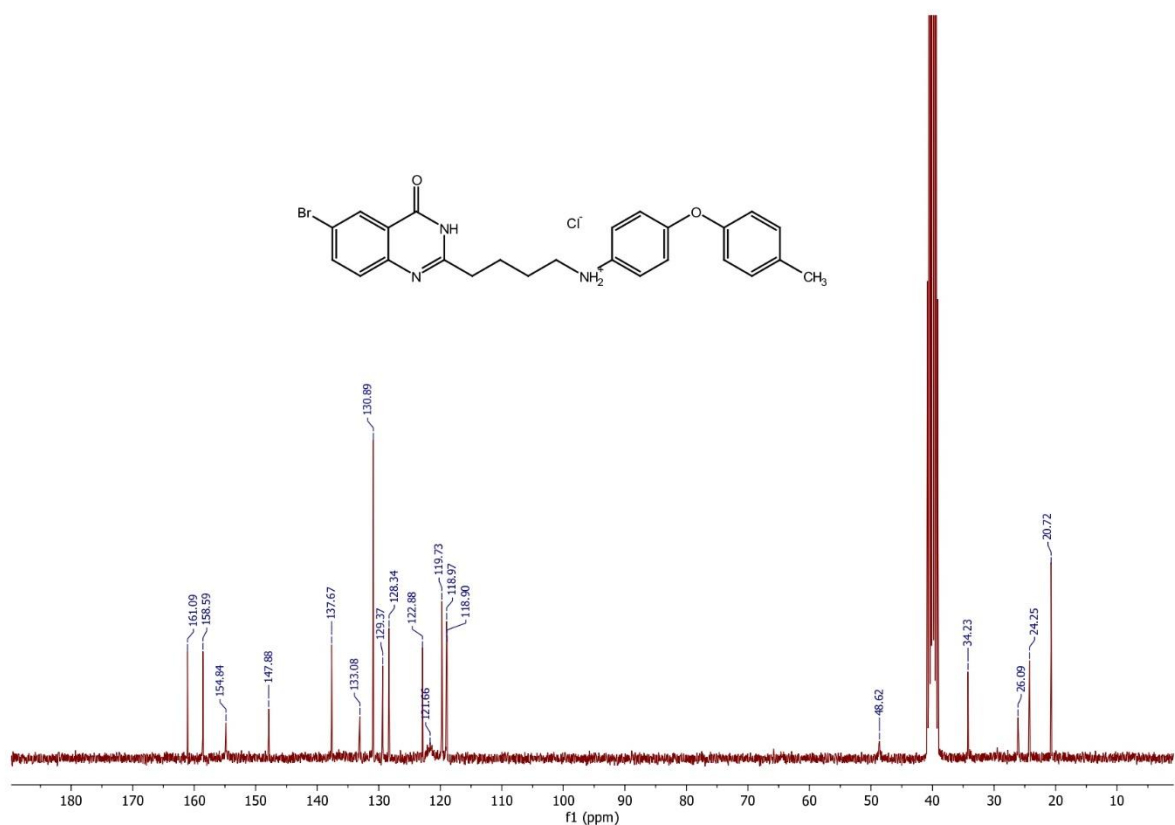


Figure 3.49 ¹³C NMR spectrum of 86k-HCl (300 MHz, DMSO-d₆)

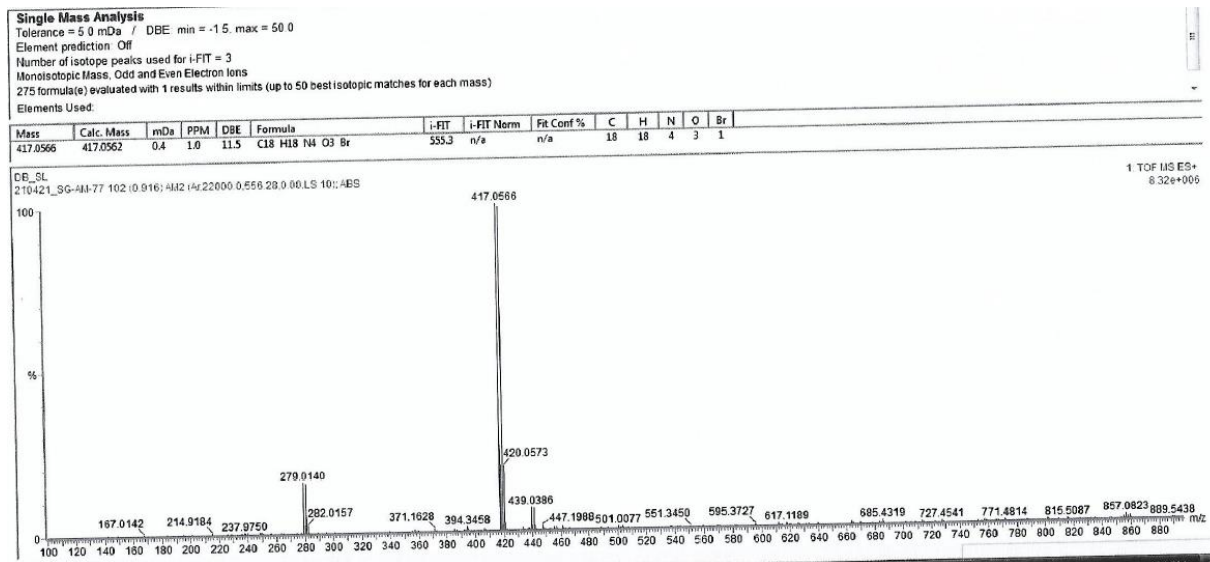


Figure 3.50 Mass spectrum of 86k-HCl (ESI-TOF), Calculated m/z for $[M+H]^+ = 417.0562$

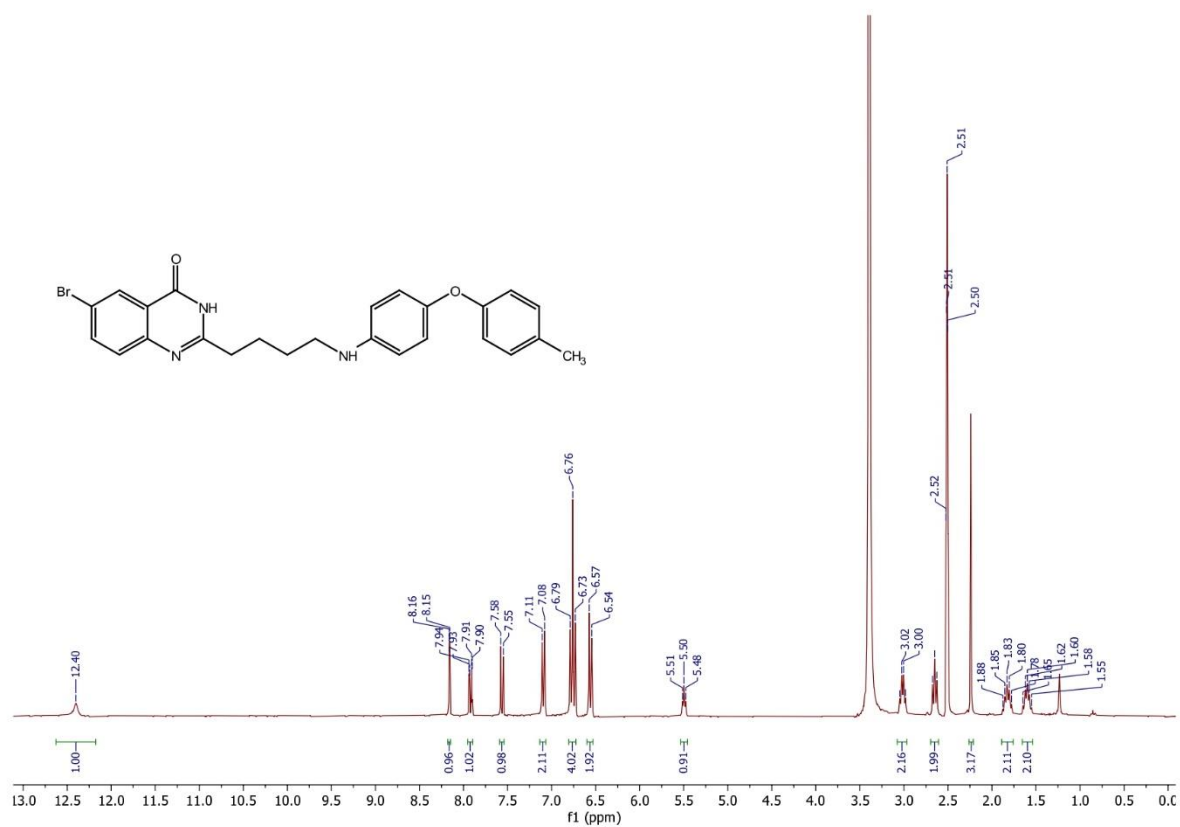


Figure 3.51 ¹H NMR spectrum of 86k (300 MHz, DMSO-d₆)

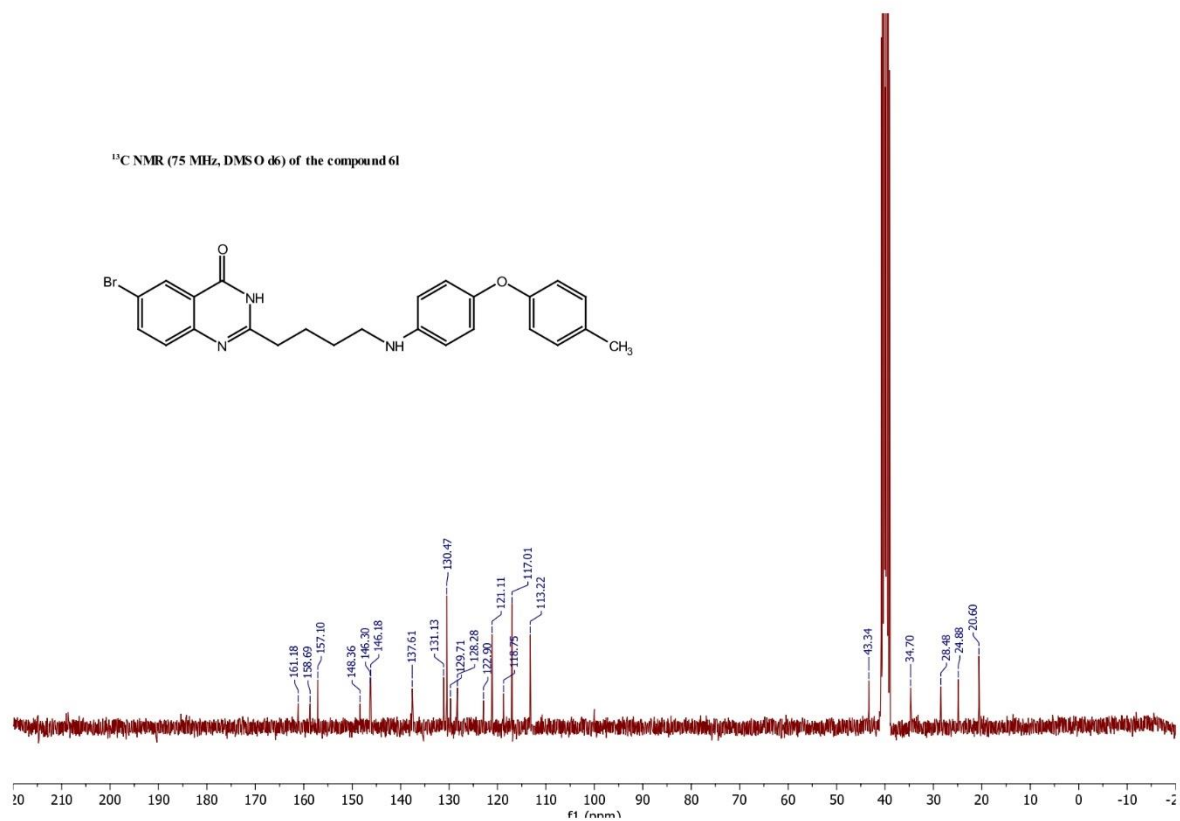


Figure 3.52 ¹³C NMR spectrum of 86k (300 MHz, DMSO-d₆)

Chapter 3

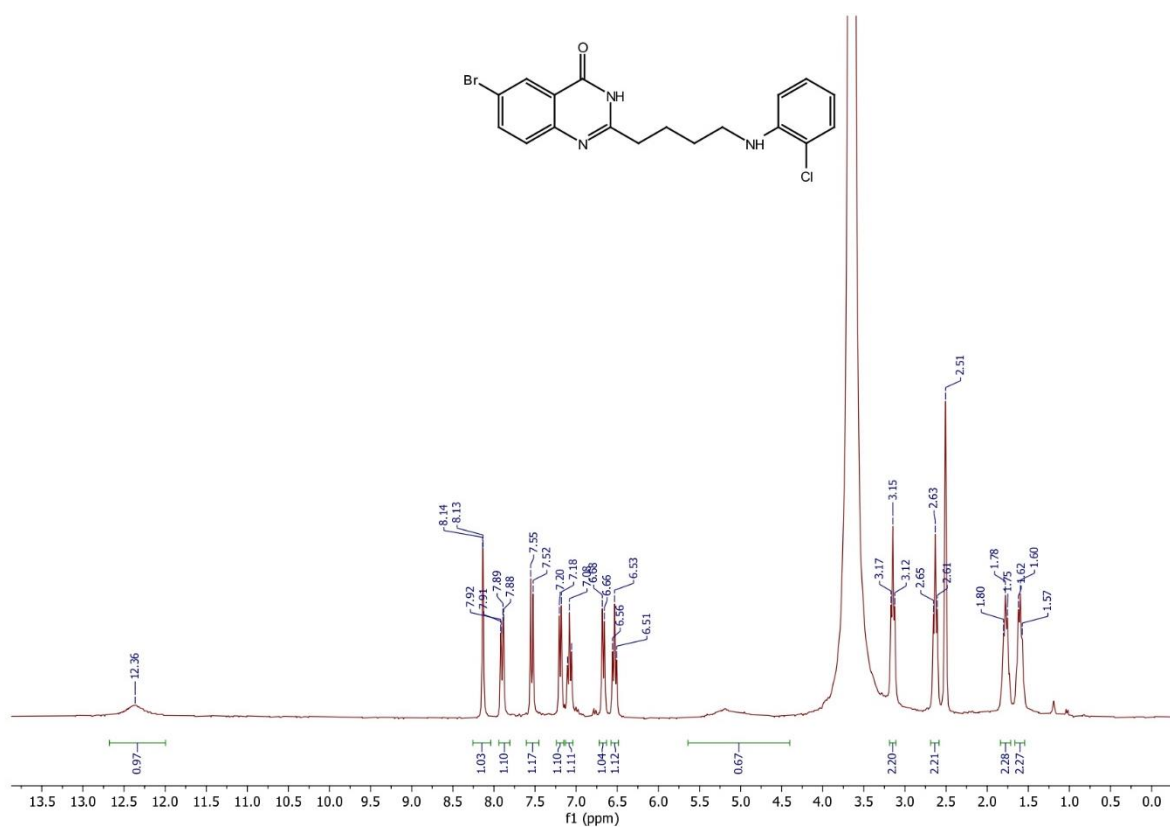


Figure 3.53 ¹H NMR spectrum of 86l (300 MHz, DMSO-d₆)

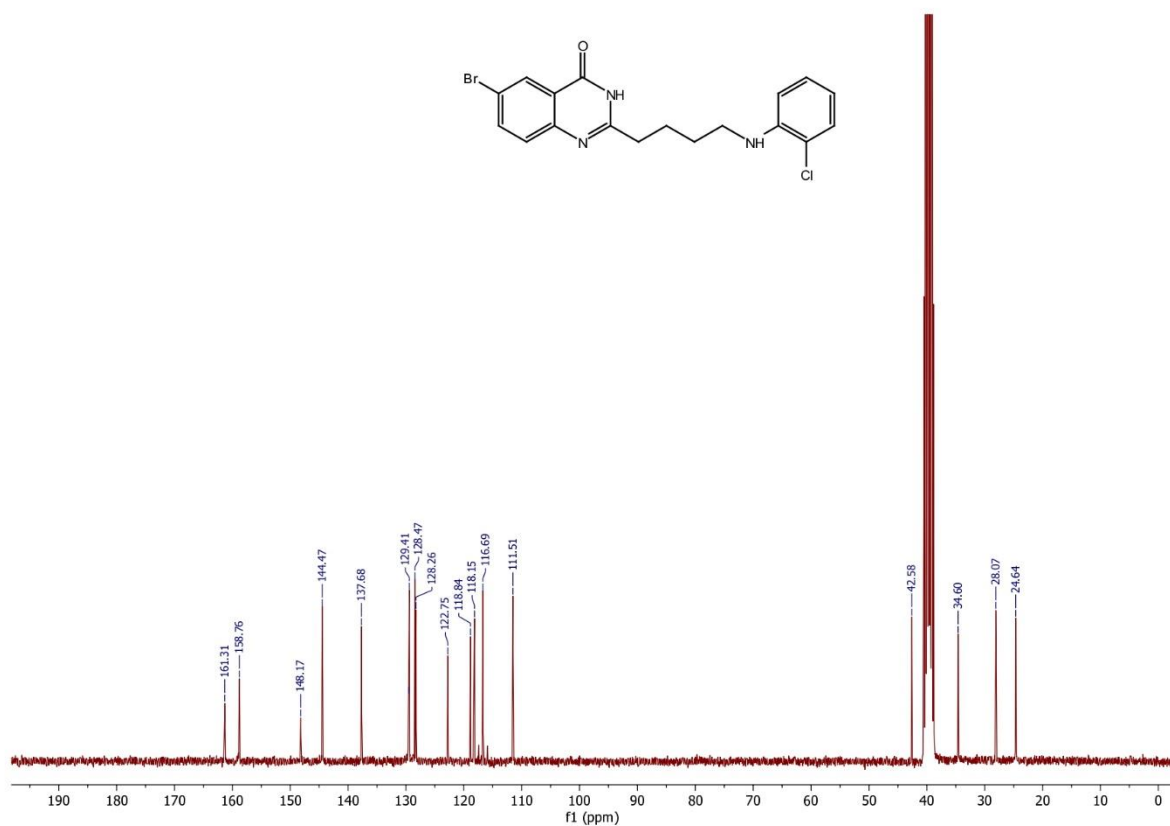


Figure 3.54 ¹³C NMR spectrum of 86l (300 MHz, DMSO-d₆)

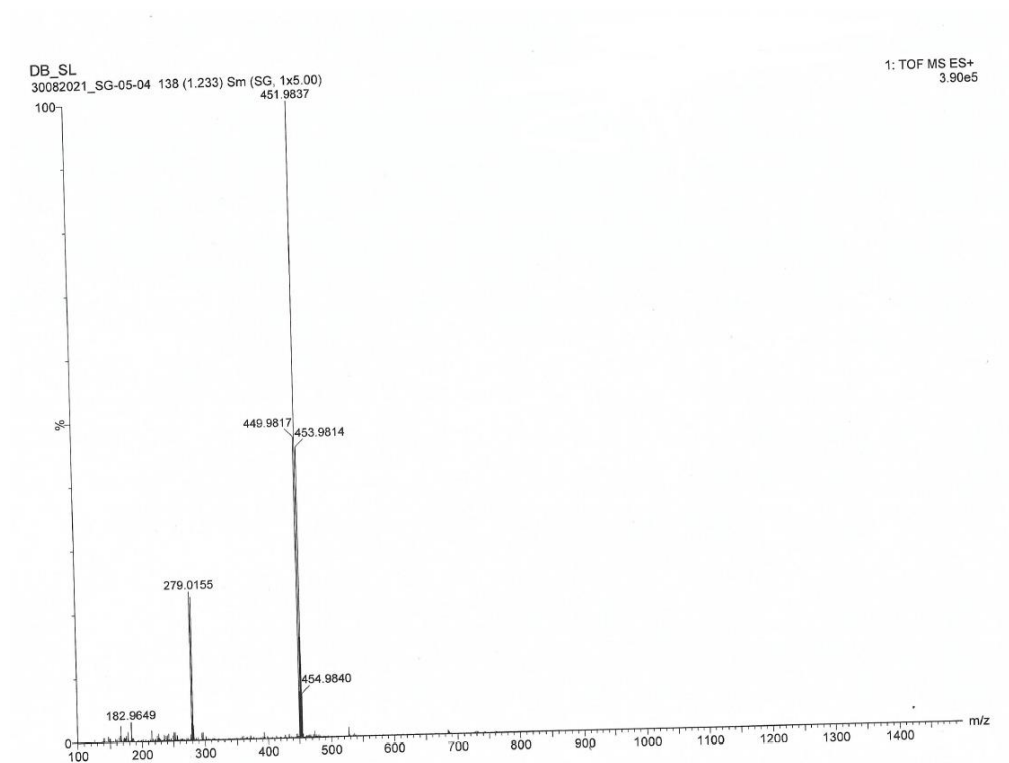


Figure 3.55 Mass spectrum of 86l (ESI-TOF), Calculated m/z for $[M+H]^+ = 449.9817$

3.8 REFERENCES

1. Panchal, N. B.; Patel, P. H.; Chhipa, N. M.; Parmar, R. S., Acridine a versatile heterocyclic moiety as anticancer agent. **2020**.
2. Marín-Ocampo, L.; Veloza, L. A.; Abonia, R.; Sepúlveda-Arias, J. C., Anti-inflammatory activity of triazine derivatives: A systematic review. *European Journal of Medicinal Chemistry* **2019**, *162*, 435-447.
3. Eguchi, S., Quinazoline Alkaloids and Related Chemistry. In *Bioactive Heterocycles I*, Eguchi, S., Ed. Springer Berlin Heidelberg: Berlin, Heidelberg, 2006; pp 113-156.
4. Kamal, A.; Ramana, K. V.; Rao, M. V., Chemoenzymatic Synthesis of Pyrrolo[2,1-b]quinazolinones: Lipase-Catalyzed Resolution of Vasicinone. *The Journal of Organic Chemistry* **2001**, *66* (3), 997-1001.
5. Grieb, P., Ueber die Einwirkung des Cyans auf Anthranilsäure. **1869**, *2* (1), 415-418.
6. Elkin, M.; Miao, H.-Q.; Nagler, A.; Aingorn, E.; Reich, R.; Hemo, I.; Dou, H.-L.; Pines, M.; Vlodavsky, I., Halofuginone: a potent inhibitor of critical steps in angiogenesis progression. **2000**, *14* (15), 2477-2485.
7. Sharma, V. M.; Adi Seshu, K. V.; Chandra Sekhar, V.; Madan, S.; Vishnu, B.; Babu, P. A.; Vamsee Krishna, C.; Sreenu, J.; Ravi Krishna, V.; Venkateswarlu, A.; Rajagopal, S.; Ajaykumar, R.; Kumar, T. S., Synthesis and biological evaluation of [4-(2-phenylethanesulfonylmethyl)phenyl]-quinazolin-4-yl-amines as orally active anti-cancer agents. *Bioorganic & Medicinal Chemistry Letters* **2004**, *14* (1), 67-71.
8. Keller, T. L.; Zocco, D.; Sundrud, M. S.; Hendrick, M.; Edenius, M.; Yum, J.; Kim, Y.-J.; Lee, H.-K.; Cortese, J. F.; Wirth, D. F.; Dignam, J. D.; Rao, A.; Yeo, C.-Y.; Mazitschek, R.; Whitman, M., Halofuginone and other febrifugine derivatives inhibit prolyl-tRNA synthetase. *Nature Chemical Biology* **2012**, *8* (3), 311-317.
9. Nathubhai, A.; Haikarainen, T.; Hayward, P. C.; Muñoz-Descalzo, S.; Thompson, A. S.; Lloyd, M. D.; Lehtiö, L.; Threadgill, M. D., Structure-activity relationships of 2-arylquinazolin-4-ones as highly selective and potent inhibitors of the tankyrases. *European Journal of Medicinal Chemistry* **2016**, *118*, 316-327.
10. Abdel-Aziz, A. A. M.; Abou-Zeid, L. A.; ElTahir, K. E. H.; Ayyad, R. R.; El-Sayed, M. A. A.; El-Azab, A. S., Synthesis, anti-inflammatory, analgesic, COX-1/2 inhibitory activities and molecular docking studies of substituted 2-mercapto-4(3H)-quinazolinones. *European Journal of Medicinal Chemistry* **2016**, *121*, 410-421.

11. Li, W.; Yin, Y.; Shuai, W.; Xu, F.; Yao, H.; Liu, J.; Cheng, K.; Xu, J.; Zhu, Z.; Xu, S., Discovery of novel quinazolines as potential anti-tubulin agents occupying three zones of colchicine domain. *Bioorganic Chemistry* **2019**, 83, 380-390.
12. Lord, A.-M.; Mahon, M. F.; Lloyd, M. D.; Threadgill, M. D., Design, Synthesis, and Evaluation in Vitro of Quinoline-8-carboxamides, a New Class of Poly(adenosine-diphosphate-ribose)polymerase-1 (PARP-1) Inhibitor. *Journal of Medicinal Chemistry* **2009**, 52 (3), 868-877.
13. Peyressatre, M.; Arama, D. P.; Laure, A.; González-Vera, J. A.; Pellerano, M.; Masurier, N.; Lisowski, V.; Morris, M. C., Identification of Quinazolinone Analogs Targeting CDK5 Kinase Activity and Glioblastoma Cell Proliferation. **2020**, 8.
14. Rahmannejadi, N.; Yavari, I.; Khabnadideh, S., Synthesis and antitumor activities of novel bis-quinazolin-4(3H)-ones. **2020**, 57 (3), 978-982.
15. Mhaske, S. B.; Argade, N. P., The chemistry of recently isolated naturally occurring quinazolinone alkaloids. *Tetrahedron* **2006**, 62 (42), 9787-9826.
16. Bogert, M. T.; May, C. E., RESEARCHES ON QUINAZOLINES (TWENTY-FIRST PAPER). ON CERTAIN QUINAZOLINE OXYGEN ETHERS OF THE TYPE —N:C(OR)— AND THE ISOMERIC —NR.CO— COMPOUNDS. *Journal of the American Chemical Society* **1909**, 31 (4), 507-513.
17. Marr, E. B.; Bogert, M. T., Researches on Quinazolines. XXXIX. The Synthesis of Quinazoline Derivatives Structurally Analogous to the Angostura Alkaloids Galiopine and Galipine1. *Journal of the American Chemical Society* **1935**, 57 (4), 729-732.
18. Mondal, S.; Panda, R.; Das, S.; Sultana, F.; Dutta, S.; Mondal, M. A., Synthesis and ctDNA binding study of a donor- π -acceptor dihydropyrimidinone fluorophore. *Journal of Molecular Structure* **2023**, 1285, 135438.
19. Mondal, S.; Sultana, F.; Dutta, S.; Mondal, M. A., Synthesis of Luotonin and Rutaecarpine Analogues by One-Pot Intramolecular Dehydrogenative Cross-Coupling and Benzylic C–H Oxidation, and In Vitro Cytotoxicity Assay. **2023**, 8 (25), e202300980.
20. Mondal, M.; Mondal, S.; Khan, A., A mechanistic insight into the acid catalyzed, one-pot synthesis of isoindole-fused quinazolin 4-ones. *Journal of Chemical Sciences* **2020**, 132.
21. Mondal, S.; Mondal, M. A., Synthesis of 3,4-dihydropyrimidin-2(1H)-one via Retro-Biginelli reaction. **2020**, 57 (12), 4175-4180.

22. Kostakis, I. K.; Elomri, A.; Seguin, E.; Iannelli, M.; Besson, T., Rapid synthesis of 2,3-disubstituted-quinazolin-4-ones enhanced by microwave-assisted decomposition of formamide. *Tetrahedron Letters* **2007**, *48* (38), 6609-6613.
23. Jahng, K. C.; Kim, S. I.; Kim, D. H.; Seo, C.; Son, J. K.; Lee, S. H.; Lee, E.-S.; Jahng, Y. J. C.; bulletin, p., One-pot synthesis of simple alkaloids: 2,3-polymethylene-4(3H)-quinazolinones, luotonin A, tryptanthrin, and rutaecarpine. **2008**, *56* 4, 607-9.
24. Zeng, F.; Alper, H., Tandem Palladium-Catalyzed Addition/Cyclocarbonylation: An Efficient Synthesis of 2-Heteroquinazolin-4(3H)-ones. *Organic Letters* **2010**, *12* (6), 1188-1191.
25. Huang, C.; Fu, Y.; Fu, H.; Jiang, Y.; Zhao, Y., Highly efficient copper-catalyzed cascade synthesis of quinazoline and quinazolinone derivatives. *Chemical Communications* **2008**, (47), 6333-6335.
26. Larraufie, M.-H.; Courillon, C.; Ollivier, C.; Lacôte, E.; Malacria, M.; Fensterbank, L., Radical Migration of Substituents of Aryl Groups on Quinazolinones Derived from N-Acyl Cyanamides. *Journal of the American Chemical Society* **2010**, *132* (12), 4381-4387.
27. Suh, C. W.; Kwon, S. J.; Kim, D. Y., Synthesis of Ring-Fused 1-Benzazepines via [1,5]-Hydride Shift/7-Endo Cyclization Sequences. *Organic Letters* **2017**, *19* (6), 1334-1337.
28. Idiris, F. I. M.; Majesté, C. E.; Craven, G. B.; Jones, C. R., Intramolecular hydride transfer onto arynes: redox-neutral and transition metal-free C(sp³)-H functionalization of amines. *Chemical Science* **2018**, *9* (11), 2873-2878.
29. Mori, K.; Isogai, R.; Kamei, Y.; Yamanaka, M.; Akiyama, T., Chiral Magnesium Bisphosphate-Catalyzed Asymmetric Double C(sp³)-H Bond Functionalization Based on Sequential Hydride Shift/Cyclization Process. *Journal of the American Chemical Society* **2018**, *140* (20), 6203-6207.
30. Mondal, M. A.; Mondal, S.; Khan, A. A., Synthesis of Functionalized Quinazolinones via Acid-Catalyzed Redox Neutral Reaction. **2021**, *6* (42), 11788-11791.
31. Misra, A.; Haque, S. K. R.; Mondal, M. A., Yttrium nitrate promoted selective cyanoethylation of amines. *Journal of Chemical Sciences* **2023**, *135* (3), 57.
32. Rozas, I.; Alkorta, I.; Elguero, J., Bifurcated Hydrogen Bonds: Three-Centered Interactions. *The Journal of Physical Chemistry A* **1998**, *102* (48), 9925-9932.
33. Culbertson, H.; Decius, J. C.; Christensen, B. E., Quinazolines. XIII. A Study of the Infrared Spectra of Certain Quinazoline Derivatives¹. *Journal of the American Chemical Society* **1952**, *74* (19), 4834-4838.

34. Beecher, C. N.; Larive, C. K., ¹H and ¹⁵N NMR Characterization of the Amine Groups of Heparan Sulfate Related Glucosamine Monosaccharides in Aqueous Solution. *Analytical Chemistry* **2015**, 87 (13), 6842-6848.
35. Khorasani-Motlagh, M.; Noroozifar, M.; Mirkazehi-Rigi, S., Fluorescence and DNA-binding spectral studies of neodymium(III) complex containing 2,2'-bipyridine, [Nd(bpy)₂Cl₃·OH₂]. *Spectrochimica Acta Part A: Molecular and Biomolecular Spectroscopy* **2010**, 75 (2), 598-603.
36. Rehman, S. U.; Sarwar, T.; Husain, M. A.; Ishqi, H. M.; Tabish, M., Studying non-covalent drug–DNA interactions. *Archives of Biochemistry and Biophysics* **2015**, 576, 49-60.
37. Akdi, K.; Vilaplana, R. A.; Kamah, S.; González-Vílchez, F., Effects of Tris and Hepes buffers on the interaction of palladium–diaminopropane complexes with DNA. *Journal of Inorganic Biochemistry* **2005**, 99 (6), 1360-1368.
38. Arjmand, F.; Parveen, S.; Afzal, M.; Toupet, L.; Ben Hadda, T., Molecular drug design, synthesis and crystal structure determination of CuII–SnIV heterobimetallic core: DNA binding and cleavage studies. *European Journal of Medicinal Chemistry* **2012**, 49, 141-150.
39. Ling, X.; Zhong, W.; Huang, Q.; Ni, K., Spectroscopic studies on the interaction of pazufloxacin with calf thymus DNA. *Journal of Photochemistry and Photobiology B: Biology* **2008**, 93 (3), 172-176.
40. Guo, L.; Qiu, B.; Chen, G., Synthesis and investigation on the interaction with calf thymus deoxyribonucleic acid of a novel fluorescent probe 7-oxobenzo[b][1,10]phenanthroline-12(7H)-sulfonic acid. *Analytica Chimica Acta* **2007**, 588 (1), 123-130.
41. Sarwar, T.; Husain, M. A.; Rehman, S. U.; Ishqi, H. M.; Tabish, M., Multi-spectroscopic and molecular modelling studies on the interaction of esculetin with calf thymus DNA. *Molecular BioSystems* **2015**, 11 (2), 522-531.
42. Jana, B.; Senapati, S.; Ghosh, D.; Bose, D.; Chattopadhyay, N., Spectroscopic Exploration of Mode of Binding of ctDNA with 3-Hydroxyflavone: A Contrast to the Mode of Binding with Flavonoids Having Additional Hydroxyl Groups. *The Journal of Physical Chemistry B* **2012**, 116 (1), 639-645.
43. Kumar, C. V.; Turner, R. S.; Asuncion, E. H., Groove binding of a styrylcyanine dye to the DNA double helix: the salt effect. *Journal of Photochemistry and Photobiology A: Chemistry* **1993**, 74 (2), 231-238.

44. Pulimamidi, R. R.; Nomula, R.; Pallepogu, R.; Shaik, H., Picolinic acid based Cu(II) complexes with heterocyclic bases – Crystal structure, DNA binding and cleavage studies. *European Journal of Medicinal Chemistry* **2014**, 79, 117-127.
45. Kakkar, R.; Garg, R.; Suruchi, Theoretical study of tautomeric structures and fluorescence spectra of Hoechst 33258. *Journal of Molecular Structure: THEOCHEM* **2002**, 579 (1), 109-113.
46. Shahabadi, N.; Hadidi, S., Spectroscopic studies on the interaction of calf thymus DNA with the drug levetiracetam. *Spectrochimica Acta Part A: Molecular and Biomolecular Spectroscopy* **2012**, 96, 278-283.
47. Parveen, M.; Malla, A. M.; Yaseen, Z.; Ali, A.; Alam, M., Synthesis, characterization, DNA-binding studies and acetylcholinesterase inhibition activity of new 3-formyl chromone derivatives. *Journal of Photochemistry and Photobiology B: Biology* **2014**, 130, 179-187.
48. Hampshire, A. J.; Rusling, D. A.; Broughton-Head, V. J.; Fox, K. R., Footprinting: A method for determining the sequence selectivity, affinity and kinetics of DNA-binding ligands. *Methods* **2007**, 42 (2), 128-140.
49. Sirajuddin, M.; Ali, S.; Badshah, A., Drug–DNA interactions and their study by UV–Visible, fluorescence spectroscopies and cyclic voltametry. *Journal of Photochemistry and Photobiology B: Biology* **2013**, 124, 1-19.
50. Rahban, M.; Divsalar, A.; Saboury, A. A.; Golestani, A., Nanotoxicity and Spectroscopy Studies of Silver Nanoparticle: Calf Thymus DNA and K562 as Targets. *The Journal of Physical Chemistry C* **2010**, 114 (13), 5798-5803.
51. Sheng, J.; Gan, J.; Huang, Z., Structure-Based DNA-Targeting Strategies with Small Molecule Ligands for Drug Discovery. **2013**, 33 (5), 1119-1173.
52. Russell, A. P.; Holleman, D. S., The thermal denaturation of DNA: average length and composition of denatured areas. *Nucleic Acids Research* **1974**, 1 (8), 959-978.
53. Mandel, M.; Marmur, J., [109] Use of ultraviolet absorbance-temperature profile for determining the guanine plus cytosine content of DNA. In *Methods in Enzymology*, Academic Press: 1968; Vol. 12, pp 195-206.
54. Tan, Z.-J.; Chen, S.-J., Nucleic Acid Helix Stability: Effects of Salt Concentration, Cation Valence and Size, and Chain Length. *Biophysical Journal* **2006**, 90 (4), 1175-1190.
55. Kutyavin, I. V.; Afonina, I. A.; Mills, A.; Gorn, V. V.; Lukhtanov, E. A.; Belousov, E. S.; Singer, M. J.; Walburger, D. K.; Lokhov, S. G.; Gall, A. A.; Dempcy, R.; Reed, M. W.; Meyer, R. B.; Hedgpeth, J., 3'-minor groove binder-DNA probes increase

- sequence specificity at PCR extension temperatures. *Nucleic acids research* **2000**, 28 (2), 655-661.
56. Bjorndal, M. T.; Fyngenson, D. K., DNA melting in the presence of fluorescent intercalating oxazole yellow dyes measured with a gel-based assay. **2002**, 65 (1), 40-44.
 57. Bridges, J. W.; Williams, R. T., The fluorescence of indoles and aniline derivatives. *Biochemical Journal* **1968**, 107 (2), 225-237.
 58. M. Carstea, E.; Levei, E. A.; Hoaghia, M.-A.; Savastru, R., Quality assessment of Romanian bottled mineral water and tap water. *Environmental Monitoring and Assessment* **2016**, 188 (9), 521.
 59. Ramana, M. M. V.; Betkar, R.; Nimkar, A.; Ranade, P.; Mundhe, B.; Pardeshi, S., In vitro DNA binding studies of antiretroviral drug nelfinavir using ethidium bromide as fluorescence probe. *Journal of Photochemistry and Photobiology B: Biology* **2015**, 151, 194-200.
 60. Li, L.; Yang, L.; Kotin, R. M., The DNA minor groove binding agents Hoechst 33258 and 33342 enhance recombinant adeno-associated virus (rAAV) transgene expression. **2005**, 7 (4), 420-431.
 61. Tao, M.; Zhang, G.; Pan, J.; Xiong, C., Deciphering the groove binding modes of tau-fluvalinate and flumethrin with calf thymus DNA. *Spectrochimica Acta Part A: Molecular and Biomolecular Spectroscopy* **2016**, 155, 28-37.
 62. Swarna, S.; Lorente, C.; Thomas, A.; Martin, C., Rate constants of quenching of the fluorescence of pterins by the iodide anion in aqueous solution. *Chemical Physics Letters* **2012**, 542, 62-65.
 63. Husain, M. A.; Ishqi, H. M.; Sarwar, T.; Rehman, S. U.; Tabish, M., Interaction of indomethacin with calf thymus DNA: a multi-spectroscopic, thermodynamic and molecular modelling approach. *MedChemComm* **2017**, 8 (6), 1283-1296.

Chapter 4

Yttrium Nitrate Promoted Synthesis of Cyanoethyl Amines

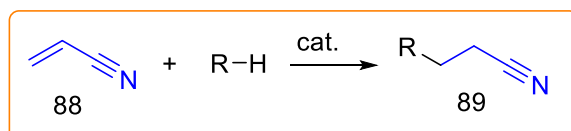
Part of the work described in this chapter is published in

J. Chem. Sci. (2023) 135:57; DOI: 10.1007/s12039-023-02173-2

Yttrium Nitrate Promoted Synthesis of Cyanoethyl Amines

4.1 INTRODUCTION

Cyanoethylation, a significant synthetic process in organic chemistry, involves the introduction of cyanoethyl groups onto various chemical substrates. Among the diverse applications of cyanoethylation, the modification of aromatic amines with acrylonitrile stands out as a pivotal transformation. Acrylonitrile, also known as vinyl cyanide, is a key building block in the production of synthetic polymers, particularly polyacrylonitrile (PAN). PAN is widely used in the textile industry for the manufacturing of acrylic fibers, and it serves as a precursor for carbon fibers, which find applications in aerospace, automotive, and other advanced material industries. This chemical transformation involves the addition of cyanoethyl groups ($-\text{CH}_2\text{CH}_2\text{CN}$) to a molecule, leading to the modification of its chemical structure and enhancing its suitability for diverse industrial applications. The produced nitrile can be subsequently transformed into amines through reduction, underscoring the significance of cyanoethylation as a pivotal reaction for generating intermediates in organic chemistry. The process is typically carried out under controlled conditions, with the choice of catalysts, reaction temperature, and other parameters influencing the efficiency and selectivity of the cyanoethylation reaction. This intriguing reaction has garnered considerable attention due to its versatility and the consequential expansion of the molecular diversity it imparts to aromatic amine derivatives.



Scheme 4.1 General way of cyanoethylation

Cyanoethylation, i.e., attachment of a cyano ethyl group at different heteroatoms (N, P, O, S) or carbons, is an essential organic transformation as it provides a crucial intermediate for synthesizing various pharmaceutically necessary materials and has commercial importance. Remarkably, *N*-cyanoethylation is important in the masking strategy of amine in a multifunctional molecule. The $-\text{CN}$ of the cyanoethyl moiety has been used as a suitable functional group for conjugation through a tetrazole spacer via click chemistry.¹ Moreover, cyanoethyl groups are attached to pharmaceuticals to attain better pharmacological scores. Apart from the use of fine chemicals preparation, the technique has also been used in the modification process of biomaterials such as carbohydrate polymers^{2, 3} cellulose,⁴ starch,⁵ chitin,⁶ nucleic acid,^{7, 8} proteins, etc. The method is reported as early in the mid-nineteenth

century,⁹ and the development of the bioorthogonal process of cyanoethylation is still a topic of interest today.¹⁰

The cyanoethylation method is catalyzed by conventional, either acidic or basic conditions. Polyacrylonitrile is a frequent by-product in cyanoethylation reactions. Acrylonitrile tends to polymerize vigorously in the presence of a base, and alkali catalysts are commonly employed in cyanoethylation.¹¹ To prevent polymerization, it is advisable to add acrylonitrile slowly. Earlier studies suggest that polyacrylonitrile is generated through alkoxide-initiated anionic polymerization and graft polymerization of acrylonitrile.¹²

4.2 LITERATURE BACKGROUND

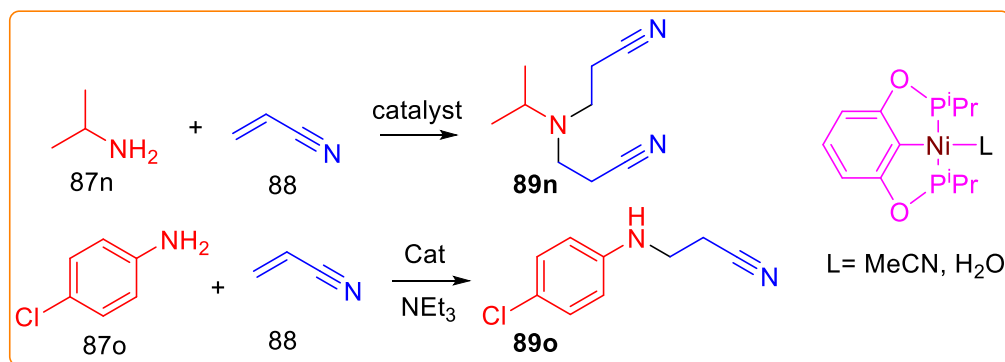
Even though cyanoethylation chemistry is considered a well-established area, ongoing research continues to unveil newer and greener methodologies applicable to the synthesis of more structurally diverse precursors related molecules has been reported in the literature. This section outlines some of the important methodologies for the cyanoethylation methodologies.

However, many transition-metal catalyzed methods are reported. The notable examples are the use of a nickel complex,^{13, 14} On-water magnetic ferrite nanoparticle,¹⁵ Al_2O_3 under alkaline condition,¹⁶ FeCl_3 /Montmorillonite,¹⁷ RuCl_3 in poly(ethylene glycol)¹⁸ polystyrene-supported aluminium chloride,¹⁹ Silicon tetrachloride,²⁰ Glycerol medium without catalyst,²¹ Platinum(II) complex,²² Copper Nanoparticles in Ionic Liquid,²³ etc. Major concerns of the reported cyanoethylation are the elevated reaction temperature, poor selectivity between the formation of mono and bis aza-Michael addition products, selectivity over N, O, S, and biomolecule compatibility. Many cyanoethylation reactions are very exothermic and require cooling or the use of an inert solvent to moderate the reaction and prevent excessive polymerization of the acrylonitrile. Some inert solvents which have been used for this purpose and to dissolve solid reactants are benzene, dioxane, pyridine, and acetonitrile.

Our previous work found that the Yttrium Nitrate efficiently catalyzed an intramolecular [1,5]-hydride transfer reaction,²⁴ to form dihydroquinazolinones,²⁵ dihydropyrimidinone,²⁶ and promote nitration of phenols.²⁷ In this chapter, we described Yttrium Nitrate as an efficient catalyst for selective mono-cyanoethylation via 1, 4-addition to acrylonitrile.

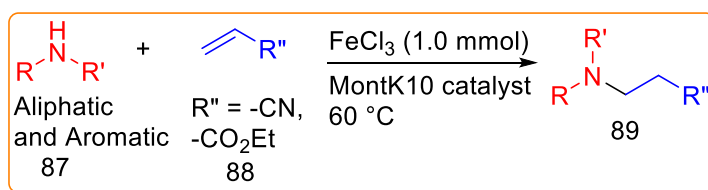
Zargarianl et al. presented a method for the anti-Markovnikov addition of nucleophiles to activated olefins, specifically the cyanoethylation of aliphatic and aromatic amines using pincer complexes of nickel (Scheme 4.2).¹³ The catalyzed additions of aliphatic amines to acrylonitrile proceed at room temperature, providing quantitative yields of bis-cyanoethylated products

through the formation of C–N bonds. In contrast, aromatic amines exhibit complete inertness and lower reactivity toward acrylonitrile, necessitating the addition of a base, elevated temperature, and extended reaction times to achieve satisfactory yields. The catalytic reactivities of Ni-Cat are attributed to the substitutional lability of the coordinated acetonitrile, allowing for competitive coordination of the nitrile moiety in the olefinic substrates. This binding enhances the electrophilicity of the C=C moiety, making them more susceptible to attack by nucleophiles.



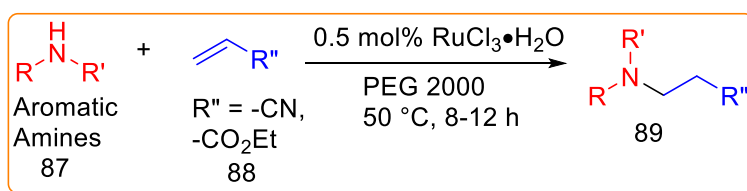
Scheme 4.2 Cyanoethylation of Amine by Ni catalyst

Patil et al. presented a straightforward protocol for the aza-Michael addition reaction of aromatic and aliphatic amines to α,β -unsaturated compounds. This reaction utilized a moisture-insensitive MontK10 supported FeCl₃ catalyst and was conducted in the absence of any solvent. The catalytic performance was found to be significantly influenced by the preheating temperature of the catalyst 120°C. (Scheme 4.3).



Scheme 4.3 Aza-Michael addition of Amine by Fe catalyst

Zhang and his group demonstrated a versatile RuCl₃-catalyzed 1,4-conjugate addition of primary, secondary, and aromatic amines, thiols, and carbamates to α,β -unsaturated compounds in poly(ethylene glycol) (PEG), resulting in the formation of desired β -substituted carbonyls in high yields (Scheme 4.4). RuCl₃-PEG exhibited low sensitivity toward moisture and oxygen, displayed high tolerance of various functional groups, and showed efficient recyclability.¹⁸



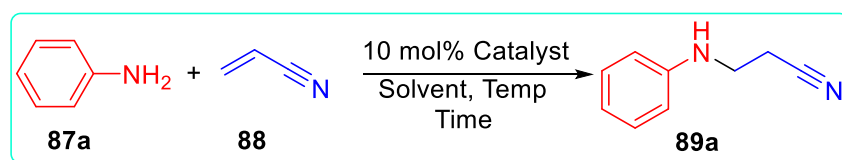
Scheme 4.4 Aza-Michael addition of Amine by Ru catalyst

Despite the promising synthetic potential of cyanoethylation of aromatic amines by acrylonitrile, certain limitations hinder its widespread application. One notable constraint lies in the demanding reaction conditions, often requiring elevated temperatures and extended reaction times. These harsh conditions can lead to reduced selectivity, decreased yields, and potential side reactions, limiting the overall efficiency of the process. Additionally, the reliance on expensive catalysts and high catalyst loadings presents an economic challenge, particularly in large-scale applications. Overcoming these limitations is crucial for enhancing the practicality and sustainability of the cyanoethylation process, prompting ongoing research efforts to develop more mild and cost-effective reaction conditions without compromising the efficiency of this important synthetic transformation.

4.3 Present Work

Our preliminary study commenced with the reaction of aniline (**87a**) with 10.0 equivalent of acrylonitrile **88** as a Michael acceptor for optimization of the reaction parameters like solvent role, catalyst loading, and reaction conditions in the presence of different catalysts (Scheme 4.5). We studied the reaction in different solvents and observed that solvents like acetone, DMF, Acetonitrile, and DCM were not suitable for the reaction as, under this condition provided low conversion. While in methanol or ethanol, good conversion of the desired product was observed. Water could be used as a solvent for the reaction, but it requires a longer reaction time as the system becomes biphasic in nature. We observed an increased reaction rate with increasing reaction temperature. For compound **89a**, the isolated yield is reported hereafter in column chromatography. Excess (10 equivalents) acrylonitrile is required to get appreciable conversion within 72 h. Several other common Lewis acids, such as CuCl_2 and FeCl_3 , were ineffective for the reaction, mostly because of the polymerization of acrylonitrile. The best result was obtained in the presence of 10 mol% $\text{Y}(\text{NO}_3)_3 \cdot 6\text{H}_2\text{O}$ at rt. Lowering the catalyst loading resulted in a lengthening of the reaction time. The progress of the reactions was monitored by TLC, and the percentage of yields was calculated based on the isolated amount of **89a** by column purification. All the products are known in the literature, and NMR spectra

were sufficient to confirm the product structure of **89a**. With the optimal conditions in hand (Table 4.1, entry 4), the substrate scope of the $Y(NO_3)_3 \cdot 6H_2O$ catalyzed Michael addition with acrylonitrile was studied in methanol at ambient temperature. The electron deficient aromatic amines and bulky aryl group give low conversion (Table 4.2, entries 4, 5, and 6). Excellent conversions were observed for electron-donating aryl amines and aliphatic amines (entries 1-3, 7-13). Aliphatic amines react faster and complete the conversion within 12 h.



Scheme 4.5 Cyanoethylation of amines

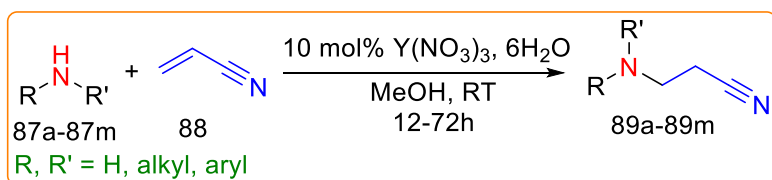
Table 4.1 Reaction Optimization

Entry	Solvents	Catalyst	Time (hrs)/temp	Conversion (%)
1	Acetone	$Y(NO_3)_3 \cdot 6H_2O$	72/RT	7
2	DMF	$Y(NO_3)_3 \cdot 6H_2O$	72/RT	Trace
3	MeCN	$Y(NO_3)_3 \cdot 6H_2O$	72/RT	10
4	MeOH	$Y(NO_3)_3 \cdot 6H_2O$	72/RT	85
5	MeOH	$Y(NO_3)_3 \cdot 6H_2O$	12/60°C	92
6	EtOH	$Y(NO_3)_3 \cdot 6H_2O$	72/RT	76
7	H ₂ O	$Y(NO_3)_3 \cdot 6H_2O$	72/RT	62
8	DCM	$Y(NO_3)_3 \cdot 6H_2O$	72	NR
9	MeOH	$CuCl_2$	12	Complex reaction mixture
10	MeOH	$FeCl_3$	12	Complex reaction mixture
11	MeOH	Without catalyst	-	No change of Starting

Note: Aniline (1 mmol) and acrylonitrile (10 mmol) are mixed in 1 mL solvent at ambient temperature. Yield was calculated after isolation of **89a** by column chromatography.

The steric properties at the nitrogen center determine the outcome of the methods. Secondary aliphatic amines and sterically demanding aliphatic primary amines yielded monocyanoethylation (Table 4.2, entries 7, 8, 10, and 13). The reaction with primary aliphatic amine without steric hindrance could not be controlled at the mono-alkylation step, even under sub-stoichiometry composition. However, it is worthwhile to mention that no bis-alkylation product was observed in the case of primary aromatic amine. Therefore, the method is selective for the monoalkylation of electron-rich aromatic amines, aliphatic secondary amines, and sterically hindered primary amines. The chemoselective nature of the reported method has also been evaluated by carrying out the different (N, O, and C) nucleophilic systems. Interestingly,

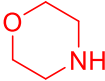
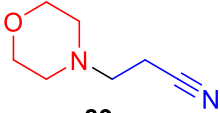

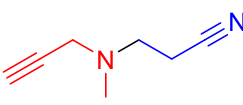
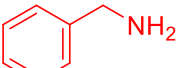
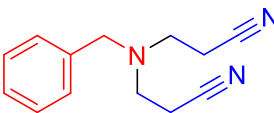

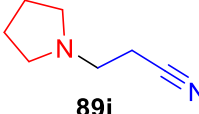
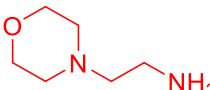
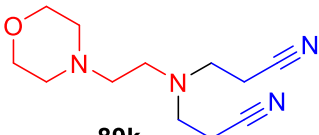
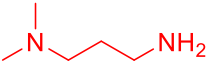
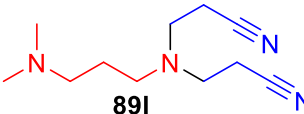
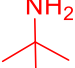
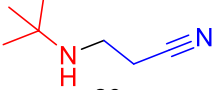
the yttrium nitrate under-reported condition does not alkylate at the phenolic OH, and active methylene centre (entry 14, 15); thus, the method specifically allows cyanoethylation at the amines in the presence of N, C, O nucleophilic centres. Thiophenol in the presence of yttrium nitrate did not provide a similar product. Presumably, it promotes polymerization of the acrylonitrile, as evident from the fact that the entire reaction mixture converted into an insoluble solid mass.



Scheme 4.6 Studies of substrate scope

Table 4.2 Studies of substrate scope.

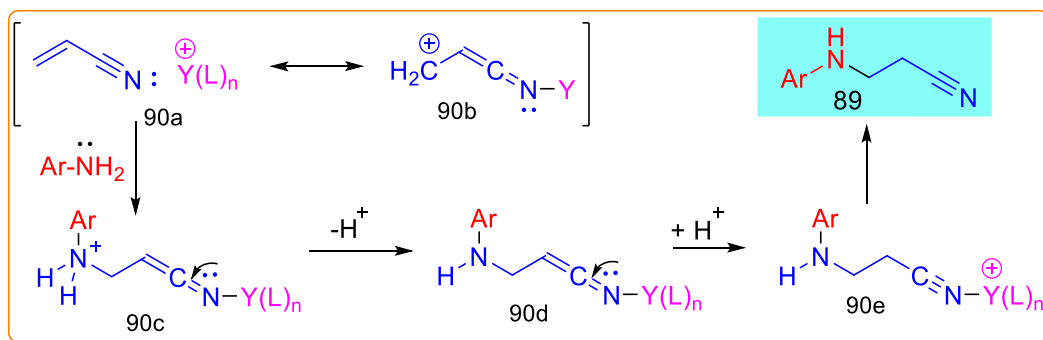
Entry	Substrate Amine	Product	Time (h)	Conversion (%)
1			72	85
2			72	Quantitative
3			72	97
4			72	19
5			72	No Conversion
6			72	64

7			12	>99
8			12	>99
9			12	>99
10			12	>99
11			12	>99
12			12	>99
13			12	>99

Note: Compound 89a was isolated by column chromatography. Yield of 89d and 89f was calculated based on the $^1\text{H-NMR}$ of the crude reaction mixture after the aqueous workup. Yield of the products 89b, 89c, 89g, and 89h-m were calculated based on the weight of the product obtained after aqueous workup, and the NMR mass spectra were recorded without further purification

4.4 MECHANISM OF AZA-MICHAEL ADDITION CATALYZED BY $\text{Y}(\text{NO}_3)_3 \cdot 6\text{H}_2\text{O}$

Considering the mild Lewis acidic nature of the yttrium ion and poor reactivity of the acrylonitrile in the absence of a catalyst and the protic solvent dependent nature of the reaction, a probable mechanism is proposed and shown in Scheme 4.7. The coordinative bond of nitrile nitrogen to the yttrium ion enhances the reactivity of the Michael acceptor²⁸ and through a protonation deprotonation mechanism via solvent, completes the cyanoethylation process. The reaction is sensitive to the steric properties at the amine centre; hence, the secondary amine **89** does not undergo further cyanoethylation. This is also evident from the result of entries 7, 8, and 10 in Table 4.2.



Scheme 4.7 A probable mechanism of cyanoethylation.

4.5 CONCLUSIONS

A potential alternative biocompatible method of cyanoethylation has been evaluated experimentally. The method is selective for mono-cyanoethylation to the electron-rich primary aromatic amines, aliphatic secondary amines, and bulky primary aliphatic amines. The method allows selective cyanoethylation of amines in the presence of -OH and carbon nucleophiles. It could be used as a potential alternative for modification of biomaterials as the yttrium ion is a stable, water-soluble mild Lewis acid, easily removable from the product.

4.6 EXPERIMENTAL SECTION

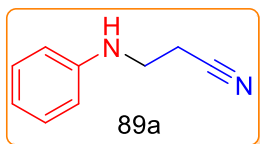
4.6.1 General information

The analytical thin layer chromatography (TLC) was carried out for monitoring the progress of the reactions using silica gel 60 F254 precoated plates. Visualizations of the spots were accomplished with a UV lamp or I₂ stain. Unless otherwise mentioned, all of the reactions were carried out in oven-dried glassware under an atmosphere of nitrogen or argon using normal solvent. All of the commercial reagents were used as received without further purification unless otherwise mentioned. Proton nuclear magnetic resonance (¹H NMR) were recorded at Bruker 300 MHz and 400 MHz. The chemical shifts were recorded in parts per million (ppm, δ) using tetramethylsilane (δ 0.00) as the internal standard. All coupling constants (*J*) are absolute values and are expressed in Hz. Splitting patterns of the ¹H NMR are mentioned as singlet (s), doublet (d), doublet of doublet (dd), doublet of triplet (dt), triplet (t), multiplet (m) etc. Proton-decoupled carbon nuclear magnetic resonance ¹³C NMR spectra were recorded at 75 MHz and 100 MHz. HRMS were obtained using (ESI) mass spectrometer (TOF).

4.6.2 Experimental Procedure and Spectral Data

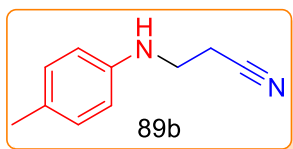
3-(phenylamino)propanenitrile (**89a**)

The mixture of aniline **87a** (50.0 mg, 0.536 mmol, 1.0 equiv), acrylonitrile **88** (56.9 mg, 1.073 mmol, 2.0 equiv) in methanol (1.5 mL) was taken in a one-necked round bottom flask under open atmosphere and 10 mol% of Yttrium Nitrate was added to it and was stirred at rt for 72 h. After completion of the reaction, the reaction mixture was diluted with water, extracted with ethyl acetate (3 × 15 mL) and dried over anhydrous Na₂SO₄. The solvent was removed under reduced pressure, which was purified by column chromatography on silica gel (100–200 mesh) using 5% ethyl acetate in petroleum ether as the eluent to obtain the pure product **89a** as a white solid in 85% yield. ¹H NMR (300 MHz, CDCl₃) δ 2.67 (t, *J* = 9.0 Hz, 2H), 3.55 (t, *J* = 6.0 Hz, 2H), 4.02 (s, 1H), 6.65 (m, 2H), 6.81 (m, 1H), 7.25 (m, 2H); (ES-TOF) *m/z*: [M+H]⁺ Calcd for C₉H₁₁N₂ is 147.0922; Found 147.3431.



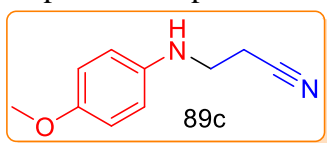
3-(p-tolylamino)propanenitrile (**89b**)

Experimental procedure is same as described for **89a**. product isolated by aqueous workup without column purification. Yield: quantitative; ¹H NMR (300 MHz, CDCl₃) δ 2.28 (s, 3H), 2.65 (t, *J* = 6.0 Hz, 2H), 3.16 (s, 1H), 3.52 (t, *J* = 9 Hz, 2H), 6.58 (d, *J* = 9 Hz, 2H), 7.05 (d, *J* = 3 Hz, 2H); ¹³C NMR (75 MHz, CDCl₃) δ 18.11, 20.41, 40.23, 113.42, 118.34, 128.05, 130.05, 143.77; (ES-TOF) *m/z*: [M+H]⁺ Calcd for C₁₀H₁₃N₂ is 161.1079; Found 161.3675.



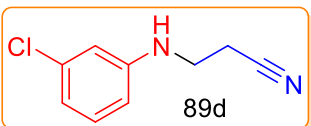
3-((4-methoxyphenyl)amino)propanenitrile (**89c**)

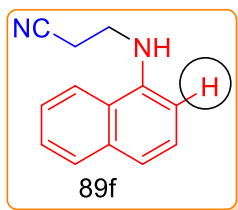
Experimental procedure is same as described for **89a**. Product isolated by aqueous workup without column purification. Yield: 97 yield; ¹H NMR (300 MHz, CDCl₃) δ 2.53 (t, *J* = 6.6 Hz, 2H), 3.39 (t, *J* = 6.6 Hz, 2H), 3.68 (s, 3H), 6.53 (d, *J* = 9 Hz, 2H), 6.73 (t, *J* = 9 Hz, 2H); ¹³C NMR (75 MHz, CDCl₃) δ 18.1, 40.8, 55.7, 114.8, 115.1, 118.3, 140.1, 153.0; (ES-TOF) *m/z*: [M+H]⁺ Calcd for C₁₀H₁₃N₂O is 177.1028; Found 177.2239.



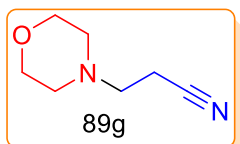
3-((3-chlorophenyl)amino)propanenitrile (**89d**)

Experimental procedure is same as described for **89a**. Product isolated by aqueous workup without column purification. Conversion: 19% (by NMR of the crude)



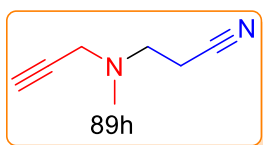
3-(naphthalen-2-ylamino)propanenitrile (89f)

Experimental procedure is same as described for **89a**. Product isolated by aqueous workup without column purification. Conversion: 64% (by NMR of the crude). Conversion measured by comparing the area under the characteristic NMR signal of the α proton of starting and product.

3-morpholinopropanenitrile (89g)

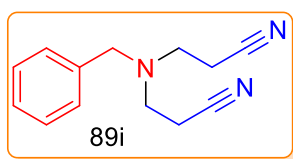
Experimental procedure is same as described for **89a**. Product isolated by aqueous workup without column purification. Yield: quantitative.

^1H NMR (300 MHz, CDCl_3) δ 2.42-2.47 (m, 6H), 2.61 ($J = 7.2$ Hz, 2H), 3.65 (t, $J = 6.9$ Hz, 4H); ^{13}C NMR (75 MHz, CDCl_3) δ 14.7, 52.0, 52.6, 65.7, 117.6.

N-methyl-N-(prop-2-yn-1-yl)but-3-yn-1-amine (89h)

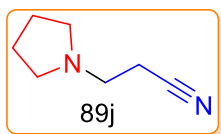
Experimental procedure is same as described for **89a**. Product isolated by aqueous workup without column purification. Yield: quantitative.

^1H NMR (300 MHz, CDCl_3) δ 2.25-2.27 (m, 1H), 2.36 (s, 3H), 2.50 (t, $J = 6.9$ Hz, 2H), 2.76 (t, $J = 7.2$ Hz, 2H), 3.40 (d, $J = 2.4$ Hz, 2H); ^{13}C NMR (100 MHz, CDCl_3) δ 16.5, 41.3, 45.3, 50.7, 118.5; (ES-TOF) m/z : $[\text{M}+\text{H}]^+$ Calcd for $\text{C}_8\text{H}_{12}\text{N}_2$ is 122.0964; Found 122.6885.

3,3'-(benzylazanediyldip)propanenitrile (89i)

Experimental procedure is same as described for **89a**. Product isolated by aqueous workup without column purification. Yield: quantitative.

^1H NMR (400 MHz, CDCl_3) δ 2.46 (t, $J = 6.8$ Hz, 4H), 2.90 (t, $J = 6.8$ Hz, 4H), 3.72 (s, 2H), 7.28-7.37 (m, 5H); ^{13}C NMR (100 MHz, CDCl_3) δ 16.8, 49.5, 58.2, 118.6, 127.7, 128.6, 128.7, 137.6; (ES-TOF) m/z : $[\text{M}+\text{H}]^+$ Calcd for $\text{C}_{13}\text{H}_{16}\text{N}_3$ is 214.1338, Found 236.1362.

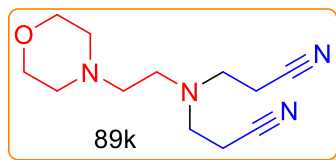
3-(pyrrolidin-1-yl)propanenitrile (89j)

Experimental procedure is same as described for **89a**. Product isolated by aqueous workup without column purification. Yield: quantitative.

^1H NMR (300 MHz, CDCl_3) δ 1.78 (t, $J = 1.2$ Hz, 4H), 2.50-2.57 (m, 6H),

2.77 (t, $J = 4.8$ Hz, 2H); ^{13}C NMR (75 MHz, CDCl_3) δ 17.5, 23.5, 51.2, 53.7, 118.8; (ES-TOF) m/z : $[\text{M}+\text{H}]^+$ Calcd for $\text{C}_7\text{H}_{13}\text{N}_2$ is 125.1073, Found 125.2051.

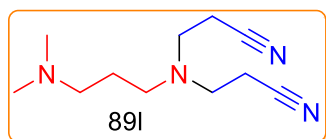
3-((3-morpholinopropyl)amino)propanenitrile (89k)



Experimental procedure is same as described for **89a**. Product isolated by aqueous workup without column purification. Yield: quantitative.

^1H NMR (300 MHz, CDCl_3) δ 2.45-2.52 (m, 10H), 2.72 (t, $J = 6.6$ Hz, 2H), 2.92 (t, $J = 6.6$ Hz, 4H), 3.70 (t, $J = 4.8$ Hz, 4H); ^{13}C NMR (100 MHz, CDCl_3) δ 17.2, 50.3, 50.7, 54.0, 57.2, 66.8, 118.5; (ES-TOF) m/z : $[\text{M}+\text{H}]^+$ Calcd for $\text{C}_{12}\text{H}_{21}\text{N}_4\text{O}$ is 237.1709; Found 237.1987.

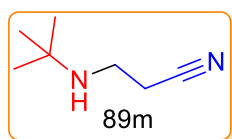
3,3'-((3-(dimethylamino)propyl)azanediyl)dipropanenitrile (89l)



Experimental procedure is same as described for **89a**. Product isolated by aqueous workup without column purification. Yield: quantitative.

^1H NMR (300 MHz, CDCl_3) δ 1.61 (m, 2H), 2.05 (bs, 1H), 2.22 (s, 6H), 2.34 (t, $J = 6.9$ Hz, 2H), 2.48 (t, $J = 6.9$ Hz, 4H), 2.58 (t, $J = 6.9$ Hz, 2H), 2.84 (t, $J = 6.9$ Hz, 4H); ^{13}C NMR (75 MHz, CDCl_3) δ 17.0, 25.4, 45.3, 49.8, 51.0, 56.7, 118.6; (ES-TOF) m/z : $[\text{M}+\text{H}]^+$ Calcd for $\text{C}_{11}\text{H}_{21}\text{N}_4$ is 209.1760; Found 209.2290.

3-(*tert*-butylamino)propanenitrile (89m)



Experimental procedure is same as described for **89a**. Product isolated by aqueous workup without column purification. Yield: quantitative.

^1H NMR (300 MHz, CDCl_3) δ 1.09 (s, 9H), 1.37(bs, 1H), 2.47 (t, $J = 6.6$ Hz, 2H), 2.84 (t, $J = 6.6$ Hz, 2H); ^{13}C NMR (100 MHz, CDCl_3) δ 19.9, 28.9, 38.5, 50.6, 118.8; (ES-TOF) m/z : $[\text{M}+\text{H}]^+$ Calcd for $\text{C}_7\text{H}_{15}\text{N}_2$ is 127.1229; Found 127.2074.

Copies of NMR and HRMS Spectra

Chapter 4

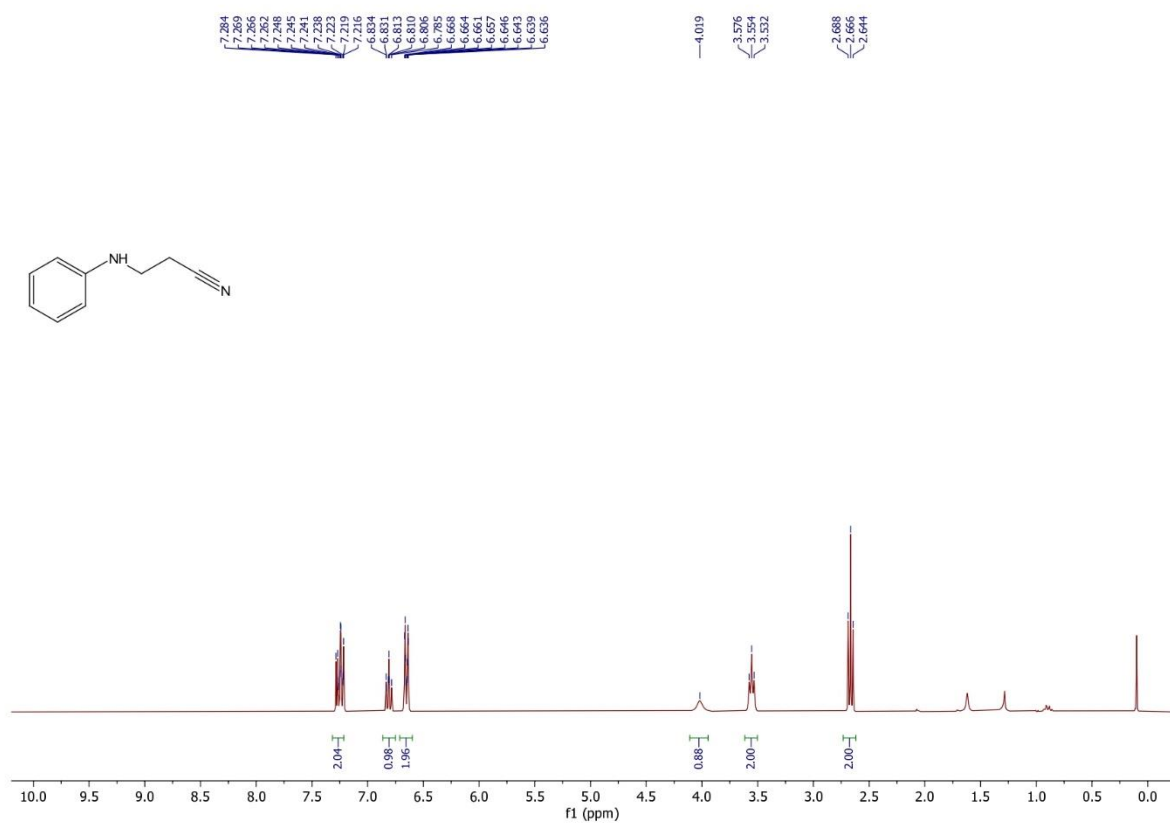


Figure 4.1 ¹H NMR spectrum of **89a** (300 MHz, CDCl₃)

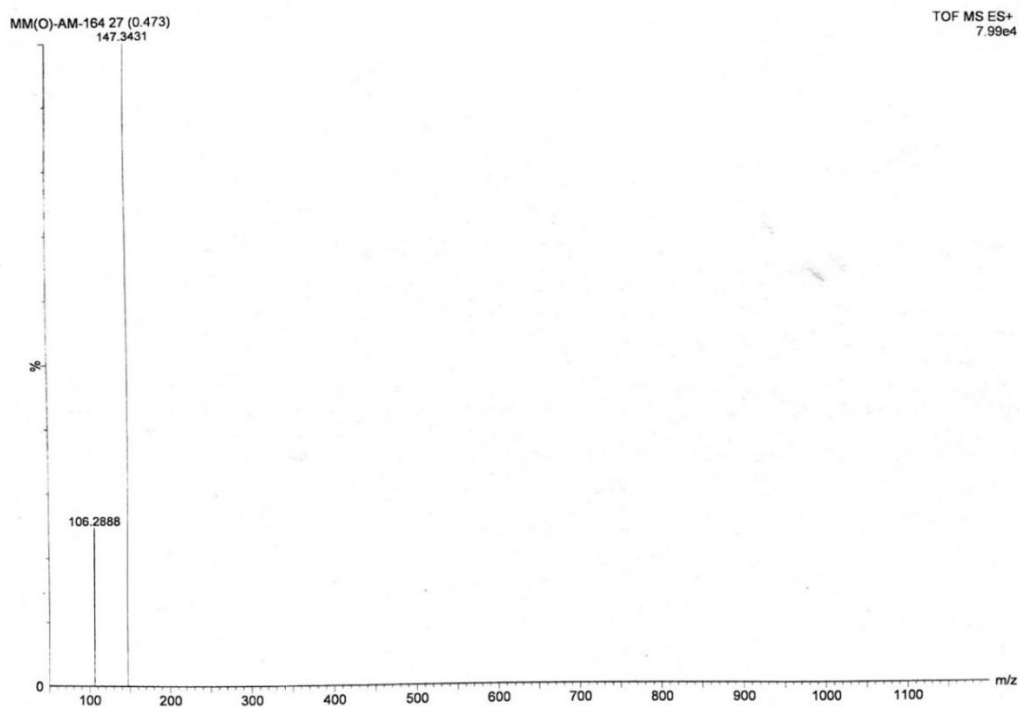


Figure 4.2 Mass spectrum of **89a** (ESI-TOF) *m/z*: [M+H]⁺

Chapter 4

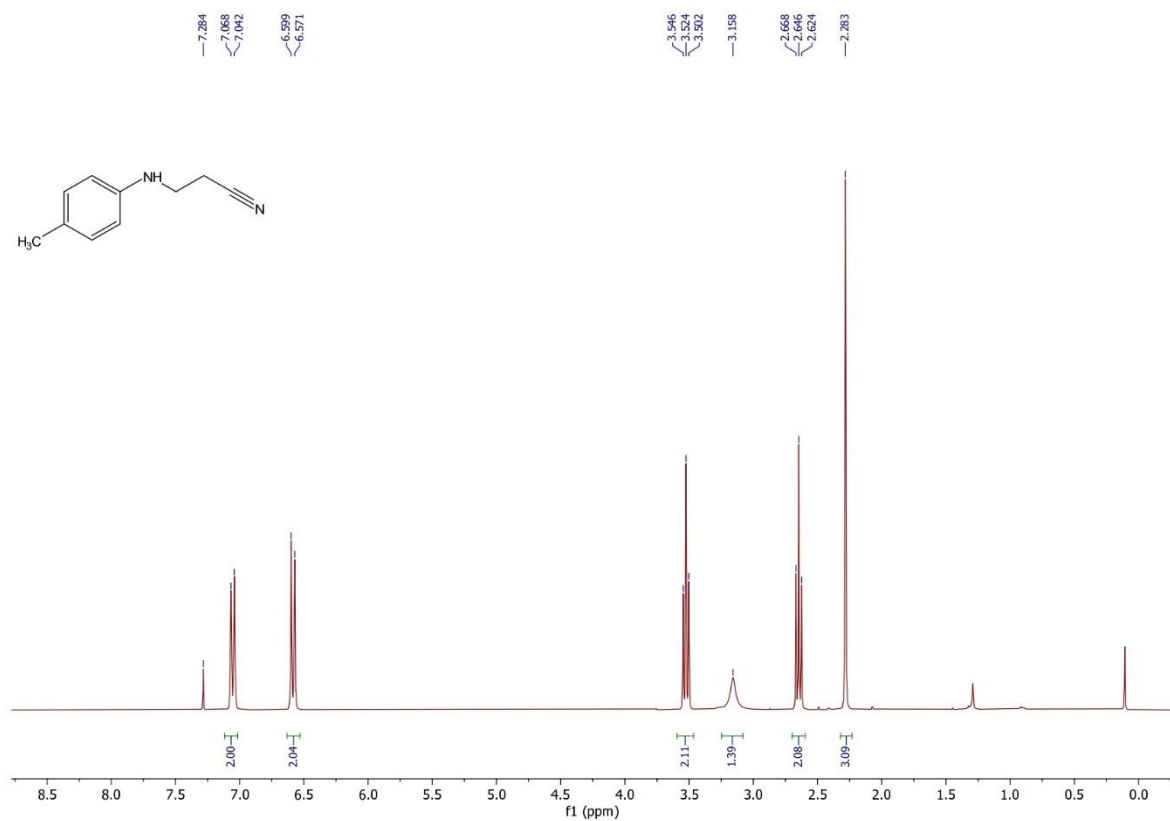


Figure 4.3 ¹H NMR spectrum of **89b** (300 MHz, CDCl₃)

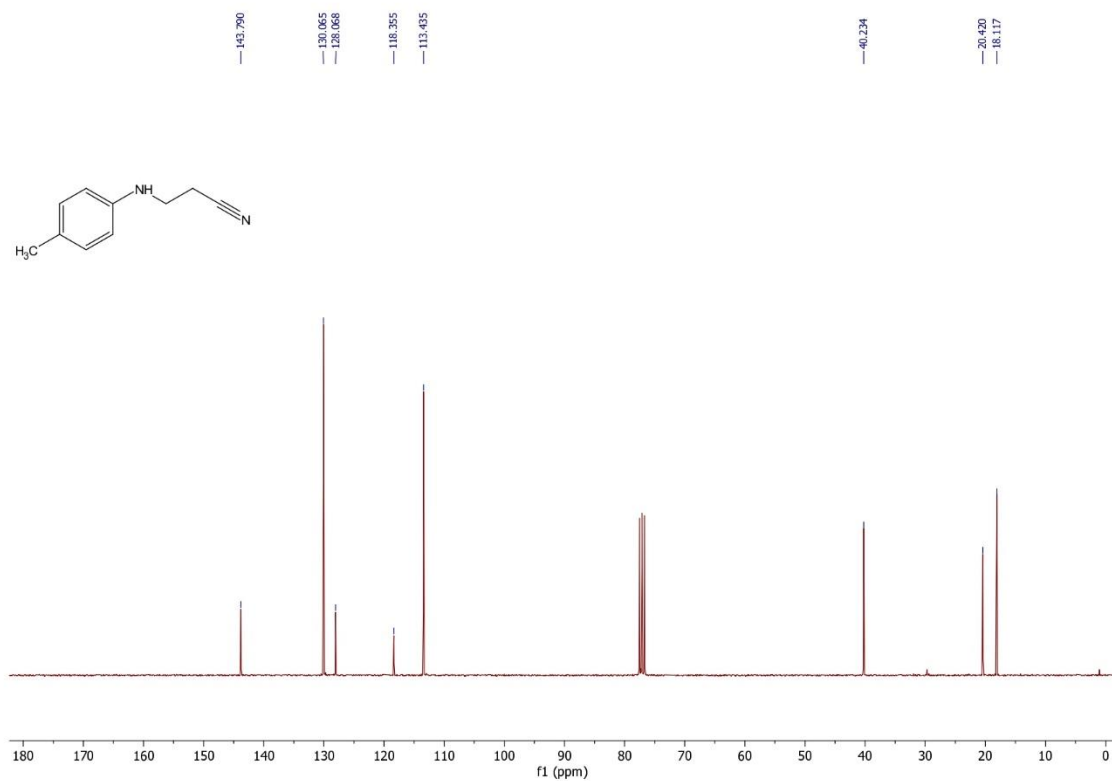


Figure 4.4 ¹³C NMR spectrum of **89b** (75 MHz, CDCl₃)

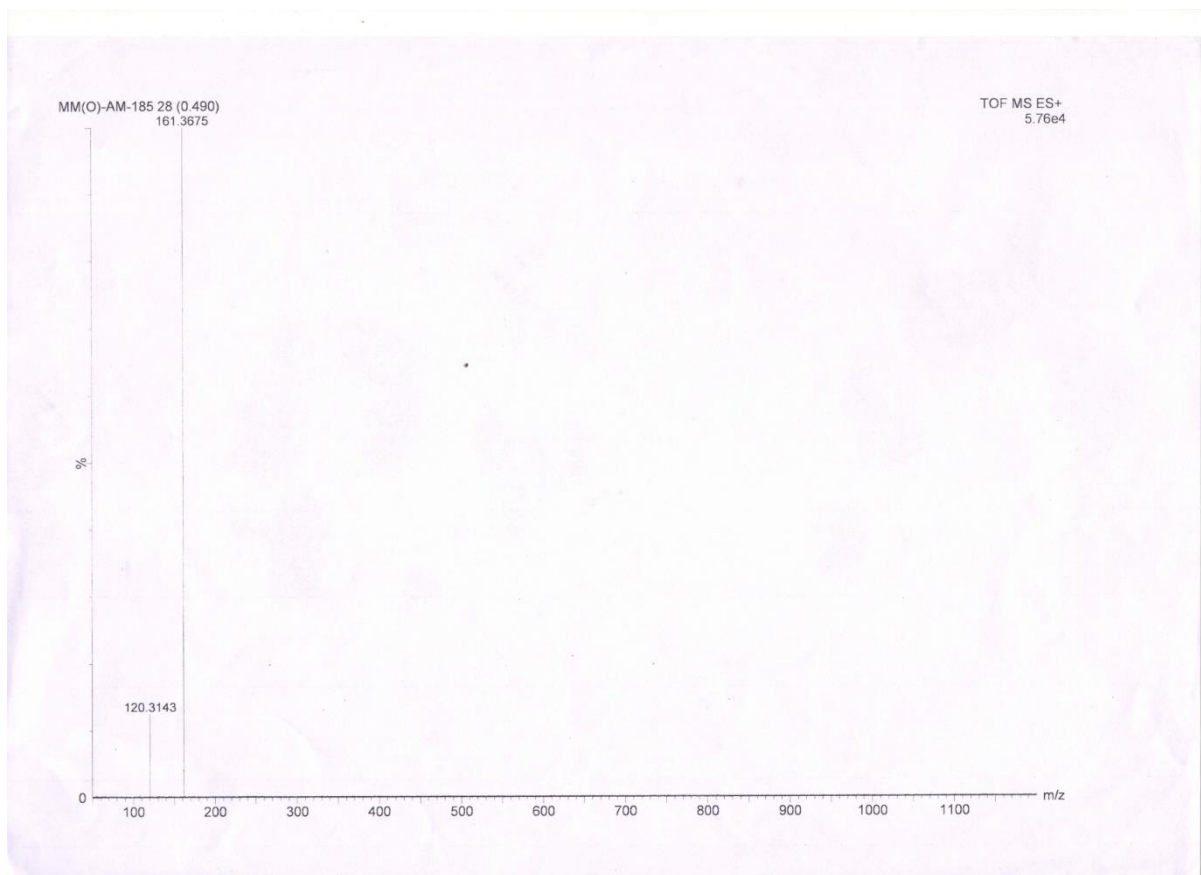


Figure 4.5 Mass spectrum of **89b** (ESI-TOF) m/z : $[M+H]^+$

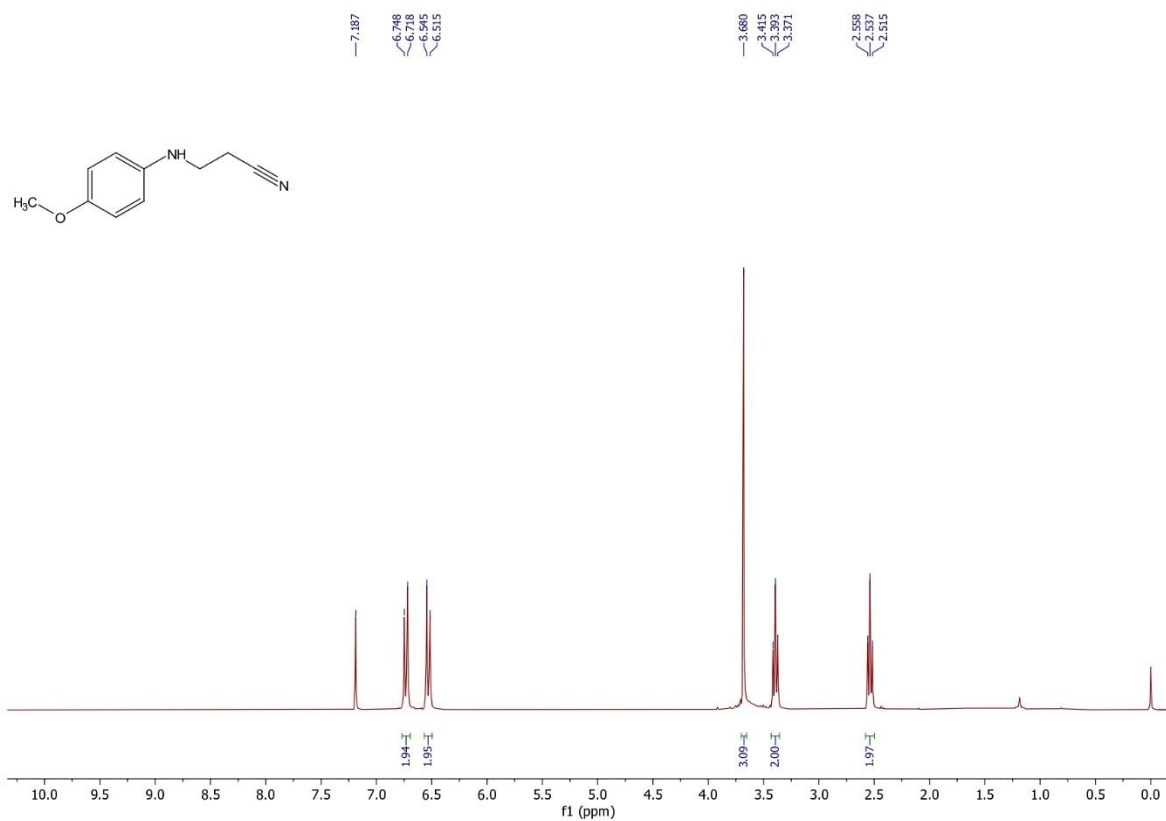


Figure 4.6 ^1H NMR spectrum of **89c** (300 MHz, CDCl_3)

Chapter 4

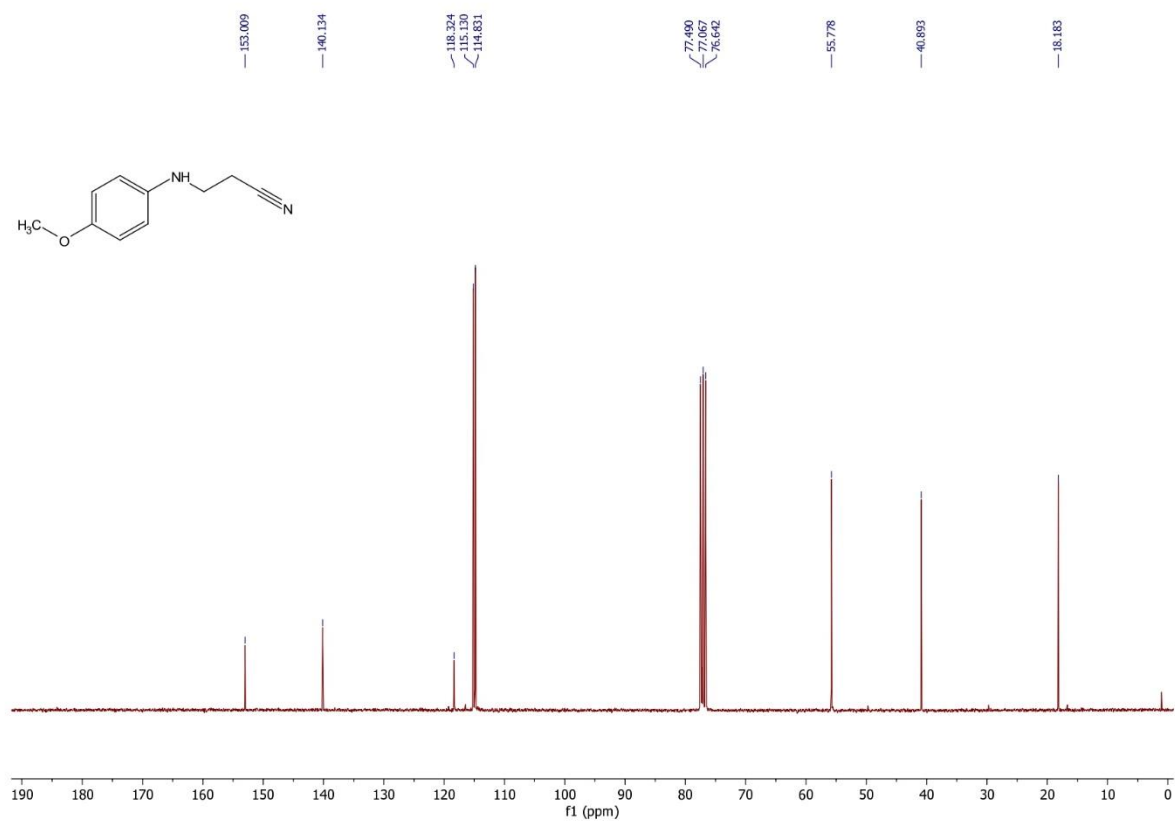


Figure 4.7 ¹³C NMR spectrum of **89c** (75 MHz, CDCl₃)

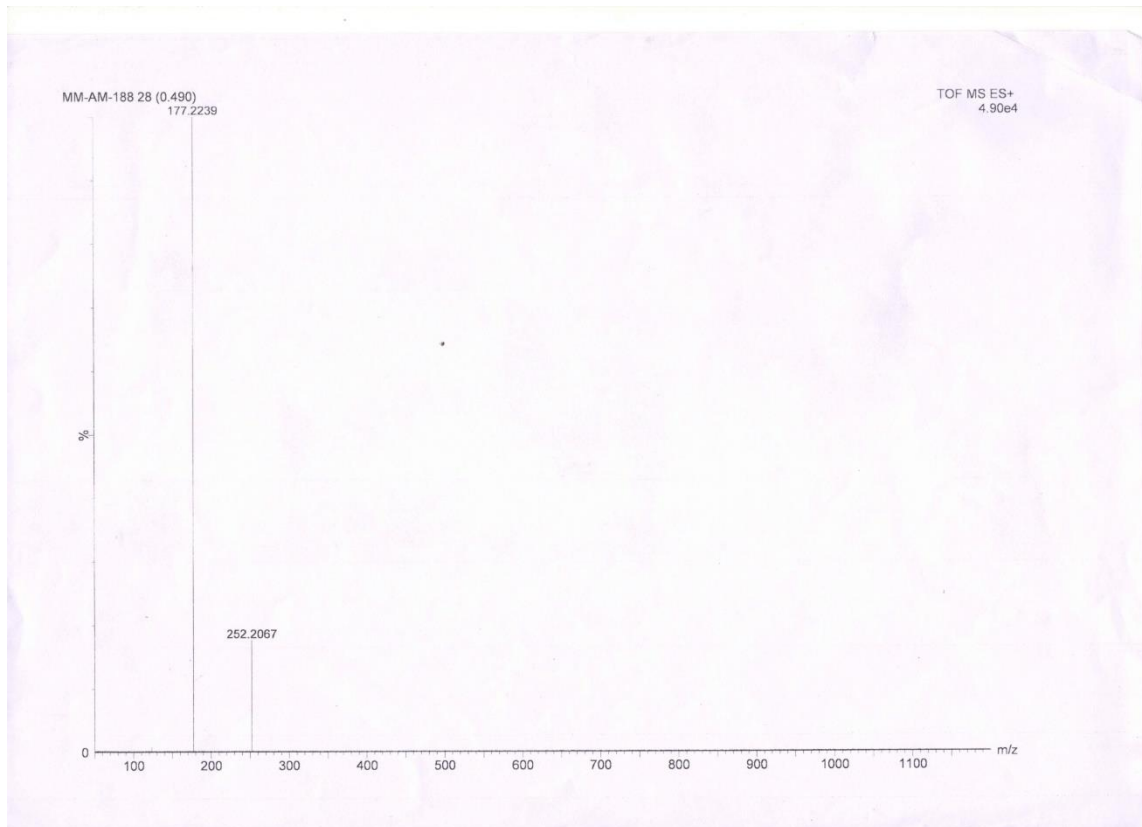


Figure 4.8 Mass spectrum of **89c** (ESI-TOF) m/z : [M+H]⁺

Chapter 4

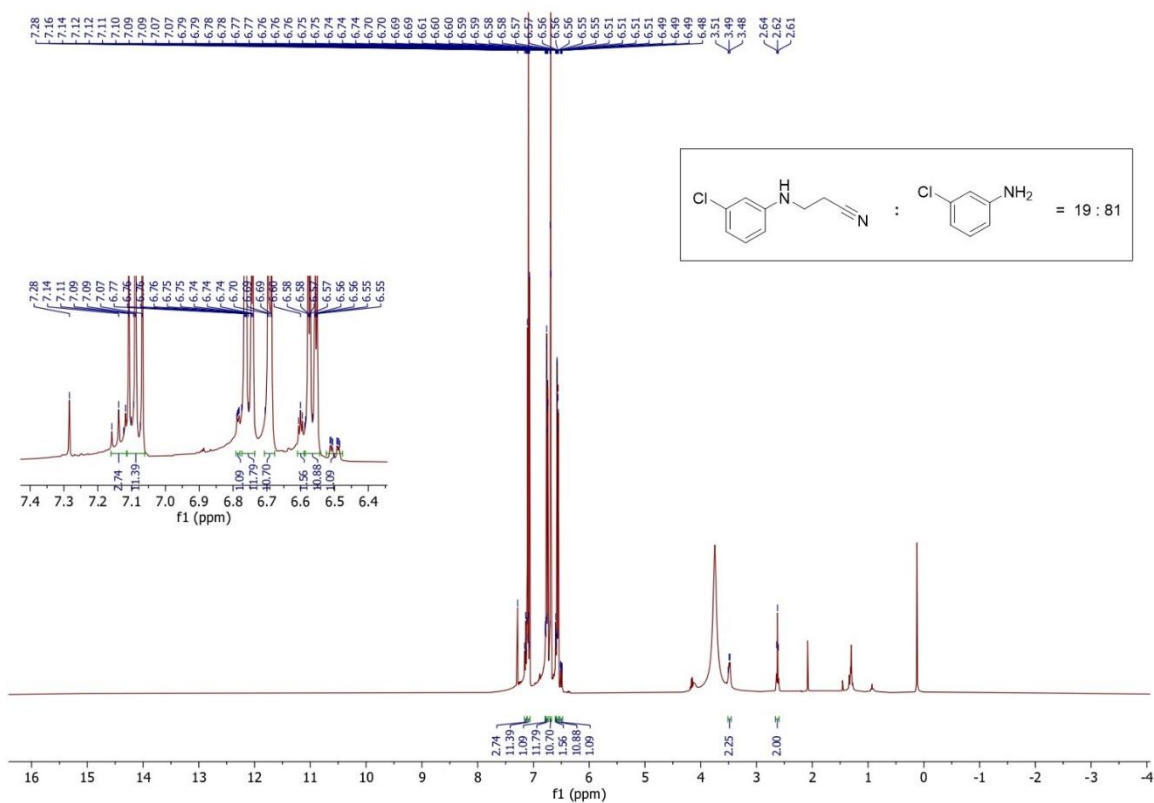
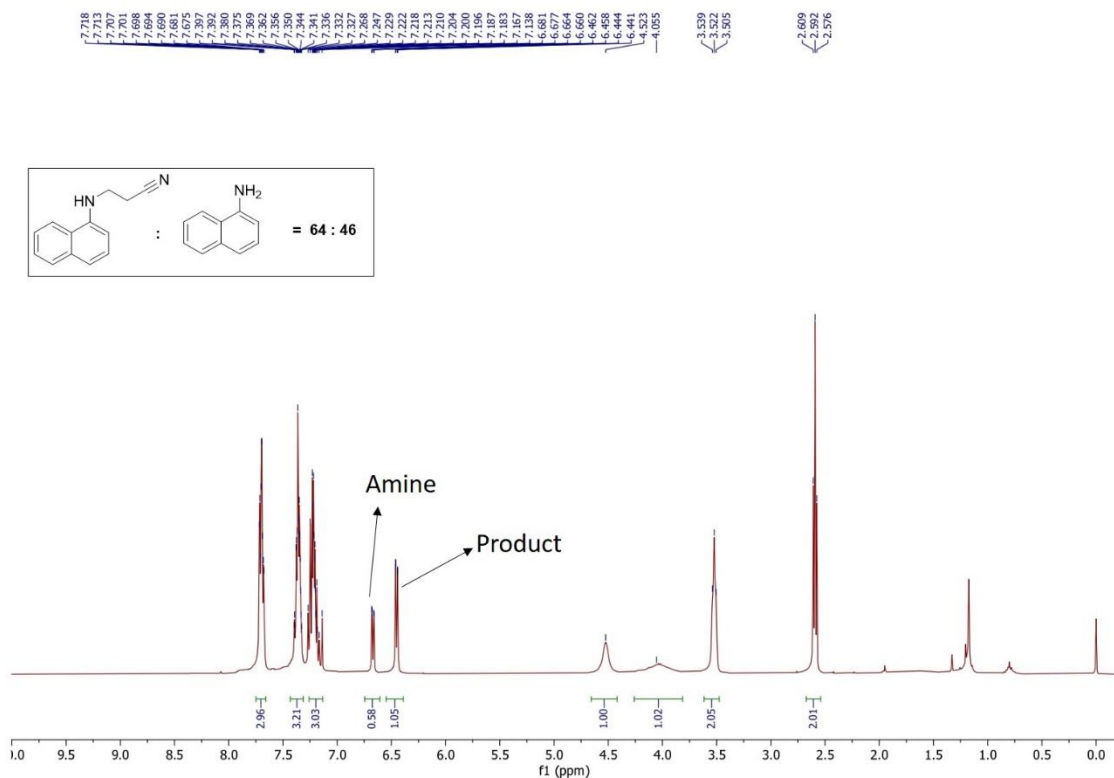


Figure 4.9 ^1H NMR spectrum of **89d** (400 MHz, CDCl_3)



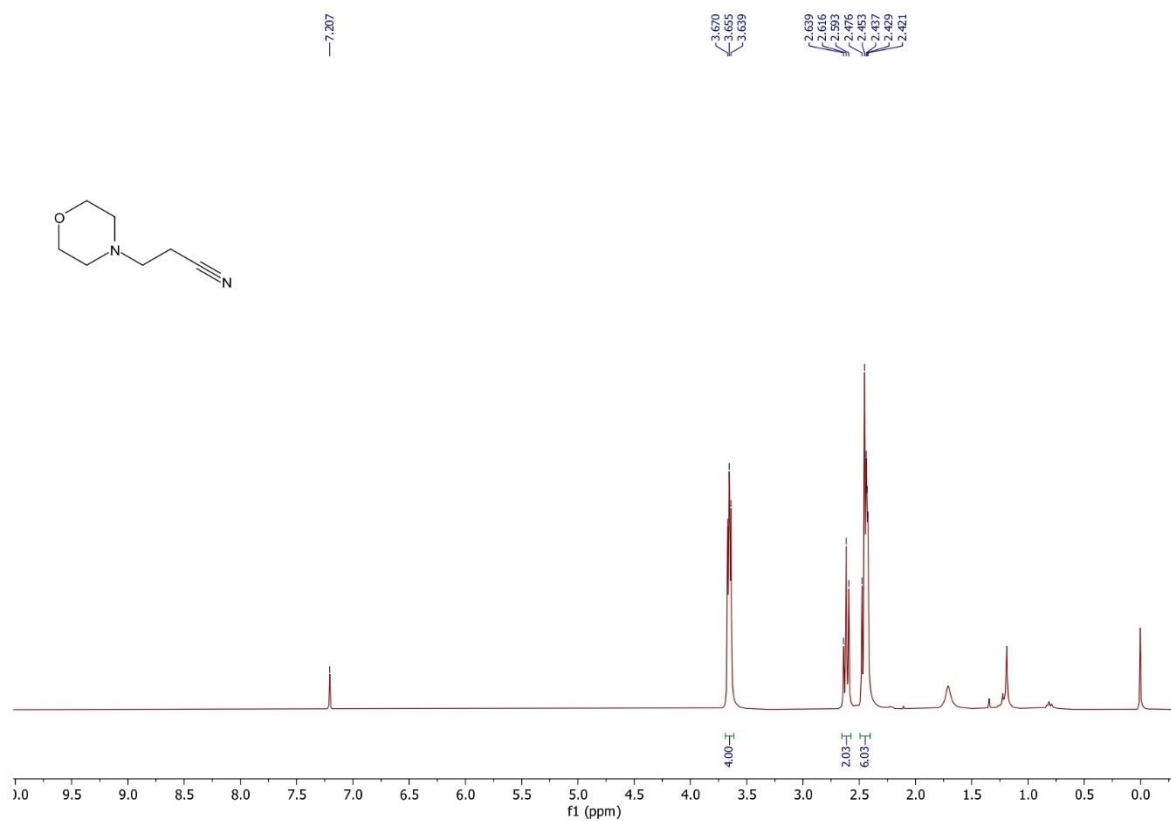


Figure 4.11 ¹H NMR spectrum of **89g** (300 MHz, CDCl₃)

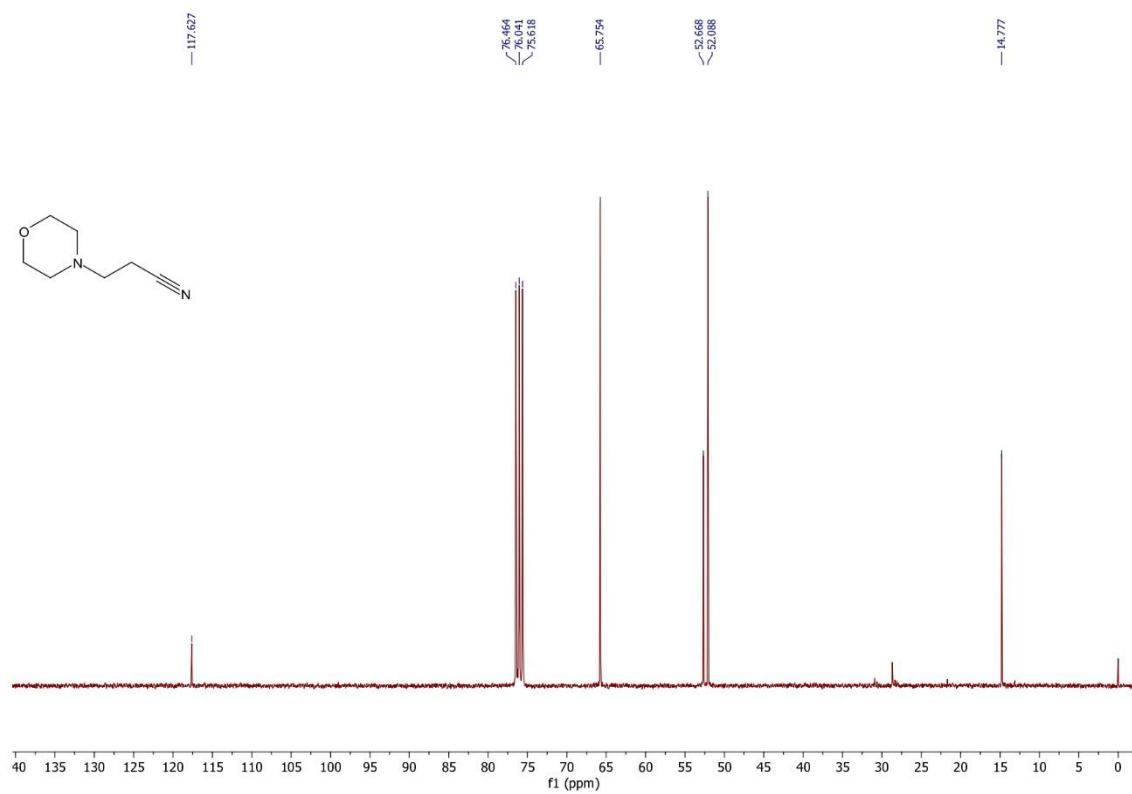


Figure 4.12 ¹³C NMR spectrum of **89g** (75 MHz, CDCl₃)

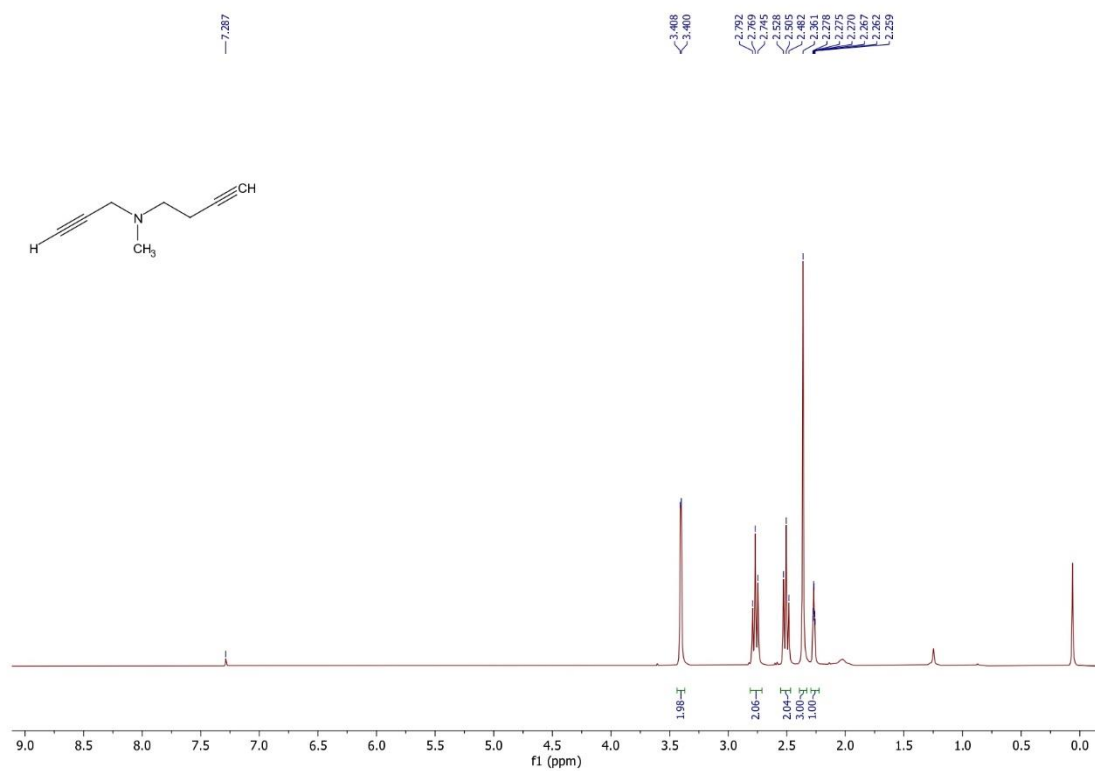


Figure 4.13 ¹H NMR spectrum of **89h** (300 MHz, CDCl₃)

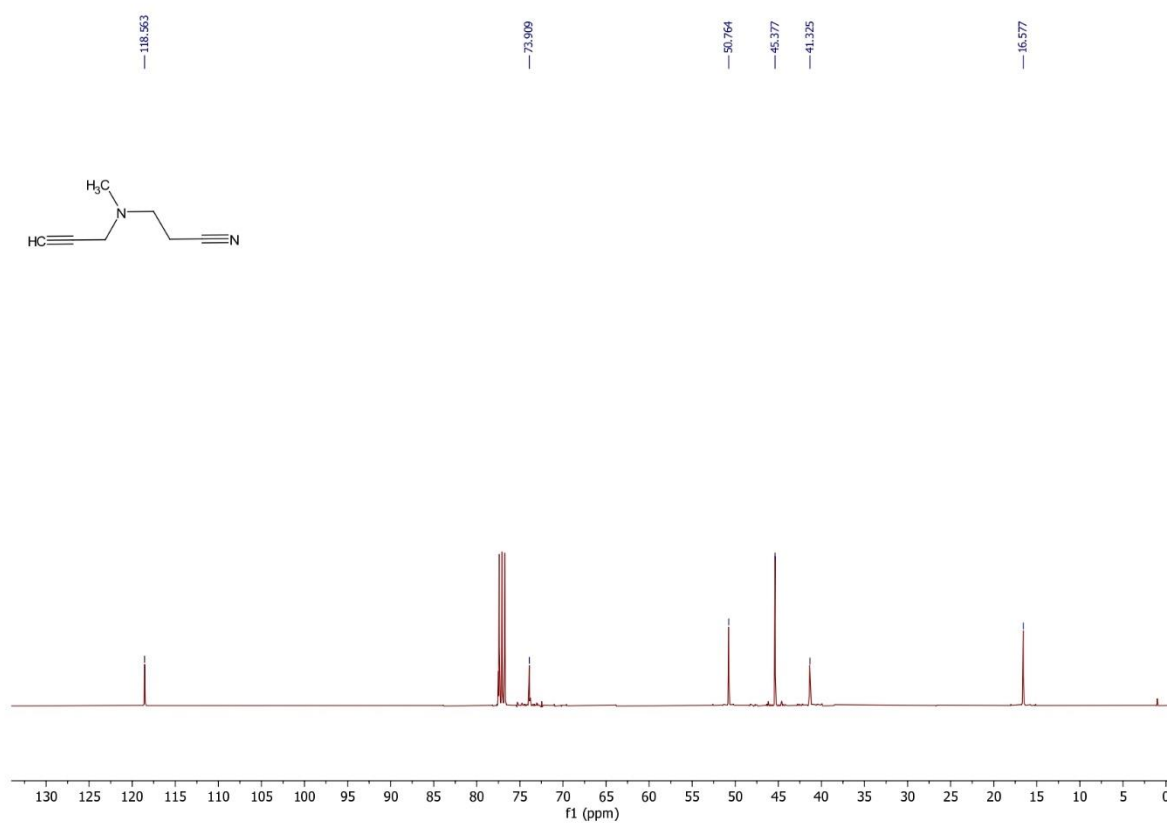


Figure 4.14 ¹³C NMR spectrum of **89h** (100 MHz, CDCl₃)

Chapter 4

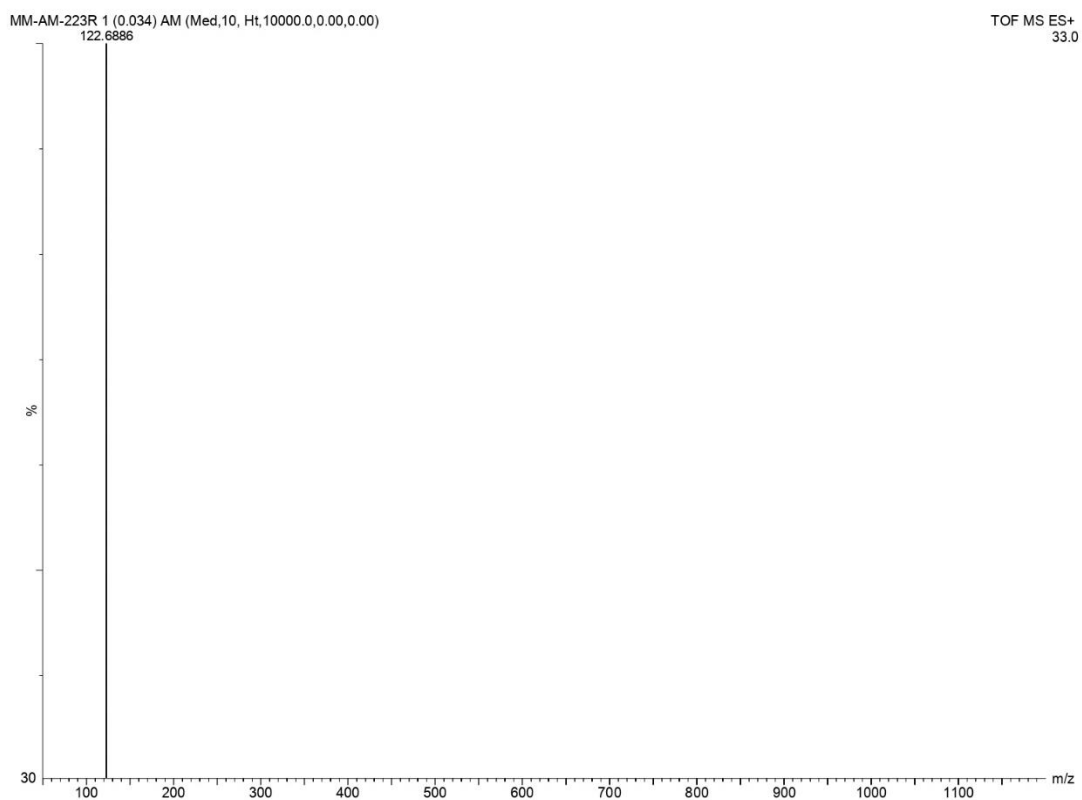


Figure 4.15 Mass spectrum of **89h** (ESI-TOF) m/z : $[M+H]^+$

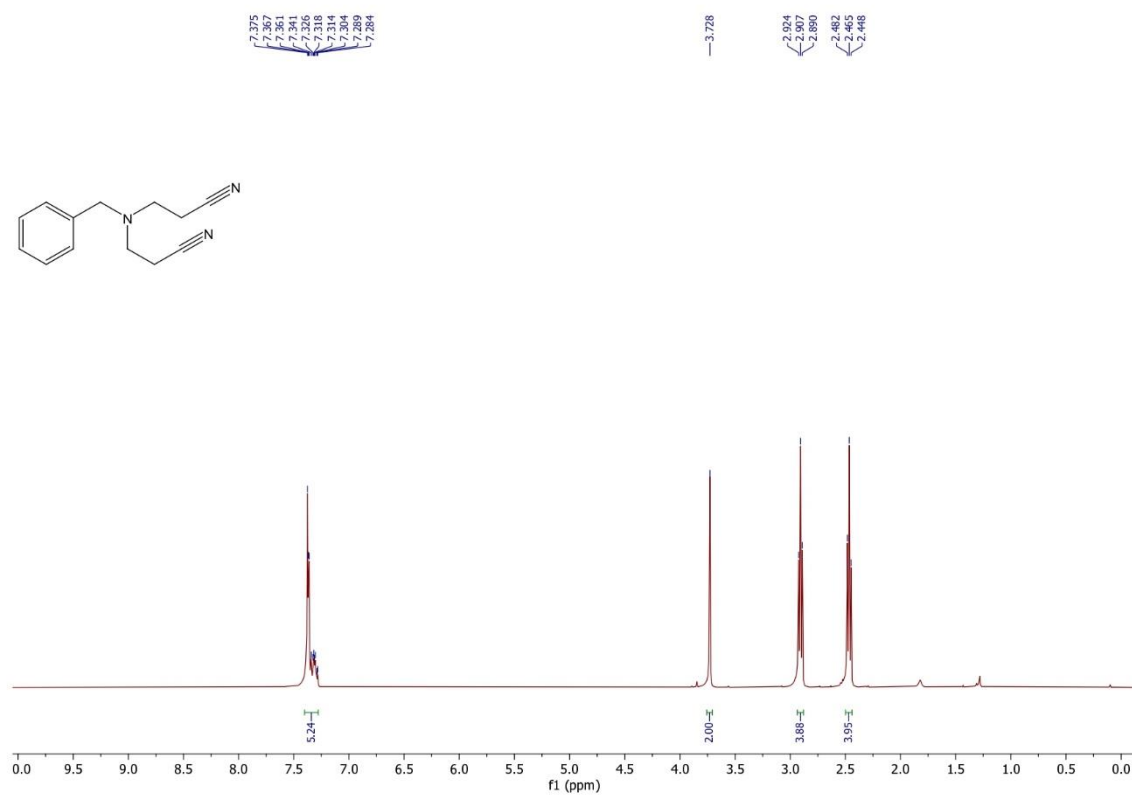


Figure 4.16 ^1H NMR spectrum of **89i** (400 MHz, CDCl_3)

Chapter 4

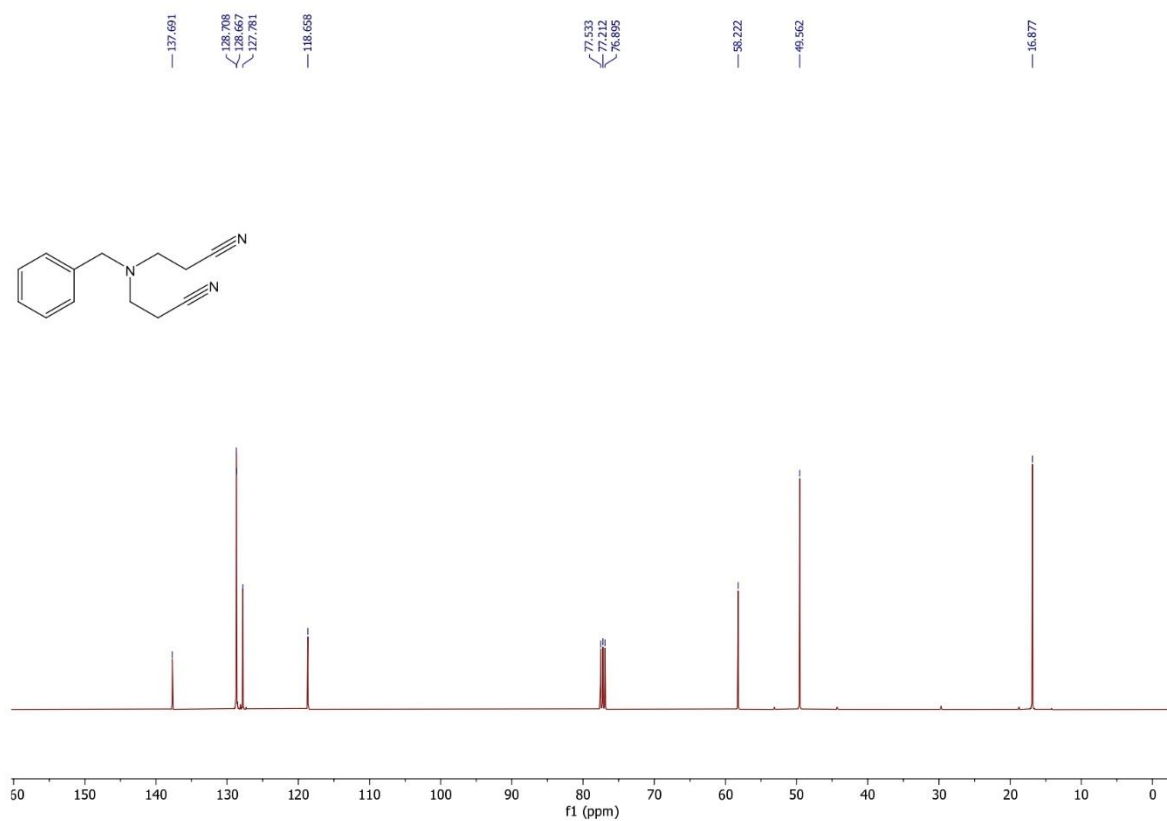


Figure 4.17 ¹³C NMR spectrum of **89i** (100 MHz, CDCl₃)

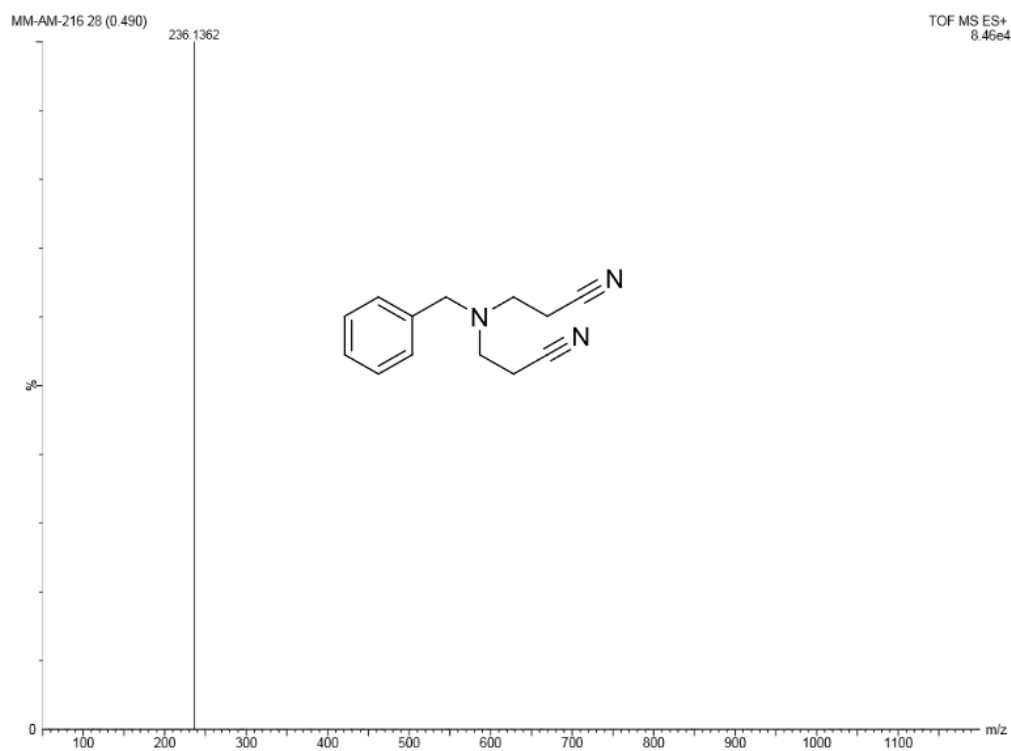


Figure 4.18 Mass spectrum of **89i** (ESI-TOF) m/z : [M+H]⁺

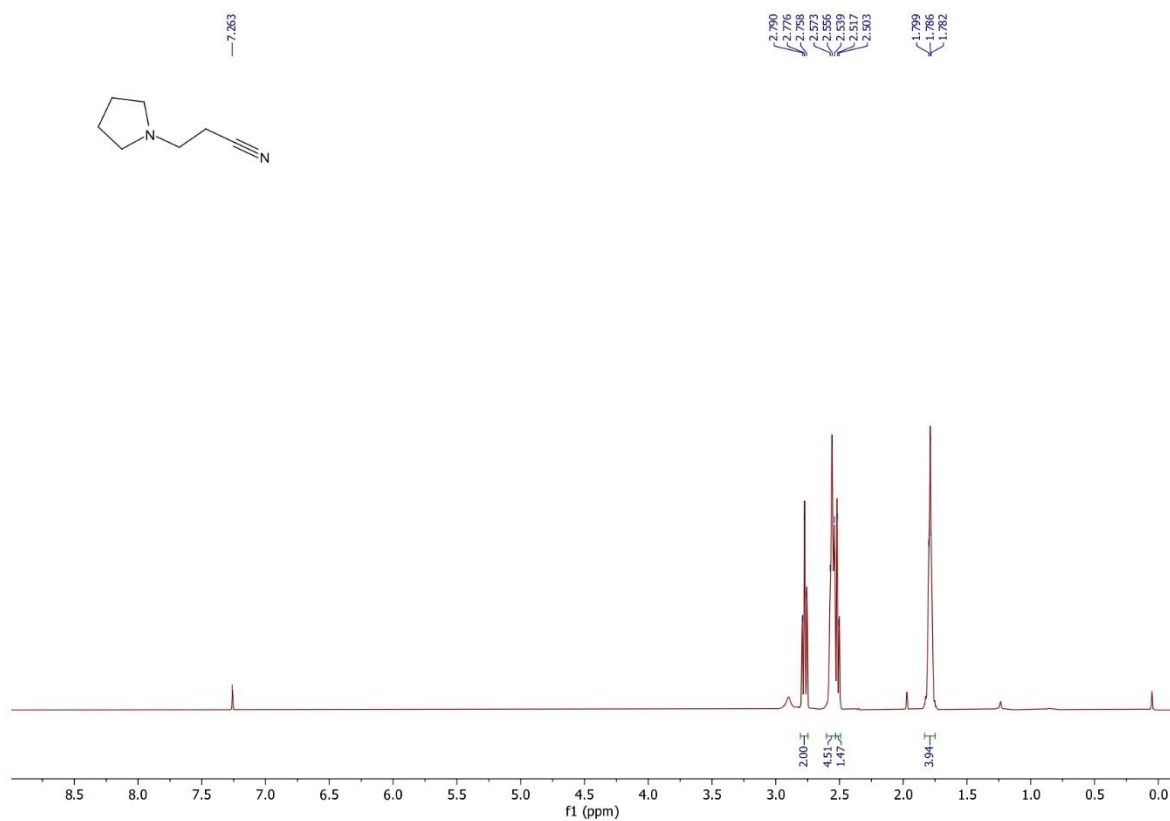


Figure 4.19 ¹H NMR spectrum of **89j** (300 MHz, CDCl₃)

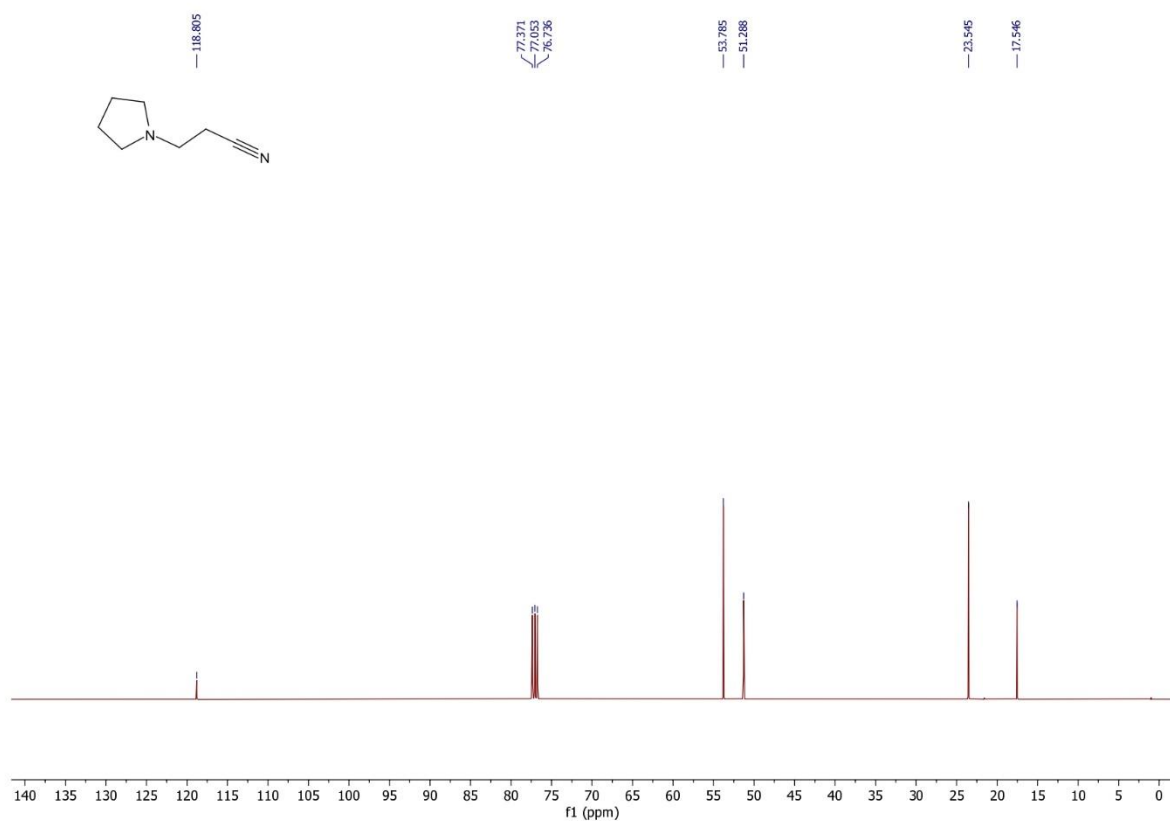


Figure 4.20 ¹³C NMR spectrum of **89j** (75 MHz, CDCl₃)

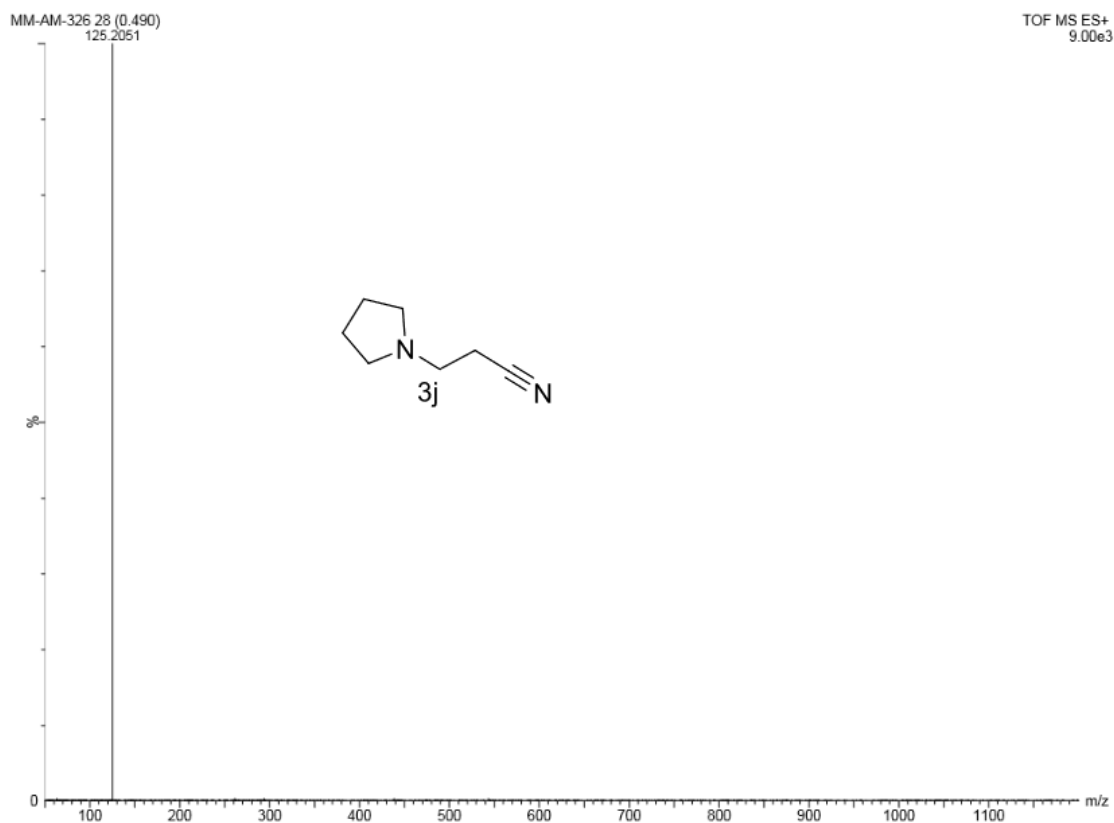


Figure 4.21 Mass spectrum of **89j** (ESI-TOF) m/z : $[M+H]^+$

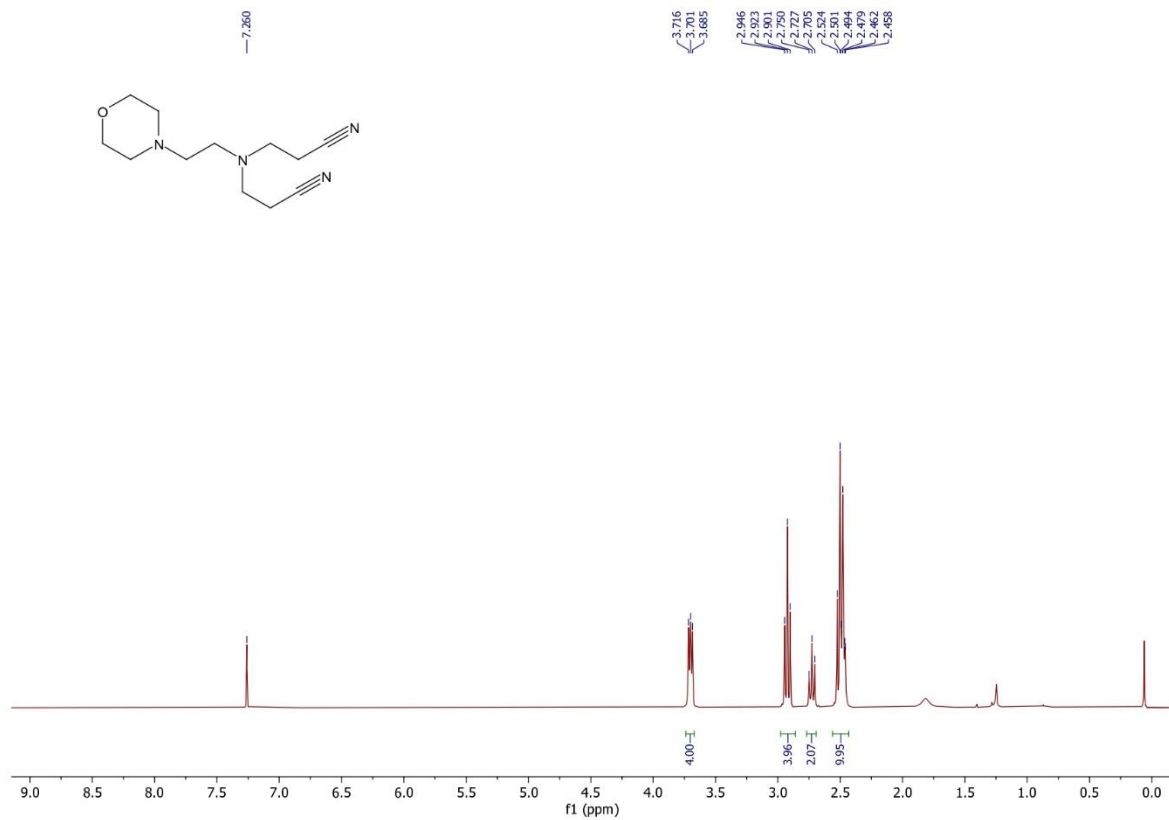


Figure 4.22 ^1H NMR spectrum of **89k** (300 MHz, CDCl_3)

Chapter 4

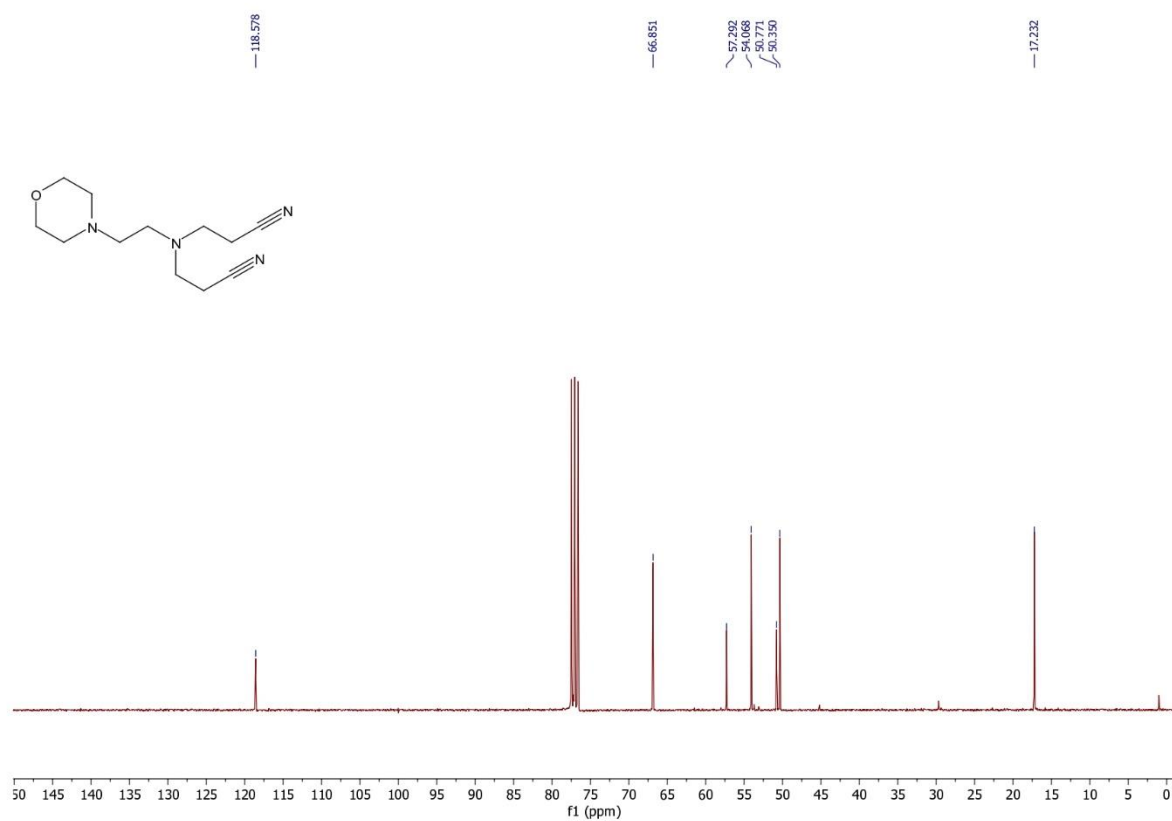


Figure 4.23 ¹³C NMR spectrum of **89k** (75 MHz, CDCl₃)

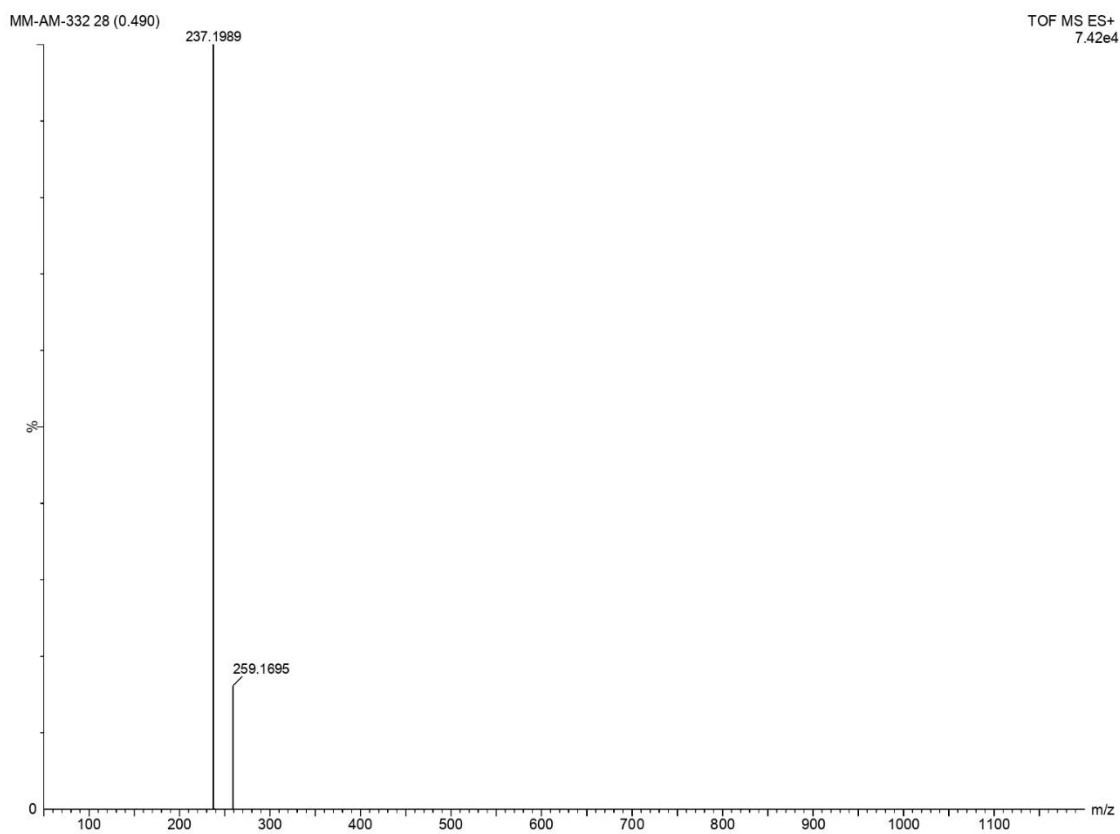


Figure 4.24 Mass spectrum of **89k** (ESI-TOF) m/z : [M+H]⁺

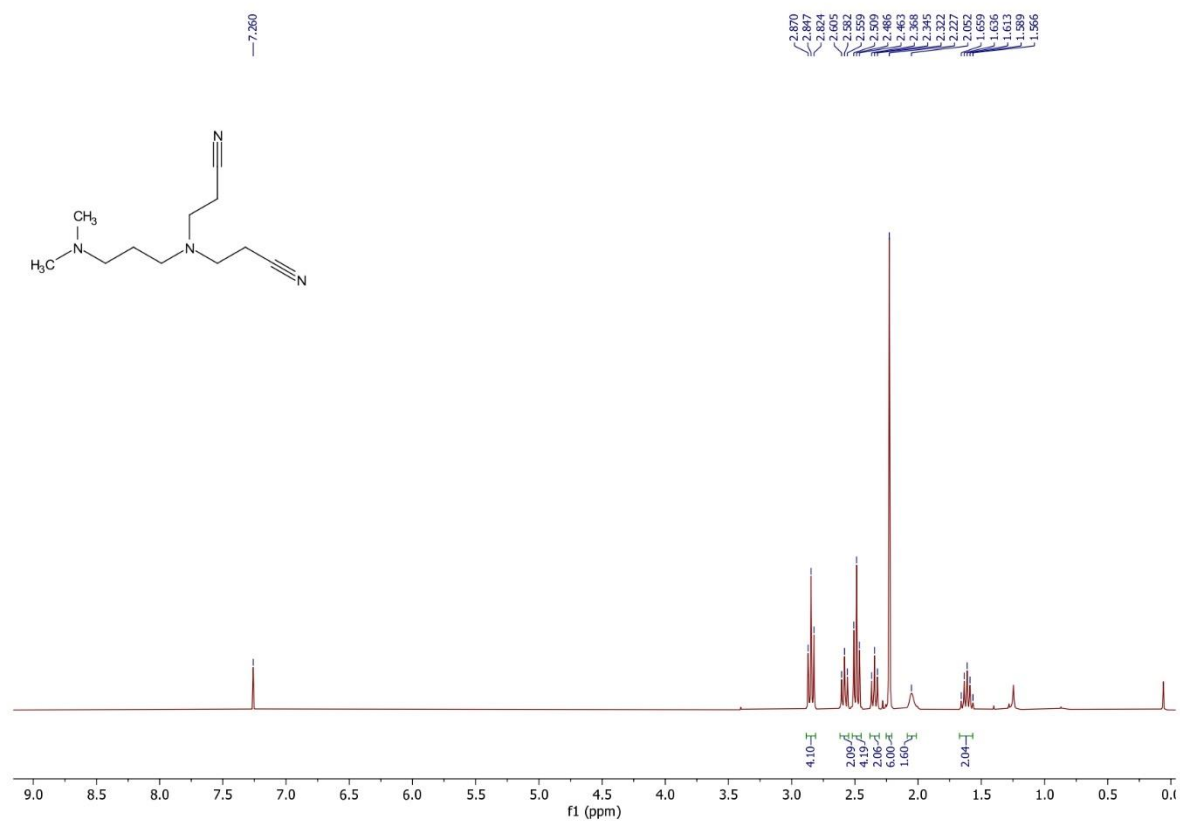


Figure 4.25 ^1H NMR spectrum of **89I** (300 MHz, CDCl_3)

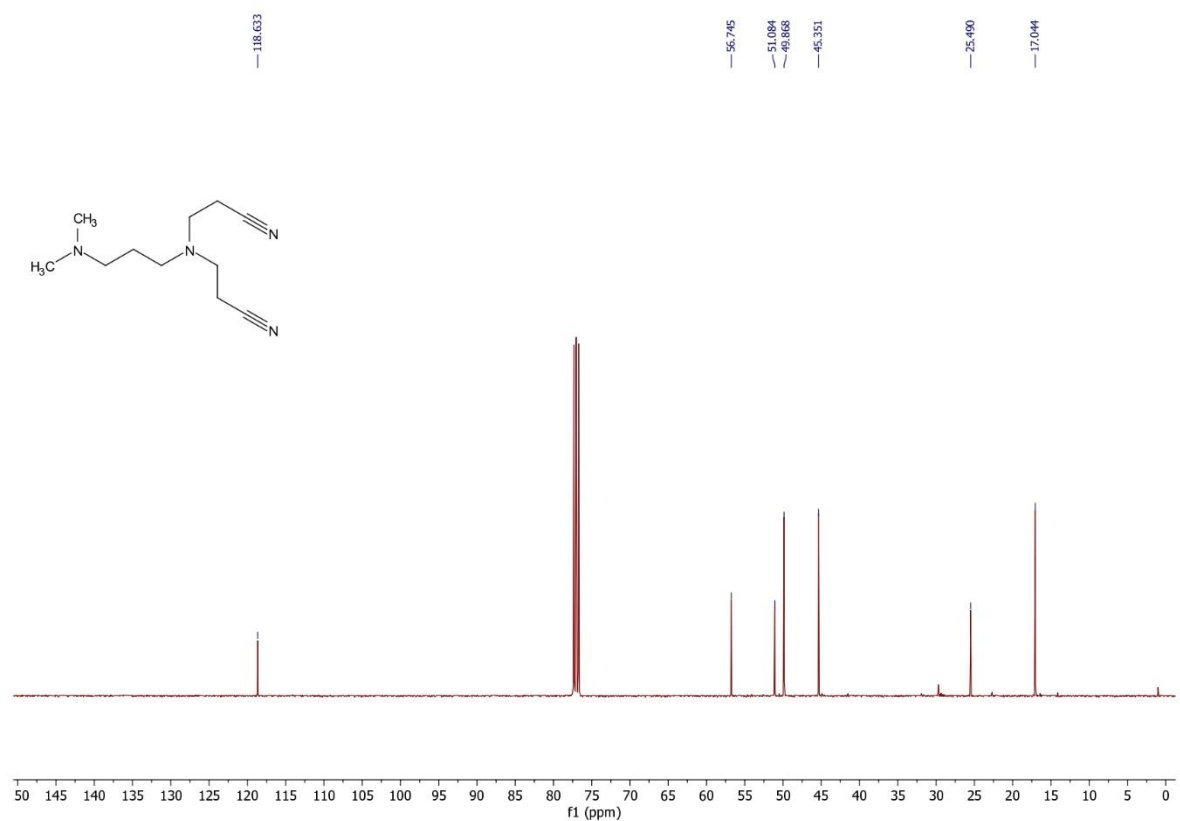


Figure 4.26 ^{13}C NMR spectrum of **89I** (100 MHz, CDCl_3)

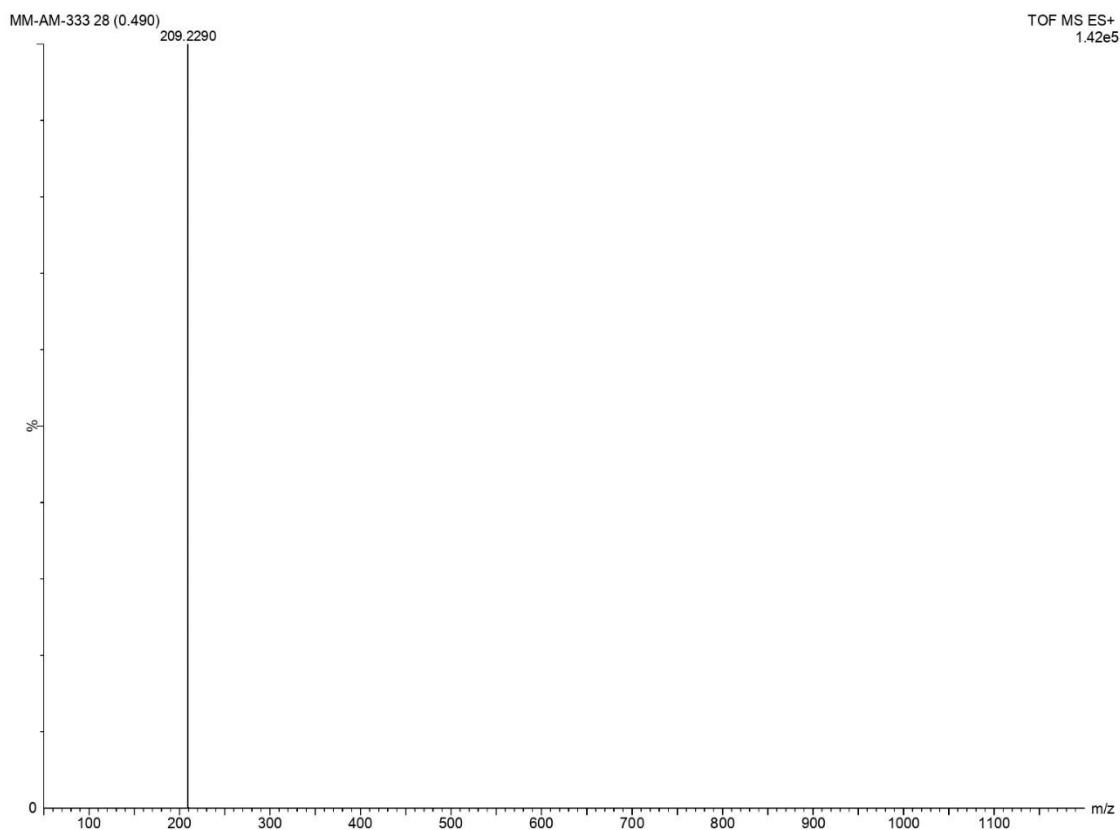


Figure 4.27 Mass spectrum of **89l** (ESI-TOF) m/z : $[M+H]^+$

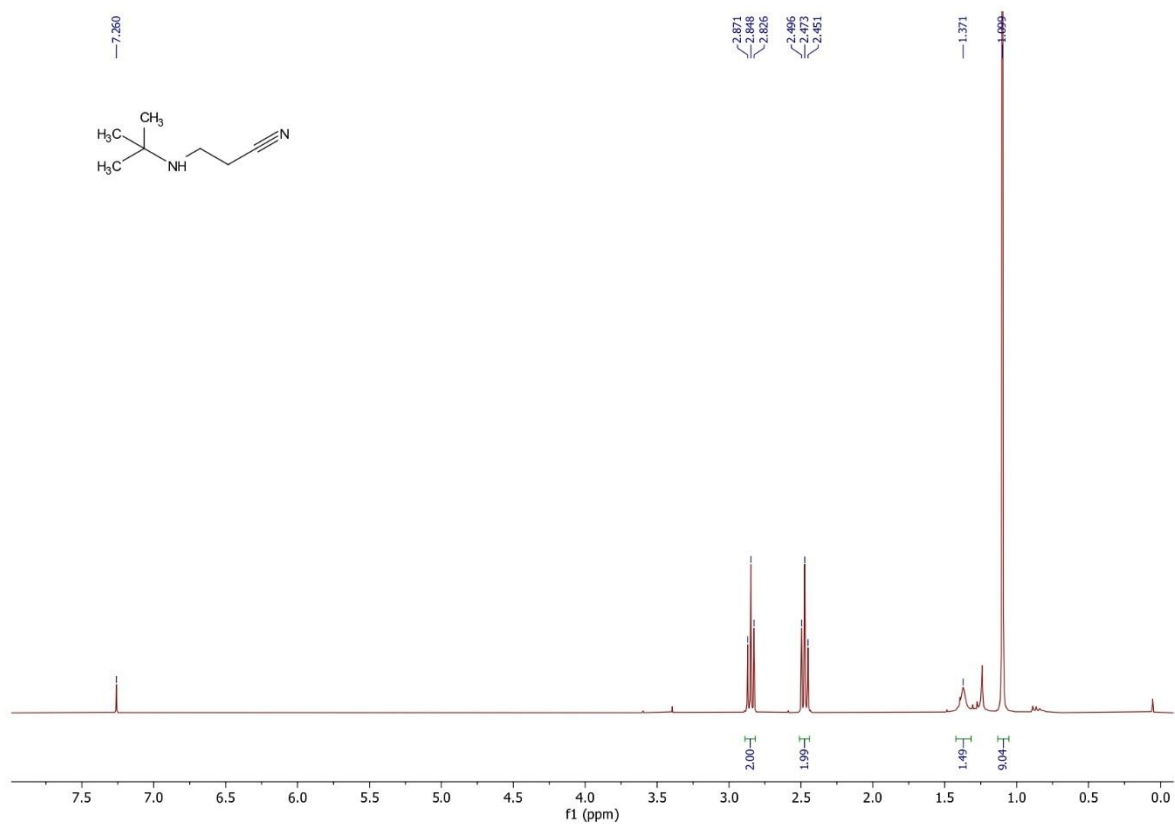


Figure 4.28 ^1H NMR spectrum of **89m** (300 MHz, CDCl_3)

Chapter 4

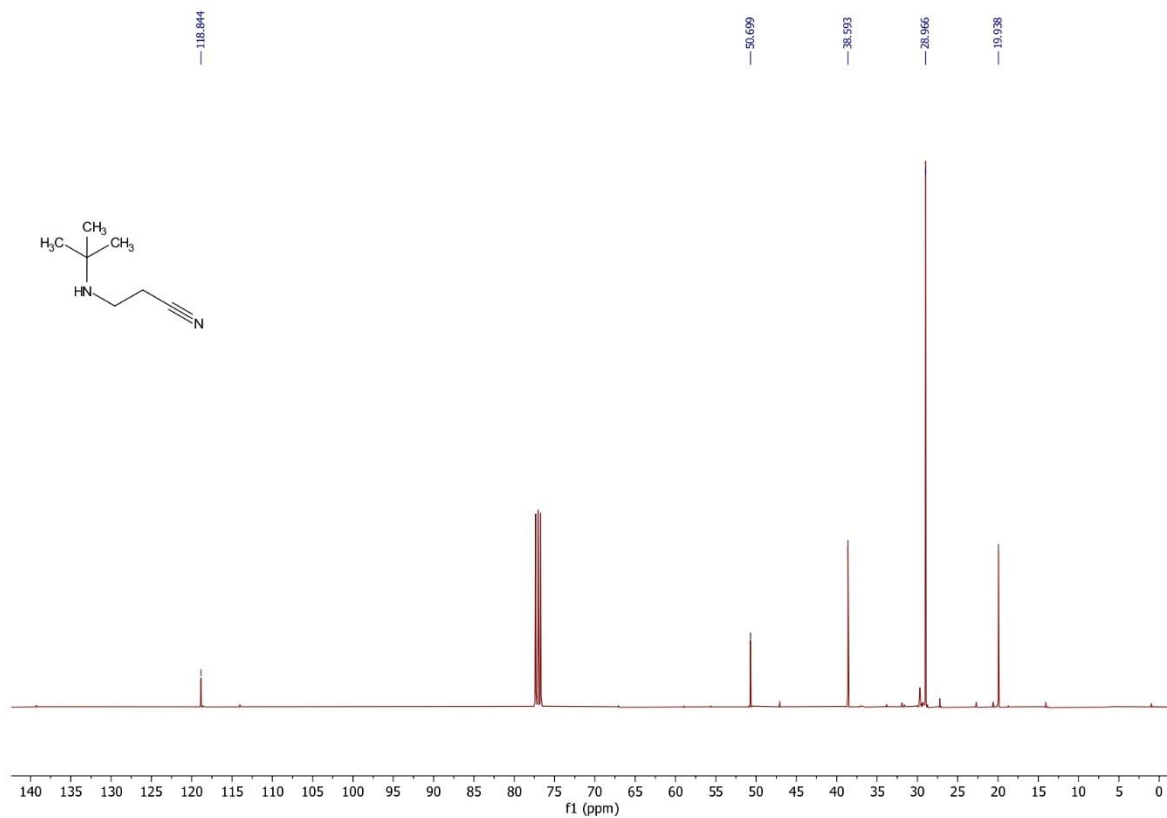


Figure 4.29 ¹³C NMR spectrum of **89m** (100 MHz, CDCl₃)

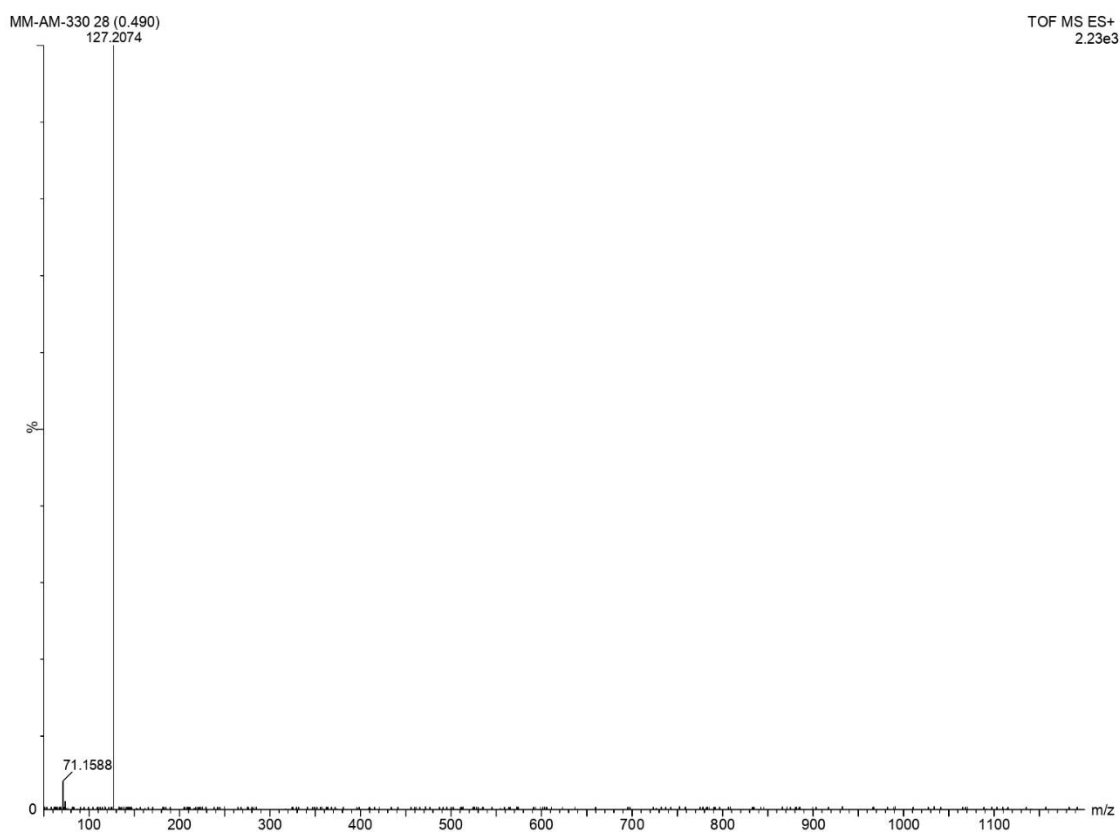


Figure 4.30 Mass spectrum of **89m** (ESI-TOF) m/z : [M+H]⁺

4.7 REFERENCES

1. Dondoni, A.; Marra, A., Addressing the scope of the azide–nitrile cycloaddition in glycoconjugate chemistry. The assembly of C-glycoclusters on a calix[4]arene scaffold through tetrazole spacers. *Tetrahedron* **2007**, *63* (27), 6339-6345.
2. Jusner, P.; Schwaiger, E.; Potthast, A.; Rosenau, T., Thermal stability of cellulose insulation in electrical power transformers – A review. *Carbohydrate Polymers* **2021**, *252*, 117196.
3. Hu, C.; Reddy, N.; Yan, K.; Yang, Y., Synthesis and characterization of highly flexible thermoplastic films from cyanoethylated corn distillers dried grains with solubles. *Journal of agricultural and food chemistry* **2011**, *59* (5), 1723-8.
4. Cao, X.; Sun, S.; Peng, X.; Zhong, L.; Sun, R., Synthesis and characterization of cyanoethyl hemicelluloses and their hydrated products. *Cellulose* **2013**, *20* (1), 291-301.
5. Nwokocha, L. M. J. J. o. A. S.; Technology, Adhesive Properties of Cyanoethyl Starch. **2011**, *25*, 893 - 902.
6. Dong, Y.; Huang, X.; Zhao, Y.; Yang, L.; Mao, W.; Bi, D.; Zhao, L., Studies on chitin-based liquid crystalline polymers - The lyotropic liquid crystallinity of low molecular weight chitosan and the influence of molecular mass on critical concentration. *Acta Polymerica Sinica* **2006**, 16-20.
7. Siddiqui, M. A. Q.; Krauskopf, M.; Ofengand, J., The function of pseudouridylic acid in transfer RNA. III. Inactivation of formylmethionine transfer RNA of E. coli by cyanoethylation with acrylonitrile. *Biochemical and Biophysical Research Communications* **1970**, *38* (1), 156-164.
8. Mengel-Jørgensen, J.; Kirpekar, F., Detection of pseudouridine and other modifications in tRNA by cyanoethylation and MALDI mass spectrometry. *Nucleic acids research* **2002**, *30* (23), e135.
9. Braunholtz, J. T.; Mann, F. G., The preparation of bis-2-cyanoethyl derivatives of aromatic primary amines, and their conversion into 1 : 6-diketotolulolidines. Part III. *Journal of the Chemical Society (Resumed)* **1954**, (0), 651-658.
10. Rajasekaran, A.; Thampi, P.; Murugesan, S., Cyanoethylation: A Vital Reaction in the Synthesis of Biologically Active Heterocycles. *Cheminform* **2004**, 35.
11. Department, A. C. C. P., *The Chemistry of Acrylonitrile*. Synthetic Organic Chemicals Department, American Cyanamid Company: 1951.
12. Feit, B.-A.; Zilkha, A., Kinetics and Mechanism of the Cyanoethylation of Alcohols. *The Journal of Organic Chemistry* **1963**, *28* (2), 406-410.

13. Lefèvre, X.; Durieux, G.; Lesturgez, S.; Zargarian, D., Addition of amines and phenols to acrylonitrile derivatives catalyzed by the POCOP-type pincer complex [$\kappa(P)\text{-}\kappa(C),\kappa(P)\text{-}2,6\text{-(i-Pr}_2\text{PO)}(2)\text{C}_6\text{H}_3\}$ Ni(NCMe)][OSO₂CF₃]. *Journal of Molecular Catalysis A: Chemical* **2011**, 335, 1–7.
14. Fadini, L.; Togni, A., Asymmetric hydroamination of acrylonitrile derivatives catalyzed by Ni(II)-complexes. *Tetrahedron: Asymmetry* **2008**, 19 (22), 2555-2562.
15. Payra, S.; Saha, A.; Banerjee, S., On-water magnetic NiFe₂O₄ nanoparticle-catalyzed Michael additions of active methylene compounds, aromatic/aliphatic amines, alcohols and thiols to conjugated alkenes. *RSC Advances* **2016**, 6 (98), 95951-95956.
16. Ai, X.; Wang, X.; Liu, J.-m.; Ge, Z.-m.; Cheng, T.-m.; Li, R.-t., An effective aza-Michael addition of aromatic amines to electron-deficient alkenes in alkaline Al₂O₃. *Tetrahedron* **2010**, 66 (29), 5373-5377.
17. Choudhary, V. R.; Dumbre, D. K.; Patil, S. K., FeCl₃/Montmorillonite K10 as an efficient catalyst for solvent-free aza-Michael reaction between amine and α,β -unsaturated compounds. *RSC Advances* **2012**, 2 (18), 7061-7065.
18. Zhang, H.; Zhang, Y.; Liu, L.; Xu, H.; Wang, Y., RuCl₃ in Poly(ethylene glycol): A Highly Efficient and Recyclable Catalyst for the Conjugate Addition of Nitrogen and Sulfur Nucleophiles. *Synthesis* **2005**, 2005 (13), 2129-2136.
19. Dai, L.-y.; Zhang, Y.; Dou, Q.; Wang, X.-z.; Chen, Y.-q. J. T., Chemo/regioselective Aza-Michael additions of amines to conjugate alkenes catalyzed by polystyrene-supported AlCl₃. **2013**, 69, 1712-1716.
20. Azizi, N.; Baghi, R.; Ghafari, H.; Bolourtchian, M.; Hashemi, M., Silicon Tetrachloride Catalyzed Aza-Michael Addition of Amines to Conjugated Alkenes under Solvent-Free Conditions. *Synlett* **2010**, 2010 (03), 379-382.
21. Kamble, S.; Kumbhar, A.; Jadhav, S.; Salunkhe, R., Aza-Michael Reaction in Glycerol as a Sustainable Hydrotropic Medium. *Materials Today: Proceedings* **2015**, 2, 1792-1798.
22. Cowan, R. L.; Trogler, W. C., Regioselective insertion of acrylonitrile into the platinum-nitrogen bond of hydrido(phenylamido)bis(triethylphosphine)platinum(II). A model step for olefin amination. *Organometallics* **1987**, 6 (11), 2451-2453.
23. Singh, P.; Kumari, K.; Katyal, A.; Thukral, R. K. T.; Chandra, R., Copper Nanoparticles in Ionic Liquid: An Easy and Efficient Catalyst for Selective Carba-Michael Addition Reaction. *Catalysis Letters* **2009**, 127, 119-125.

24. Mondal, M. A.; Mondal, S.; Khan, A. A., Synthesis of Functionalized Quinazolinones via Acid-Catalyzed Redox Neutral Reaction. **2021**, *6* (42), 11788-11791.
25. Khan, A.; Mitra, K.; Mandal, A.; Baildya, N.; Mondal, M., Yttrium nitrate catalyzed synthesis, photophysical study, and TD-DFT calculation of 2,3-dihydroquinazolin-4(1H)-ones. *Heteroatom Chemistry* **2017**, 28.
26. Khan, A. A.; Mitra, K.; Mondal, M. A., Microwave Promoted $Y(NO_3)_3 \cdot 6H_2O$ Catalyzed Biginelli Synthesis of Dihydropyrimidin-2-ones. *Asian Journal of Chemistry* **2016**, *29* (3), 529-534.
27. Mondal, M.; Mandal, D.; Mitra, K., Yttrium Nitrate mediated Nitration of Phenols at room temperature in Glacial Acetic acid. *Journal of Chemical Sciences* **2017**, 129.
28. Guo, B.; Zijlstra, D. S.; de Vries, J. G.; Otten, E., Oxa-Michael Addition to α,β -Unsaturated Nitriles: An Expedient Route to γ -Amino Alcohols and Derivatives. **2018**, *10* (13), 2868-2872.

LIST OF PUBLICATIONS

1. **Misra, A.**, Mondal, S. & Mondal, M.A. Ferric Chloride mediated one pot Synthesis and Photophysical Studies of Isoindoloindolones. *Tetrahedron* 155 (2024) 133887; DOI: 10.1016/j.tet.2024.133887
2. **Misra, A.**, Mondal, S. & Mondal, M.A. Synthesis of 11*H*-benzo[b]fluoren-11-one via an unprecedented cascade reaction of *o*-phthaldehyde. *Polycyclic aromatic compounds* (2023); DOI: 10.1080/10406638.2023.2270124
3. **Misra, A.**, Das, S. & Mondal, M.A. Design, Synthesis, and Calf-Thymus DNA binding properties of highly functionalized Quinazolinones. *ChemistrySelect* 2024, 9, e202303740; DOI: 10.1002/slct.202303740
4. **Misra, A.**, Haque, R. & Mondal, M.A. Yttrium nitrate promoted selective cyanoethylation of amines. *J. Chem. Sci.* (2023) 135:5; DOI: 10.1007/s12039-023-02173-2
5. **Misra, A.**, Mondal, M.A. Design, Synthesis of highly conjugated azaheterocycles and their applications in organic electronics (under communication)

PUBLICATIONS ABSTRACT

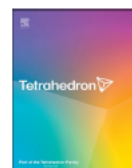
Tetrahedron 155 (2024) 133887



Contents lists available at ScienceDirect

Tetrahedron

journal homepage: www.elsevier.com/locate/tet



Ferric chloride mediated one pot synthesis and photophysical studies of isoindoloindolones

Arunava Misra, Sudipta Mondal, Mohabul Alam Mondal^{*}

Department of Chemistry, Jadavpur University, Kolkata 700032, India

ARTICLE INFO

Keywords:

Ferric chloride
Tandem reaction
Annulative coupling
Intramolecular charge transfer
Isoindoloindolone
Polycyclic aromatic compound

ABSTRACT

We have explored a one-pot, tandem protocol for constructing a linear tetracyclic aromatic core isoindoloindolone via FeCl₃-mediated annulative coupling of 2-aminoacetophenones with *ortho* phthalaldehyde (OPA). This report describes a detailed optimizations of the method, substrate scope, and characterization of the synthesized compounds by NMR, XRD, etc.,. Spectroscopic analysis of one of the synthesized compounds (1a) revealed that the intramolecular charge-transfer state formation is responsible for PL in solution. In contrast, emission resulted predominately from the locally excited state in the crystalline state. Tailoring the isoindoloindolone moiety by placing different substituents on the 2-amino acetophenone part and its effect on photophysical properties are also evaluated.

POLYCYCLIC AROMATIC COMPOUNDS
<https://doi.org/10.1080/10406638.2023.2270124>



Taylor & Francis
Taylor & Francis Group



Synthesis of 11*H*-Benzo[*b*]Fluoren-11-One via an Unprecedented Cascade Reaction of *O*-Phthalaldehyde

Arunava Misra, Sudipta Mondal, and Mohabul A. Mondal

Department of Chemistry, Jadavpur University, Kolkata, India

ABSTRACT

Developing multicomponent reactions in a cascade manner is a long-standing interest to chemists to access valuable organic materials more economically. Herein, we described a simple, economically viable method for synthesizing 11*H*-benzo[*b*]fluoren-11-one, a dual-state organic fluorophore, starting from *ortho* phthalaldehyde (OPA) in DMSO solvent. Simple and rapid product isolation, high atom economy, short reaction time, and scalability are the attractive features of the method. During the optimization of the reaction condition, we observed that DMSO, DMF, and acetone served one carbon to form the said compound besides their role as solvents. A plausible mechanism has been proposed based on the evidence obtained from LCMS analysis of the incomplete reaction mixture.

ARTICLE HISTORY

Received 5 July 2023
Accepted 29 September 2023

KEYWORDS

Ortho phthalaldehyde;
benzo fluorenone;
mechanistic study; tandem
aldol condensation

Please check the marked (■) text passages carefully, if any are present.

www.chemistryselect.org

Aromatic Amine attached Quinazolinones: Synthesis Characterization and DNA Binding Properties

Arunava Misra,^[a] Soumya Das,^[a] and Mohabul Alam Mondal^{*,[a]}

A facile intramolecular [1,5] hydride transfer reaction in a Dihydroquinazolin-4(1H)-one moiety synthesized from anthranilamide, glutaraldehyde, and aromatic amines is described in isopropanol medium in the presence of catalytic HCl. Based on that, we have designed a simple, efficient strategy for conjugating quinazolinone, a pharmaceutically active moiety, with an aromatic amine through an aliphatic spacer. The use of

isopropanol as a reaction medium at RT and isolation of the product without rigorous column purification make the process a step ahead towards sustainability. One of the synthesized compounds was evaluated as a small molecule DNA binder. Detailed binding properties were investigated by the multi-spectroscopy methods.

J. Chem. Sci. (2023)135:57
<https://doi.org/10.1007/s12039-023-02173-2>

© Indian Academy of Sciences

REGULAR ARTICLE



Yttrium nitrate promoted selective cyanoethylation of amines

ARUNAVA MISRA, SK RAJIBUL HAQUE and MOHABUL A MONDAL^{* ①}

Department of Chemistry, Jadavpur University, Kolkata 700032, India
E-mail: mohabula.mondal@jadavpuruniversity.in

MS received 13 February 2023; revised 13 April 2023; accepted 18 April 2023

Abstract. The catalyst $Y(NO_3)_3 \cdot 6H_2O$ exhibited remarkable activity in the aza-Michael addition of various aromatic and aliphatic amines with acrylonitrile at ambient temperature in a protic solvent. The method is selective for the monocyanoethylation of primary aromatic amines, aliphatic secondary amines, and sterically hindered aliphatic amines. Phenols and active methylene compounds do not undergo cyanoethylation. Thiophenol, in the presence of yttrium nitrate, promotes the polymerization of acrylonitrile. The water solubility and high catalyst stability make the process of removing the catalyst from the product easy. Direct aqueous workup of the reaction mixture could lead to the isolation of cyanoethylation products up to 99.9% purity.

Keywords. Aza-Michael Addition; Yttrium Nitrate; Amines; Biocompatible cyanoethylation.

ORAL PRESENTATION IN CONFERENCE

1. International conference on Advance Research in Molecular and Material Science (ARM2S-2022) on March, 2nd and 3rd, 2022. Organized by Sikkim Manipal Institute of Technology in association with Indian Chemical Society, Kolkata.

Title of the Presentation: “Design and Synthesis of 6-bromo-2-(4-(arylamino)butyl)quinazolin-4(3*H*)-one via 1,5-hydride shift to a distal Imine”

LIST OF SEMINAR ATTENDED

1. International Virtual Conference on Advances in Molecular Materials Research (AMMR-2021) 3-5 Feb, 2021 at Visva-Bharati, Santiniketan, India. Organised by Visva-Bharati; India, Osaka University; Japan and Jadavpur University, India.
2. International conference on Advance Research in Molecular and Material Science (ARM2S-2022) on March, 2nd and 3rd, 2022. Organized by Sikkim Manipal Institute of Technology in association with Indian Chemical Society, Kolkata.
3. One Day International Seminar On Recent Developments in Chemistry-2023 (RDC-2023) December 8, 2023. Organised by Department of Chemistry in Collaboration with IQAC, Malda College, Malda.